H2020 Work Programme

D1.6 – REPORT ON H/C RECOVERY / STORAGE TECHNOLOGIES AND RENEWABLE TECHNOLOGIES

Lead Contractor: UoB

Date: 11/03/2021

This project has received funding from the European Union's Horizon 2020 research and innovation programme under grant agreement No 847097. The content of publication is the sole responsibility of the author(s). The European Commission or its services cannot be held responsible for any use that may be made of the information it contains.

Horizon 2020
European Union Funding
for Research & Innovation

This project has received funding from
the European Union's Horizon 2020 research and innovation
programme under grant agreement No 847097

Project title Supporting new Opportunities for Waste Heat And cold valorisation Towards EU decarbonization			
Project acronym	SO WHAT	**Start / Duration**	June 2019 (36 months)
Coordinator	RINA Consulting - RINA-C		
Website	www.sowhatproject.eu		

Deliverable details			
Number	1.6		
Title	Report on H/C recovery/storage technologies and renewable technologies		
Work Package	1		
Dissemination level[1]	PU = Public	**Nature**	Report
Due date (M)	29/02/2020	**Submission date (M)**	29/02/2020
Deliverable responsible	University of Birmingham - UoB		

[1] PU = Public
CO = Confidential, only for members of the consortium (including Commission Services)

Horizon 2020
European Union Funding
for Research & Innovation

This project has received funding from
the European Union's Horizon 2020 research and innovation
programme under grant agreement No 847097

	Beneficiary
Deliverable leader	Adriano Sciacovelli (University of Birmingham)
Contributing Author(s)	Adriano Sciacovelli (UoB), Giovanni Manente (UoB), Francisco Morentin (CAR), Giorgio Bonvicini (RINA-C), Carolina Ferrando (RINA-C)
Reviewer(s)	RINA-C, 2GOOUT
Final review and quality approval	Francesco Peccianti (29/02/2020)
	Update F. Peccianti (11/03/2021)

Document History			
Date	**Version**	**Name**	**Changes**
14/02/2020	1.0	Adriano Sciacovelli	Initial draft for review
28/02/2020	2.0	Adriano Sciacovelli, Giovanni Manente	Final Version
29/02/2020	Final	Francesco Peccianti	Quality check
10/03/2021	Update	G. Manente	Update according to feedback from external reviewers (notably chapters 2.7 and 5.6)

Horizon 2020
European Union Funding
for Research & Innovation

This project has received funding from
the European Union's Horizon 2020 research and innovation
programme under grant agreement No 847097

Executive summary

A wide range of waste heat and cold (WH/C) recovery technologies in industry are presently available. They greatly differ in terms of operating principle and operating conditions, target applications, development stage, costs and benefits. The overarching aim of this deliverable is therefore to publicly provide to stakeholders a comprehensive and unified view of the currently existing portfolio of WH/C recovery technologies and provide a robust basis for the SO WHAT tool development and specific applications. The specific objectives of this document are: i) systematically classify WH/C recovery technologies; ii) review the features and state-of-the-art performance of each technology considered; iii) examine the typical industrial applications of each technology; iv) identify emerging near-to-market WH/C recovery technologies and their potential. The document is structured into five main sections, each one dedicated to a macro category of WH/C recovery technology:

1. Heat-to-Heat technologies;
2. Thermal Energy Storage technologies;
3. Heat-to-Cold technologies;
4. Heat-to-Power technologies;
5. Heat upgrade technologies.

Within the section of each macro-category, the individual technologies are reviewed with a focus on operating principle, performance, typical applications and development stage. Where available technological advancement from recent H2020 projects are highlighted.

A mixture of consolidated and near-to-market WH/C recovery technologies has emerged from the systematic review carried out here, which demonstrate the long-stading utilization of WH/C technologies but also the need and the ongoing effort in technological development for difficult-to-recover WH/C. Most of the passive WH/C recovery technologies, which use heat/cold directly or at a lower temperature level, are already consolidated from technological and commercial point of view. This is the case for heat-to-heat technologies such as conventional heat exchangers, recuperators/regenerators, economizers and waste heat boilers which have been extensively used to valorise medium-to-high grade heat. In this area the technological development is primarily directed at maximize the heat transfer performance to increase WH recovery capacity as well as reduce space requirements. An example of such emerging technology is the case of heat pipe heat exchangers.

Active technologies (Heat-to-Power class and Heat Upgrade class) which transform or upgrade WH see a blend of consolidated and emerging technologies. High temperature power cycles (steam Rankine cycles) for conversion of WH into electricity are well consolidated Heat-to-Power technologies, with both technology suppliers and extensive know-how available from the power sector industries. Mid-to-low temperature power cycles see a mixture of niche commercial applications and of near-to-market solutions that necessitate further development mainly aimed at reducing specific costs due to intrinsically lower thermodynamic performance. This is the case for Organic Rankine Cycles (ORCs) and Kalina cycles. MW-scale ORCs are commercially available via a selected number of suppliers. Conversely, commercial applications of small scale ORCs (kW scale) remains prohibitive due to cost-performance limitations. Here, technological development is primarily aimed at developing more efficient expanders and evaporators in order to increase overall cycle performance. On the other hand, Kalina technology appears to be commercially available but only from one supplier which possess both IP rights as well as the specialized knowledge to design and installation of the technology. Further near to market Heat-to-power technologies have been also

Horizon 2020
European Union Funding
for Research & Innovation

This project has received funding from
the European Union's Horizon 2020 research and innovation
programme under grant agreement No 847097

identified. These includes thermoelectric technologies for direct conversion of WH through Seebeck effect and cryogenic technologies using the phase change (vaporization) of cryogenic working fluids (for example liquid nitrogen) to generate mechanical power as well as cooling effect as a by-product.

The class of Heat Upgrade technologies is dominated by Heat Pumps (HPs). Air source, ground source and water source HPs are widely commercially available and already employed for valorisation of WH by increasing the temperature at which it is available. The vast majority of HPs commercially available are electrical-driven vapour compression systems. Such feature creates further opportunity for WH valorisation and energy flexibility through coupling of thermal and electrical supply/demand. Most of the technological advancement in HPs technology is centred on the development of high temperature HPs for heat upgrade/supply above 140-160°C. A limited number of high temperature HPs is currently commercially for industrial applications.

Within the context of Heat upgrade and cooling production, Absorption heat pumps (AHP), absorption heat transformers (AHT) and absorption chiller are attractive options for valorisation of WH/C. Absorption technologies are thermally driven with minimal or negligible electricity consumption. Therefore, they can be driven purely through a suitable stream of WH. Technological development is mostly concentrated around AHTs with near-to-market systems currently available.

Thermal energy storage (TES) class also see a mixture of well established (sensible thermal energy storage), and near-to-market (latent heat and thermochemical energy storage) technologies. Within the context of WH/C valorisation, TES technologies provide a portfolio of possible functions. In its simplest implementation TES can operate as a passive technology by storing WH/C and make it available when heat/cold demand is present. Such type of TES operation has been implemented for WH/C recovery within the site of industrial processes. Mobile TES applications have been also envisioned with the aim of store WH/C from an industrial site to then deliver it to a nearby user (up to about 20 km from the WH source). Latent TES and thermochemical TES are particularly promising in this regard since they enable higher energy storage density compare to sensible TES.

More advanced applications of TES technology involve the synergic integration of TES with WH/C source, other WH/C recovery technologies and the demand side. In such context TES is an enabling technology that allows to recover WH/C through other technologies which would be otherwise not possible. This is the case, for example, when WH/C fluctuates in times and WH/C utilization or valorisation does not match the WH/C availability. From technological prospective, sensible TES is well established and commercially available particularly for temperatures below 100°C (hot water tanks). For higher temperatures, options (such as molten salts tanks) are available from the solar thermal industry, although currently not utilized in industrial processes for the purpose of WH/C recovery. Latent heat TES using phase change materials (PCMs) is an attractive option which has drawn significant attention and has developed to a near-to-market stage. A limited number of suppliers exists with products mostly for domestic applications but suitable for low-grade WH. Thermochemical TES is currently at Research & Development although pilot systems (TRL 5) have been show-cased for both stationary and mobile application. A few technological challenges around thermochemical TES still remain unsolved, although the technology remains the most promising one due to high theoretical energy storage density, ability to store WH/C with near-zero losses and wide range of storage temperatures.

Horizon 2020
European Union Funding
for Research & Innovation

This project has received funding from
the European Union's Horizon 2020 research and innovation
programme under grant agreement No 847097

Abbreviations

AHP: Absorption Heat Pump
AHT: Absorption Heat Transformer
ASHP: Air Source Heat Pump
BF: Blast Furnace
BTES: Borehole Thermal Energy Storage
CAES: Compressed Air Energy Storage
CAPEX: Capital Expenditure
CHP: Combined Heat and Power
COP: Coefficient of Performance
CSP: Concentrating Solar Power
DEN: Dearmean Engine
DH: District Heating
DHN: District Heating Network
DHW: Domestic Hot Water
DL: Dual loop ORC layout
DP: Dual pressure ORC layout
EAF: Electric Arc Furnace
ECO: Economizer
EGR: Exhaust gas Recirculation
HER: Exhaust Heat Recovery
GSHP: Ground Source Heat Pump
GT: Gas Turbine
HC: Hydrocarbon
HE: Heat Exchanger
HFC: Hydrofluorocarbon
HP: Heat Pump
HPHE: Heat Pipe Heat Exchanger
HRSG: Heat Recovery Steam Generator
HRVG: Heat Recovery Vapour Generator
HS: Heat Source
HT: High Temperature
HTF: Heat Transfer Fluid
HTHP: High Temperature Heat Pump
HVAC: Heating, Ventilation and Air Conditioning
ICE: Internal Combustion Engine
KC: Kalina Cycle
LAES: Liquid Air Energy Storage
LHTES: Latent Heat Thermal Energy Storage
LN: Liquid Nitrogen
LNG: Liquefied Natural Gas
LP: Low Pressure
LT: Low Temperature
M-TES: Mobilized Thermal Energy Storage
MW: Molecular Weight

Horizon 2020
European Union Funding
for Research & Innovation

This project has received funding from
the European Union's Horizon 2020 research and innovation
programme under grant agreement No 847097

NG: Natural Gas
NGCC: Natural Gas Combined Cycle
NTU: Number of Transfer Units
OCGT: Open Cycle Gas Turbine
ORC: Organic Rankine Cycle
OTSG: Once-through heat recovery steam generator
PBT: Payback time
PCM: Phase Change Material
PHE: Plate Heat Exchanger
PHES: Pumped Heat Energy Storage
PSHE: Plate and Shell Heat Exchanger
PTES: Pit Thermal Energy Storage
PV: Photovoltaic
RC: Recuperated ORC layout
REC: Recuperator
REG: Regenerator
SE: Stirling Engine
SIC: Specific Investment Cost
Q: Heat duty
sCO2: Supercritical CO_2 power cycle
SHE: Spiral Heat Exchanger
SPHE: Spiral Plate Heat Exchanger
SRC: Steam Rankine Cycle
SSHT: Single Stage Heat Transformer
STES: Sensible Thermal Energy Storage
STHE: Shell and Tube Heat Exchanger
T: Temperature
Tamb: Ambient Temperature
TCES: Thermochemical Energy Storage
TE: Thermoelectric
TEG: Thermoelectric generator
TES: Thermal Energy Storage
TMC: Transport Membrane Condenser
TPV: Thermophotovoltaic
TRL: Technology Readiness Level
TTES: Tank Thermal Energy Storage
VCHP: Vapour Compression Heat Pump
VHTHP: Very High Temperature Heat Pump
WF: Working Fluid
WGTES: Water Gravel Thermal Energy Storage
WH: Waste Heat
WHB: Waste Heat Boiler
WH/C: Waste Heat/Cold
WHTP: Waste Heat to Power
WHR: Waste Heat Recovery
WHRB: Waste Heat Recovery Boiler

Horizon 2020
European Union Funding
for Research & Innovation

This project has received funding from
the European Union's Horizon 2020 research and innovation
programme under grant agreement No 847097

WHTH: Waste Heat to Heat
WSHP: Water Source Heat Pump
WtE: Waste to Energy
Z: Figure of merit of a thermoelectric generator
ZT: Dimensionless figure of merit of a thermoelectric generator

Horizon 2020
European Union Funding
for Research & Innovation

This project has received funding from
the European Union's Horizon 2020 research and innovation
programme under grant agreement No 847097

TABLE OF CONTENTS

Horizon 2020
European Union Funding
for Research & Innovation

This project has received funding from
the European Union's Horizon 2020 research and innovation
programme under grant agreement No 847097

Horizon 2020
European Union Funding
for Research & Innovation

This project has received funding from
the European Union's Horizon 2020 research and innovation
programme under grant agreement No 847097

Horizon 2020
European Union Funding
for Research & Innovation

This project has received funding from
the European Union's Horizon 2020 research and innovation
programme under grant agreement No 847097

1 Introduction

This section has two main objectives: i) introduce the systematic classification of the WH/C recovery technologies adopted in this document and ii) illustrate the systematic approach adopted to review the existing literature in order to gather specific and quantitative information about each individual technology. In the following a subsection is dedicated to each one of the two objectives.

1.1 Definition and classification of waste heat and waste cold recovery technologies

The diagram of Figure 1 illustrates the classes of WH/C recovery technologies considered in this document, as well as the specific technologies within each class. Technologies within each class are further grouped depending on the level of technological and commercial maturity. The following five classes were identified in order to cover all the WH/C recovery options currently technically feasible:

1. Waste Heat-to-Heat (WHTH) technologies;
2. Thermal Energy Storage (TES) technologies;
3. Waste Heat-to-Cold (WHTC) technologies;
4. Waste Heat-to-Power (WHTP) technologies;
5. Heat Upgrade (HU) technologies.

The individual technology within each class share the same fundamental underlying working principle. It is worthy therefore here to briefly define more precisely each class:

Waste Heat-to-Heat (WHTH): class of passive WH/C recovery technologies designated to transfer a waste heat or waste cold stream to a lower temperature sink so that it can be reutilized by heat. No conversion or upgrade of the WH/C stream takes place. *Example of WHTH technology*: heat exchangers.

Thermal energy storage (TES): class of passive technologies designate to store thermal energy (heat and cold options available) for subsequent use in time, bridging mismatch between thermal energy availability and thermal energy demand. This is a class of enabling technologies. TES can capture waste heat or waste cold for its subsequent reutilization but more advanced uses are possible by integrating TES with other WH/C recovery technologies. *Example of TES technology*: hot water storage tanks.

Waste Heat-to-Cold (WHTC): class of technologies designated to produce cooling from WH. This is a class of active technologies which transforms the original WH stream. The WH stream is used to provide the energy necessary to drive the cooling process. The latter typically takes advantage of sorption phenomena involving a sorbent-sorbate pair. *Example of WHTC technology*: water-lithium bromide vapour absorption chiller.

Waste Heat-to-Power (WHTP): class of technology designated to produce an electrical power output from WH. This is a class of active technologies which transform the nature of the original WH stream. More specifically, the WH stream is used to drive an energy conversion process. The latter can be of different nature; options include power cycles and thermo-electric materials, the suitability of which largely depend of the size of the WH sources as well as the WH temperature. *Example of WHTP technology*: steam Rankine power cycles.

Horizon 2020
European Union Funding
for Research & Innovation

This project has received funding from
the European Union's Horizon 2020 research and innovation
programme under grant agreement No 847097

Waste Heat upgrade (HU): class of technology designated to upgrade the original WH source. This means lifting the temperature at which WH is originally available. This is an active technology which alters the conditions at which WH is available but do not transform it into a different form of energy. In the most common instances HU requires an expenditure of electrical energy to uplift WH temperature, although HU technologies purely driven by heat are available. In such instance a cooling effect is also provided as by product. *Example of HU technology*: vapour compression heat pumps.

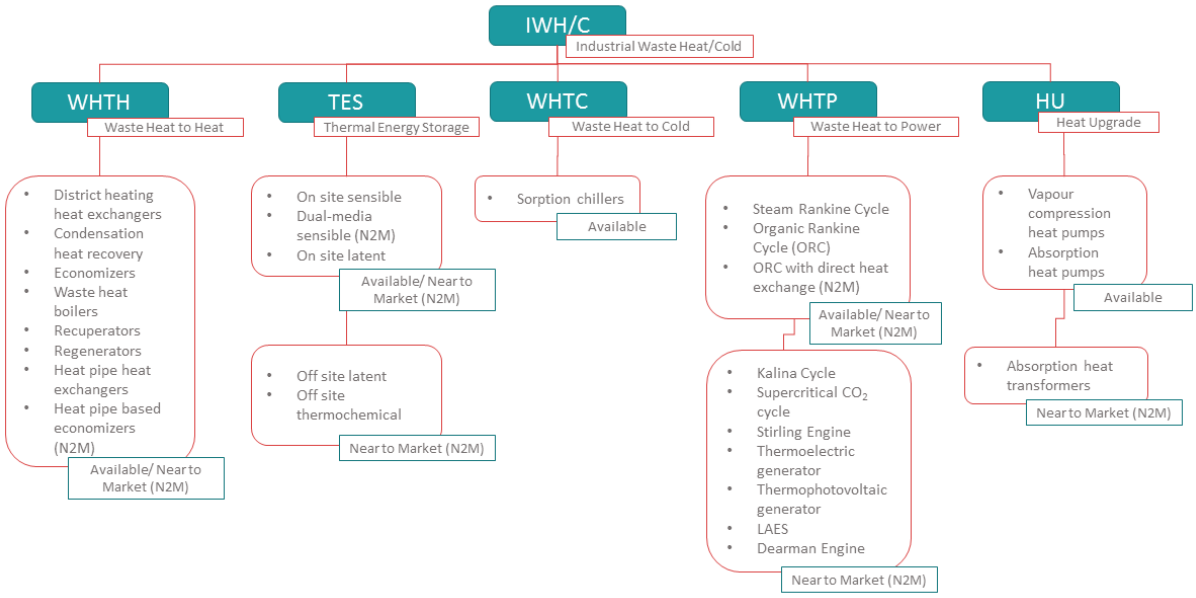

Figure 1: Classification of the technologies for recovery of industrial waste heat and waste cold.

1.2 Literature review methodology and main literature sources

A systematic approach was adopted to accurately capture the technological specifications, the typical performance, industrial applications and, where available, the costs of each individual technology listed in Figure 1. In this regard the literature was searched systematically. Three main categories of sources were considered:

Peer-reviewed scientific publications: Scopus and Web of Science Database were used to sieve the publications in top-tier journal of energy research such as *Applied Energy, Energy, Energy Conversion & Management, Applied Thermal Engineering, Renewable and Sustainable Energy Reviews*. With the articles initially retrieved a forward and backward search was performed to identify further relevant papers that were cited.

Technical reports from research institutions, governmental institutions and relevant research projects: online search was performed to identify and retrieve technical report which previously addressed WH/C recovery technologies and/or relevant topic in the proximity, for example energy efficiency in industrial processes. The search was directed at retrieving published work from highly esteemed institutions such as the US Department of Energy (DoE), UK Carbon Trust or the Department for Business, Energy & Industrial Strategy (BEIS). EU Cordis portal was also employed to identify recent or ongoing relevant projects and the corresponding public deliverables available.

Horizon 2020
European Union Funding
for Research & Innovation

This project has received funding from
the European Union's Horizon 2020 research and innovation
programme under grant agreement No 847097

Technical literature from technology manufacturers, suppliers and distributors. For each WH/C recovery technology already commercially available the main suppliers were identified. Where available technical literature from suppliers' official websites was retrieved to obtain technical specifications of the technologies provided.

Horizon 2020
European Union Funding
for Research & Innovation

This project has received funding from
the European Union's Horizon 2020 research and innovation
programme under grant agreement No 847097

2 Waste heat to heat (WHTH) technologies

2.1 District Heating Heat Exchangers (DH HEs)

According to (Frederiksen & Werner, 2013), the fundamental idea of district heating is to use local fuel or heat resources that would otherwise be wasted, in order to satisfy local customer demands for heating, by using a heat distribution network. Traditional excess heat resources are Combined Heat and Power (CHP) plants, Waste-to-Energy (WtE) plants, and industrial processes (S. Werner, 2017b). Industrial excess heat recovery from industrial processes (chemical industry, oil refineries) and recovered gases (e.g., black furnace gases) are in operation at about seventy locations in Sweden (S. Werner, 2017a). The enabling technology to recover the waste heat from industrial processes and transfer it to the district heating network (DHN) is the District Heating Heat Exchanger (DH HE). Several designs of Heat Exchangers (HEs) are available and currently used in the industrial sites to recover the waste heat. The Shell and Tube heat exchanger (STHE) and Plate heat exchanger (PHE) are the most common. In the following, the main features and operating conditions of these HEs are summarized. The focus is on the heat exchanger where heat is recovered from the industrial site. However, a brief paragraph is given about the typical design of HEs used in the district heating substations.

2.1.1 Technological features and performance

The main types of heat exchangers for district heating are the shell and tube HE, the plate HE (gasketed, brazed and welded), fin and tube coil, plate and shell and the spiral HE.

2.1.1.1 Shell and Tube Heat Exchangers (STHEs)

STHEs are built of round tubes mounted in a cylindrical shell with the tubes parallel to the shell (Kakac, Liu, & Pramuanjaroenkij, 2012). One fluid flows inside the tubes, while the other fluid flows across and along the axis of the exchanger. The major components of this exchanger are tubes (tube bundle), shell, front-end head, rear-end head, baffles, and tube sheets (Kakac et al., 2012). The simplest flow pattern through the tubes is for the fluid to enter at one end and exit at the other. This is a single-pass tube arrangement (Figure 2). To improve the heat transfer rate, higher velocities are preferred. This is achieved by increasing the number of tubeside passes. The number of tubeside passes generally ranges from one to eight (Thulukkanam, 2013). The standard design has one, two, or four tube passes. Longitudinal baffles divide the shell into two or more sections, providing multipass on the shellside. For exchangers requiring high effectiveness, multipassing on the shell side is adopted (Thulukkanam, 2013), but multipassing on the shell with longitudinal baffles will reduce the flow area per pass compared to a single pass on the shellside. This drawback is overcome by shells in series (up to six in heat recovery applications) which is also equivalent to multipassing on the shellside (Thulukkanam, 2013). STHEs employ low-finned tubes to increase the surface area on the shellside when the shellside heat transfer coefficient is low compared to the tubeside coefficient (e.g., when shellside fluid is highly viscous liquids, gases, or condensing vapours). STHEs provide relatively large ratios of heat transfer area to volume and weight and they can be easily cleaned. They offer great flexibility to meet almost any service requirement. STHEs can be designed for high pressures relative to the environment and high-pressure differences between the fluid streams (Kakac et al., 2012).

Horizon 2020
European Union Funding
for Research & Innovation

This project has received funding from
the European Union's Horizon 2020 research and innovation
programme under grant agreement No 847097

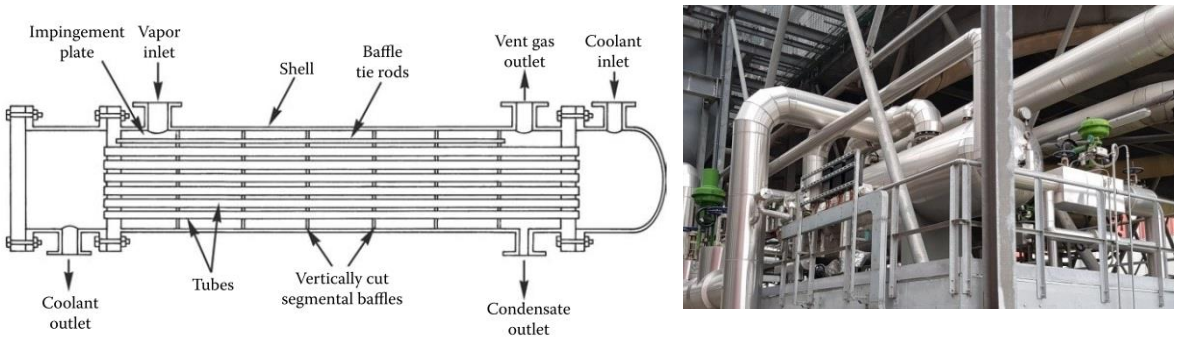

a) b)

Figure 2: STHE: a) Schematic of a shell side condenser (Kakac et al., 2012); b) Picture of a STHE installed in a CHP district heating plant (G. Manente et al., 2018).

2.1.1.2 Plate heat exchangers (PHEs)

PHEs are built of thin plates forming flow channels. The fluid streams are separated by flat plates. PHEs are used for transferring heat for any combination of gas, liquid, and two-phase streams (Kakac et al., 2012). However, the characteristics of PHEs are such that they are particularly well suited to liquid–liquid duties, whereas they are not recommended for gas-to-gas applications (Thulukkanam, 2013). These heat exchangers can further be classified as gasketed plate, brazed plate and welded.

- **Gasketed Plate Heat Exchangers**

A gasketed PHE is usually comprised of a stack of corrugated metal plates in mutual contact, each plate having four apertures serving as inlet and outlet ports, and seals designed so as to direct the fluids in alternate flow passages (Figure 3). The flow passages are formed by adjacent plates so that the two streams exchange heat while passing through alternate channels. The number and size of the plates are determined by the flow rate, physical properties of the fluids, pressure drop, and temperature program (Thulukkanam, 2013). The plate corrugations promote fluid turbulence and support the plates against differential pressure. The stack of plates is held together in a frame by a pressure arrangement (Figure 4). The periphery of each plate is grooved to house a moulded gasket, each open to the atmosphere. Table 1 shows the main design features and parameters of the gasketed PHEs and Table 2 reports their main advantages.

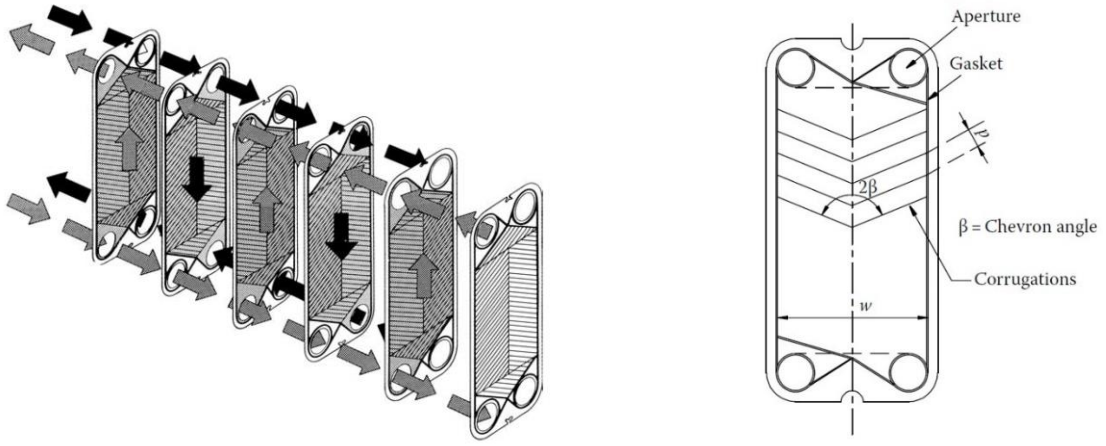

a) b)

Figure 3: a) Diagram showing the flow paths in a gasketed PHE (Kakac et al., 2012); b) Schematic showing a Chevron plate (Thulukkanam, 2013).

Horizon 2020
European Union Funding
for Research & Innovation

This project has received funding from
the European Union's Horizon 2020 research and innovation
programme under grant agreement No 847097

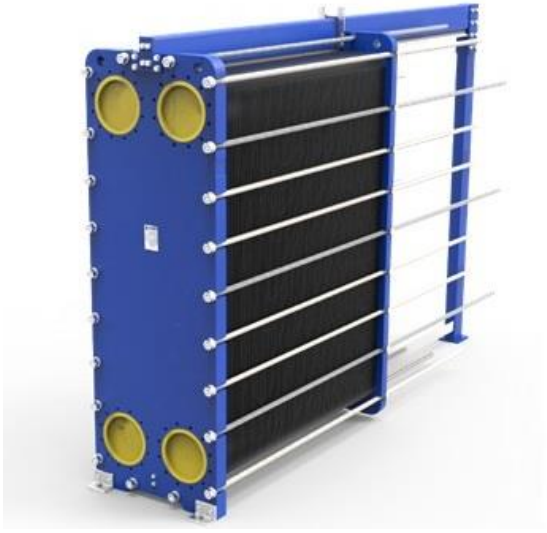

Figure 4: Gasketed PHE ("Sondex - Plate heat exchanger," 2020).

Table 1: Geometrical features, operational data and performance of gasketed PHEs (Thulukkanam, 2013).

Parameter	Value
Maximum operating pressure (bar)	25÷30
Maximum temperature (°C)	160÷200
Maximum flow rate (m^3/h)	3600
Heat transfer area (m^2)	0.1÷2200
Number of plates	<700
Minimum temperature approach (°C)	≈ 1
Heat recovery (%)	< 93
Common plate materials	Stainless steel, Inconel, Cupronickel, Hastelloy, Incoloy, Titanium, Aluminium brass

Table 2: Main features and benefits of gasketed PHEs (Thulukkanam, 2013).

Feature	Comment
High turbulence and high heat transfer performance	Very high heat transfer coefficients
Reduced fouling	Less need for frequent cleaning
Cross-contamination eliminated	The space between gaskets is vented to atmosphere
True counterflow	Possibility to reach higher temperatures of the heating medium
Close approach temperature	≈ 1°C
Multiple duties with a single unit	It is possible to heat or cool two or more fluids within the same unit
Expandable	Due to the modular construction
Easy to inspect and clean and less maintenance	It can be easily opened
Lightweight	Reduced liquid volume space and less surface area for a given application
High-viscosity applications	High-viscosity fluids in turbulent flow

Horizon 2020
European Union Funding
for Research & Innovation

This project has received funding from
the European Union's Horizon 2020 research and innovation
programme under grant agreement No 847097

- **Brazed Plate Heat Exchangers**

Brazed PHE evolved from the conventional PHE in answer to the need for a compact PHE for high-pressure and high-temperature duties. Like the gasketed PHE, the brazed PHE is constructed of a series of corrugated metal plates but without the gaskets (Thulukkanam, 2013). The plates are brazed together in a vacuum oven to form a complete pressure-resistant unit. Brazed PHEs accommodate a wide range of temperatures, from cryogenic to 200°C (Thulukkanam, 2013), and pressures up to 30 bar (Hesselgreaves, Law, & Reay, 2017). Because of the brazed construction, the units are not expandable.

- **All-Welded Plate Heat Exchangers**

This design entirely eliminates the gaskets and by developing a fully welded plate exchanger further enhances the reliability as well as the temperature and pressure limits. Only chemical cleaning is possible. The absence of gaskets allows operational temperatures to 350°C and pressures up to 40 bar (Hesselgreaves et al., 2017).

2.1.1.3 Compact Fin and Tube Coils

Tube-fin HEs are widely used throughout the industry in a variety of applications. They are employed when one fluid stream is at a higher pressure and/or has a significantly higher heat transfer coefficient compared to the other fluid stream (Kakac et al., 2012). For example, in a gas-to-liquid exchanger, the heat transfer coefficient on the liquid side is generally very high compared to the gas side. Fins are used on the gas side to increase surface area. The most common materials for tubes and fins are copper, aluminium, and steel. For instance, Kelvion HE coils are manufactured with copper tubes and aluminium or copper fins ("Kelvion - Coils," 2020).

a) *b)*

Figure 5: a) Schematic of a tube-fin HE (Kakac et al., 2012); b) Fin and tube coils manufactured by Kelvion ("Kelvion - Coils," 2020).

2.1.1.4 Plate and Shell Heat Exchangers (PSHEs)

PSHEs combine the compact and counter current advantages of PHEs with the high pressure ratings of STHEs provided by the cylindrical shell ("Gesmex," 2020). The core of this heat exchanger is a fully welded plate pack enclosed in a strong shell structure, which eliminates the need for a gasket ("Vahterus," 2020). This exchanger utilises a welded pack of corrugated plate pairs of circular planform with ports for one fluid at the extremes of a diameter, so that this fluid finds its own flow path within the plate planform. The other fluid is introduced through ports in the cylindrical shell and

Horizon 2020
European Union Funding
for Research & Innovation

This project has received funding from
the European Union's Horizon 2020 research and innovation
programme under grant agreement No 847097

is ducted across the plate pack in counterflow, as shown in Figure 6 (Hesselgreaves et al., 2017). Because of the feature of a cylindrical shell, the containment pressures are higher than for other plate types, with design pressures over 100 bar being quoted. The units sold by Alfa Laval are all-welded heat exchangers designed for use with liquids, gases and two-phase mixtures at temperatures up to 540°C (Hesselgreaves et al., 2017). This plate-and-shell unit works well with aggressive media (e.g., organic solvents) that are beyond the capabilities of gasketed heat exchangers. Besides Alfa Laval, other manufacturers are Gesmex ("Gesmex," 2020) and Vahterus ("Vahterus," 2020). The main operating parameters reported by these manufactures are shown in Table 3.

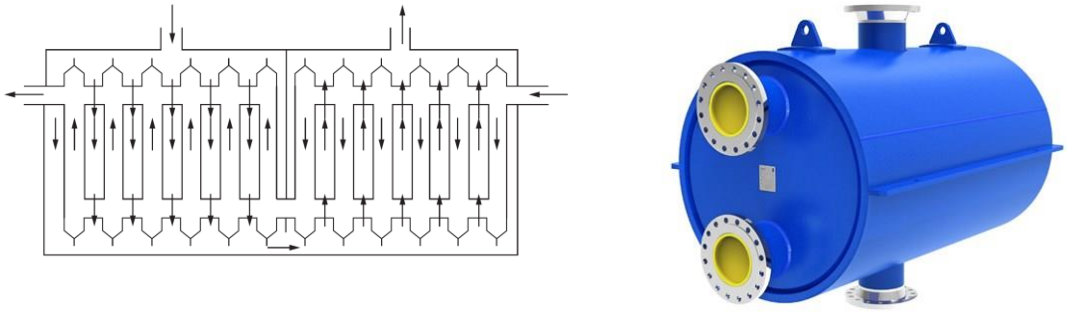

a) *b)*

Figure 6: a) Schematic of the flow pattern in a PSHE (Hesselgreaves et al., 2017); b) Picture of a PSHE manufactured by Sondex ("Sondex - Plate and shell HX," 2020).

Table 3: Operating parameters of PSHEs ("Gesmex," 2020) ("Vahterus," 2020)("Alfa Laval - Plate and Shell HXs," 2020).

Parameter	Value
Heat transfer surface (m^2)	1÷1000
Heat duty (kW)	10÷100000
Maximum operating pressure (bar)	100÷400
Maximum operating temperature (°C)	450÷600
Minimum operating temperature (°C)	-200

2.1.1.5 Spiral heat exchangers (SHEs)

SHEs are formed by rolling two long, parallel plates into a spiral using a mandrel and welding the edges of adjacent plates to form channels (Kakac et al., 2012). One fluid enters the centre of the unit and flows towards the periphery. The other fluid enters the unit at the periphery and moves towards the centre ("Alfa Laval - Spiral heat exchangers," 2020) (Figure 7). The different media flow counter-currently in these channels with no risk of intermixing. The channels are curved and have a uniform cross section. The two spiral paths introduce a secondary flow, increasing the heat transfer and reducing fouling deposits. These heat exchangers are quite compact but are relatively expensive due to their specialized fabrication. The SHE is particularly effective in handling sludge, viscous liquids, and liquids with solids in suspension including slurries (Kakac et al., 2012). The main features are shown in Table 4.

Horizon 2020
European Union Funding
for Research & Innovation

This project has received funding from
the European Union's Horizon 2020 research and innovation
programme under grant agreement No 847097

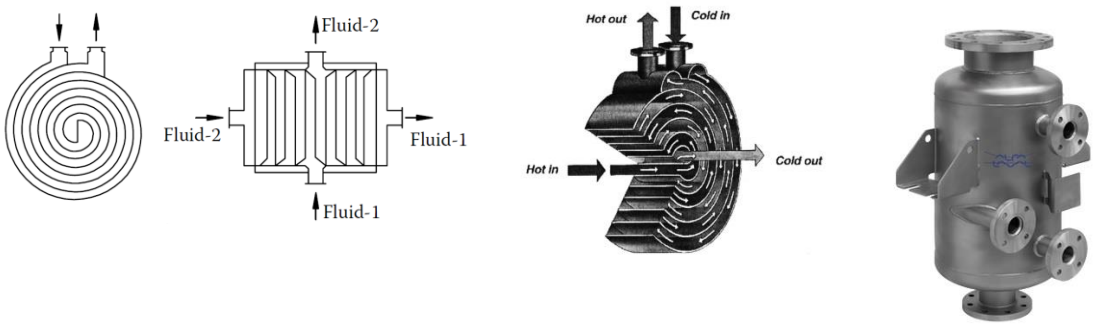

a) b) c)

Figure 7: Spiral heat exchanger: a) Schematic of the flow pattern (Thulukkanam, 2013); b) Schematic of the flow pattern (Hesselgreaves et al., 2017); c) Spiral heat exchanger manufactured by Alfa Laval ("Alfa Laval - Spiral heat exchangers," 2020).

Table 4: Main features of spiral HXs (Kakac et al., 2012)("Alfa Laval - Spiral heat exchangers," 2020).

Parameter	Value
Heat transfer surface (m²)	0.5÷2500
Maximum operating temperature (°C)	400÷500
Maximum operating pressure (°C)	15÷100

2.1.1.6 Heat exchangers in the building substations

The HE in the building is used to transfer the energy from the DH heating distribution system (primary system) to the building distribution system (secondary system). The heat exchanger provides the interface between the primary and secondary systems and ensures hydraulic separation is maintained at all times (Skagestad & Mildenstein, 2002). PHEs generally have a cost advantage and require less space compared with most standard STHEs. They require significantly less surface area, for the same operating conditions, than shell and tube units because they have much higher heat transfer rates. With plate exchangers, the approach temperature between the primary return and the secondary return is closer, generally 1÷2°C, compared with 6÷7°C for most STHEs (Skagestad & Mildenstein, 2002). For this reason, DH operators often favour the plate type. Brazed PHEs tend to be smaller than gasketed PHEs as more surface area is devoted to heat exchange. They also do not require the level of maintenance required by the gasketed option. STHEs are still being used in some DH systems but are gradually being phased out, as they do not provide sufficiently low approach temperatures between primary and secondary side water. They also take up a lot of space. Shell and spiral tube heat exchangers do not share the disadvantages of other types of shell and tube heat exchangers, and are excellent for district heating applications (Skagestad & Mildenstein, 2002).

2.1.2 Technology readiness level and examples of applications

In the following the main experiences and studies reported in the literature of WHR from industrial sites and heat supply to the DHN are summarized. The aim of this section is to highlight some heat recovery option with high potential that have been implemented or investigated only recently.

- **Steel industry**

1) Heat recovery from slag. In (Yemao Li, Xia, Fang, Su, & Jiang, 2016) a scheme was proposed to integrate the surplus heat of two steel plants into a large-scale DHN. The steel plants purchase iron ore as raw material and produce steel products in four major processes: sintering, iron-making, steel-

Horizon 2020
European Union Funding
for Research & Innovation

This project has received funding from
the European Union's Horizon 2020 research and innovation
programme under grant agreement No 847097

making, and steel-rolling. Three sources of surplus heat were identified as suitable for the district heating: 1) slag-flushing water of blast furnace (BF); 2) cooling water of blast furnace; 3) low-pressure mixed saturated steam produced in processes of steel-making and steel-rolling. The heat in cooling water and low-pressure steam are directly recovered by using conventional water-to-water and steam-to-water HEs having efficiencies close to 100%. Instead, the heat in slag-flushing water is recovered according to the scheme shown in Figure 8, where two main energy losses can be identified. The BF slag is quenched by water and is cooled from 1450°C to approximately 100°C. Putting the hot slag into the water leads to local boiling and a part of water flashes into steam. The rest heat of BF slag will be absorbed by the water resulting in temperature rise. The mixture of water and slag will flow into the sedimentation tank. The heat recovery efficiency, which is defined as the proportion of heating potential, is experientially estimated at approximately 52%, because heat is lost unavoidably during the quenching and the depositing. The demonstration project conducted since 2014 showed that the slag flushing water can provide up to 90.5 MW for DH and 15 MW for factory heating.

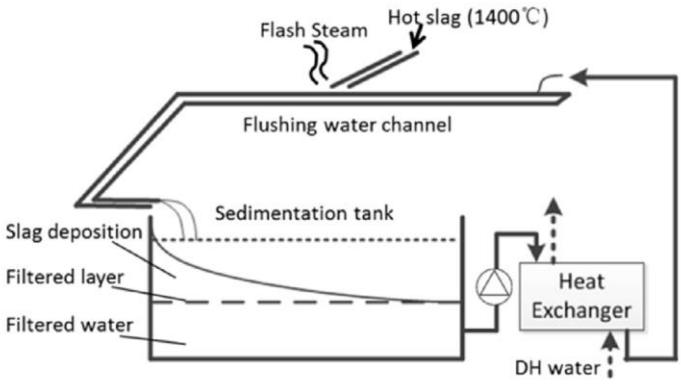

Figure 8: Heat recovery from the blast furnace flushing water (Yemao Li et al., 2016).

2) Electric Arc Furnace (EAF) off gas. Depending on the EAF operation and input materials, approximately 30% of the total energy input is dissipated to the off gas. The off gas is cooled down from approximately 1000°C by a water-cooled duct, followed by a second-stage gas cooler before entering the filter plant and the stack. In this cooling process, most of the energy is dissipated to the ambient (Fleischanderl, Steinparzer, & Trunner, 2017). Waste heat can be recovered by replacing the conventional water-cooled hot gas line by a heat recovery duct. In this case, the off gas cooling is done with pressurized water at elevated temperatures. As part of a revamp of the dedusting system of the EAF at a steel plant in Sweden, the recovered waste heat was used to generate hot water for DH. To equalize fluctuations of the EAF and to supply constant heat flow to the DHN, a thermocline-type buffer tank was implemented (Fleischanderl et al., 2017). In a recent project led by SIJ Metal Ravne (Slovenian steel group) the waste heat generated by the cooling system of the EAF is recovered by the installation of a 4.2 MW PHE (Figure 9). The recovered heat is used for space heating and domestic hot water heating (Konovšek et al., 2017) for the community of Ravne na Koroškem (Slovenia).

Horizon 2020
European Union Funding
for Research & Innovation

This project has received funding from
the European Union's Horizon 2020 research and innovation
programme under grant agreement No 847097

Figure 9: PHE (4.2 MW) for WHR from an EAF in a steel plant (Konovšek et al., 2017).

3) Cooling process of hot steel slabs. The recovery of surplus heat from a cooling facility at a steel mill in Aviles (Spain) is investigated in (Villar, Parrondo, & Arribas, 2014). Hot slabs enter into the last building at about 500°C and are progressively removed when their temperature has decreased at least 250°C. Cooling of the slab stacks typically occurs by thermal radiation toward the building boundaries and by natural convection to the surrounding air. The proposed WHR solution, shown in Figure 10, is formed by: a) Hoods in the cooling facility above the lines of slab stacks to accumulate and collect hot air (above 180°C); b) Thermally insulated air duct and fan to drive hot air from hoods through the primary HE; c) STHE to heat the DH water.

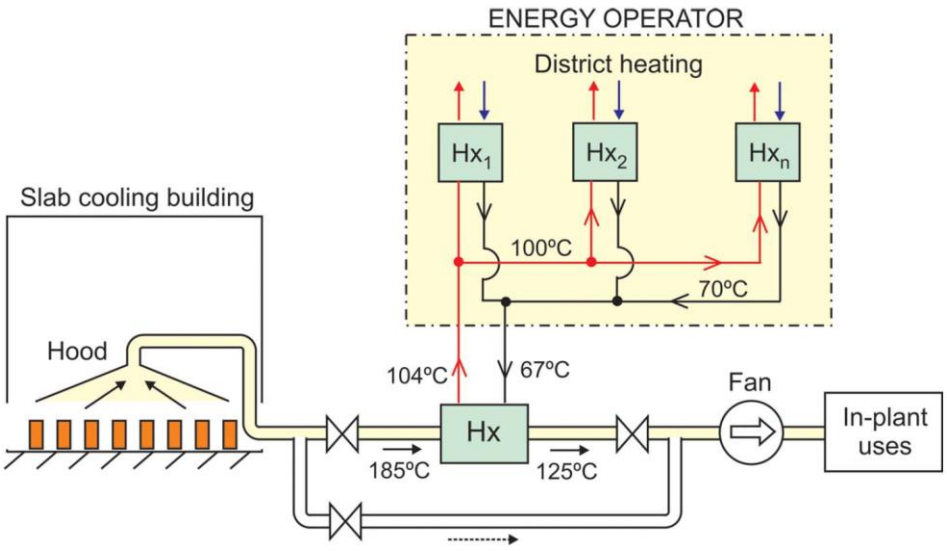

Figure 10: WHR from hot steel slabs and heat supply to the DHN (Villar et al., 2014).

Horizon 2020
European Union Funding
for Research & Innovation

This project has received funding from
the European Union's Horizon 2020 research and innovation
programme under grant agreement No 847097

Table 5: WHR from the steel industry and heat supply to DHNs.

TRL	Plant	Location	Heat source/s	T heat sources (°C)	Q heat sources (MW)	Reference
9	Steel	Ravne na Koroškem (Slovenia)	Cooling system EAF	/	4.2	(Konovšek et al., 2017)
9	Steel	Sweden	Off gas from EAF	≈1000	/	(Fleischanderl et al., 2017)
7	Steel	Qianxi (China)	1) Slag-flushing water 2) Cooling water of BF 3) Low-pressure steam (4 bar)	1) <100 2) 35÷45 3) 143	1) 188.4 2) 156.7 3) 52	(Yemao Li et al., 2016)
N/A	Steel	Aviles (Spain)	Cooling air steel slabs	180	1.1	(Villar et al., 2014)

- **Gas refinery plant**

In the gas refinery plant reported in (Zebik, Baliko, & Mont, 1997) there was a potential of 54.2 MW of recoverable waste heat from different waste heat sources as shown in Table 6. Figure 11 shows the T-Q chart of waste heat that can be utilized for DH. On the basis of Figure 11, it can be seen that in case of heating to 80°C all the heat can be utilized in theory. Instead, in case of heating to 100°C and 130°C it is impossible to use all the available heat sources. For instance, when utilization of waste heat is assumed with a minimum Δt = 10°C between the heating and cooling mediums, then the available heat at temperature of 100°C is 42.14 MW. The resulting heat transfer network of maximum energy recovery is quite complex. A much simpler heat transfer network can be obtained leaving out the heat flows from both the gas engine and the electric motor-driven compressors, as shown in (Zebik et al., 1997).

Table 6: Waste heat recovery from a gas refinery plant and heat supply to DHNs.

TRL	Location	Plant	Heat sources	Tin / Tout (°C)	Q (MW)	Reference
N/A	Budapest (Hungary)	Gas refinery	1) Cold water circuit 2) Condensers 3) Hot water circuit 4) Gas cooling from compressors 5) Flue gas from boiler house 6) Flue gas from pipe kiln 7) Exhaust gas from gas compressors 8) Torch-gas	1) 50/45 2) 53÷ 70/53÷70 3) 83/75 4) 100÷120/50 5) 160/130 6) 320/30÷130 7) 450/130 8) 1000/500	1) 3.2 2) 19.8 3) 5.7 4) 8.6 5) 0.9 6) 4.25 7) 5.3 8) 6.5	(Zebik et al., 1997)

Horizon 2020 European Union Funding for Research & Innovation

This project has received funding from the European Union's Horizon 2020 research and innovation programme under grant agreement No 847097

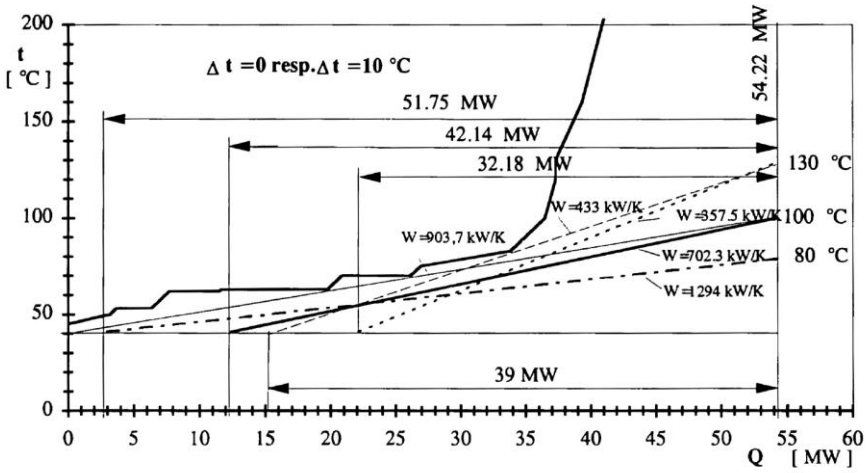

Figure 11: T-q diagram of waste heat utilization in the gas refinery plant for three different district heating supply temperatures (80°C, 100°C and 130°C) and a return temperature of 40°C.

- **Aluminium industry**

Primary aluminium production takes place in three major stages: bauxite mining, alumina refining and aluminium smelting (Fleer, Lorentsen, Harvey, Palsson, & Saevarsdottir, 2010). The aluminium smelting process reduces the alumina to aluminium in electrolytic cells, also called reduction cells or pots. The process is called Hall-Héroult process. In the Hall-Héroult process liquid aluminium is produced by the electrolytic reduction of alumina (Al_2O_3) dissolved in an electrolyte bath. A typical reduction cell consists of an anode and a cathode to apply a continuous high amperage and low voltage current to the electrolyte bath (Figure 12 left). During normal cell operation, the electrolyte bath has a temperature of around 955-965°C (Fleer et al., 2010). Below the electrolyte bath there is a pool of liquid aluminium, which is contained in a carbon lining. The carbon lining is thermally insulated by refractory and insulation materials inside a steel shell. As a result of the Hall-Héroult process, solid and gaseous emissions are released while aluminium is produced in the cells. Thus, each cell is covered by a hooding system which is connected to an individual exhaust duct (Fleer et al., 2010). The exhaust gas from the cells is collected in ductwork, which leads to one or more fume treatment plants. Figure 12 left provides a schematic representation of the distribution of energy flow and the main heat losses in the aluminium production highlighted using yellow arrows. Approximately 30-45% of the total waste heat is carried away by the exhaust gas which is drawn from the cell (M. Yu, 2018). During the production of aluminium, exhaust gas is collected from each cell and transported to a gas treatment unit where the pollutant gases are removed. The exhaust gas enters the gas treatment unit at 110°C and exit at 95°C through the stack (Haraldsson, 2019). In the investigated WHR scheme shown in Figure 12 (right) the district heating HE was placed upstream of the gas treatment unit (position A) taking into account the higher temperature and other successful experiences of installation of HEs on the dirty side. More than 20 MW of waste heat could be recovered by cooling the gases from 110°C to the acid dew point of 84°C. Figure 13 shows the integration of the DH HEs into the plant where only half of the exhaust gases are used to fulfil the limited users` demand. The exhaust gases leaving the pot rooms at 110°C are cooled to 98°C and admitted to the gas treatment unit. On the cold side, the return water is heated up to 80°C and supplied to the DHN. The overall heat duty of the HE units is 5.2 MW. A vertical counterflow shell and tube design is selected where the dirty exhaust gas flows inside the tubes and the water is heated on the shell side, to avoid fouling (vertical) and simplify the cleaning

Horizon 2020
European Union Funding
for Research & Innovation

This project has received funding from
the European Union's Horizon 2020 research and innovation
programme under grant agreement No 847097

process (gas in tube). It was demonstrated on the real field (STHE in Mosjøen, Norway) that the placement of this type of STHE on the dirty side is possible without having to clean it for 8+ years running, while still maintaining an acceptable heat transfer coefficient (Haraldsson, 2019).

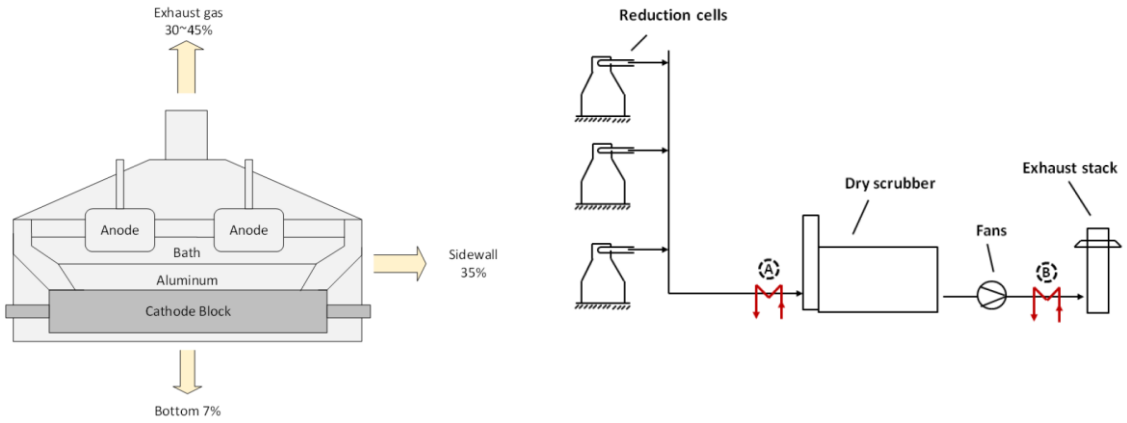

a) b)

Figure 12: a) Heat losses from a typical Hall-Héroult cell (M. Yu, 2018); b) Possible locations (A or B) for a DH HE linked to a pot line (Fleer et al., 2010).

Table 7: WHR from an aluminium plant and heat supply to DHNs.

TRL	Plant	Location	Heat source	Inlet T (°C)	Q (MW)	Reference
N/A	Aluminium	Fjarðaál (Iceland)	Exhaust gas (dirty)	110	5.2	(Haraldsson, 2019)

Horizon 2020
European Union Funding
for Research & Innovation

This project has received funding from
the European Union's Horizon 2020 research and innovation
programme under grant agreement No 847097

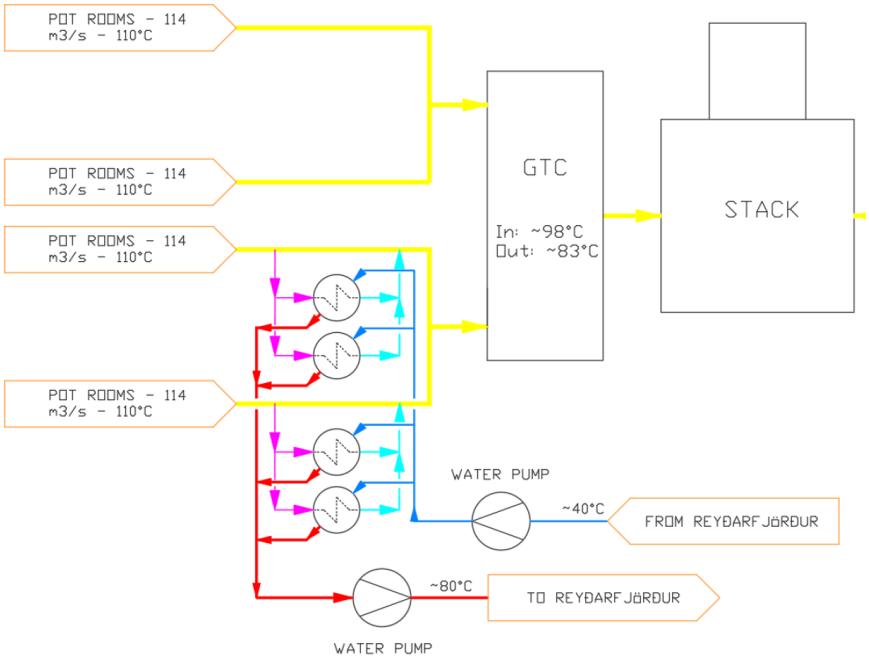

Figure 13: Heat recovery from the exhaust gas of an aluminium plant and heat supply at 80°C (Haraldsson, 2019).

- **Data centres**

The temperature of captured waste heat depends on the location where it is captured and on the cooling technology. In air-cooled data centres waste heat can generally be captured between 25 °C and 35 °C. In liquid cooled stations, waste heat can be captured closer to processors, where operating temperatures are higher and therefore the captured waste heat is of a higher temperature, e.g. 50÷60 °C (Wahlroos, Pärssinen, Manner, & Syri, 2017)(Davies, Maidment, & Tozer, 2016a). In low-temperature district heating networks (LT DHNs) water supply temperature can be lower than 50°C and the return temperature close to 20°C. Since the supply water temperatures are below 50 °C, waste heat from liquid cooled data centres could be directly fed to the LT DHN without the heat pump (HP), especially for data centres with modern cooling technologies, which allow high WHR temperatures (Wahlroos et al., 2017).

- **Pulp mill**

The Kraft pulping process is the prevalent manufacturing process, on a world scale, by which wood chips are reduced to paper pulp, the intermediate material from which the paper products are made. The core of the Kraft process is a chemical delignification step in which the individual cellulosic fibres are separated to form the pulp. The thermal energy required for the various process operations is produced in recovery boilers where the spent liquor and the wood residues are burnt to generate process steam (Figure 14a). In an efficient mill an excess steam production capacity is available that could be used to supply the heat demand of an adjacent DHN, as investigated in (Marinova, Beaudry, Taoussi, Trépanier, & Paris, 2008). The main transfer station in Figure 14b includes a HE where heat from steam desuperheating and condensation is transferred to the hot water which circulates in the distribution network. The distribution network consists of two parallel main ducts, one for the outgoing hot water (110°C) from the main transfer station and one for the returning cooled water (90°C). An exemplary utilization of the the excess heat in a pulp mill to feed a DHN is Södra Cell Värö

Horizon 2020
European Union Funding
for Research & Innovation

This project has received funding from
the European Union's Horizon 2020 research and innovation
programme under grant agreement No 847097

plant on the west coast of Sweden that has been supplying district heat to the Varberg municipality for almost 20 years. The heat from the mill's wastewater and that recovered from the boiler's flue gases almost meet Varberg's entire district heating demands (ABB, 2012).

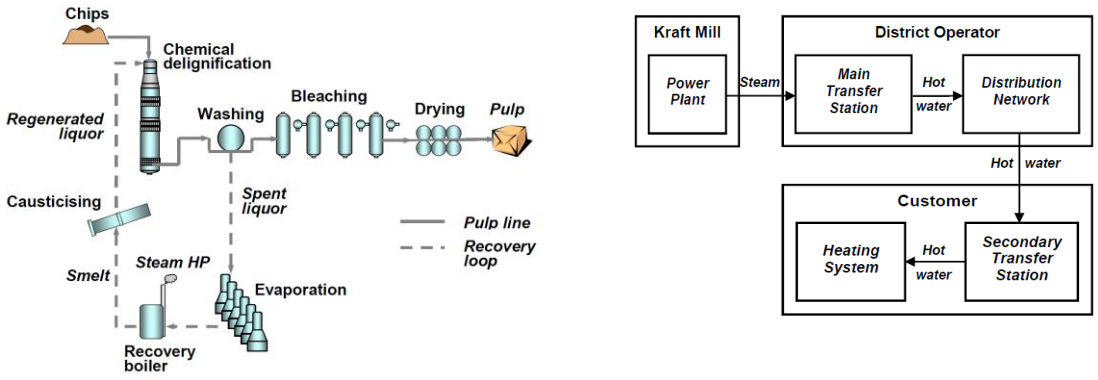

a) *b)*

Figure 14: a) Schematic of the Kraft pulping process and steam production; b) Utilization of the excess steam in the DHN.

Table 8: WHR from a pulp mill plant and heat supply to DHNs.

TRL	Plant	Location	Heat source/s	Heat source inlet T (°C)	Heat supply T to the DHN (°C)	Heat duty (MW)	Reference
9	Pulp mill	Varberg (Sweden)	1) mill`s wastewater 2) flue gases	/	<90	29	(ABB, 2012)
N/A	Pulp mill	Eastern Canada	Excess high pressure steam (31 bar)	370	110	/	(Marinova et al., 2008)

- **Copper plant**

The industrial waste heat in a copper plant mainly comes from the cooling water of different production processes. Based on an investigation of the waste heat and evaluation of the feasibility of recovery, the usable waste heat sources of a copper plant in Chifeng City (Northern China) are listed in Table 9 (Xia, Zhu, & Jiang, 2016). The waste heat is used in a DHN to serve a residential area of the city during the heating season. Thanks to the low return water temperature (30°C) the theoretical maximum outlet temperature of the heat-collecting water can reach 84.7 °C (Figure 15). With a simplified heat exchanger network the supply temperature is 83.7°C (Xia et al., 2016). To recover the considerable amount of waste heat released into the environment during the non-heating season a borehole sensible TES system was added in 2016 (L. Xu, Torrens, Guo, Yang, & Hensen, 2018). A DHN utilizing the waste heat of a copper industry has been recently built in Hamburg (Germany). The copper producer Aurubis AG supplies industrial waste heat to heat the Hamburg port quarter HafenCity Ost. The company extracts heat that is formed when sulphur dioxide (a by-product of copper smelting) is converted into sulphuric acid ("Copper Alliance - Aurubis," 2020). Eight state-of-the-art PHEs made of special Hastelloy materials were installed.

Horizon 2020
European Union Funding
for Research & Innovation

This project has received funding from
the European Union's Horizon 2020 research and innovation
programme under grant agreement No 847097

Table 9: Industrial waste heat sources in a copper plant located in Chifeng City of Northern China (Xia et al., 2016).

TRL	Plant	Location	Heat source	Q (kW)	Tin/Tout (°C)
9	Copper	Chifeng City (China)	1) Acid desiccation-1 2) Acid absorption-1 3) Acid desiccation-2 4) Acid absorption-2 5) Furnace cooling	3910 7802 7819 15603 26527	65/45 100/80 65/45 100/80 70/40

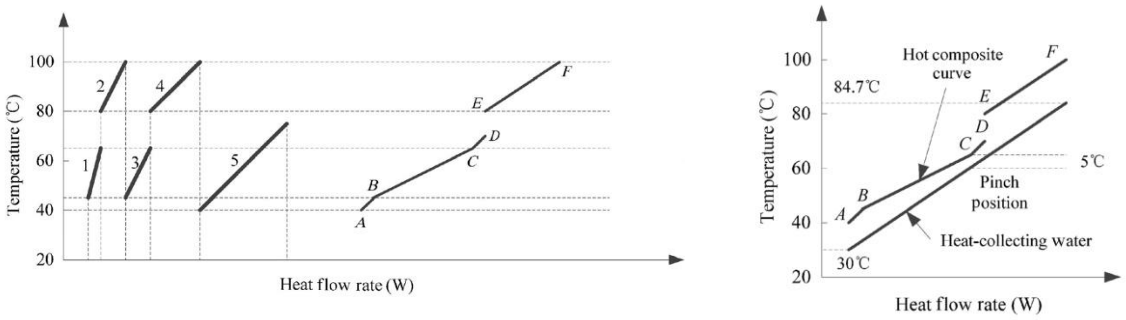

a) *b)*

Figure 15: a) Waste heat streams in a copper plant and hot composite curve. b) Heat transfer between hot composite curve and district heating water (Xia et al., 2016).

Table 10: WHR from copper plants and heat supply to DHNs.

TRL	Plant	Location	Heat sources	Heat sources inlet T (°C)	Heat supply T to the DHN (°C)	Q (MW)	Reference
9	Copper	Chifeng City, Inner Mongolia (China)	see Table 9	see Table 9	70	100	(L. Xu et al., 2018)
9	Copper	Hamburg (Germany)	/	/	/	/	("Copper Alliance - Aurubis," 2020)

- **Cement plant**

1) Flue gas. One of the main sources of waste heat in cement plants is the flue gas from the white kilns. In the Aalborg (Denmark) Portland cement factory the solution to this energy loss was to implement a WHR system, in which the flue gas from the five white kilns are utilized in HE installations to transfer the thermal energy to Aalborg's DHN ("Aalborg Portland's supply of surplus heat from production in the form of district heating," 2020).

2) Rotary kiln. The heat recovery from a rotary kiln was theoretically investigated in (Söğüt, Oktay, & Karakoç, 2010) for a cement plant in Turkey. The surface temperature of the rotary kiln varies between 200 and 300 °C. A heat recovery exchanger was modelled to make use of this energy (Figure 16). The temperature of the air between the surface of the rotary kiln and the heat exchanger is approximately 160°C. The water flowing in the tubes was heated up to temperatures between 90 and 140°C depending on the flow rate. The optimum water flow is determined with respect to the kind of

Horizon 2020 European Union Funding for Research & Innovation
This project has received funding from the European Union's Horizon 2020 research and innovation programme under grant agreement No 847097

heating project. The total heat transfer from the rotary kiln's waste heat to the water flowing through exchanger was calculated equal to 3 MW. The schematic layout of a district heating system using this waste heat is shown in Figure 17.

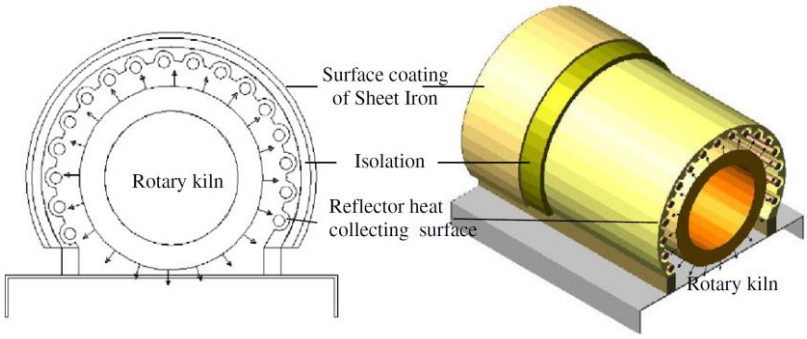

Figure 16: Cross sectional picture of the waste recovery heat exchanger from a rotary kiln (Söğüt et al., 2010).

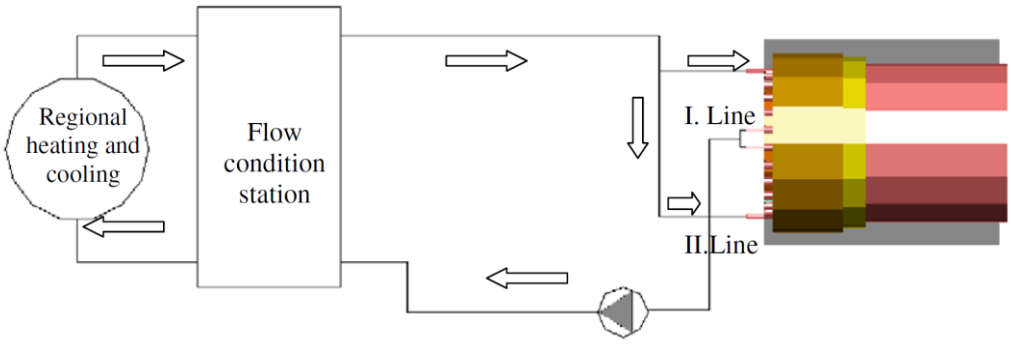

Figure 17: Utilization of the thermal energy recovered from the cement kiln for district heating (Söğüt et al., 2010).

Horizon 2020
European Union Funding
for Research & Innovation

This project has received funding from
the European Union's Horizon 2020 research and innovation
programme under grant agreement No 847097

2.2 Condensation heat recovery

2.2.1 Technological features and performance

In industrial combustion systems, the combustion usually takes place in a steam boiler followed by an air heater to preheat the combustion air. The exit temperature of flue gases is maintained above the acid dew point to avoid corrosion from the condensate and to ensure buoyancy of the flue gases. However, similarly to domestic condensing boilers, by the use of suitable materials (PTFE, aluminium, etc.), the flue gases could be cooled to about 30°C with the recovery of both latent and sensible heat (Q. Chen et al., 2012). In the case of natural gas, which contains a significant proportion of hydrogen in the molecule, this heat represents about 15÷20% of the fuel`s energy content. In the case of biomass such as wood chips, this heat represents 6–8% of the fuel calorific value due to the hydrogen in the fuel, and up to half the calorific value of the raw fuel due to its 50% moisture content. For the coal fired power plants, water vapour exits with the flue gases at a volume percentage 12÷16%. Other industrial processes such as drying, wet scrubbers, dry scrubbers, dewatering, and water chilling, produce flue gases with 20÷90% moisture content. Typically, the water vapour along with its substantial latent heat is exhausted into the atmosphere, limiting the thermal efficiency of these processes. If 40÷60% of this water vapour and its latent heat could be recovered, thermal efficiency would increase more than 5% for most of these processes (D. Wang, Bao, Kunc, & Liss, 2012).

The condensing heat exchangers (also called condensing economizers) represent the enabling technology for the recovery of the latent heat from the combustion gases. There are two main types of condensing economizers: indirect and direct contact (U.S. Department of Energy, 2007):

- An indirect contact condensing economizer (see Figure 18 left) recovers the sensible and latent heat from hot flue gases by passing them through one or more shell-and-tube or tubular heat exchangers. This economizer can heat fluids to a temperature of 93°C (200°F) while achieving exit gas temperatures as low as 24°C (75°F). The condensing economizer must be designed to withstand corrosion from condensed water vapour produced by the combustion of hydrocarbon fuels (natural gas, light oils, etc.).
- A direct contact condensing economizer (see Figure 18 right) consists of a vapour-conditioning chamber followed by a countercurrent spray chamber. In the spray chamber, small droplets of cool liquid come into direct contact with the hot flue gas. The liquid droplets cool the stack gas and condense the water vapour. The spray chamber may be equipped with packing to improve contact between the water spray and hot gas. Since they operate close to atmospheric pressure the maximum outlet water temperature is limited to 60°C (140°F).

Horizon 2020
European Union Funding
for Research & Innovation

This project has received funding from
the European Union's Horizon 2020 research and innovation
programme under grant agreement No 847097

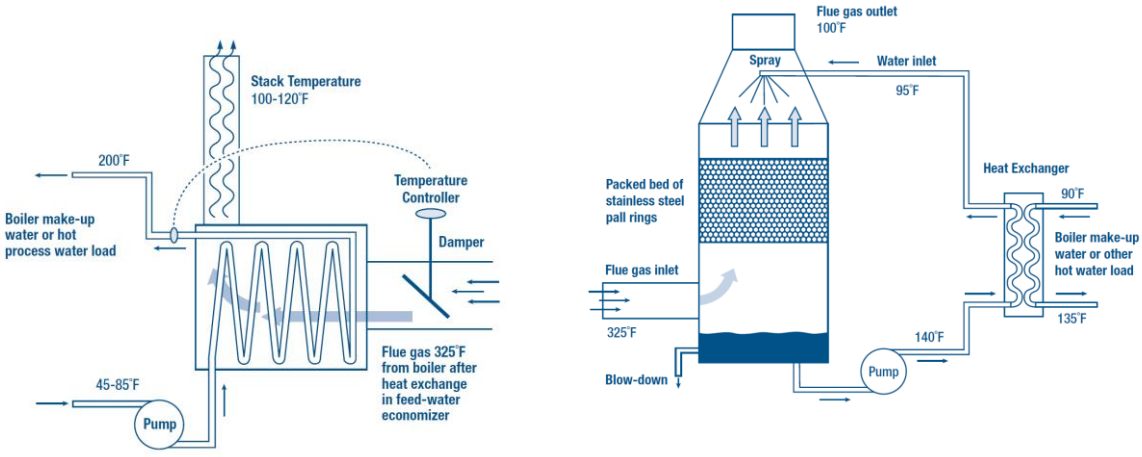

a) *b)*

Figure 18: Condensing economizer designs: a) indirect contact; b) direct contact (U.S. Department of Energy, 2007).

Natural gas. The relationship between the outlet temperature of the flue gas and the utilization efficiency of the natural gas (LHV based) at different excess air ratios (α) is shown in Figure 19. When the flue gas outlet temperature decreases from 100°C to the dew point, the utilization efficiency of natural gas varies linearly with it and only the sensible heat of the flue gas is recovered. When the flue gas outlet temperature is below the dew point, the relationship between the utilization efficiency and the outlet temperature is nonlinear and there will be condensation in the flue gas. Both the sensible and latent heat of the flue gas are recovered at the same time, and the amount of waste heat per temperature drop increases significantly. Note that when the excess air ratio of the gas boiler is relatively high, the dew point of the flue gas is lower, which negatively affects the practical recovery of the latent heat. The excess air coefficients of gas boilers and gas ICEs are 1.05÷1.3 and 1.5÷2.0, respectively. The excess air coefficient of gas turbines of CHP units is about 2.6÷3.1, which is higher than that of natural gas boilers (X. Zhao, Fu, Sun, Wang, & Wang, 2017). This explains why the condensing HE technology is typically implemented in combination with natural gas boilers rather than with gas internal combustion thermal engines.

Horizon 2020
European Union Funding
for Research & Innovation

This project has received funding from
the European Union's Horizon 2020 research and innovation
programme under grant agreement No 847097

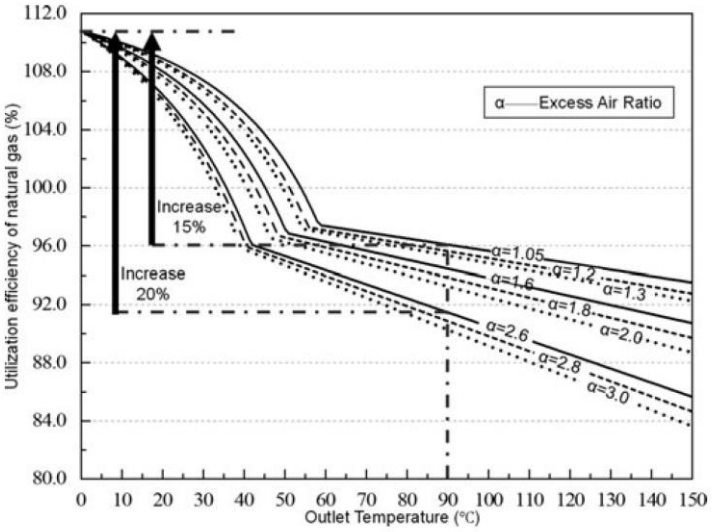

Figure 19: Outlet temperatures of flue gas versus utilization efficiency of natural gas (X. Zhao et al., 2017).

A key performance indicator of condensing HE called "condensation efficiency" was introduced in (K. Jeong, Kessen, Bilirgen, & Levy, 2010). It is defined as the weight percentage ratio of total condensation rate (i.e., flow rate of water condensed) to inlet water vapour flow rate. Figure 20 shows the strong dependence of condensation efficiency on inlet cooling water temperature. The condensation efficiency linearly decreased from 74 to 46 wt.% as the inlet cooling water temperature increased from 24.4°C to 38.1°C.

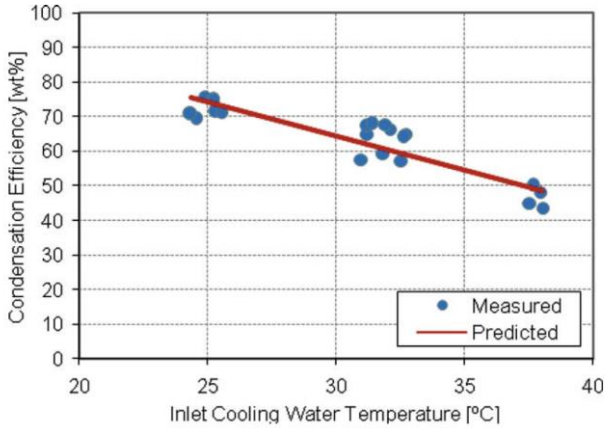

Figure 20: Effect of inlet cooling water temperature on condensation efficiency for coal flue gas condensation (K. Jeong et al., 2010).

A different performance indicator was used in (E. Vigants, Prodanuks, Vigants, Veidenbergs, & Blumberga, 2017) to assess the dependence of the performance of the condensing HE on the water inlet temperature. This was defined as the ratio between the condensing HE load and the boiler load. Basically, it shows the part of the boiler capacity that can be recovered by the deep cooling of flue gas. Figure 21 shows that this performance indicator increases as the water return temperature from the DHN decreases. The experimental data were collected from the flue gas condenser-unit of the direct contact condensing HE installed at the woodchip boiler of the Ludza city (Latvia) heating system (G.

Horizon 2020
European Union Funding
for Research & Innovation

This project has received funding from
the European Union's Horizon 2020 research and innovation
programme under grant agreement No 847097

Vigants, Galindoms, Veidenbergs, Vigants, & Blumberga, 2015). The positive impact of decreased DHN return temperature on the condensing HE shows that the introduction of the 4th generation of DH systems will increase the energy efficiency of the condensing HE.

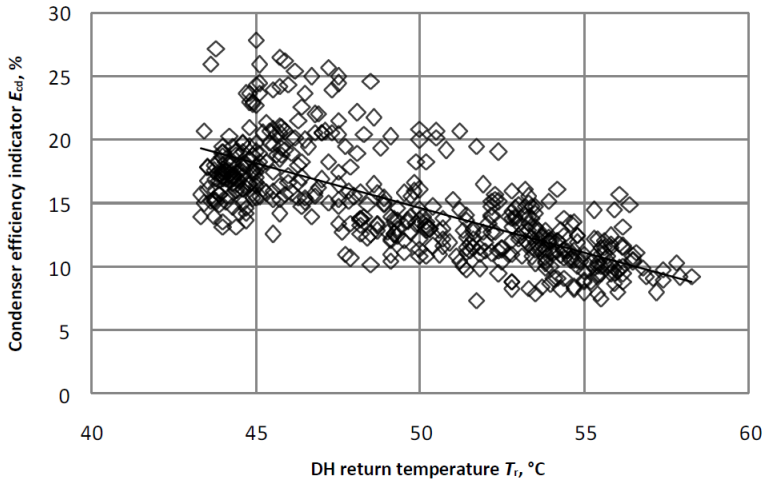

Figure 21: Changes in condenser efficiency depending on DH network return temperature (E. Vigants et al., 2017).

2.2.2 Technology readiness level and examples of applications

Examples of the application of the condensing HE technology in several fields are reported in the following.

- **Milk powder production plant**

Standard industrial steam boilers for milk powder production operate at 40 bar (250°C saturated) and are fitted with an economiser that preheats pressurised boiler feed water before it enters the main evaporation tubes. The installation of an additional condensing economiser was investigated in (Walmsley, Atkins, Walmsley, Philipp, & Peesel, 2018) to capture more flue gas heat. Extracting additional heat, both sensible and latent, maximises boiler efficiency and minimises fuel use. The temperature - heat load (T-q) diagram in Figure 22 shows that the condensation heat of the flue gases (red curved line) is only partially used due to the lack of low temperature heat sinks in the plant`s site.

Horizon 2020
European Union Funding
for Research & Innovation

This project has received funding from
the European Union's Horizon 2020 research and innovation
programme under grant agreement No 847097

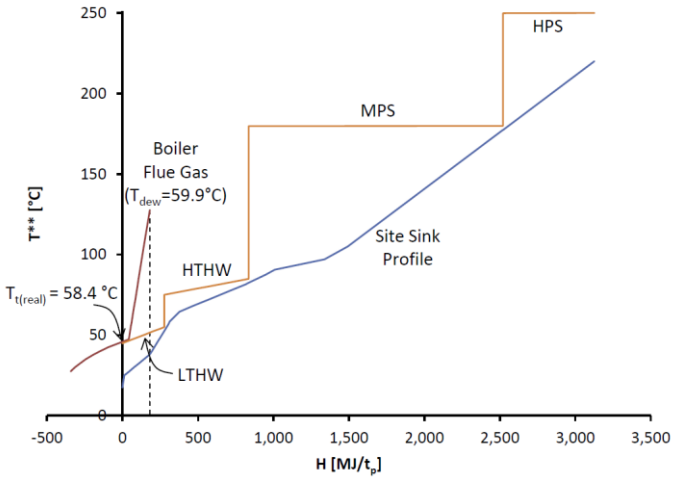

Figure 22: Coupling between heat sources and heat sinks in a milk powder production plant. The cooling thermal profile of the flue gases in the condensing economizer is shown using a red colour (Walmsley et al., 2018).

- **Biomass fired boilers (indirect contact condensing HE)**

The adoption of condensing HEs to fully exploit the heat of flue gases is highly investigated in the biomass sector and similar solutions could be adopted in the industrial WHR sector. In (Q. Chen et al., 2012) the thermal design of a flue gas condenser was carried out for one of the largest biomass-fired heating station in Finland. Wood chips are burned in a fluidised-bed boiler having a thermal output of 40 MWt at full load. After the electrostatic precipitator (ESP) the flue gases enter the condensing HE where the temperature of flue gases is decreased from 150°C to 35 °C (Figure 23). In the condensing HE most of water vapour is condensed to water (the dew point of the flue gas being 64.3 °C) and about 12 MWt of heat is produced and delivered to the district. This increases the boiler output to 52 MWt and the boiler efficiency to 118% (LHV based). Table 11 shows the operating conditions of the condensing HE.

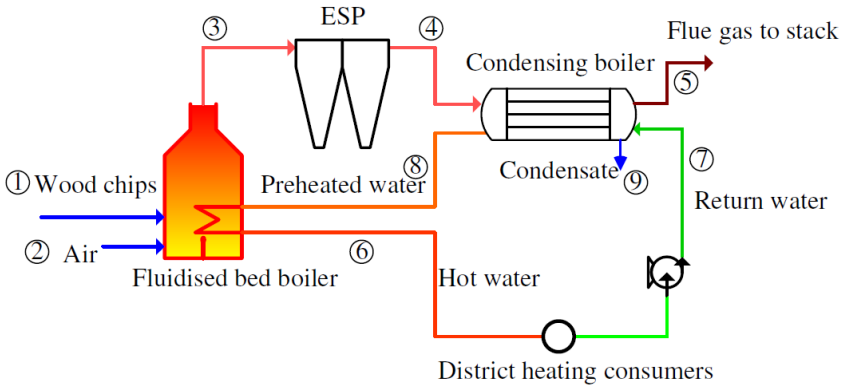

Figure 23: Process diagram of the biomass fired heating plant with condensing HE (Q. Chen et al., 2012).

Horizon 2020
European Union Funding
for Research & Innovation

This project has received funding from
the European Union's Horizon 2020 research and innovation
programme under grant agreement No 847097

Table 11: Operating conditions of the condensing HE.

TRL	Application	Tin gas (°C)	Tout gas (°C)	Tin water (°C)	Tout water (°C)	Q (kW)	Reference
9	Biomass fired heating plant	150	35	30	55	12000	(Q. Chen et al., 2012)

An indirect-contact condensing HE with a shell-and-tube design was chosen in (Q. Chen et al., 2012) due to its relative simplicity. The flue gas was on the shell-side and the return water (i.e., feed water to the boiler) on the tube-side. The flue gas thermal profile in the condensing HE (Figure 24) shows the de-superheating process (A-B) and the condensation process (B-E). The latter occurs at variable temperature due to the presence of non-condensable gases.

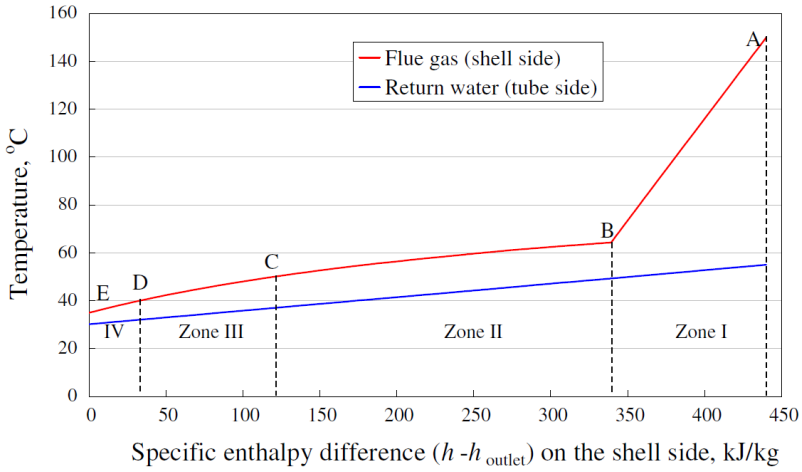

Figure 24: Heat transfer profiles of flue gases and feed water in the condensing HE (Q. Chen et al., 2012).

- **Biofuel fired boilers (direct contact condensing HE)**

A condensing heat utilizer of flue gases produced by XILO ECO (Figure 25) was installed downstream of a biofuel boiler (Ionkin, Roslyakov, & Luning, 2018). In the flue gas chambers made of stainless steel, water was introduced through special sprayers. Wet flue gases were cooled to the dew point, so that the water vapour contained in them could condense and fall out of the gas stream in the form of a liquid (condensate). The resulting condensate transferred its heat energy in a PHE to another heat carrier (water for a centralized heating system). The installation of such condensing HE unit made it possible to increase the efficiency of the boiler up to 25% with low return-water temperatures, due to the high water vapour content in the biofuel combustion gases (Ionkin et al., 2018).

Horizon 2020
European Union Funding
for Research & Innovation

This project has received funding from
the European Union's Horizon 2020 research and innovation
programme under grant agreement No 847097

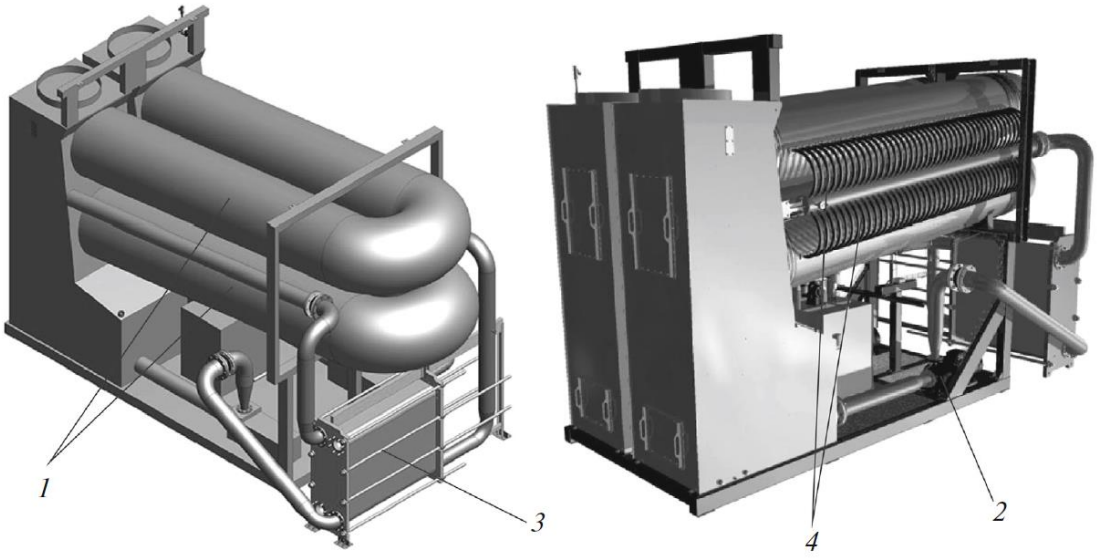

Figure 25: Condensing heat utilizer of flue gases XILO ECO. (1) Flue gas chambers, (2) the pump, (3) PHE, (4) water supply to sprayers (Ionkin et al., 2018).

- **Industrial natural gas condensing boilers**

In (Che, Liu, & Gao, 2004) a 2.8 MW natural gas fired boiler was retrofitted into a condensing boiler by adding a surface-type condensing HE. The boiler efficiency (LHV based) at various exit flue gas temperatures is shown in Figure 26. The boiler efficiency varies relatively gradually in the temperature range of 60÷180 °C, then it changes very rapidly in the temperature range of 20÷60 °C, because the latent heat takes a greater role than the sensible heat. It was demonstrated in (Che et al., 2004) that the shortest payback period was obtained for an exit flue gas temperature of 40÷55 °C, because too low an exit flue gas temperature gave rise to a great increase of the HE surface area and cost.

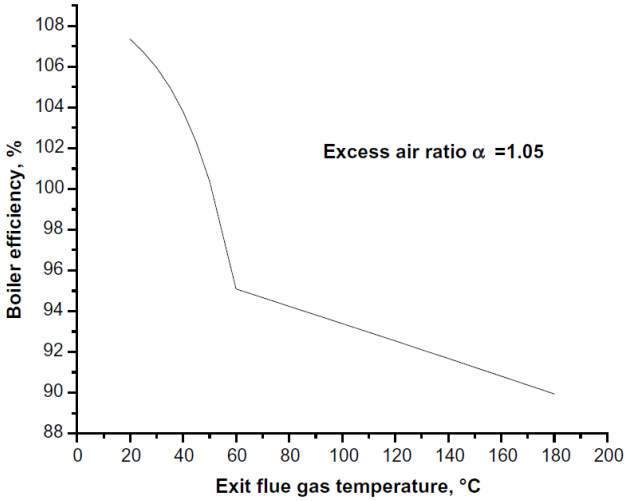

Figure 26: Variation of the boiler efficiency (LHV based) with the exit flue gas temperature for a natural gas boiler (Che et al., 2004).

- **Condensing HE and DHN**

Horizon 2020
European Union Funding
for Research & Innovation

This project has received funding from
the European Union's Horizon 2020 research and innovation
programme under grant agreement No 847097

In November 2009 the 116 MW gas-fired boiler of the Imanta plant in Riga (Latvia) was retrofitted by installing a 10 MW condensing economizer inside the flue gas channel downstream of the boiler (Ziemele, Blumberga, Talcis, & Laicane, 2012). Return water from the district heating (DH) network was preheated in the condensing economizer before entering the boiler (Figure 27). The flue gas cooling process released sensible heat and also latent when the temperature was lower than the dew point (57÷58°C). In the system schematic shown in Figure 27 (Ionkin et al., 2018) return network water with temperature 38°C is fed to the condensing HE where it is heated to 43°C before admission to the boiler. The installation of the condensing HE allowed for the increase in the efficiency of the hot-water boiler by 8÷9%. Such a high efficiency of utilizing the condensation heat in this unit was ensured by a low return-water temperature as a result of the reconstruction of the DHN. The project payback period was 2÷3 years (Ziemele et al., 2012).

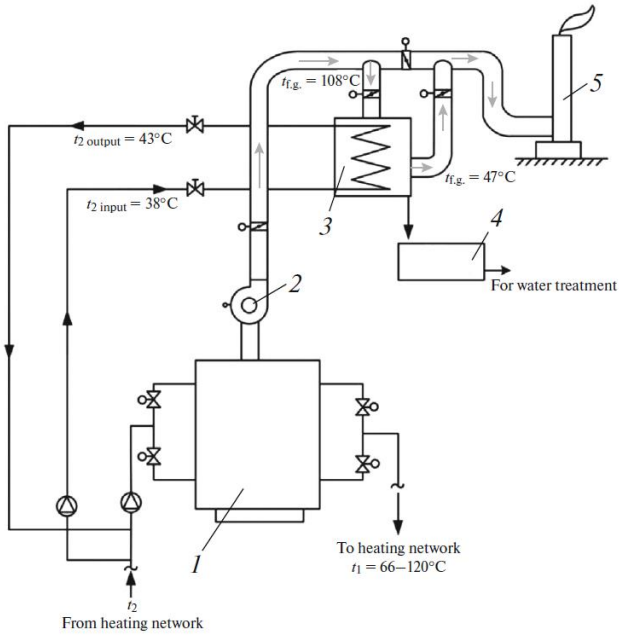

Figure 27: Installation of a condensing HE downstream of a natural gas boiler: (1) 116-MW hot-water boiler, (2) smoke exhauster, (3) condensing HX with a capacity of 10 MW, (4) collection of condensate, (5) chimney (Ionkin et al., 2018).

- **Condensing HE plus humidifier and DHN**

A more complicated but more efficient "condenser and humidifier" scheme is shown in Figure 28a. Preliminary humidification of the air supplied for combustion is applied. Due to its cooling by air and partial evaporation, the water return temperature from the DHN is reduced from 50°C to 35°C. Since the water temperature is much lower than it would be in the absence of a humidifier, the temperature of the outgoing flue gases (43°C) can be lower than that of the return water (50°C). Condensing heat utilizer systems equipped with humidifier were installed on two boilers (each 64 MW thermal capacity) at Rosenlunds thermal power station in Göteborg (Sweden) in the mid-90s of the last century (Figure 28b). Introduction of the condenser technology allowed achieving additional heat recuperation of waste gases by 12÷14% and reduction of NOx emissions by 50÷60%. The payback period was 4 years. At present, these condenser units are still operating smoothly (Ionkin et al., 2018).

Horizon 2020
European Union Funding
for Research & Innovation

This project has received funding from
the European Union's Horizon 2020 research and innovation
programme under grant agreement No 847097

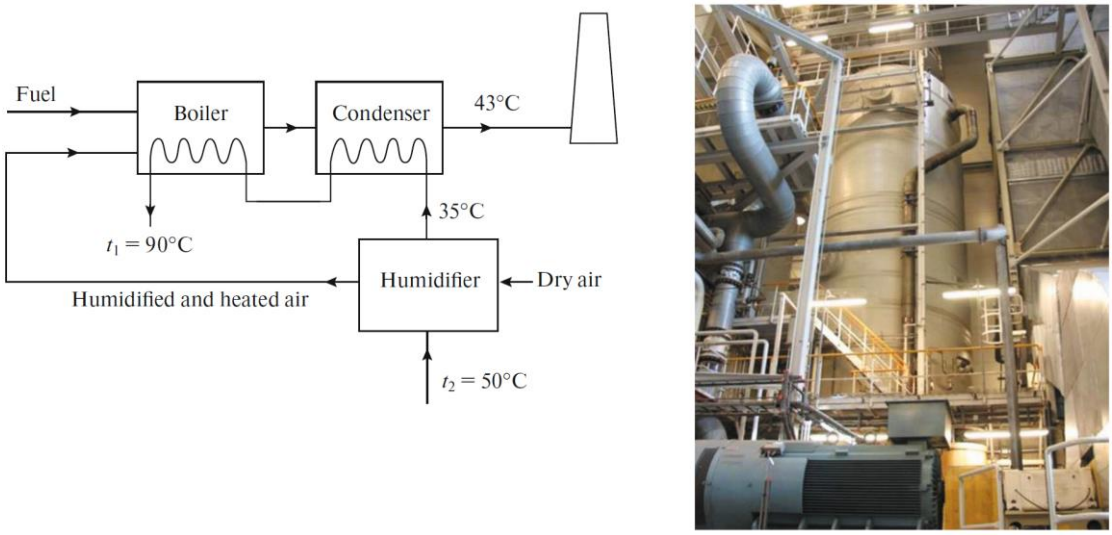

a) b)

Figure 28: Condensing heat utilizer at the Rosenlunds thermal power plant in Göteborg (Sweden).

In 2008, at the thermal power plant of the Carlsberg brewery in Fredericia (Denmark) a heat recuperation system was installed on three natural gas boilers having a thermal capacity of 14 MW each (Ionkin et al., 2018). At this facility, a three-stage solution for heat recuperation of waste gases and humidification of air supplied for combustion in boilers was realized. The installation was carried out in the form of three separate HE: a contact humidifier and two recuperative HEs. Each of the HEs had three water circuits, one of which ensured the humidifier operation while the rest ensured the production of three water streams at different temperatures for the brewery process. The scheme of the system is shown in Figure 29. This system allowed receiving an additional 5 MW of heat (Ionkin et al., 2018).

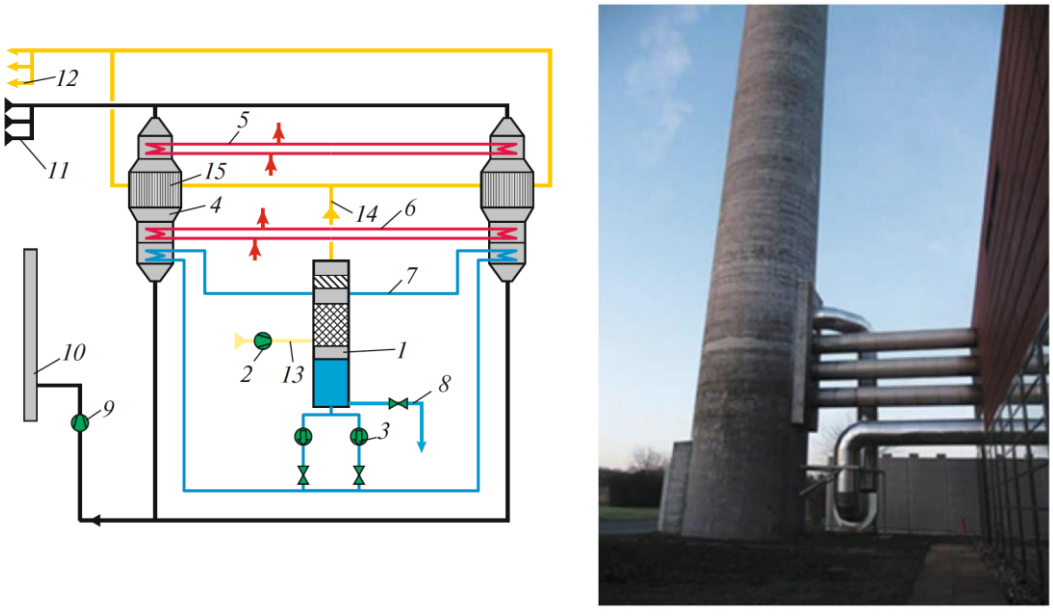

a) b)

Figure 29: Scheme of the condensation HE units installed at the thermal power station of the Carlsberg brewery (Ionkin et al., 2018).

Horizon 2020
European Union Funding
for Research & Innovation

This project has received funding from
the European Union's Horizon 2020 research and innovation
programme under grant agreement No 847097

- **Condensing HE plus AHP and DHN**

Moisture condensation from the flue gases requires them to be cooled below their dew point (55÷65°C for natural gas). Thus, as already shown in the previous sections, low temperature heat sinks are required to capture the latent heat. If the return water from a DHN is not cool enough to directly serve as a heat sink, heat pumps can be coupled with condensing boilers (Q. Chen et al., 2012). The evaporation duty of the HP decreases the temperature of the cooling water and enables a deep recovery of the latent heat of the flue gases. For instance, the new system developed in (K. Zhu, Xia, Xie, & Jiang, 2014) combines absorption heat pump (AHP) and condensing (direct-contact) HE. When the system is running, the flue gas exiting the boiler flows into the condensing HE instead of the main flue. The AHP is driven by natural gas and its flue gas flows into the condensing HE as well (Figure 30). The evaporation process in the AHP generates cooled water, which is pumped into the direct-contact HE. The cooled water is sprayed out by nozzles and cools down the flue gas. At last, the cooling water will go back to the evaporator of the AHP, carrying the recovered heat as the low-temperature heat source for the AHP. The return water from the DHN goes into the AHP at first, and then into the gas boiler to reach the desired supply temperature.

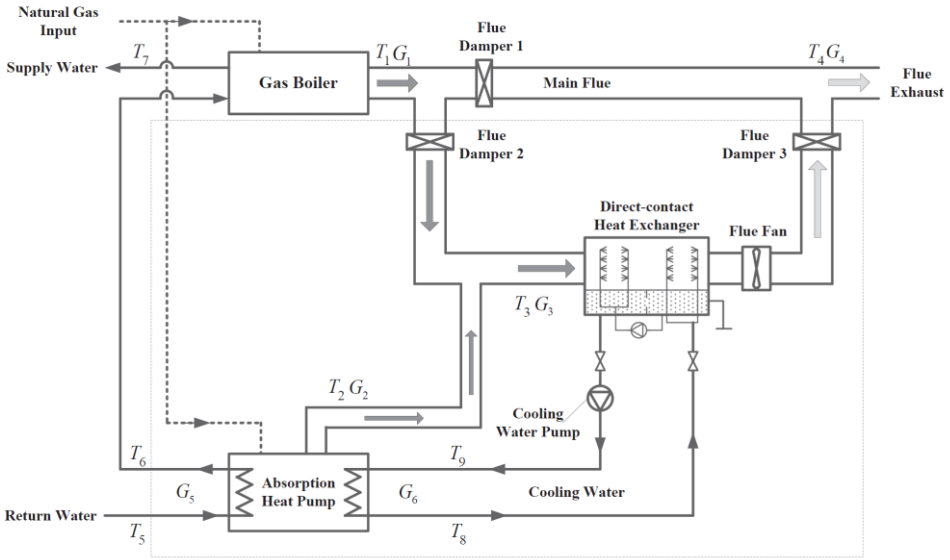

Figure 30: Combination of AHP and condensing HE for deep heat recovery from the flue gases of a natural gas boiler (K. Zhu et al., 2014).

The performance of this technology has been tested in a demonstration project in (K. Zhu et al., 2014). If the excess air ratio of the gas boiler is within a reasonable range (i.e., low), the total heat capacity can be improved by 12% and the flue gas can be cooled below 30°C. Nearly 70% of vapour can be condensed and most of the condensing heat is recovered. Table 12 shows the measured data at design conditions (100% load of the boiler) where the excess air ratio was 1.2 and the dew point of flue gas was 55°C. A payback period of less than half year was reported (K. Zhu et al., 2014).

Horizon 2020
European Union Funding
for Research & Innovation

This project has received funding from
the European Union's Horizon 2020 research and innovation
programme under grant agreement No 847097

Table 12: Operational data of the condensing HE – AHP system (K. Zhu et al., 2014).

TRL	T flue gas in (°C)	T flue gas out (°C)	T cooling water in (°C)	T cooling water out (°C)	Heat recovered (kW)	Condensing heat recovered (kW)
5	116	35	20	30	1800	1200

The flue-gas WHR system shown in Figure 31 was constructed in a heating gas boiler room in Beijing (Figure 32) to recover the flue-gas waste heat from a 29 MW boiler. The exhaust flue gas temperature from the boiler and AHP was lowered to 27.4°C by heating the cold water in the direct-contact HE. The flue gas heat recovery was 2.7 MW, which resulted in a heating efficiency improvement of 11.5%. The gas-fired AHP supplied 7.2 MW for increasing the return-water temperature from 55 to 65 °C (L. Feng, Lin, Lin, & Xiling, 2019).

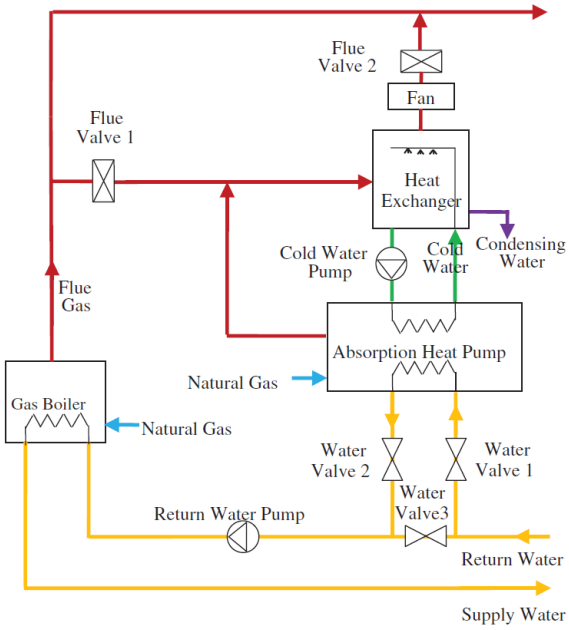

Figure 31: Flue gas WHR system with direct contact condensing HE and AHP (L. Feng et al., 2019).

a) b)

Figure 32: a) Connection between the chimney and the WHR system; b) WHR system composed by the direct-contact condensing HE and the AHP.

Horizon 2020
European Union Funding
for Research & Innovation

This project has received funding from
the European Union's Horizon 2020 research and innovation
programme under grant agreement No 847097

- **Membrane condenser for simultaneous latent heat recovery and purified water recovery**

A new technology based on a nanoporous ceramic separation membrane was developed by GTI (Gas Technology Institute) to extract a portion of the water vapour and its latent heat from flue gases (Gas Technology Institute, 2013). This is achieved through the use of a Transport Membrane Condenser (TMC). Water vapour passes through the membrane and then is condensed in direct contact with a low-temperature water stream. Contaminants are inhibited from passing through the membrane by its high selectivity. The TMC has been developed and proven at industrial demonstration scale for gas-fired package boilers and commercial laundry applications, and already commercialized by Cannon Boiler Work ("Cannon Boiler Works," 2020) under the trade name "Ultramizer". Figure 33 depicts the TMC concept for boiler applications with exhaust gas flowing on one side of a nanoporous ceramic membrane tube and cold boiler feed water flowing countercurrent on the opposing side. Water vapour from the flue gas is transported through the membrane structure. Condensed water along with its latent heat combines with the cold boiler feed water, helping to raise its temperature prior to entering the boiler. A 40% recovery of the exhaust water vapour and an increase of more than 5% in efficiency have been achieved. Figure 34 shows the membrane and its installation in a boiler.

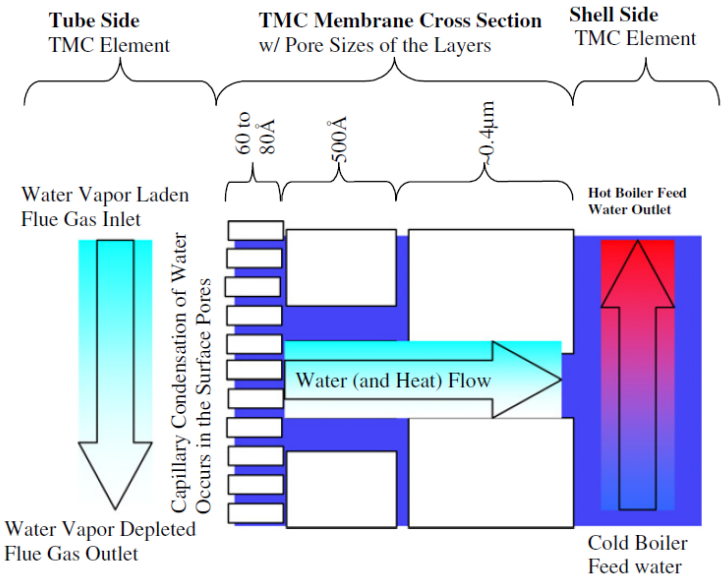

Figure 33: Schematic concept of a Transport Membrane Condenser (TMC) (Gas Technology Institute, 2013).

Horizon 2020
European Union Funding
for Research & Innovation

This project has received funding from
the European Union's Horizon 2020 research and innovation
programme under grant agreement No 847097

a)

b)

Figure 34: a) Membrane module; b) Installed TMC unit for a 150 kW boiler (Gas Technology Institute, 2013).

2.2.3 Cost aspects

The specific investment cost of condensing HEs for industrial applications varies in the range 130÷370 €/kWt (Table 13). Some detailed quotations were reported in (Vnukov & Rozanova, 2013). The selling price for one condensing economizer with the heating surface of 1000 m² and thermal output of 4.65 MW is about 1 million US dollars. The installation cost of the condensing economizer at the Imanta CHP plant (Riga, Latvia) inclusive of steel insert into the chimney stack was 1.51 millions US dollars (Vnukov & Rozanova, 2013). According to (Vnukov & Rozanova, 2013) the material typically used for manufacturing condensing economizers is austenitic (heat resistant) chromium-nickel steel of the 8/18 type, which is more expensive than chromium stainless steel. In (Q. Chen et al., 2012) carbon steel and stainless steel have been considered as materials for the condensing heat HE. In order to use carbon steel in the condensing boiler, the outer surface of the tubes and the inner surface of the shell were coated with polypropylene as the corrosion-resistant material. As stainless steel is more expensive, the capital cost for the stainless steel condenser is about 2.5 times higher than the carbon steel condenser. However, due to corrosion, the expected life for a carbon steel HE is usually 5 years much shorter than a stainless steel one (10–15 years). Polymers in condensing HEs have been considered to avoid the cost and corrosion concerns of metallic designs. Polymers offer the advantage of corrosion resistance and cost, however, lower thermal conductivity have limited their application. More recent developments have introduced thermally conductive polymers which now offer promising conductivity values. The HE with helical geometry presented in (Trojanowski, Butcher, Worek, & Wei, 2016) included a polymer matrix with fillers for thermal conductivity improvement.

Table 13: Specific investment costs of condensing heat exchangers.

Material	Cost of the condensing HE (€)	Installed cost of the condensing HE (€)	Q (kWt)	Specific investment cost (€/kWt)	Reference
Stainless steel	2300000	4380000	12000	365	(Q. Chen et al., 2012)
Carbon steel	810000	1780000		148	
Austenitic Chromium-nickel steel	900000	1060000	4650	228	(Vnukov & Rozanova, 2013)
	/	1360000	10000	136	

Horizon 2020 European Union Funding for Research & Innovation

This project has received funding from the European Union's Horizon 2020 research and innovation programme under grant agreement No 847097

2.3 Economizers (ECOs)

2.3.1 Technological features and performance

Economizer (ECO) is a device typically used to recover the waste heat from the flue gas to preheat the boiler feed water. The economizer is so-called because it economizes the fuel usage by extracting the low-grade heat. For every 22°C reduction in flue gas temperature by passing through an economizer, there is 1% saving of fuel in the boiler. In other words, for every 6°C rise in feed water temperature through an economizer, there is 1% saving of fuel in the boiler (Thulukkanam, 2013).

Due to the gas-liquid heat transfer, the ECO has nearly three to four times greater heat-transfer coefficient than an air heater (i.e., a gas-gas HE). ECO heat transfer is governed by gas-side coefficient only (Rayaprolu, 2009). Bare tube ECOs (Figure 35 left) are reliable and effective for applications in dusty environment and eliminate uncertainties associated with finned tubes (fouling and fin erosion). However, to minimize the cost and space, various types of extended-surface (i.e., finned tube) ECOs (Figure 35 right) are available, with helical, plate or rectangular and longitudinal fins (Rayaprolu, 2009). Figure 36 shows the picture of a real ECO unit with finned tubes.

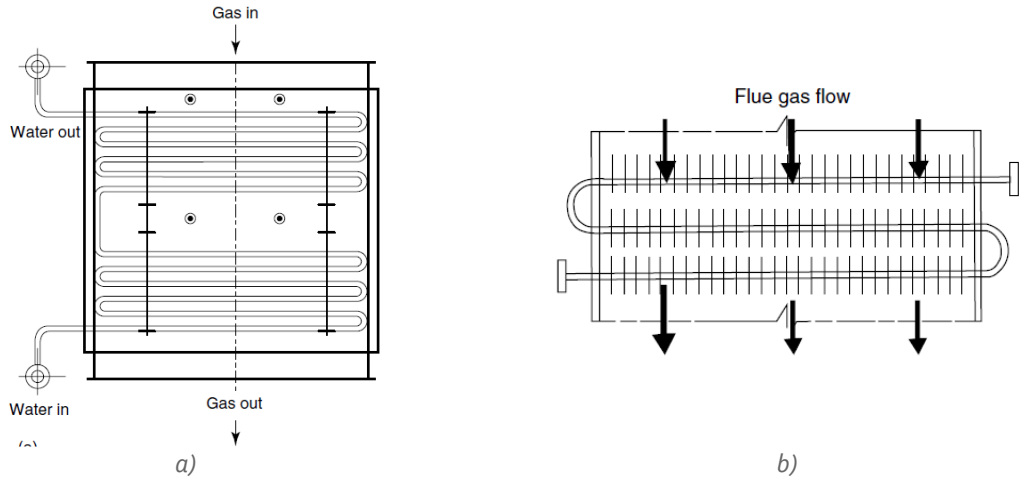

Figure 35: Schematic of an economizer with: a) bare tubes; b) finned tubes. (Rayaprolu, 2009).

Horizon 2020
European Union Funding
for Research & Innovation

This project has received funding from
the European Union's Horizon 2020 research and innovation
programme under grant agreement No 847097

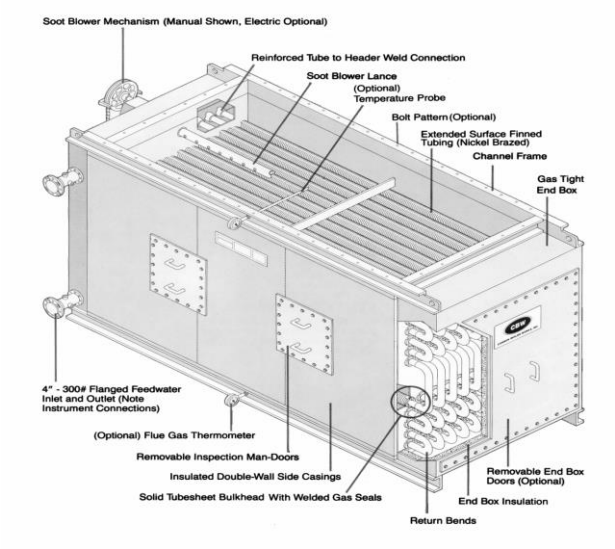

Figure 36: Economizer (heavy duty) commercialized by Cannon Boiler Works for operation with dirty flue gases ("Cannon Boiler Works," 2020).

Table 14 shows the typical working conditions of ECOs. They are typically installed to recover the waste heat of the flue gases at the outlet of industrial steam boilers at temperatures around 200÷250°C. The recovered heat is used to preheat the feedwater entering the boiler up to 100÷150°C. The addition of ECO in the UK industrial installations reported in ("ThermTech," 2020) resulted in a 5÷6% increase in boiler efficiency and a payback time of less than 1÷3 years.

Table 14: Examples of the operating conditions of ECOs installed for WHR from the flue gases of natural gas fired steam boilers ("ThermTech," 2020).

Location / Industry	Boiler steam pressure (bar)	Tin gas (°C)	Tout gas (°C)	Tin water (°C)	Tout water (°C)	Increase in boiler efficiency	Payback time (years)
Noble's Hospital on the Isle of Man	11	240	160	110	135	5%	3
UK based specialty chemicals production facility	23	245	138	87	120	6%	<1
UK based textiles manufacturer	9	240	135	75	109	6%	≈1

2.3.2 Technology readiness level and examples of applications

There are many manufactures involved in the design and commercialization of ECOs from very small sizes up to very large sizes such as those installed in coal-fired and combined cycle power plants. Table 15 shows the main features and application ranges of two leading companies active in this field. The typical industrial applications cover thermal duties in the range hundreds of kWs to a few MWs and water pressures up to 60 bar ("Cannon Boiler Works," 2020). Higher thermal duties and pressures are more typical of the power industry.

Horizon 2020
European Union Funding
for Research & Innovation

This project has received funding from
the European Union's Horizon 2020 research and innovation
programme under grant agreement No 847097

Table 15: Main features, operating conditions, size and applications of commercialized ECOs.

Manufacturer	Tube type	Water pressure (bar)	Water flowrate (ton/hr)	Thermal duty (MW)	Applications	Reference
Green Power Limited	Smooth tube, Spiral tube, H-fin design	10 ÷ 320	10 ÷ 2800	1 ÷ 100	a) Power stations (coal fired, WtE, biomass). b) Industrial plants (pulp and paper or steel mills, chemical producers and food processors)	("Green`s Power Economisers," 2019)
Cannon Boiler Works	Finned	1 ÷ 60	7 ÷ 70	0.3÷3.4	a) Boilers (Natural gas, oil, propane, upgraded land fill gas, coal, oil, wood). b) WHR from gas turbine and hydrogen fuel cell	("Cannon Boiler Works," 2020)

Some interesting case studies reported in the literature about the integration of ECOs in the process, manufacturing and power industry are described in the following. The case studies refer to the milk production process, textile industry, steel industry and power industry.

- **Milk production plant**

In a pasteurized milk plant, hot water at temperatures higher than 72°C is mainly required to kill virus and bacteria in raw milk. Furthermore, heat is also utilized to sterilize piping systems and equipment before and after production. Hence, a boiler is mostly employed to supply thermal energy in terms of steam or hot water for these processes. In the ECO the waste heat in the exhaust gases is typically recovered by preheating the boiler's feed water.

Outlet from a LPG boiler. A newly designed ECO was devised in (Niamsuwan, Kittisupakorn, & Mujtaba, 2013) to achieve high heat recovery in a pasteurized milk plant. ECOs are normally designed with single-pass or double-pass of the exhaust gas flowing over the water tube bank. The novel ECO improves the heat transfer on the gas side by using a new gas flow pattern with double pathway and triple pass (see Figure 37 left). The ECO consists of the single rectangular shell and eight rows of tubes in the gas flow direction and six tubes per row connected to header. For real implementation, the newly designed ECO is placed into the chimney of the existing LPG boiler as shown in Figure 37 right. The outlet preheated water is delivered from the bottom of the header to the boiler. The efficiency of heat recovery is higher than that achieved by a single pass mode-economizer due to the higher retention time for the exhaust gas.

Horizon 2020 European Union Funding for Research & Innovation

This project has received funding from the European Union's Horizon 2020 research and innovation programme under grant agreement No 847097

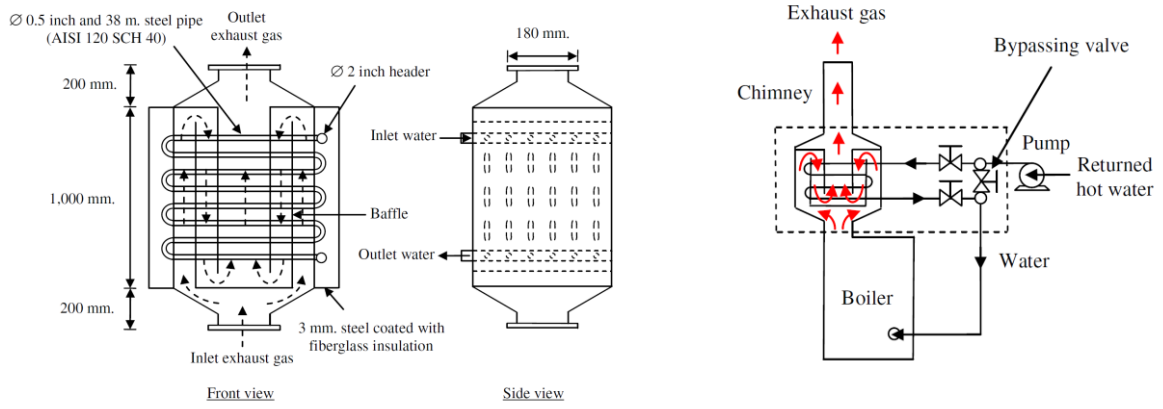

a) b)

Figure 37: Economizer for WHR from the exhaust gas of a milk production plant: a) Drawing of newly designed ECO (Niamsuwan et al., 2013); b) Installation of the ECO into the existing boiler system (Niamsuwan et al., 2013).

Outlet from a WHR boiler. The CHP system shown in Figure 38 is installed in a milk production plant. The exhaust gas (EFG) of the gas engine is first used to generate steam at 7 bar in a WHR boiler (STHE) and then in the ECO to preheat the feed water entering the deaerator. In this way less steam is needed for oxygen removal in the deaerator and more steam is available for the end users. The reported payback time was less than half a year (Martić, Budimir, Mitrović, Maslarević, & Marković, 2016).

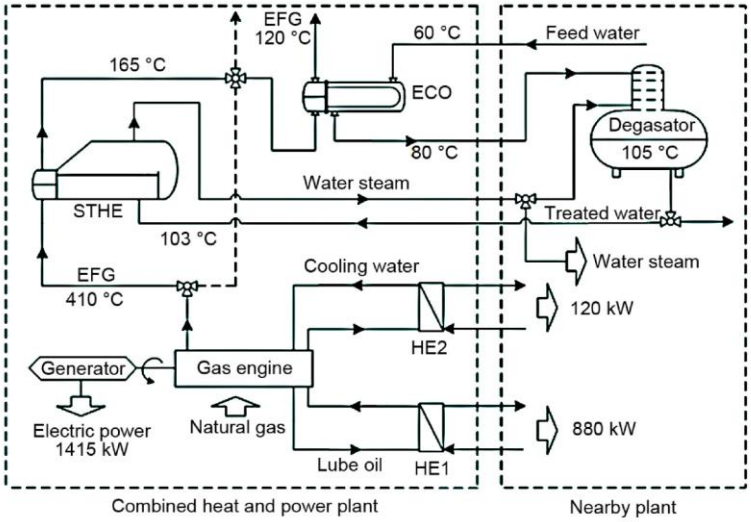

Figure 38: Installation of an economizer downstream of a waste heat recovery boiler (Martić et al., 2016).

- **Textile industry**

A textile industry in Narsingdi (Bangladesh) with four NG boilers having a total rated steam production capacity of ≈40 ton/h was investigated in (Rakib, Saidur, Mohamad, & Afifi, 2017). The results of boilers' combustion test showed high exhaust gas temperatures between 186 and 209 °C and revealed significant amount of waste-heat presented in boiler's exhaust. Thus, ECOs were installed in order to utilize the waste heat and reduce the NG consumption (Figure 39). The feed water temperature was raised by approximately 25°C following the installation of the economizers. Preheated feed water

Horizon 2020
European Union Funding
for Research & Innovation

This project has received funding from
the European Union's Horizon 2020 research and innovation
programme under grant agreement No 847097

required less energy to produce steam compare to normal temperature feed water. The overall energy saving was found to be 4.9% of the energy used and the payback period was estimated equal to 2.1 years (Rakib et al., 2017).

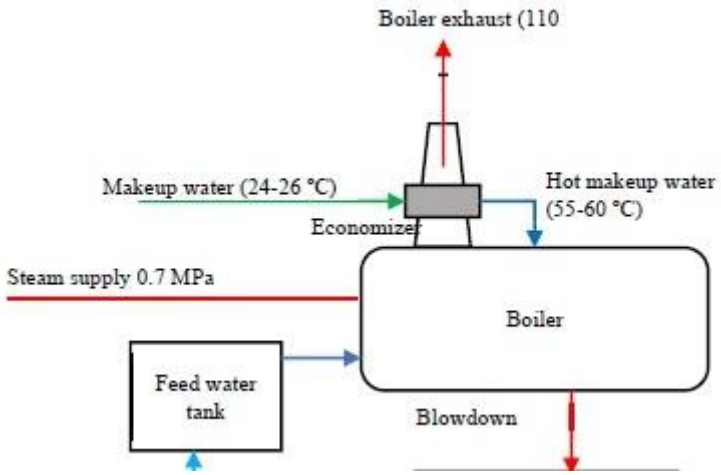

Figure 39: Installation of an economizer in a textile industry (Rakib et al., 2017).

- **Steel industry**

In an integrated iron and steel plant, one of the most intensive energy consumers is the reheating furnace. Reheating furnaces work continuously and they are used in hot rolling mills to heat the steel stock (billets, blooms or slabs) at the temperature around 1050÷1300°C (Figure 40 left). At the reheating furnace, blast furnace gas and coke-oven gas are used as a fuel and burned with preheated combustion air. With the heat generated by combustion the slab is heated from ambient temperature up to 1100÷1200 °C. The combustion gas is discarded from chimney by transferring a part of its energy to the combustion air in the recuperator (Figure 40 right). The residual heat of the flue gas after the recuperator could be recovered using an ECO. In (Kilinc¸ et al., 2014) the temperature of the flue gas leaving the recuperator at 330÷380°C was reduced to 215°C by using the economiser. The produced hot water at 90°C was used in bathrooms and buildings of the plant to meet the need of hot water and heating. A payback period of only 3 months was reported.

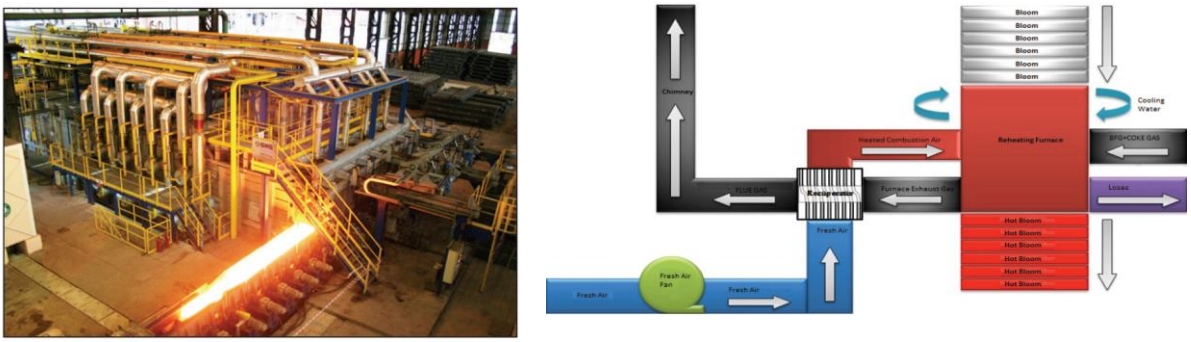

a) *b)*

Figure 40: Reheating furnace: a) Photo of the reheating furnace; b) Working principle of the reheating furnace. The ECO was installed in the chimney after the recuperator (Kilinc¸ et al., 2014).

Horizon 2020
European Union Funding
for Research & Innovation

This project has received funding from
the European Union's Horizon 2020 research and innovation
programme under grant agreement No 847097

- **Refinery**

Two ECO designs were investigated in (Chucherd & Kittisupakorn, 2017) for WHR from a coal-fired industrial boiler (thermal oil heater) in a palm oil refinery plant: the existing gas-in-tube and the new water-in-tube. The gas-in-tube exchanger was a STHE where the flue gas flowed inside the tubes (Figure 41 left). Instead, in the water-in-tube design the water flows inside the tubes (Figure 41 right) and the flue gases follow a double pass flow pattern. The new design was preferred because it reduced the fouling and the pressure drops compared to the gas-in-tube design.

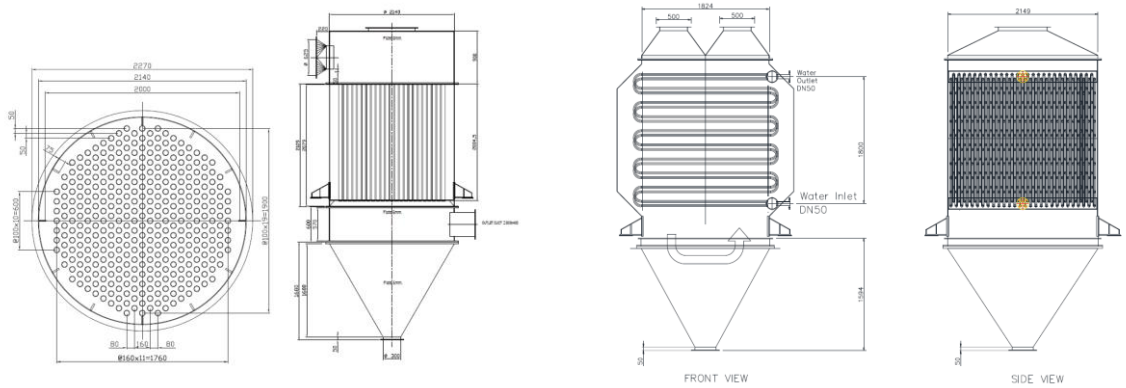

a) b)

Figure 41: Two ECO designs for WHR from the flue gases of a coal-fired boiler: a) gas-in-tube; b) water-in-tube.

Figure 42 shows the integration of the novel ECO in the system. The function of the ECO is to control the flue gas temperature before entering the bag filter while recovering the waste heat to preheat feed water up to 100÷110°C (Chucherd & Kittisupakorn, 2017). The flue gas leaving the air preheater at 230°C needs to be cooled because the filter cloth is unable to resist to temperatures above 170°C. On the other hand, the flue gas temperature should not be lower than 120°C, to avoid the acid dew point temperature.

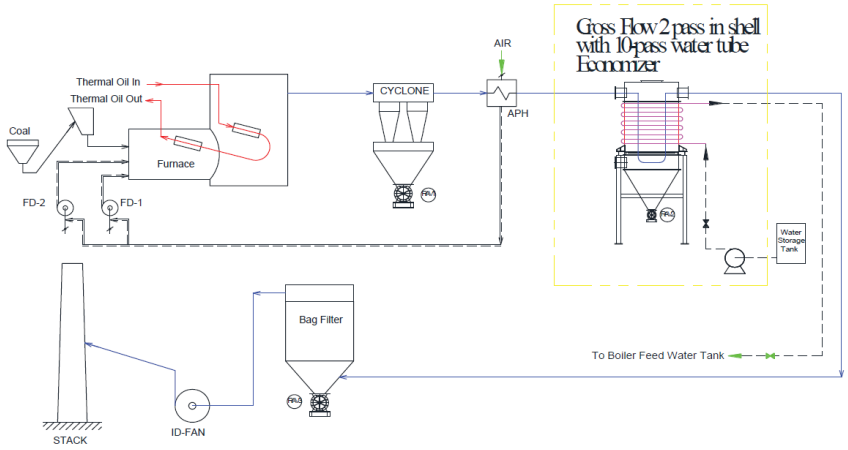

Figure 42: Installation of the ECO in the thermal oil heater plant (Chucherd & Kittisupakorn, 2017).

- **Power industry (coal-fired power plants)**

When a low pressure economizer (LP ECO) is installed in a coal-fired power plant, part of the exhaust heat of the flue gas is recovered and utilized to heat the low temperature feed water, replacing a

Horizon 2020
European Union Funding
for Research & Innovation

This project has received funding from
the European Union's Horizon 2020 research and innovation
programme under grant agreement No 847097

portion of the heat from steam extracted from the steam turbine. The saved steam expands through next stages of the steam turbine and produces more power. In this way, the low-grade heat of the exhaust flue gas is utilized and upgraded. The LP ECO is commonly installed in the flue gas side between the ESP (electrostatic precipitator) and the desulfurizer. On the water side, the LP ECO was positioned between feed water preheaters 6 and 7 in both the 600 MW unit investigated in (C. Wang et al., 2012) (Figure 43 left) and the 350 MW unit investigated in (C. Wang, He, Yan, Pei, & Chen, 2014) (Figure 43 right). This made the average working temperature of the LP ECO exchanger surface slightly higher than the acid dew point (98.5°C).

Table 16: Investigated operating conditions for ECOs in large coal-fired power plants.

TRL	Type of plant	Tin gas (°C)	Tout gas (°C)	Tin water (°C)	Tout water (°C)	Heat load (kW)	Reference
9	600 MW Coal fired	122.8	98.2	81.9	97.7	25170	(C. Wang et al., 2012)
9	350 MW Coal fired	146	119.1	88.2	109.1	18307	(C. Wang et al., 2014)

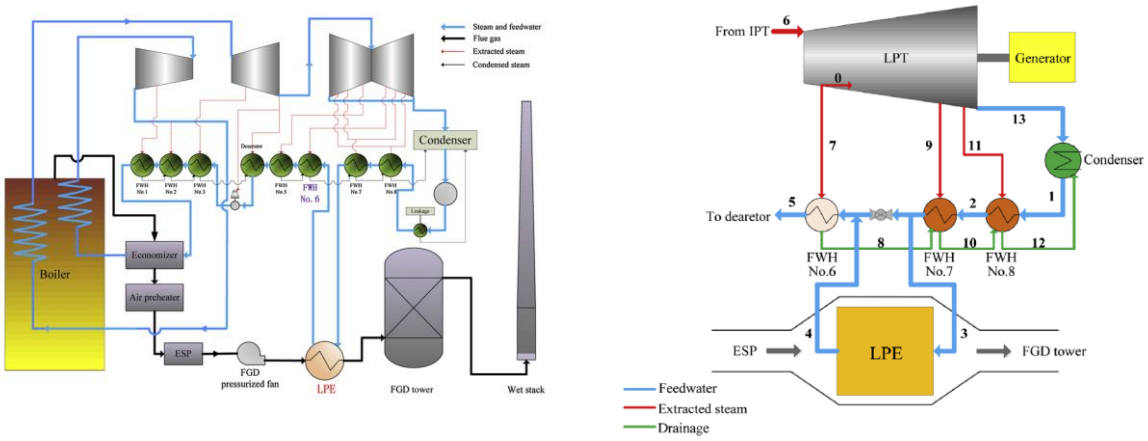

a) b)

Figure 43: Installation of a low pressure economizer (LPE) to recover the residual heat of the flue gases: a) Layout of the 600 MW coal fired power plant (C. Wang et al., 2012); b) Integration of the LPE in a 350 MW coal fired plant (C. Wang et al., 2014).

Horizon 2020
European Union Funding
for Research & Innovation

This project has received funding from
the European Union's Horizon 2020 research and innovation
programme under grant agreement No 847097

2.4 Waste heat boilers (WHBs)

2.4.1 Technological features and performance

Waste heat boilers (WHBs) are multiphase flow thermal systems to recover medium-to-high grade WH (typically in the range 300÷1000°C) in order to generate steam as output. The technology is fully established and widely commercially available. WHBs are commonly known as Heat Recovery Steam Generators (HRSGs) in power plants, and Waste Heat Recovery Boilers (WHRBs) in process industries (Rayaprolu, 2009). Figure 44 shows the key elements of a WHB: the system consists of a bundle of tubes in thermal contact with the WH stream, typically hot flue gases coming from other subprocesses of the industrial site (Hussam Jouhara et al., 2018). The tubes are fed with water typically through a steam drum, and the water circulates through the tubes where it boils by recovering heat from the WH steam. Such configuration is commonly referred as water-tube WHB. As a result of the heat transfer process, the gas stream is cooled from the given inlet temperature to the design outlet temperature, eventually for further processing. At the tube-side water boils and the steam is collected at the top of the steam drum.

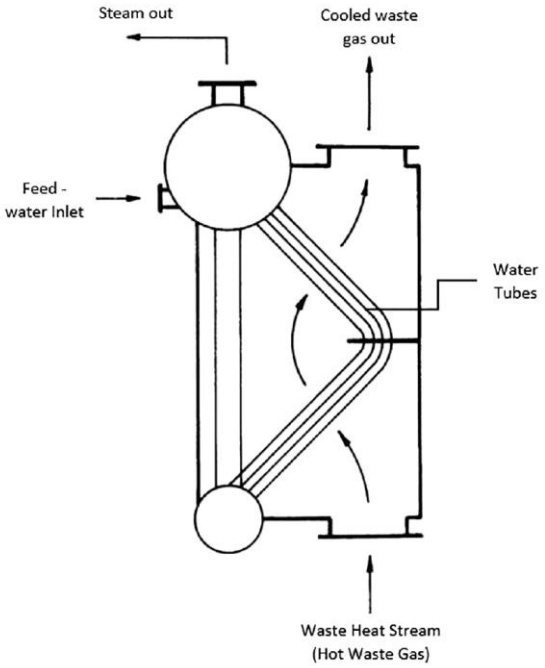

Figure 44: Schematic of a water tube WHB (Hussam Jouhara et al., 2018).

Figure 45 illustrates the classification of WHBs proposed in (Ganapathy, 2014). The extent of the classification criteria results from the wide variety of WHB options currently available. The main classification criterion is the intended purpose of the WHB (Ganapathy, 2014): in "energy recovery" applications the main objective is to maximize the recovery of thermal energy (compatible with low-temperature corrosion issues), with the flue gas being vented to the stack beyond the boiler exit. Typical examples are incinerators, heat recovery from outlet of gas turbines, kiln exhausts. In "process" applications the purpose of the WHB is to cool gas streams to a design temperature in order to enable further processing of the gas stream, for example desulfurization.

Horizon 2020
European Union Funding
for Research & Innovation

This project has received funding from
the European Union's Horizon 2020 research and innovation
programme under grant agreement No 847097

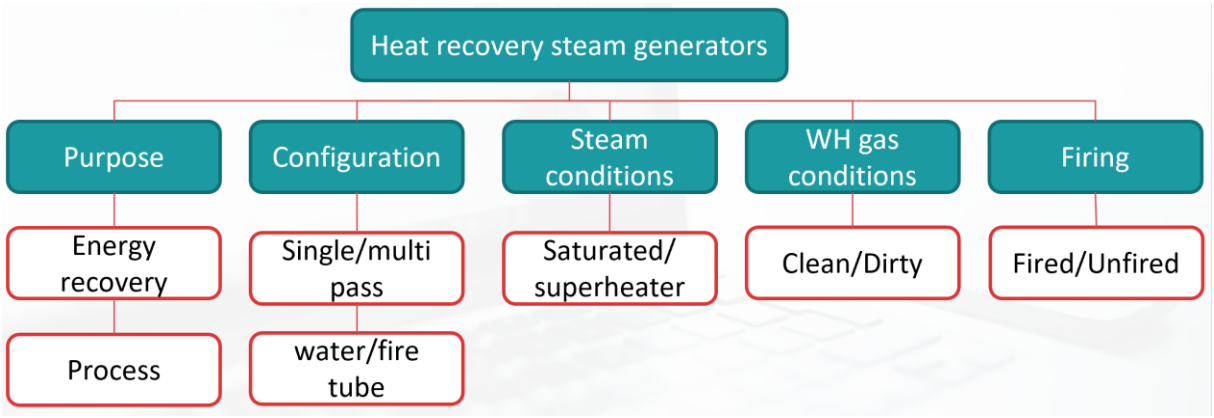

Figure 45: Classification of WHBs (Ganapathy, 2014).

WHBs are commercially available in a wide range of capacities, from less than 1000 m^3/h to 10^6 m^3/h of flue gas intake (Doty & Turner, 2013). Such wide range of flow rates has led to different types of WHB configurations. Water tube WHBs (Figure 44) are typically suitable for large capacities – in the range of millions of kg/h of WH steam flow rate. In such configuration water flows in the tubes of the WHB. On the other hand, for low capacities, fire tube WHBs are the preferred choice. In this case the flue gases flow inside the tubes while water surrounds the tubes bundle. This configuration closely resembles a STHE equipped with steam drum (Figure 46).

If the inlet gas temperature is above 700°C, a single-pressure WHB is adequate to cool the flue gas to about 130°C÷150°C (Ganapathy, 2014). However, if the inlet gas temperature is lower, like in gas turbine applications (500÷600°C) or in cement plant applications (300÷350°C) the flue gas cannot be cooled to 130÷150°C with generation of medium/high pressure steam in a single pressure WHB due to pinch point limitations dictated by the constant temperature evaporation. That is why multiple-pressure steam generation is required to fully recover the thermal energy of the exhaust streams of gas turbines or cement plants.

It is important to emphasize the heterogeneous nature of WHB technology and the wide variety of solutions which fall under this technology. Figure 46 and Figure 47 provide a visual comparison of a small scale fire tube WHRB and a large scale water tube HRSG. Fire tube are compact units (relatively to large capacity water tube WHB) and offer opportunity for retrofitting into existing industrial processes. Applications of small scale WHBs can be found in a variety of industries that need process steam such as food, paper and textile ("Cannon Bono Energia," 2019). On the other end of the spectrum, large capacity WHBs are typically bespoken, large scale engineering infrastructures which require to be planned, designed and built on site in parallel with the industrial site. Large scale HRSGs are employed in power plants for electricity production through steam Rankine cycles. Examples include WtE plants, combined cycle power plants and cogeneration plants. In Table 17 a quantitative comparison of fire (i.e., flue gas) tube and water tube WHBs is provided. Generally, water tube boilers are suitable for large gas flows in the range of hundred thousands or millions of kg/h and can handle high steam pressures and temperatures suitable for power generation. Fire tube boilers are suitable for low steam pressures, because they require large thickness as the steam pressure increases and thus become uneconomical. While multiple-pressure modules are easy to build with water tube boilers, they are rarely seen with fire tubes.

Horizon 2020
European Union Funding
for Research & Innovation

This project has received funding from
the European Union's Horizon 2020 research and innovation
programme under grant agreement No 847097

Figure 46: Fire tube WHB with a capacity of 3000 kg/h and a thermal power output of 2 MW for various industrial applications (WHR from engines, thermal oxidizers, gasifiers, etc.) ("Cochran UK," 2019).

a) *b)*

Figure 47: HRSG for combined cycle power plants: a) Photo of the combined cycle power plant; b) Layout of an horizontal three pressure level HRSG downstream of a 250 MWe gas turbine ("AC Boilers," 2019) (Volpi, Penati, & Silva, 2005).

Table 17: Comparison of fire tube and water tube HRSGs (Ganapathy, 2014).

Category	Fire (Gas) tube	Water tube
WH gas flow rate (kg/h)	< 30000÷40000	30000 ÷ 1000000
WH gas inlet temperature (°C)	Any (from low to adiabatic combustion)	Any (from low to adiabatic combustion)
WH recovery capacity	~100 kW to ~10 MW	~tens MW
Steam pressure (bar)	<35	<150
Steam temperature (°C)	<500	<570
Multiple pressure	No	Yes
Heat transfer surface	Plain tubes	Plain/finned tubes
Thermal efficiency (%)	70 ÷ 85	70 ÷ 85

The large scale water tube WHB (i.e., the HRSG) consists of three heat exchanger sections: Economizer, Evaporator and Superheater. In the Economizer, the feedwater is heated up to a temperature close to its saturation point. In the Evaporator, feedwater is evaporated at constant

Horizon 2020
European Union Funding
for Research & Innovation

This project has received funding from
the European Union's Horizon 2020 research and innovation
programme under grant agreement No 847097

temperature and pressure. The water and saturated steam are separated in the drum and the steam is fed to the superheater where it is superheated to the desired live-steam temperature (Kehlhofer, Hannemann, Stirnimann, & Rukes, 2009). The heat exchange in an HRSG can take place on one, two and three pressure levels, depending on the desired amount of energy and exergy to be recovered. HRSGs can be built in two basic configurations, based on the direction of the exhaust gas flow through the boiler (Kehlhofer et al., 2009):

1) Vertical HRSGs: The direction of the exhaust gas flow is vertical whereas the heat transfer tubes are horizontal, suspended from uncooled tube supports located in the gas path. In the past, vertical HRSGs were most often known as forced-circulation HRSGs because of the use of circulating pumps to provide positive circulation of boiler water through the evaporator sections.
2) Horizontal HRSGs: The direction of the exhaust gas flow is horizontal whereas the heat transfer tubes are vertical, and essentially self-supporting. The horizontal HRSG is typically also known as a natural-circulation HRSG because circulation through the evaporator takes place entirely by gravity, based on the density difference of water and boiling water mixtures.

Today most of the plants are equipped with horizontal natural-circulation HRSGs but the presence of both technologies on the market indicates that both of them meet customer expectations. The most common HRSGs use a steam drum for water/steam separation. In the Once-Through Steam Generator (OTSG), the economizer, evaporator, and superheater are basically formed by one tube (i.e., water enters at one end and steam leaves at the other end) eliminating the drum and the circulation pumps. This design has advantages at higher steam pressures because the absence of the drum does not impose limits during start-ups and load changes (Kehlhofer et al., 2009). Both horizontal and vertical HRSGs can be built with the once-through circulation principle.

2.4.2 Technology readiness level and examples of applications

WHB is a fully commercialized technology supported with an extensive and international supply chain. The global market of this technology is estimated to be around 5.78 US billion $ in 2018. Under the pressure of necessary energy-efficient solutions the demand for WHBs is expected to grow at a rate of 6.4% (compound annual growth rate) in the period 2019÷2027 (The Insight Partners, 2019). Key global suppliers of WHBs include Bosch, Viessmann, and Siemens. Table 18 and and Table 19 summarize the main products commercially available, distinguishing small scale (off-the-shelf) boilers (Table 18) from bespoken solutions (Table 19).

Table 18: Selection of small/medium scale WHBs.

Manufacturer	Model	WHB type	Boiler output		Application	Reference
			kW	kg/h		
Viessmann	VITOMAX 200-RS	Fire tube	300 ÷ 2600	/	Meat processing, beverage, laundries, small scale industries	("Viessmann Vitomax 200-RS - waste heat boiler for generating steam," 2020)
Bosch	UNIVERSAL HRSB	Fire tube	/	400 ÷ 4100	Waste heat sources	("Bosch Thermotechnology," 2019)
Cochran	ST95	Fire tube	200 ÷ 2200	300 ÷ 3200	Gas turbines, engines, incinerators, gasifiers, thermal oxidizers	("Cochran UK," 2019)

Horizon 2020 European Union Funding for Research & Innovation
This project has received funding from the European Union's Horizon 2020 research and innovation programme under grant agreement No 847097

Thermax and Danstoker	/	/	<15000	<15000	Diesel Engines, Gas turbines, Ferrous (Sponge, Coke, Furnaces), Non Ferrous (Copper, Zinc), Cement, Chemicals, Glass, Refinery fluid catalytic cracker, Sulfur, Hydrogen	("Thermax - Waste heat recovery boilers," 2019) ("Danstoker - Waste heat recovery boilers (WHRB)," 2019)
Alfa Laval	Aalborg XW	Water tube, forced circulation	100 ÷ 21000	200 ÷ 17000	Exhaust gases from marine Diesel engines	("Alfa Laval - Waste heat recovery," 2020)
Byworth	/	Fire tube	9600	<16000	CHP boiler projects, incineration and hot air dryers	("Byworth - Waste heat boilers," 2020)

Table 19: Selection of large scale WHBs (HRSGs).

Manufacturer	Model	HRSG type	Boiler output		Application	Reference
			kW	kg/h		
Siemens	H-BASIC, H-FAST, NEM-Fast	Horizontal and vertical HRSG	10000 ÷ 70000	/	Thermal power plants	("Siemens - Heat Recovery Steam Generators," 2020)
GE	/	Horizontal drum, vertical drum, horizontal once through	/	/	Combined cycle power plants	("GE Power - Heat recovery steam generators," 2020)
Mitsubishi	/	/	/	/	Power plants, marine engines	("Mitsubishi Heavy Industries - waste heat recovery systems," 2020)
Ansaldo Boilers	/	Horizontal natural circulation drum type, Horizontal once-through, Vertical assisted circulation	/	/	Combined cycle power plants	("AC Boilers," 2019)

Horizon 2020 European Union Funding for Research & Innovation

This project has received funding from the European Union's Horizon 2020 research and innovation programme under grant agreement No 847097

2.5 Recuperators (RECs)

2.5.1 Technological features and performance

Recuperators (RECs) are medium-to-high temperature gas-to-gas HEs used to recover WH from exhaust gas, for example from furnaces, to preheat combustion air. This practice reduces the amount of fuel used in the process, hence increasing the overall efficiency and abating the CO_2 emissions. RECs find therefore application in furnaces, ovens, incinerators and burners (BCS, 2008). More in general, a REC is a convective heat transfer-type HE where the two fluids are separated by a conduction wall through which heat transfer takes place due to convection or a combination of radiation and convection (Thulukkanam, 2013). This more broad definition includes other types of heat exchange (gas-to-liquid, liquid-to-liquid, solid-to-gas, etc.) under the recuperator heading. In the RECs the fluids flow simultaneously, remain unmixed and there are no moving parts. Some examples of RECs are tubular, plate-fin, and extended surface HEs. RECs are typically used when the flue gas is clean and uncontaminated (Thulukkanam, 2013). Several designs of RECs are available. However, they can be classified into two major categories on the basis of the heat transfer mode: convective RECs and radiant RECs (BCS, 2008)(Gorog, 2007).

Convective RECs. In these RECs convective heat transfer is the main mode of heat transfer between the exhaust gas and the air stream. Such RECs operate similarly to conventional HEs and employ similar flow arrangements. Exhausts flow through tubes or channels while the other fluid flows over the tubes (or vice versa depending on the requirements of the specific application). Parallel, counter or cross flow configurations are possible. Figure 48 shows the schematics of a parallel flow (left) and a cross flow (right) convective REC. Figure 49 shows a picture of a commercialized convective recuperator.

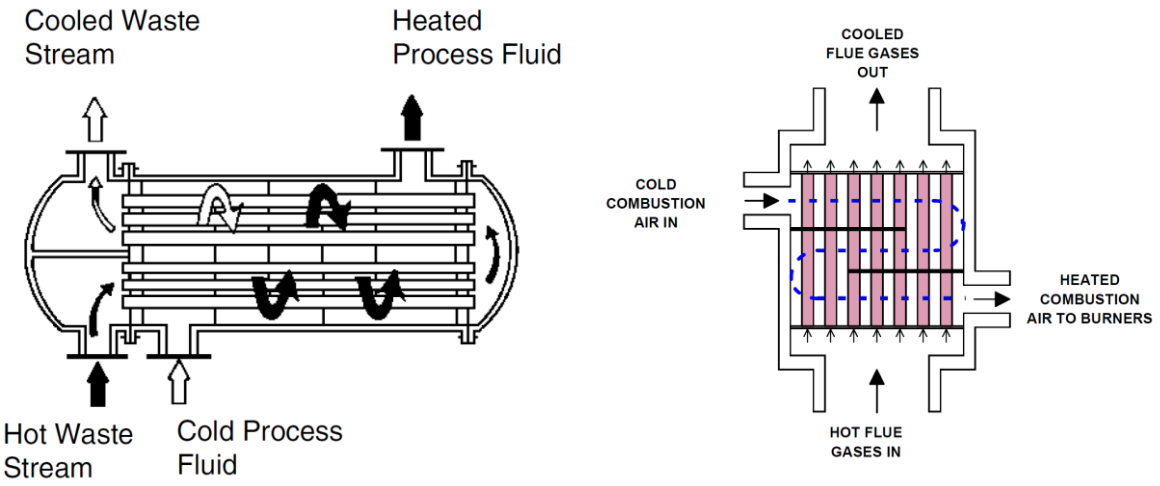

a) b)

Figure 48: Schematics of convective recuperators: a) parallel flow recuperator (EPRI, 2010); b) cross flow recuperators (Gorog, 2007).

Horizon 2020 European Union Funding for Research & Innovation
This project has received funding from the European Union's Horizon 2020 research and innovation programme under grant agreement No 847097

Figure 49: Commercial convective REC ("Kalfrisa - Convective recuperators," 2020).

Radiant RECs. In these RECs radiative heat transfer is the main mode of heat transfer between the WH stream and the secondary fluid. This class of REC is most suitable to operate in the high temperature range (>700°C) where radiation becomes the dominant heat transfer mode in comparison to convection. In its simplest implementation radiative RECs consist of two concentric cylinders as illustrated in Figure 50. As the high temperature WH stream flows through inner duct it emits thermal radiation (due to its high temperature) toward the inner pipe of the duct. The colder secondary gas (air) flows through the outer shell and it is progressively heated. In comparison to convective recuperators, radiant recuperators (Figure 51) have simpler geometry (no need of extended heat transfer surfaces), resulting in lower pressure drops and less issues with fouling/blockage of exhausts flow cross sections (BCS, 2008). On the other hand, the high working temperature requires the adoption of suitable construction materials, for example ceramics.

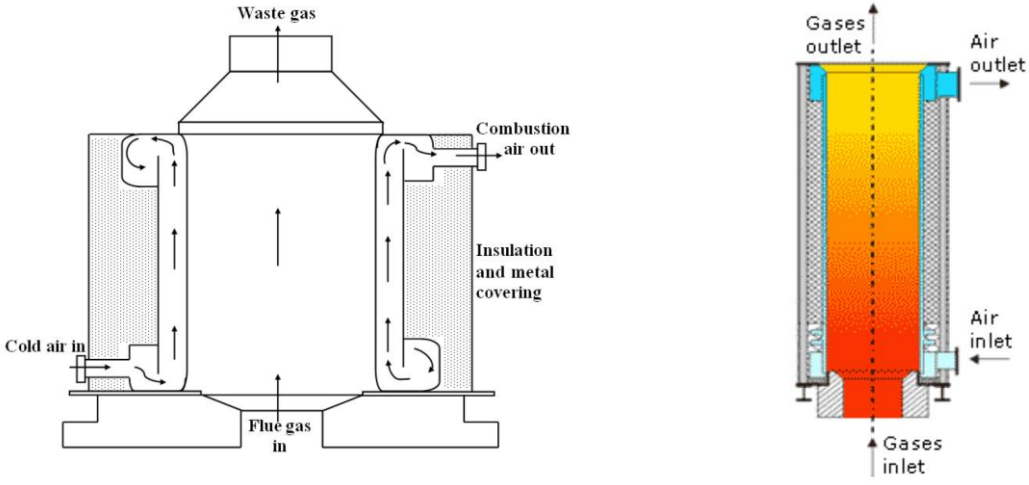

a) *b)*

Figure 50: Schematics of radiant RECs: a) Literature source (H. Sharma, Kumar, Varun, & Khurana, 2014) *(EPRI, 2010) ; b) Literature source ("Kalfrisa - Radiation recuperators," 2020).*

Horizon 2020
European Union Funding
for Research & Innovation

This project has received funding from
the European Union's Horizon 2020 research and innovation
programme under grant agreement No 847097

Figure 51: Commercial radiant REC ("Wabtec corporation - Radiation recuperators," 2020).

Recuperative burners. Recuperative systems are also available as an integral part of the burners. Such burners (called recuperative burners) incorporate the HE surfaces and the combustion chamber in a single device. The design is such that both WH from the hot flue gases from the burner and the waste heat from the body of the burner is recovered. The recovered heat is used to preheat the combustion air before it is mixed with the fuel in the burner. This results in an overall improvement of the combustion efficiency, and therefore the overall increase efficiency of the burner. A schematic of a recuperative burner is presented in Figure 52.

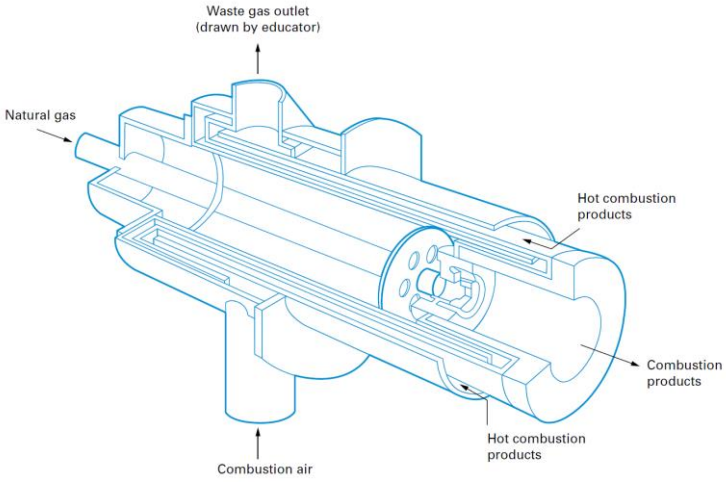

Figure 52: Schematic of a recuperative burner (Carbon Trust, 2019).

By recovering heat from the flue gases of fired heaters, furnaces or boilers and using the recovered heat to preheat the combustion air to the burners considerable savings can often be made. Figure 53 shows the reduction in fuel consumption which can be achieved by means of combustion air preheating for a final flue gas temperature of 180°C (Nicholson, 1983) and different initial temperatures in the range 200÷600°C. The saving increases with the initial flue gas temperature and with the excess air. For instance, in a typical refinery furnace with a flue gas exit temperature of 400°C

Horizon 2020
European Union Funding
for Research & Innovation

This project has received funding from
the European Union's Horizon 2020 research and innovation
programme under grant agreement No 847097

and an excess air of 40% the percentage reduction of fuel consumption achievable by preheating air in a convective REC could reach 15÷16%. The saving is significant and higher than 10% even for a more efficient burner with a low excess air of 10%.

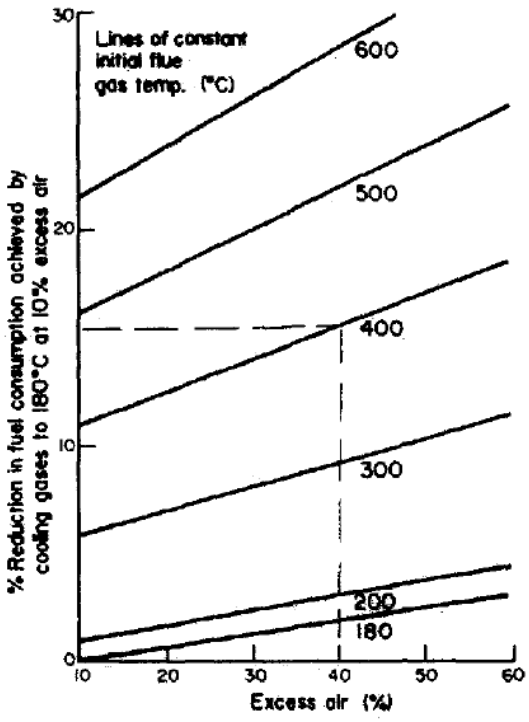

Figure 53: Potential fuel savings by combustion air preheat for different flue gas temperatures (180÷600°C) and excess air (10÷60%), considering a minimum flue gas temperature of 180°C (Nicholson, 1983).

2.5.2 Technology readiness level and examples of applications

RECs recover exhaust gas waste heat in medium-to-high temperature applications such as soaking or annealing ovens, melting furnaces, afterburners, gas incinerators, radiant tube burners, and reheat furnaces (BCS, 2008). Regarding materials, RECs are usually constructed in either metallic material for applications up to 800÷1100°C (2000°F) or ceramic materials for applications up to about 1600°C (2800°F) (EPRI, 2010) (BCS, 2008).

A variety of convective RECs is currently available commercially. They have been designed and manufactured largely on the basis of design guidelines for HEs. For medium-to-high temperature (up to about 800°C) conventional parallel-plate and shell-and-tube configurations can be adopted. Higher working temperatures might necessitate tailored designs; these are clustered under "Convective" type in Table 20 and Table 21.

Efficiency of RECs might vary depending on the specific operating conditions. Commonly, the efficiency of RECs can be estimated through established methods for HEs, for example effectiveness-NTU method (Thulukkanam, 2013). Table 20 summarizes the performance of different types of RECs. Table 21 presents and compares their typical applications.

Table 20: Operating temperature and performance of RECs (Carbon Trust, 2019).

Type of REC	Maximum operating T (°C)	Efficiency (%)	Resistance to fouling
Radiant	1400	10÷20	Good
Convective	1200	30÷50	Moderate

Horizon 2020
European Union Funding
for Research & Innovation

This project has received funding from
the European Union's Horizon 2020 research and innovation
programme under grant agreement No 847097

Plate	800	40÷60	Poor
Shell and tube	550	70÷90	Moderate

Table 21: Examples of applications of RECs.

Type of REC	Temperature range	Sources of waste heat	Typical uses	Type of heat exchange
Radiant	High	Soaking or annealing ovens, melting furnaces, incinerators, radiant-tube burners, reheat furnace	Combustion air preheat	Gas-Gas
Convective	Medium / High			
Plate	Low / Medium	Exhaust from boilers, incinerators and turbines. Drying, curing and baking ovens	Combustion air preheat, space heating	Gas-Gas Liquid-Liquid
Shell and tube	Low / Medium	Refrigeration condensates, waste steam distillation condensates, coolants from engines, air compressors, bearings and lubricants	Liquid feed flows requiring heating	Gas-Liquid Liquid-Liquid

A selected number of industrial applications of RECs reported in the literature is described in the following: they refer to the magnesium, steel, glass/fiberglass, aluminium and textile industries.

- **Magnesium production plant (rotary kiln)**

The improvement of the energy efficiency of a rotary kiln by the use of heat loss from its mantle was investigated in (Karamarković, Marašević, Karamarković, & Karamarković, 2013). The kiln is used for calcination of dolomite in a magnesium production plant. The waste heat is used in a REC to preheat air up to 300°C for the combustion of fuel in the kiln. In the first part of the rotary kiln, where the surface temperatures are the highest (and reach a peak of 364°C), a several meters long annular duct is installed through which air flows to subtract from the kiln thermal power equal to the one dissipated by the bare kiln in ambient air (Figure 54). Air, which enters the annulus from both ends, is preheated and then extracted over that section of the kiln with the highest temperature by a fan for the combustion of fuel inside the kiln. The implementation of the REC enabled a 12% saving of heavy fuel oil consumption (Karamarković et al., 2013). A short payback period of less than 6 months was reported.

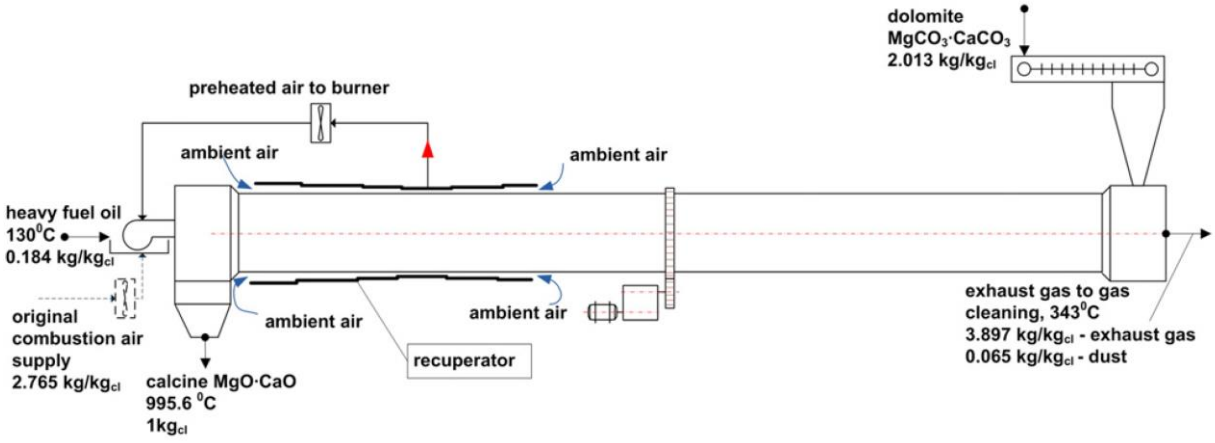

Figure 54: Schematic of the rotary kiln with the annular REC used for air preheating from the waste heat of the kiln shell (Karamarković et al., 2013).

- **Steel industry**

Horizon 2020
European Union Funding
for Research & Innovation

This project has received funding from
the European Union's Horizon 2020 research and innovation
programme under grant agreement No 847097

1) *Directly fired heat treating furnace*. The Allino furnace is a NG fired furnace where the steel billets are heated. The furnace consists of several gas burners distributed along the furnace in four heating zones. An integrated REC increases the combustion air temperature up to 280°C (Figure 55). The temperature of the flue gas at the outlet of the REC is still high (≈400°C) and its mass flow rate is highly variable. In the ETEKINA EU project ("ETEKINA H2020," 2020) this residual waste heat was recovered using the heat pipe HE technology in order to reach a preheating air temperature of 400°C at the outlet of the REC (Egilegor et al., 2019).

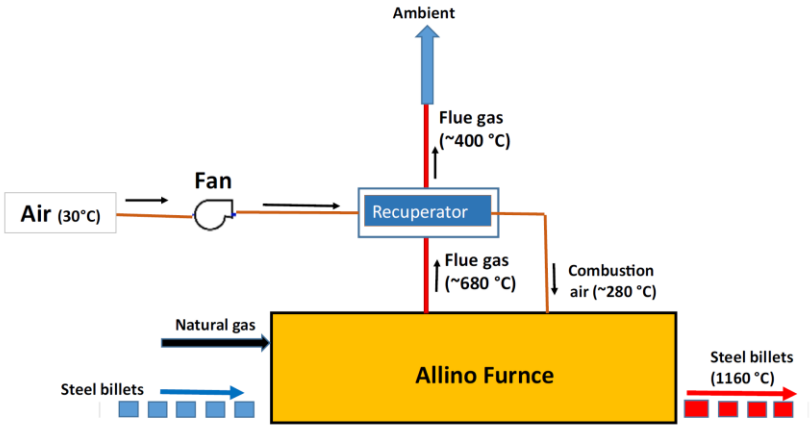

Figure 55: Integration of a REC to recover the flue gas from a billet heating furnace of a steel processing industry (Egilegor et al., 2019).

2) Indirectly-fired heat treating (austenitization/quench hardening) furnace. The quench hardening furnace (Figure 56 left) investigated in (Ganesh, Ezekoye, Edgar, & Baldea, 2019) is heated indirectly using radiant-tube burners (fired with NG) to prevent surface oxidation of the parts. The furnace operates at temperatures above 727°C (1000 K). Part of the heat in the burner exhaust gases is recovered to preheat the air fed to the burners using a shell and tube radiant REC that is fitted at the exhaust section of each burner (Figure 56 right). The maximum temperature of the preheated air was limited to 260°C to limit NO_x emissions. The results of an accurate simulation model showed that the furnace equipped with RECs requires 16% less fuel compared to the base case without RECs (Ganesh et al., 2019).

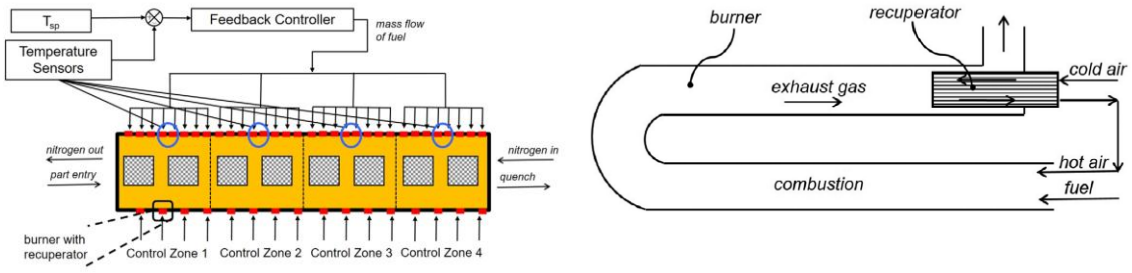

a) *b)*

Figure 56: Implementation of a REC in an indirectly heated furnace: a) austenitization furnace; b) U-tube burner with REC (Ganesh et al., 2019).

- **Glass industry (glass and fiberglass)**

Horizon 2020
European Union Funding
for Research & Innovation

This project has received funding from
the European Union's Horizon 2020 research and innovation
programme under grant agreement No 847097

A typical arrangement of a recuperative glass furnace is shown in Figure 57 (left). A recuperative glass furnace is essentially a direct-fired furnace that has been fitted with a REC to recover heat from the exhaust gases (Pellegrino, 2002). It can be fired with either NG or oil and it is used mostly in smaller operations. Heat is recovered from the flue gas to preheat combustion air to 540÷815°C (Pellegrino, 2002). The REC can be of double-shell or tubular design, and is constructed from stainless steel or Inconel. Recovering heat nearly doubles the thermal efficiency of the furnace to as much as 25÷40%. Radiant RECs with diameters lower than 1.3 m and heights lower than 10 m are typically used. Figure 57 (right) shows a recuperative fiberglass furnace. Fiberglass is melted at lower temperatures compared to glass and the flue gas enters the radiant recuperator at 1200°C (H. Sharma et al., 2014).

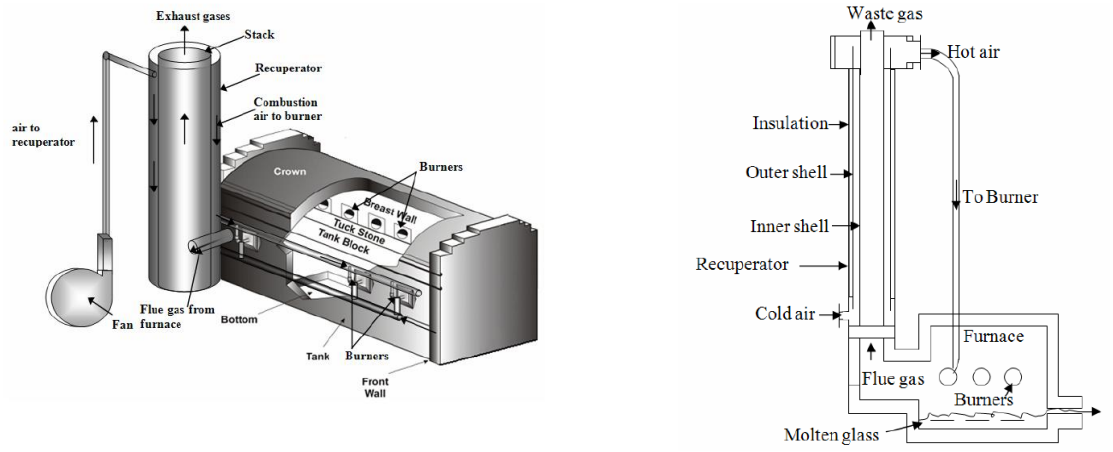

a) *b)*

Figure 57: Direct fired furnaces with radiant RECs: a) glass production; b) fiberglass production (H. Sharma et al., 2014).

- **Aluminium industry**

The system investigated in the early paper by (Incropera, Prescott, & Voelkel, 1985) recovers heat from the flue gas of an aluminium melting furnace at temperatures up to 1315°C and it is composed by the combination of a radiant REC and a SRC. Both series and parallel flow configurations were considered. Since the radiant REC is only effective for high gas temperatures (>1350°C), it is placed upstream of the WHB in the series arrangement (Figure 58 left). In the parallel arrangement (Figure 58 right), the furnace exhaust gas is divided into two streams which are separately routed to the two heat recovery systems (REC and WHB). The series arrangement was found to be superior to the parallel arrangement because the REC exhaust gas temperatures are still high (due to the radiant REC`s low typical efficiencies) and the additional heat recovery unit positioned downstream of the REC substantially enhances the total heat recovery (Incropera et al., 1985).

Horizon 2020
European Union Funding
for Research & Innovation

This project has received funding from
the European Union's Horizon 2020 research and innovation
programme under grant agreement No 847097

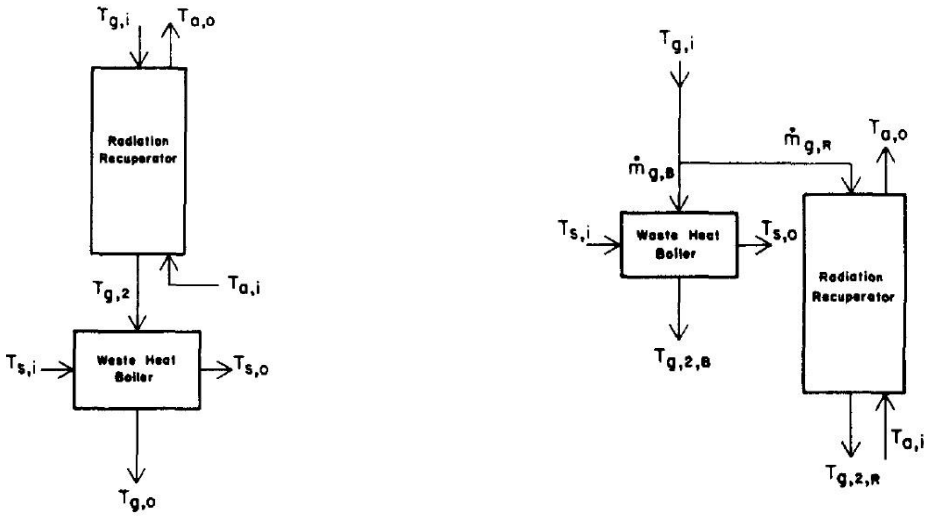

a) *b)*

Figure 58: Cascade WHR from the exhaust gas of an aluminium melting furnace: a) series arrangement of radiant REC and WHB; b) parallel arrangement of radiant REC and WHB (Incropera et al., 1985).

- **Textile industry (indirect heat recovery using a water loop)**

In textile industrial driers warm air or combustion gases are impinged on the humid fabric and then vented to the atmosphere. This heat can be recovered to preheat the fresh dry air to be continuously circulated to the drying process (Fiaschi, Manfrida, Russo, & Talluri, 2017). Direct heat recovery from the exhaust stream to the inlet air has proven to be troublesome, due to the contamination of the exhaust with dyes, oil and textile fragments. Moreover, the air inlet is distributed in several points and this makes, on the whole, this solution unpractical. Thereby, indirect heat recovery systems were developed, typically recovering heat from the exhaust and transferring it to a water circuit/storage vessel; hot water can then be distributed to HEs for air preheating (Figure 59). Water within the circuit is pressurized (typically to 3÷3.5 bar) in order to maintain liquid conditions at temperatures slightly exceeding 100°C. The heat recuperation from the exhaust stream is done through flow of water across the external annulus of the exhaust pipes (Fiaschi et al., 2017).

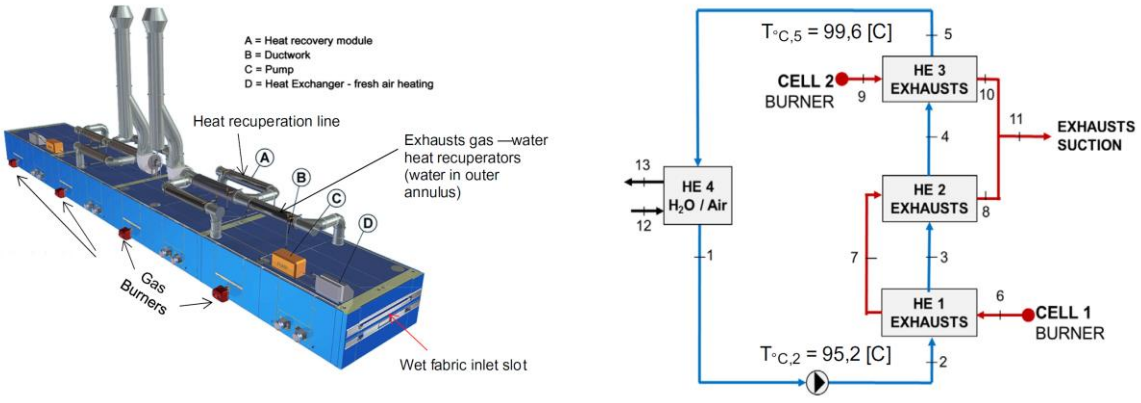

a) *b)*

Figure 59: WHR from the combustion gases in a textile industry: a) textile plant; b) heat recovery loop (Fiaschi et al., 2017).

Horizon 2020 European Union Funding for Research & Innovation
This project has received funding from the European Union's Horizon 2020 research and innovation programme under grant agreement No 847097

2.6 Regenerators (REGs)

2.6.1 Technological features and performance

A regenerator (REG) consists of a matrix through which the hot stream and cold stream flow periodically and alternatively. Firstly, the hot fluid exchange heat to the REG. In a second phase, the cold fluid flows through the same passage, picking up the stored heat. Thus, by regular reversals, the matrix is alternatively exposed to the hot and cold gas streams, and the temperature of the packing, and the gas, at each position fluctuates with time. After a number of cycles following the start-up of the regenerator, a condition of cyclic equilibrium is reached where the variations of temperature with time are the same during successive cycles and the time period of hot fluid and cold fluid flow ensures sufficient time to absorb and release heat (Thulukkanam, 2013).

REGs use a high temperature mass, typically a metallic/ceramic matrix, that is cyclically heated through the WH stream (WH capture) and cooled by the secondary fluid (WH recovery) (Carbon Trust, 2019). REGs can be classified into two general categories: fixed matrix and rotary regenerators.

1) *Fixed matrix REGs*. The fixed matrix REG shown Figure 60 consists of a pair matrix structure made of bricks through which hot air (WH stream) and cold air alternatively flow. When combustion products flow through a one of the structure, heat is absorbed and the temperature of the bricks increases, effectively storing in sensible heat from the WH carried by the combustion products. The flow is then redirected such that combustion air (i.e. the secondary stream) passes through the now hot structure. As air passes through, heat is transferred from the bricks to the air before it enters the combustion chamber, completing the cycle for WH recovery. In the system illustrated in Figure 60 two matrix structures of bricks are employed such that combustion process can be operated continuously, as while one matrix absorbs heat from combustion products the other one release heat to the air flow. The role of the two matrices is swapped every 20 minutes (BCS, 2008). Some examples of fixed matrix regenerators are air preheaters for blast furnace stoves, glass furnaces, and open hearth furnaces (Thulukkanam, 2013).

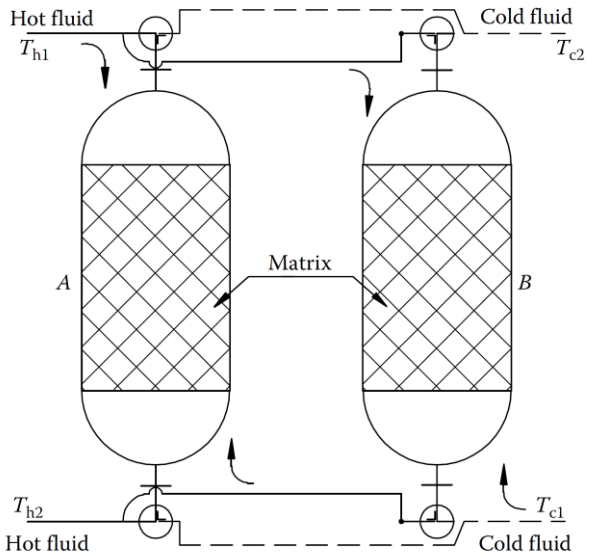

Figure 60: Fixed matrix regenerator of dual-bed valved type (Thulukkanam, 2013).

2) *Rotary REGs*. Beside fixed matrix structures cyclically heated/cooled by alternating direction of hot/cold streams, REGs can be also implemented by using rotary (i.e., moving) matrices, commonly called rotary REGs or "heat wheels". Rotary REGs use a round porous matrix made of a

Horizon 2020
European Union Funding
for Research & Innovation

This project has received funding from
the European Union's Horizon 2020 research and innovation
programme under grant agreement No 847097

high thermal capacity material which rotates perpendicularly to the direction of the hot and cold streams (BCS, 2008). A schematic of a rotary REG is shown in Figure 61 (left). The disc, by rotating along its axis, transfers the heat from the hot WH stream to the colder secondary fluid (air). Thus, at any instant of time during operation, the wheel is divided into two halves. A hot zone exposed receiving heat from the hot WH stream and a colder zone which transfer heat to the secondary stream.

Generally, the utilization of rotary REGs is limited to low-medium temperature differences between the hot and cold streams in order to avoid issues with thermal stresses and thermal expansion of the wheel, compromising the mechanical integrity of the system (BCS, 2008). Another challenge with rotary REGs is avoiding any leakage of the hot WH stream toward the cold stream, leading to contamination issues particularly in cases where the WH stream consists of flue gases from combustion processes. Furthermore, the rotary REGs present a higher level of complexity compared to RECs, due to the presence of moving parts and electric motors necessary to move the heat wheel. This generally makes conventional RECs/HEs more economical than rotary REGs.

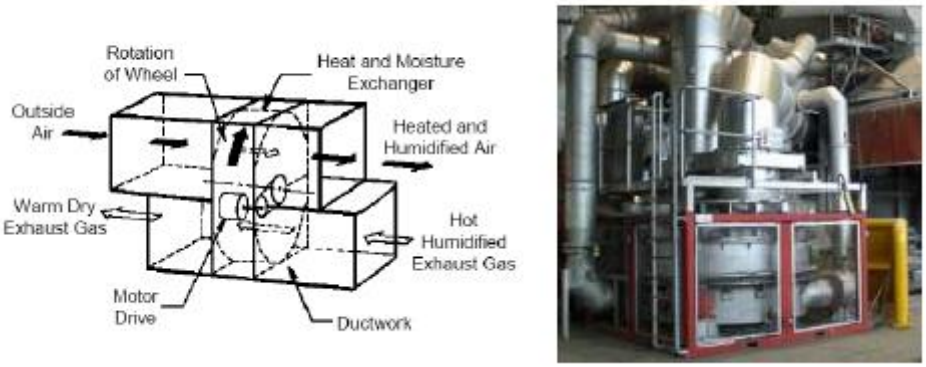

Figure 61: Schematic of a rotary REG (left) and picture of a rotary REG installed on a furnace (right) (BCS, 2008).

The "disk-type" matrix consists of alternate layers of corrugated, flat, thin metal strips wrapped around a central hub or ceramic pressing in a disk shape. Gases flow normal to the disk (Figure 62 left). The porous matrix provides a long, tortuous path and hence large area of contact for the flowing fluids. Depending upon the applications, disk-type REGs are variously referred to as heat wheel, thermal wheel, Munter wheel, or Ljungstrom wheel (Figure 62 right) (Thulukkanam, 2013). Process heat recovery applications of rotating REGs are many and varied, ranging from small units of 0.5÷1 m in diameter on dryers, to the large wheels in 660 MW power station boilers, where diameters of 15 m are typical (Reay, 1981).

Horizon 2020
European Union Funding
for Research & Innovation

This project has received funding from
the European Union's Horizon 2020 research and innovation
programme under grant agreement No 847097

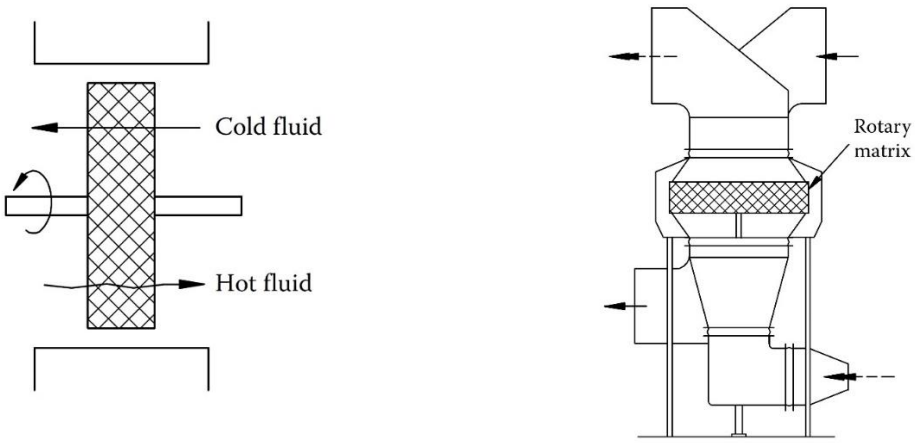

Figure 62: Disk type rotary REG: a) fluid flow across the wheel; b) Ljungstrom type REG.

2.6.2 Technology readiness level and examples of applications

The REGs are designed to cover a wide operating temperature range from cryogenic applications (-20°C) to very high temperatures of 1500°C and over. Metal REGs are used for operating temperatures up to about 870°C, wheras ceramic REGs are used for higher temperature, up to about 2000°C. The typical operating pressures for WHR applications are close to the atmospheric pressure (1÷1.5 bar). Table 22 shows the typical operating temperatures and efficiency of different types of REGs. REGs can generally operate at higher temperatures and are more efficient than RECs, but are much more expensive to install and are far bulkier (Carbon Trust, 2019). Table 23 shows the typical applications of rotary REGs. Rotary REGs are also particularly suitable for air conditioning applications (i.e., very low grade WH) where it is possible to transfer both heat as well as humidity from the hot to the cold stream. In such applications the matrix of the wheel is a hygroscopic material (e.g. silica, zeolite) which can capture heat and moisture from the hot stream and transfer it to a dry and cold stream (BCS, 2008).

Table 22: Operating temperature and performance of REGs (Carbon Trust, 2019).

Type of REG	Maximum operating T (°C)	Efficiency (%)	Resistance to fouling
Static	1000÷1500	70÷90	Good
Rotary	1000÷1700	70÷90	Poor
Compact	1000÷1500	70÷90	Moderate

Table 23: Typical applications of rotary REGs (BCS, 2008).

Type of REG	Temperature range	Sources of waste heat	Typical uses	Type of heat exchange
Metallic	Low-Medium	Boiler exhaust, curing and drying ovens	Combustion air preheating, space heating	Gas-Gas
Ceramic	Medium-High	Large boilers, incinerators exhaust, melting furnaces	Combustion air preheating	Gas-Gas

The integration of the rotary REG (heat wheel) in different industrial plants is presented in the following. For the glass production plants the heat wheel is considered as a way to further enhance the heat recovery compared to what is already achievable using the fixed matrix REG. Most of the

Horizon 2020
European Union Funding
for Research & Innovation

This project has received funding from
the European Union's Horizon 2020 research and innovation
programme under grant agreement No 847097

examples are taken from the early paper by (Warren, 1982), which still represents one of the most comprehensive reviews about the WHR in the industrial sector using rotary REGs. On the other hand, the developments at material level achieved in the last thirty-forty years have disclosed new opportunities for the integration of REGs at higher temperatures in the industrial sites.

- **Cement industry**

In the schematic shown in Figure 63 the combustion air is preheated in two stages: 1) by the kiln exhaust gas (leaving the limestone preheater at ≈450°C) through the introduction of a rotary REG (heat wheel); 2) by the cooler exhaust air in a shell and tube REC. By using two separate pieces of equipment (REG and REC) for the two heat sources, the mixing of the cooling air (lime dust laden) with the kiln exhaust gases (containing SO_3) and the consequent chemical reaction taking place between the two gases are avoided (Warren, 1982).

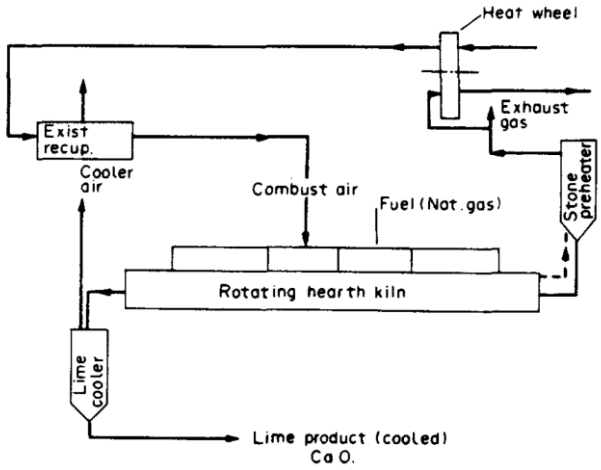

Figure 63: Integration of a rotary REG (heat wheel) for WHR from the exhaust gas in a cement plant (Warren, 1982).

- **Steel industry**

Figure 64 shows the installation of a heat wheel within the chimney combustion air system of a billet reheating furnace. The flue gases leaving the furnace at 900°C are diluted with entrained air and then pass through a heat wheel to raise the combustion air temperature to approximately 450°C. Even allowing for the fact that the full flue gas temperature was not handled, the fuel savings due to air preheating were significant (Warren, 1982).

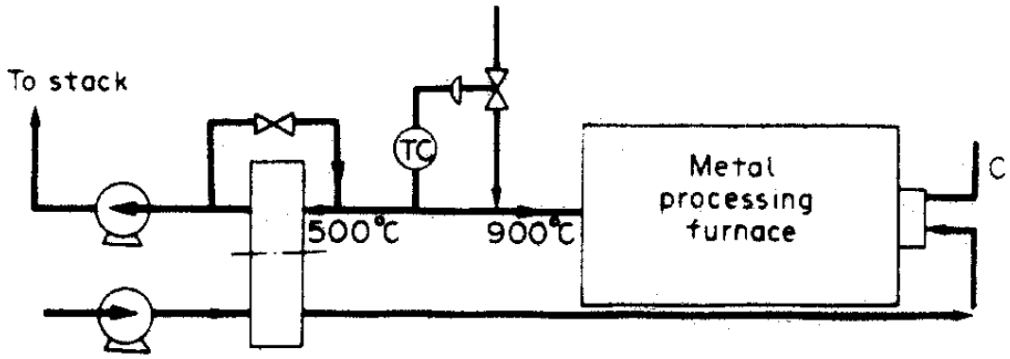

Figure 64: Installation of a regenerator (heat wheel) within the chimney combustion air system of a billet reheating furnace (Warren, 1982).

Horizon 2020
European Union Funding
for Research & Innovation

This project has received funding from
the European Union's Horizon 2020 research and innovation
programme under grant agreement No 847097

- **Glass industry**

The glass industry has long recovered heat from the flue gases and used it to preheat the combustion air using brick static REGs. At the beginning of 2000 regenerative furnaces accounted for about 42 percent of glass furnace population (Pellegrino, 2002). Capacities in these furnaces are high (100÷1000 tons per day), and they are relatively efficient (up to 65% thermal efficiency) when compared with direct-fired or recuperative furnaces (Pellegrino, 2002). The static REG consists of two chambers filled with a refractory brickwork packing. Hot exhaust gases pass through one chamber, heating up the refractory, whilst the air passes through the other in the opposite direction, being heated up by the refractory (Nicholson, 1983). The flow is reversed after a short period of time (usually 15-20 minutes), which alternates the inlet and exhaust ports (Figure 65b). The flame burns above the surface of the glass inside the space under the top of the melter (combustion space). The temperature of the melt is about 1430°C (2600°F) and combustion air preheating temperatures can reach as high as 1260°C (2300°F).

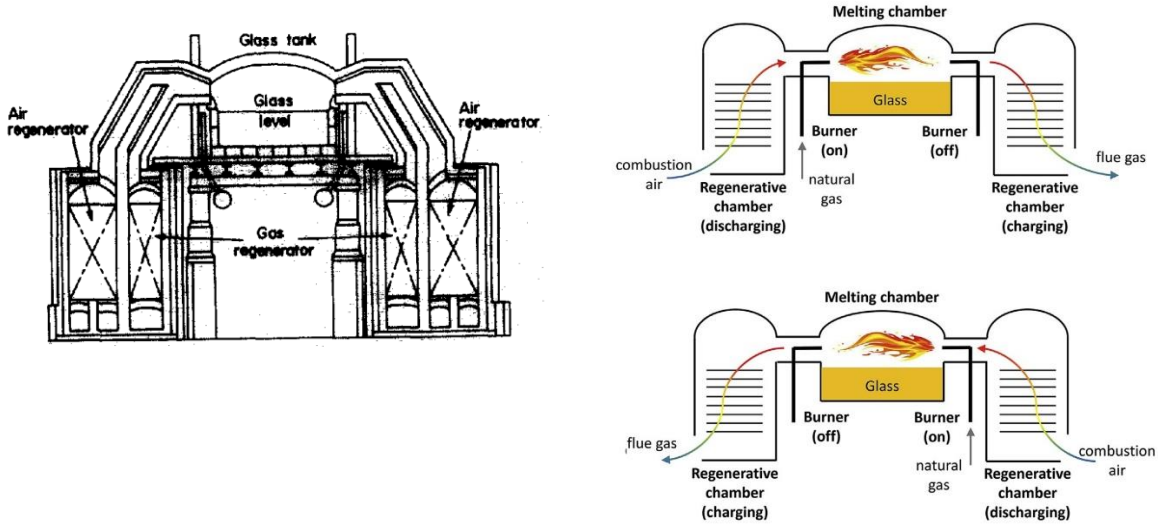

a) *b)*

Figure 65: Regenerative glass furnace with fixed matrix regenerators: a) Schematic (Nicholson, 1983); b) Operating principle (Danieli, Rech, & Lazzaretto, 2019).

Because of the high temperatures involved, the final flue gas temperature leaving the static REG is still high around 600÷700°C. Figure 66 shows a scheme where the air entering the checkerwork REG (i.e., the fixed REG) is raised from ambient to approximately 500°C by means of a stainless steel design of rotary REG which is able to accept gases at 700°C, with the final flue gas temperature being reduced to around 400°C (Warren, 1982).

Horizon 2020
European Union Funding
for Research & Innovation

This project has received funding from
the European Union's Horizon 2020 research and innovation
programme under grant agreement No 847097

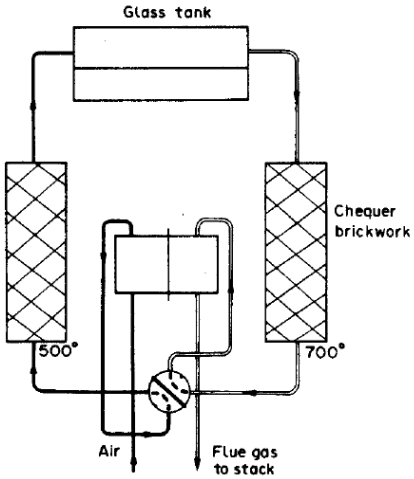

Figure 66: Integration of a static REG (stack of bricks) and a rotary REG (stainless steel) for WHR from a glass melting furnace (Warren, 1982) (Reay, 1981).

- **Ceramic industry**

In the brick industry it is normal for the clay to be dried by taking the warm cooling air coming from the adjacent Hoffmann kiln and further raising its temperature by means of a direct fired heater. It is possible via a rotary REG (in this case a Howden design) to exchange heat from the kiln exhaust gases (at 170°C) to warm the cooling air (Figure 67) and thereby reducing the load or even eliminate the load on the direct fired heater (butane burner) (Warren, 1982).

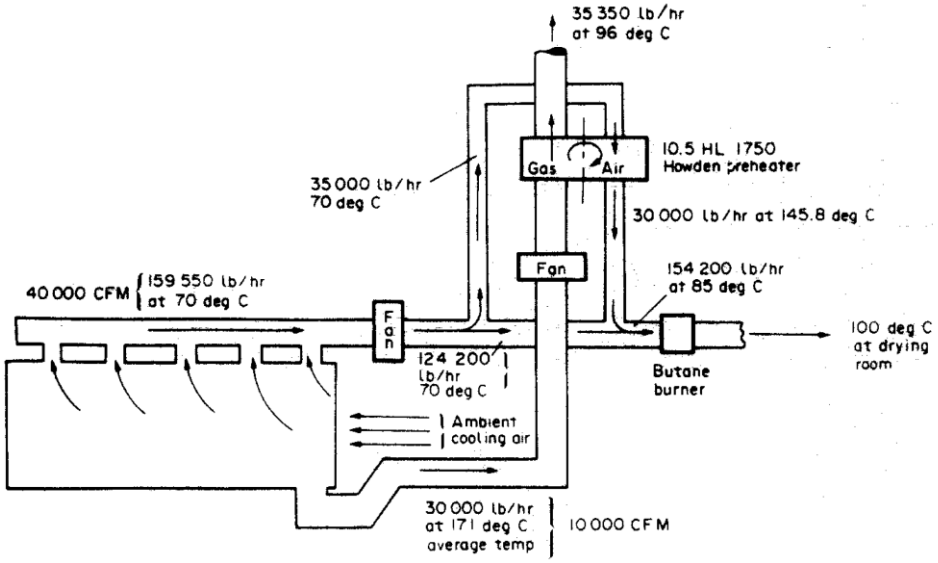

Figure 67: Installation of a rotary REG (Howden preheater) on modified Hoffman kiln ceramic works (Warren, 1982).

- **Drying processes**

In the schematic shown in Figure 68 the gas leaving the dryer at ≈110°C is used to preheat the ambient air to 70°C (Figure 68). The preheated air is used in a direct fired air heater (Warren, 1982).

Horizon 2020
European Union Funding
for Research & Innovation

This project has received funding from
the European Union's Horizon 2020 research and innovation
programme under grant agreement No 847097

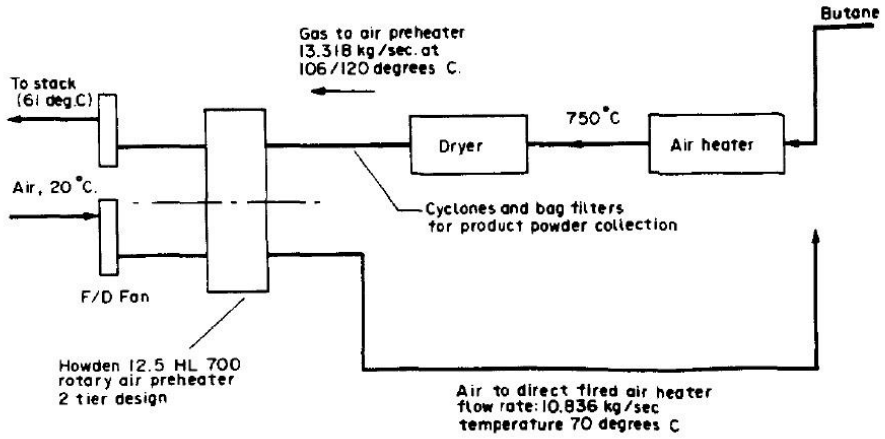

Figure 68: Integration of a thermal wheel in a dryer (Warren, 1982).

- **Petrochemical industry**

The air preheating in the petrochemical industry using rotary REGs is widespread. Table 24 shows several examples of processes where the regenerative air preheating up to 260÷440°C led to significant fuel savings in the range 8÷21% (Warren, 1982).

Table 24: Examples of air preheating using rotary REGs in the petrochemical industry (Warren, 1982).

Plant	Fuel	T gas in (°C)	T gas out (°C)	T air in (°C)	T air out (°C)	Fuel saving (%)
Ultraformer - Ultrafiner	Natural gas	563	199	4.4	438	21.4
Crude distillation unit	Heavy fuel oil	499	196	4.4	357	17.6
Ammonia (cracking)	Naphtha	356	171	16	272	9.15
Naphtha reformer	Natural gas	438	240	10	329	11.8
Crude distillation unit	Natural gas	499	201	4	362	17.4
Crude and vacuum	Heavy fuel oil	474	201	15.6	343	15.8
Unifiner and platformer	Heavy fuel oil	552	268	15.6	413	17.3
Crude distillation unit	Natural gas	282	136.4	-5	335	7.9
Methanol plant	Naphtha	375	187	25	260	9.4
Methanol plant	Natural gas	390	132	4	350	14.1

Horizon 2020
European Union Funding
for Research & Innovation

This project has received funding from
the European Union's Horizon 2020 research and innovation
programme under grant agreement No 847097

2.7 Heat pipe heat exchangers (HPHEs)

2.7.1 Technological features and performance

A significant portion of industrial processes generates WH in the form of gas streams (exhausts) under challenging operating conditions (Miró, Gasia, & Cabeza, 2016). The latter can be characterized as follows:

- Large mass flow rates/high temperatures;
- High content of particulate/abrasive substances causing fouling and wear&tear;
- Coresidents due to presence of SO_2, SO_3, NO_3, etc.

Such conditions may pose technical and economic barriers to the adoption of traditional heat exchangers (HEs) for process reintegration of WH into the industrial process. In particular, the operating conditions listed above could lead to:

- Higher CAPEX (corrosion resistant and abrasion resistant materials required);
- Reduced returns (more frequent maintenance/cleaning of equipment);
- Increased risks (higher probability of malfunctioning);
- Faster ageing of WH recovery equipment (higher corrosion and abrasion rates).

Heat pipe heat exchangers (HPHEs) are a class of HEs designed to meet harsh operating conditions, enabling WH recovery in industrial processes where the use of traditional HEs would be technically and/or economic not viable. Professor Hussam Jouhara at Brunel University (London) and his collaborators designed and tested several types of heat pipe heat exchangers for applications in various industrial contexts: ceramic industry ((Hussam Jouhara et al., 2021)(Brough et al., 2020)(Delpech, Axcell, & Jouhara, 2019)(Delpech et al., 2018)), steel industry (Hussam Jouhara et al., 2017) as well as aluminium industry ((Brough & Jouhara, 2020)(Egilegor et al., 2019)), which represent a subset of all the application fields reviewed in (H. Jouhara et al., 2017).

Figure 69 presents a typical configuration of an HPHE and allows to appreciate how such class of HEs differs from conventional HEs. An HPHE is constituted of two main compartments, which keep separate the WH exhaust stream from the cold fluid stream, which is heated due to the process of WH recovery. The Separator Plate (Figure 69) prevents WH exhausts and the cold stream to physically mix. Crucially, the two streams are in thermal contact (i.e., they exchange heat) *only* via a series of components called "heat pipes", which are oriented transversally to the flow direction of the two streams. No significant amount of heat is transferred between the two streams through the separating plate. Such feature is the main difference between the conventional HEs and HPHEs. Indeed, in conventional HEs heat transfer occurs by convection and conduction through metallic surfaces (for example fins). Conversely, in HPHEs the WH stream compartment and the cold stream compartment are kept thermally isolated (no heat transfer across metallic surfaces) with only the heat pipes acting as thermal bridges that transfer heat from the WH exhaust to the cold stream.

Horizon 2020
European Union Funding
for Research & Innovation

This project has received funding from
the European Union's Horizon 2020 research and innovation
programme under grant agreement No 847097

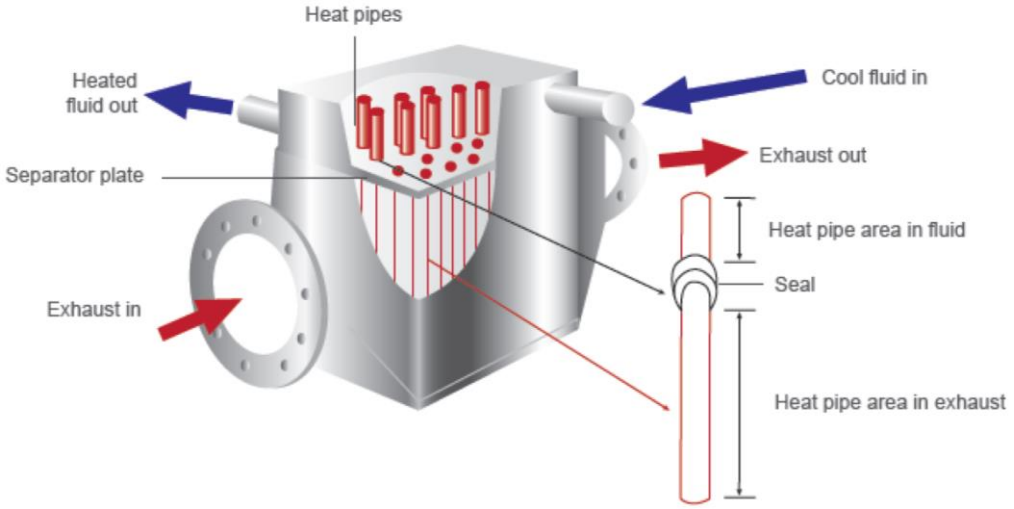

Figure 69: Heat pipe heat exchanger configuration (Hussam Jouhara, 2016).

Figure 70 and Figure 71 illustrate the structure of a heat pipe. Each individual heat pipe is a passive thermal device. It consists of a sealed shell, a wick structure and a certain amount of working fluid that transfers heat from the hot side to the cold side through continuous vaporization and condensation (Hussam Jouhara et al., 2018). Three main sections can be identified: heating section, adiabatic section and cooling section. The heating section is in contact with the WH stream, which causes the working fluid inside the heat pipe to evaporate. Consequently, the vapour pressure generated in the heat pipe drives the transport of the vapour through the adiabatic section to the cooling section. Here, vapour condensation occurs and the corresponding latent heat of condensation is released to the cold fluid. The condensed fluid is then captured by the wick structure and it returns to the heating section by capillary effect. By relying on evaporation/condensation heat transfer phenomena, rather than single phase convection/conduction, enables heat pipes to achieve very high effective thermal conductivities, up to 5000 ÷ 200000 W/m-K (("BOYD corporation - Heat Pipe Technology," 2020)(Hussam Jouhara et al., 2018)).

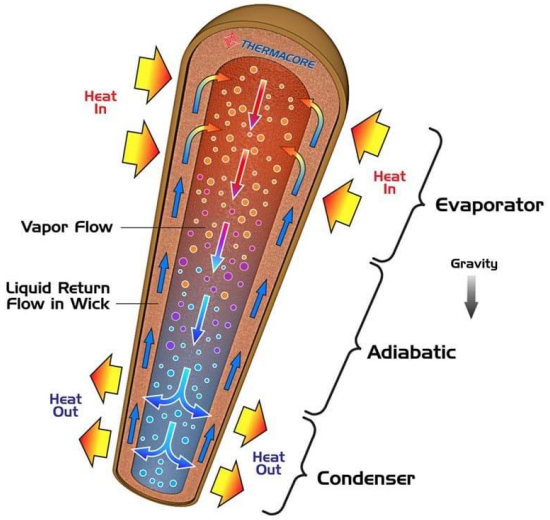

Figure 70: Structure and working principle of a heat pipe ("jhc specialized solutions," 2019)(Hussam Jouhara et al., 2018).

Horizon 2020
European Union Funding
for Research & Innovation

This project has received funding from
the European Union's Horizon 2020 research and innovation
programme under grant agreement No 847097

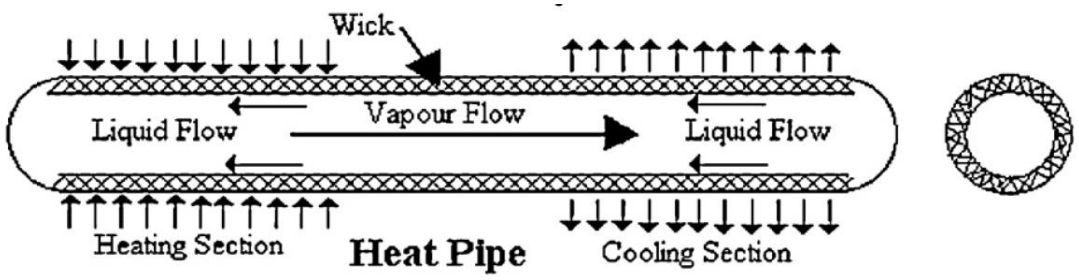

Figure 71: Schematic of a heat pipe structure (Chaudhry, Hughes, & Ghani, 2012).

A range of working fluids, materials and wick structures for heat pipes have been proposed. The selection of the working fluid largely relies on the WH stream temperature and the cold sink temperature (cold fluid stream temperature). For applications in the range 30÷300°C, water, ammonia, acetone and refrigerant-type working fluids have been used (Hussam Jouhara et al., 2018). Furthermore, selected working fluids should also meet cost, safety and physio-chemical stability criteria. Similarly to working fluids, the material selection of heat pipe shell is largely dictated by the temperature of the WH stream and the compatibility of the material with the WH stream. Aluminium, stainless steel, titanium and Inconel are examples of heat pipe materials ("ACT - Advanced Cooling Technologies," 2020). Finally, the wick typically consists of a mesh structure made of copper or stainless steel and expanded against the heat pipe shell in order to adhere to it. Grooved structures consisting of dents orthogonal to the heat pipe wall have been also employed.

Heat pipe heat exchanger configurations and Technology readiness level

HPHEs are currently commercially available in a few different configurations, mostly depending on the type of cold working fluid used and the heat duty of the HPHE. Although commercially deployed, it appears that the supply chain of HPHEs is presently limited, with Econoterm ("Econotherm," 2020) and Spirax Sarco ("Spirax Sarco," 2020) being the main suppliers.

The H2020 project "I-ThERM" (Grant Agreement ID: 680599) ("I-Therm H2020," 2019) proposed the following HPHEs classification:

- Standard cross flow HPHEs:
  - Air preheaters;
  - Gas-to-water;
  - Gas-to-thermal oil;
  - Steam generators.
- Modular cross flow HPHEs:
  - Gas-to-water;
  - Gas-to-thermal oil.
- Through-flow HPHEs.

Standard HPHEs are available for applications where the secondary fluid (i.e., the cold stream) is gas (air) or liquid (water, oil). Steam generation is also possible; in this instance the WH stream is used to transform water (the secondary fluid) in steam. A detailed view of a standard cross flow HPHE designed and tested in (Brough et al., 2020) is illustrated in Figure 72. Heat pipes are illustrated in red and they are in cross flow configuration with respect to the direction of the WH gas stream. The secondary fluid (water) flows in the top part of the HE and it is in thermal contact with the cooling section of the heat pipes. Multiple cross flow sections of heat pipes can be combined together. Figure

Horizon 2020
European Union Funding
for Research & Innovation

This project has received funding from
the European Union's Horizon 2020 research and innovation
programme under grant agreement No 847097

73 shows a Modular cross flow configuration with two heat pipe sections. Similarly, the cold fluid circuit is separated in two main sections. The modular configuration allows to achieve higher WHR rates due to the larger number of heat pipes used and the better temperature matching between the hot and cold streams. Depending on the number and length of the heat pipes used, the heat duty of HPHEs can reach about 1÷6 MW. Finally, Through-flow HPHEs are configurations suitable for exhaust temperatures higher than 500°C. Figure 74 shows the internal configuration of a Through-flow HPHE. The heat pipes are arranged in a cylindrical bundle while the WH stream and the cold stream flow in tangential and radial direction rather than in cross flow.

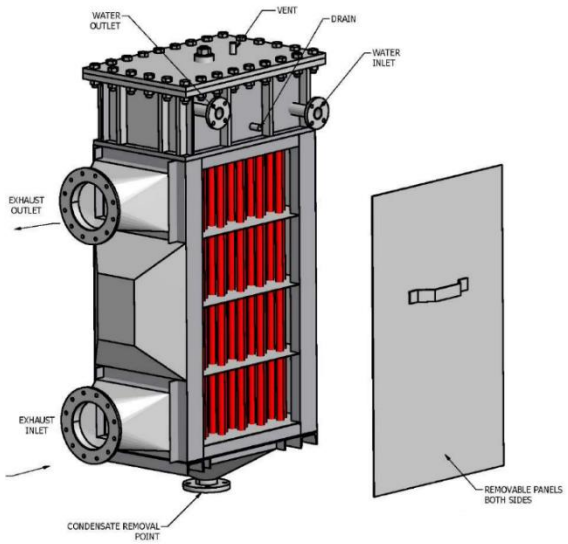

Figure 72: Cross flow HPHE (Brough et al., 2020). *Heat duty: 19 kW; gas stream inlet/outlet temperature: 203°C/50°C; water inlet/outlet temperature 20°C/51°C; Exhaust/water flow rate: 375 kg/h, 500 kg/h.*

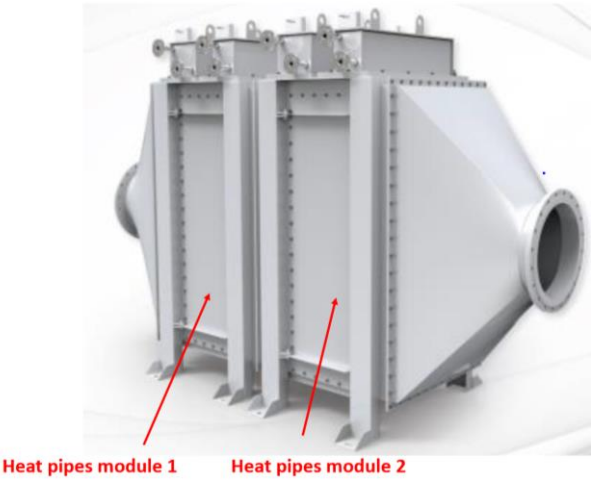

Figure 73: Modular cross flow HPHE (Hussam Jouhara, 2016).

Horizon 2020
European Union Funding
for Research & Innovation

This project has received funding from
the European Union's Horizon 2020 research and innovation
programme under grant agreement No 847097

Figure 74: Through-flow HPHE (Hussam Jouhara, 2016).

2.7.2 Examples of applications and cost aspects

A series of HPHE applications and case studies is presented in this Section. Where possible, available technical specifications and costs are reported. The applications listed in this Section have been reported by Econotherm Ltd ("Econotherm," 2020), a leading manufacturer in HPHEs and currently associate company of Spirax Sarco, which commercially supplies HPHEs in the range kW to MW heat duty ("Spirax Sarco," 2020).

- **WHR from furnace exhaust to preheat air (Automotive industry, Aluminium Furnace)**

Figure 75: Gas-to-air HPHE ("Econotherm," 2020).

The main technical and economic data for this application are reported in Table 25. The HPHE unit allowed to recover heat from an exhaust gas with high particulate concentration (furnace exhaust). The use of smooth heat pipes reduced the risk of fouling, increasing the reliability of the unit and eased the cleaning procedure. The reported payback period was less than two years, which is particularly attractive for industrial applications.

Horizon 2020
European Union Funding
for Research & Innovation

This project has received funding from
the European Union's Horizon 2020 research and innovation
programme under grant agreement No 847097

Table 25: Technical and economic data for Gas-to-air HPHE case study.

Parameter	Value
Exhaust inlet/outlet temperature (°C)	400/266
Air inlet/outlet temperature (°C)	30/293
Exhaust/air flow rate (kg/h)	12000/6374
Waste heat recovery rate (kW)	528
Specific investment cost (€/kW)	110÷255 €/kW

- **WHR from thermal oxidizer to process water (Gas extraction industry)**

Figure 76: Gas-to-water HPHE ("Econotherm," 2020).

Table 26 summarizes the main data for this application. The unit was mounted on a truck for travelling around Canada, which demonstrates an interesting mobilized application of HPHEs. A through-flow design was employed due to the very high inlet temperature of the WH stream. Removable panels facilitated the access to the bundles of heat pipes for cleaning and maintenance purposes, increasing the reliability of the unit. A heat duty of 2.2 MW was attained which led to a very short payback time of less than three months.

Table 26: Technical and economic data for Gas-to-water HPHE case study.

Parameter	Value
Exhaust inlet/outlet temperature (°C)	816/150
Water inlet/outlet temperature (°C)	5/16
Exhaust/water flow rate (kg/h)	11016 / 180000
Waste heat recovery rate (kW)	2260
Specific cost (€/kW)	32

Horizon 2020
European Union Funding
for Research & Innovation

This project has received funding from
the European Union's Horizon 2020 research and innovation
programme under grant agreement No 847097

- **WH recovery from pyrolysis plant (Power industry – thermochemical conversion of biomass)**

Figure 77: Gas-to-oil HPHE ("Econotherm," 2020).

Table 27 summarizes the main data for this exhaust-to-oil application. A through-flow configuration was used in order to deal with very high temperature (1000°C) of the furnace exhaust gases containing a very high content of particulate matter (Figure 77). The secondary fluid (oil) was then utilized to provide heat to an organic Rankine cycle for power production. A combination of smooth and finned heat pipes were installed in the HPHE.

Table 27: Technical and economic data for Gas-to-oil HPHE case study.

Parameter	Value
Exhaust inlet/outlet temperature (°C)	1000/250
Oil inlet/outlet temperature (°C)	135/280
Exhaust/oil flow rate (kg/h)	4150/9200
Waste heat recovery rate (kW)	940
Specific cost (€/kW)	27÷32

Horizon 2020
European Union Funding
for Research & Innovation

This project has received funding from
the European Union's Horizon 2020 research and innovation
programme under grant agreement No 847097

- **WHR in the food industry for steam generation and water pre-heating (Power industry – biochemical conversion of biomass)**

Figure 78: Gas-to-steam multi-stage HPHE ("Econotherm," 2020).

Table 28 summarizes the main data for this application. The unit is composed of two modules for water pre-heating (on the right of the unit) and one module for steam generation (on the left hand side) connected in series (Figure 78). The modules could be removed individually for cleaning and maintenance purposes. The WH stream from an anaerobic digester genset (i.e, from a reciprocating internal combustion engine fed by biogas) was recovered. The payback period was one year.

Table 28: Technical and economic data for Gas-to-water HPHE case study.

Parameter	Value
Exhaust inlet/outlet temperature (°C)	420/160
Water inlet/outlet temperature (°C)	160/198 (steam at 12 bar)
Exhaust/water flow rate (kg/h)	11484/900
Waste heat recovery rate (kW)	520
Specific cost (€/kW)	43

Horizon 2020
European Union Funding
for Research & Innovation

This project has received funding from
the European Union's Horizon 2020 research and innovation
programme under grant agreement No 847097

2.8 Summary - Waste heat to heat recovery technologies

The systematic review carried out in this Chapter indicated that the waste heat-to-heat class includes well developed and fully commercialized technologies which have been adopted extensively for WHR. This class of technologies fundamentally derives from heat exchangers (HEs) technology, from which it adopts several types of designs (e.g., shell-and-tube HEs) as well as methods for integration and operation. Gas-to-Gas HEs make a substantial part of the waste heat-to-heat technologies. This is due to the fact that high temperature flue gases and combustion products are a typical stream of WH, which can be recuperated/valorised when a heat sink (e.g., combustion air, water, steam) is available in the proximity of the flue gases streams. Such practice of process reintegration of WH is common in energy intensive industries which extensively use waste heat-to-heat technologies. As a result, supply chain, regulation standards, certification of performance and short payback periods are the strengths of waste heat-to-heat technologies. On the other hand, such technologies allow WH recovery/valorisation only when heat sinks and a demand of process heat are present in the premises of the WH stream to enable process reintegration. Alternatively, specialized HEs can be utilized to connect the WH source with a district heating infrastructure if the latter is present. Finally, the systematic review identified Heat pipe HEs as a promising near-to-market technology. They allow to meet harsh operating conditions (e.g., fouling, gas-liquid phases), enabling WHR where traditional heat exchangers would not be technically and/or economically viable. In conclusion, Table 29 lists and summarizes the key benefits and drawbacks of the waste heat-to-heat technologies.

Table 29: Summary of waste heat-to-heat technologies.

Waste heat to heat technologies		
Technology	**Benefits**	**Disadvantages**
District heating heat exchangers	Well proven technology based on conventional heat exchangers; used on a wide scale and fully commercially available.	District heating infrastructure needs to be in place and it needs to reach waste heat sources
Condensation heat recovery	Direct and indirect condensing economizers are available commercially; well proven.	Stream of condensed liquid need to be handled adequately and disposed if necessary
Economizers	Well proven technology based on conventional gas-liquid heat exchangers	Use limited to preheat boilers feed water; possible large foot print due to heat transfer limitations
Waste heat boilers	Well proven technology with fully developed supply chain	Technological option only feasible when there is a demand of steam to be met
Recuperators and Regenerators	Medium to high temperature heat exchangers to recover WH from flue gases; proven technology with several designs available	Possible issues with high operating temperatures and fouling. Moving parts for certain type of designs
Heat pipe heat exchangers	Near to market technology, about 300 full scale installations. Higher recovery capacity compared with traditional heat exchangers	Limited number of suppliers; specialized knowledge needed for design and installation

Horizon 2020
European Union Funding
for Research & Innovation

This project has received funding from
the European Union's Horizon 2020 research and innovation
programme under grant agreement No 847097

3 Thermal energy storage (TES) technologies

3.1 Sensible thermal energy storage (STES)

3.1.1 Technological features

Sensible thermal energy storage (STES) is the most deployed TES technology, widely commercialized and used at scale for a broad range of temperatures. All the STES are based on the same operating principles: raising or lowering the temperature of a suitable storage medium (liquid or solid) to capture heat from a process (charging) or release it to a process (discharging) ((Ease & EERA, 2017);(G. Li, 2016)). STES is also suitable for cold thermal energy, where cold is stored by lowering the temperature of the storage medium, and vice versa for release of cold.

Water is the most widely, cost-effective storage medium and it is commonly used up to about 120°C (pressurized water in DH systems ((Sartor & Dewallef, 2018); (Giovanni Manente, Lazzaretto, Molinari, & Bronzini, 2019)). Diathermic oils and molten salts are adopted as thermal storage media for temperature up to 250°C (oils) (H. Zhang, Baeyens, Cáceres, Degrève, & Lv, 2016) and around 300-400°C (molten salts) (Strasser & Selvam, 2014), respectively.

More recently STES in solid media (bricks, pebbles, rocks, concrete) has become increasingly attractive and has reached near-to-market status ("EnergyNest," 2019) ("Eco-Tech Ceram," 2019) (Odenthal, Klasing, & Bauer, 2017)(Libby, 2010), as well as focus of present H2020 projects (*Smartrec H2020*, 2019). An example of STES with solid storage medium developed by Energy Nest is presented in Figure 79. The major benefit of this option is the ability to store heat at high temperature (>400°C) and through direct contact between the heat transfer fluid (gas) and the storage medium. Solid media are applicable for low temperature STES too; this is the case of borehole TES (BTES) where heat is injected/retrieved into/from the ground through the use of boreholes which carry the heat transfer fluid pipeline.

Figure 79: Thermal battery module and storage system based on solid materials (EnergyNest 2019).

3.1.2 Examples of applications and technological maturity

The vast majority of STES technologies is very mature (TRL9) and they have been in use for decades (Ease & EERA, 2017). Water tanks are widely used at building, process and district scale, spanning storage sizes from few kWh to tens of MWh. Underground STES has been used in Scandinavian countries and for seasonal storage purposes in DHNs (Bott, Dressel, & Bayer, 2019). For high temperature applications, two-tank and single tank molten salts are the most adopted solution,

Horizon 2020
European Union Funding
for Research & Innovation

This project has received funding from
the European Union's Horizon 2020 research and innovation
programme under grant agreement No 847097

particularly in CSP plants, although the maturity of the technology allows its application also in high-temperature industrial processes. STES in bricks and solid media is available at small scale for domestic applications ("Dimplex," 2019), while is at advanced pilot stage for large scale applications, including waste heat capture, both stationary and mobile TES systems. This is the case of Energy Nest (TES in cement) ("EnergyNest," 2019), Eco-Tech Ceram (TES in ceramic materials) ("Eco-Tech Ceram," 2019) and Lumenion (TES is steel) ("Lumenion," 2019). These systems are near-to-market and aim to provide TES function for energy intensive industries, and potential power-to-heat provision. Finally, Table 30 summarizes the typical applications of STES.

Table 30: Example of stationary applications of STES systems.

Application	Reference
District heating; thermal load peaks shaving or seasonal thermal storage; District cooling.	(Ease & EERA, 2017)(Sartor & Dewallef, 2018)(Giovanni Manente et al., 2019)(Marguerite, Andresen, & Dahl, 2018)
Single building: low temperature TES (water tanks) for renewable storage or electricity price arbitrage (power to heat)	(Ease & EERA, 2017)(Beausoleil-Morrison, Kemery, Wills, & Meister, 2019)(Louvet et al., 2019)
High temperature STES for on-site generation flexibility (e.g., CHP)	(Ease & EERA, 2017)(W. D. Steinmann, Bauer, Jockenhöfer, & Johnson, 2019)
Industrial processes: increased flexibility and energy efficiency	(Köfinger et al., 2018)
STES with solid medium for heat recovery applications	("Reslag H2020," 2019) (Strasser & Selvam, 2014) (Libby, 2010)(H. Zhang et al., 2016)(Dinker, Agarwal, & Agarwal, 2017)("EnergyNest," 2019) ("Eco-Tech Ceram," 2019)
Seasonal storage for both small communities to districts: Pit TES, Aquifer TES, Borehole STES	(Dahash, Ochs, Janetti, & Streicher, 2019)(Bott et al., 2019)(Nilsson & Rohdin, 2019)(Böhm & Lindorfer, 2019)
Power to heat applications; STES coupled with heat pumps from residential to large district scale	("Dimplex," 2019) (Smallbone, Jülch, Wardle, & Roskilly, 2017) (Marini, Buswell, & Hopfe, 2019)

3.1.3 Characteristics and costs of sensible thermal energy storage

Table 31 reports the key performance metrics of STES around costs and storage efficiency. The following parameters are considered:

- Storage capacity range [m^3];
- Storage capacity range [MWh];
- Typical energy storage density [kWh/m3];
- CAPEX [€/m^3]: Capital costs per unit of volume;
- CAPEX [€/kWh]: Capital costs per unit of thermal energy stored.

Horizon 2020
European Union Funding
for Research & Innovation

This project has received funding from
the European Union's Horizon 2020 research and innovation
programme under grant agreement No 847097

Table 31: Storage capacity, volumetric energy density and CAPEX of the STES systems.

STES technology	Storage volume (m^3)	Storage capacity (MWh)	Energy density (kWh/m^3)	CAPEX		Reference
				(€/m^3)	(€/kWh)	
Water tank TES (water TTES)	300 ÷ 12000	/	35 ÷ 70	117 ÷ 477	1.3	(Bott et al., 2019) (Böhm & Lindorfer, 2019)(Delta Energy & Environment Ltd, 2016)
Water pit TES (water PTES)	800 ÷ 203000	/	60 ÷ 80	24 ÷ 406	0.4 ÷ 1	
Water gravel TES (WGTES)	1050 ÷ 8000	/	/	/	/	
Borehole TES (BTES)	4470 ÷ 15800	/	15 ÷ 30	14 ÷ 93	/	(Böhm & Lindorfer, 2019) (Nilsson & Rohdin, 2019)(Delta Energy & Environment Ltd, 2016)
Medium temperature (liquid) Two tanks	/	100 ÷ 3500	50 ÷ 430	/	13 ÷ 245	(Strasser & Selvam, 2014)(Libby, 2010) (H. Zhang et al., 2016) (Carlson, Davidson, Tran, & Stein, 2019) (Gil et al., 2010)
Medium temperature (liquid) Thermocline with filling solid material	/	100 ÷ 3500	/	/	30.3 ÷ 219	(Strasser & Selvam, 2014)(Libby, 2010)
Medium-high temperature in solids	/	/	58 ÷ 600	/	0.8 ÷ 31.2	(Carlson et al., 2019)(Ahmed, Elfeky, Lu, & Wang, 2019)(Gil et al., 2010)

Horizon 2020 European Union Funding for Research & Innovation

This project has received funding from the European Union's Horizon 2020 research and innovation programme under grant agreement No 847097

3.2 Latent heat thermal energy storage (LHTES)

3.2.1 Technological features

Latent heat thermal energy storage (LHTES) technology exploits the process of melting and solidification (i.e., phase change) of the storage media in order to store heat or cold. The storage media employed in LHTES are commonly referred as phase change material (PCMs) (Zalba, Marín, Cabeza, & Mehling, 2003)(Reddy, Mudgal, & Mallick, 2018)(Farid, Khudhair, Razack, & Al-Hallaj, 2004). During the energy storage process, heat transfer occurs between the PCM and suitable heat transfer fluid (HTF). During the charging process heat is supplied by the HTF to the PCM, causing the latter to melt; thermal energy is therefore stored in the form of latent heat of fusion. Conversely, during the discharge process heat is transferred from the PCM to the HTF. This causes the PCM to solidify, thus releasing the corresponding latent heat of fusion. The energy released by the PCM is then carried by the HTF and made available to the end-user (e.g., batch industrial process, building, heat network, etc.). Figure 80 and Figure 81 summarize the fundamental working principle of LHTES; T_m is the PCM melting temperature, $T_{HTF,C}$ is the HTF temperature during charging process and $T_{HTF,D}$ the HTF temperature during the discharge process. Finally, ΔT is the temperature difference which drives the heat transfer process between the PCM and the HTF. ΔT for charging can differ from the one for discharging depending on the specific requirements of the industrial process in which LHTES system is integrated.

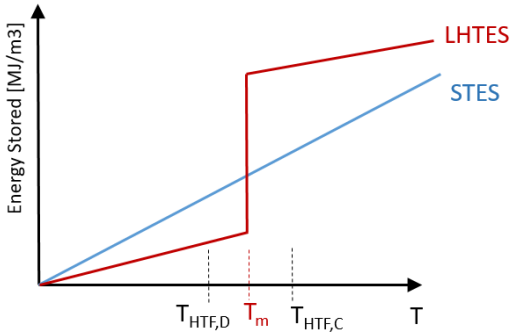

Figure 80: Thermal energy stored versus temperature increase: difference between latent TES (LHTES, red line) and sensible TES (STES, blue line).

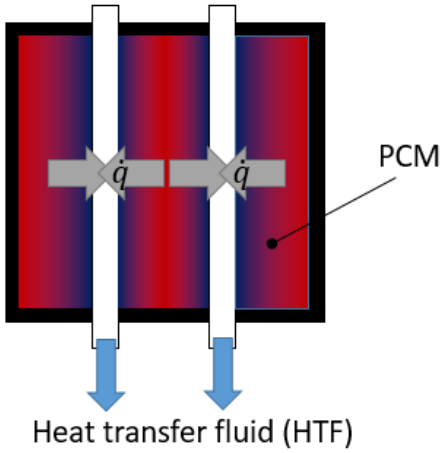

Figure 81: Heat transferred from the phase change material (PCM) to the heat transfer fluid (HTF) during the discharging process.

Horizon 2020
European Union Funding
for Research & Innovation

This project has received funding from
the European Union's Horizon 2020 research and innovation
programme under grant agreement No 847097

In LHTES technology most of the energy is stored around T_m, i.e. the melting point of the PCM, and in the form of latent heat. PCM selection it is therefore crucial since it largely dictates the operating temperature of the LHTES system and the energy stored per unity of volume (or mass), that is the energy storage density (R. K. Sharma, Ganesan, Tyagi, Metselaar, & Sandaran, 2015)(Abhat, 1983). In the context of WH/C, storage of waste heat streams requires therefore to match PCM melting temperature with the temperature at which the streams are available.

Table 32 and Table 33 present the most common classes of PCMs, for the low and the medium/high temperature range. Broadly speaking, low temperature range PCMs are mostly constituted by organic materials such as paraffins and fatty acids. Commercial products are available in this category ("Rubitherm," 2019)("PCM Products Ltd," 2019). Molten salts populate the class of medium/high temperature PCMs and they are available typically from the same supply chain for CSP plants, where they are used as HTF (B. Xu, Li, & Chan, 2015)(Gil et al., 2010). Molten salts can be used as PCM both in pure form or as in the form of mixtures, typically as in eutectic compositions. This allows to formulate PCMs with a target melting temperature, thus with the benefit of being more suitable for applications where there are sources of WH at available at specific temperatures. Finally, metallic materials are currently explored as high temperature PCMs. However, their commercial application remains prohibitive due to technological challenges such as corrosiveness, rapid oxidation and safety issues (Kenisarin, 2010)(Wei et al., 2018)(Alva, Lin, & Fang, 2018).

Table 32: Latent heat, melting temperature and energy density of the selected materials for low temperature latent TES.

Low temperature phase change materials						
Category	**Latent heat (kJ/kg)**	**Melting temperature (°C)**	**Energy density (MJ/m³)**	**Examples**	**Chemical formula**	**References**
Salt hydrates	113 ÷ 266	28 ÷ 117	200 ÷ 385	Calcium chloride hexahydrate	$CaCl_2 \cdot 6H_2O$	(C. Pan et al., 2018) (Farid et al., 2004) (Pereira da Cunha & Eames, 2016)
				Sodium acetate trihydrate (SAT)	$CH_3COONa \cdot 3H_2O$	(Y. Wang, Yu, & Ling, 2019) (T. X. Li, Xu, Wu, He, & Wang, 2019) (IRENA, 2013)
Paraffins	152 ÷ 259	-9.5 ÷ 80	115 ÷ 230	n-Dodecane	$C_{12}H_{26}$	(G. Li, Hwang, Radermacher, & Chun, 2013) (Y. Song et al., 2019)
				Rubitherm RT82	mixture	(Merlin, Soto, Delaunay, & Traonvouez, 2016) ("Rubitherm," 2019)
Fatty Acids	171 ÷ 220	23 ÷ 64	150 ÷ 220	Lauric acid	$C_{12}H_{24}O_2$	(Reddy et al., 2018) (R. K. Sharma et al., 2015) (Pereira da Cunha & Eames, 2016)
				Myristic acid	$C_{14}H_{28}O_2$	
Alcohols	240 ÷ 340	80 ÷ 167	280 ÷ 500	Erythritol	$C_4H_{10}O_4$	(S. Guo et al., 2018) (Crespo, Barreneche, Ibarra, & Platzer, 2019)(IRENA, 2013)

Horizon 2020 European Union Funding for Research & Innovation

This project has received funding from the European Union's Horizon 2020 research and innovation programme under grant agreement No 847097

Table 33: Latent heat, melting temperature and energy density of the selected materials for medium-to-high temperature latent TES.

Medium/high temperature phase change materials						
Category	**Latent heat (kJ/kg)**	**Melting temperature (°C)**	**Energy density (MJ/m3)**	**Examples**	**Chemical formula**	**References**
Molten salts	140 ÷ 270	270 ÷ 850	185 ÷ 700	Sodium nitrate	$NaNO_3$	(Seitz, Johnson, & Hübner, 2017) (Laing, Bauer, Breidenbach, Hachmann, & Johnson, 2013) (Bellan et al., 2015)
				Potassium nitrate	KNO_3	(M. Wu, Xu, & He, 2014) (Y. Lin, Alva, & Fang, 2018)
				Sodium carbonate	Na_2CO_3	(Reddy et al., 2018) (B. Xu et al., 2015)
Molten salt mixtures	160 ÷ 460	150 ÷ 480	360 ÷ 900	Sodium and potassium nitrates	$NaNO_3/KNO_3$	(Bayón, Rojas, Valenzuela, Zarza, & León, 2010) (P. Zhang, Ma, & Xiao, 2016) (C. Guo & Zhang, 2008)
				Sodium carbonate/ lithium carbonate	Na_2CO_3/Li_2CO_3	(C. Li, Li, & Ding, 2019b)(C. Li, Li, & Ding, 2019a)
				Lithium carbonate/ potassium carbonate	Li_2CO_3/K_2CO_3	(Dadollahi & Mehrpooya, 2017)(B. Xu et al., 2015) (Zhao Ma, Yang, Yuan, Jin, & He, 2017)
Metallics	140 ÷ 560	340 ÷ 800	440 ÷ 1500	Aluminium-silicon	Al-Si (88-12)	(Rea, Oshman, Singh, et al., 2018) (Kotzé, Von Backström, & Erens, 2013) (He, 2001)
				Magnesium-zinc	Mg-Zn (49-51)	(Blanco-Rodríguez, Rodríguez-Aseguinolaza, Risueño, & Tello, 2014)(Blanco-Rodríguez et al., 2015)

Finally, Figure 82 and Figure 83 compare the melting points of low and medium/high temperature PCMs, respectively. It is important to emphasize that the melting point largely affects the specific application of LHTES technology. In particular, it is crucial that PCM melting temperature lies between the hot thermal source and cold thermal sink available in the industrial processes and coupled with the LHTES system. Heat from the hot source should be above the melting point temperature to allow charging of LHTES, while the cold sink should stay below the melting point to allow discharge of the thermal energy previously stored in the LHTES system.

Horizon 2020
European Union Funding
for Research & Innovation

This project has received funding from
the European Union's Horizon 2020 research and innovation
programme under grant agreement No 847097

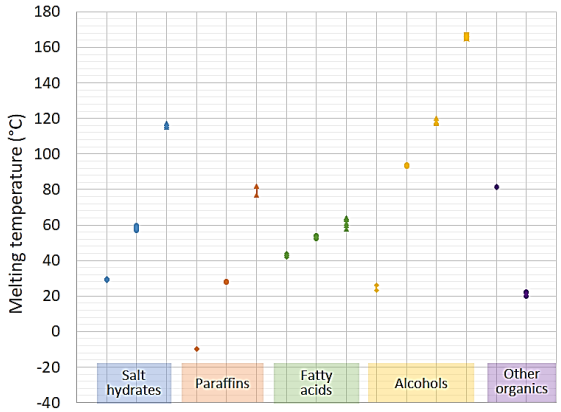

Figure 82: Melting temperatures of the selected low temperature PCMs.

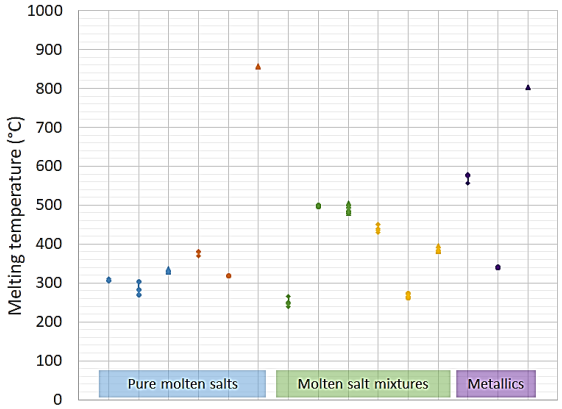

Figure 83: Melting temperature of the selected medium/high temperature PCMs.

3.2.2 Examples of application and technology maturity

The state of development of LHTES technology largely depends on the application temperature range (Ease & EERA, 2017). Low temperature systems, in the range 10÷80°C, have already found niche market applications. Rubitherm, PCM products, Phase energy, Climator, Pluss, Teap, Cristopia are examples of businesses commercializing either PCMs or LHTES units ("Rubitherm," 2019)("PCM Products Ltd," 2019)("Phase energy Ltd," 2019)("Climator," 2019)("PLUSS," 2019)("Teap," 2019)("Cristopia," 2019). Medium-to-high temperature LHTES are, broadly speaking, at the demonstration/pilot stage up to TRL 7, with pilots in the range of 50-700 kWh (Bayón et al., 2010)(Laing et al., 2013). High thermal power LHTES systems are at the research and development stage (Zhao Ma et al., 2017)(Q. He & Zhang, 2001)(Rea, Oshman, Singh, et al., 2018)(X. Wang, Liu, Zhang, Di, & Jiang, 2006). Table 34 lists applications of LHTES; applications developed in the context of WH/C recovery are also reported in the tables. Table 34 focuses on stationary applications of LHTES. In such case LHTES is located on-site (i.e., not mobile) and integrated with the process to which it provides storage functions.

Horizon 2020
European Union Funding
for Research & Innovation

This project has received funding from
the European Union's Horizon 2020 research and innovation
programme under grant agreement No 847097

Table 34: Example of stationary applications of LHTES systems.

Application	Reference
Thermal storage of renewable heat	(Ease & EERA, 2017)
Thermal storage in solar water/air heating systems (space heating, DHW)	(Reddy et al., 2018) (Y. Lin et al., 2018) (R. K. Sharma et al., 2015)
Thermal energy storage integrated in buildings (passive systems)	(Ease & EERA, 2017)(Reddy et al., 2018) (Y. Lin et al., 2018)(R. K. Sharma et al., 2015)
Increasing the flexibility of baseload power plants	(Carlson et al., 2019)
Improvement in dynamics of generation assets (CHP) or heat pumps	(Ease & EERA, 2017) (W. D. Steinmann et al., 2019)(Lizana, Friedrich, Renaldi, & Chacartegui, 2018)
Cold applications, HVAC flexibility and supply of process cold	(C. Pan et al., 2018)(Zeinelabdein, Omer, & Gan, 2018) (G. Li et al., 2013)(Y. Song et al., 2019)(Alva et al., 2018) (S. F. Li, Liu, & Wang, 2019)
Storage in district heating networks	(Colella, Sciacovelli, & Verda, 2012)(Thomson & Claudio, 2019)
Heat recovery from genset (e.g., ICE)	(Miró et al., 2016)
Storage for solar driven steam generation	("EERA TES Technologies," 2018)(Blanco-Rodríguez et al., 2014) (W.-D. Steinmann, Laing, & Tamme, 2010)
Food industry	(Merlin et al., 2016)
Waste heat capture from furnaces	(Miró et al., 2016) (*Smartrec H2020*, 2019) (Nardin, Meneghetti, Dal Magro, & Benedetti, 2014)
Thermal storage in concentrated solar systems	(B. Xu et al., 2015)(Y. Lin et al., 2018) (Crespo et al., 2019)(Gil et al., 2010) (F. Ma & Zhang, 2017)(Rea, Oshman, Olsen, et al., 2018) (Riahi, Jovet, Saman, Belusko, & Bruno, 2019)(Wei et al., 2018)(Hoshi, Mills, Bittar, & Saitoh, 2005) (Kotzé et al., 2013)
Off-peak electricity utilization	(T. X. Li et al., 2019)
Industrial heat recovery	(Y. Lin et al., 2018)(Ji, Qin, Dubey, Choo, & Duan, 2017) (S. Guo et al., 2018)(Nomura, Okinaka, & Akiyama, 2010) (Dal Magro, Savino, Meneghetti, & Nardin, 2017)
Power to heat	(X. Wang et al., 2006)

3.2.3 Mobilized latent heat thermal energy storage

The relative large energy density of LHTES systems compared to sensible TES allows to conceive also mobilized thermal energy storage (M-TES) applications. In this case the TES system allows to thermally connect two processes/industrial sites which are separated in space (from hundreds of meters to kilometers). The M-TES is typically installed on a truck and adequately equipped with inlet-outlet ports to capture/release heat or cold from the sources. These ports allow therefore to charge the M-TES in one location and then discharge it at a different location. Potential PCMs candidates for M-TES applications include sugar alcohols, alkalies and hydrated salts. Similarly, various designs like those including shell-and-tube, macro encapsulation and direct contact HEs have been considered for the mobile container (S. Guo et al., 2018). The potential PCM candidates should show large latent heat of fusion in order to maximize the amount of heat transported. Similarly, the container designs should be as light as possible and compact, as well as provide good heat transfer performance.

Energy storage performance, energy density and overall economic viability are key metrics to successfully apply M-TES technology. The utilization of M-TES requires an adequate analysis of benefits and drawbacks. Recover of heat otherwise wasted, increased efficiency of the processes thermally connected and reduction of primary energy consumption. Such benefits can be particularly relevant in cases where the development of district heating (to connect heat supply with demand) is

Horizon 2020 European Union Funding for Research & Innovation
This project has received funding from the European Union's Horizon 2020 research and innovation programme under grant agreement No 847097

not feasible due to the low heat demand density. On the drawbacks side the operation strategy of M-TES requires particular attention. It is in fact necessary to consider the cost of transportation and the associated emissions, ensuring that application of M-TES leads to an overall reduction of emissions as well as energy efficiency/energy saving for the linked system (heat source, heat sink and M-TES). Table 35 reports M-TES applications with a focus on industrial waste heat.

Table 35: Examples of mobile applications of LHTES systems.

Heat source (supply)	Heat sink (demand)	Reference
Aluminium factory / waste incineration	Industrial drying, air conditioning	(Storch & Hauer, 2006) (Miró et al., 2016)
Steelworks	Chemical plant	(Nomura et al., 2010)(Miró et al., 2016)
CHP plant	DH network	(W. Wang, 2010)(W. Wang et al., 2014)(W. Wang, Hu, Yan, Nyström, & Dahlquist, 2010)(Miró et al., 2016)

Figure 84 illustrates the typical features of a M-TES application based on LHTES (Trans-heat container). The process consists in using PCMs to store industrial WH for its transportation into cities and utilization as heat source for DHW and space heating (IEA-ECES, 2018). The heat was transported for 28 km. Such application is a retrofitting case where M-TES allows, on one side, WH recovery improving industrial process efficiency, and on the other side, a more effective utilization of existing heating systems in buildings. The M-TES illustrated in Figure 85 contained about 15 tons of PCM (erythritol, storage temperature about 120°C). A direct-contact heat transfer container was considered; this was achieved using thermal oil as HTF which is immiscible with the PCM. Such technical solution allowed to achieve rapid charge/discharge rates, which are crucial for M-TES applications.

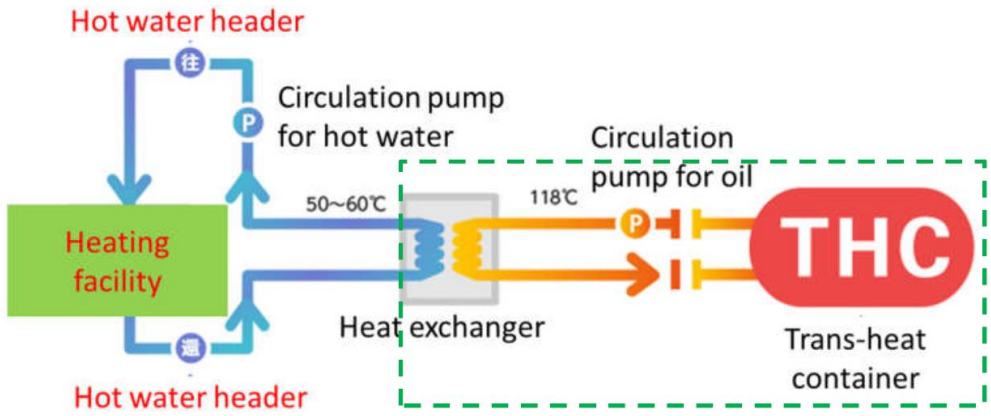

Figure 84: Schematic of M-TES unit (THC) for heating of buildings (IEA-ECES, 2018).

Horizon 2020
European Union Funding
for Research & Innovation

This project has received funding from
the European Union's Horizon 2020 research and innovation
programme under grant agreement No 847097

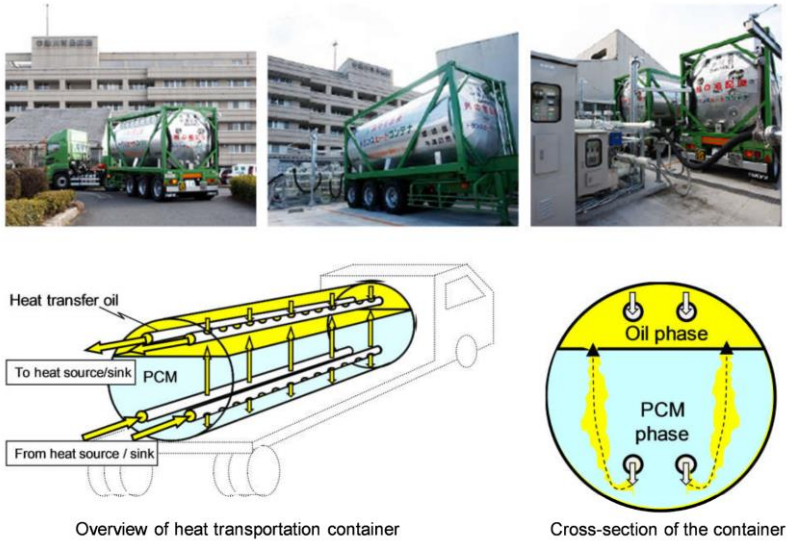

Figure 85: Pictures and schematic of the M-TES unit (IEA-ECES, 2018).

3.2.4 Characteristics and costs of latent thermal energy storage

Table 36 reports the key performance metrics of LHTES around costs and storage efficiency. The following definitions are adopted:

- Storage capacity range [MJ];
- Typical energy storage density [MJ/m^3];
- CAPEX [€/MJ]: Capital costs per unit of thermal energy stored.

Table 36: Storage capacity, energy density and specific investment cost of the LTES systems.

Technology	Storage capacity (MJ)	Energy storage density (MJ/m^3)	CAPEX (€/MJ)	Reference
Low temperature LTES	22 ÷ 53000	200 ÷ 500	4.6 ÷ 72.2	(S. Guo et al., 2018)(S. Guo et al., 2017)(Ahmed et al., 2019)(Merlin et al., 2016)
Medium/high temperature LTES with molten salts	2500 ÷ > 1 million	155 ÷ 750	4.9 ÷ 22.2	(Seitz et al., 2017)(M. Liu et al., 2016)(B. Xu et al., 2015)

Horizon 2020
European Union Funding
for Research & Innovation

This project has received funding from
the European Union's Horizon 2020 research and innovation
programme under grant agreement No 847097

3.3 Thermochemical energy storage (TCES)

3.3.1 Technological features

Thermochemical energy storage (TCES) takes advantage of reversible chemical reactions to store and release heat. This principle is illustrated by the reversible general reaction reported in Equation 1. Reactions suitable for TCES typically involve two main chemical components A and B, which under suitable conditions can exist in either compounded form AB or in dissociated form A+B. During the charging process thermal energy is used to dissociate the compound AB into A+B, which are then kept separate. Conversely, during the discharge process A+B are recombined to form AB. Such process releases the corresponding heat of reaction ΔH_R. Thus, the previously stored energy is recovered.

$$AB + \Delta H_R \leftrightarrow A + B \qquad 1$$

In comparison with sensible and latent TES, the use of reversible reactions has the theoretical advantage of higher energy storage density and loss-free storage (Yan, Wang, Li, Wang, & Fred, 2015) (Pardo et al., 2014). This because heat is stored in chemical form, rather than in the physical way.
Reactions suitable for TCES fall into two main categories: sorption reactions and gas-solid reactions (Z. H. Pan & Zhao, 2017). Table 37 summarizes some candidate reactions that have been considered in TCES pilot systems and in the few commercial installations built until now. The sorption systems exploit the heat associated to absorption process (e.g., NaOH into water) or adsorption process (water vapour onto zeolites, or salt hydrates). In general sorption TCES systems are suitable for low-to-medium temperatures, up to about 200°C and thus have been considered and demonstrated in pilot systems targeting TES for buildings ("MERITS FP7," 2015)("E-Hub FP7," 2013)(Hauer, 1997) or low temperature WH (Krönauer, Lävemann, Brückner, & Hauer, 2015). Conversely, high temperature TCES necessitate gas-solid reactions, such as oxidation reactions (X. Chen, Zhang, Qi, Ling, & Peng, 2018).

Table 37: Materials, energy density and reactions for TCES.

Category	Temperature range	Energy density (MJ/m3)	Examples of materials	Example of reactions	References
Low temperature	50 ÷ 200°C	150 ÷ 2800	Zeolites Salt hydrates NaOH	$Na_2S{\cdot}5H_2O+\Delta H_r \leftrightarrow Na_2S{\cdot}0.5H_2O+4.5H_2O$ $SrBr_2{\cdot}6H_2O+\Delta H_r \leftrightarrow SrBr_2{\cdot}1H_2O+5H_2O$ $MgCl_2{\cdot}6H_2O+\Delta H_r \leftrightarrow MgCl_2{\cdot}2H_2O+4H_2O$	(N. Yu, Wang, & Wang, 2013) (Scapino, Zondag, Van Bael, Diriken, & Rindt, 2017) (Krese, Koželj, Butala, & Stritih, 2018) (IEA, Task 32, 2007) (Lefebvre & Tezel, 2017)
Medium/high temperature	200 ÷ 1200°C	600 ÷ 7000	Calcium hydroxide Calcium carbonate Magnesium hydride Cobalt oxide	$Ca(OH)_2+\Delta H_r \leftrightarrow CaO+H_2O$ $CaCO_3+\Delta H_r \leftrightarrow CaO+CO_2$ $MgH_2+\Delta H_r \leftrightarrow Mg+H_2$ $2Co_3O_4+\Delta H_r \leftrightarrow 6CoO+O_2$	(X. Chen et al., 2018) (Z. H. Pan & Zhao, 2017) (Manickam et al., 2019) (S. Wu, Zhou, Doroodchi, Nellore, & Moghtaderi, 2018)(Wong, DOE, 2011)

Horizon 2020 European Union Funding for Research & Innovation
This project has received funding from the European Union's Horizon 2020 research and innovation programme under grant agreement No 847097

3.3.2 Example of applications and technology maturity

Thermochemical energy storage is the least developed TES technology and it currently remains object of research activities. A key barrier for TCES are the high costs (X. Chen et al., 2018)(Pardo et al., 2014). Sorption systems are at a more advanced stage, and recent H2020 projects currently focus on pilot demonstration in relevant environment. For example H2020 CREATE has been focusing on the implementation of sorption based storage for buildings ("CREATE H2020," 2020). Similarly, FP7 COMTES project developed solid sorption as well as liquid sorption systems for seasonal thermal energy storage in buildings with renewable heat supply ("Comtes FP7," 2016). The systems developed in such projects are in the range of 660 kWh ÷ 1 MWh, supply heat at <75°C and reach TRL values of 5÷7 at the completion of the projects. TCES have also the capability to provide waste heat upgrade, for example by resorption processes. For such reason hybrid systems (storage+upgrade) have been studied and demonstrated at lab scale (Jiang et al., 2017)(Esaki, Yasuda, & Kobayashi, 2017).
As for the medium/high temperature TCES, SaltX is a Swedish company that has developed near to market medium/high temperature TCES units based on calcium hydroxide. The SaltX system can deliver heat up to 400°C. A pilot system of about 10 MWh scale is currently operational in Berlin which is charged with electricity from the grid and discharges high-quality heat into the Berlin district heating network ("SaltX," 2019). High temperature TCES systems using oxides or high temperature reactions have reached TRL 4÷6 and mostly developed for application in CSP plant. A promising option is Calcium Looping (CaL) due to its relative low costs. For example, H2020 SOCRATCES project ("SOCRATCES H2020," 2020) aims to demonstrate the feasibility of a CaL pilot system using low price limestone as well as mature components, such as fluidized bed reactor, to abate costs. Therefore CaL appears an attractive option also for integration into energy-intensive industries for WH recovery and energy efficiency. Finally, one of the key technologies demonstrated in the H2020 SCORES project ("SCORES H2020," 2020) is a power-to-heat concept based on the reactions of metals. In the chemical looping combustion "heat battery" the metal core is oxidized using air and the heat generated is used for supplying DHW and space heating. After the reaction, the core is regenerated by supplying hydrogen produced by renewable electricity ("SCORES PROJECT - 'Self Consumption Of Renewable Energy by hybrid Storage systems,'" 2019). The developed heat batteries have the potential to store heat with a very high storage density (~6 GJ/m^3 on material level) at very competitive cost (<20 €/MJ storage capacity) (*SCORES - D 2.3 Market analysis on hybrid storage components*, 2019).
Table 38 summarizes the envisioned applications for TCES.

Table 38: Examples of applications of TCES systems.

Application	Reference
Concentrated solar thermal / high temperature heat	("SOCRATCES H2020," 2020) (Bayon et al., 2018) (Ortiz, Valverde, Chacartegui, Perez-Maqueda, & Giménez, 2019) ("RESTRUCTURE FP7," 2016)
Seasonal storage in buildings	("CREATE H2020," 2020)("Comtes FP7," 2016)("MERITS FP7," 2015)(De Jong, Van Vliet, Hoegaerts, Roelands, & Cuypers, 2016)("E-Hub FP7," 2013) (Zondag, Kikkert, Smeding, Boer, & Bakker, 2013)(Krese et al., 2018) (Hui, Edem, Nolwenn, & Luo, 2011)(Zhiwei Ma, Bao, & Roskilly, 2019)
Flexibility of CHP plants	("SaltX," 2019)(Fopah Lele, Kuznik, Opel, & Ruck, 2015) (Angerer, Djukow, Riedl, Gleis, & Spliethoff, 2018)(Wuerth, Becker, Ostermeier, Gleis, & Spliethoff, 2019)
Low grade industrial process heat (storage and upgrade)	(Jiang et al., 2017)(Esaki et al., 2017) (Chan, Ling-Chin, & Roskilly, 2013) (Krönauer et al., 2015)(Spoelstra, Haije, & Dijkstra, 2002) (Miró et al., 2016)(Scapino et al., 2017)

Horizon 2020 European Union Funding for Research & Innovation
This project has received funding from the European Union's Horizon 2020 research and innovation programme under grant agreement No 847097

Storage in DHN	(Böhm & Lindorfer, 2019)(Hauer, 2002) (Krese et al., 2018)
Thermal management (e.g., vehicles)	(Narayanan et al., 2015)(Narayanan et al., 2017)
Power-to-heat	(Angerer, Becker, et al., 2018)(Fernández, Ortiz, Chacartegui, Valverde, & Becerra, 2019)("SaltX," 2019)("SCORES H2020," 2020)
High grade industrial waste heat	(Bogdanović, Ritter, Spliethoff, & Straßburger, 1995a)(Miró et al., 2016) (Ding, Wang, Gu, Wang, & Lu, 2019)

3.3.3 Mobilized thermochemical energy storage

TCES technology has the highest theoretical energy storage density among the available TES options (Sensible, Latent, Thermochemical). It is possible to achieve energy storage density 3 to 10 times higher than sensible storage (Yan et al., 2015)(N. Yu et al., 2013)(Van Essen et al., 2009). This makes TCES particularly attractive for M-TES applications. In such instance, the storage volume corresponds to the volume of a trailer or shipping container which can be transported within a limited distance by a heavy truck. Maximizing the stored energy is therefore crucial to ensure the economic feasibility of M-TES as well as to displace any possible emission due to the transportation. Table 39 summarizes the M-TES applications for TCES technology. Such applications focus on WHR and valorisation between two industrial sites. Figure 86 illustrates the M-TES demonstrator developed by ZAE Bayern (Krönauer et al., 2015). The system uses zeolite material to store heat by solid sorption process. Steam from a waste incinerator was used to charge the M-TES system. The system was discharged at an industrial drying process 7 km far away to provide heat at about 130°C. Figure 87 illustrates in more detail the charging and discharging processes. It is important to notice that in order to take place the thermochemical reaction necessitates specific conditions for the inlet stream of air. During charging dry air is necessary at the inlet in order to ensure that desorption of zeolite could take place. Conversely, in order to discharge the M-TES, humid air is required at the inlet to activate the adsorption reaction of the zeolite. This demonstrates that, differently from latent M-TES systems, careful analysis about reaction conditions, in particular equilibrium temperature, pressure and concentrations are necessary in order to identify suitable operating conditions.

Table 39: Examples of mobile applications of TCES systems.

Heat source (supply)	Heat sink (demand)	Reference
Steelworks	Utility plant	(Miró et al., 2016) (Hauer et al., 2010)
Incineration	Industrial drying	(Storch & Hauer, 2006)(Krönauer et al., 2015)(S. Guo et al., 2018)
CHP plant	DH network	(W. Wang, 2010)(W. Wang et al., 2014)(W. Wang et al., 2010)(Miró et al., 2016)

Horizon 2020
European Union Funding
for Research & Innovation

This project has received funding from
the European Union's Horizon 2020 research and innovation
programme under grant agreement No 847097

Figure 86: M-TES prototype tested by ZAE research centre (Krönauer et al., 2015).

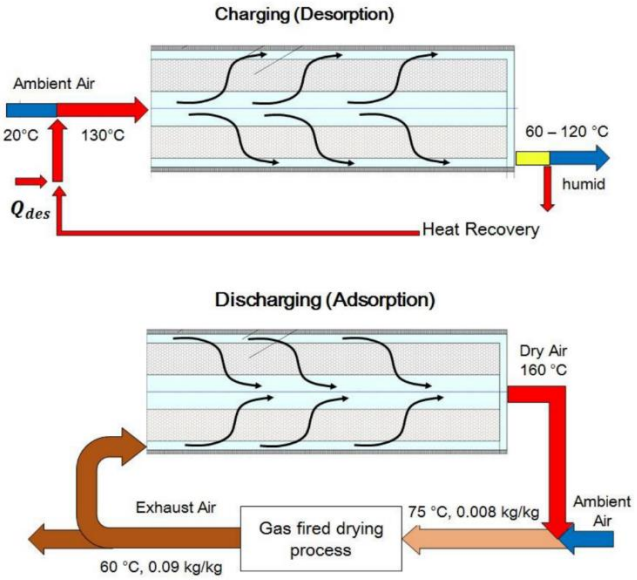

Figure 87: Schematics of the charging (above) and discharging (below) processes for the mobilized TCES developed by ZAE (Krönauer et al., 2015).

3.3.4 Characteristics and costs of thermochemical energy storage

Table 40 reports the key performance metrics of TCES around costs and storage efficiency. The following metrics were adopted:

- Storage capacity range [MJ];
- Typical energy storage density [MJ/m^3];
- CAPEX [€/MJ]: Capital costs per unit of thermal energy stored.

Table 40: Storage capacity, energy storage density and specific investment cost of TCES systems.

Stationary thermochemical energy storage				
Technology	**Storage capacity (MJ)**	**Energy storage density (MJ/m^3)**	**CAPEX (€/MJ)**	**Reference**
Low temperature TCES (zeolites, salt hydrates)	500 ÷ 5000	120 ÷ 1000	5 ÷ 11.9	(Michel, Neveu, & Mazet, 2014)(Zondag et al., 2013)(IEA Task 32, 2007)(Scapino et al., 2017)(De Jong et al., 2016)(Hauer, 1997)

Horizon 2020
European Union Funding
for Research & Innovation

This project has received funding from
the European Union's Horizon 2020 research and innovation
programme under grant agreement No 847097

Medium/High temperature TCES	36000 ÷ few millions	340 ÷ 1860	3 ÷ 38	(Schaube, Wörner, & Tamme, 2011)(Alovisio, Chacartegui, Ortiz, Valverde, & Verda, 2017)(Bogdanović, Ritter, Spliethoff, & Straßburger, 1995b)("SaltX," 2019)(Corgnale et al., 2014)(DOE, 2011)
Mobile Applications				
Low temperature TCES (zeolites)	8400	210 ÷ 440	10.8	(Krönauer et al., 2015)(Scapino et al., 2017)

3.4 Summary – Thermal energy storage technologies

The thermal energy storage (TES) technological class contains three sub categories: sensible TES, latent heat TES and thermochemical energy storage. Overall, development and increase in TES applications has been found across the whole TES technology class. This was found mainly due to the inherent nature of the technology class itself. TES finds application as a passive WHR technology, but more importantly and attractively, also as an enabling technology which facilitates the use of other WHR options which would not be possible without the thermal storage function. These include heat upgrade (e.g., heat pumps), heat conversion (e.g., power cycles) and heat-electricity sector coupling. Table 41 summarizes the benefits and drawbacks of TES technologies.

STES. Sensible TES is a fully commercial technology for low temperatures (<100°C); in this regard hot water tanks have been used extensively across industries to mitigate fluctuations in heat demand/supply and/or to capture intermittent WH released from batch processes. High temperature sensible TES is commonly used in the solar thermal industry (e.g., CSP plants), taking advantage of suitable liquids such as diathermic oils or molten salts. However, applications of high temperature sensible TES remain limited in the field of industrial WHR. Transfer of knowledge, expertise and skills from solar thermal industry can therefore accelerate the update of WHR applications. Near-to-market sensible TES systems based on solid storage medium (e.g. rocks, ceramics) are also emerging.

LHTES. Latent heat TES is approaching commercialization with a number of phase change materials already available, particularly in the range of -20°C to 90°C, which make them suitable for low grade WHR applications or for integration with HVAC systems. Regarding high temperature application inorganic PCMs are emerging as well as the use of molten salts as PCMs. The relatively high heat of fusion makes latent heat TES a good candidate also for mobilized thermal energy storage (M-TES) solutions. It was indeed found that M-TES has been demonstrated at pilot scale for transportation and utilization of waste heat up to about 30 km. Overall, costs of latent heat TES are higher than sensible TES and thus cost-benefit analysis is particularly relevant for this technology, which however expands significantly the range of TES applications compared with sensible TES technology.

TCES. Thermochemical energy storage is presently at development stage with some relevant pilot testing. This technology exploits reversible reactions to store heat in the form of chemical energy. Multiple candidate reactions have been identified and tested at laboratory scale. Presently, sorption reactions (e.g., zeolites material) and hydration/dehydration reaction (e.g., salt hydrates material) have reached the pilot stage and they have been under trial in multiple EU projects. The high energy density and the ability of storing energy indefinitely (without losses) make this class particularly attractive for long duration storage as well as mobilized thermal energy storage applications, with the latter being already trialled on the field using zeolite materials.

Horizon 2020 European Union Funding for Research & Innovation
This project has received funding from the European Union's Horizon 2020 research and innovation programme under grant agreement No 847097

Table 41: Summary of thermal energy storage technologies.

Thermal energy storage technologies		
Technology	**Benefits**	**Disadvantages**
Sensible	Well proven technology; Used at scale for T < 100°C (water tanks) and T ≈ 300 ÷ 500°C (molten salt tanks); Near to market solid media systems (rocks, concrete).	Possible low energy storage density and self-discharge (heat losses).
Latent	Higher energy storage density; Wide range of storage temperature (included cold thermal storage); It can provide energy flexibility opportunities (e.g., peak/off peak).	Storage materials (PCMs) commercially available mostly in the range -20 ÷ 120°C; Require specialists for fully engineered system; Higher costs that sensible storage.
Thermochemical	Highest energy storage density; No thermal losses with possibility of long duration storage of heat; Suitable and demonstrated for mobile applications.	Currently at pilot scale with limited number of suppliers; Possible high system complexity; Development and demonstration needed to abate costs and establish long term performance.

Horizon 2020
European Union Funding
for Research & Innovation

This project has received funding from
the European Union's Horizon 2020 research and innovation
programme under grant agreement No 847097

4 Waste heat to cold (WHC) technologies

This section aims to present the cold production equipment from waste heat, thus achieving its recovery and valorisation. The operating principles are also described.

4.1 Sorption chillers

4.1.1 Technological features and performance

A technological review of the methods for the production of cold from heat flows which might come from WH was carried out in (Florides, Tassou, Kalogirou, & Wrobel, 2002). The methods were clustered into three main categories: sorbent systems (absorption and adsorption), mechanical systems and specific systems. The focus of this Section is on sorbent cooling systems. Sorbents are materials that have the ability to attract and hold other gases or liquids. Sorption chillers can be defined as those equipment that through a sorption process (gas-on-liquid absorption or gas-on-solid adsorption) are able to establish two levels of pressure through which the refrigerant can condense and evaporate and therefore produce the required cooling effect. Absorption cooling based on the gas-on-liquid absorption is widely used for cold production.

The applications of the sorption chillers are fundamentally two: refrigeration and air conditioning. In the first case, the operating temperatures must be close to or below zero degrees Celsius. However, for air conditioning it is sufficient to operate in the environment of 10°C. Note that the operating temperatures in the cycle (evaporator, condenser and generator) will condition the power and performance of the equipment. Figure 88 presents the cycle schematic and hardware schematic of a water/lithium bromide absorption chiller, which is the most widespread technology for air conditioning applications. The absorption chiller uses WH at low/medium temperatures, typically in the range 65÷200°C, at the desorber (Q_d) and produces the cooling effect (Q_e) in the evaporator. The low grade heat streams released in the condenser (Q_c) and absorber (Q_a) are commonly rejected to the environment.

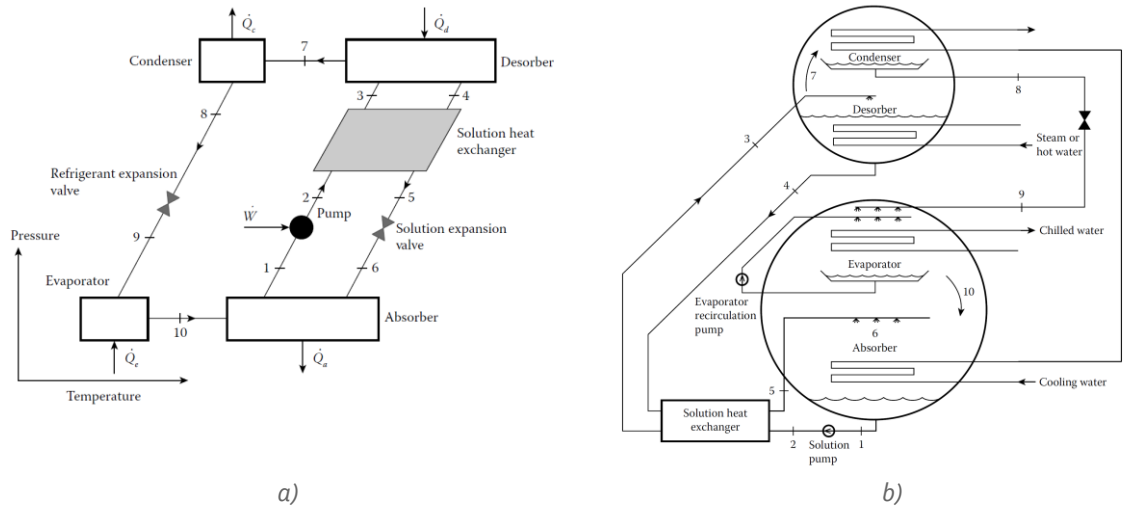

a) b)

Figure 88: Single-effect water/lithium bromide absorption chiller: a) Cycle schematic; b) Hardware schematic (Herold, Radermacher, & Klein, 2016).

Horizon 2020 European Union Funding for Research & Innovation
This project has received funding from the European Union's Horizon 2020 research and innovation programme under grant agreement No 847097

The implementation of the first absorption machine was carried out by Ferdinand Carré (1857) with its presentation at the universal exhibition in London which caused great expectation since the production of cold from heat was firstly considered. Recently, Altarmirano et al. (Altamirano, Pierrès, & Stutz, 2019) have done a review of the absorption technologies. For air conditioning applications with cold water use, the technology that provides better performance is that using the lithium bromide – water working pair, which allows to obtain cooling temperatures around 10ºC with relatively low generator (i.e., desorber) temperatures. However, this technology requires the use of cooling towers to condense. The utilization of lithium bromide together with the use of water as a refrigerant, makes this type of facilities (Figure 89) to have a low environmental impact index.

Figure 89: Absorption chiller (model Yazaki WFC10) ("Cartif," 2020).

Table 42 shows a selection of commercial technologies available using lithium bromide - water absorption cooling with the range of generator temperatures and performance (COP). Seven representative systems have been considered in (U.S. Department of Energy, 2017a) where systems 1 to 3 correspond to single-stage machines and systems 4 to 7 are double-stage systems.

Table 42: Summary of absorption chiller architectures and performance using LiBr-water (U.S. Department of Energy, 2017a).

	System						
Description	**1**	**2**	**3**	**4**	**5**	**6**	**7**
Design	Single stage			Two Stage			
Heat Source	Hot Water		Steam (low pressure)	Steam (high pressure)		Exhaust Fired	
Cooling power nominal (kW)	175	1540	4620	1155	4620	1155	3520
Waste Heat in							
Hot water inlet (ºC)	88	98	100	/	/	/	/
Hot water outlet (ºC)	82	88	90	/	/	/	/
Steam pressure (bar)(T_{sat}ºC)	/	/	2 (120ºC)	9 (175ºC)	9 (175ºC)	/	/
Exhaust gas T (ºC)	/	/	/	/	/	275	450
Heat Required (Waste Heat) (kW)	250	2081	5848	813	3254	856	2550
Chilled Water							

Horizon 2020
European Union Funding
for Research & Innovation

This project has received funding from
the European Union's Horizon 2020 research and innovation
programme under grant agreement No 847097

Inlet T (ºC)	12						
Outlet T (ºC)	6						
Cooling COP	0.70	0.74	0.79	1.42	1.42	1.35	1.38

The COP parameter is calculated as the ratio between the cold energy produced and the thermal energy introduced into the chiller from the waste heat sources. Single effect chillers require lower activation temperatures than double and triple effect chillers. However, double and triple effect chillers have higher values of performance (i.e., higher COP). Additionally some double effect chillers can be used in a dual way. When there is available hot water with waste heat origin (or solar thermal), the machines work as single effect chillers with lower performance but free cost in terms of fuel supply. When the hot water is not available, the machine is equipped with a natural gas direct fired burner that activates the second effect. Therefore, the machines operate with higher performance but with higher economic cost due to the natural gas consumption. Furthermore, there is a development that takes advantage of the crystallization of lithium chloride for the production of cold developed by the Swedish company Climatewell.

However, if air-condensation is required and therefore at higher temperatures or it is applied to the production of refrigeration with uses that have temperatures below 0ºC, other technologies, usually based on ammonia (ammonia-water or lithium-nitrate ammonia) must be used (Table 43). Some advances made in these technologies allow improving performance using GAX and Branched-GAX cycles.

Table 43: Summary of working pairs for absorption chillers.

Working pair	Reference
Lithium bromide - water (LiBr-H_2O)	(Herold et al., 2016) (Chahartaghi, Golmohammadi, & Shojaei, 2019) (F. Sun et al., 2020) (Z. Liu, Xie, & Yang, 2020)(Shiue, Hu, & Chiang, 2018)
Lithium chloride - water (LiCl-H_2O)	(Oberweis & Al-Shemmeri, 2012)(Bellos, Tzivanidis, Pavlovic, & Stefanovic, 2017) (Konwar & Gogoi, 2018)(Konwar, Gogoi, & Das, 2019)
Ammonia - water (NH_3-H_2O)	(Cervantes, Sauceda, Velázquez, Lara, & Pando, 2016)(Le Lostec, Galanis, & Millette, 2012)(Jakob, Spiegel, Pink, Manager, & Gmbh, 2008)(Garimella, Ponkala, Goyal, & Staedter, 2019) (Boudéhenn et al., 2016)(Matjanov, 2020)
Lithium nitrate - ammonia ($LiNO_3$-NH_3)	(Jiménez-García & Rivera, 2018)(Ventas, Lecuona, Zacarías, & Venegas, 2010)(Llamas et al., 2007) (Zamora, Bourouis, Coronas, & Vallès, 2015)(Ventas, Lecuona, Vereda, & Rodriguez-Hidalgo, 2017)

4.1.2 Technology readiness level and examples of applications

Absorption chillers have traditionally been linked to their use with solar energy, although references on WH driven systems can be found in the scientific literature. Three technologies have been classically developed: NH_3-H_2O, NH_3-$LiNO_3$ and H_2O-LiBr. References of the three of them are shown in Table 44 and are briefly summarized in the following.

Table 44: In-lab developed prototypes.

TRL	Working pair	Driving heat source		Cooling		$Q_{cooling}$	COP	Reference
		Application	Tin (°C)	Application	Tout (°C)	(kW)		
7	NH_3-H_2O	Geothermal	125	Heating and cooling	-10	10.5	0.4	(Ayala Delgado, 1992)

Horizon 2020 European Union Funding for Research & Innovation
This project has received funding from the European Union's Horizon 2020 research and innovation programme under grant agreement No 847097

7	NH_3-H_2O	Exhaust gases	180	Heating and cooling	0	7	0.255	(Koehler, Tegethoff, Westphalen, & Sonnekalb, 1997)
7	NH_3-H_2O	Combustion module	180	Heating and cooling	9.5	3.5	0.53	(Garimella et al., 2016)
7	NH_3-H_2O	Combustion module	183	Heating and cooling	7.9	7	0.51	(Staedter & Garimella, 2018)
7	NH_3-H_2O	Waste heat from Diesel generator	398.9	Heating and cooling	19.8	1.91 ÷ 2.71	0.55	(Goyal, Staedter, Hoysall, Ponkala, & Garimella, 2017)
7	NH_3-$LiNO_3$	Electric heater	90	Heating and cooling	15	9.3	0.6	(Zamora, Bourouis, Coronas, & Vallès, 2014)
7	NH_3-$LiNO_3$	Electric heater	90	Heating and cooling	15	10.16	0.67	Zamora et al., 2014
7	H_2O-LiBr	Electric heater	75	Heating and cooling	15	10.2	0.76	(Kühn et al., 2005) (Kühn, Meyer, & Ziegler, 2008)
7	H_2O-LiBr	Electric heater	90	Heating and cooling	15	50	0.8	(Kühn, 2013)

As for the NH_3-H_2O technology, a prototype was constructed at the Cerro Prieto Geothermal Field (Mexico) to cool a small storage unit at negative temperatures (-10 °C) at generator temperatures of 125 °C from geothermal energy (Ayala Delgado, 1992). Some years later Koehler et al. (Koehler et al., 1997) simulated, constructed, and tested a refrigeration system for food transport using the exhaust gases from a truck. Garimella et al. (Garimella et al., 2016) developed a prototype of 3.5 kW of cooling with a COP of 0.53. After, Staedter and Garimella (Staedter & Garimella, 2018) constructed a 7 kW system based on the same concept that delivered chilled water at 7.2°C with a COP of 0.51. Finally, Goyal et al. (Goyal et al., 2017) constructed a waste-heat-driven and air-cooled chiller designed for a thermal COP of 0.55. The absorption machine provided between 1.91 and 2.54 kW of cooling at ambient temperatures between 29.7°C and 44.2°C. There are some prototypes of NH3-$LiNO_3$ absorption cooling systems, developed in laboratories and their operating conditions are shown in Table 44. At T_{amb} = 41 °C, the air-cooled chiller could still provide 64% of its nominal capacity (obtained at T_{amb} = 35 °C) (Zamora et al., 2014). As for the H2O-LiBr pair, Kühn et al. (Kühn et al., 2008) presented a compact 10 kW chiller for low driving temperature (75°C). At nominal conditions, the system produced chilled water at 15°C with a COP of around 0.76 (Kühn et al., 2005). Later (Kühn, 2013), she developed a compact system with low heat losses with 50 kW, which can get COPs of around 0.8 supplying 44 kW of office cooling driven by district heating and 35 kW of data centre cooling.

There are many examples of application with CHP systems. From airports, hospitals, military facilities, educational centres, hotels, etc. Three examples of application of absorption machines for the use of WH from cogeneration plants are presented in the following.

BMW- Spartanburg. The BMW manufacturing plant in Spartanburg (SC, USA) uses landfill gas, a local opportunity fuel, from Waste Management's Palmetto Landfill. The gas travels through a 15 km long pipeline to the plant. At the BMW facility, two 5.5 MW gas-fired combustion turbines burn this gas to produce 11 MW of electricity, while heat is recovered from the thermal engines and used in the facility as process steam. This system produces 30% of the plant's electrical need and 60% of the plant's thermal needs (Figure 90).

Horizon 2020 European Union Funding for Research & Innovation
This project has received funding from the European Union's Horizon 2020 research and innovation programme under grant agreement No 847097

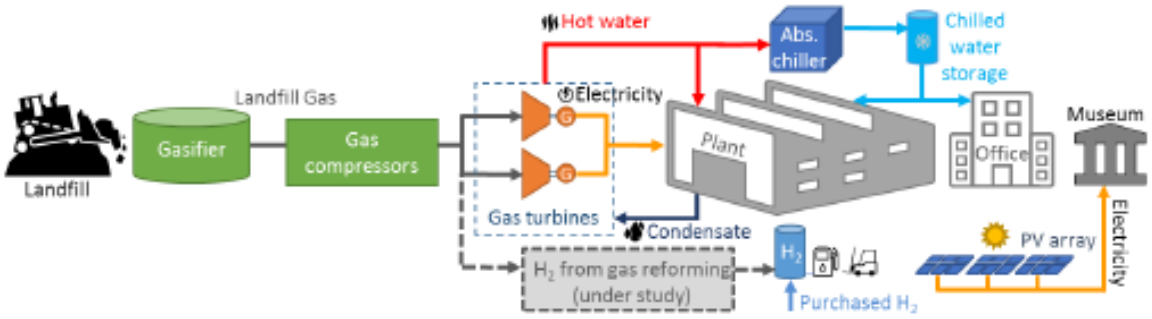

Figure 90: Diagram of the BMW Spartanburg plant in the US (RETD, 2017).

Heat recovered from the turbines is used to produce 275˚C pressurized hot water for a thermal treatment bath process and for refrigeration. Part of the hot water is used by one 3.5 MW and one 2.1 MW absorption chillers to provide refrigeration to the campus facilities. Chilled water thermal storage is also used to help provide the 53 MW peak refrigeration loads, in order to reduce peak electrical load for refrigeration.

F-D-S Manufacturing Company. F-D-S Manufacturing Company is a family-owned, West Coast manufacturer of Industrial and Agricultural Packaging in Pomona (CA, USA). They produce high quality and eco-friendly standard and custom packaging. F-D-S uses extrusion, thermoforming, injection molding and unique paper converting processes to manufacture recyclable polyethylene terephthalate (PET) clamshells and fruit trays and PET rolls. The facility is equipped with a CHP plant formed by 6 micro gas turbines Capstone C65 of 390 kW of electric power each (Figure 91).

Figure 91: Capstone Micro-turbines (U.S. Department of Energy, 2017b).

Prior to the plastic extrusion process, recyclable plastic is dried using diluted air heated by the exhaust from two Capstone micro-turbines connected to two air to air heat exchangers. Exhaust air of the remaining four micro-turbines are connected in parallel and operated in full heat recovery mode to produce 165°C hot water via an air-water heat exchanger. The hot water stream is then pumped to the Thermax absorption chiller (LT10C) to produce 350 kW of chilled water that cools the plastics during the extrusion process.

Simonds International. Simonds International's facility in Fitchburg (MA, USA) was constructed in 1935 and primarily manufactures metal blades for band saws from steel coils. Simonds installed combined heat and power (CHP) in 2011 for a project cost of $6.5 million. The system consists of three 600 kW MWM engines running on natural gas, with emissions reduced using selective catalytic reduction

Horizon 2020
European Union Funding
for Research & Innovation

This project has received funding from
the European Union's Horizon 2020 research and innovation
programme under grant agreement No 847097

(SCR). In addition to the engines, the system also includes switchgear, eight new air handlers units and a 1.4 MW Carrier absorption chiller (Figure 92).

Figure 92: Absorption chiller Carrier and engines MWM in Simonds Plant (U.S. Department of Energy, 2017a).

The recovered heat from the engines is recycled back to the eight air handlers units to maintain the proper temperature in the manufacturing facility. Additionally, the recovered heat is used to raise the closed hot water loop to 90°C. During the summer, the recovered heat is used to power the absorption chiller, providing space cooling.

4.1.3 Cost aspects

It is important to remark that most of the sorption chillers use inorganic natural substances (water, lithium bromide, ammonia, silica gel, etc.) that are environmentally friendly and do not harm the ozone layer. Table 45 reports the key performance metrics of absorption chillers around costs based on Table 42. The first column (i.e, system "0") is based on CARTIF data, and the other columns are based on U.S. Department of Energy. The specific investment cost of the equipment of large units in the MW or multi-MW range is the range 200÷350 € per kW of cooling capacity. Higher equipment costs above 500 €/kW are shown by the smaller units. The installed cost is 2 to 3 times the cost of the bare equipment due to the costs associated with construction and installation.

Table 45: Performance metrics of absorption chillers (LiBr-H_2O) around costs (U.S. Department of Energy, 2017a).

	System							
Description	**0(*)**	**1**	**2**	**3**	**4**	**5**	**6**	**7**
Design	Single stage				Two Stage			
Heat Source	Hot Water			Steam (low pressure)	Steam (high pressure)		Exhaust Fired	
Power nominal (kW)	35	175	1540	4620	1155	4620	1155	3500
Waste Heat Required (kW)	50	250	2081	5848	813	3254	856	2550
Equipment Cost (€/kW)	857	523	242	213	309	260	346	242
Installed cost (€/kW)	1957	1560	598	468	780	572	858	520
O&M Costs (c€ /kWh)	2.1	2.1	0.7	0.4	1.1	0.4	1.1	0.4

(*) CARTIF Data ("Cartif," 2020).

Absorption chiller emissions depend on the heat producer. If the chiller is integrated with CHP facilities, there are no incremental emissions from the absorption chiller. If the absorption chiller is a standalone unit that is direct fired, emissions will depend on the fuel used to produce thermal energy to drive the system and the specific combustion technology used for direct firing. Natural gas, which

Horizon 2020
European Union Funding
for Research & Innovation

This project has received funding from
the European Union's Horizon 2020 research and innovation
programme under grant agreement No 847097

is relatively low cost and clean burning, is a common fuel used for direct firing. For direct firing, absorption chillers can use low NO_x burner technologies and other emission control measures to comply with local air quality requirements as needed.

4.2 Summary – waste heat to cold technologies

The systematic review identified that this class of technologies is largely dominated by sorption refrigeration systems, also commonly called sorption chillers. They take advantage of gas-liquid sorption or gas-solid sorption phenomena to convert heat (e.g., WH stream) into a cooling effect. Sorption chillers are therefore thermally driven systems suitable to meet refrigeration or air conditioning demand where sources of WH are also available. Absorption cooling systems using lithium bromide-water or ammonia-water working pairs are commercially available in different cycle arrangements (e.g., from single stage to triple stage) and thermal COPs in the range 0.7÷1.4, and dominate this class of WH valorisation technologies. Absorption chillers are a commercially available technology that has been primarily used in conjunction with solar energy, although references in using WH as thermal source are available in the literature. Multiple applications of sorption chillers with combined heat and power (CHP) systems have been found in order to deliver heat, electricity and cooling (trigeneration systems).

Horizon 2020
European Union Funding
for Research & Innovation

This project has received funding from
the European Union's Horizon 2020 research and innovation
programme under grant agreement No 847097

5 Waste heat to power technologies

This Section covers a wide range of technologies for power production from waste heat sources. The SRC, ORC, KC, sCO2 and SEs generate power using a direct thermodynamic cycle (Rankine, Kalina, Brayton-Joule or Stirling). The TEG and TPV generators directly generate power from heat and thermal radiation, respectively, using solid state devices. Finally, the cryogenic generators are novel conversion systems that produce power through thermal streams available at cryogenic temperatures. The technological features and performance of each technology are described along with their applications in different industrial contexts.

5.1 Steam Rankine Cycles (SRCs)

5.1.1 Technological features and performance

The most commonly used system for power generation from WH involves using the heat to generate steam in a WHB, which then drives a steam turbine. Steam turbines are a mature and versatile technology, and have been in use for more than 100 years (U.S. Environmental Protection Agency, 2012). In WHR applications, the capacity of steam turbines can range from 50 kW to several hundred MWs. WHB/steam turbine systems operate thermodynamically as a Rankine Cycle. In the SRC, the working fluid — water— is first pumped to elevated pressures before entering a WHB. The pressurized water is vaporized by the hot exhaust and then expanded to lower temperatures and pressures in a turbine, generating mechanical power that can drive an electric generator. The low-pressure steam is then exhausted to a condenser at vacuum conditions, where heat is removed by condensing the vapour back into a liquid. The condensate from the condenser is then returned to the pump and the cycle continues (Figure 93).

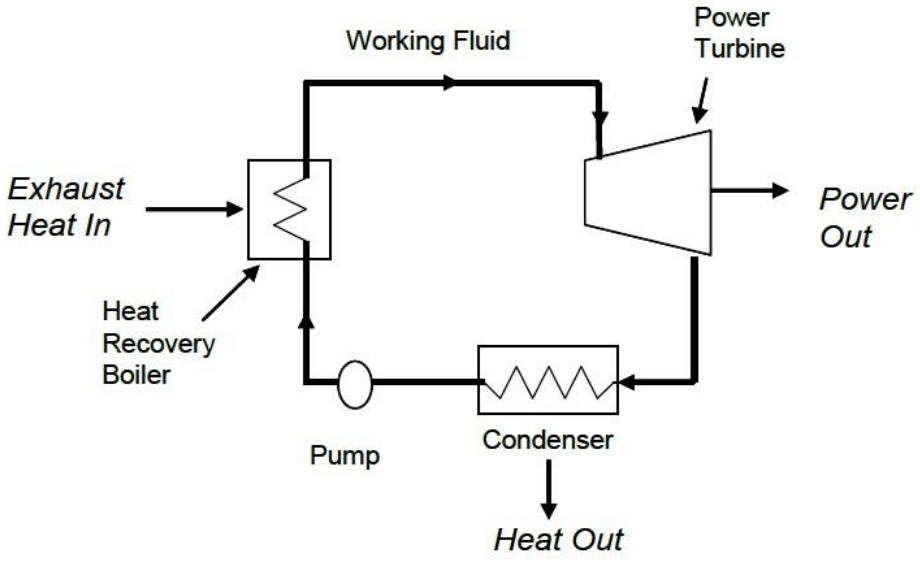

Figure 93: Schematic of a Rankine cycle heat engine (EPRI, 2010).

Horizon 2020
European Union Funding
for Research & Innovation

This project has received funding from
the European Union's Horizon 2020 research and innovation
programme under grant agreement No 847097

The traditional SRC is the most efficient option for WHR from exhaust streams with temperatures above 340÷370°C. At lower WH temperatures, SRCs become less cost effective, since low pressure steam will require bulkier equipment. Moreover, low temperature WH may not provide sufficient energy to superheat the steam, which is a requirement for preventing steam condensation and erosion of the turbine blades. Thus, low temperature heat recovery applications are better suited for the ORC or Kalina cycle, which use fluids with lower boiling point temperatures compared to steam (BCS, 2008).

Generally, two types of SRC systems with different evaporation pressure levels are reported: the single-pressure SRC system (Figure 94 left) and the more efficient dual-pressure SRC system (Figure 94 right) (S. Zhu, Zhang, & Deng, 2019).

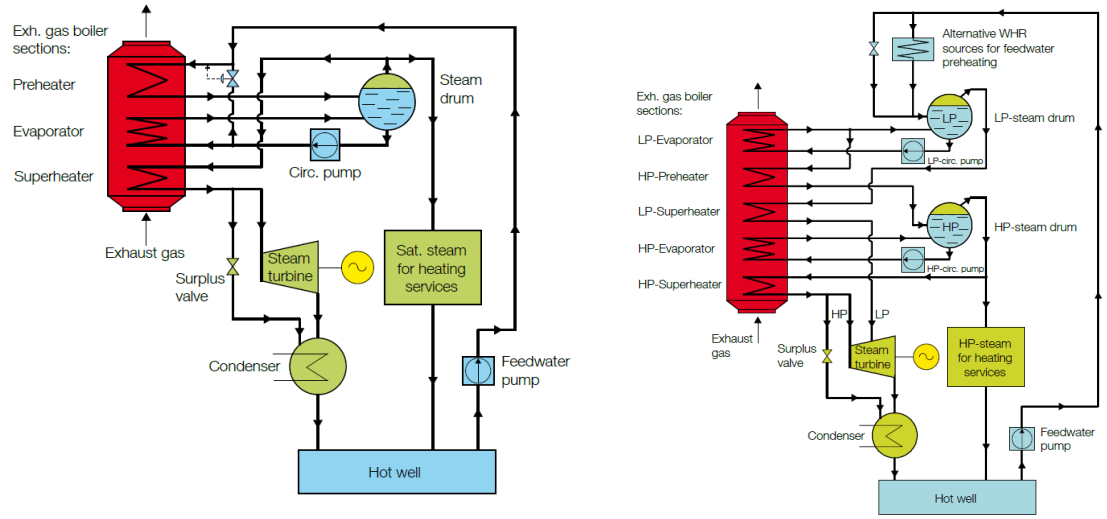

a) *b)*

Figure 94: SRCs for WHR from the exhaust gas: a) single pressure layout; b) dual pressure layout (MAN Diesel & Turbo, 2014).

5.1.2 Examples of applications, technology maturity and cost-performance of SRCs

The SRC is widely adopted as bottoming cycle of gas turbines in natural gas combined cycle power plants (NGCCs). Smaller SRC units are employed for WHR from the exhaust of Diesel engines for stationary or marine applications. In the industrial sector it is used in the cement, steel, chemical and other industries where large flow rates of flue gases at medium/high temperature are available. In the following, a selection of examples of the integration of the SRC for WHR in the industrial sector and EHR in the power sector are reported.

- **Steel, Silicon, chemical and petrochemical industries**

One of the largest examples of industrial WHR using the SRC is a series of seven integrated projects serving Arcelor/Mittal Steel in northwest Indiana (USA). Another large project is for silicon producer West Virginia Alloys where WH from the silicon process produces 40÷44 MW of electrical power, offsetting one-third of the host facility's electricity needs. An additional notable project is Port Arthur Steam Energy LP in Texas (Figure 95). This project captures high temperature flue gas heat from a

Horizon 2020
European Union Funding
for Research & Innovation

This project has received funding from
the European Union's Horizon 2020 research and innovation
programme under grant agreement No 847097

petroleum coke calcining operation to produce high pressure steam that is used to produce 5 MW of electricity (Table 46).

Table 46: Main features of the WHP projects using the SRC ("Heat is Power Association," 2019).

TRL	Industry	Project name	Location	Type heat source	Temperature heat source (°C)	Power output (kW)
9	Steel	North Lake	East Chicago (Indiana, USA)	Flue gases from the combustion of by product fuel from a blast furnace	815	90000
9	Petrochemical	Port Arthur Steam Energy LP (PASE)	Port Arthur (Texas, USA)	Flue gas from petroleum coke calcining kilns	980 ÷ 1090	5000
9	Chemical (Fertilizer Manufacturing)	Simplot	Pocatello (Idaho, USA)	Excess heat from the sulphuric acid plant	≈ 450	15900

Figure 95: WHB/steam turbine WHP project at a petroleum coke plant in Port Arthur, Texas (U.S. Environmental Protection Agency, 2012).

- **Cement industry**

In the energy audit analysis of a dry type rotary kiln system working in a cement plant in Turkey performed in (Engin & Ari, 2005) it was found that about 40% of the total input energy was being lost through hot flue gas (19.2%), cooler stack (5.6%) and kiln shell (15.1% convection plus radiation). For the first two losses, a WHR with a SRC system was proposed. In the SRC layout analysed in (Karellas, Leontaritis, Panousis, Bellos, & Kakaras, 2013) one stream of feed water is evaporated and superheated utilizing the energy from the exhaust gases, whereas the other stream of feed water follows the same process utilizing the hot air heat source (Figure 96).

Horizon 2020
European Union Funding
for Research & Innovation

This project has received funding from
the European Union's Horizon 2020 research and innovation
programme under grant agreement No 847097

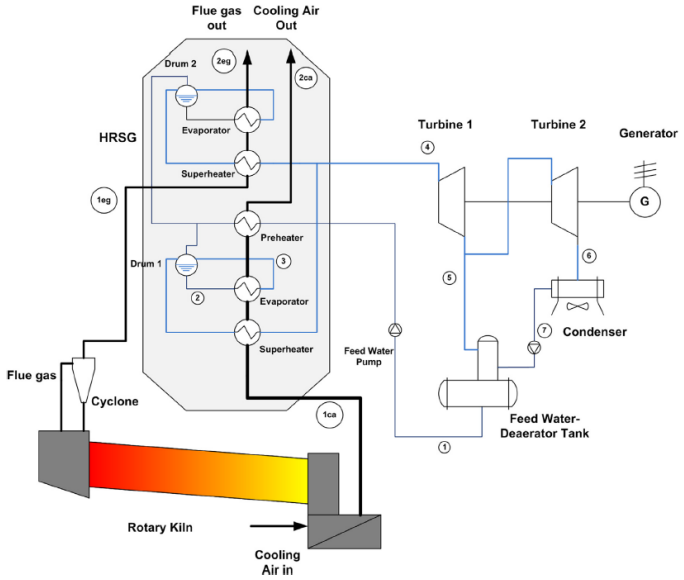

Figure 96: WHR using a double pressure SRC in a cement plant (Karellas et al., 2013).

The SRC layout for WHR from the Mazandaran cement plant in Iran considered in (Sanaye, Khakpaay, Chitsaz, Hassan Yahyanejad, & Zolfaghari, 2020) is basically the same as that presented in (Karellas et al., 2013) but applied to two production lines. The feed water is preheated using the hot air and then it is split into two streams in parallel which are evaporated and superheated using the hot air and exhaust gases, respectively. The two steam flows are merged and expanded in the steam turbine (Figure 97).

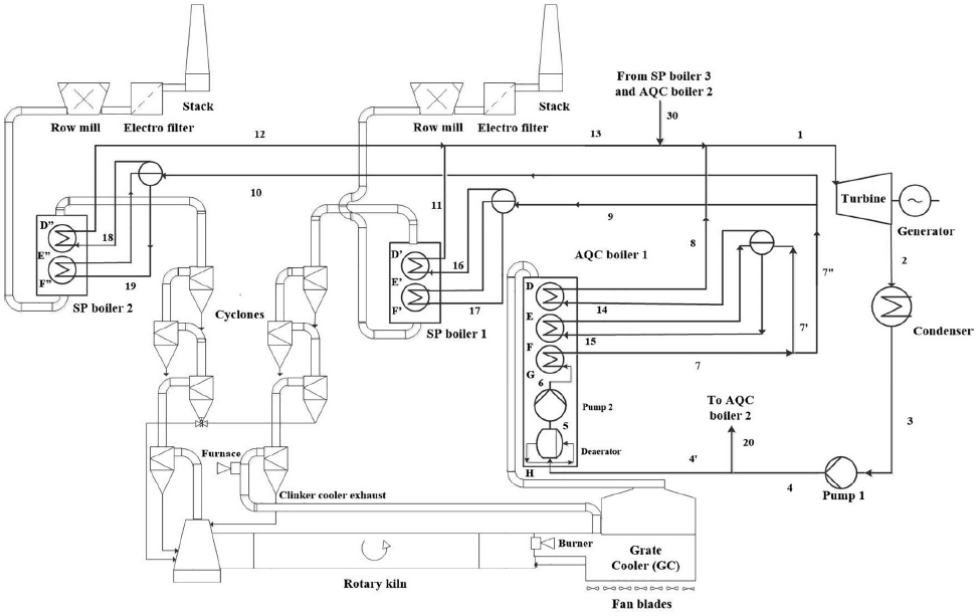

Figure 97: WHR from grate cooler exit hot air and from exit hot gas leaving the cyclone investigated for the Mazandaran cement plant in Iran (Sanaye et al., 2020).

The SRC for WHR from a cement plant in Iran analysed in (Amiri Rad & Mohammadi, 2018) uses the higher temperature of the exhaust gases for steam superheating and reheating (Figure 98 right). It

Horizon 2020
European Union Funding
for Research & Innovation

This project has received funding from
the European Union's Horizon 2020 research and innovation
programme under grant agreement No 847097

shows a lower system efficiency due to the higher condensation temperature dictated by the use of an air-cooled condenser. Table 47 summarizes the main features and performance of SRCs for WHR in cement plants reported in the literature. The power output varies in the range 4÷16 MW and the thermal efficiency in the range 16÷26%.

Table 47: Main features and performance of the SRC for WHR in cement plants.

TRL	Type heat source/s	T heat source/s (°C)	Power (kW)	Thermal efficiency (%)	Reference
9	a) exhaust gases b) hot air clinker cooler	a) 410 b) 230	16200	/	(Cunningham & Chambers, 2002)
N/A	a) exhaust gases; b) exit hot air grate cooler	a) 305 b) 290	9140	/	(Sanaye et al., 2020)
N/A	a) exhaust gases b) hot air	a) 325 b) 220	/	25.7	(Madlool, Saidur, & Rahim, 2012)
N/A	a) exhaust gases b) hot air	a) 380 b) 360	6260	23.6	(Karellas et al., 2013)
N/A	a) exhaust gases b) hot air	a) 380 b) 315	≈4300	16	(Amiri Rad & Mohammadi, 2018)
N/A	a) exhaust gases b) hot air	a) 350 b) 320	/	22	(Ghalandari, Majd, & Golestanian, 2019)
N/A	Hot air clinker cooler	320	≈4000	19.75	(Ren & Wang, 2019)

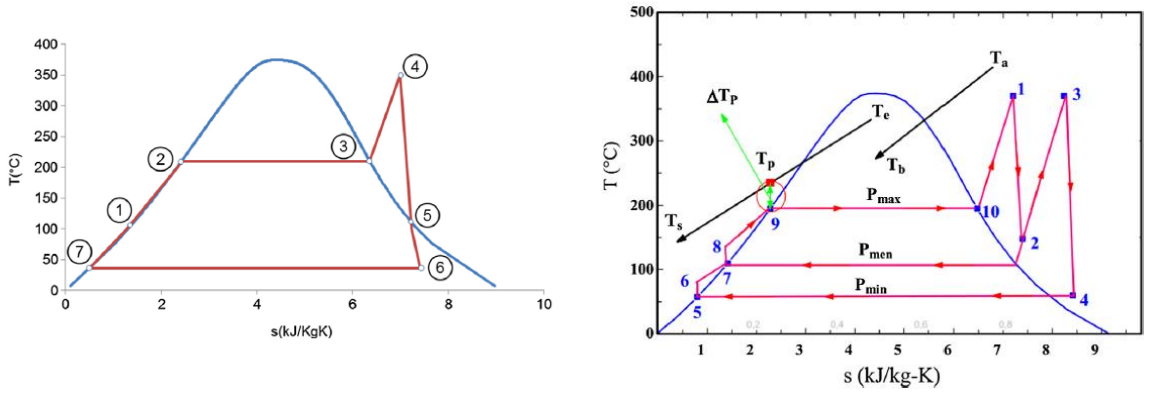

a) *b)*

Figure 98: T-s diagram of SRCs for WHR from cement plants: a) SRC with steam superheating (Karellas et al., 2013); b) SRC with steam superheating and reheating (Amiri Rad & Mohammadi, 2018).

- **Internal combustion engines**

The engine exhaust gas is typically selected as the only heat source for the single-pressure SRC system. To avoid acid condensation in the exhaust boiler, the minimum steam pressure of 7 bar with the evaporation temperature of 165°C is suggested by manufacturers (S. Zhu et al., 2019). With respect to the dual-pressure SRC system, steam pressures in the high-pressure (HP) and low-pressure (LP) stages are recommended to be 10÷11 bar and 4÷5 bar, respectively (Figure 99). Considering the sulphuric acid corrosion and wet soot deposits on boiler tubes, the LP steam with a low saturated temperature should not be preheated with exhaust gas, and the feedwater has to be preheated with supplementary WH sources available in the engine, like the jacket water and scavenge air. Because of the integrated design of the two-stage steam turbine, only marginal or even no superheat is mandatory for the LP steam (S. Zhu et al., 2019).

Horizon 2020
European Union Funding
for Research & Innovation

This project has received funding from
the European Union's Horizon 2020 research and innovation
programme under grant agreement No 847097

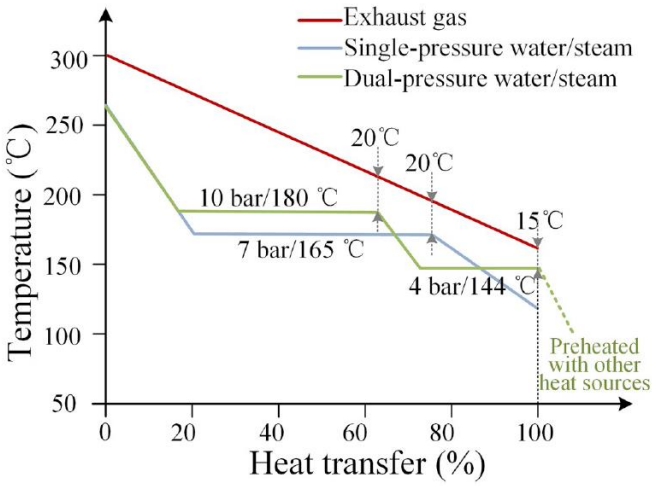

Figure 99: Heat transfer diagram of single and dual-pressure SRC systems for WHR from engines (S. Zhu et al., 2019).

It is shown in (G. Shu, Wang, & Tian, 2016) that water shows the highest power output and thermal efficiency for WHR from the exhaust gases of a gas engine (Figure 100) compared to a wide set of organic fluids. For evaporating pressures of 20÷30 bar the thermal efficiency of the SRC reaches the maximum value of 22÷23%, which is approximately 3%-points higher than the best organic fluid (toluene). On the other hand, the power output of water is only slightly higher compared to toluene, due to the better capability of the latter in heat extraction from the exhaust gases.

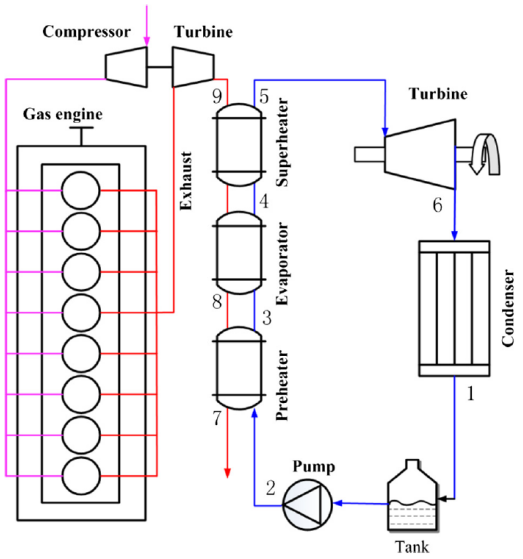

Figure 100: Schematic diagram of a WHR system from the exhaust gases of a turbocharged engine based on a single pressure SRC (G. Shu et al., 2016).

In order to avoid the complexity of a cascaded (dual loop) layout made of a topping SRC and a bottoming ORC, only the highest temperature heat sources (i.e., exhaust gas, EGR gas, aftercooler) were recovered in the optimum design proposed in (Dolz, Novella, García, & Sánchez, 2012) using a SRC (Figure 101).

Horizon 2020
European Union Funding
for Research & Innovation

This project has received funding from
the European Union's Horizon 2020 research and innovation
programme under grant agreement No 847097

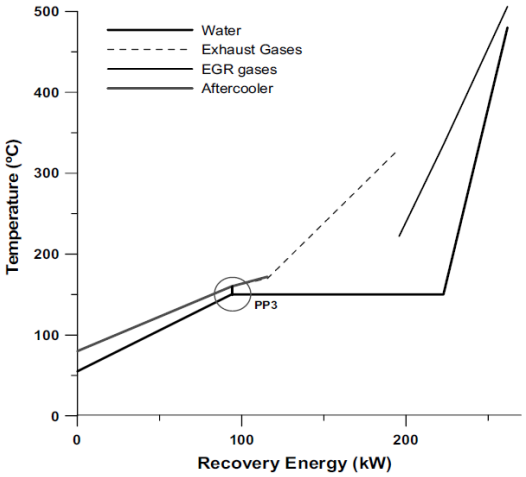

Figure 101: T-q diagram in the WHR of the high temperature heat sources from a Diesel engine using a SRC.

Table 48 summarizes the main features and performance of selected studies reported in the literature about the WHR from ICEs using the SRC. The thermal efficiency exceeds 20% for WHR from the exhaust gas.

Table 48: Main features and performance of the SRC for WHR from internal combustion engines.

TRL	Type ICE	Power ICE (kW)	Type heat source/s	T heat source/s (°C)	WHB type	Power (kW)	Thermal efficiency (%)	Reference
N/A	Diesel	/	Exhaust gas	292	Single pressure	4000	/	(Zheshu Ma, Yang, & Guo, 2012)
N/A	Gas	1000	Exhaust gas	540	Single pressure	154	23	(G. Shu et al., 2016)
N/A	Diesel	310	a) EGR cooler b) Exhaust gases c) Aftercooler	a) 509 b) 330 c) 172	Single pressure	46	17.8	(Dolz et al., 2012)

- **Gas turbine exhaust**

While the use of SRCs (double and triple pressure) is widespread for WHR from the exhausts of utility size gas turbines, the focus of this Section is on WHR from small/medium size gas turbine systems.

Offshore gas turbines. The NGCC on the offshore installation in Oseberg Field Centre (North Sea) consists of two gas turbines with a once-through heat recovery steam generator (OTSGs) located downstream of each gas turbine (L. O. Nord & Montañés, 2018) (Figure 102). The drum-based HRSGs were replaced by OTSGs in the years 2011/2012 for increased compactness, lower weight and higher reliability (L. Nord & Bolland, 2012). One steam turbine received the combined steam mass flow from the two steam generators. The two OTSGs were designed for a live steam pressure of 16.5 bar with a live steam temperature of 430°C. The power generated at the design point was 16 MW (Table 49).

Horizon 2020
European Union Funding
for Research & Innovation

This project has received funding from
the European Union's Horizon 2020 research and innovation
programme under grant agreement No 847097

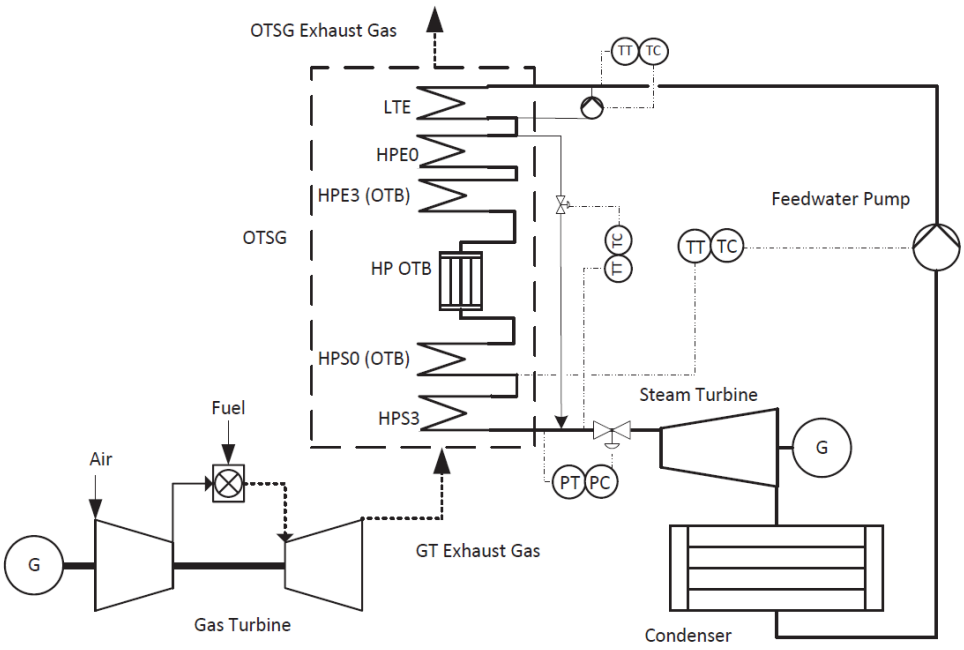

Figure 102: WHR from the gas turbine exhaust using a SRC (L. O. Nord & Montañés, 2018).

Table 49: Main features and performance of SRCs for WHR from the gas turbine exhausts.

TRL	Site	Power of GT (kW)	T heat source (°C)	Layout	Power output (kW)	Thermal efficiency (%)	Reference
9	Oseberg Field Centre (North Sea)	2 × 30000	506	Single pressure	16.1	/	(L. O. Nord & Montañés, 2018)

5.1.3 Cost aspects

The consulting and technology services company ICF ("ICF International," 2019) recently reviewed in-house data, published literature, and held discussions with industry stakeholders to develop cost estimates for commercially available SRC systems. The results of ICF's cost analysis are shown in Table 50 extracted from (Oak Ridge National Laboratory, 2015). SRC capital costs range from 1080 to 2700 €/kW as a function of the capacity. O&M costs range from 0.45 to 1.17 cents €/kWh. The installed capital costs likely do not contain contingency for site specific characteristics that can significantly increase costs for actual installations.

Table 50: Capital costs and O&M costs of SRCs in WHR applications (Oak Ridge National Laboratory, 2015).

Electric capacity of the WH SRC (kW)	Installed capital cost (€/kW)	Operation and maintenance costs (c€/kWh)
50 ÷ 500	2700	1.17
500 ÷ 1000	2250	0.81
1000 ÷ 5000	1620	0.72
5000 ÷ 20000	1350	0.54
>20000	1080	0.45

Horizon 2020
European Union Funding
for Research & Innovation

This project has received funding from
the European Union's Horizon 2020 research and innovation
programme under grant agreement No 847097

5.2 Organic Rankine Cycles (ORCs)

5.2.1 Technological features and performance

In its simplest implementation the ORC layout is identical to a conventional SRC and comprises pump, evaporator, expander and condenser, as illustrated in Figure 103. The working fluid with low boiling point is pumped to the evaporator, where it is heated and vaporized by the exhaust heat. The generated high pressure vapour flows into the expander and its heat energy is converted to work. Simultaneously, the expander drives the generator and electric energy is generated. Then, the exhaust vapour exits the expander and is led to the condenser where it is condensed by the cooling water. The condensed WF is pumped back to the evaporator and a new cycle begins (C. He et al., 2012). Depending on the temperature at which WH is available and presence of pinch points, the organic WF at the outlet of the evaporator can be saturated or in superheated conditions.

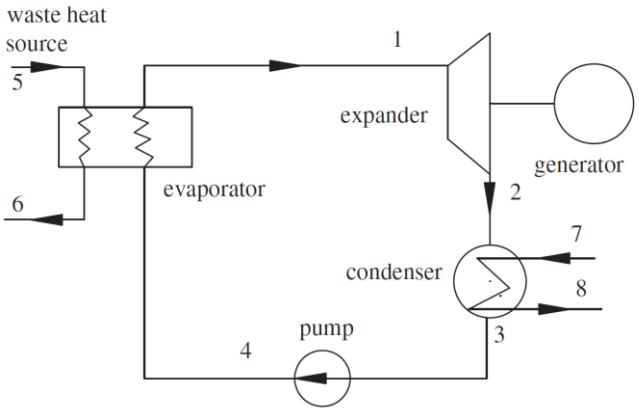

Figure 103: Schematic diagram of the ORC (C. He et al., 2012).

ORC technology uses organic substances as WFs which typically have a lower boiling point and critical temperature than that of water (G. Qiu, 2012). The low boiling point of ORC WFs enables the conversion of low/mid-grade WH in the range 80÷300°C into power. Since the critical pressure of most organic fluids is in the range 30÷40 bar, the ORC system operates at moderate pressures, which is often limited to 20÷25 bar (Bao & Zhao, 2013). Moreover, the condensing pressure is often higher than the atmospheric pressure, which reduces the issues related to air leakage into the system. The vaporization heat of organic fluids is much lower than that of water, hence a better thermal match can be obtained with the sensible heat source. The low enthalpy drop in the expansion process of organic fluids makes the turbine design easy, so that a single stage turbine may be used instead of a multi-stage turbine, as required for steam. Turbine erosion is avoided due the positive slope of the saturated vapour pressure curve of the vast majority of organic fluids, which implies expansion in the dry vapour region. Accordingly, even for medium-temperature heat sources around 400°C, significantly higher output and simpler design is usually achieved by choosing an organic fluid instead of water when the output of the plant is below 1÷2 MW (Larjola, 1995). Water shows good efficiency at high pressure requiring increased safety measures which are not economically feasible for small plants (Drescher & Brüggemann, 2007). This is one of the main reasons why ORCs are preferred also in biomass-fired applications or other high temperature WH applications. All the above mentioned aspects define an application range of capacities and temperatures of the heat source that is conveniently covered by ORCs. Such range is called "mainstream ORC systems" in Figure 104.

Horizon 2020
European Union Funding
for Research & Innovation

This project has received funding from
the European Union's Horizon 2020 research and innovation
programme under grant agreement No 847097

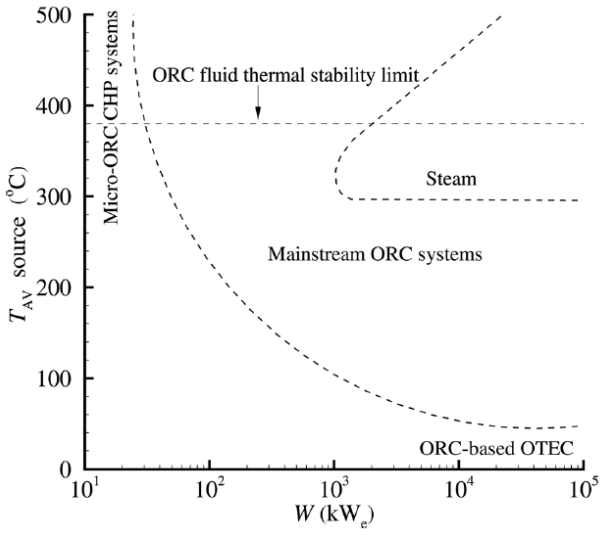

Figure 104: Current and future fields of application of ORC versus SRC in terms of average temperature of the energy source and power capacity of the system (Colonna et al., 2015).

While fluid selection studies in the scientific literature cover a broad range of WFs (Bao & Zhao, 2013), only a few fluids are actually used in commercial ORC power plants (Colonna et al., 2015), as shown in Table 51.

Table 51: Main properties of the most common working fluids currently in use in ORC power plants (Colonna et al., 2015).

Working fluid	Chemical formula	Category	MW (kg/kmol)	Critical temperature Tcr (°C)	Critical pressure pcr (bar)	Normal boiling temperature Tboil(°C)
R134a	C2H2F4	HFC	102.0	101.1	40.59	-26.1
Isobutane	C4H10	HC	58.1	134.7	36.29	-11.8
R245fa	C3H3F5	HFC	134.0	154.0	36.51	15.1
Solkatherm SES36	Mixture	HFC	184.9	176.1	28.49	35.3
Isopentane	C5H12	HC	72.1	187.2	33.78	27.8
N-pentane	C5H12	HC	72.1	196.6	33.70	36.1
Cyclopentane	C5H10	HC	70.1	238.5	45.15	49.2
MM	C6H18OSi2	Siloxane	162.4	245.5	19.39	100.2
MDM	C8H24Si3O2	Siloxane	236.5	290.9	14.15	152.5
Toluene	C7H8	HC	92.1	318.6	41.26	110.6

ORC performance is commonly described by the "thermal efficiency" (η_{th}) that is defined as the ratio between the net power output (W_{net}) and the rate of waste heat captured by the ORC system (Q_{in}):

$$\eta_{th} = \frac{\dot{W}_{net}}{\dot{Q}_{in}} \qquad 2$$

The thermal efficiency exclusively depends on the state points of the cycles (condensation and evaporator pressures/temperatures and superheat degree) and does not account for the extent of

Horizon 2020
European Union Funding
for Research & Innovation

This project has received funding from
the European Union's Horizon 2020 research and innovation
programme under grant agreement No 847097

utilization of the heat source. However, due to pinch point limitations, the heat supplied to the ORC system (Q_{in}) is lower than the maximum heat (Q_{av}) that could be recovered if the heat source was cooled down to the ambient temperature. Thus, in WHR applications the information about η_{th} should be complemented with some information about the extent of utilization of the heat source. A useful index is the heat recovery effectiveness (ε) defined as the ratio between Q_{in} and Q_{av}, which depends on the outlet temperature of the heat source stream (Braimakis & Karellas, 2018):

$$\varepsilon = \frac{\dot{Q}_{in}}{\dot{Q}_{av}} = \frac{T_{in} - T_{out}}{T_{in} - T_{amb}} \qquad 3$$

Since the final aim in a WHR application is to generate the maximum power output from the available heat source, the most meaningful metric is the so-called "system efficiency" (also called "total-heat recovery efficiency") that combines the two sub-metrics. The system efficiency (η_{sys}) is the ratio of the net power to the maximum allowable heat rate from the WH source:

$$\eta_{sys} = \frac{\dot{W}_{net}}{\dot{Q}_{av}} = \eta_{th} \cdot \varepsilon \qquad 4$$

The system efficiency can be a few percentage points lower than the thermal efficiency and the discrepancy typically increases as the WH temperature decreases.
An extensive open-access database of more than 100 ORC experiments collected from about 175 scientific literature references was published in 2017 (Landelle, Tauveron, Haberschill, Revellin, & Colasson, 2017). Prototypes from the database covered a wide range of conditions, going from a few Watts to 1 MW of gross output power with hot source temperatures ranging from 60 to 675 °C. This first database was merged with a second database containing commercial ORC references presented in (Tauveron, Colasson, & Gruss, 2015) without duplicates. The overall result are the two maps presented in (Landelle et al., 2017) that show the variation of ORC thermal efficiency with the ORC power (Figure 105 left), and the variation of ORC thermal efficiency with the heat source temperature (Figure 105 right). The centred sliding average provides the mean trend. Thermal efficiency of ORCs varies in the range 5÷25%. Such low values as well as the spread across a relatively large range should not come at a surprise. Indeed, ORC technology convert WH available in a wide temperature range between 80÷500°C, and it is inherently less efficient than other power cycles (e.g., SRC) which operate at higher temperatures.

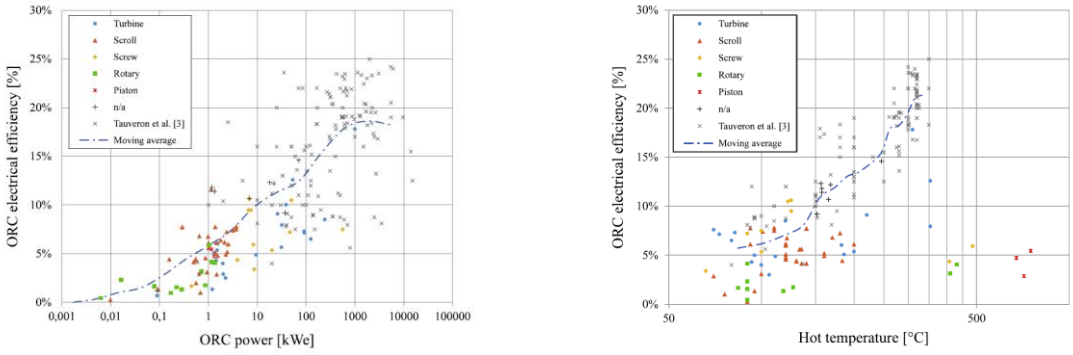

a) b)

Figure 105: a) Variation of ORC thermal efficiency (η_{th}) with the power of the system (Landelle et al., 2017); Variation of ORC thermal efficiency with the heat source temperature (Landelle et al., 2017).

Horizon 2020
European Union Funding
for Research & Innovation

This project has received funding from
the European Union's Horizon 2020 research and innovation
programme under grant agreement No 847097

The relatively low thermal efficiency requires to carefully consider cost-effectiveness aspects, therefore, advanced ORC cycle architectures have been developed to maximize ORC performances. Most common architectures proposed include (Lecompte, Huisseune, Van Den Broek, Vanslambrouck, & De Paepe, 2015):

- B: Basic (See Figure 103).
- RC: Addition of a recuperator. A HE is added in order to reuse the heat after expansion to preheat the working fluid prior to evaporation (Toffolo, Lazzaretto, Manente, & Paci, 2014).
- MP: Multiple pressure. The evaporation of the working fluid is staged in two or more pressure levels to improve the thermal match with the heat source (G. Manente, Lazzaretto, & Bonamico, 2017).
- DL: Dual loop or cascade. The system is composed by two separate ORC cycles working at different temperature levels and with different working fluids. The condenser of the upper cycle acts as the evaporator of the lower cycle (Zhi, Hu, Chen, & Zhao, 2019).
- TLC: Trilateral cycle. Boiling of the working fluid is avoided to overcome limitations with pinch points; a two-phase expander is used (Giuseppe Bianchi et al., 2018). The TLC was recently demonstrated for low grade (70÷100°C) WHR applications within the H2020 I-Therm project ("I-Therm H2020," 2019).
- RG: Regenerative ORC. Turbine bleeding together with direct contact heat exchanger is used to preheat the fluid prior to the evaporator, increasing thermal efficiency (Branchini, De Pascale, & Peretto, 2013).
- ZM: Use of zeotropic mixtures. To improve temperature matching between WH source and working fluids and thus reduce thermal inefficiencies (Y. Feng et al., 2015).
- TC: Transcritical/supercritical cycle. ORC fluid is pumped above supercritical pressure to bypass two-phase boiling and attain better temperature matching between WH source and working fluid (Yağli, Koç, Koç, Görgülü, & Tandiroğlu, 2016).

Currently, saturated and superheated cycle configurations with or without REC are common (Colonna et al., 2015). The supercritical and trilateral cycle configurations have been adopted only in few exemplary/experimental cases (Lecompte et al., 2015). Multiple (two and three) pressure levels in the evaporator have been adopted only in large geothermal power plants (Bronicki, 2007).

5.2.2 Examples of applications, technology maturity and cost-performance of ORCs

ORCs can be driven by multiple kinds of heat sources and currently find applications in WH recovery, geothermal energy, biomass and solar thermal energy (Tchanche, Lambrinos, Frangoudakis, & Papadakis, 2011). Information about more than 700 ORC projects were collected in (Tartière & Astolfi, 2017) and showed that 13.9% of the global installed ORC capacity was in WHR plants. Focusing on WHR, ORCs find application mostly in recovery of thermal energy from stationary ICEs and gas turbines or from a variety of industrial processes, as shown in the pie chart in Figure 106.

Horizon 2020
European Union Funding
for Research & Innovation

This project has received funding from
the European Union's Horizon 2020 research and innovation
programme under grant agreement No 847097

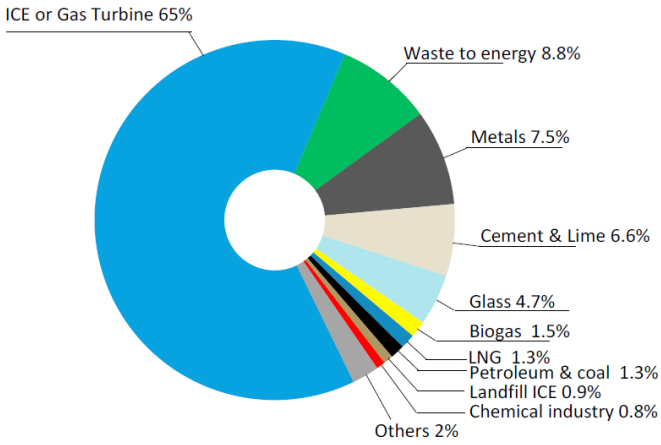

Figure 106: Shares of ORC installed capacity per WHR application (Tartière & Astolfi, 2017).

Table 52 summarizes the capacity and WFs of real ORC systems installed by different manufacturers in various applications (solar, geothermal, biomass and waste heat). Fluids having lower critical temperatures (like refrigerants) are used in geothermal and low grade WH applications. Instead, WFs having higher critical temperatures (like cyclopentane, toluene and siloxanes) are used in high temperature WH or biomass applications.

Table 52: Overview of the main characteristics of commercial ORC power plants commissioned in the period 1995÷2015 (Colonna et al., 2015).

Manufacturer	Power output (kW)	Working fluid	Energy source	Number of units
Atlas Copco	2100 22500 3600 22500	R134a n-butane isobutane n-butane	WH GEO GEO GEO	1 2 1 2
GE oil and gas	17000	Cyclopentane	WH	6
GE energy	125	R245fa	Biomass, WH	>100
Ormat	1200 400÷3500 4000÷6500 1000÷25000	n-pentane n-pentane/isopentane n-pentane/cyclo-pentane n-pentane/n-butane	Solar GEO WH GEO	1 70 20 159
Turboden	100 200÷500 500÷1000 1000÷1500 1500÷2000 2000÷4000 4000÷13000	Siloxanes Siloxanes Siloxanes/R134a Siloxanes/Isobutane Siloxanes Siloxanes/solkatherm n-pentane/cyclo-pentane/R134a/245fa	Solar Biomass, WH, GEO Biomass, WH, GEO Biomass, WH, GEO Biomass, WH, GEO, Solar Biomass, WH, GEO Biomass, WH, GEO	1 28 131 67 16 17 11
Tri-O-Gen	80÷160	Toluene	WH, Biomass	30

As illustrated in Table 52, WH recovery from energy intensive processes by ORCs has been demonstrated at MW-scale, and commercially available from suppliers such as Turboden, Ormat, GE oil and gas, etc. For a more complete list of manufacturers the reader is referred to (Tartière & Astolfi, 2017). In such applications the WH, commonly available in the form of hot exhausts, is transferred to the ORC evaporator typically through an indirect loop with thermal oil in order to avoid contact with

Horizon 2020
European Union Funding
for Research & Innovation

This project has received funding from
the European Union's Horizon 2020 research and innovation
programme under grant agreement No 847097

exhausts gases. When possible, however, it is beneficial to attain direct heat transfer contact between the WH stream and the ORC fluid, as in the small units commercialized by Tri-O-Gen. This reduces the number of HEs needed and abates thermal inefficiencies. In such context, the recently completed H2020 TASIO project ("TASIO H2020," 2019) developed ORCs with direct contact HEs. Small scale ORCs (<100÷200kW) remain under research development; the main challenge is cost reduction and performance increase. The primary focus in on the development of efficient expansion devices as they play a critical role in determining the cycle efficiency (Rahbar, Mahmoud, Al-Dadah, Moazami, & Mirhadizadeh, 2017). Current interest is in developing expanders that can tolerate two-phase flow, have low cost and meet lubrication requirements.

In the following the main features of the ORC plants for WHR in various industrial sectors are summarized. The industrial sectors considered are: steel, chemical and petrochemical, glass, ceramic, cement and food. Instead, only a brief presentation is given about the EHR from ICEs and gas turbines.

- **Steel industry**

Table 53 summarizes the main features and the performance of real installations, prototypes and case studies for the integration of ORC units in the steel industry reported in the literature. A more detailed description is reported in the following for each plant.

Table 53: Main features and performance of ORCs for WHR in the steel industry.

TRL	Type heat source	T heat source (°C)	Location	HTF loop fluid and T (°C)	ORC Layout	Working fluid	Power output (kWe)	Thermal efficiency (%)	Reference
9	Exhaust gas from an electric arc furnace	505	Brescia (Italy)	Steam (181÷224)	RC	MM	1283[a]	21.7[a]	(Ramirez et al., 2017) ("FP7 PITAGORAS," 2017)
9	Cooling water of the skids of the furnace	122 ÷ 132	Turkey	Pressurized water	Basic	R245fa	200÷ 250	8.8 ÷ 10.2	(Kaşka, 2014)
5	Flue gases from a thermal oxidizer (RTO)	137	/	Pressurized water	Basic	R245fa	177	9.6	(Sung et al., 2016)
N/A	Underfiring exhaust gas stream coke oven	221	UK	/	Basic	benzene	2310	11	(Walsh & Thornley, 2012)
N/A	Flue gases reheating furnace	200	/	/	/	R245fa	200	9.4	(Y. P. Lin et al., 2016)

[a] average during the operating period.

1) Residual heat of flue gases from a thermal oxidizer. The steel processing plant analysed in (Sung et al., 2016) produces painted steel sheets and includes a regenerative thermal oxidizer (RTO) to remove harmful volatile organic compounds (VOCs). The hot combustion gases at 850°C generated in the RTO are partially used for in-plant purposes, and the remaining heat is released through a chimney at flue gas temperatures (177÷265°C) that are well above the acid dew point (≈140°C). In the WHR system installed in the steel processing plant (Figure 107) the WH of the flue gases is recovered using a heat transfer loop of pressurized water having a maximum temperature of 140°C. The hot pressurized water is used to evaporate R245fa that operates as the WF. The heat transfer loop consists

Horizon 2020 European Union Funding for Research & Innovation
This project has received funding from the European Union's Horizon 2020 research and innovation programme under grant agreement No 847097

of the flue gas HE (fin-tube HE), a thermal storage tank and a hot water pump. Two bypass valves control the flue gas flow from the main chimney to the sub-chimney where the HE was installed. A thermal storage tank with 1-ton capacity was installed to suppress the variation of the heat source (Sung et al., 2016).

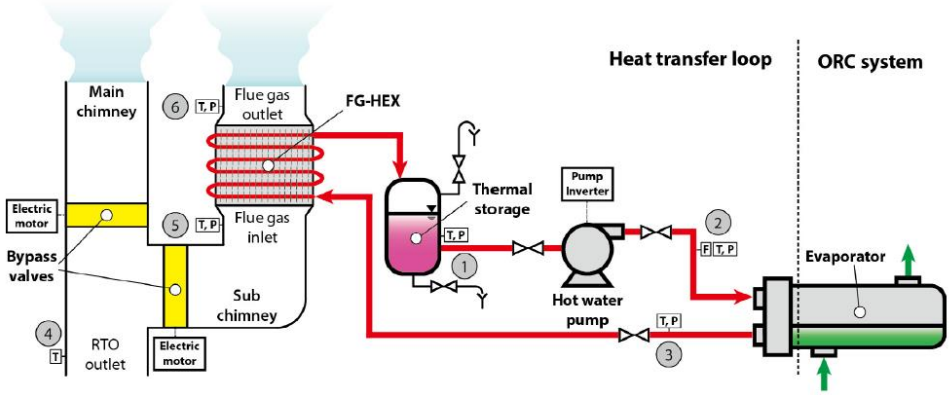

Figure 107: WHR from the flue gases in a steel processing plant (Sung et al., 2016).

2) Exhaust gas from an electric arc furnace. A real scale pilot plant was implemented within the European project PITAGORAS ("FP7 PITAGORAS," 2017) at the steel mill owned by ORI Martin located in Brescia (Italy). The ORC unit recovers heat from the off-gas of an EAF. Originally, the exhaust gases from the melting process were cooled in a quenching tower, filtered in a bag-filter and expelled through the chimney. With the implementation of the WHR system the exhaust gases are first passed through the WHR Unit (WHRU) where thermal energy is transferred to the water producing saturated steam. Steam is used as heat carrier between the heat source (EAF) and the ORC evaporator as shown in Figure 108. The main challenge to overcome was the discontinuous availability of the WH because the EAF works as a batch process due to the melting phase and the tapping phase. During tapping and when the roof of the furnace is open, for bucket scrap charging or for repairing, the thermal power at the primary off gas duct is close to zero. Thus, in order to smooth the fluctuations in the steam supply and provide the required quality of heat input to the ORC-generator, a steam accumulator with a volume of 150 m^3 (storage capacity of 6 MWh) was added to the process (Ramirez et al., 2017). A similar ORC power plant with a capacity of 2400 kW was installed by the same company (Turboden) in another still mill in Riesa (Germany) as described in (Bause et al., 2015) meeting all the expected performance targets.

Horizon 2020
European Union Funding
for Research & Innovation

This project has received funding from
the European Union's Horizon 2020 research and innovation
programme under grant agreement No 847097

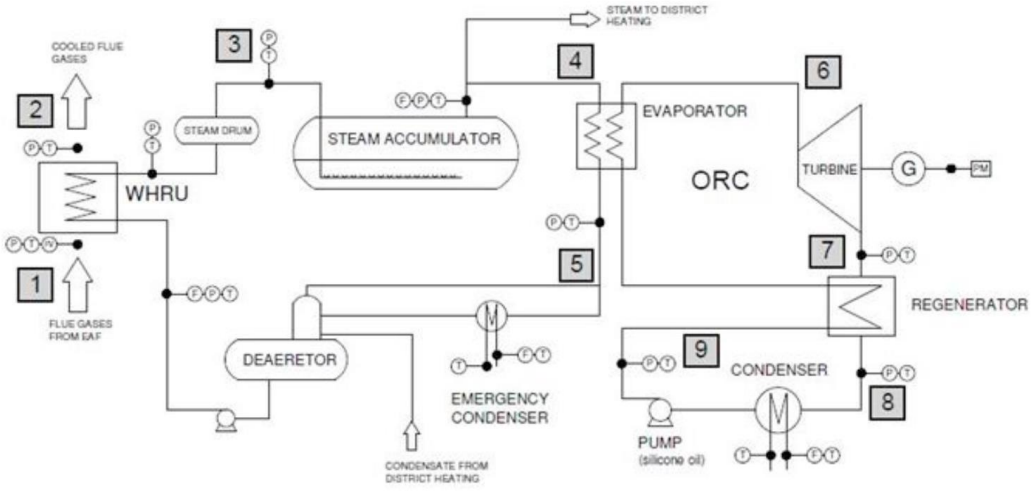

Figure 108: WHR from the exhaust gas of an electric arc furnace (Ramirez et al., 2017).

3) *Stacks from a coke oven*. Coke is the most important reducing agent in hot metal production and it is produced in ovens by the pyrolysis of coal. The potential application of an ORC to generate electricity from low grade WH from the stacks of a coke oven used in steel production was investigated in (Walsh & Thornley, 2012). The authors highlighted that the low grade WH represents an underused resource in the steel industry but that an attractive payback period of between 3 and 6 years can be obtained.

4) *Flue gas from the reheating furnace*. The bloom and billet produced in an EAF steel making plant are typically reheated to 1150÷1250 °C in a reheating furnace for various types of rolling mills. The first ORC power plant recovering heat from a rolling mill of a reheating furnace (700 kW) went into operation in 2013 in Singapore. The heat transfer was performed by direct exchange between the exhaust gas and the ORC WF at temperatures around 400 °C (Colonna et al., 2015). In (Y. P. Lin et al., 2016) the flue gas of the reheating furnace after the regenerative HE are utilized for electricity generation using an ORC system.

5) *Cooling water of the skids of the furnace*. The ORC system described in (Kaşka, 2014) was installed to produce electricity by using the WH of a slab reheat furnace. A semi-closed loop evaporative cooling system is used to cool the skids of the furnace. Water is circulated through the furnace to cool the walking beam skids and leaves the furnace as a saturated liquid–vapour mixture (wet steam). ORC units use the water from the furnace as the heat source. Four ORC units, with around 250 kW net power capacity, are installed for WHR from the reheat furnace.

- **Chemical and petrochemical industry**

Table 54 summarizes the main features and the performance of real installations and case studies for the integration of ORC units in the chemical and oil refining industry reported in the literature. A more detailed description is reported in the following for each plant.

Table 54: Main features and performance of ORCs for WHR in the chemical and petrochemical industry.

TRL	Type heat source	T HS (°C)	Location	ORC Layout	Working fluid	Power (kW)	Thermal efficiency (%)	Reference
9	Waste hot water	81.5	Mailiao (Taiwan)	Basic	R134a	194	4.7	(Lee, Liu, Chang, &

Horizon 2020 European Union Funding for Research & Innovation
This project has received funding from the European Union's Horizon 2020 research and innovation programme under grant agreement No 847097

								Hsieh, 2017)
9	Sewage	110	Binzhou (China)	Basic	TY-1	220 ÷ 280	4.6 ÷ 6.7	(H. Yang et al., 2020)
N/A	a) Bottom oil of xylene; b) Xylene products; c) Evaporation tower; d) Reforming tower; e) Benzene tower	a) 215 b) 205 c) 147 d) 104 e) 98	Shijiazhuang Refining & Chemical Company (China)	DP	R141b	3325	10.2	(J. Song, Li, Gu, & Zhang, 2014)
N/A	Vapours condenser distillation column	140	/	Basic	isobutane, butane, isopentane, pentane (pure and binary mixtures)	440 ÷ 600	8.0 ÷ 9.1	(Varga & Csaba, 2018)
N/A	Stream of liquid kerosene from vacuum column distillation	105÷ 140	New Zealand Refining Company Limited (Refining NZ)	Basic	Isobutane Butane/pentane mixture	250	6.8÷7.6	(Jung, Krumdieck, & Vranjes, 2014)

Condensate stripping tower. In the original styrene monomer chemical plant in Taiwan the thermal energy of the steam condensate leaving the stripping tower at 82°C was rejected to the environment. In the implemented WHR system (Lee et al., 2017) the heat is transferred to the WF (R134a) of an ORC that generates 200 kW. Through the ORC, the condensate temperature decreases from 81.5°C to 63°C reducing the load on the cooling tower. Since the hot water contained a certain amount of in-process polymerized substances that tended to adhere easily onto the HE, the shell-and-tube-type design was preferred to the plate design thereby facilitating onsite cleansing and descaling operations. While the thermal efficiency is very low (less than 5%) due to the low temperature of the heat source, yet the estimated payback time was less than 5 years. This is a clear example of the capability of the ORC technology to generate power from low grade heat sources that are commonly wasted.

Sewage heat recovery. An ORC system using evaporative condenser was designed and built for WHR from sewage in a petrochemical industry in China (H. Yang et al., 2020). In the evaporative condenser the WF is condensed into the condenser tubes. The cold water is pumped from a water basin at the bottom of evaporative condenser and sprayed over the condensing coil. The outside air is drawn and blown up through the condenser tube at the same time. Some of the water on the condenser tubes evaporates into the air. The un-evaporated water falls into the bottom of evaporative condenser and then flows back to the sprayers using the pump. The evaporative condenser enhances the heat rejection process by utilizing the evaporation cooling effect and therefore can improve the annual energy conversion efficiency. The real plant data showed that the penalty in thermal efficiency of the system was 2.1%-points as the ambient temperature increased from 0°C to 30°C.

Horizon 2020
European Union Funding
for Research & Innovation

This project has received funding from
the European Union's Horizon 2020 research and innovation
programme under grant agreement No 847097

Waste heat from a catalytic reforming unit. The recovery of five different WH sources at temperatures in the range 98÷215°C from the catalytic reforming unit in Shijiazhuang Refining & Chemical Company (Hebei Province, China) was investigated in (J. Song et al., 2014). A dual pressure ORC system was found as the most promising. The higher temperature WH sources (a,b,c) are used to evaporate the WF (R141b) at the higher temperature level (120°C), whereas the lower temperature WH sources (d,e) are used to evaporate the WF at the lower temperature (≈80°C) (Figure 109).

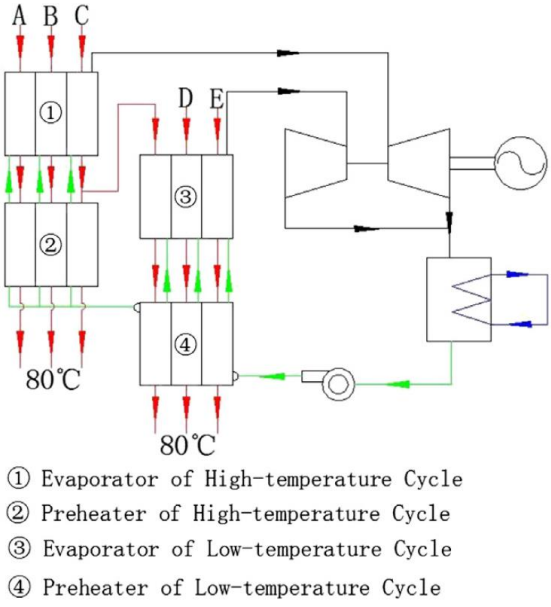

Figure 109: Optimum ORC layout (dual pressure) for WHR from five waste heat streams (a,b,c,d,e) in a petroleum refining industry (J. Song et al., 2014).

Condenser distillation column. The possible utilization of the heat content of a condenser connected to the main column of a residue upgrading unit was investigated in (Varga & Csaba, 2018). The ORC was used to substitute an air cooler applied as a condenser connected to the main distillation column of a vacuum residue processing unit. This HE condenses and cools down vapours entering at 140 °C and leaving at 50 °C, meantime dissipating heat of 6.5 MW into the environment. By using isobutane as WF in an ORC system a maximum power output of 600 kW could be obtained.

Cooling of hot kerosene from a distillation column. In a vacuum distillation process, the refinery uses a kerosene stream to control indirectly the column vacuum and cut-point via the temperature control at the top section of the distillation column (Figure 110). In the common design the liquid kerosene is drawn off from the column and flows through two forced air cooling banks where heat is rejected to the environment (Figure 110 left). In the upgraded design the WH of hot kerosene is recovered using an ORC unit (Figure 110 right) installed in a bypass line between the pump and the cooler (Jung et al., 2014).

Horizon 2020
European Union Funding
for Research & Innovation

This project has received funding from
the European Union's Horizon 2020 research and innovation
programme under grant agreement No 847097

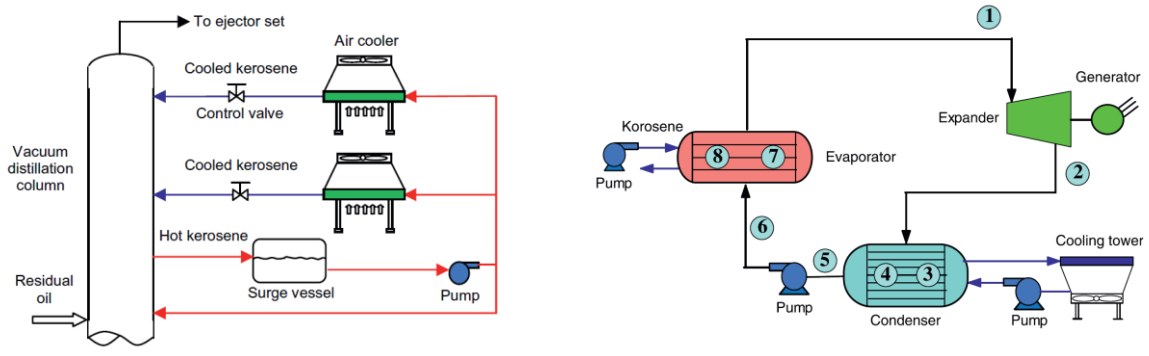

Figure 110: WHR from hot kerosene leaving a vacuum distillation column: a) Kerosene cooling process for controlling distillation column temperature at refinery NZ facility; b) ORC integration (Jung et al., 2014).

- **Glass industry**

The glass industry also offers vast opportunities for WHR by means of indirectly heated ORC power systems. An intermediate heat transfer loop can collect thermal energy from the hot gas exiting the oven that melts and refines the raw materials. The exhaust gas temperatures are relatively high (400÷500 °C) so that high thermal efficiencies can be obtained. Since 2012 one such system (1.3 MWe) is in operation at the AGC floating glass production site in Cuneo (Italy) and reached a thermal efficiency of 23.6% (Table 55). In September 2018 a new 6.2 MW unit started operation in Turkey to convert the off-gas WH from the two float glass production lines ("Turboden," 2019). In this plant thermal oil is heated up to 315°C and heat is transferred to the ORC system.

Table 55: Main features and performance of ORCs for WHR in the glass industry.

TRL	Type heat source	T heat source (°C)	Location	HTF loop fluid and T(°C)	ORC Layout	Working fluid	Power output (kW)	Thermal efficiency (%)	Reference
9	Exhaust gas	500	Cuneo (Italy)	Thermal oil (307°C)	/	/	1200	23.6	(Altieri R., Campana F., 2014)

- **Ceramic industry**

Exhaust gases from a furnace. The recovery of the WH from the exhaust gases of a ceramic furnace was described in (Peris, Navarro-Esbrí, Molés, & Mota-Babiloni, 2015). Specifically, the WH was recovered from the cooling air (rather from the exhaust) due to the moderate temperature and non-corrosive composition (Navarro-Esbrí, Peris, Collado, & Molés, 2013), and the thermal efficiency was lower than 11% (Table 56). The recovery facility (Figure 111 below) was mainly composed by a recuperator HE, located in the bypass of the cooling air, and a heat transfer loop with thermal oil that transported the thermal energy from the heat source to the ORC module (Navarro-Esbrí et al., 2013). In the early design proposed in (Casci et al., 1981) the heat recovery was from the exhaust gases (Figure 111) and a special design of the ORC preheater and evaporator was undertaken to prevent the decomposition of the WF at high temperatures and to address the presence of dust in the exhaust gases.

Horizon 2020 European Union Funding for Research & Innovation
This project has received funding from the European Union's Horizon 2020 research and innovation programme under grant agreement No 847097

Table 56: Main features and performance of ORCs for WHR in the ceramic industry.

TRL	Type heat source	T heat source (°C)	Location	HTF loop fluid and T(°C)	ORC Layout	Working fluid	Power output (kWe)	Thermal efficiency (%)	Reference
9	Hot air	287	Spain	Thermal oil (165)	RC	R245fa	18.5	10.9	(Peris et al., 2015)

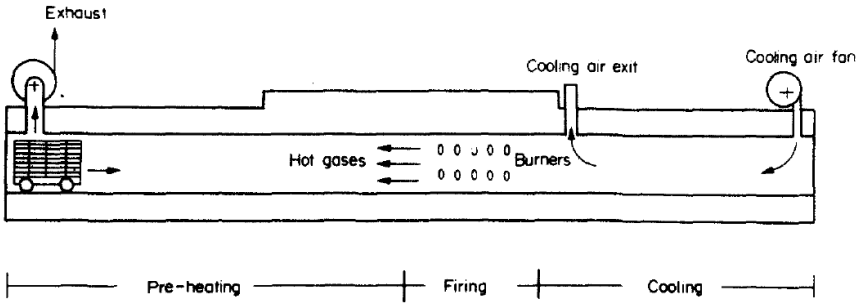

a)

b)

Figure 111: WHR from ceramic kilns: a) Schematic of a tile tunnel kiln showing the exhaust gases and the hot cooling air as potential heat sources for the ORC (Casci et al., 1981); b) photo of the recovery facility implemented in Spain composed by a recuperator (located in the bypass line of the cooling air) and a heat transfer loop with thermal oil (Navarro-Esbrí et al., 2013).

- **Cement industry**

Table 57 summarizes the main features and the performance of real installations and case studies for the integration of ORC units in the cement industry reported in the literature. A more detailed description is reported in the following for each plant.

Table 57: Main features and performance of ORCs for WHR in the cement industry.

TRL	Type heat source	T heat source (°C)	Location	HTF loop and T(°C)	ORC Layout	Working fluid	Power output (kW)	Thermal efficiency (%)	Reference
9	Cooler exhaust air	275	Lengfurt, Germany	Thermal oil 230°C	Basic	Pentane	1500	18.3	(Legmann, 2002)
N/A	a) Exhaust gas b) Hot air from	a) 310 b) 440	Quixeré, Brazil	No	Basic; REC	R141b R123	4500 ÷ 5500	18.8 ÷ 22.4	(Moreira & Arrieta, 2019)

Horizon 2020 European Union Funding for Research & Innovation
This project has received funding from the European Union's Horizon 2020 research and innovation programme under grant agreement No 847097

	clinker cooler								
N/A	Exhaust gas from the rotary kiln	350	/	Thermal oil	Basic	Cyclohexane benzene toluene	1050 ÷ 1570	/	(Fergani, Touil, & Morosuk, 2016)
N/A	Dry air at the kiln cooler outlet	220	/	/	Basic	hexane, isohexane, R601, R123	1020 ÷ 1090	18.0 ÷ 19.1	(Huarong Wang, Xu, Yang, Miao, & Yu, 2015)
N/A	a) Exhaust gas b) Clinker cooler exhaust	a) 340 b) 320	/	/	Basic	R123	8650	20.6	(Jiangfeng Wang, Dai, & Gao, 2009)

Real plants. The first ORC applied in the cement industry was the 1.5 MW unit installed at the Heidelberger Zement AG Plant in Lengfurt (Germany) in 1998 by Ormat (Legmann, 2002). The budget restrictions imposed that only the cooler exhaust air was used as the heat source for the ORC. Due to the variable temperature and flow rate of the grate cooler air, the ORC system was preferred to the more common SRC. The WH from the clinker cooler air was transferred to the ORC by a thermal oil loop. The grate cooler air temperature fluctuated between 340°C and 180°C causing the thermal oil to fluctuate between 230°C and 120°C. Coping with such fluctuations, the power generated varied in the range 0.4÷1.5 MW (Legmann, 2002). Similar plants are under construction or in the commissioning phase such as a 4 MW ORC plant in Alesd, (Romania), a 5 MW plant in Rohoznik (Slovakia) and a 1.9 MW plant in Untervaz (Switzerland) (Colonna et al., 2015). Most of these installations use an intermediate thermal oil loop to transfer the thermal energy to the ORC working fluid.

Theoretical investigations and case studies. The thermodynamic and economic performance of basic and RC ORCs working under subcritical and subcritical conditions were investigated in (Moreira & Arrieta, 2019) for WHR in Brazilian cement factories. The main sources of WH used for the ORC were thermal energy from the suspension preheater exhaust gas and hot air from the clinker cooler discharge. The authors showed that the best WF was R141b (i.e., the WF having the highest critical temperature among those considered) both in the basic and RC configurations. The gain in power output deriving from the RC configuration was significant (around 20%) compared to the simple layout. In the analysis carried out by (Fergani et al., 2016) an intermediate heat transfer loop with thermal oil was used to transfer heat from the kiln exhaust gas to the WF. Fluids with high critical temperatures in the range 280÷320°C were selected for the analysis. The results of the optimization showed that cyclohexane provided the highest power output. In (Huarong Wang et al., 2015) only the hot dry air at the kiln cooler outlet was considered as the WH source for the ORC. The authors found that the best WF was R601. In the ORC system analysed in (Jiangfeng Wang et al., 2009) the WF at the outlet of the pump is split into two streams that are preheated, vaporized and superheated by the exhaust gas and by the clinker cooler in parallel.

- **Food industry**

Chips manufacturing. The potential of recovering the WH from both the fryer section and exhaust stream sent to the stack of a typical potato crisps/chips manufacturing plant using an ORC was investigated in (Aneke, Agnew, Underwood, Wu, & Masheiti, 2012). Crisps frying involve passing the crisps through hot cooking oil, which is heated using heat from the combustion chamber. After

Horizon 2020 European Union Funding for Research & Innovation
This project has received funding from the European Union's Horizon 2020 research and innovation programme under grant agreement No 847097

heating the oil, the flue gases are emitted from the process through the industrial exhaust stack. Also during the cooking operation, some hot polluted air (foul gas which is mainly hot vaporized cooking oil) is emitted from the fryer. This is either recycled back into the combustion chamber or emitted into the environment (Figure 112). Different ORC systems were analysed to maximize the power output from the two WH streams. The maximum power output was obtained when the foul gas was used to preheat the WF, whereas the exhaust gas was used to complete the preheating process and to evaporate the WF (Table 58).

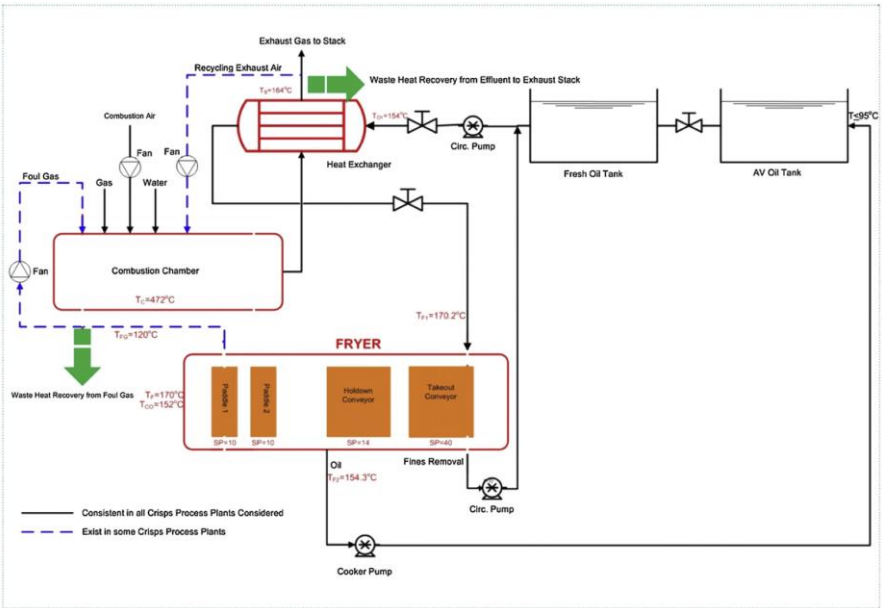

Figure 112: Process flow diagram of crisps manufacturing process showing the two WH streams available for the ORC (Aneke et al., 2012).

Coffee roasting. Coffee roasting is a process that converts green coffee beans into beans that can be ground, brewed and consumed with a complex aroma and flavour. In the case of batch coffee roasters, the roasting happens in cycles in which the green coffee beans enter the roasting drum and are heated to the desired temperature of 200÷250 °C before being transferred to a cooling chamber (Figure 113a). Coffee roasting is a highly energy intensive process wherein a large quantity of heat is discharged from the stack at medium/high temperatures (350÷400°C). Much of the heat is released from the afterburner, which is required to remove volatile organic compounds and other pollutants from the flue gases. In (Pantaleo, Fordham, Oyewunmi, De Palma, & Markides, 2018) the WHR from the hot flue gases using an ORC was investigated. The operation of the ORC system was decoupled from the intermittent heat source using a pressurized water STES (Figure 113b). The economic results were satisfactory, with PBT ranging between 5 and 11 years, only for roasting plants with high production capacities (18 hours per day).

Horizon 2020
European Union Funding
for Research & Innovation

This project has received funding from
the European Union's Horizon 2020 research and innovation
programme under grant agreement No 847097

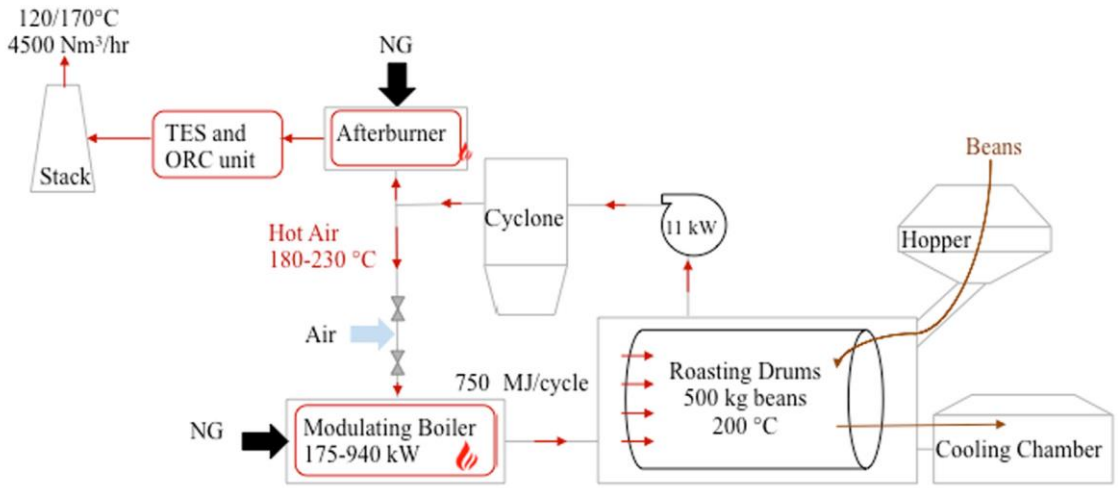

a)

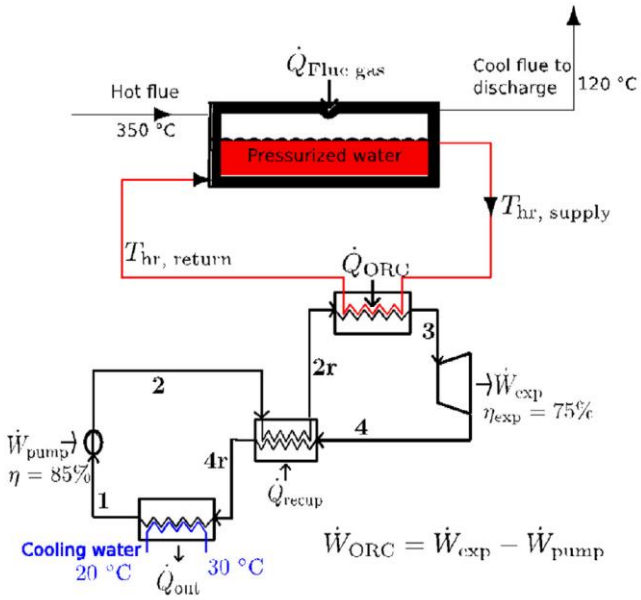

b)

Figure 113: a) Schematic of the coffee roasting process with WHR from the flue gases using an ORC; b) Schematic of the pressurized-water heat recovery unit and the ORC system with the RC layout (Pantaleo et al., 2018).

Table 58: Main features and performance of ORCs for WHR in the food industry.

TRL	Process	Type heat source	T heat source (°C)	HTF loop and T(°C)	ORC Layout	Working fluid	Power output (kW)	Thermal efficiency (%)	Reference
N/A	Chips frying	a) Foul gas from the fryer b) Exhaust gas	a) 120 b) 164	/	Basic	R245fa	213	15	(Aneke et al., 2012)

Horizon 2020
European Union Funding
for Research & Innovation

This project has received funding from the European Union's Horizon 2020 research and innovation programme under grant agreement No 847097

N/A	Coffee roasting	Flue gases exiting the afterburner	350 ÷ 400	Pressurized water (100÷ 150°C)	RC	butane, pentane, R227ea, R245fa, and R1234ze	25 ÷ 33	9.0 ÷ 11.5	(Pantaleo et al., 2018)

- **ICE exhausts**

Table 59 summarizes the main features and the performance of selected real installations and case studies for WHR from ICEs using ORC units. A more detailed description is reported in the following for each plant. In this application the main issue is related to the effective utilization of heat from the two main heat sources (exhaust gases and engine coolant) having very different temperature levels. The real application reported in (Linnemann, Priebe, Heim, Wolff, & Vrabec, 2020) demonstrates that the dual loop (i.e., cascade) ORC layout is close to commercialization.

Table 59: Main features and performance of ORCs for WHR from the engine exhausts.

TRL	Type ICE	Power of ICE (kW)	Type heat source	T heat source (°C)	HTF loop	Layout	Working fluid	Power (kW)	Thermal efficiency (%)	Reference
9	Biogas	600	a)Exhaust gas b)Engine coolant	a)468÷519 b) 90	No	DL	Toluene (HT) Solkatherm SES36 (LT)	85	15	(Linnemann et al., 2020)
N/A	Gas	1000	a)Exhaust gas b)Jacket water	a) 540 b) 80	Yes	Basic	R123, R245fa, R114 and R141b	80 ÷ 120	9 ÷ 14	(G. Shu et al., 2016)
N/A	Gas	1000	a)Exhaust gas b)Jacket water	a) 540 b) 80	No	Basic	benzene, toluene, decane, cyclohexane, D4 and MDM	130 ÷ 150	16 ÷ 19	(G. Shu et al., 2016)
N/A	Gas	23375	a) Charge air b)Jacket water c) Lubricating oil	a) 170 b) 80 c) 75	Yes	Basic; RC; DP	R134a, R125, R236fa, R245ca, R245fa, R227ea	430 ÷ 820	6÷8	(Soffiato, Frangopoulos, Manente, Rech, & Lazzaretto, 2015)

In (G. Shu et al., 2016) the WFs were classified in two categories according to their decomposition temperature. The low temperature WFs (e.g., R245fa) required an intermediate heat transfer loop between exhaust gases and WF to prevent their decomposition (Figure 114 left). Instead, a direct heat transfer between exhaust gases and WF (Figure 114 right) was possible when using WFs with a high decomposition temperature (e.g., cyclohexane and siloxanes). The authors showed that the high temperature WFs (especially toluene and benzene) outperform the low temperature ones in term of thermal efficiency and power output from the engine. On the other hand, the condensation pressures of the high temperature WFs are much lower than the atmospheric pressure, which implies an expensive multi-stage turbine design and operational issues to keep the vacuum in the condenser. Thus, they finally suggested the dual loop (i.e., cascaded) ORC system as the best design that is composed by a topping ORC cycle using toluene and a bottoming ORC cycle using R245fa. The low

Horizon 2020 European Union Funding for Research & Innovation
This project has received funding from the European Union's Horizon 2020 research and innovation programme under grant agreement No 847097

temperature ORC recovers heat from the condensation heat of the topping cycle, the jacket water and the residual heat of the exhaust gas (G. Shu et al., 2016).

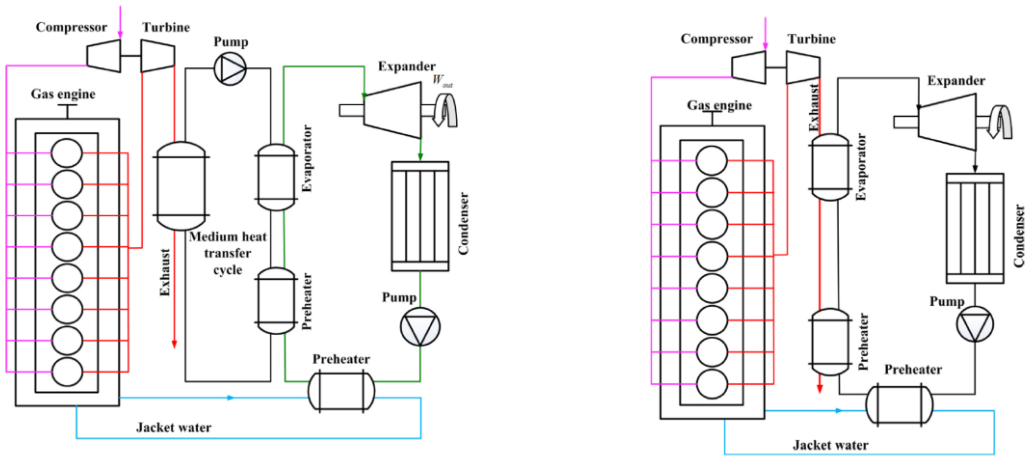

a) *b)*

Figure 114: Schematic diagram of a simple ORC for WHR from an engine: a) ORC with heat transfer loop between exhaust gases and organic fluid; b) ORC with direct heat transfer between exhaust gases and working fluid (G. Shu et al., 2016).

Biogas engine. A dual loop (i.e., cascade) ORC plant was designed, built and field tested to improve the WHR from a biogas engine (Linnemann et al., 2020). Figure 115 shows the schematic of the cascaded ORC. Heat from the exhaust gas is utilized with a high temperature ORC (HT-ORC), where toluene is employed as the WF. The heat discharged from the HT-ORC as well as heat from the engine coolant and additional heat from the exhaust gas is supplied to a low temperature ORC (LT-ORC) with the WF Solkatherm SES36. A direct evaporator (process 2–3 in Figure 115) is used in the HT-ORC where the WF is directly heated from the exhaust gas. A fan is used to take off a part of the cooled exhaust gas after HE 1 and mix it with the hot exhaust gas in front of the direct evaporator. Thus, the mass flow rate was increased, which led to a better heat transfer, while a lower temperature of the exhaust gas decreased the risk of thermal decomposition of the WF in the direct evaporator. Instead in the LT-ORC the heat is transferred to the evaporator using a water loop (IC in Figure 115), which allows for a higher degree of independence between the two working cycles and therefore to an improved operational behaviour (Linnemann et al., 2020).

Horizon 2020
European Union Funding
for Research & Innovation

This project has received funding from
the European Union's Horizon 2020 research and innovation
programme under grant agreement No 847097

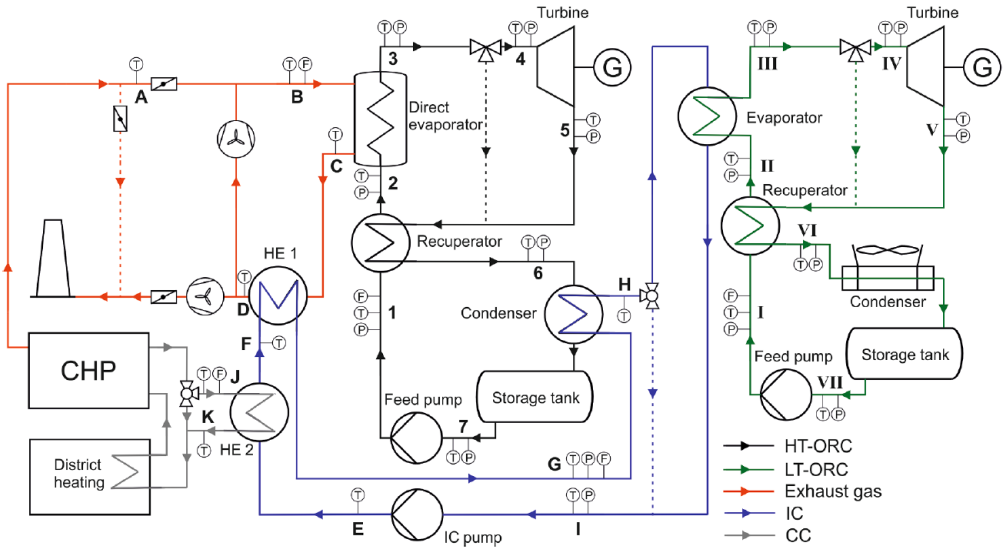

Figure 115: Process flow diagram of the cascaded ORC plant for WHR from a biogas engine (Linnemann et al., 2020).

Marine engines. The WHR from large size ICEs installed in large ships was investigated in (Soffiato, Frangopoulos, Manente, & Lazzaretto, 2014). Since the exhaust gas was already used in WHB for steam generation for ship internal uses, the available heat sources for the ORC were the jacket water, the lubricating oil and the charge air. Due to the low temperature of the WH streams and the segmented form of the hot composite curve the thermal efficiency was less than 10%. However, when also the exhaust gas is available for WHR higher efficiencies can be achieved. The German company Orcan Energy AG sells ORC units (commercialized under the name of "Efficiency Pack") for WHR from marine ICEs. These off-the-shelf units have an input power of ≈ 1 MWt thermal and can use as heat sources: Exhaust gas (max. 550 °C), saturated steam (120÷180 °C), thermal oil (120÷180 °C) and warm water (e.g., from jacket cooling, 75÷109 °C) ("Orcan Energy AG," 2020). Smaller ORC units (200÷500 kW of thermal input) for industrial WHR are sold by the same company. They use liquid heat sources above 80°C (ideal 140°C) and gaseous heat sources above 150°C ("Orcan Energy AG," 2020).

- **Gas turbine exhaust gases**

Two case studies of WHR from gas turbines using ORC systems are reported in Table 60. The choice of an ORC unit in place of the more common SRC can be justified by the small size of the system. For larger power capacities the selection of WFs having high critical temperatures (like toluene) can provide relevant thermal efficiencies.

Table 60: Main features and performance of ORCs for WHR from the gas turbine exhausts.

TRL	Application of gas turbine (kW)	T heat source (°C)	Layout	Working fluid	Power output (kW)	Thermal efficiency (%)	Reference
9	NG compression station	416	Basic and RC	Cyclohexane, Benzene	1900 ÷ 2200	15÷19	(Khatita, Ahmed, Ashour, & Ismail, 2014)
9	NG compression station	446 ÷ 548	RC	Cyclopentane, MM	700 ÷ 7000	16.4 ÷ 24	(M. Bianchi et al., 2019)
9	Offshore platforms	510	Basic and RC	Toluene	11900 ÷ 13400	24.6 ÷ 28.4	(Reis & Gallo, 2018)

Horizon 2020
European Union Funding
for Research & Innovation

This project has received funding from
the European Union's Horizon 2020 research and innovation
programme under grant agreement No 847097

Gas turbines in NG compression stations. An existing upstream gas treatment facilities in Egypt treats NG extracted from a number of offshore wells. Gas compression from 5.5 bar to the network delivery pressure (50÷55 bar) is obtained via a two stage intercooled compressor driven by a gas turbine that typically runs at 70% load. It was shown in (Khatita et al., 2014) that the recovery of the exhaust gases using an ORC system generates a power output of 2 MW using cyclohexane or benzene and a RC plant configuration. In (M. Bianchi et al., 2019) commercial gas turbine models, in the size range 3÷30 MW, were taken into account as representative of mechanical driver units in NG compressor stations. ORC configurations with and without an intermediate thermal oil loop were modelled and compared considering a RC layout and two WFs having high crtitical temperatures. The estimated PBT for WHR from a mid-size GT (11 MW) was 7 years. Fifteen ORC plants manufactured by ORMAT for WHR in NG compression stations were installed in North America since 1999 for a total electric power greater than 75 MW (Gómez-Aláez et al., 2017) .

Gas turbines in offshore platforms. In the WHR from the gas turbines equipping an offshore oil platform, thermal efficiencies as high as 28% were calculated for a large scale (12 MW) ORC unit using toluene as WF, a RC layout and a turbine inlet temperature of 300°C (Reis & Gallo, 2018).

5.2.3 Cost aspects

Figure 116 displays a review of published data on estimated ORC investment costs presented in (Lemmens, 2016). The references concern estimates of ORC costs because reporting on real ORC costs still remains rather scarce. The specific investment costs (SIC) are presented as a function of capacity (kW). The data has been categorized according to the scope of the system and the heat source. The scope refers to either an ORC module (M), which comprises only the essential components of the ORC itself without integration or installation, or an ORC project (P), including all expenses needed to integrate and install the ORC module. The heat sources are classified into four groups: geothermal, biomass, waste heat recovery (green marks), and solar. To allow for comparison, the costs were converted to Euros and updated to 2014 values. The WHR ORC systems are more represented in the middle power range, with estimated module costs around 2780 €/kW and averaging project costs of 3414 €/kW.

Horizon 2020
European Union Funding
for Research & Innovation

This project has received funding from
the European Union's Horizon 2020 research and innovation
programme under grant agreement No 847097

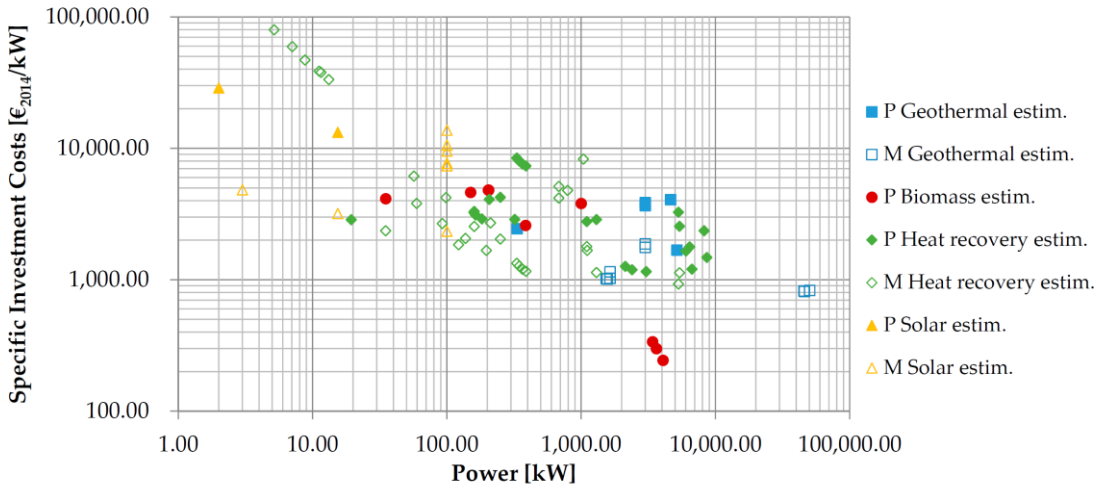

Figure 116: Estimated costs of ORC Projects (P) and Modules (M) in the literature. The WHR applications are reported using green marks (Lemmens, 2016).

A similar map was presented previously in (Quoilin, Broek, Declaye, Dewallef, & Lemort, 2013) using data from scientific publications and from ORC manufacturers. This map, reported in Figure 117, shows that the WHR applications have the lowest investment costs among all the applications of ORCs. The module cost reported was between 1000÷2000 €/kW for installations having a capacity higher than a few hundred kWs. On the other hand, the total cost (that includes engineering, buildings, process integration, etc.) was two to three times higher than the module cost.

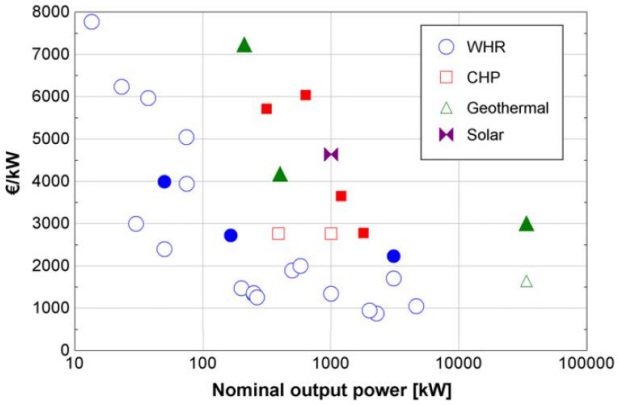

Figure 117: Module (empty dots) and total (full dots) cost of ORC systems depending on the target application and on the net electrical power (Quoilin et al., 2013).

The consulting and technology services company ICF ("ICF International," 2019) recently reviewed in-house data, published literature, and held discussions with industry stakeholders to develop cost estimates for commercially available ORC systems. The results of ICF's cost analysis are shown in Table 61 extracted from (Oak Ridge National Laboratory, 2015). ORC capital costs range from 1890 to 4050 €/kW as a function of capacity. O&M costs range from 0.9 to 1.8 cents €/kWh. The installed

Horizon 2020
European Union Funding
for Research & Innovation

This project has received funding from
the European Union's Horizon 2020 research and innovation
programme under grant agreement No 847097

capital costs likely do not contain contingency for site specific characteristics that can significantly increase costs for actual installations.

Table 61: Capital costs and O&M costs of ORCs in WHR applications (Oak Ridge National Laboratory, 2015).

Electric capacity of the WH ORC (kW)	Installed capital cost (€/kW)	Operation and maintenance costs (c€/kWh)
50÷500	4050	1.8
500÷1000	3600	1.35
1000÷5000	2700	1.17
5000÷20000	2250	1.08
>20000	1890	0.9

Horizon 2020
European Union Funding
for Research & Innovation

This project has received funding from
the European Union's Horizon 2020 research and innovation
programme under grant agreement No 847097

5.3 Kalina cycles (KCs)

5.3.1 Technological features and performance

Kalina cycles (KCs), similarly to SRC and ORC technology, belong to the class of power cycles for conversion of low/medium temperature WH into electricity. The main feature of KCs is the use of the ammonia-water zeotropic mixture as WF in order to maximize the conversion of WH into power (Saghafifar, Omar, Mohammadi, Alashkar, & Gadalla, 2019). Several architectures of KC have been developed to optimize the power output from WH sources or renewable resources at different temperature levels. Figure 118 illustrates the typical KC architectures for: a) low temperature application (Figure 118 left) called KC system 34 (KCS34); b) medium-high temperature applications (Figure 118 right) called KC system 12 (KCS12).

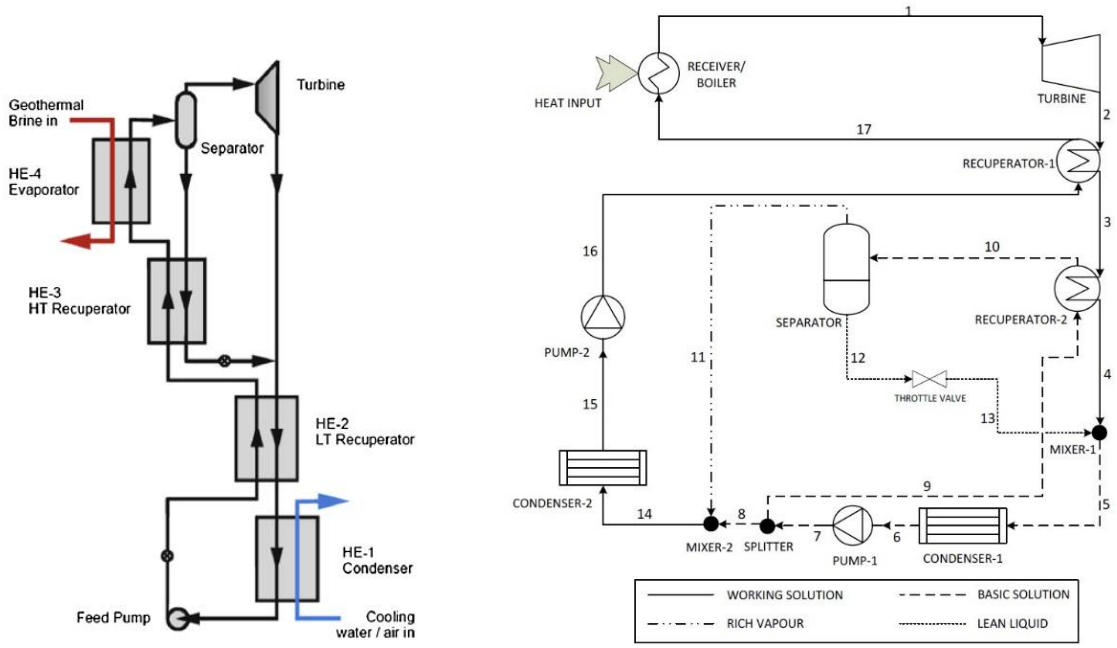

a) b)

Figure 118: Typical layouts of the Kalina cycle for: a) low temperature application (KCS34) (E. Wang & Yu, 2016); b) medium-high temperature applications (KCS12) (Modi, Knudsen, Haglind, & Clausen, 2014)).

The ammonia–water mixture has varying evaporation and condensing temperatures. For instance, Figure 119 shows the variation of the evaporation temperature for different ammonia water-mixtures (from pure ammonia to pure water) considering an evaporation pressure of 30 bar. The mixture of ammonia and water boils at a variable temperature depending on its composition. The higher the fraction of ammonia in the mixture, the lower is its boiling temperature (Ogriseck, 2009). When the liquid mixture is heated, the more volatile ammonia tends to vaporize first and at a lower temperature than does pure water. This property of the ammonia-water mixtures enables a better match to the enthalpy-temperature curve of a hot gas heat source, such as a gas turbine exhaust (Marston, 1989).

Horizon 2020 European Union Funding for Research & Innovation
This project has received funding from the European Union's Horizon 2020 research and innovation programme under grant agreement No 847097

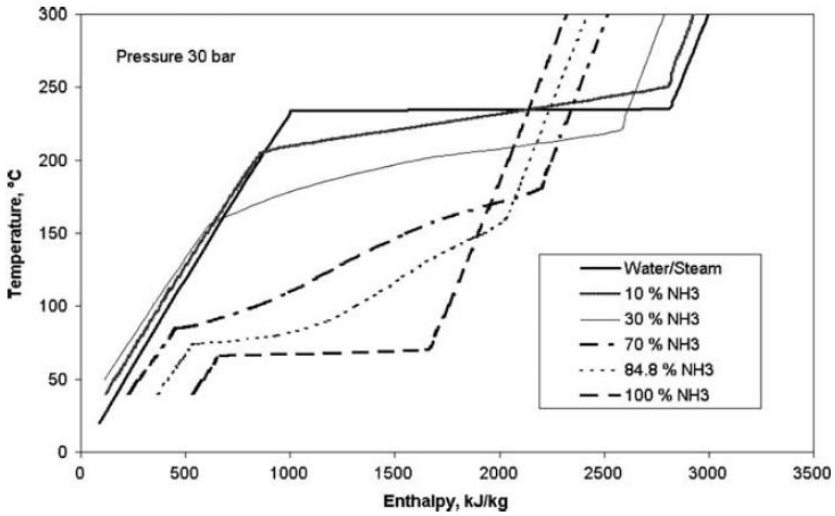

Figure 119: Comparison between boiling of pure water and different ammonia–water mixtures at 30 bar (Ogriseck, 2009).

Besides the improved thermal match with the heat source, one of the key feature of the KC technology, especially for medium/high temperature applications, consists in the ability to vary the ammonia-water concentration throughout the power plant system to optimize energy conversion, and to add heat recuperative stages for increased efficiency. In KCS12 (Figure 118 right) the composition of the working fluid is varied through the use of a distillation subsystem, providing a richer concentration in the heat acquisition stage (HRVG) and leaner composition in the low-pressure condenser (M. D. Mirolli, 2005).

5.3.2 Examples of applications, technology maturity and performance of KCs

Typically, KC technology has been considered for recovery of WH available in the temperature range 90÷600°C (Saghafifar et al., 2019). Presently, a limited number of commercial-scale installations of KC have been operated. Most of the KC installations were developed by Global Geothermal Ltd (Global Geothermal - Advanced Waste Heat Engineering, 2019) which, together with Kalina Power Ltd ("Kalina Power," 2019), appears to hold most of the patents around KC technology and be the major suppliers of KC solutions. These companies provide build and operation tailored KC solutions for energy intensive industries (Steel, Cement, Glass, etc.). Further KC applications for WHR have been proposed in the scientific literature. Estimation of techno-economic performance for KC technology also comes primarily from scientific literature. However, the vast majority of the investigations are either theoretical or modelling work, with limited experimental/pilot demonstration and validation. Table 62 reports applications of KC technology for WHR in the industrial sector and the corresponding features of the heat source and performance parameters. In the following the integration of the KC in these different industrial contexts is summarized with a special focus on the real systems (TRL=9).

Horizon 2020
European Union Funding
for Research & Innovation

This project has received funding from
the European Union's Horizon 2020 research and innovation
programme under grant agreement No 847097

Table 62: Kalina cycle plants for WHR in the industrial and power sectors: features of the heat source and performance.

TRL	Type of industry/system	Type heat source	Temperature heat source (°C)	Power output (kW)	Thermal efficiency (%)	Reference
9	Steel (Kashima Steel Works, Japan)	Oxygen converter gas	98	3450	10.4	(Global Geothermal, 2019)
9	Petrochemical (Fuji Oil, Japan)	Condensing overhead vapours	116	3300	7.1[a] 8.0[b]	(K. Matsuda, 2013)
9	Cement (DGKhan, Pakistan)	a) Exhaust gas and b) clinker cooler	≈360	8600	/	(McCaffrey, 2018)
9	Cement (Star Cement, UAE)	Clinker cooler only	/	4750	/	(M. Mirolli & Gibbons, 2012)
N/A	Chemical (Benzene, toluene, p-xylene separation)	Overhead vapour	179	1362	20.0	(Chew, Reddy, & Rangaiah, 2014)
N/A	Industry (generic)	Thermal oil	200	278	11.7	(Hua, Chen, Wang, & Roskilly, 2014)
N/A	Industry (generic)	/	300	739.4	21.7	(Hua, Chen, Wu, Zhi, & Dong, 2015)
N/A	Power	Flue gases from coal combustion	150 (inlet) 130 (outlet)	320÷440	12.3÷17.1[a] 13.5÷18.8[b]	(Ogriseck, 2009)
N/A	Cement	exhaust gases of the cyclone preheater of the rotary kiln	390	2430	23.3	(Júnior, Arrieta, Arrieta, & Silva, 2019)
N/A	Engine	Diesel engine a) exhaust gases and b) coolant	a) 524.9 b) 86.8	21.7	25.6	(Mohammadkhani, Yari, & Ranjbar, 2019)
N/A	Engine	Exhaust gas	439	217	18.8	(Yue, Han, Pu, & He, 2015)
N/A	Engine	Exhaust gas	346	1615	19.7	(Bombarda, Invernizzi, & Pietra, 2010)
5	Gas turbine	Exhaust gas	566	3137	28.6	(A. I. Kalina & Leibowitz, 1988)
N/A	Gas turbine	Exhaust gas	550	/	30÷33	(Nag & Gupta, 1998)
			522	86136	35.6	(A. I. Kalina, Leibowitz, Markus, & Pelletier, 1991)
			550	/	30.7÷32.7	(Marston, 1989)
			560	2700	32.9	(A. I. Kalina, 1984)

[a] net thermal efficiency; [b] gross thermal efficiency.

Horizon 2020 European Union Funding for Research & Innovation

This project has received funding from the European Union's Horizon 2020 research and innovation programme under grant agreement No 847097

- **Cement industry**

Heat recovery from the exhaust gases. The KC layout considered in (Júnior et al., 2019) for WHR from the exhaust gases of the cyclonic preheater of the rotary kiln in a cement industry is shown in Figure 120 (left). The ammonia/water mixture is heated in the economizer, evaporated in the evaporator and sent to a liquid/vapour separator. The ammonia-rich vapour leaving the separator is superheated and expanded through the turbine to generate power. The exhaust vapour from the turbine is mixed into the depressurized ammonia-poor liquid leaving the separator. This mixture is first cooled in the low temperature recuperator and then it is condensed by rejecting heat in the condenser. The liquid is pressurized in the pump and is preheated in the low and high-temperature regenerators before returning to the economizer.

Heat recovery from both the exhaust gases and the hot air. Figure 120 (right) shows the schematic of the KC configuration investigated in (M. D. Mirolli, 2005) and (M. D. Mirolli, 2007) for WHR from the preheater exhaust gases and the clinker cooler hot exit air. Two HRVGs are provided, one for the exhaust gases (HRVG-1) and one for the hot air (HRVG-2). A rich mixture of water and ammonia is boiled and superheated in the HRVGs and the superheated vapour is expanded in the turbine. Since the turbine exhaust is too rich (high ammonia concentration) to condense, it is cooled and diluted with the bottoms from the vapour separator/demister, and is then fully condensed in the low pressure condenser (LPC). At this stage, part of the WF is sent to the vapour separator/demister through recuperative HEs and part of the WF is mixed with the high ammonia concentration vapour stream from the vapour separator/demister. This process restores the WF to the optimum ammonia-water concentration for the heat acquisition stage of the cycle. The WF is then condensed in the high pressure condenser (HPC) and returned to the HRVGs (M. D. Mirolli, 2005). The 8.6 MW Kalina cycle installed at the DG Khan Cement plant at Khairpur (Pakistan) reaches a fluid temperature of 340°C and recovers WH from the preheater exhaust and from the clinker cooler using the KCS12 layout which is especially suited for the cement industry (McCaffrey, 2018).

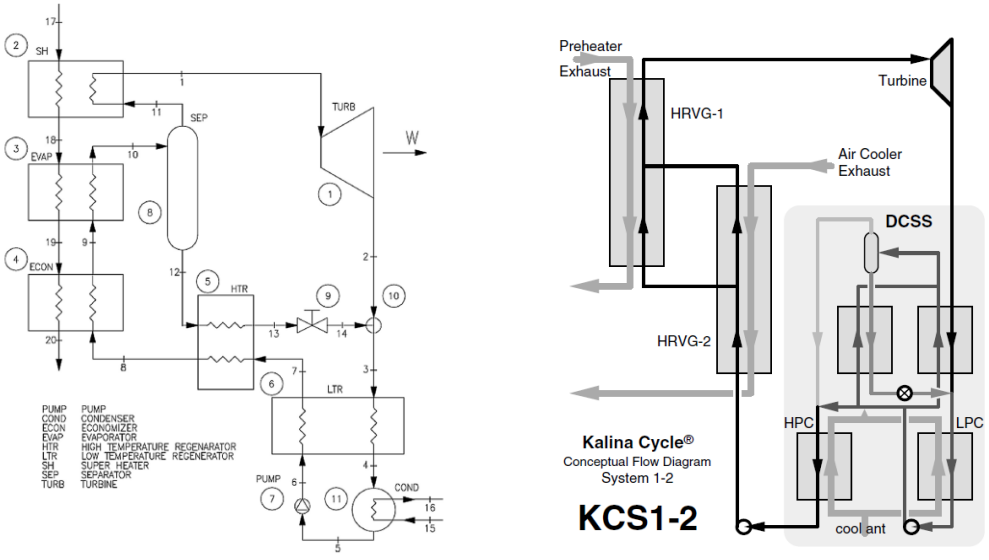

a) *b)*

Figure 120: Kalina cycle for WHR in cement industry: a) WHR from the exhaust gases (Júnior et al., 2019); b) WHR from the exhaust gases and clinker cooler hot air (M. D. Mirolli, 2005) (M. D. Mirolli, 2007).

Horizon 2020
European Union Funding
for Research & Innovation

This project has received funding from
the European Union's Horizon 2020 research and innovation
programme under grant agreement No 847097

- **Steel industry**

The KC power plant installed at Kashima Steel Works (Figure 121) is based on the low temperature KC layout shown in Figure 122. The ammonia-water mixture is partially evaporated in the evaporator by using the cooling water at 98°C from the OCGR (Oxygen Converter Gas Recovery) of the steel-making plant as the heat source. The ammonia-rich vapour leaving the top of the separator at 95°C drives the turbine to generate electric power and after the expansion it enters the condenser. The liquid leaving the bottom of the separator exchanges heat in the preheater and enters into the condenser where it absorbs the ammonia rich vapour exhausted from the turbine and condenses. The liquid leaving the condenser is pumped and fed back to the evaporator via the preheater. The performance of the Kalina plant exceeded the design specifications and operated trouble-free with an operating rate above 96% (Global Geothermal, 2019).

Figure 121: Photo of the low temperature 3.5 MWe Kalina power plant installed in a steel industry (Kashima Steel Works) in Japan (Global Geothermal, 2019).

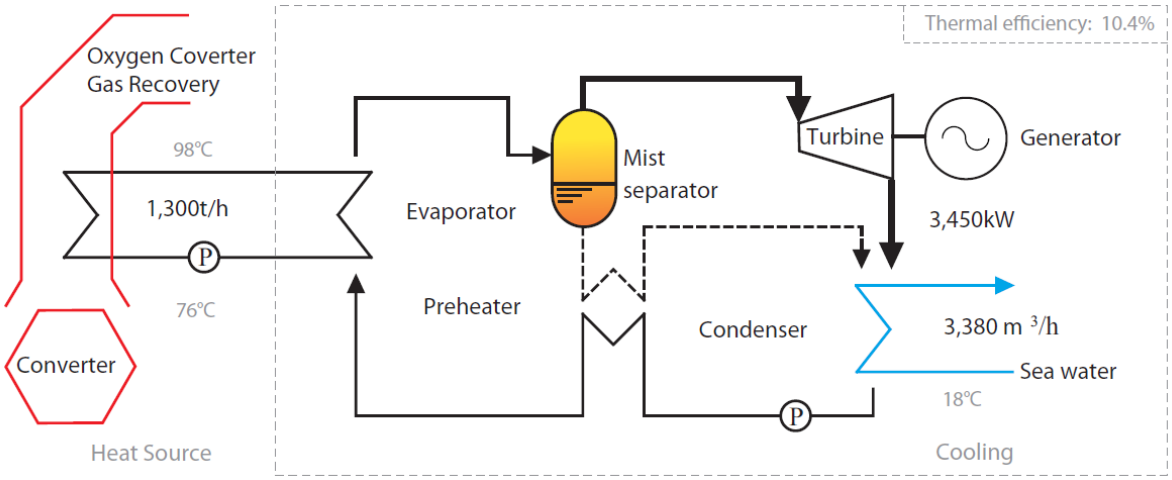

Figure 122: Schematic layout of the low temperature Kalina cycle for WHR from a steel industry (Kashima Steel Works) in Japan (Global Geothermal, 2019).

Horizon 2020 European Union Funding for Research & Innovation

This project has received funding from the European Union's Horizon 2020 research and innovation programme under grant agreement No 847097

- **Petrochemical and chemical industry**

Oil refining. The Fuji Oil 4 MW Kalina plant (Figure 123) uses heat from two sources, a lightweight hydrocarbon vapour and a low-pressure steam (Pilodia, Wanve, Maheshwari, & Kumar, 2018). A schematic of the plant flowsheet is shown in Figure 124. The overhead vapour is used as heat source in the evaporator where the ammonia-water mixture is heated and vaporized at a pressure of approximately 30 bar. After the separator, the high-pressure ammonia-rich vapour is superheated by low pressure steam that in summer often becomes surplus in the industrial site. The superheating is beneficial in increasing the power generation and reducing the amount of the liquid drop entrainment which otherwise would cause erosion in the turbine (Kazuo Matsuda, 2014). The KC installed at the Fuji oil plant was able to perform continuously, safely and reliably, despite fluctuating conditions reaching an annual operating rate of 97%.The multi-stage structure of the KC was required because the plot area for the power generation system was limited (20 m x 24 m) and the Kalina cycle utilized a high elevation vapour line for the evaporator (Kazuo Matsuda, 2014).

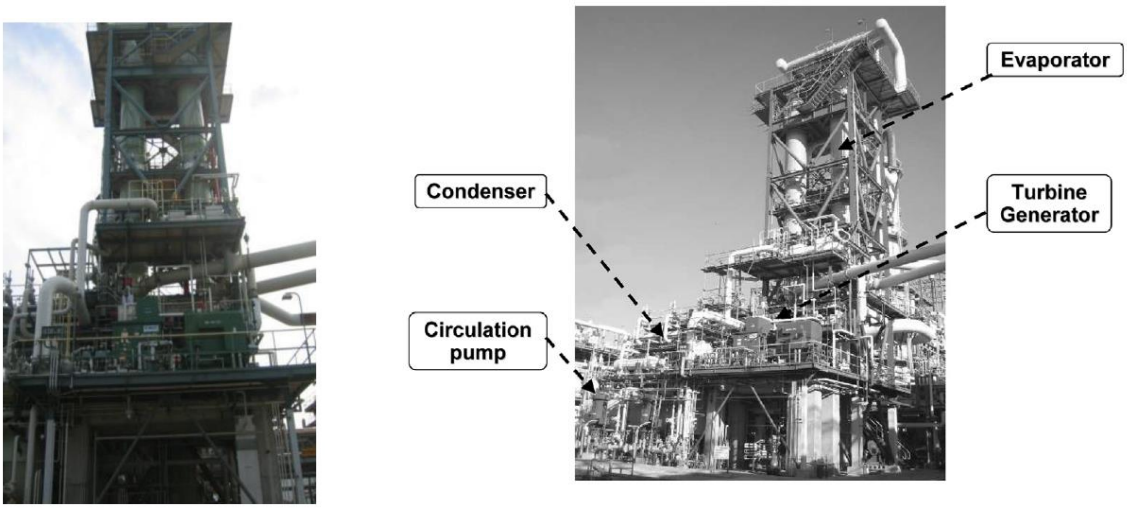

a) *b)*

Figure 123: Photos of the 4 MW Kalina plant installed in a petrochemical plant (Fuji Oil) in Japan: a) front view (Recurrent Engineering LLC, 2013); b) black and white photo with the main components (Kazuo Matsuda, 2014).

Horizon 2020
European Union Funding
for Research & Innovation

This project has received funding from
the European Union's Horizon 2020 research and innovation
programme under grant agreement No 847097

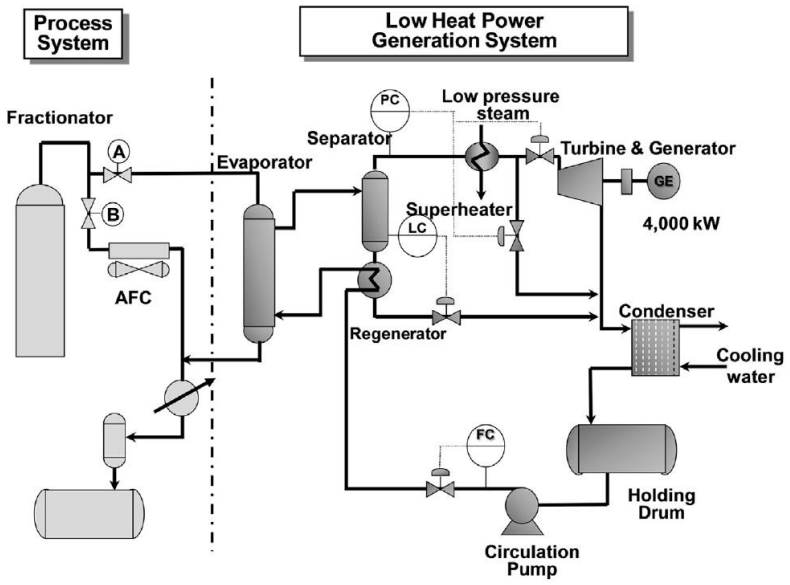

Figure 124: Schematic layout of the low temperature KC for WHR from a petrochemical industry (Fuji Oil) in Japan (K. Matsuda, 2013).

Separation processes. In a distillation column, the latent heat of condensation of the overhead is available at the condenser as significant WH, which can be recovered to generate electric power. The potential of the KC for WHR from three industrial-scale distillation applications for separation of ternary mixtures was investigated in (Chew et al., 2014). These applications are: 1) alkanes separation; 2) benzene, toluene, ethylbenzene (BTE) separation; 3) benzene, toluene, p-xylene (BTX) separation. The temperatures of the vapour overhead in the first two separation applications (93°C and 97.3°C, respectively) were considered too low for profitable electricity generation. Instead, the WHR using the KC was considered for the third separation process (i.e., BTX). The schematic layout is shown in Figure 125 where the heat input for the KC is provided by the condenser of the distillation column.

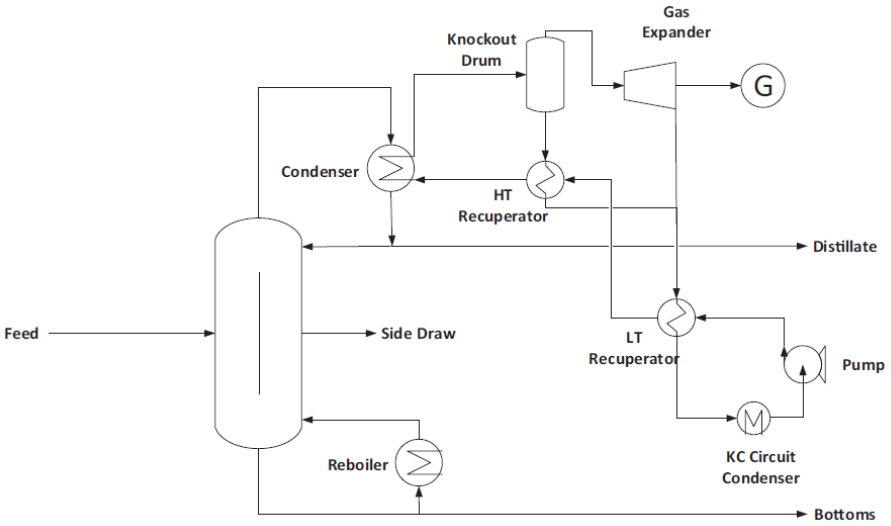

Figure 125: Kalina cycle for WHR from the vapour overhead in the distillation processes in the chemical industry (Chew et al., 2014).

Horizon 2020 European Union Funding for Research & Innovation
This project has received funding from the European Union's Horizon 2020 research and innovation programme under grant agreement No 847097

- **Power industry**

The application of a low temperature KC for WHR from a coal fired CHP plant at the Industrie-park Hoechst in Frankfurt (Germany) was investigated in (Ogriseck, 2009). In the original plant the flue gas was cooled down from 150 to 130°C with water injection before entering the dry flue gas treatment system. In the retrofitted plant the temperature range between 150 and 130°C was considered suitable for WHR using the KC. The author considered the same low temperature KC layout implemented at the geothermal plant in Husavik (KCS34, Figure 118 left) but considered higher evaporation pressures up to 70 bar due to the higher temperature of the heat source (Figure 126).

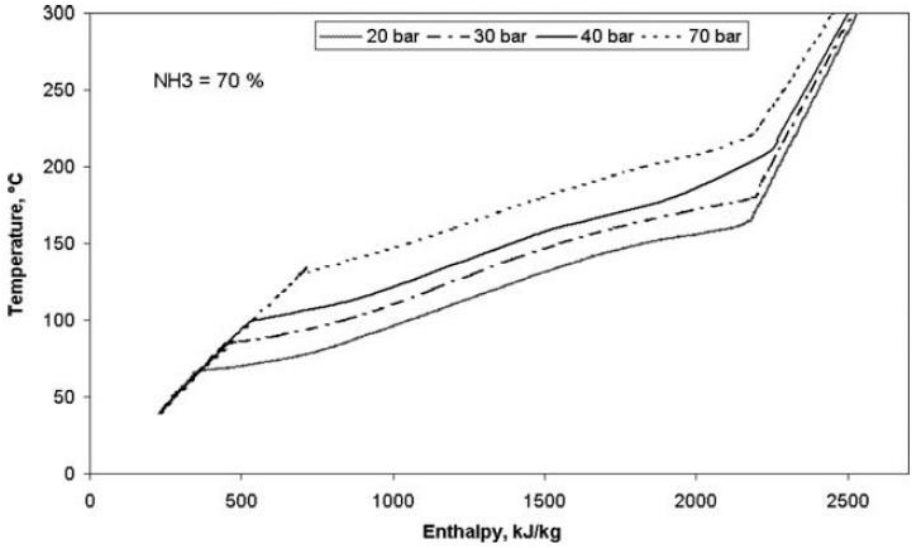

Figure 126: Variation of the evaporation temperature of the ammonia-water mixture (70 NH_3/30 H_20) for different evaporation pressures (20÷70 bar)(Ogriseck, 2009).

- **Exhaust gases from gas turbines**

The KC was originally conceived for the utilization of WH of the gas turbine in a NGCC power generation system (A. I. Kalina, 1984) with a WF composition of 70% ammonia/ 30% water in the evaporator. However, the envelope of peak efficiencies obtained in (Marston, 1989) suggested that operation with somewhat lower ammonia concentration at the turbine inlet could improve performance. Also in (Nag & Gupta, 1998) it was shown that the maximum cycle efficiency is obtained at moderate ammonia mass fractions (<70%) in the liquid mixture and high temperatures of the vapour entering the turbine. The main technological features and design performance of the first Kalina plant built in the late eighties in Canoga Park (California) is reported in (A. I. Kalina & Leibowitz, 1988). Due to its small size (3.1 MW) and some techno-economic constraints in the design, the plant had a design thermal efficiency of 28.6%, which is lower than the value calculated for optimized utility scale installations (≈33÷36%) (Table 62).

- **Waste heat from internal combustion engines**

The high temperature Kalina layout (KCS12, Figure 118 right) was selected by (Mohammadkhani et al., 2019) for the WHR from the exhaust gases and coolant of a turbocharged Diesel engine (Figure 127 left). The engine coolant was used to preheat the ammonia-water mixture leaving the feed pump before the high temperature recuperator. A similar KC plant scheme suited for high temperature WHR

Horizon 2020
European Union Funding
for Research & Innovation

This project has received funding from
the European Union's Horizon 2020 research and innovation
programme under grant agreement No 847097

was selected in (Bombarda et al., 2010) for WHR from the exhaust gases of two large maritime Diesel engines. Instead, the simpler KCS34 layout was considered in (Yue et al., 2015) for WHR from the exhaust gases (Figure 127 right).

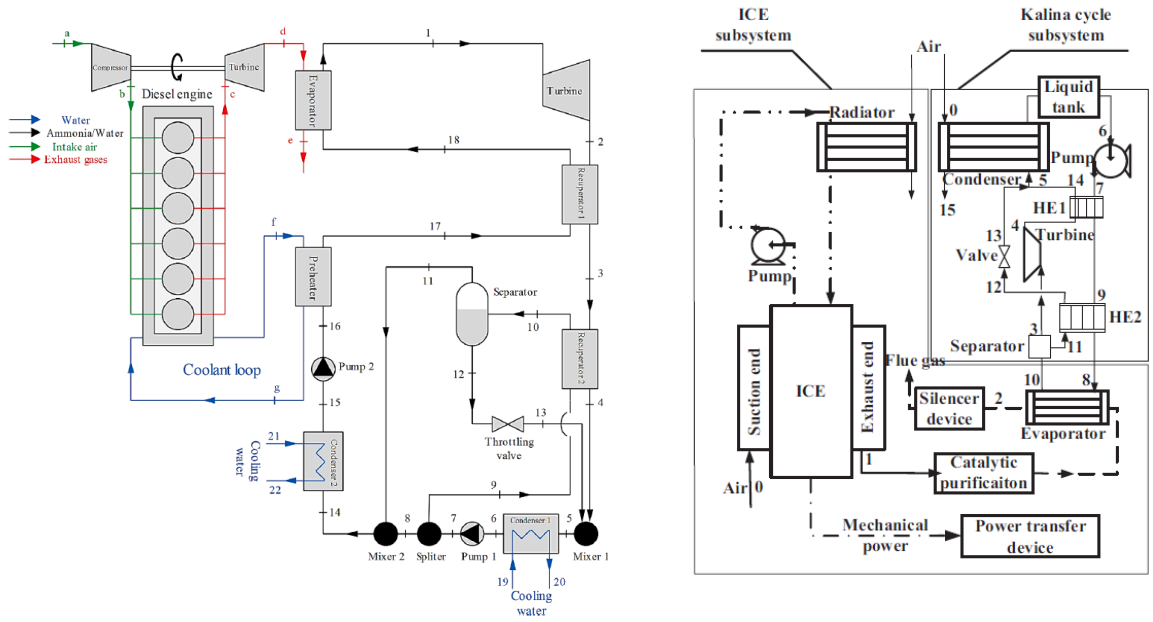

a) *b)*

Figure 127: Kalina cycles for WHR from ICEs: a) high-temperature KC for WHR from the exhaust gases and cooling water of a turbocharged Diesel engine (Mohammadkhani et al., 2019); b) Simpler layout considered by (Yue et al., 2015) for WHR from the exhaust gases.

- **Geothermal energy**

Another relevant commercial demonstration of KC technology is the Husavik facility installed in Iceland. In this instance the heat source driving the KC is a geothermal water flow with a temperature of 120°C (Mlcak, Mirolli, Hjartarson, Húsavíkur, & Ralph, 2002). The plant has operated reliably since 2002 generating a power output of 1.6 MW. The layout of the KC used for the Husavik plant is the Kalina Cycle System 34 (KCS-34) (Figure 128 centre). KCS34 features a brine evaporator that produces 70% quality vapour (Leibowitz & Micak, 1999). In a patent dated 2007 by Siemens the location of the recuperator in a KCS34 Kalina was changed to generate a new power cycle called KSG-1 (Figure 128 right) that can achieve high cycle efficiency and only requires a single-stage turbine (E. Wang & Yu, 2016). The KSG-1 layout was used in the more recent Kalina geothermal plant in Unterhaching, Germany (Figure 129), as presented in (Dawo, Wieland, & Spliethoff, 2019). A KC system designed for the utilization of relatively high temperature (above 148°C) geothermal sources is KC System 11 (KCS-11), a flow diagram of which is presented in Figure 128 (left). KCS-11 is not, in fact, fully a KC, as the composition of the WF does not vary throughout the cycle (A. Kalina, Kaiina, Dickson, & Moore, 2014).

Horizon 2020
European Union Funding
for Research & Innovation

This project has received funding from
the European Union's Horizon 2020 research and innovation
programme under grant agreement No 847097

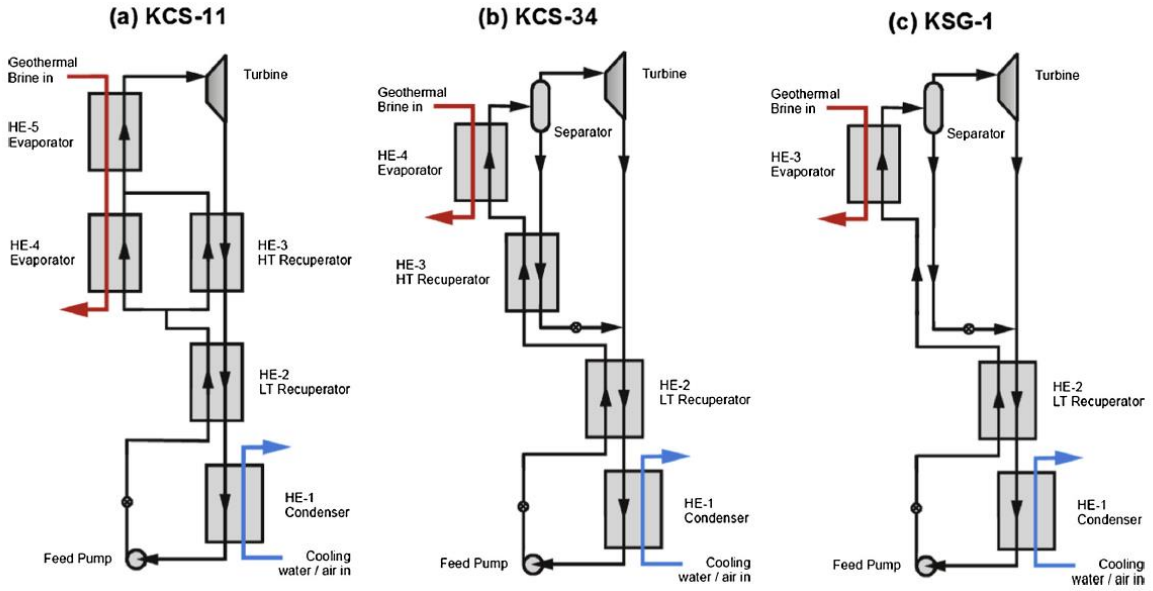

a) *b)* *c)*

Figure 128: Layouts of Kalina cycles for geothermal power plants (E. Wang & Yu, 2016): a) KCS-11; KCS-34 (Husavik); KSG-1 (Unterhaching).

Figure 129: Geothermal Kalina cycle at the Unterhaching site ("Unterhaching," 2019).

Similar to the ORC technology, the thermal conversion efficiency is the main performance parameter for KC technology. For the utilization of low temperature geothermal sources, claims in the literature indicate that KC has the potential to produce 15÷40% more power output that ORC technology for the same WH input (Lewis & Ralph, 2002) (Leibowitz & Micak, 1999). However actual data have so far demonstrated an increase of only about 3% (DiPippo, 2004). The main performance data of

Horizon 2020
European Union Funding
for Research & Innovation

This project has received funding from
the European Union's Horizon 2020 research and innovation
programme under grant agreement No 847097

geothermal KCs are shown in Table 63 where it appears that the typical thermal efficiency for a low temperature geothermal source is around 10÷11%.

Table 63: Main features and performance of the geothermal Kalina plants.

TRL	Type heat source	Temperature heat source (°C)	Power output (kW)	Thermal efficiency (%)	Reference
9	Geothermal (Husavik)	122	1700	10.6	(DiPippo, 2004) (Mlcak et al., 2002)
9	Geothermal (Unterhaching)	123.9	2360	/	(Dawo et al., 2019)
1	Geothermal	120	200.6	10.5	(S. Li & Dai, 2014)
1	Geothermal (EGS)	90÷140	5÷30	5÷11	(Campos Rodríguez et al., 2013)

- **Solar energy**

The KC for solar energy has been considered in combination with different solar thermal technologies: solar tower (Modi, Andreasen, Kærn, & Haglind, 2015); parabolic through collectors (Babaelahi, Mofidipour, & Rafat, 2019) (Ashouri, Khoshkar Vandani, Mehrpooya, Ahmadi, & Abdollahpour, 2015)(Jiangfeng Wang, Yan, Zhou, & Dai, 2013); evacuated collectors (Wasabi Energy Limited, 2010). Figure 130 shows a schematic of a KCS34 driven by the solar heat collected in a parabolic trough system. The solar KC power plant installed at EXPO 2010 (Figure 131 left) was the first demonstration of the KC technology in a solar thermal application. One of the major technological breakthroughs achieved by this plant involves successfully achieving effective power generation from a non-concentrating solar arrays composed of low-cost evacuated solar collectors (Figure 131 right). The main features and performance parameters of the solar KCs are reported in Table 64.

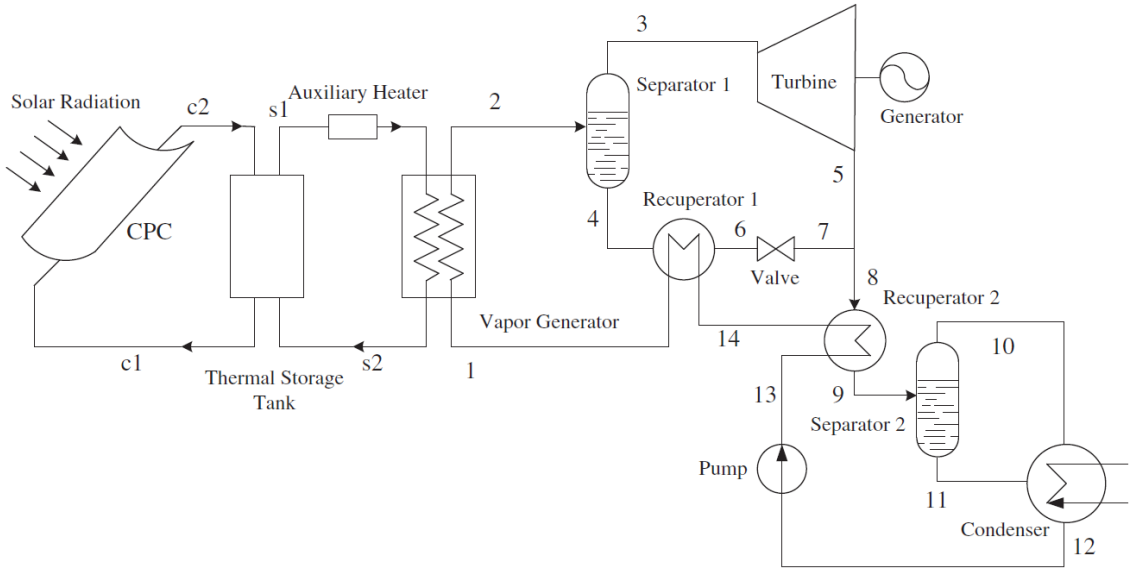

Figure 130: Schematic diagram of KC driven by solar energy (Jiangfeng Wang et al., 2013).

Horizon 2020 European Union Funding for Research & Innovation

This project has received funding from the European Union's Horizon 2020 research and innovation programme under grant agreement No 847097

a) b)

Figure 131: Solar thermal Kalina cycle demonstration plant built at EXPO 2010 Shanghai (China): a) construction of the power plant; b) evacuated solar collectors installed on the roof of the EXPO Pavilion (Wasabi Energy Limited, 2010).

Table 64: Main features and performance of the Kalina cycle for solar applications.

TRL	Solar field technology	Temperature heat source (°C)	Max temperature fluid (°C)	Power output (kW)	Thermal efficiency (%)	Reference
7	Evacuated collectors	90÷95	/	50	/	(Wasabi Energy Limited, 2010)
1	Parabolic collectors	122.5	106	10.9	7.55	(Jiangfeng Wang et al., 2013)
1	Parabolic collectors	320	300	233	27.3	(H. Hong et al., 2017)
1	Solar tower	/	500	/	29.6	(Modi et al., 2015)

5.3.3 Cost aspects

Table 65 shows the cost of KCs for different applications. References in the literature show capital costs of between 2000 and 3000 €/kW for small Kalina plants with an electric power capacity of less than 500 kW (Ogriseck, 2009). The capital costs for plants in the MW and multi-MWs range should be comparable to that of a conventional Rankine power plant (M. D. Mirolli, 2005). In one of the early papers by Kalina (A. I. Kalina et al., 1991) reporting a detailed cost comparison between a utility size KC and a baseline two-pressure SRC, it was shown that the cost of the KC was 1058 US$/kW against 1033 US$/kW of the SRC. While these cost estimates are dated and would need an accurate update, still they provide a first of order magnitude of the KC cost at different sizes. The more updated cost estimate provided in (Campos Rodríguez et al., 2013) for a low temperature geothermal application shows a specific cost consistent with the other sources. It includes the cost of the binary unit and the cost of interconnections, civil works and installation.

Table 65: Specific investment costs of the Kalina cycle for different sizes and applications.

Application	Size (kW)	Specific cost (€/kW)	Reference
Geothermal	<500	2000 ÷ 3000	(Ogriseck, 2009)
Geothermal	1850	1745	(Campos Rodríguez et al., 2013)
Cement plant	6000	1335	(M. D. Mirolli, 2005)
Bottoming cycle of a gas turbine	86000	940	(A. I. Kalina et al., 1991)

Horizon 2020 European Union Funding for Research & Innovation

This project has received funding from the European Union's Horizon 2020 research and innovation programme under grant agreement No 847097

5.4 Supercritical CO2 power cycles (sCO2)

5.4.1 Technological features and performance

The sCO2 power cycle is a closed Brayton cycle operating with CO_2 as the working fluid. CO_2 is compressed, heated up to the maximum cycle temperature, expanded in the turbine and cooled down to the lowest cycle temperature. The compressor inlet state is close to the CO_2 critical point (73.8 bar; 30.98°C). In this region the real gas effects are significant and a marked reduction in compression work can be achieved. The high CO_2 critical pressure necessarily requires low pressure ratios (around 2÷3) to limit the maximum cycle pressures, and the cycle configuration is regenerative to improve thermal efficiency. The flowsheet of the simple sCO2 cycle and the thermodynamic processes in the temperature-entropy (T-s) diagram are shown in Figure 132. The CO2 leaving the compressor is first heated by regenerative heat transfer in the recuperator and then heated up to the turbine inlet temperature by the external waste heat source. Heat energy is introduced through a waste (primary) HE installed into the exhaust stack of a gas turbine or a furnace or the flue gas exhaust of an industrial process with 200°C to greater than 650°C operating temperature range (T. Held, Zdankiewicz, Kacludis, & Persichilli, 2012). While the lower temperature applications (200÷350°C) are basically a variation of the ORC where CO_2 is used as WF, the higher temperature applications (350÷650°C) are of particular interest as they represent an alternative to the SRC. The focus in this Section is on these higher temperature applications of the sCO2 technology.

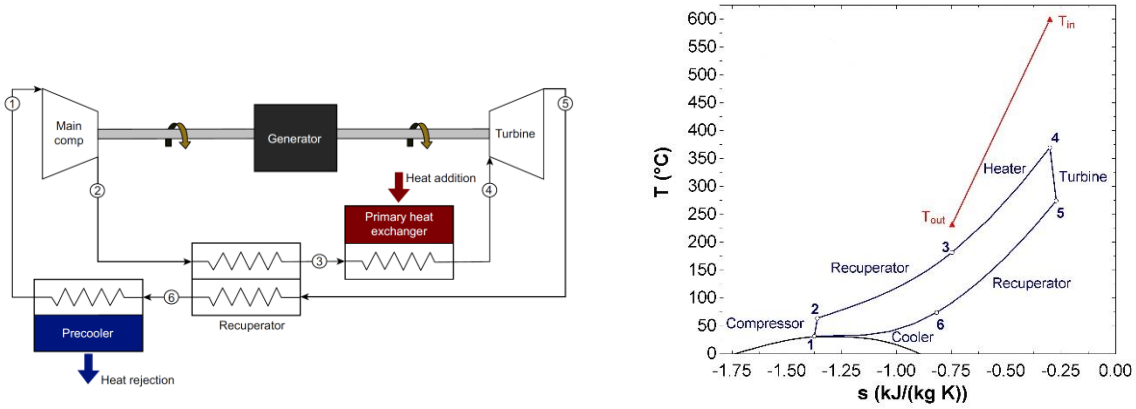

a) *b)*

Figure 132: sCO2 power cycle: Process flow diagram (Brun, Friedman, & Dennis, 2017)*; b) T-s diagram of the sCO2 cycle and cooling profile of the WH source* (Giovanni Manente & Fortuna, 2019).

- **Advantages of sCO2 power cycle compared to the SRC**

The sCO2 heat engine is a platform technology scalable from 250 kW_e to greater than 50 MW_e and is suitable with a wide range of heat sources for energy recovery with efficiencies up to 30%. Compared to ORC and SRC systems, sCO2 can achieve higher efficiencies over a wide temperature range of heat sources with compact components resulting in a smaller system footprint, lower capital and operating costs (T. Held et al., 2012). This is mainly due to properties of the WF, namely supercritical CO_2, that is a low-cost WF non-toxic, non-flammable, non-corrosive and readily available. Its thermo-physical features enable a more compact and efficient design for the main plant`s components compared to use of water/steam as explained in the following.

Horizon 2020
European Union Funding
for Research & Innovation

This project has received funding from
the European Union's Horizon 2020 research and innovation
programme under grant agreement No 847097

1) *Compact turbines*. The high fluid density of supercritical CO_2 enables extremely compact turbomachinery designs. Figure 133 compares a 10 MW_e CO_2 turbine to a 10 MW_e steam turbine. Supercritical CO_2 turbines are very compact and highly efficient with simpler, single casing body designs. Instead, steam turbines usually require multiple turbine stages (i.e., high, medium and low-pressure) and associated casings with a corresponding increase in systems complexity (T. Held et al., 2012).

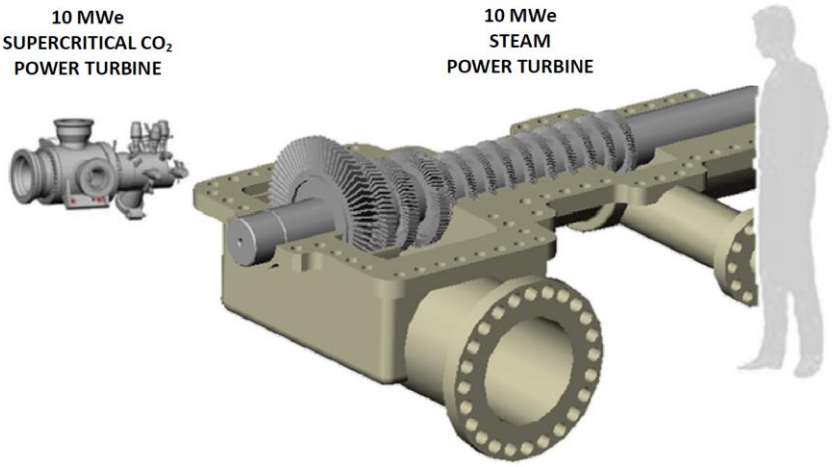

Figure 133: Comparison between a 10 MWe sCO2 power turbine and a 10 MWe steam turbine (T. Held et al., 2012).

2) *Compact recuperator HE*. The high density of supercritical CO_2 on both sides of a recuperating HE permits the use of highly compact, microchannel-based HE technology or printed circuit HEs. The dimensions and weight of these compact HEs are much lower compared to a conventional STHE for the same heat duty.
3) *Improved thermal match with the WH source*. Carbon dioxide more effectively captures heat from a sensible heat source compared to water/steam. This is due to the character of its heat capacity in the supercritical region, which provides superior matching to the heat source temperature profile compared to the boiling process of water/steam (Figure 134). Accordingly, a higher fluid temperature and thermal efficiency can be achieved for the same heat source. Instead, the boiling process in steam systems limits the maximum fluid temperature and requires multiple pressures (e.g., double and triple-pressure HRSG systems) to achieve close approach to the exhaust or flue gas temperature.

Horizon 2020
European Union Funding
for Research & Innovation

This project has received funding from
the European Union's Horizon 2020 research and innovation
programme under grant agreement No 847097

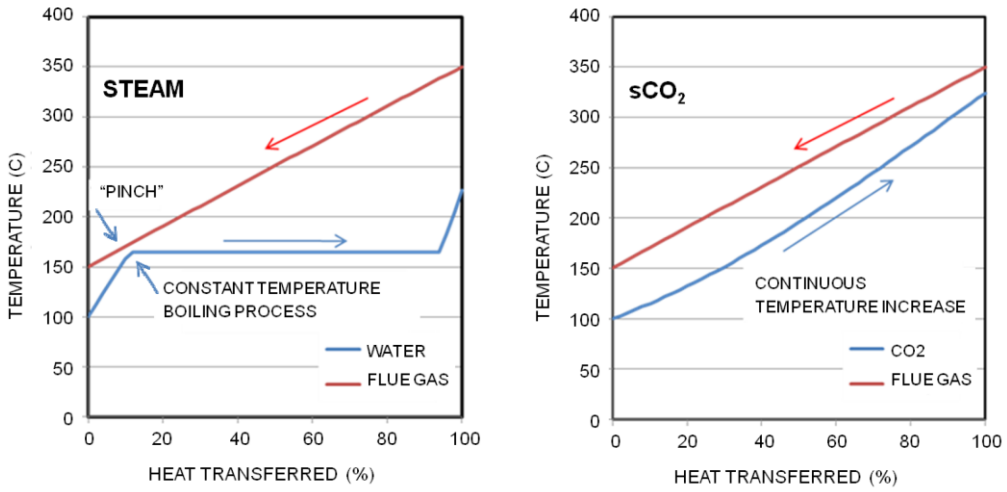

a) *b)*

Figure 134: Thermal match between WH source (flue gas) and WF: a) the WF is water/steam; b) the WF is supercritical CO_2. (T. Held et al., 2012).

Waste heat exchanger. The single phase nature of supercritical CO_2 allows for the design of simple, single phase, single pressure exhaust HEs (Figure 135) with low gas-side pressure drop. Due to the superior thermal stability and non-flammability of CO_2, direct heat exchange from high temperature sources is possible, permitting higher working fluid temperature (and thus higher cycle efficiency).

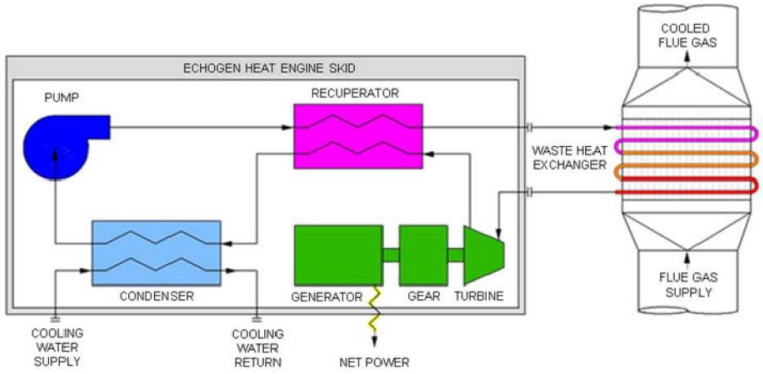

Figure 135: Waste heat exchanger and connection to the system (T. Held et al., 2012).

Fast start-up time. The growing trend to operate NGCC plants on an as-needed, cyclical basis can cause severe HRSG hardware damage and premature life end. Because supercritical CO_2 is a single-phase WF, it does not create the associated thermal fatigue or corrosion problems due to two-phase flow within the system components. The compact equipment gives a fast start-up time (approximately 20 minutes to full power for the EPS100 system (T. Held et al., 2012)), enabling application in peaking duty and for industrial WH with variable inlet conditions.

- **Drawbacks of sCO2 power cycle**

Challenging operating conditions for the compressor and high sensitivity of sCO2 performance to the compressor inlet state. Operation of the sCO2 cycle near the critical point provides the optimum

Horizon 2020
European Union Funding
for Research & Innovation

This project has received funding from
the European Union's Horizon 2020 research and innovation
programme under grant agreement No 847097

efficiency. However, operation at this point is difficult and challenging due to the rapid changes in thermophysical properties of the CO_2 near the critical point and the potential for entering the two-phase dome (gas-liquid) and having both liquid and gas in the flow. A conventional compression system is not able to handle this two-phase (gas-liquid) flow, and the wet gas compression technology is still in its infancy and never been used with CO_2. Because of this, industry designers have stayed away from operating on the critical point. However, a deviation of the compressor suction state from the critical point (31°C, 73.8 bar) to a nearby state with (40°C, 76.9 bar) implies a thermal efficiency decay as high as 6 percentage points (Melissa Poerner, Musgrove, & Beck, 2016).

Significant drop of performance during the warm season. The previous point also implies that a significant drop of performance is to be expected in the warm season especially when a dry cooling system is used. Indeed, the higher temperature of the available heat sinks (ambient air, water recirculated from a cooling tower) in the warm season might not allow the operation in the close proximity of the critical point.

Challenging operating conditions for the HEs. The high thermal efficiency of sCO2 is highly dependent on the recuperators` performance (i.e., the effectiveness). Due to the low cycle pressure ratio and relatively high turbine outlet temperature, the sCO2 system must recuperate a large amount of heat to increase the thermal efficiency. The common HE types (STHEs, PHEs, PSHEs, etc.) described in Section 2.1 are not suitable as recuperators for sCO2 due to their pressure and temperature limitations. On the other hand, various compact HEs with high compactness (up to 10 times compared to STHE), such as a Printed Circuit Heat Exchanger (PCHE) and microchannel heat exchangers (MCHE) have been commercialized and can be considered for application in the sCO2 cycle due to their very high pressure and temperature ratings (Figure 136). However, these new recuperator designs must face significant mechanical, thermo-mechanical and thermo-hydraulic challenges. For instance, the potential for flow maldistribution in MCHEs is a design concern and drops of HE effectiveness of 30% are possible due to flow maldistribution (Lance & Carlson, 2018).

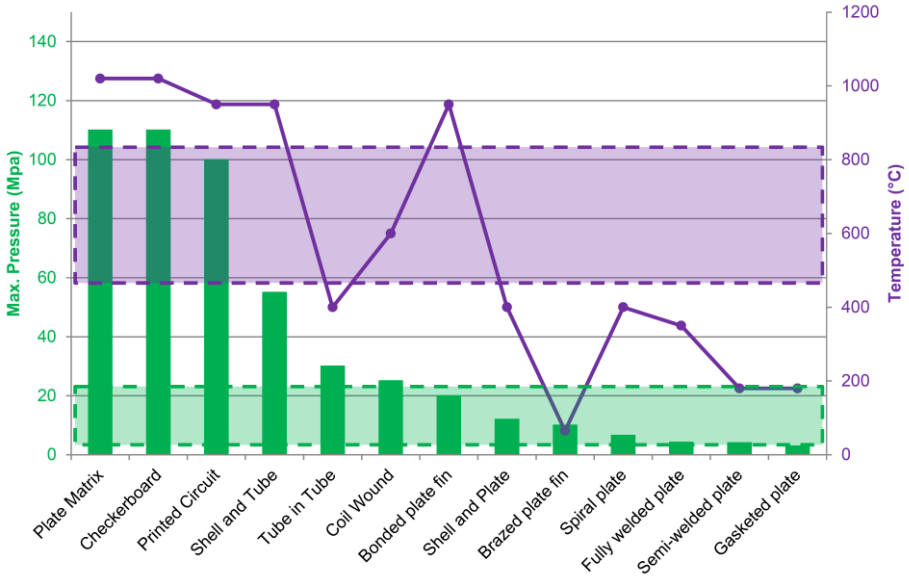

Figure 136: Temperature and pressure ranges of different HE types (Musgrove, Le Pierres, & Nash, 2014).

Horizon 2020
European Union Funding
for Research & Innovation

This project has received funding from
the European Union's Horizon 2020 research and innovation
programme under grant agreement No 847097

Advanced architectures required for WHR applications. Quite complex sCO2 architectures are required to enable an effective heat extraction from the WH source. These include a higher number of components (e.g., two turbines, two recuperators, two or three heaters) compared to the simple recuperated layout, as well as one or more flow splits. This increase the complexity and cost of the sCO2 systems for WHR. These advanced architectures required to maximize the power output in WHR applications are described in the following Section.

5.4.1.1 Traditional layouts and advanced layouts of sCO2 for WHR applications

The sCO2 cycle was originally proposed in the late 1960s to overcome the thermodynamic and technological limitations of the Rankine and Brayton cycles. Nuclear power was considered as the foremost application and it is still considered one of the most relevant applications of sCO2, as also demonstrated by the H2020 sCO2-HeRo project ("sCO2-HeRo H2020," 2018). In the meantime, the renewed interest in CSP and, in particular, on the central receiver layout suggested the sCO2 power cycle as a suitable power block substitute for the SRC due to its higher thermal efficiency and compactness. For these applications (nuclear, solar), the most promising layout is the "recompression" layout (Figure 137 right) that achieves a thermal efficiency of 45% for a turbine inlet temperature of 550°C. The recompression cycle improves by 5÷6%-points the thermal efficiency of the simpler single recuperated cycle (Figure 137 left) (G. Manente & Lazzaretto, 2014).
Figure 138 compares the maximum thermal efficiency achievable by several architectures of sCO2 considering a turbine inlet temperature of 500°C. It clearly appears that the recompression cycle layout outperforms the other layouts. However, in the recovery of WH the maximization of net power output rather than of thermal efficiency is to be pursued. Accordingly, other layouts are to be preferred in WHR applications, such as the preheating or the turbine split flow, which show a higher capability of heat extraction from the heat source (i.e., a more effective cooling of the heat source). Indeed, one key difference between sCO2 cycles for WHR and sCO2 cycles for solar and nuclear applications is the thermodynamic implication of how heat is added to the cycle (Mohagheghi & Kapat, 2013). For those applications (solar, nuclear) in which heat is added via a closed loop system the amount of added heat to the cycle is equal to the heat generated by the heat source. This type of heat sources (solar receiver or nuclear reactor) is usually in the form of heat flux source in which the heat utilization is not constrained by temperature variation (Mohagheghi & Kapat, 2013). In contrast, for WHR applications, the heat input is applied through a heat exchange process between the WF (carbon dioxide) and the hot waste gas. In such arrangements, the temperature of the waste gas stream decreases as the heat is transferred to the cycle's WF. The remaining thermal energy in the waste gas stream is ultimately discharged to the environment via the stack. This implies that a portion of thermal energy in the waste gas stream is recovered in the heat exchanger and the rest is still wasted through the stack (Mohagheghi & Kapat, 2013).

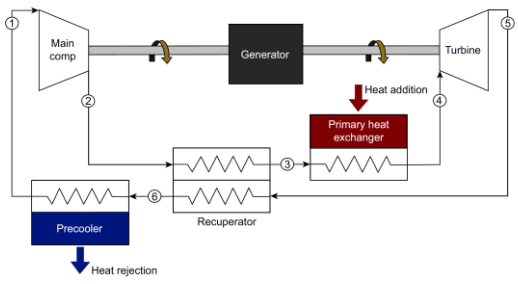

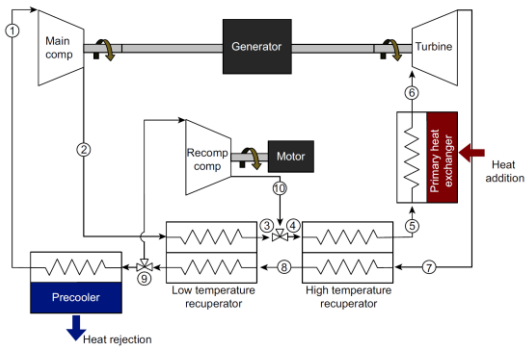

Horizon 2020
European Union Funding
for Research & Innovation

This project has received funding from
the European Union's Horizon 2020 research and innovation
programme under grant agreement No 847097

a) b)

Figure 137: Traditional sCO2 power cycles (Brun et al., 2017)*: a) single recuperated cycle; b) recompression cycle.*

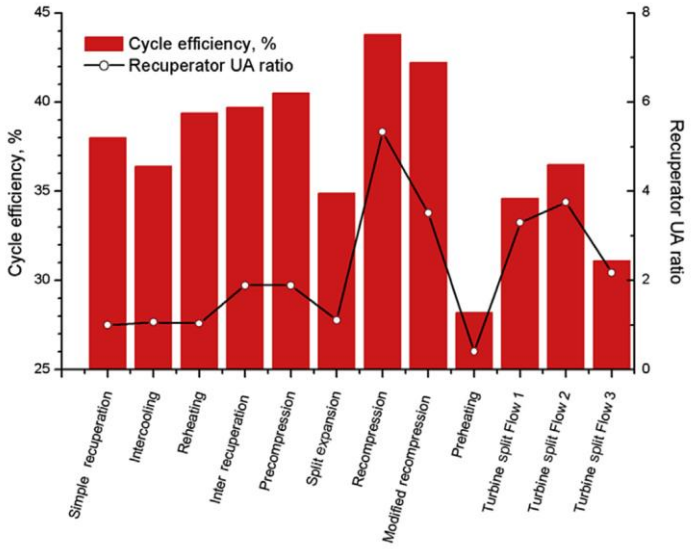

Figure 138: Performance comparison of different sCO2 layout for a maximum cycle temperature of 500°C (Ahn et al., 2015).

The most promising sCO2 cycle architectures specifically developed in the last decade for WHR applications are shown in Figure 139 and are briefly described in the following:

1) *Single flow split with dual expansion* (also called "cascade cycle" in (Kimzey, 2012) or "turbine split flow" in (Ahn et al., 2015)) (Figure 139a). The CO_2 flow to the higher temperature turbine (HTT) is heated by the WH source, whereas the CO_2 flow to the lower temperature turbine (LTT) is heated in low and high temperature recuperators by recovering internally the exhaust heat of the sCO2 turbines.
2) *Dual flow split with dual expansion* (Figure 139b). This cycle includes a dual splitting of the total CO_2 flow, in order to increase the mass flow rate of CO_2 heated in the low temperature recuperator and finally improve the thermal match with the exhausts of CO_2 turbines.
3) *Dual recuperated* (also called "dual stage" in (Walnum, Nekså, Nord, & Andresen, 2013)) (Figure 139c): This cycle includes a higher temperature turbine (HTT) and a lower temperature turbine (LTT), exhausting to a high temperature recuperator (HTR) and low temperature recuperator (LTR), respectively.
4) *Partial heating* (also called "preheating" in (S.A. Wright, Davidson, & Scammel, 2016)) (Figure 139d): A fraction of CO_2 is heated by the exhaust gases in a low temperature heater in parallel with the recuperator. This enables a better thermal match in the recuperator and a more effective cooling of the heat source.

The patents related to the WHR application of sCO2 cycles belong to Echogen (Ohio, USA) and General Electric (New York, USA)(Ahn et al., 2015). Architectures (1) and (3) were first proposed in a patent by Echogen Power Systems (Patent No. WO 2011/119650 A2, 2011). Architecture (2) was developed by EPRI (Kimzey, 2012). Architecture (4) was first described in mid-nineties by professors of Politecnico of Milan (Steven A Wright, Davidson, & Husa, 2018). Other architectures were developed by GE for the simultaneous utilization of multiple WH sources (Lehar & Michelassi, 2013). A detailed analysis of the thermodynamic performance and costs of these novel layouts in a wide range of temperature of the WH source between 400°C and 800°C has been recently carried out by

Horizon 2020
European Union Funding
for Research & Innovation

This project has received funding from
the European Union's Horizon 2020 research and innovation
programme under grant agreement No 847097

one of the current author in (Giovanni Manente & Fortuna, 2019) and (Giovanni Manente & Costa, 2020). Another interesting comparison between traditional and advanced sCO2 layouts for WHR is the recent paper by (Matteo Marchionni, Bianchi, & Tassou, 2018), which is one of the outcomes of the H2020 EU project I-Therm ("I-Therm H2020," 2019).

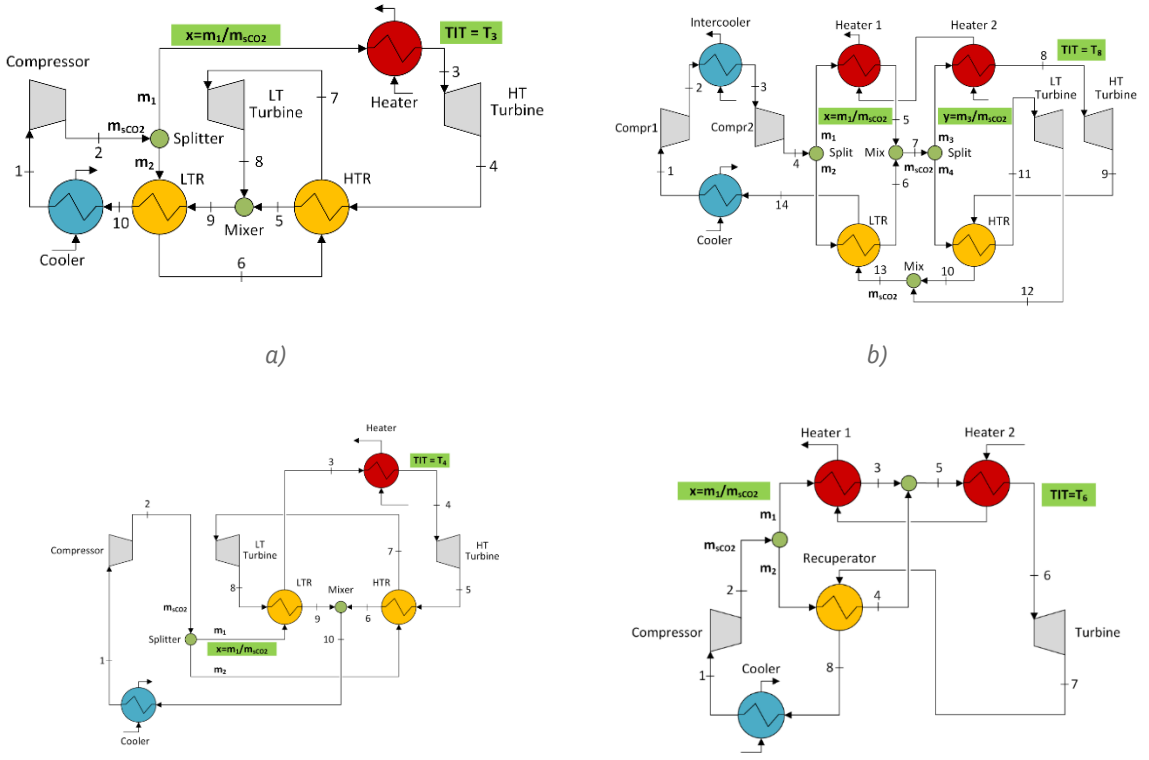

a) *b)*

c) *d)*

Figure 139: Advanced sCO2 architectures specifically developed for WHR applications: a) Single flow split with dual expansion; b) Dual flow split with dual expansion; c) Dual recuperated; d) Partial heating (Giovanni Manente & Fortuna, 2019)(Giovanni Manente & Costa, 2020).

5.4.2 Examples of applications, technology maturity and performance of sCO2

There are many possible applications of sCO2 power cycles: nuclear, CSP, fossil fuels, geothermal and WHR (Ahn et al., 2015)(Brun et al., 2017). Figure 140 shows the application fields of the sCO2 technology, namely the temperature – power output ranges where the sCO2 power cycles can outperform the more conventional/mature technologies based either on the steam or organic Rankine cycles. The ongoing U.S. DOE STEP (Supercritical Transformational Electric Power) project (U.S. Department of Energy, 2020) targets large-scale and high temperature nuclear, solar and fossil applications. The European H2020 sCO2-Flex project ("sCO2flex H2020," 2019) targeted large coal/lignite fired power plants with higher operational flexibility (i.e., fast load changes, fast start-ups and shut-downs). Focusing on the WHR application, Figure 140 shows that the sCO2 power cycle can provide a higher efficiency compared to the ORC for heat source temperatures higher than 350°C. Moreover, it is preferred to steam when the power output is lower than 20÷30 MW_e.

Horizon 2020
European Union Funding
for Research & Innovation

This project has received funding from
the European Union's Horizon 2020 research and innovation
programme under grant agreement No 847097

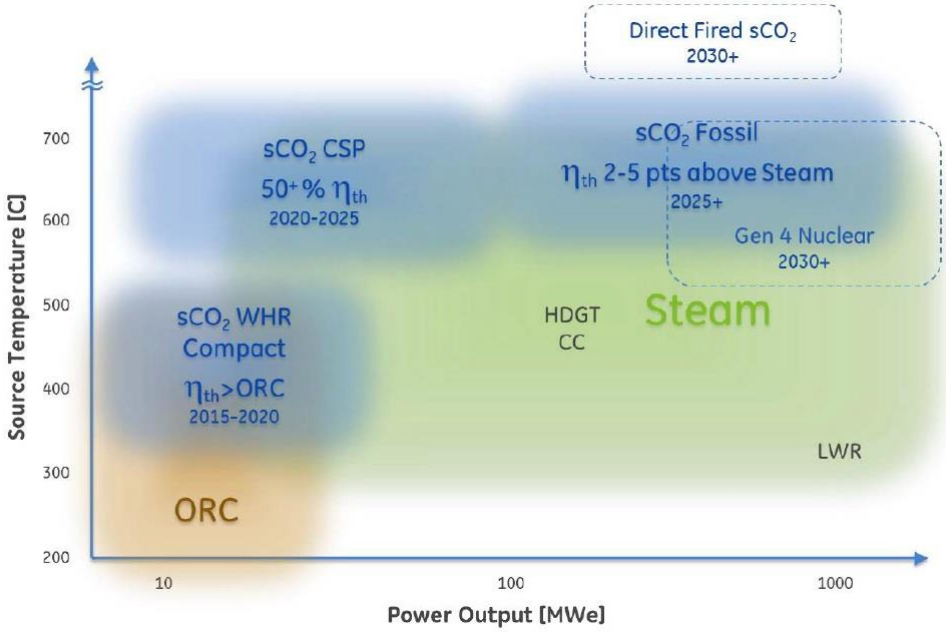

Figure 140: Application fields of the sCO2 power cycle (Wilkes, 2018).

The main applications of sCO2 power cycles for industrial WHR are in the cement, steel and glass industry (Brun et al., 2017). Other applications include EHR from small/medium scale gas turbines and ICEs. The relevant information reported in the literature for these WHR applications is reported in the following. Special attention is about the comparison of sCO2 against the more mature SRC and ORC technologies.

- **Cement industry**

The potential application of a WH to power recovery system at the cement plant (Figure 141) in Gmunden (Austria) was investigated in (A. Werner, Klemencic, Flegkas, Haider, & Helmut Leibinger, 2016). The authors found that the power output of the sCO2 cycle outperforms that of a dual pressure SRC, whereas it is only slightly higher than that achievable by an ORC using cyclopentane as WF. The power gain over the SRC and ORC was 21.5% and 2.3%, respectively. Similar results were obtained in (Kizilkan, 2020) for a cement plant in Turkey where the performance of the existing SRC was compared against that achievable by a simple recuperated sCO2 cycle (Figure 142). The power gain of sCO2 over the SRC was estimated equal to 13%. The heat source temperatures involved and performance are shown in Table 66.

Table 66: Features and performance of sCO2 power cycles for WHR in cement plants.

TRL	Heat sources	Heat source temperature (°C)	Layout	Thermal efficiency (%)	Power output (kW)	Reference
8	1) off-gas from the rotary kiln 2) cooling air from the grate cooler	1) 295 2) 410	Simple recuperated	20.8	4000	(A. Werner et al., 2016)
8	1) flue gas 2) hot air	1) 376 2) 451	Simple recuperated	27.6	9360	(Kizilkan, 2020)

Horizon 2020
European Union Funding
for Research & Innovation

This project has received funding from
the European Union's Horizon 2020 research and innovation
programme under grant agreement No 847097

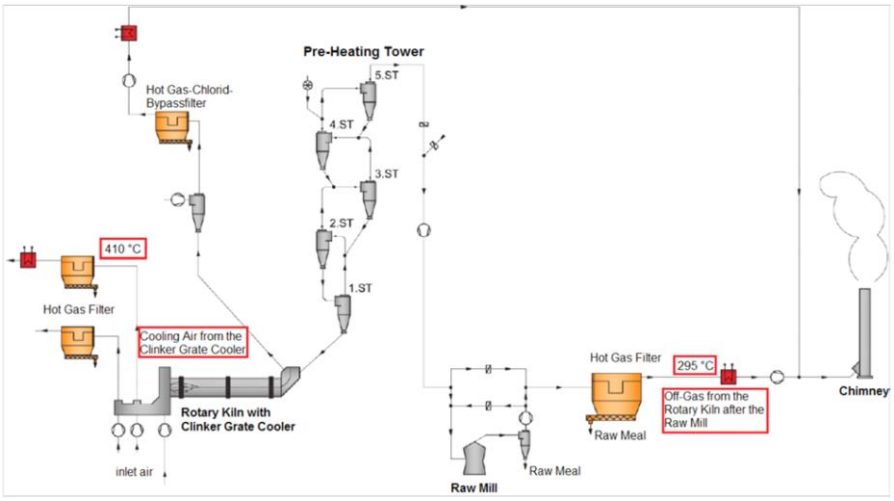

Figure 141: Simplified schematic of the cement plant with highlighted in red the two heat sources considered for WHR (A. Werner et al., 2016).

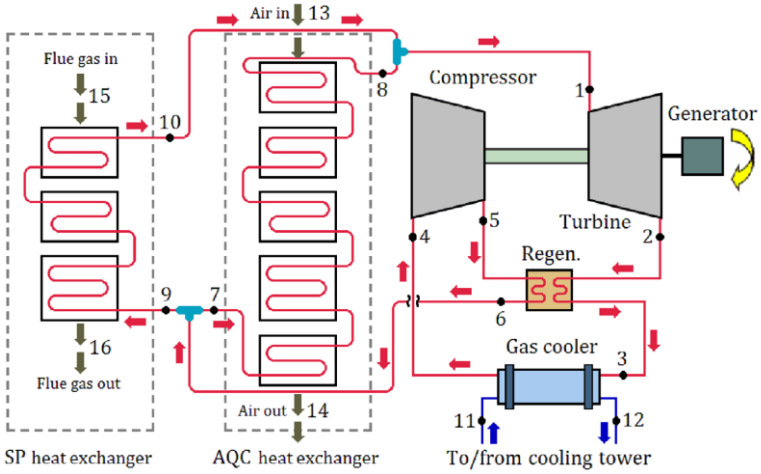

Figure 142: sCO2 power cycle integration in a cement plant (Kizilkan, 2020).

- **Steel industry**

The integration of a sCO2 power cycle for WHR from the reheat furnace flue gas in a steel plant was investigated in (Kacludis, Lyons, Nadav, & Zdankiewicz, 2012). In a hot strip steel mill, steel slabs are reheated prior to hot rolling. The flue gas, after preheating furnace combustion air in a recuperator, is typically discharged to the atmosphere at a high temperature (540°C). A direct flue gas-to-sCO2 waste HE installed downstream of the existing combustion air heater absorbs WH energy that is converted into electrical power using a sCO2 power cycle. The advanced sCO2 cycle architecture (Echogen) enables the maximum extraction of the WH from the flue gas, which leaves the stack at only 110°C, and converts the recovered WH with an efficiency of 22.5% (Table 67). The estimated PBT without any subsidy was 4 years (Kacludis et al., 2012). The WHR from a coke oven plant using a sCO2 was recently considered in (Sathish et al., 2019) as an alternative to the baseline SRC.

Horizon 2020
European Union Funding
for Research & Innovation

This project has received funding from
the European Union's Horizon 2020 research and innovation
programme under grant agreement No 847097

Table 67: Features and performance of sCO2 power cycles for WHR in steel plants.

TRL	Heat sources	Heat source temperature (°C)	Layout	Thermal efficiency (%)	Power output (kW)	Reference
8	Flue gas from a reheating furnace (downstream the air preheater)	540	Advanced (Echogen)	22.5	3730	(Kacludis et al., 2012)
8	Flue gas in a coke oven plant	≈600	Simple recuperated	28÷29	15000	(Sathish et al., 2019)

- **Glass industry**

The performance of different WHR systems from the flue gas of a regenerative hollow glass furnace was investigated in (Danieli et al., 2019). The regenerative furnace is composed of a melting chamber and two regenerative chambers. NG is injected in the melting chamber by two burners generating a non-premixed flame, which operate alternately with periodic switches of the main flow every 20 min. The regenerative chambers recover heat from the hot gas exiting the melting chamber to preheat the combustion air. The sCO2 power cycle exploits the heat of flue gas exiting the regenerative chamber at 470°C (Figure 143) and reaches a thermal efficiency of 20.4% (Table 68). The power output of the sCO2 cycle was found 10% lower than that achievable by an ORC system using cyclopentane as WF (Danieli et al., 2019). Indeed, the high temperature of CO_2 at the outlet of the recuperator prevented the full extraction of the heat of the flue gas that exited the plant at 212°C. The replacement of the traditional sCO2 with a more advanced sCO2 layout could markedly improve the performance.

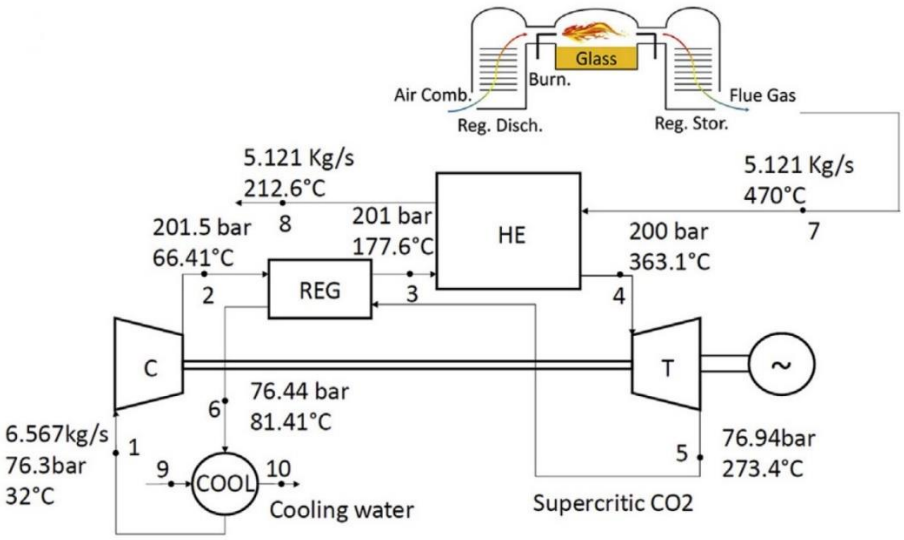

Figure 143: sCO2 power cycle for WHR from the flue gas of a glass furnace (Danieli et al., 2019).

Table 68: Features and performance of sCO2 power cycles for WHR in glass furnaces.

TRL	Heat sources	Heat source temperature (°C)	Layout	Thermal efficiency (%)	Power output (kW)	Reference
8	Flue gas from a glass regenerative furnace	470	Simple recuperated	20.4	322	(Danieli et al., 2019)

Horizon 2020
European Union Funding
for Research & Innovation

This project has received funding from
the European Union's Horizon 2020 research and innovation
programme under grant agreement No 847097

- **Gas turbines**

The large gas turbine units (e.g. above 120 MW_e size) are typically installed for utility-scale power generation and are usually configured for combined cycle service with large heat recovery steam generators for bottom cycling. The small to medium size gas turbine units are typically sold as simple cycle units because of the difficulties and economics in scaling down steam systems for combined cycle service. Thus, the small to medium gas turbine market makes sense for other bottoming cycle technologies such as the sCO2 power cycle (T. Held et al., 2012). Figure 144 shows a performance comparison between the steam cycles (single and dual pressure) and the advanced sCO2 cycle (EPS100) as bottoming units in a small/medium scale NGCC based on a commercial 22 MW gas turbine (LM2500). The power output of the advanced sCO2 cycle significantly exceeds that of the single-pressure SRC and is comparable to the double-pressure SRC. The gain is significant at low ambient temperatures and gradually vanishes at warm ambient temperatures. The net power on 20÷50 MW_e gas turbines could be increased by up to 30%.

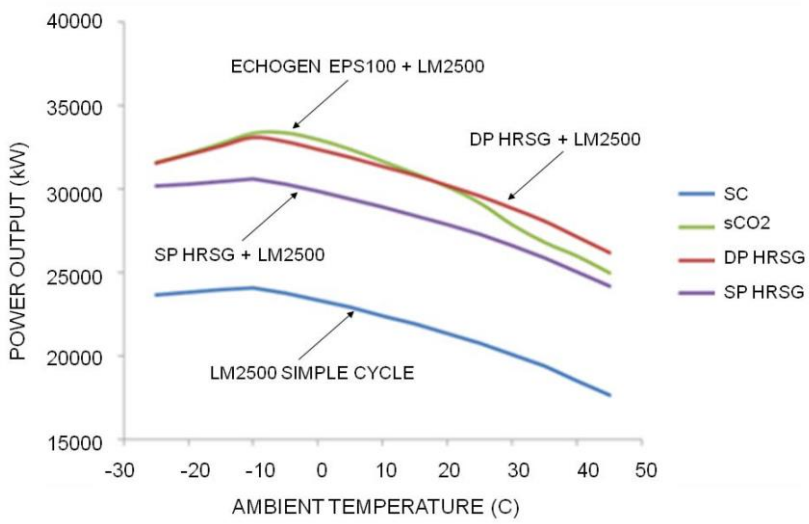

Figure 144: Power output versus ambient temperature of small/medium NGCC based on a LM2500 gas turbine (T. Held et al., 2012): 1) violet line: single pressure steam bottoming cycle; 2) red line: dual pressure steam bottoming cycle; 3) green line: advanced sCO2 bottoming cycle (EPS100).

Figure 145 compares the power output for a standalone LM2500 power generation turbine against the power output of the LM2500 integrated with various heat recovery technologies including the ORC using n-pentane as WF. The modeling results show that the sCO2 cycle (Echogen layout) exceeds the power output of single pressure steam-based and ORC systems by a factor of 1.13 and 1.48, respectively (Persichilli, Held, Hostler, & Zdankiewicz, 2011).

Horizon 2020
European Union Funding
for Research & Innovation

This project has received funding from
the European Union's Horizon 2020 research and innovation
programme under grant agreement No 847097

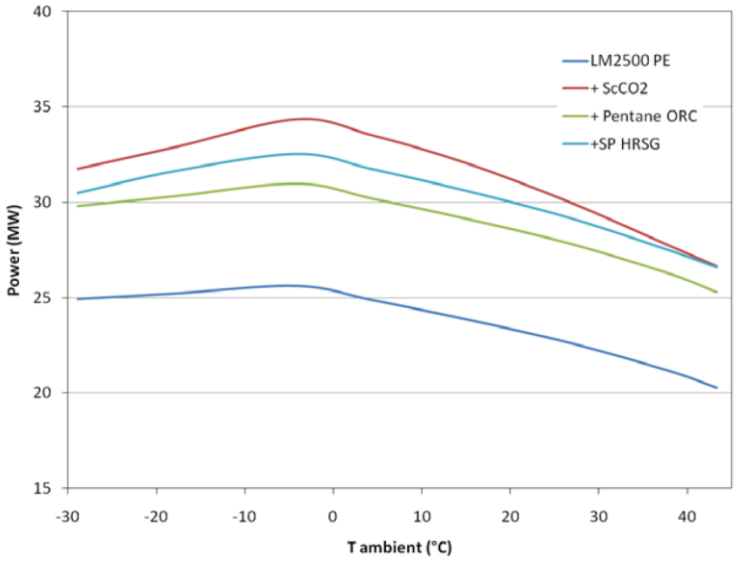

Figure 145: Power output comparison between the sCO2 cycle (Echogen layout), single pressure SRC and ORC as bottoming cycles of a small/medium scale gas turbine (Persichilli et al., 2011).

The dual recuperated layout (Figure 146 right) was first investigated in (Walnum et al., 2013) for WHR for an off-shore gas turbine and compared against the traditional single recuperated layout (Figure 146 left). The availability of cooling water at 10 °C throughout the year enabled transcritical operation with heat rejection at subcritical pressures. The dual recuperated layout improved by 9.5% the power output compared to the simple recuperated cycle due to the better capability of heat extraction from the exhaust (Table 69).

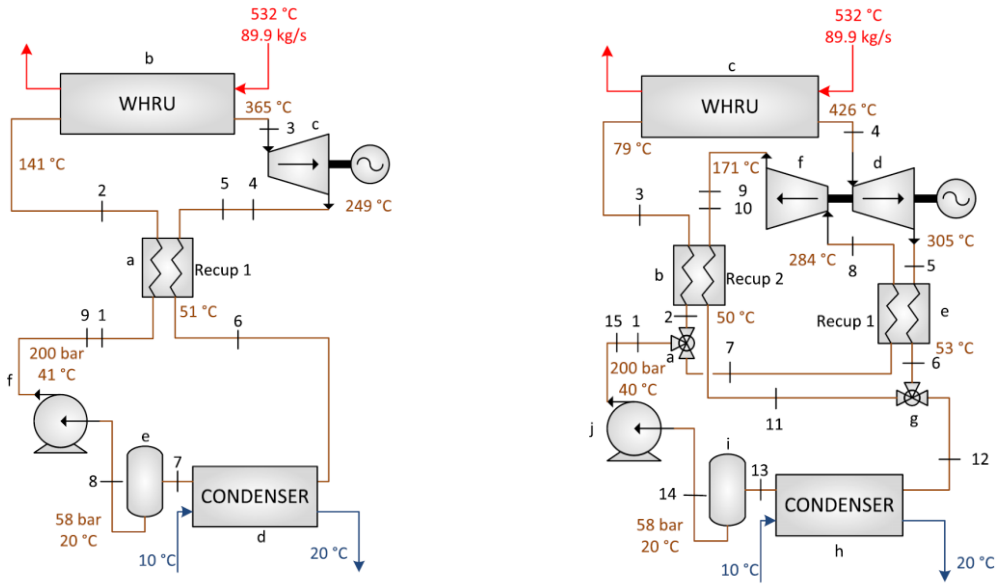

a) b)

Figure 146: sCO2 cycles for WHR from a small/medium scale gas turbine: a) Single recuperated layout, b) Dual recuperated layout (Walnum et al., 2013).

Horizon 2020
European Union Funding
for Research & Innovation

This project has received funding from
the European Union's Horizon 2020 research and innovation
programme under grant agreement No 847097

Table 69: Features and performance of sCO2 power cycles for WHR from gas turbine exhaust.

TRL	Heat source	Temperature heat source (°C)	Layout	Power output (MW)	Thermal efficiency (%)	Reference
8	Gas turbine exhaust	530	Single recuperated	9.5	26÷27	(Walnum et al., 2013)
			Dual recuperated	10.4		

- **Internal combustion engines**

For distributed generation applications, reciprocating ICEs fuelled by NG or Diesel fuel are a widespread and well-known technology. Typical distributed generation applications include on-site gensets at industrial facilities. The sCO2 cycle scales well into smaller sizes from both a performance and economic perspective for bottom cycling reciprocating engine gensets (Kacludis et al., 2012). The application of traditional and advanced sCO2 power cycles for WHR from internal combustion engines (Figure 147) was investigated in (Chuang Wu et al., 2016) and (S. sen Wang, Wu, & Li, 2018). The results obtained in (S. sen Wang et al., 2018) for WHR from a 2.9 MW_e genset using simple and dual recuperated cycles are shown in Table 70. The significant gain in power output of the dual recuperated cycle is due to the more effective heat extraction from the exhaust gas which leave the heater (GH) at 120°C (versus 237°C in the simple recuperated cycle).

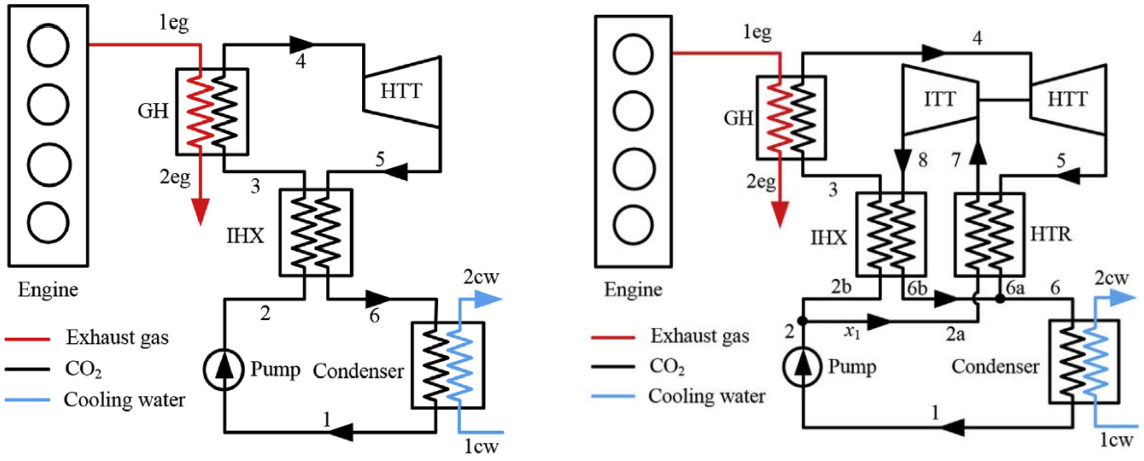

a) *b)*

Horizon 2020
European Union Funding
for Research & Innovation

This project has received funding from
the European Union's Horizon 2020 research and innovation
programme under grant agreement No 847097

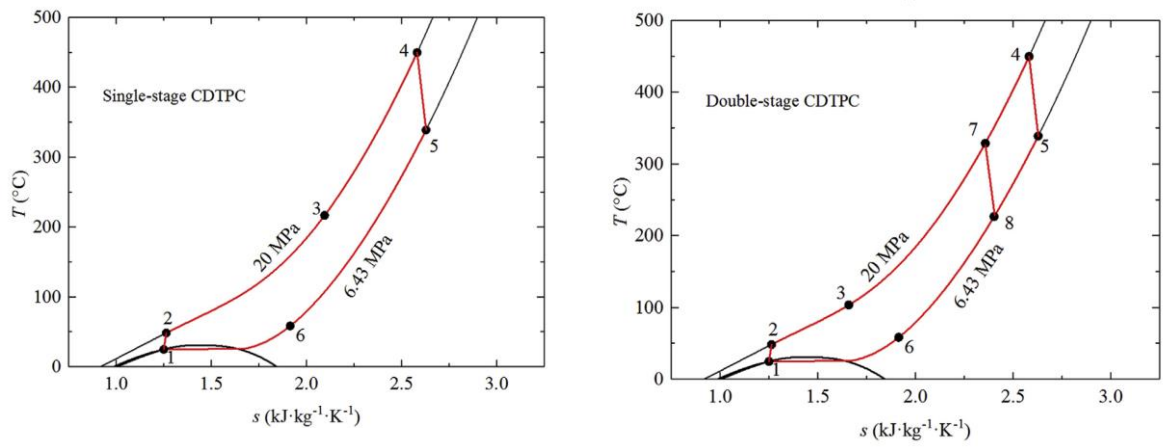

c) d)

Figure 147: sCO2 for WHR from the exhaust of internal combustion engines (S. sen Wang et al., 2018)*: a) single recuperated cycle layout; b) dual recuperated cycle layout; c) T-s diagram of the single recuperated cycle; d) T-s diagram of the dual recuperated cycle.*

Table 70: Features and performance of sCO2 power cycles for WHR from ICE exhaust.

TRL	Heat source	Temperature heat source (°C)	Layout	Power output (kW)	Thermal efficiency (%)	Reference
8	Engine exhaust	470	Single recuperated	357	28÷30	(S. sen Wang et al., 2018)
			Dual recuperated	484		

- **Technology maturity**

Up to very recently, Echogen Power Systems LLC (Akron, OH U.S.A.) ("Echogen Power Systems," 2020) was the only manufacturer worldwide of sCO2 cycles for WHR applications. Echogen has developed and is continuing to refine commercial-scale sCO2 cycles and systems specifically for moderate temperature thermal power conversion, including industrial WHR and exhaust heat recovery (EHR) applications. These applications are characterized by heat source temperatures in the range 300÷600°C, and heat that is in the form of sensible enthalpy (T. J. Held, 2015). The Echogen 250 kW thermal engine (Figure 148) was the first demonstration unit built and tested in the years 2010÷2011. As the first step in commercialization of sCO2 cycles, Echogen designed the EPS100 (Figure 149), a 7 to 8 MW class heat recovery engine, targeted at small-scale CCGT (~30MW_e total output) applications and large industrial waste heat utility applications. EPS100 is the first commercial-scale sCO2 engine. The EPS100 uses supercritical CO2 and incorporates an advanced power cycle (see Figure 139) that maximizes utilization of exhaust thermal energy by reducing the exhaust temperature to a minimum practical limit. The design of EPS100 system was completed in 2011 and by 2015 all phases of testing were completed at the Dresser-Rand/Siemens facility in Olean (NY, USA) (Figure 150). A maximum electrical power output of 3.1 MW_e was achieved and was only limited by available heat on the test rig ("Dresser-Rand & Supercritical CO2," 2016) (T. J. Held, 2014).

Horizon 2020
European Union Funding
for Research & Innovation

This project has received funding from
the European Union's Horizon 2020 research and innovation
programme under grant agreement No 847097

Figure 148: Echogen 250 kWe demonstration system tested in 2011 at the American Electric Power (AEP) Dolan Technology Center (Groveport, OH, USA) (Persichilli et al., 2011).

Figure 149: 6÷8 MW advanced sCO2 heat engine (EPS100), process and power skids (T. J. Held, 2015).

a) *b)*

Figure 150: EPS100 test installation at the Dresser-Rand compressor test facility in Olean (NY, USA) (T. J. Held, 2014).

The 50 kW_e sCO2 demonstrator (Figure 151) built at Brunel University (UK) within the H2020 I-Therm project ("I-Therm H2020," 2019) was the first sCO2 experimental facility in EU academia. Unlike existing experimental sCO2 facilities, where the heat input to the WF is provided through electrical

Horizon 2020
European Union Funding
for Research & Innovation

This project has received funding from
the European Union's Horizon 2020 research and innovation
programme under grant agreement No 847097

resistance heaters, a novel feature of the research was the investigation and development of direct recovery HEs using flue gas as heat source (Miol et al., 2018). Indeed, the devised applications for sCO2 power cycle in the I-Therm project were steel, cement and glass industry (G. Bianchi & Tassou, 2019).

a) b)

Figure 151: sCO2 power cycle demonstrator for industrial WHR built at Brunel University within the I-Therm H2020 project (M. Marchionni, Saravi, Bianchi, & Tassou, 2019).

5.4.3 Cost aspects

A cost estimate of the fully-installed 6÷8+ MW_e sCO2 system (EPS100) for a gas turbine application has been performed by Echogen and compared to a double-pressure bottoming steam system (Figure 152). The installed cost is between 1800÷1900 €/kW_e. The specific investment cost is up to 40% less compared to the more conventional steam bottoming cycle. The lower installed cost is the result of the simplicity of the sCO2 system, its smaller footprint, and reduced auxiliary system requirements. The economics for a sCO2 system installation in a steel plant was reported in (Kacludis et al., 2012) as shown in Table 71. The specific investment cost is aligned with the costs of the gas turbine application. The Operation and Maintenance (O&M) costs are not available due to the early commercialization phase of the sCO2 power cycle compared to the SRC and ORC. However, the O&M costs of the sCO2 system are projected to be significantly lower compared to the SRC (T. Held et al., 2012) due to the properties of CO2 that is clean, non-scaling, non-fouling, and provided it is maintained in a dry condition, it is non-corrosive.

Horizon 2020
European Union Funding
for Research & Innovation

This project has received funding from
the European Union's Horizon 2020 research and innovation
programme under grant agreement No 847097

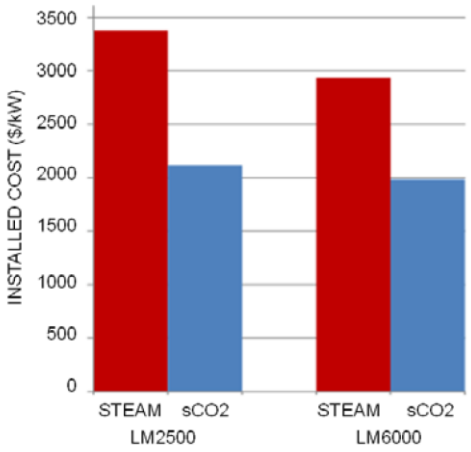

Figure 152: Specific investment cost of a sCO2 heat engine as compared to a steam bottoming cycle (T. Held et al., 2012).

Table 71: Specific investment cost of sCO2 power cycles.

TRL	Industry	Power output (kWe)	Installed cost (€)	Specific investment cost (€/kW)
8	Steel	3730	7380000	1980
8	Power (Gas Turbine	6000÷8000+	/	1800÷1900

Horizon 2020
European Union Funding
for Research & Innovation

This project has received funding from
the European Union's Horizon 2020 research and innovation
programme under grant agreement No 847097

5.5 Stirling Engines (SEs)

5.5.1 Technological features and performance

The Stirling engine is a reciprocating, externally-heated engine. The heat is transferred to the working gas and is then converted to work via expanding the gas inside the cylinder. Heat is added continuously and at constant temperature to the expanding gas. Since heat is supplied externally to the SE, a wide variety of heat sources can be used (EPRI, 2002):

- Heat of combustion of any gaseous, liquid, or solid fuel;
- Concentrated solar radiation;
- WH from industrial processes (e.g., metal casting, glass manufacturing, etc.);
- WH from thermal engines (e.g., from ICE exhaust).

The ideal Stirling cycle combines four processes, two constant-temperature processes and two constant-volume processes. Because more work is done by expanding high-pressure/high-temperature gas than is required to compress low-pressure/low-temperature gas, the Stirling cycle produces net work, which can drive an electric alternator. The heat rejected during the constant volume heat rejection is reused in the constant volume heating process. Heat is, therefore, only added or rejected in efficient constant-temperature processes, which is the basis for the extremely high performance potential of the Stirling cycle (William B. Stine and Richard B. Diver, 1994). However, due to the complex architecture of the engine and the strong irreversible processes occurring during the system operation, the actual values of efficiency achievable by the existing machines are always lower than 30÷40% (Figure 153) (M. Bianchi & De Pascale, 2011).

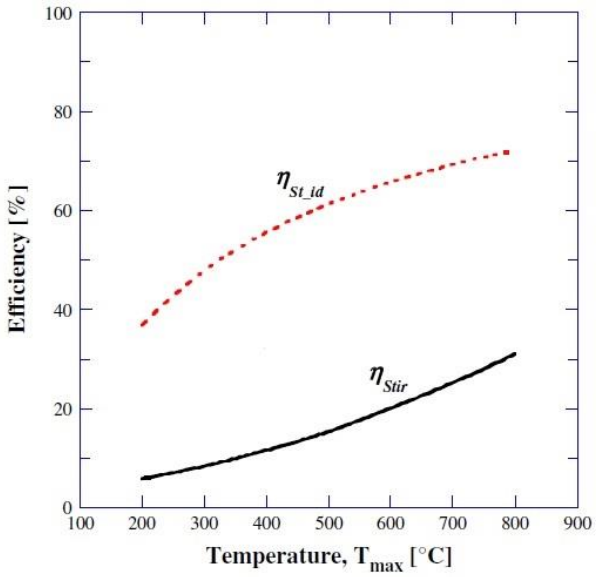

Figure 153: Variation of the efficiency of the Stirling engine versus the hot side temperature. Red dashed line: ideal efficiency; Black solid line: real efficiency calculated using a simplified model (M. Bianchi & De Pascale, 2011).

Kinematic and free piston engines

Hundreds of SE designs have been developed over the years that embody the basic thermodynamic concept. These SE designs can be classified by their mechanical configurations in kinematic or free-piston engines (EPRI, 2002). Kinematic engines have a crankshaft and a mechanical linkage to the power piston. Electricity is generated with a rotating synchronous, permanent magnet, or induction

Horizon 2020
European Union Funding
for Research & Innovation

This project has received funding from
the European Union's Horizon 2020 research and innovation
programme under grant agreement No 847097

generator. Free-piston engines typically generate electric power with a linear alternator formed by the oscillatory travel of the power piston in a magnetic field. The power piston of a free-piston SE is not mechanically connected to an output shaft. It bounces alternately between the space containing the working gas and a spring (usually a gas spring). In most designs, the displacer piston is also free to bounce on gas or mechanical springs. Piston frequency and the timing between the two pistons are established by the dynamics of the spring/mass system. To extract power, a magnet is attached to the power piston and electric power is generated as it moves past stationary coils (William B. Stine and Richard B. Diver, 1994).

Alpha, Beta and Gamma-type Stirling engines

A Stirling engine is a heat engine that operates in a closed-cycle between two heat reservoirs. The engine consists of three main parts: 1) the hot volume, 2) the cold volume, and 3) the regenerator. A gaseous working fluid (mostly air) moves between hot and cold volumes during expansion and compression. Heat is transferred to the working gas through a HE in the hot volume. Heated working fluid expands and pushes the pistons in the hot and cold cylinders. The regenerator absorbs some of the heat of the working gas during expansion, as the gas moves through the hot volume to the cold volume. During compression, the pistons move in the opposite direction and the working fluid is compressed. While passing toward the hot volume, the cooled working gas absorbs the stored heat in the regenerator. The hot and the cold pistons move with a phase difference, determined by the crank mechanism. The hot and cold volumes consist of two sub-volumes. The region where the pistons move is called "swept volume", and the clearance of the cylinders and pipes between cylinders are called "dead volume" (Güven, Bedir, & Anlaş, 2019).

The location of the hot and cold volumes determines the engine type. The engine in Figure 154 is an Alpha-type, with two separate cylinders for the hot and cold volumes. In a Beta-type engine, the hot and cold volumes are located in one cylinder and separated from each other by a displacer. The displacer is connected to the crank mechanism for supporting the transfer of working gas between the hot and cold volumes (Figure 155). Gamma-type engine, which is similar to Beta-type, has its cold volume and compression piston in a shifted cylinder (Figure 156). Among these three categories, the Beta-type engine has higher power density than the other two types.

The ratio of the shaft power output to the input heat transfer rate represents the thermal efficiency of the SE.

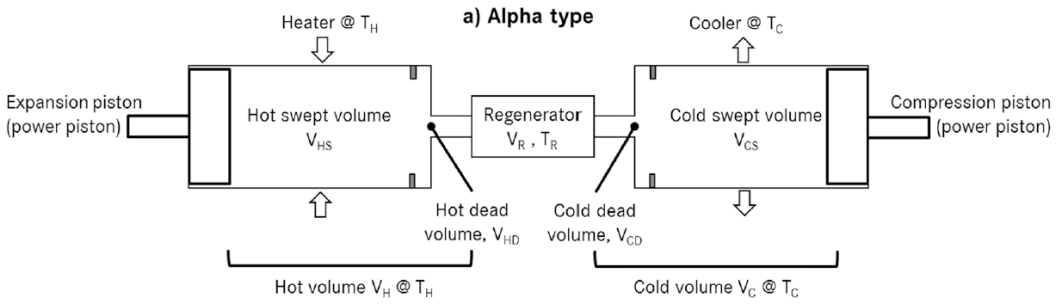

Figure 154: Alpha type Stirling engine (Güven et al., 2019).

Horizon 2020
European Union Funding
for Research & Innovation

This project has received funding from
the European Union's Horizon 2020 research and innovation
programme under grant agreement No 847097

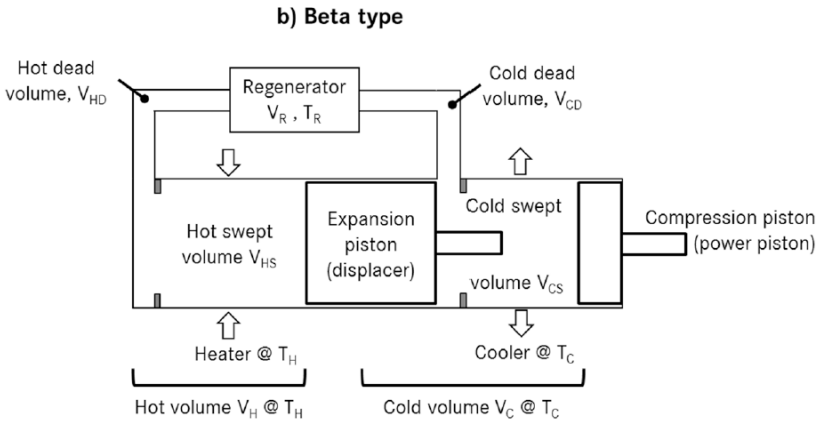

Figure 155: Beta type Stirling engine (Güven et al., 2019).

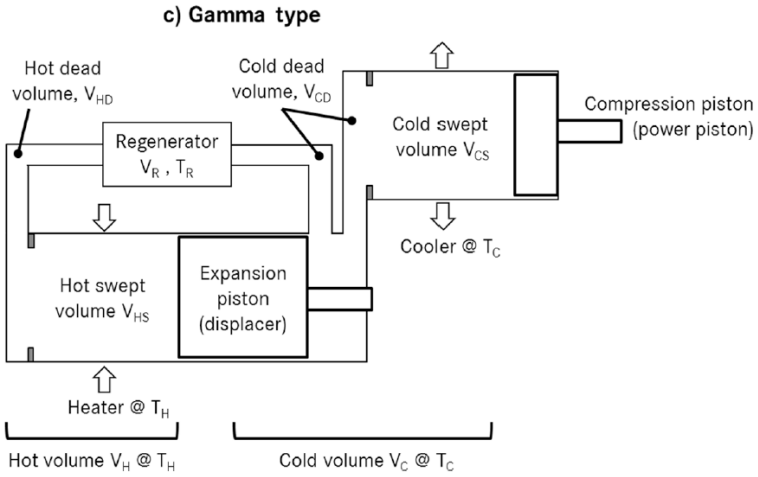

Figure 156: Gamma type Stirling engine (Güven et al., 2019).

The principles of operation of a SE are described in the following (EPRI, 2002). The displacers and power pistons reciprocate in sealed cylinders filled with a fixed charge of the working gas, typically helium, hydrogen, nitrogen, or air. All external heat is transferred to the working gas at the cycle maximum temperature and rejected at the cycle minimum temperature. The regenerator absorbs heat from the working gas as the gas passes through it from the hot end to the cold end. The heat stored in the regenerator is then returned to the working gas on its return from the cold end to the hot end with minimal thermal loss. As the displacer reciprocates, it shuttles the working gas through the regenerator between the hot and cold regions of the engine. The pressure oscillations created by varying the average working gas temperature in a fixed volume are applied to the power piston, thus reciprocating it. The displacers and power pistons are phased so that more work is put into the power piston in the expansion stroke (when most of the working gas is in the hot space), than the work that the piston returns to the working gas a half cycle later (to compress the mostly cold working gas). The net surplus of expansion work less compression work is extracted as useful work by the power piston (EPRI, 2002).

Selection of the working gas

Horizon 2020
European Union Funding
for Research & Innovation

This project has received funding from
the European Union's Horizon 2020 research and innovation
programme under grant agreement No 847097

The use of hydrogen or helium leads to higher efficiencies than the use of heavier working gases due to the low viscosities and high thermal conductivities of these gases. Instead, the higher viscosity and lower thermal conductivity of air and nitrogen tend to reduce the ability to achieve high cycle efficiencies (EPRI, 2002).

The performance of a prototype Beta-type SE with rhombic-drive mechanism was investigated in (Cheng, Yang, & Keong, 2013) considering heating temperatures in the range 650÷850°C, two working gases (air and helium) and charging pressures in the range 4÷8 bar. The authors showed that the shaft power is 1.5÷1.7 higher when using helium in place of air at the same heat source temperature and gas pressure. The reason for the improvement in engine performance with helium is that helium possesses higher thermal diffusivity and lower viscosity than air. The highest power output of 390 Watts was obtained at the highest heating temperature (850°C) and charged pressure (8 bar) and at an optimum engine speed (1400 rpm). Figure 157 shows the experimental results obtained (Cheng et al., 2013).

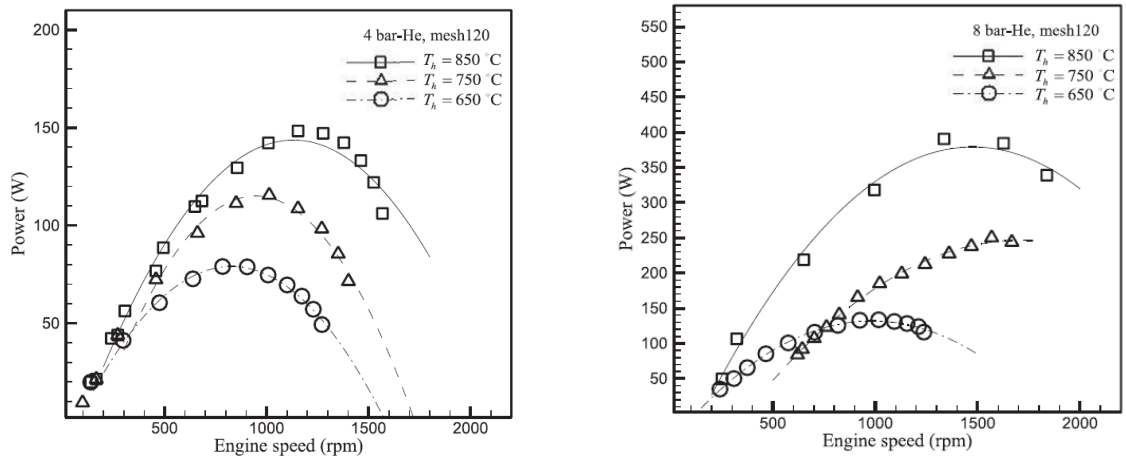

a) *b)*

Figure 157: Variation of the power output of a Beta-type prototype Stirling engine with the engine speed and heating temperature using helium as working gas: a) 4 bar charging pressure; b) 8 bar charging pressure. (Cheng et al., 2013)

In (Bert, Chrenko, Sophy, Le Moyne, & Sirot, 2014) a Gamma-type Stirling engine was investigated and a comparison was performed between air and helium. The authors showed that the power output using helium is much higher compared to air at high engine speeds (approximately higher than 500÷600 rpm), whereas it is lower at low engine speeds. Air has a better heat storage capacity but a lower thermal conductivity than helium. This explains that for low engine speed (i.e., the gases have time to exchange with the wall) air has the capacity to store more energy than helium, but when the engine speed increases the air has not enough time to store heat. Moreover, helium benefits from its convective exchange coefficient which increases with the engine speed.

5.5.2 Examples of applications, technology maturity and performance of SEs

Table 72 summarizes the performance achieved by SE prototypes in different applications. The main applications are electricity production from combustion of natural gas or biomass and CSP. Emerging applications of particular interest for this project are the WHR from exhaust gases and from flue gases.

Horizon 2020
European Union Funding
for Research & Innovation

This project has received funding from
the European Union's Horizon 2020 research and innovation
programme under grant agreement No 847097

Table 72: Applications, operating temperatures, working gas and performance of Stirling engines.

TRL	Heating system	Application or devised application	T hot side/ T source Th (°C)	T cold Tc (°C)	Working gas	Type of Stirling engine	Power output (kW)	Thermal efficiency (%)	Reference
N/A	Heavy-duty truck Diesel engine (315 kW)	Exhaust gas	294	50	Helium	Alpha Beta Gamma	3	/	(Güven et al., 2019)
4	Electric	/	850	/	Air Helium	Beta	0.39[a]	32.2[a]	(Cheng et al., 2013)
9	Natural gas	Combustion gases	700	30	Helium	Alpha	4.6 ÷ 8.5	20	(Rogdakis, Antonakos, & Koronaki, 2012)
4	Electric	Heating resistances	200 ÷ 700	25	Air Helium	Gamma	1	/	(Bert et al., 2014)
4	LPG flame	Solar (domestic scale)	200	27	Air	Beta	0.05	15[b]	(Karabulut, Yücesu, Çinar, & Aksoy, 2009)
4	Gasoline engine	Exhaust gases	550	15	Helium	Beta	3.48	≈25	(T. Li et al., 2012)
4	Electric	Biomass combustion	355	25	Air	Beta	0.09	4.2	(ISSHIKI et al., 2008)
4	Electric	Biomass combustion	750 ÷ 850	20÷50	/	Alpha	2 ÷ 3	25÷30	(Schneider, Müller, & Karl, 2018)
4	Natural gas or lean gas	Combustion gases	676 ÷ 745	/	Helium	Alphagamma (G6ooi)	6.5 ÷ 7.7	38.8÷40.6	("Frauscher thermal motors," 2019)
4	Electric heater	/	184	26	Air	Gamma free-piston	0.016	20.7	(Der Minassians & Sanders, 2011)
N/A	Solar	Nonimaging compound parabolic collectors	130	27	Air	Gamma free-piston	2÷3	16	(Der Minassians & Sanders, 2011)
4	Solar	Dish	850	≈10	/	/	10.9	39.4[c] 34.3[d]	(Reinalter et al., 2008)
4	Solar	Electrical heaters	350 ÷ 500	35	Air	Beta	0.1	5.5 ÷ 9.35	(Sripakagorn & Srikam, 2011)

[a] maximum; [b] internal thermal efficiency (i.e., without considering mechanical losses); [c] thermal-to-mechanical; [d] thermal-to-electrical.

- **Waste fuels combustion**

Many industrial applications produce by-products in the form of gases (residual gas) that are currently burned without harnessing its energy content. For instance in a ferrochrome industry in South Africa the typical fuel composition is: CO (65 %) - H_2 (13 %) - CO_2 (8 %) - O_2 (1 %) - N_2 (13 %). The producers have tried to recover the energy using ICEs or gas turbines, but all solutions have failed. Due to its external combustion the SE is almost insensitive to the type and the quality of gas that is burned. In 2019 the company commissioned their first commercial PWR BLOK 400-F (Figure 158) at Afarak

Horizon 2020 European Union Funding for Research & Innovation
This project has received funding from the European Union's Horizon 2020 research and innovation programme under grant agreement No 847097

Mogale (a Ferrochrome Manufacturer) in South Africa. In July of same year an exclusivity agreement was signed to finalise an installation of 25 PWR BLOK 400-F units for a 9.9 MW power generation facility at Glencore's smelter in Lydenburg in South Africa. ("Swedish Stirling AB," 2019).

Figure 158: One of the seven PWR BLOK 400-F units delivered to a ferrochrome plant in South Africa ("Swedish Stirling AB," 2019).

- **Exhaust gases**

In (Güven et al., 2019) the application of a SE for WHR from the exhaust gas of a heavy duty Diesel engine (Mercedes-Benz Actros tractor with OM470 engine) was investigated. The HE to transfer heat from the exhaust gas to the SE was placed after the after-treatment unit where the exhaust gas temperature was approximately 300°C. The Beta-type Stirling engine could reach the target power (3 kW) with less volume (3525 cm^3) than the other two types, due to overlap volume. The authors showed that the greatest obstacle of SE is the low power-to-weight ratio (30 kg/kW).
As a consequence of closed cycle operation, the heat energy driving a SE must be transferred from the heat source to the working gas by HEs. For small (low-power) SEs the heater or hot-side HE may consist simply of the walls of a hot vessel, but for larger power requirements the HE has to have a greater heating surface area. Hence, in a typical implementation the heater is composed of multiple small-bore tubes in which the working gas (air, hydrogen or helium) flows, usually at high pressure and velocity (Z. Song, Chen, & Yang, 2015). In (T. Li et al., 2012) a SE prototype with output shaft power of several kilowatts driven by mid-high temperature waste gases was developed. The heater was made by a high number (46) of U-shape stainless steel tubes and a swirling flow of the gases was created to increase the gas turbulence and improve the heat transfer between waste gas and helium. A similar design of heater was adopted in (Z. Song et al., 2015) (Figure 159) and, to further reduce the heat transfer resistance on the flue gas side, a heat-resistant steel wool was placed into the space between the outside of the tubes.

Horizon 2020
European Union Funding
for Research & Innovation

This project has received funding from
the European Union's Horizon 2020 research and innovation
programme under grant agreement No 847097

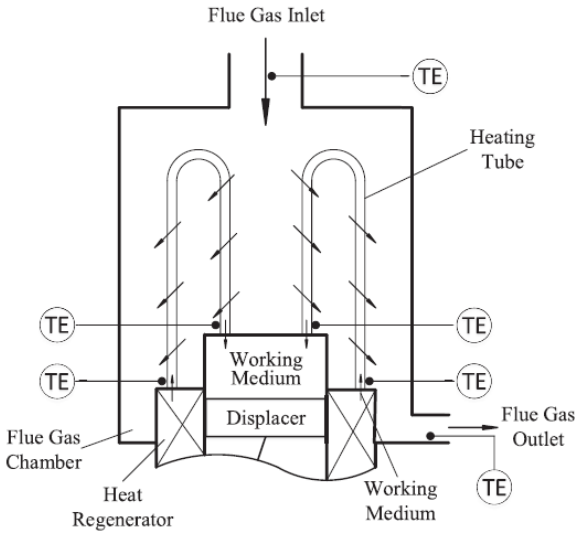

a) *b)*

Figure 159: Heater of a Stirling engine composed of multiple small-bore tubes: a) Layout of the heater tubes; b) Schematic diagram of the heater structure (Z. Song et al., 2015).

- **Concentrating solar power (CSP)**

There are two major directions of SE development in the CSP sector: the high temperature and the low temperature designs.

High temperature solar applications of Stirling engines (Dish/Stirling)

Stirling engines implemented in Dish/Stirling systems generally operate at the thermal limits of the materials used for their construction. Typical temperatures range from 650°C to 800°C resulting in SE conversion efficiencies in the range 25÷40%. Because of their high heat-transfer capabilities, hydrogen and helium have been used as the working gas. Hydrogen, thermodynamically a better choice, generally results in more efficient engines than does helium. Helium, on the other hand, has fewer material compatibility problems and is safer to work with. To maximize power, engines typically operate at high pressure, in the range of 50 to 200 bar (William B. Stine and Richard B. Diver, 1994).

1) *Early Dish/Stirling systems*. Most of the engines used in dish/Stirling applications are kinematic. These include the United Stirling AB (USAB) 4-95 engine and the USAB 4-275 engine, the Stirling Power Systems (SPS)/Solo V-160 engine, the Aisin Seiki NS30A engine, and the Stirling Thermal Motors STM4-120 engine. Instead, Cummins Power Generation developed a free piston engine. The main features and performance of these engines that were designed and manufactured in the eighties and beginning of the nineties are reported in Table 73.

Table 73: Main features and performance of the commercial Stirling engines implemented in high temperature solar dish/Stirling applications (William B. Stine and Richard B. Diver, 1994).

Engine model	Gas temperature (high) (°C)	Coolant temperature (max) (°C)	Working gas	Power (rated) (kW_e)	Efficiency (%)	Manufacturer	Year
4-95	720	50	Hydrogen	25	41	United Stirling AB, Malmo (Sweden)	1984
4-275	620	65	Hydrogen	50	42		1984
Solo V-160	630	/	Helium	9	30	Solo Kleinmotoren,	1991

Horizon 2020 European Union Funding for Research & Innovation
This project has received funding from the European Union's Horizon 2020 research and innovation programme under grant agreement No 847097

						Sindelfingen (Germany)	
NS30A	683	50	Helium	30	25	Aisin Seiki, Kariya City (Japan)	1989
STM4-120	720	45 ÷ 70	Helium or hydrogen	25	40 ÷ 45[a]	Stirling Thermal Motors, Ann Arbor (Michigan, USA)	1988
Free piston	629	/	Helium	9	28 ÷ 33	Cummins Power Generation, Columbus (Indiana, USA)	1992

[a] projected.

2) *More recent Dish/Stirling systems*. The "EuroDish" dish/Stirling system with a nominal power output of 10 kW was developed in a joint European project from 1998 to 2001. A second development step was made in the project "Envirodish" (funded by Germany) introducing many improved components to the system and ending with the erection of three "country reference units" erected in 2004. The measurements on the reference unit in Odeillo (France) (Figure 160) were carried out within the EU "Solface" program and reported in (Reinalter et al., 2008). The measurement campaign was aimed at determining the optical and thermodynamic efficiency of the system. The thermal power into engine was calculated equal to 31.6 kW and the measured electrical power and shaft power outputs were 10.9 kW and 12.3 kW, respectively. Thus, the thermal efficiency of the Stirling engine approached 40% and the electrical efficiency approached 35%. Considering all the losses, the overall system efficiency for the conversion of solar radiation to net electric power was calculated equal to 22.5% (Reinalter et al., 2008).

Figure 160: The 11 kW$_e$ Dish/Stirling system built in France in 2004 (Reinalter et al., 2008).

Low temperature solar applications of Stirling engines

1) *Combination with parabolic trough collectors*. In (Sripakagorn & Srikam, 2011) a 100 W prototype SE (Figure 161 left) working at the moderate temperature range was developed to demonstrate the potential of the moderate temperature SE as an option for the parabolic trough solar collector technology. The moderate temperature difference allows the use of low cost materials and

Horizon 2020 European Union Funding for Research & Innovation

This project has received funding from the European Union's Horizon 2020 research and innovation programme under grant agreement No 847097

simplified mechanical designs. It was shown that the thermal efficiency of a SE increased by almost 4%-points as the heater temperature increased from 350°C to 550°C (Figure 161 right).

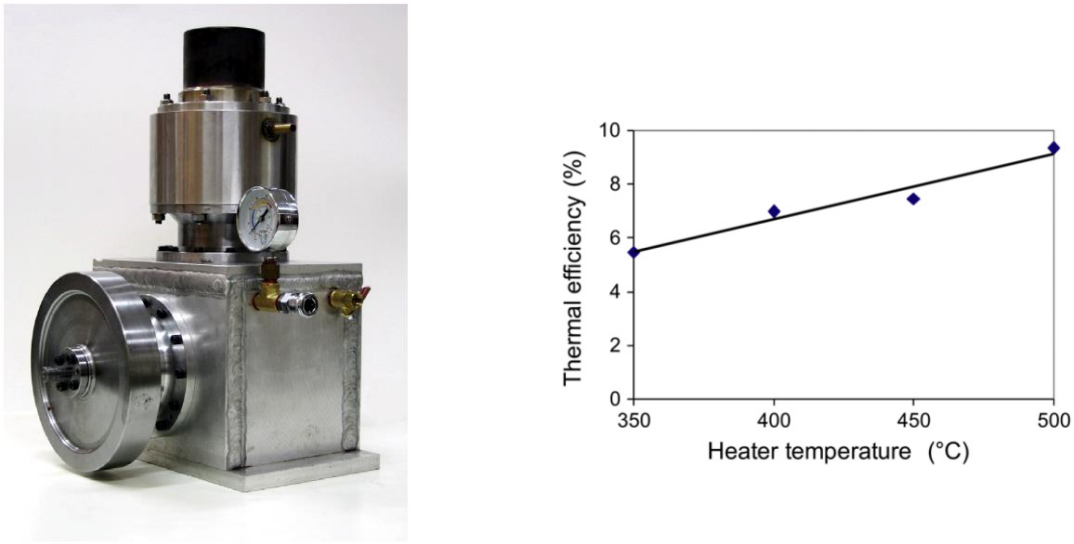

a) *b)*

Figure 161: Stirling engine for medium temperature solar applications: a) the 100 Watt engine prototype; b) variation of thermal efficiency with heater temperature (Sripakagorn & Srikam, 2011).

2) *Combination with evacuated tube collectors*. The free piston SE developed in (Der Minassians & Sanders, 2011) was conceived to operate with collector temperatures in the range of 120°C to 150°C, which is consistent with the use of stationary solar thermal collectors employing low-concentration nonimaging reflectors that are cheaper compared to tracking collectors with high concentration ratios. The use of low-temperature heat limits the theoretical maximum thermodynamic efficiency achievable by the heat engine. This disadvantage, however, can be compensated by lower costs in materials and in reduced maintenance. The efficiencies of a representative solar collector (Schott ETC 16), the Stirling engine, and the overall system are plotted as a function of temperature in Figure 162. Based on the experimental results obtained for a small prototype, a higher power Stirling engine with 2÷3 kW output power was proposed with a thermal efficiency of 16%.

Horizon 2020
European Union Funding
for Research & Innovation

This project has received funding from
the European Union's Horizon 2020 research and innovation
programme under grant agreement No 847097

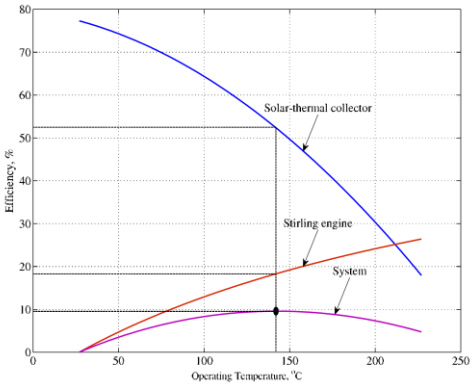

Figure 162: Variation of the efficiency of the solar collector, Stirling engine and overall system as a function of the operating temperature (Der Minassians & Sanders, 2011).

- **Biomass combustion and gasification**

The Stirling engine can be used for electricity generation from the flue gases generated by the combustion of solid biomass or the combustion of syngas produced in biomass gasifiers.

Stirling engine driven by the flue gas of biomass combustion. Stirling engines especially designed for CHP plants using solid biomass fuels have been developed at the Technical University of Denmark since the early nineties. The flue gases from the biomass combustion are used to heat the working gas of the SE according to the schematic shown in Figure 163. A 35 kW unit was put in operation in 2002 in Mawera (Austria) as shown in Figure 164. The SE was mounted downstream of the secondary combustion chamber and the surface temperature of the SE heater was 780°C. An automatic cleaning system was developed to remove fly ash particles from the SE heater. The air preheater and the economizer were placed on the top of the furnace to achieve a compact plant design. During test runs the plant achieved an overall plant electric efficiency (LHV based) of 12% (Obernberger, 2010).

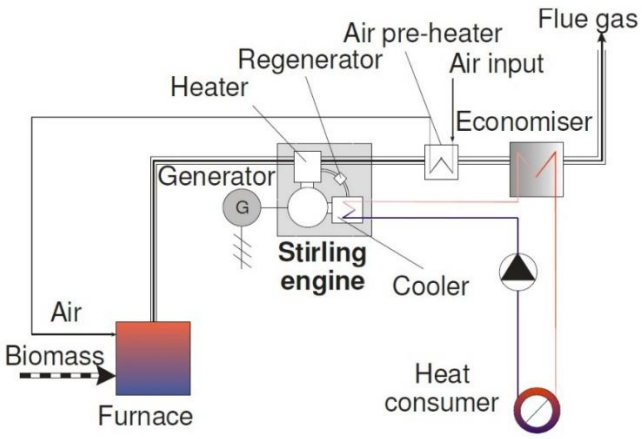

Figure 163: Schematic of a CHP plant based on Stirling engine and biomass combustion (Obernberger, 2010).

Horizon 2020
European Union Funding
for Research & Innovation

This project has received funding from
the European Union's Horizon 2020 research and innovation
programme under grant agreement No 847097

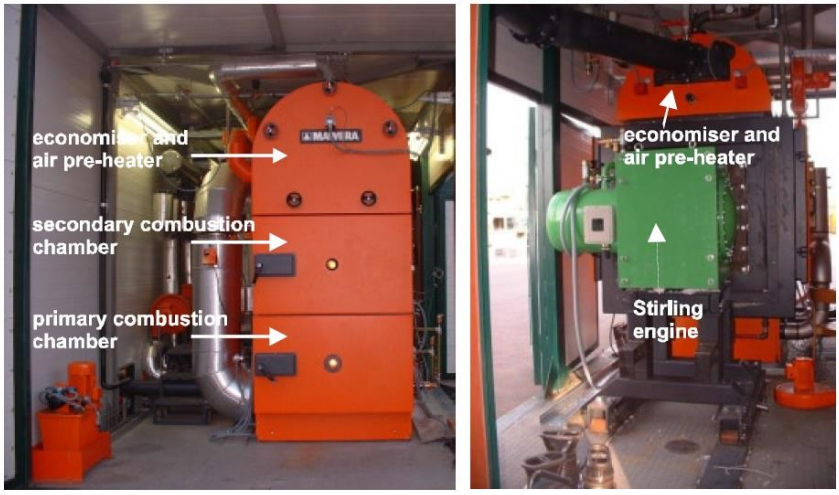

Figure 164: Photo of the CHP plant based on Stirling engine and biomass combustion (Obernberger, 2010).

Fluidized bed fired Stirling engine. An innovative micro-scale CHP plant concept was developed at the Friedrick –Alexander University Erlangen-Nurnberg (Germany) combining a small fluidized bed combustion with a Stirling engine. An efficient cooling of the combustion zone through an in-bed heat exchanger (e.g., of a Stirling engine) gets possible without exceeding ash melting temperatures. Tests in lab environment already showed promising results regarding the Stirling performance and in the EU project "BioWasteStirling" this concept will be transferred to a pilot plant scale for long-term testing with different woody fuels as well as various solid biogenic residues in a field test environment (Schneider et al., 2018). The objective of the "BioWasteStirling" project will be the development and field testing of a highly efficient, fuel flexible pilot CHP-system consisting of a 45 kW_t fluidized bed combustion and a 5 kW_e Stirling engine.

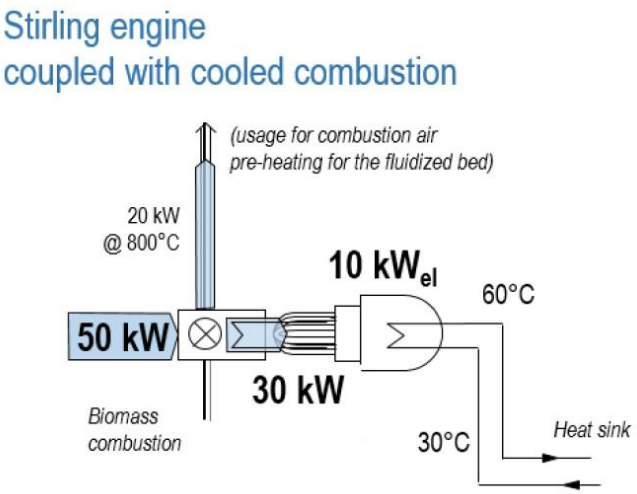

Figure 165: Biomass fired CHP system with Stirling engine (Schneider et al., 2018).

Horizon 2020
European Union Funding
for Research & Innovation

This project has received funding from
the European Union's Horizon 2020 research and innovation
programme under grant agreement No 847097

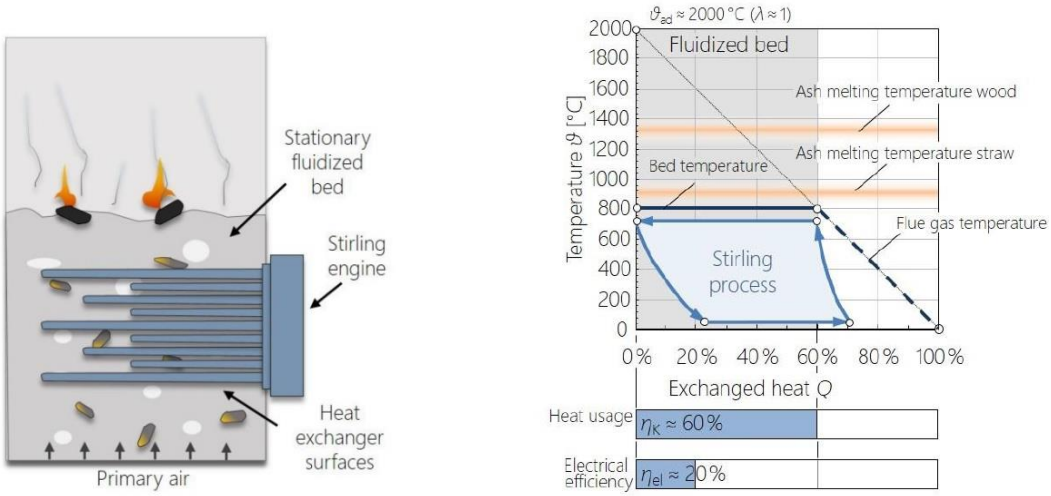

a) *b)*

Figure 166: Fluidized bed fired Stirling engine: a) Direct placement of the Stirling engine heater into a fluidized bed; b) T-q diagram of the heat transfer between combustion gases and the engine (Schneider et al., 2018).

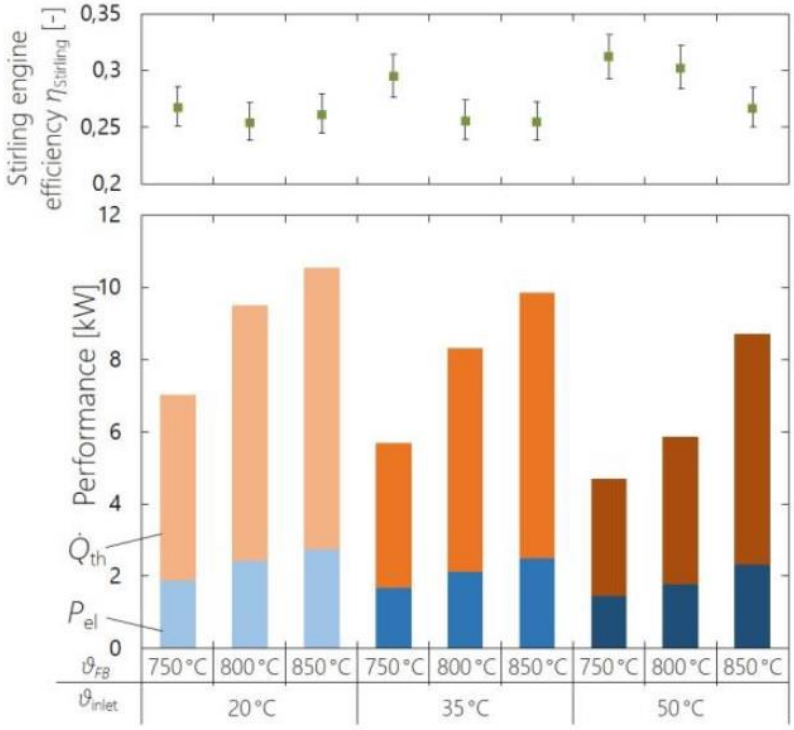

Figure 167: Variation of the efficiency of the Stirling engine as a function of the fluidized bed temperature (750÷850°C) and cooling temperature (20÷50°C).

Horizon 2020
European Union Funding
for Research & Innovation

This project has received funding from
the European Union's Horizon 2020 research and innovation
programme under grant agreement No 847097

Figure 168: HE surfaces of the Stirling engine heater before and after the tests (Schneider et al., 2018).

CHP plant based on biomass gasification. The system is made of three main parts: the updraft gasifier, the combustion chamber and the Stirling engine (Figure 169). The product gas from an updraft gasification process contains significant amounts of tar and the net calorific value is approximately 10% of the heating value of natural gas. Its combustion in an internal combustion engine would require cleaning, tar removal or gas conditioning. Instead in the combustion chamber it is directly burned along with the tar. The SE is mounted opposite the burner in the other end of the combustion chamber. The heater of the SE transfers 125 kW of heat from radiation and convection to the working gas (helium) that produces an electrical power output of 35 kW. This results in a net electrical efficiency of the SE equal to 28%. The SE heater reduces the flue gas temperature from 1350°C to 650÷750°C. Then the flue gas flows through an air preheater and an economizer and leaves the plant at around 120÷140°C (Marinitsch, Bovin, Gørtz, Mygind, & Carlsen, 2011). The achieved overall electrical plant efficiency (defined as the ratio between electrical output and fuel input) measured on an existing biomass Stirling CHP plant was around 17.5%. The authors showed that an increase of the operating temperature of the heater would increase the SE efficiency but would reduce the heat that can be taken from the flue gas (Figure 170). In (Groth, Marinitsch, & Newman, 2012) the combined thermal output from the economizer and the SE was used to drive an absorption chiller.

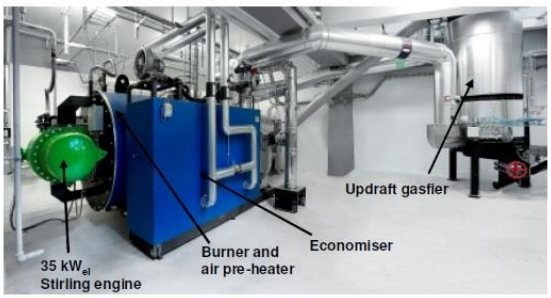

Horizon 2020
European Union Funding
for Research & Innovation

This project has received funding from
the European Union's Horizon 2020 research and innovation
programme under grant agreement No 847097

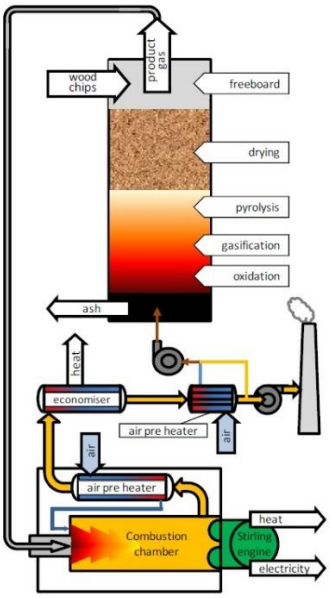

a) *b)*

Figure 169: Stirling engine CHP plant using updraft gasification: a) Flow diagram (Marinitsch et al., 2011); b) Picture of the system (Obernberger, 2010).

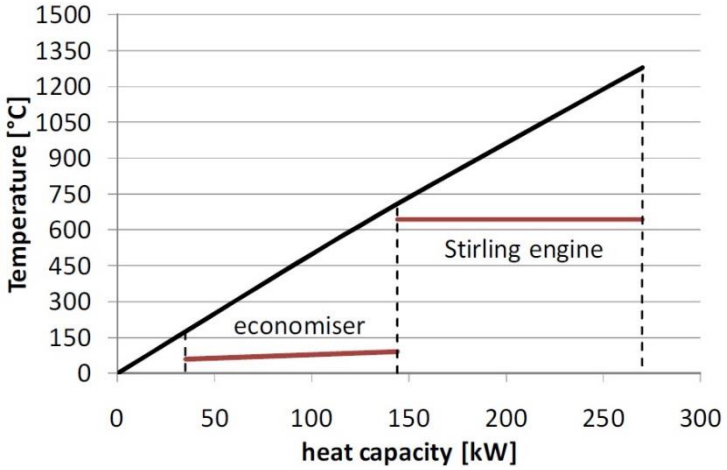

Figure 170: T-q diagram of the heat transfer between flue gas and the two heat sinks (helium in the Stirling engine and water in the economizer). The air preheating is not considered.

- **Manufacturers of Stirling engines**

The main active manufacturers of Stirling engines are Frauscher Thermal Motors, Microgen Engine Corporation, Qnergy and Swedish Stirling. The main features and applications of their engines are briefly summarized in the following.

1) *Frauscher Thermal Motors*. The measurements made in the course of the research project "Lean Gas CHP" showed a high level of development of the prototype Stirling machine G60oi (Figure 171) both in natural gas and lean gas operation. The engine uses a novel layout (called Alphagamma) and has a power output of 7 kW. The SE efficiency was in the range 39÷40% operating with helium at maximum temperatures in the range 680÷740°C. The overall efficiency of the system, defined as the ratio between the electric power output and the fuel input (LHV

Horizon 2020
European Union Funding
for Research & Innovation

This project has received funding from
the European Union's Horizon 2020 research and innovation
programme under grant agreement No 847097

based), was 31% for operation with NG and varied in the range 26÷30% for operation with lean gas (e.g., biogas) having a low methane content (<50%). ("Frauscher thermal motors," 2019).

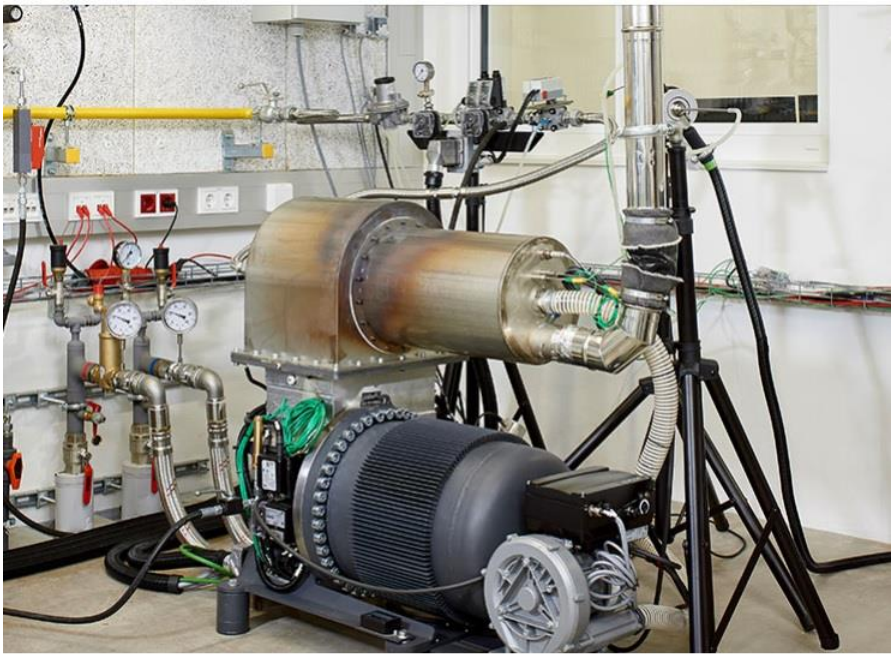

Figure 171: Photo of the 8 kW alphagamma® Stirling engine model G60oi ("Frauscher thermal motors," 2019).

2) *Microgen Engine Corporation (MEC)*. Microgen Engine Corporation started serial production and sales of the 1 kW Free Piston SE in 2010 (Figure 172). Combined with the burner, controllers and HE, the MEC 1 kW engine has been applied in thousands of domestic CHP applications that have been installed by heating companies around Europe (Viessmann, Vaillant and Boesch, ÖkoFEN, etc.). For instance, ÖkoFEN sells a pellet-CHP system with a 1 kW_e free-piston Stirling from Microgen, integrated in the freeboard of one of their commercial pellet boilers ("OkoFEN," 2019).

a) *b)*

Figure 172: Microgen Stirling engine: a) 1 kW Stirling engine; b) serial production of Stirling engines ("Microgen Engine Corporation," 2019).

Horizon 2020
European Union Funding
for Research & Innovation

This project has received funding from
the European Union's Horizon 2020 research and innovation
programme under grant agreement No 847097

3) *Qnergy*. Based on Qnergy's no-maintenance and highly reliable PCK series SE (Figure 173), the generator package can work with a variety of fuel supplies including: natural gas, propane, ethane, biogas, and multiple associated gas streams. ("Qnergy," 2019).

Figure 173: Qnergy QB80 series engine ("Qnergy," 2019).

4) *Swedish Stirling*. Swedish Stirling was founded in 2008 and during its first years, the company focused on developing the SE to be used with solar energy. In September 2017, Swedish Stirling launched its new product named PWR BLOK 400-F (Figure 158). It is a container-based solution in which SEs are used to harness energy from flare and industrial residual gas combustion. The PWR BLOK 400-F contains 14 Stirling engines and delivers a net electrical output of 400 kW. The working gas inside the SE is hydrogen (H_2) and the net efficiency of the Stirling engine is around 30%.

5.5.3 Cost aspects

For high temperature SEs the specific investment cost is in the range 1250÷1500 €/kW for large customized systems having a capacity of hundreds kW, like that recently installed in the ferrochrome industry in South Africa ("Swedish Stirling AB," 2019). Instead, the estimated cost for low temperature 2÷3 kW mass produced SEs can easily be 300 US$/kW or even less (Der Minassians & Sanders, 2011). In low temperature systems the metal (e.g., copper) content of the SE can be reduced by replacing many metallic parts with plastics (Der Minassians & Sanders, 2011).

Table 74: Specific cost of Stirling engines.

Model	Cost (€)	Power (kW)	Number of Stirling engines	Specific cost (€/kW)	Reference
PWR BLOK 400-F	500000 ÷ 600000	400	14	1250÷1500	("Swedish Stirling AB," 2019)

Horizon 2020 European Union Funding for Research & Innovation

This project has received funding from the European Union's Horizon 2020 research and innovation programme under grant agreement No 847097

5.6 Thermoelectric generators (TEGs)

5.6.1 Technological features of thermoelectric generators

Thermoelectric materials converts heat directly into electricity by exploiting the Seebeck effect. Electricity generation persists as long as the thermoelectric material is exposed to a temperature difference. In its simplest form, a thermoelectric generator (TEG) is composed by two distinct thermoelectric materials (Figure 174). The electromotive force (voltage) generated by the TEG is given by:

$$V = S(T_1 - T_2) \qquad 5$$

Where S is the Seebeck coefficient.

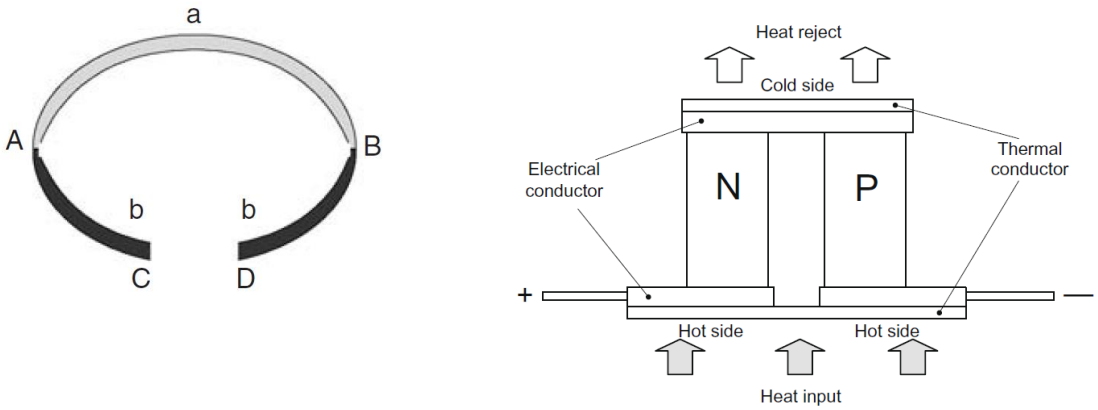

a) b)

Figure 174: a) Basic schematic of a thermocouple (Rowe, 2006); b) Schematic of a TEG generator formed by a single TEG couple (C. Yu & Chau, 2009).

The efficiency of the TEG is defined as the ratio of the electrical power delivered to the heat absorbed. The maximum efficiency of thermoelectric generation is determined by a parameter called "Figure-of-merit" (Z), which is defined as follows:

$$Z = \frac{S^2\sigma}{\lambda} \qquad 6$$

where S is the Seebeck coefficient, σ is the electrical conductivity and λ is the thermal conductivity of the two arms of the junction. It can be demonstrated (see e.g., (Rowe, 2006)) that the maximum conversion efficiency is:

$$\eta_{TEG} = \frac{T_H - T_C}{T_H} \cdot \frac{\sqrt{1 + ZT_M} - 1}{\sqrt{1 + ZT_M} + \frac{T_C}{T_H}} = \eta_c \cdot \gamma \qquad 7$$

where T_H and T_C are the absolute temperatures of the heat source and heat sink, respectively and T_M is the mean temperature between T_H and T_C. So, the maximum conversion efficiency is bounded by the Carnot efficiency (η_c) and a parameter (γ) that embodies the properties of the materials.

Horizon 2020
European Union Funding
for Research & Innovation

This project has received funding from
the European Union's Horizon 2020 research and innovation
programme under grant agreement No 847097

The thermoelectric efficiency increases with the dimensionless figure of merit ($ZT_M = ZT$). Commercial thermoelectric materials today typically reach effective figures of merit *ZT* around unity, while figures of merit up to *ZT*=3.5 have been published (Zheng, Liu, Yan, & Wang, 2014). A more realistic midterm assumption is that materials with a maximum *ZT* of up to 2 may be commercialized in the near future (Bode et al., 2017) and technology roadmaps project *ZT* value up to 3.0 by 2030 (Kishita et al., 2016). The corresponding conversion efficiency is shown in Figure 175 considering *ZT* values up to 2÷3 or even higher. Using a heat source at 280°C the conversion efficiency could increase from the current 7.2% to values higher than 15% if new materials with *ZT* as high as 3 are developed.

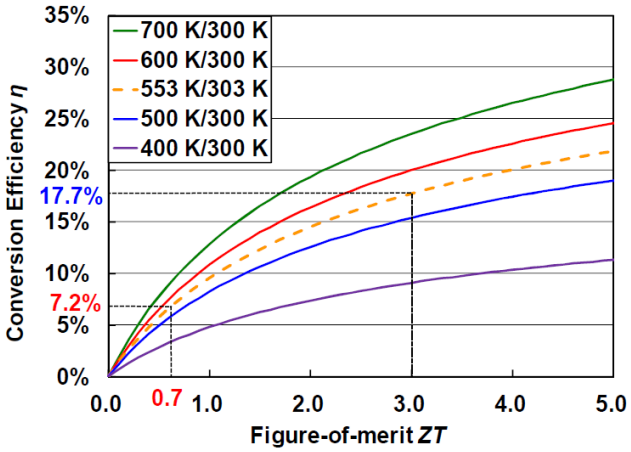

Figure 175: Relationship between the dimensionless figure of merit (*ZT*) and the conversion efficiency (Kishita et al., 2016).

5.6.2 Commercially available thermoelectric materials and modules

Semiconductors which lie between metals and insulators are the best for thermoelectric properties (Ravindra, 2019). In spite of intense studies, Bi_2Te_3, with a dimensionless figure of merit as high as 1, still remains among the most performant thermoelectrics since its discovery six decades ago (Ravindra, 2019). Several companies worldwide sell thermoelectric modules based on Bi-Te alloys (Table 75). These modules operate between a hot side temperature in the range 200÷300°C and a cold side temperature of 30÷50°C and show a maximum efficiency around 5%. The power output of each single module is in the range 2÷20 Watts. The efficiency curve in Figure 176 of a 20 Watt commercialized module by a U.S. company (Hi-Z Technology, 2019) shows that the module efficiency increases with the temperature difference between hot and cold side and reaches the maximum at an optimum ΔT.

Table 75: Performance of commercial thermoelectric modules based on Bi-Te alloys.

Temperature hot side (°C)	Temperature cold side (°C)	Power (Watt)	Maximum efficiency (%)	Company
230	50	2.71 ÷ 7.95	4.97 ÷ 5.03	(Marlow Industries, 2019)
300	30	5.1 ÷ 14.6	/	(TECTEG, 2019)
300	30	5 ÷ 22	5.6 ÷ 5.9	(TEGMART, 2019)
250	50	2.3÷20	≈ 5	(Hi-Z Technology, 2019)

Horizon 2020
European Union Funding
for Research & Innovation

This project has received funding from
the European Union's Horizon 2020 research and innovation
programme under grant agreement No 847097

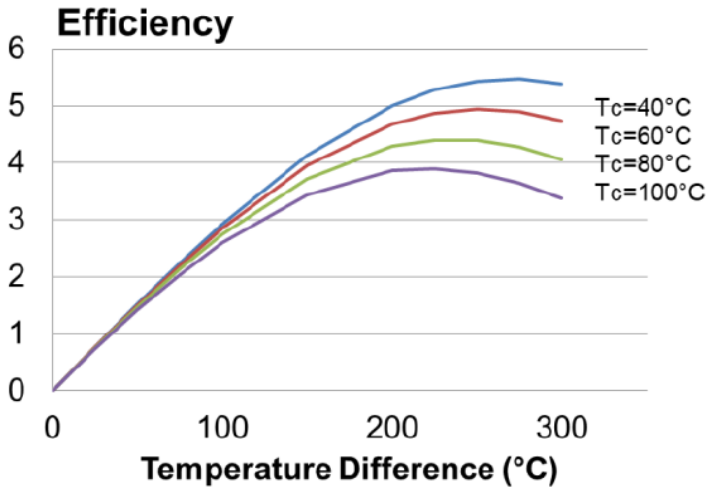

Figure 176: Efficiency curve of a commercial 20 Watt thermoelectrical module (Hi-Z Technology, 2019).

5.6.3 Novel high efficient thermoelectric materials for medium-high temperature applications

Over the past 10 years new state of the art materials with high *ZT* have been developed as shown in Figure 177 (Pineda, 2017). However, no TE material is currently mass-produced, beside bismuth telluride and lead telluride. In particular, all materials shown in Figure 177 operating with hot-side temperature in the range of 500°C are not available commercially. While they can be fabricated using industry-standard powder metallurgy processes, the necessary manufacturing infrastructures are not in place to support commercialization of TE heat-to-power conversion (D. Crane et al., 2013). In recent years, strong efforts have been devoted to improve the manufacturing process and accelerate the mass production of two classes of novel materials that have demonstrated significant promise for WHR in the medium temperature range: 1) half Heuslers alloys and 2) skutterudites. These materials are low-cost, based on most earth-abundant elements and eco-friendly materials. For instance, the recently completed European H2020 project INTEGRAL has focused on half-Heusler alloys. (INTEGRAL H2020, 2019). The ongoing European H2020 project MAGENTA concentrates on the newly discovered thermal-to-electric energy conversion capacity of ionic-liquids and ferrofluids (i.e., colloidal dispersions of magnetic nanoparticles in ionic liquids) (MAGENTA H2020, 2019).

Figure 177 clearly shows that every thermoelectric material operates at its maximum figure-of-merit at a specific temperature. Consequently, when operating over a wide temperature range the majority of the thermoelement material is operating below its potential maximum performance (Rowe, 2006). In these cases the thermoelectric performance can be improved by "segmentation". In this arrangement two materials are joined or segmented together, each with its figure-of-merit optimized for a different temperature range. For segmented generators, high *Z* materials need to be selected, which have similar "compatibility factors" (see (Jeffrey Snyder, 2006) for the definition). As a rule of thumb, the compatibility factors of segmented materials should be within about a factor of two. Outside this range are materials which are incompatible where the efficiency will be substantially less than that expected from *Z* (Jeffrey Snyder, 2006). The compatibility factor is therefore, like *Z*, a thermoelectric property essential for an efficient segmented thermoelectric device.

Horizon 2020
European Union Funding
for Research & Innovation

This project has received funding from
the European Union's Horizon 2020 research and innovation
programme under grant agreement No 847097

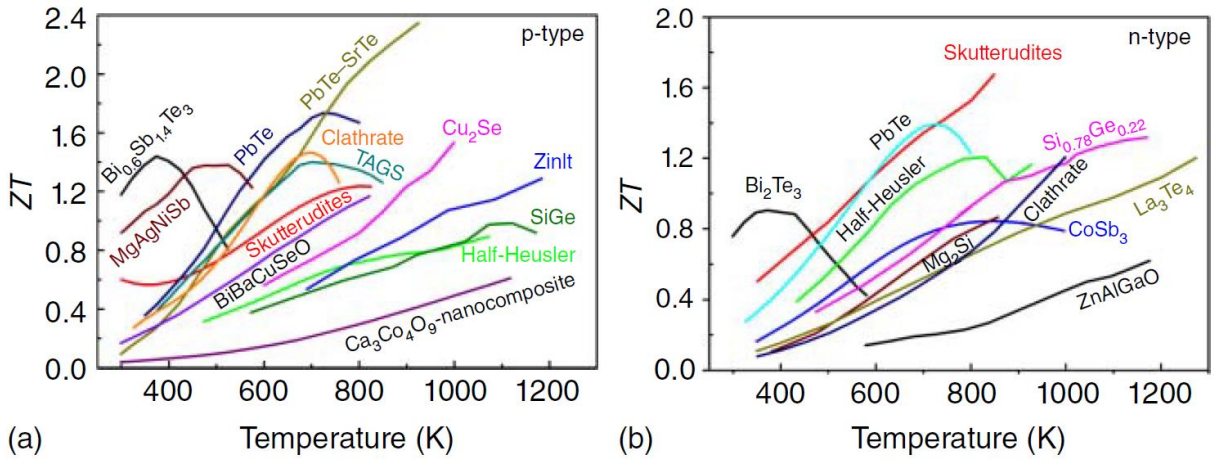

Figure 177: Dimensionless figure of merit (*ZT*) as a function of temperature for state-of-the-art thermoelectric materials: (a) p-type materials and (b) n-type materials (Pineda, 2017).

5.6.4 Application of TEG for recovery of waste heat

Table 76 summarizes the main features and performance of TEG systems for WHR in various industries (steel, cement, chemical and manufacturing).

- *Steel industry*. One of the recently emerging applications for TEG is the recovery of radiant heat form sources such as hot steel slabs in steel casting processes. In Figure 178 a thermoelectric energy conversion system is installed above the casting belt, facing down towards the belt, so that the radiant heat is transferred and absorbed at the heat collection plate of the TE system. The absorbed heat is then converted to electricity by the TE module.

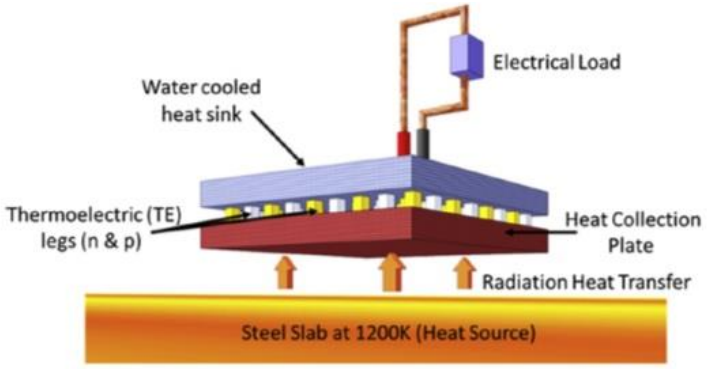

Figure 178: Schematic of a thermoelectric module suspended over the radiating steel slab (Ghosh, Margatan, Ahn, & Bahk, 2018).

The 10 kW grid-connected TEG system installed in a continuous casting line in Japan (Figure 179) is composed by 56 TEG units each containing 16 modules. The size of the TEG system is about 4 m × 2 m, with a distance between the slab and the TEG units of about 2 m. The heat collection plates of the TEG units are heated by radiant heat from continuous casting slab and the side face of the heat collection plate is approximately 250°C (Kuroki et al., 2015). Using a nanostructured Bi-Te alloy with a high dimensionless figure of merit (*ZT*=1.4 for p-type and ~1.0 for n-type, both at 400 K) Ghosh estimated that a maximum power density as high as 1.5 kW/m² could be achieved (Ghosh et al., 2018).

Horizon 2020
European Union Funding
for Research & Innovation

This project has received funding from
the European Union's Horizon 2020 research and innovation
programme under grant agreement No 847097

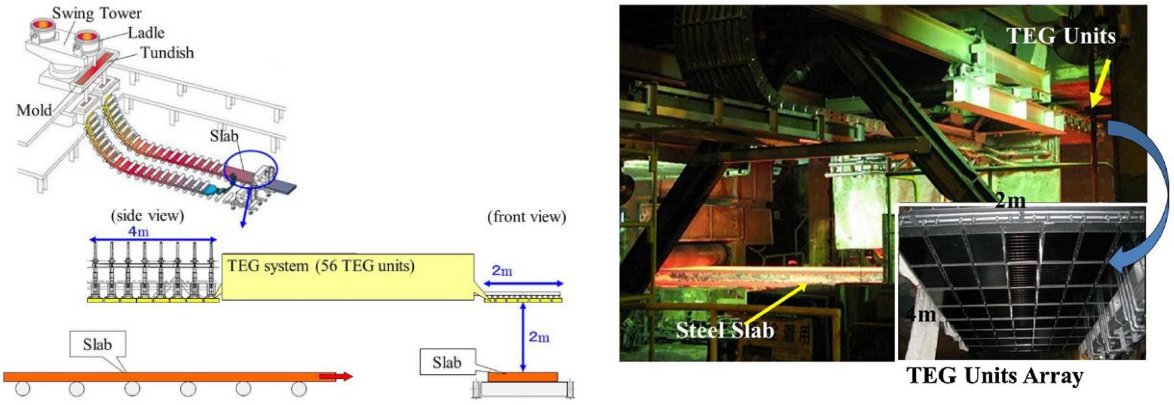

a) b)

Figure 179: TEG system installed in a continuous casting line in Japan (Kuroki et al., 2015): a) Schematic of the system; b) photo of the installed system.

- *Cement industry*. Rotary kilns are the main equipment used for large-scale industrial cement production. Substantial amounts of heat are consumed in the rotary kilns, and approximately 8÷15% of the total input energy is lost through the kiln shell. The configuration proposed in (Q. Luo et al., 2015) recovers convection and radiation WH from the secondary shell coaxial of rotary kiln (Figure 180). Two different kinds of TE material with different operating temperatures were chosen to better suit the different temperatures along the longitudinal direction: a Bi-Te alloy in the first and third zone having a maximum surface outer temperature of 300°C, and a Pb-Te alloy in the middle zone having a higher outer temperature around 400°C. The calculated TE efficiency varied in the range 2.0÷3.7% depending on the axial position.

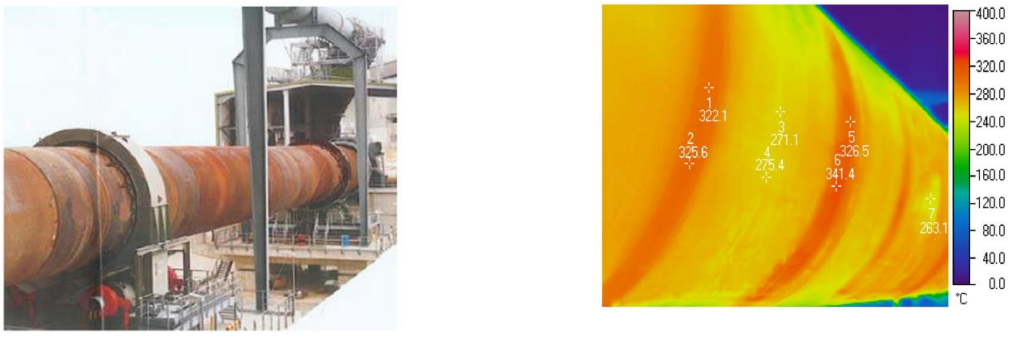

a) b)

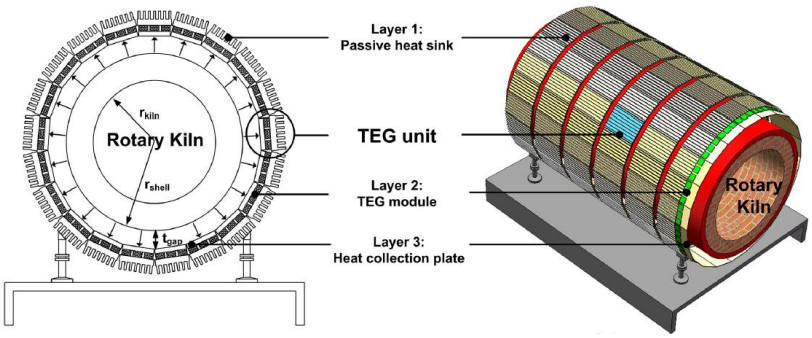

Horizon 2020
European Union Funding
for Research & Innovation

This project has received funding from
the European Union's Horizon 2020 research and innovation
programme under grant agreement No 847097

c)

Figure 180: a) Rotary kiln for cement production; b) External surface temperature of the rotary kiln as shown by infrared thermal imaging; c) Configuration of thermoelectric WHR system analysed by (Q. Luo et al., 2015).

- *Combustion of waste fuel gases*. In the TEG system installed at a carburizing furnace in Japan the residual carburizing gas composed of CO and H_2 was burned, and the flame constantly heated up the hot side of TEG (Figure 181). However, only 20% of the total combustion heat (which means 4 kW out of 20 kW) could be used to drive the TEG due to the poor performance of the heat capturing elements (plain plate or fin structure). The generated electric output power charged a set of storage batteries and then through DC/AC inverters powered LED light tubes inside the factory (H. Kaibe, Makino, Kajihara, Fujimoto, & Hachiuma, 2012).

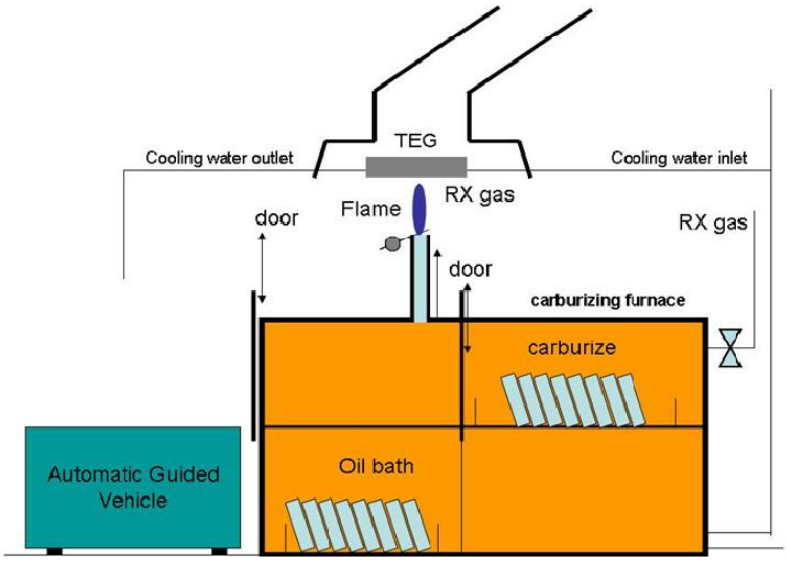

Figure 181: Thermoelectric generating system set up at a carburizing furnace. TEG is placed over blue flame (H. Kaibe et al., 2012).

- *Exhaust pipes, ducts and chimneys*. In the case study concerning an industry in Spain (manufacturing of stone wool insulation products) WH from a 30-meter-long exhausts pipeline at 230°C was in part recovered using TEGs. (Araiz, Casi, Catalán, Martínez, & Astrain, 2020). The energy company AEInnova (AEInnova, 2019) born from the European Life project HEAT-R (HEAT-R, 2019) installed similar TEG systems in industrial chimneys (Figure 182).

Figure 182: Examples of TEG systems installations in chimneys (AEInnova, 2019).

Horizon 2020
European Union Funding
for Research & Innovation

This project has received funding from
the European Union's Horizon 2020 research and innovation
programme under grant agreement No 847097

Table 76: Industrial WHR applications using TEGs: real systems and case studies.

TRL	Application	Temperature source (°C)	Material	TE efficiency (%)	Power (kW)	Power density (kW/m²)	Reference
9	Radiant heat from molten metal in a continuous casting line	Steel slab T (915)	Bi-Te	7.2[a]	10	1.2	(Kuroki et al., 2015)(Kuroki et al., 2014)
9	Heat of flames in the afterburner of a carburizing furnace	Flame T (>1000)	Bi-Te	5.4	0.214	1.8	(Hiromasa Kaibe, Kajihara, & Fujimoto, 2011)(H. Kaibe et al., 2012)
N/A	Radiant heat from hot steel casting slabs	Steel slab T (927)	Nanostructured Bi-Te alloys	8	/	1.5	(Ghosh et al., 2018)
N/A	Heat losses from the outer surface of a cement rotary kiln	200 ÷ 400	Bi_2Te_3 PbTe	2.8	211	≈0.2	(Q. Luo et al., 2015)
N/A	Hot gas flow in a stone wool manufacturing plant	120 ÷ 230	Bi-Te	3.3	≈50	/	(Araiz et al., 2020)

[a] maximum conversion efficiency of the single module.

5.6.4.1 WHR from internal combustion engines

Recovery of WH from ICEs is another promising application of TEG. Figure 183 shows a typical schematic of a TEG integrated with exhaust pipeline for WH recovery from the exhaust gas. The arrangement consists of hot-gas channels for the exhaust gas and cooling water channels for the coolant flow. TE modules are arranged between the hot and the cold channels. The heat transfer in the hot side channels is usually enhanced by fins. When the exhaust gas from the ICE flows along the pipeline, WH is transferred to the hot side of TEGs, part of which is directly converted into electric power and the remaining dissipated into the surrounding air or is taken away by liquid as shown in Figure 184 (Shen, Tian, & Liu, 2019).

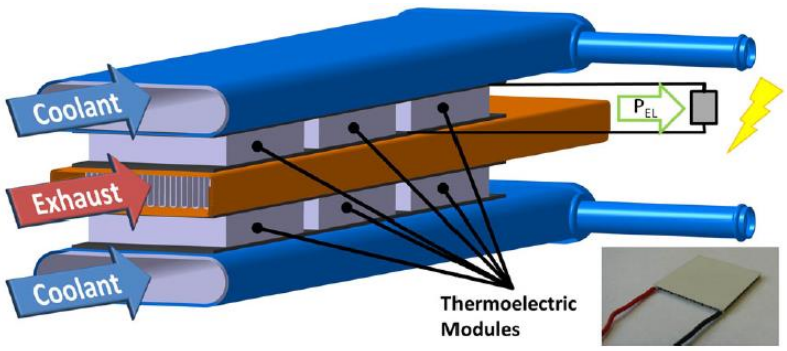

Figure 183: Schematic of a TEG for exhaust gas applications.

Horizon 2020 European Union Funding for Research & Innovation
This project has received funding from the European Union's Horizon 2020 research and innovation programme under grant agreement No 847097

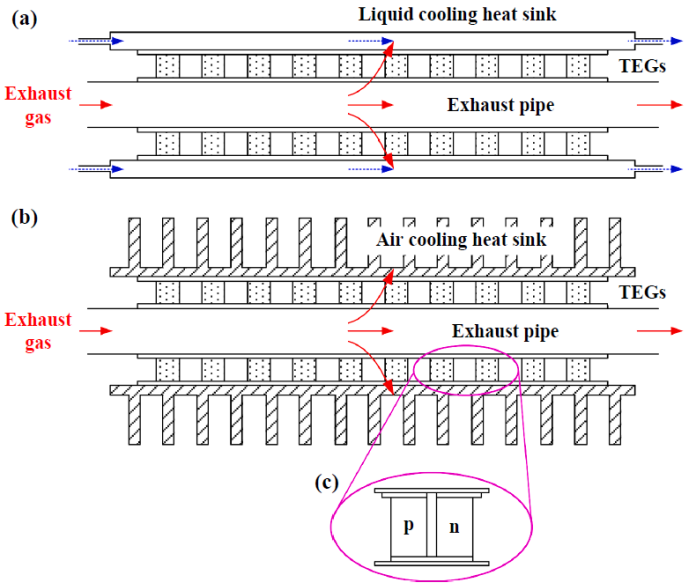

Figure 184: Operation principle and construction of a TEG for automotive applications: a) liquid cooled TEG; b) air cooled TEG (Shen et al., 2019).

Table 77 summarizes the main features and performance of TEG prototypes for WHR from ICEs. One of the first TEG generator coupled to the exhaust gas of a turbocharged Diesel engine was built at the beginning of the nineties in the U.S. and reported in (Bass, Elsner, & Leavitt, 1995). It generated 1 kW using 72 Bi-Te modules. The main purpose was to provide auxiliary electric power for a class 8 Diesel truck engine instead of using the engine driven alternator. In the modern engines the TEG is typically integrated into the exhaust gas line behind the exhaust gas aftertreatment, in order not to lower the temperature within the aftertreatment catalytic converters.

In the prototype shown in Figure 185 (Frobenius, Gaiser, Rusche, & Weller, 2016) the TEG is positioned at the central muffler. The TEG is arranged in longitudinal direction and a bypass pipe protects the TE materials from exceeding temperatures. In the European FP7 project HEATRECAR (HEATRECAR FP7, 2013) the TEG system was able to deliver 0.5 kW at the design point, with inlet gas at 450°C. A thermoelectric by-pass was included to limit the highest TE modules temperature at 270°C to prevent the damage of the Bi-Te modules. In the DOE sponsored program summarized in (D. Crane et al., 2013) a high temperature TEG made of segmented TE elements consisting of half-Heusler at the hot side and Bi_2Te_3 at the cold side (D. T. Crane, Koripella, & Jovovic, 2012) was integrated into two-passenger vehicles (a BMW X6 and a Lincoln MKT) and over 0.6 kW was produced in on vehicle tests. A 1 kW TEG containing 400 nanostructured bulk half Heuslers modules for a Diesel engine of a military tank was reported in (Meda, Romzek, Zhang, & Cleary, 2016) and shown in Figure 187. A TEG system based on the same materials was developed, engineered, and fabricated at the Oak Ridge National Laboratory capable of generating up to 0.3 kW for a gasoline passenger sedan application (Szybist, Davis, Thomas, & Kaul, 2018). For the EGR (exhaust gas recirculation) WHR a TE assembly made of skutterudite was fabricated in a joint collaboration between Michigan State University (MSU) and NASA-JPL aimed at enhancing the technology-readiness level of skutterudites to facilitate mass manufacturing similar to that of Bi-Te alloys. Recently, a consortium of three UK universities supported by industry partners have demonstrated skutterudite materials in an engine WHR application (Stobart & Yang, 2018).

Horizon 2020
European Union Funding
for Research & Innovation

This project has received funding from
the European Union's Horizon 2020 research and innovation
programme under grant agreement No 847097

Table 77: Waste heat recovery from engine exhaust gases using TEGs: prototypes using low and high temperature thermoelectric materials.

TRL	Application	Position of TEG	Temperature source (°C)	Material	TE efficiency (%)	Power (kW)	References
4	Exhaust gases of a heavy duty truck	a) Exhaust gas path b) EGR path	a) 300 b) ≈500	Bi-Te	a) 2.3 b) /	a) 0.416 b) 0.400	(Frobenius et al., 2016)(Risseh et al., 2017)
4	Exhaust gases from an automobile engine	Exhaust gas between catalytic converter and muffler	310	Bi-Te	/	0.94	(X. Liu, Deng, Li, & Su, 2015)
4	Exhaust gases from a Diesel light duty truck	Exhaust gas path	450	Bi-Te	/	0.17 ÷ 0.50	(HEATRECAR FP7, 2013)
4	Exhaust WH from an automotive gasoline engine	Between catalyst and middle muffler	/	Segmented TE elements: half-Heusler (hot side) and Bi-Te (cold side)	/	0.600 ÷ 0.700	(D. Crane et al., 2013)
4	Diesel engine of a military tank	Exhaust gas path	553	nanostructured bulk half-Heusler	/	1.0	(Meda et al., 2016)
4	Exhaust WH from an automotive Diesel engine	Exhaust gas path	550	nanostructured bulk half-Heusler alloys	2.1	1.0	(Yanliang Zhang et al., 2015)

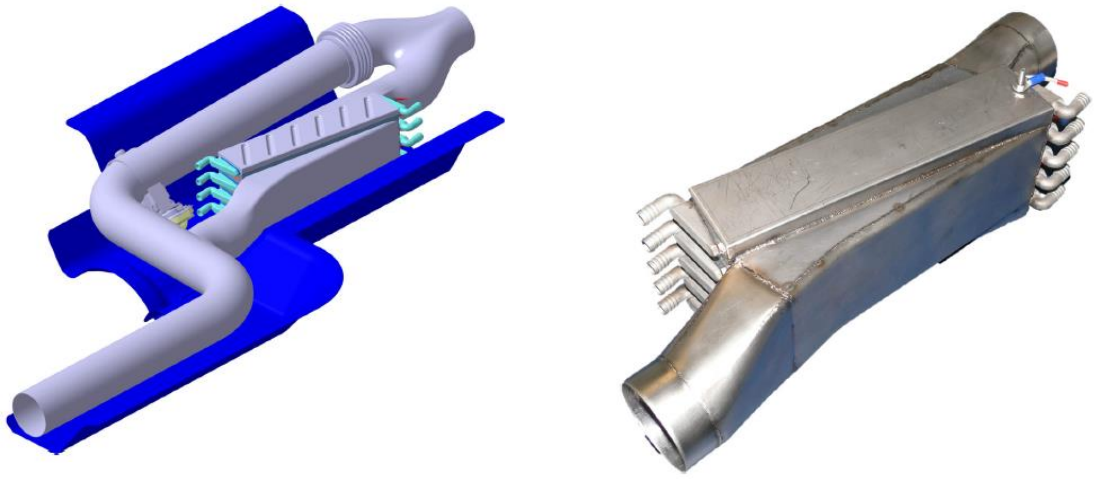

a) *b)*

Figure 185: TEG prototype for a passenger car application: a) integration of TEG and bypass line; b) TEG prototype. (Frobenius et al., 2016)

Horizon 2020
European Union Funding
for Research & Innovation

This project has received funding from
the European Union's Horizon 2020 research and innovation
programme under grant agreement No 847097

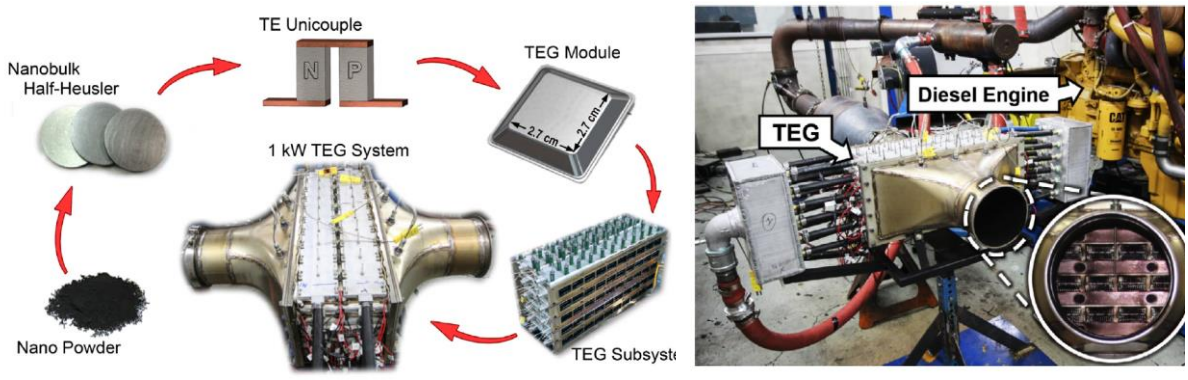

a) *b)*

Figure 186: a) High-performance TEG fabricated using nanobulk half-Heusler alloys and installed at the exhaust of a Diesel engine; b) TEG installed at the exhaust pipe of a Diesel engine. (Yanliang Zhang et al., 2015)

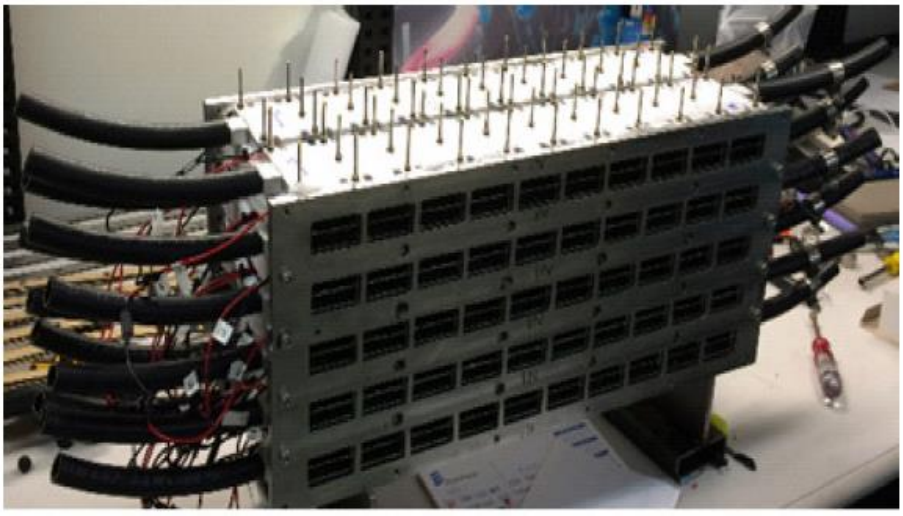

Figure 187: The 1 kW TEG includes 5 layers of exhaust HEs, 10 layers of half Heuslers TE materials with 40 modules on each layer, and 6 layers of cold HE. (Meda et al., 2016)

5.6.5 Cost aspects

The cost of the TE modules varies within the range 9 ÷ 74 € per module, depending on the generated power and operating temperature (Table 78). Considering an average electric power of the single module equal to 10 Watt, the specific cost is roughly 900÷7400 €/kW. Lower costs can be obtained from the suppliers for purchase of quantities higher than 50÷500 modules. The cost of a complete TEG generator having a capacity of 100÷250 Watts is in the range 5400÷8400 €/kW as shown in Table 79.

Table 78: Cost of commercial thermoelectric modules supplied by different manufacturers.

Quantity	Price per module (€)	Power (Watt)	Company
1 ÷ 120	21.5 ÷ 36.1	2.7 ÷ 8	(Marlow Industries, 2019)
1 ÷ 100	17.8 ÷ 73.9	5.1 ÷ 14.6	(TECTEG, 2019)
1 ÷ 499	14.4 ÷ 50.7	5 ÷ 22	(TEGMART, 2019)
1 ÷ 50	8.9 ÷ 44.5	2.3 ÷ 20	(Hi-Z Technology, 2019)

Horizon 2020
European Union Funding
for Research & Innovation

This project has received funding from
the European Union's Horizon 2020 research and innovation
programme under grant agreement No 847097

Table 79: Cost of thermoelectric generators.

Source	TRL	Power (W)	Quantity	Price (€)	Specific cost (€/kW)	Reference
Gas, wood or coal stove or industrial WHR	9	100	1 ÷ 499	543 ÷ 639	5400 ÷ 6400	(TEGMART, 2019)
Exhaust gases from a Diesel light duty truck	5	250	/	/	8400	(HEATRECAR FP7, 2013)

Horizon 2020
European Union Funding
for Research & Innovation

This project has received funding from
the European Union's Horizon 2020 research and innovation
programme under grant agreement No 847097

5.7 Thermophotovoltaic generators (TPVs)

5.7.1 Technological features of TPVs

Thermophotovoltaic (TPV) conversion involves the generation of electric power by the interaction of thermal radiation from a heated body and photocells. A TPV converter system involves a heat source, emitter, photocells, and spectral control as its four primary components (Figure 188). TPV devices convert radiation using exactly the same principles as do photovoltaic (PV) devices; namely photons of radiation are absorbed by a semiconductor p/n junction (a diode), which causes the generation of excess electrical charge. The excess photogenerated positive and negative charge is separated by a combination of diffusion to and drift across the electrostatic junction. This process establishes a potential difference between the two sides of the junction (Coutts, 1999).

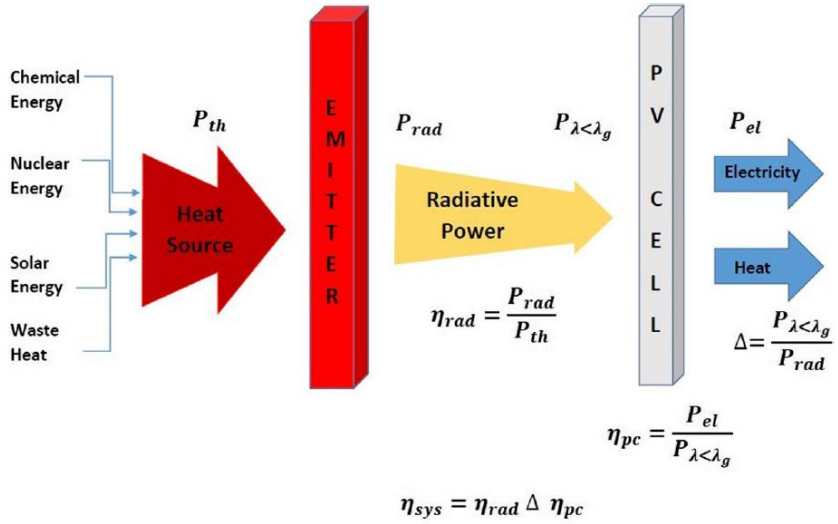

Figure 188: Energy sources, principal components and definition of system efficiency of a TPV generator system (Daneshvar, Prinja, & Kherani, 2015).

Power generation by TPV is quite similar to power conversion by conventional photovoltaics, except that radiation of a different wavelength is used (Butcher et al., 2011). A TPV device receives radiation from a surface at a temperature of 1027÷1527°C (1300÷1800 K) and at a distance of only a few centimetres. While the power received by a solar cell is of the order of 1 kW/m², that received by a TPV converter is likely to be 50÷300 kW/m² depending on the radiator temperature. Thus, the power density output from a TPV converter is expected to be significantly greater than that from a non-concentrating PV converter (Coutts, 1999).

The electrical efficiency of a TPV system is the ratio between the electrical power and the energy input from the heat source. The electrical efficiency versus the generated electrical power of TPV systems in the literature is shown in Figure 189 (Ferrari, Melino, Pinelli, & Spina, 2014). Both measured and predicted values are reported. The electric efficiency increases with TPV system size. With the exception of very small TPV units, most prototypes have an electric power in the range of 10÷300 Watts and the measured electric efficiency ranges from some percentage points up to 7.5%. Only the JX Crystals Inc. product, with a 66 W electric power, claims a 10.9% electric efficiency and also envisions a 12.3% electric efficiency, if the size is increased to 1.5 kW (L. M. Fraas, Avery, & Huang, 2003).

Horizon 2020
European Union Funding
for Research & Innovation

This project has received funding from
the European Union's Horizon 2020 research and innovation
programme under grant agreement No 847097

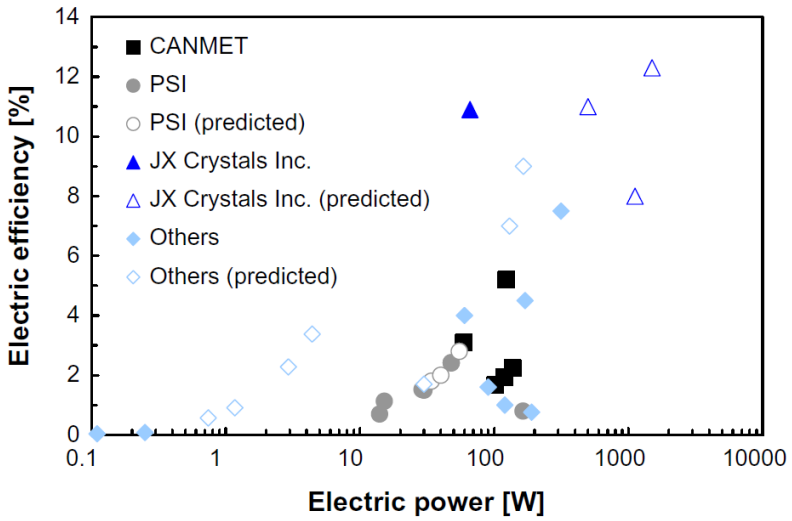

Figure 189: TPV electrical efficiency as a function of generated electrical power (Ferrari et al., 2014).

5.7.2 Thermophotovoltaic cells

TPV cells are the core component to realize the conversion process. At present, TPV cells are generally classified into two categories: commercial solar cells represented by Si (E_g = 1.12 eV) and low bandgap cells mainly represented by GaSb and InGaAsSb (Jianxiang Wang, Ye, Wu, Wang, & Xu, 2013).

Table 80: Material and energy gap of the low bandgap cells compared to the silicon photocells.

Material photovoltaic cell	Energy band gap E_g (eV)
Si	1.12
GaSb	0.72
InGaAsSb	0.53
InAsSbP	0.45
PbS	0.41
GaInAsSbP	0.35

Silicon photocells can be used to produce electric power from incident light with wavelengths shorter than 1 µm. In TPV applications, the emitter temperature is significantly lower than that of the sun. Thus, the black body emission spectrum is shifted to longer wavelengths in TPV systems. Gallium antimonide (GaSb) photocells, which respond to wavelengths of 1.7 µm and shorter are therefore preferred. To appreciate the advantage of using low-bandgap cells like those based on GaSb, consider that for a typical TPV emitter with a temperature of 1400°C, the black body emissive power between 0 and 1 µm is 12 kW/m², while the emissive power between 0 and 1.7 µm is 106 kW/m², which is 8.8 times higher (Butcher et al., 2011).
Figure 190 shows the variation of the percentage of convertible blackbody radiation with the bandgap of the semiconductor, the temperature of the radiator being treated parametrically. For low temperatures, the percentage is relatively small for even low-bandgap materials, but for silicon it is less than 1%. As the bandgap decreases the convertible percentage increases but the power density output is far less (Coutts, 1999).

Horizon 2020
European Union Funding
for Research & Innovation

This project has received funding from
the European Union's Horizon 2020 research and innovation
programme under grant agreement No 847097

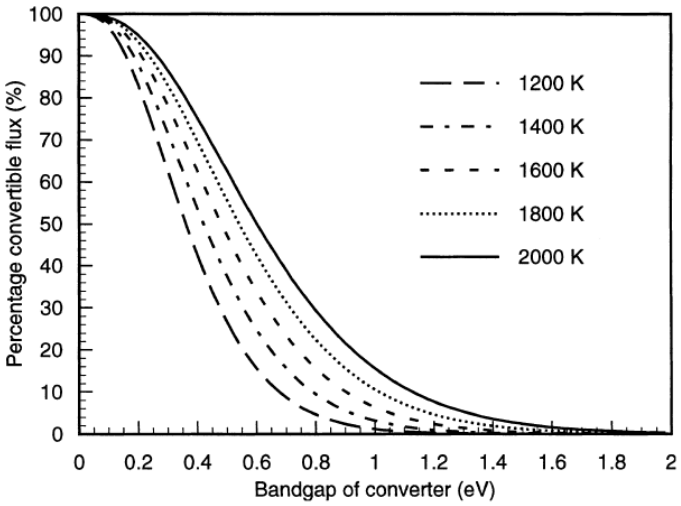

Figure 190: Percentage of convertible flux from blackbody radiators at the temperatures shown, with the bandgap of the converter (Coutts, 1999).

The U.S. company JX Crystals (JX Crystals, 2019) fabricates the GaSb cells, shingled circuits and shingled circuits with infrared filters. The circuit area is approximately 125 cm^2 and the power produced is as high as 150 W per circuit demonstrating that these circuits are capable of producing over 10 kW/m^2 (Figure 191). The GaSb cells can also be mounted on a cylindrical circuit as shown in Figure 192.

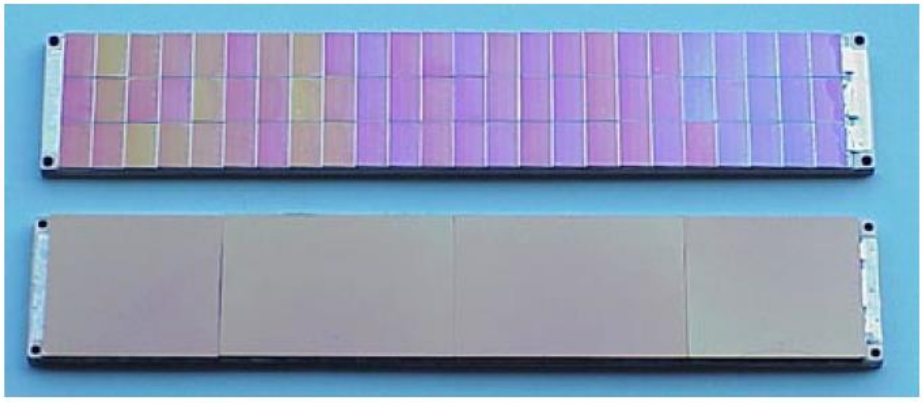

Figure 191: 72 GaSb cells (63 cells) mounted on a flat circuit measuring 5 cm by 26 cm. The circuit shown at the bottom is covered with planar filter covers (L. M. Fraas et al., 2003).

Horizon 2020
European Union Funding
for Research & Innovation

This project has received funding from
the European Union's Horizon 2020 research and innovation
programme under grant agreement No 847097

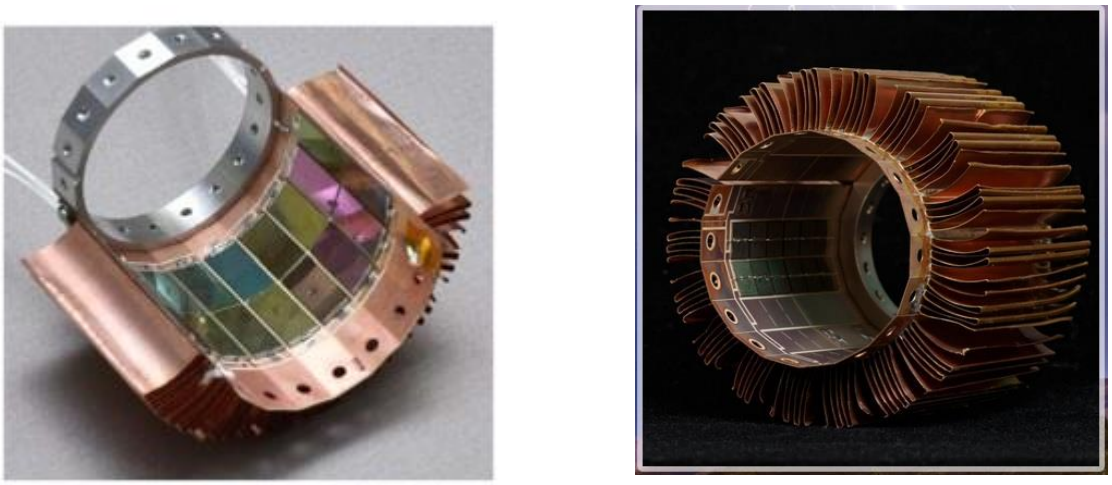

a) b)

Figure 192: GaSb cells mounted on a cylindrical circuit generating a power of 50 or 100 Watts (JX Crystals, 2019).

Figure 193 (left) shows the experimental results presented in (Utlu, 2019) in the testing of a TPV system made of GaSb cells. The TPV system efficiency steeply increases with the radiation temperature up to ≈1300÷1500°C and then reaches a plateau. The maximum efficiency of 21.57% is obtained at a radiation temperature around 2000÷2200°C and at the minimum cell temperature of 27°C. The impact of the cell temperature on the cell efficiency is significant: an increase from 300K (27°C) to 400K (127°C) implies approximately halving the cell efficiency. Similar results were obtained in (Shoaei, 2016) in the testing of a GaSb cell for a constant emitter temperature of 1200°C and a variable cell temperature between 27 and 107°C (Figure 193 right). This shows that cooling is very important in improving the cell and, in turn, the TPV system efficiency.

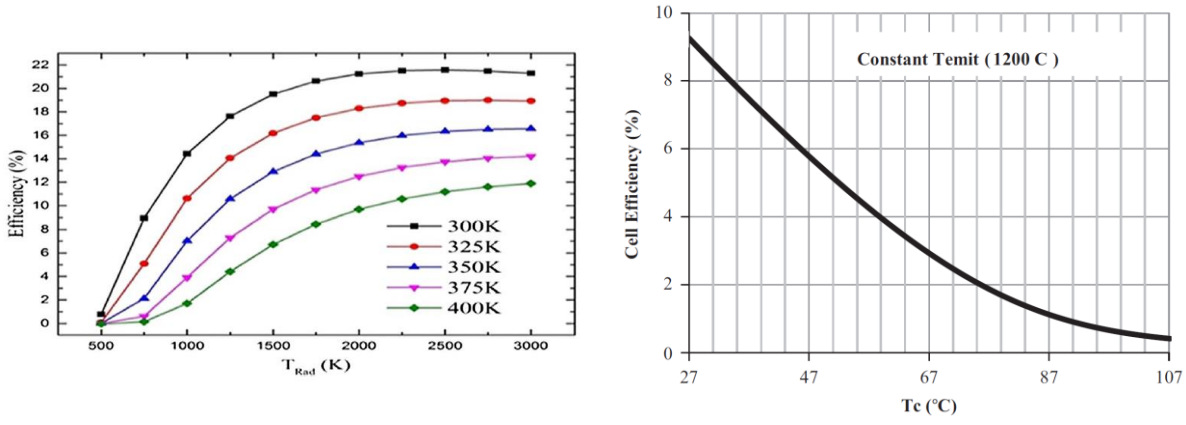

a) b)

Figure 193: Impact of cell temperature: a) Variation of TPV system efficiency with radiation temperature (500÷3000 K) and cell temperature (300÷400 K) (Utlu, 2019); b) variation of cell efficiency with cell temperature (27÷107°C) for a constant emitter temperature of 1200°C (Shoaei, 2016).

5.7.3 Applications of TPV systems for WHR from the steel and glass industries

Industrial WHR using TPV conversion was proposed by Coutts at the end of 1990s (Coutts, 1999). The author argued that the greatest potential for TPV generation of electricity is in its application to industrial WH, especially in the glass, steel and aluminium industries. The high-temperature processes

Horizon 2020
European Union Funding
for Research & Innovation

This project has received funding from
the European Union's Horizon 2020 research and innovation
programme under grant agreement No 847097

in these industries share the common schematic shown in Figure 194. The energy entering the chamber can be derived from electrical heating or combustion of a fuel with an oxidant. Within the process chamber, the temperature exceeds 1023°C (1300K). There are three principle locations for heat recovery, namely product (1), flue gas (2) and wall heat recovery (3).

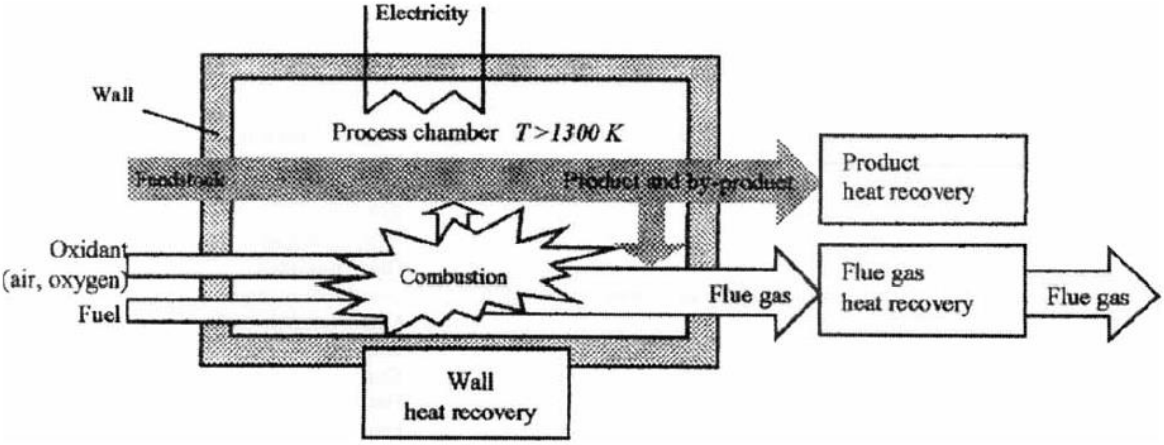

Figure 194: Schematic of an industrial high temperature process (Bauer, Forbes, & Pearsall, 2004).

- **Glass industry**

Figure 195 illustrates a schematic of a glass melting process with an estimate of the energy distribution. The energy content of the fuel is only partially transferred to the glass, other parts are lost in the structure (mainly through the furnace walls) and carried out by the flue gas. There are three areas where a TPV heat recovery system could be placed, which are: 1) secondary processes; 2) the furnace and 3) the regenerator.

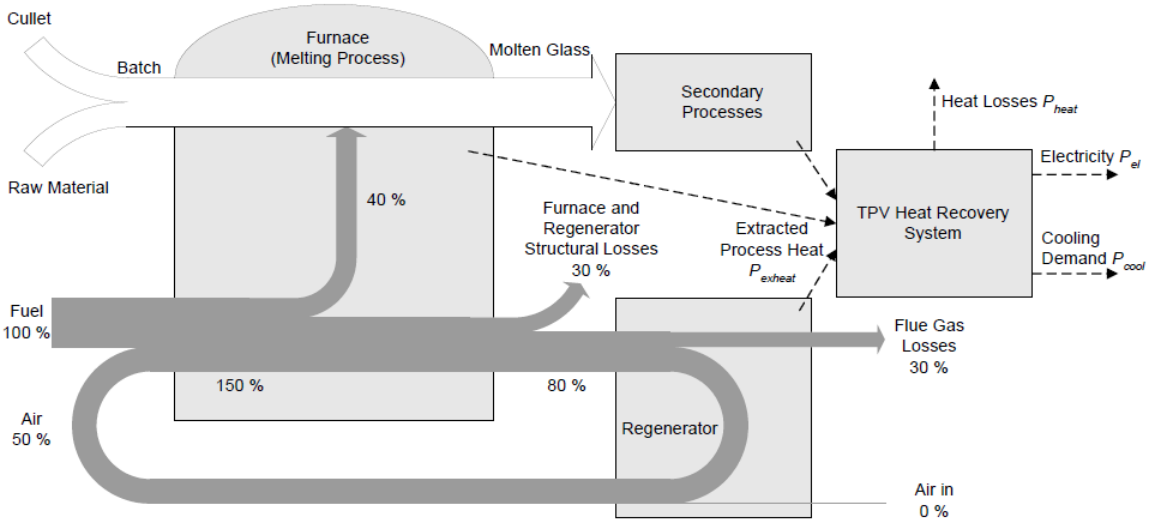

Figure 195: Energy diagram of a typical NG glass furnace showing where TPV system could be sited for WHR (Bauer, Forbes, Penlington, & Pearsall, 2003).

Horizon 2020
European Union Funding
for Research & Innovation

This project has received funding from
the European Union's Horizon 2020 research and innovation
programme under grant agreement No 847097

- **Steel industry**

Johansson (Johansson & Söderström, 2011) included the TPV systems among the WH to power technologies in the steel industry sector. 1) The steel products (blast furnace slag and slabs from the continuous casting); 2) hot flue gases from a blast furnace (down to 1000°C, with the remaining heat availably for other heat recovery methods) and 3) wall heat recovery (water-cooled areas in a blast furnace or a reactor for ladle metallurgy and the water-cooled panels on the roof and sides of an electric arc furnace) were considered suitable for TPV conversion.

Product heat recovery. The utilization of TPV systems in the steel industry to use the radiant heat of steel billets from the extruded temperature of 1400°C down to 1100°C was investigated technically and economically in (Lewis M. Fraas, 2014). Assuming a minimum TPV operation temperature of 1027°C (1300 K) Bauer et al. (Bauer et al., 2004) estimated that an amount of energy of about 0.7 MJ per kg steel for continuous casting is in principle available for TPV conversion. They identified as the most suitable location for TPV operation the support area where the strand with its solidified skin and liquid core is supported by rollers and is traditionally cooled by water sprayers. The TPV could replace the water sprayers, and could also be beneficial in overcoming the limitations of the water sprayers related to the closed arrangement of the rollers and the changes in the quality of the steel product due to changes in the heat transfer rate in the cooling process.

Figure 196: Steel billets after continuous casting (Utlu, Paralı, & Gültekin, 2018).

Wall heat recovery. Electric arc furnaces (EAFs) are cylindrical refractory lined vessels which are used to produce carbon and alloy steels in a batch process. Water-cooling for the roof and sidewall panels of EAF furnaces is becoming common practice. In principle, these panels could be replaced by a TPV heat recovery system, where the already-available water supply could be used for PV cell cooling. Other potential processes are the metallurgical reactor for secondary refining and water-cooled areas in the blast furnace.

Table 81 summarizes the main features of the prototypes and case studies for WHR in the steel and glass industries. In the TPV device analysed in (Jianxiang Wang et al., 2013) the high temperature slag or products are made to get through the radiant pipe by a transmission device (Figure 197). The radiant energy emitted by the heated radiator is absorbed by the cells to generate electricity. The cooling system has eight water cooled plates, each of which has a PV circuit with 8 cells mounted in series. It was shown that the Yb_2O_3 radiator is propitious to decrease the Si cell temperature and

Horizon 2020
European Union Funding
for Research & Innovation

This project has received funding from
the European Union's Horizon 2020 research and innovation
programme under grant agreement No 847097

improve the cell performance. The system electric efficiency of 3.1% reported in Table 81 was reached using an Yb_2O_3 radiator.

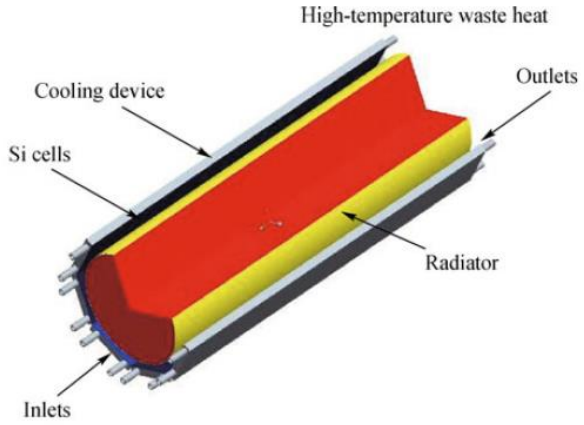

Figure 197: Schematic of a TPV system for WHR from the slag or products of a glass industry

In the theoretical model developed in (Shoaei, 2016) validated against the real data of JX-Crystals cells, a maximum system efficiency of 4.12% was obtained considering a distance of 1 cm between the cell and the slab. Furthermore, note that the TPV system electrical efficiency was calculated as the ratio between generated electrical energy and radiant energy from the source in (Shoaei, 2016), whereas it included at the denominator the view factor of the cell module toward the radiator in (Jianxiang Wang et al., 2013).

Table 81: Features and performance of TPV systems for waste heat recovery in the steel and glass industries.

TRL	Source	Source emitter temperature (°C)	Cell temperature (°C)	Material photovoltaic cell	Power output (kW)	Cell efficiency (%)	System efficiency (%)	Reference
4	Slabs (steel plates)	1257	27	GaSb	/	9.7 ÷ 10.9	4.12	(Shoaei, 2016)
4	Slag or product glass industry	1300	50	Si	0.196	/	3.1	(Jianxiang Wang et al., 2013)

5.7.4 TPV applications for micro-cogeneration

An interesting application of the TPV systems is the micro-cogeneration. In the combustion of a fuel (natural gas, butane, etc.) the radiant heat at the highest temperature is converted into electricity by a TPV system coupled with the burner, whereas the heat at lower temperature is used to meet the heating demand of the users. This improves the boiler efficiency and enables the co-generation of the electricity. In the microcogeneration sector the TPV technology has reached the highest level of maturity with even commercialized products like the JX Crystals' MidnightSun® TPV stove (L. M. Fraas et al., 2003). The main prototypes developed are presented in the following.

Figure 198 shows the TPV furnace–generator design presented in (L. M. Fraas et al., 2003) in which a cylindrical photovoltaic converter array (PCA) surrounds an infrared emitter on the outside surface of a section of a radiant tube burner. The SiC radiant tube burner (pointing downward) consists of an

Horizon 2020
European Union Funding
for Research & Innovation

This project has received funding from
the European Union's Horizon 2020 research and innovation
programme under grant agreement No 847097

outer tube closed at its bottom end with a concentric tube inside it (Figure 198). Fuel and air are mixed and burned inside the middle of the inner tube. The hot combustion gases then flow down inside the inner tube and then turn around and flow up between the inner tube and the outer emitter support tube. They then flow through a recuperator section at the top of the radiant tube burner preheating the combustion air. The commercial SiC radiant tube burners are capable of operating at temperatures up to 1250°C.

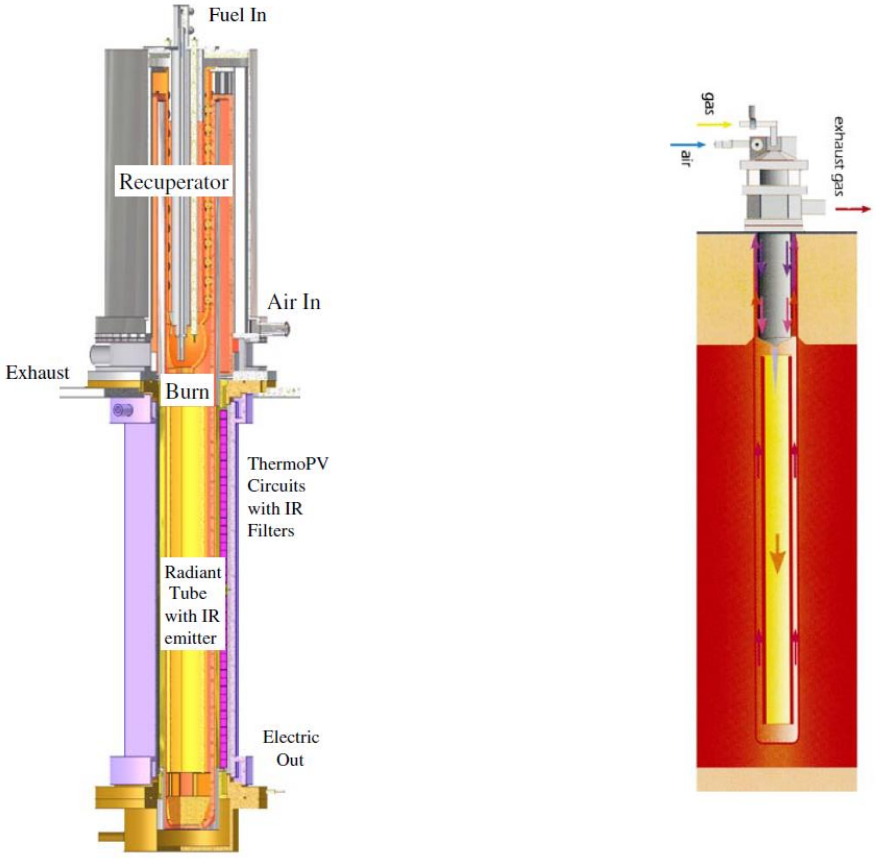

a) *b)*

Figure 198: TPV generator prototype (left) with an electric output of 1.5 kW and a heat output of 12 kW (thermal), using a radiant tube burner (right) (L. M. Fraas et al., 2003).

In the residential oil fired boiler described in (Butcher et al., 2011) the cells were separated from the combustion chamber by three layers of quartz which acted as radiation shields to reduce the long wavelength thermal load on the cells (Figure 199). Those frequency ranges that are not converted to electricity can raise the temperature of the TPV cells, degrading performance and in some cases cause damage. The porous foam emitter (through which 100% of the combustion products leaving the combustion chamber passed) was made of a SiC/Alumina composite and achieved slightly higher power density than direct flame radiation.

Horizon 2020
European Union Funding
for Research & Innovation

This project has received funding from
the European Union's Horizon 2020 research and innovation
programme under grant agreement No 847097

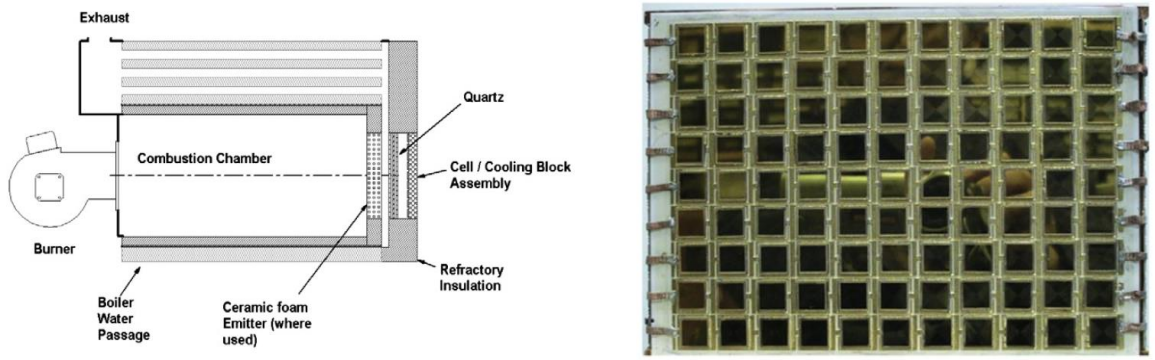

a) *b)*

Figure 199: Residential oil-fired boiler equipped with a 99 cell TPV converter array (Butcher et al., 2011). Each cell has an active area of 1 cm², and each row is connected in series.

In the 0.5 kW prototype described in (Horne, 2003) heat from the combustion of Diesel fuel is coupled to the inside wall of a cylindrical SiC emitter. The outer wall of the emitter then radiates blackbody energy at the design temperature of 1400°C. The cylindrical emitter is enclosed in a glass envelope that separates it from the photovoltaic cells. The array consists of 216 1 cm² GaSb cells into series and parallel arrays. An array of heat pipes couple the PV cell arrays to a HE which is cooled by forced air convection. Finally, one of the best TPV prototype systems developed at the Paul Scherrer Institute (Durisch, 2003) was based on high efficiency silicon cells and reached a system efficiency of 2.4% (2.8% with air preheating). The ytterbia emitter was heated using a butane burner.

Table 82: Features and performance of TPV systems for micro-cogeneration.

TRL	Source	Source emitter temperature (°C)	Cell temperature (°C)	Material photovoltaic cell	Power output (kW)	Power output density (kW/m²)	Energy conversion efficiency (%)	Reference
5	Hot combustion gases	1260	50	GaSb	1.5	/	12.3	(L. M. Fraas et al., 2003)
4	Flame of an oil-fired boiler	1600	/	GaSb	0.119	12	/	(Butcher et al., 2011)
4	Flame from the combustion of Diesel fuel	1200	/	GaSb	0.185	/	7.5	(Horne, 2003)
4	Flame temperature	/	20.6 ÷ 23.6	Si	0.048	/	2.4 ÷ 2.8	(Durisch, 2003)

5.7.5 Theoretical investigations about the applications of TPV systems for WHR at medium temperatures

Waste heat from solid oxide fuel cells (SOFC). The TPV system for WHR from a solid oxide fuel cell (Figure 200) theoretically investigated in (Liao, Cai, Zhao, & Chen, 2016) is composed of an emitter operating at 800°C and a PV cell with integrated back surface reflector (BSR). The SOFC acts as the heat source of the TPV system to generate additional power output. The role of the regenerator in the hybrid device is to preheat the incoming air and fuel by using the high-temperature exhaust gas of the SOFC.

Horizon 2020
European Union Funding
for Research & Innovation

This project has received funding from
the European Union's Horizon 2020 research and innovation
programme under grant agreement No 847097

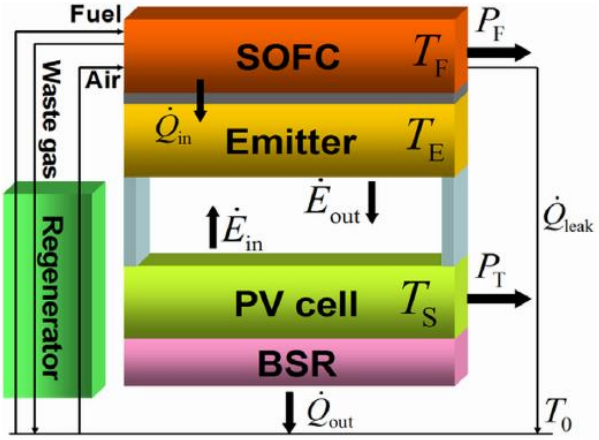

Figure 200: TPV application for WHR from a solid oxide fuel cell (SOFC) (Liao et al., 2016)

Waste heat from engine exhaust. The TPV system driven by the automobile exhausts at 500°C theoretically investigated in (Z. Yang et al., 2018) is composed of a cylindrical exhaust gas pipe covered by an emitter, a PV cell array, and a vacuum gap between the PV cell array and the emitter (Figure 201). The PV cell array includes the back surface reflector (BSR) used to reflect non-absorbed radiation back to the emitter. The optimum bandgap to maximize the power output from the engine exhausts was found lower than those typical of the low bandgap materials (such as GaInAsSbP, PbS and InAsSbP shown in Table 80). Ultra-low bandgap photocells with bandgap energies as low as 0.2÷0.3 eV have been recently developed but are extremely expensive (Daneshvar et al., 2015).

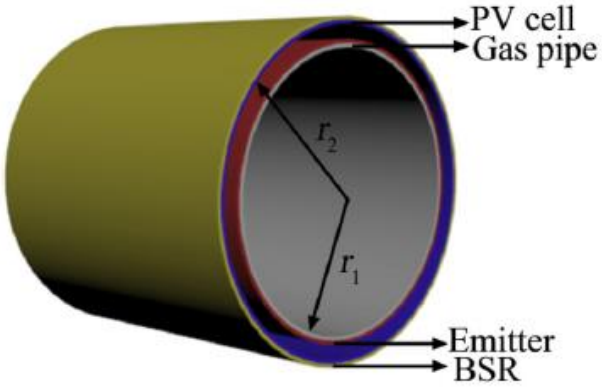

Figure 201: Schematic of the TPV for WHR from the automobile exhausts (Z. Yang et al., 2018).

5.7.6 Cascading of TPV and TEG for WHR from the flue gases

In the flue gas heat recovery (Figure 194) it is thought that TPV flue-gas heat recovery would typically operate in a cascaded manner, where the TPV system would make use of the "high quality" heat from the actual flue gas temperature down to 1027°C (1300 K) and other heat recovery methods would utilise the remaining heat (Bauer et al., 2004). The concept of cascading TPV and TE power generation was proposed in (K. Qiu & Hayden, 2012) in order to increase system electrical efficiency (Figure 202).

Horizon 2020
European Union Funding
for Research & Innovation

This project has received funding from
the European Union's Horizon 2020 research and innovation
programme under grant agreement No 847097

In the cascading power generation system, the residual heat stream leaving the TPV is applied as input to a TEG system. The developed prototype generated 123.5 Watts from the TPV cells and 306.2 Watts from the TEG generator. The overall electrical efficiency of the cascading system was 5.2%.

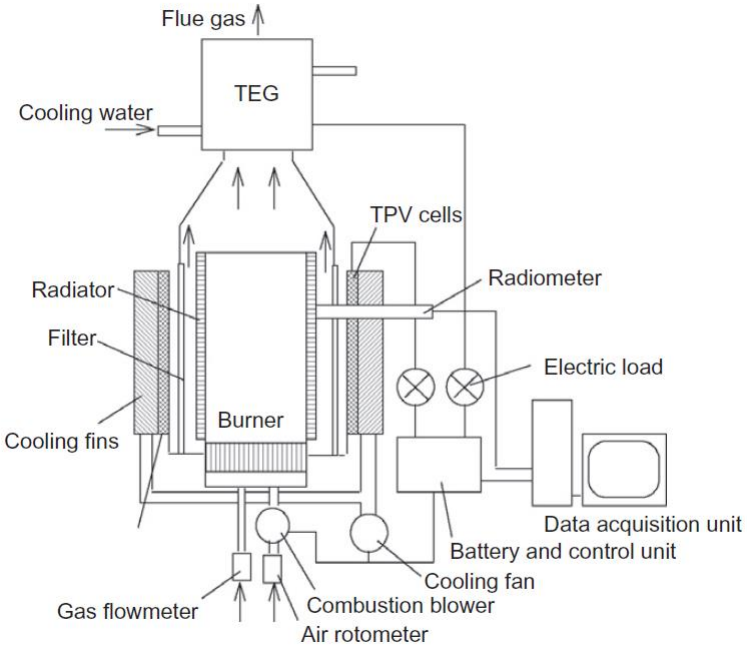

Figure 202: Schematic diagram of cascading TPV and TE power generation system (K. Qiu & Hayden, 2012).

5.7.7 Cost aspects

The cost of the TPV system heavily relies on the choice of the cell material, as shown in Table 83. When using commercial Si cells the costs of the radiator and the cooling device are the key factors affecting the system cost of a TPV system (Jianxiang Wang et al., 2013). The scenario is different when using GaSb cells that have not still reached high production volumes.

The cost of the gallium and antimony in a GaSb chip was 14 cents per cm^2 at the beginning of the 2000 and in order to make GaSb cells at low cost, processes were considered that parallel the silicon solar cell manufacturing process (L. M. Fraas et al., 2003). Assuming that the cells can reach a high power density of 10 kW/m^2 when installed in a furnace-generator, the cost could be reduced to values lower than 1000 €/kW considering a high production volume (>10 MW_e). The trend shown in Figure 203 is a projection for the GaSb cell cost from ABB given input from JX Crystals (L. M. Fraas et al., 2003).

Horizon 2020
European Union Funding
for Research & Innovation

This project has received funding from
the European Union's Horizon 2020 research and innovation
programme under grant agreement No 847097

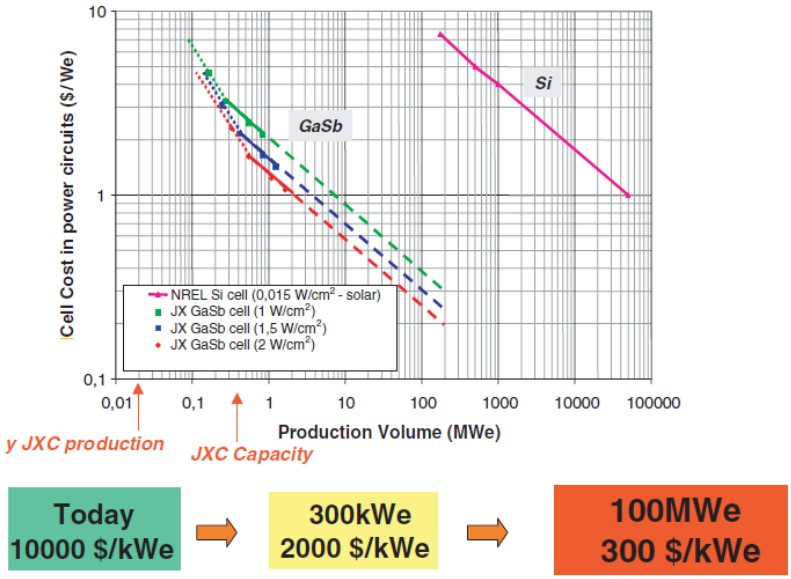

Figure 203: Achievable GaSb cell costs versus cumulative production volume (L. M. Fraas et al., 2003).

The theoretical economic analysis in (Shoaei, 2016) for WHR from a steel industry reported an investment cost of 16 million US$ for the installation of 324870 GaSb cells. Thus, the unit cost of a GaSb cell is equal to approximately 45 €. Assuming a maximum power output of 1 Watt per cell for a WHR installation (i.e., a power density of 10 kW/m²), the specific cost is 45000 €/kW which appears prohibitive and demonstrates that in the last 15÷20 years the production capacity has not achieved the required volumes to make TPV systems competitive.

Table 83: Estimated installation cost of TPV systems reported in the literature.

Cell materials	Cost (€/kW)	Reference
Si	6730	(Jianxiang Wang et al., 2013)
GaSb	45000	Calculated from (Shoaei, 2016)

Horizon 2020
European Union Funding
for Research & Innovation

This project has received funding from
the European Union's Horizon 2020 research and innovation
programme under grant agreement No 847097

5.8 Cryogenic generators: Liquid Air Energy Storage and Dearmean engine

This class encompasses technologies which take advantage of processes and working fluids that operate at cryogenic temperatures, commonly below -50°C. Such low-temperature processes also constitute in principle an ideal heat sink for any WH source, particularly for otherwise difficult to recover low-grade waste heat available at near ambient temperature. As a result, cryogenic processes often offer opportunities for process integration and synergies with other industrial processes; on one side WH is recovered from the industrial process, making the latter more efficient, on the other side the overall efficiency is also improved due to the injection of WH into the process. In this section two near-to-market cryogenic technologies are presented: Liquid Air Energy Storage (LAES) and Dearmean Engine (DEN). Furthermore their use for WH recovery is also discussed.

5.8.1 Liquid Air Energy Storage (LAES)

5.8.1.1 LAES: Technological features and performance

LAES is a cryogenic process for large scale storage of electrical energy. The technology is suitable for power capacity of 10 MW or above and energy storage capacity in the order of MWh (Mark Akhurst, Andy Atkins, Ian Arbon, & michael Ayres et al., 2013). Differently from other storage technologies (e.g. batteries, hydropower), LAES stores energy through a thermo-mechanical process. It is such thermo-mechanical nature of the process that provides opportunities for WH recovery and integration with large scale industrial processes. Figure 204 illustrates a schematic of a LAES system, including WH recovery opportunity. The system comprises three main stages of thermo-mechanical processes.

A charging stage, through which air drawn from the atmosphere is liquefied (liquefaction temperature -190°C at ambient pressure). The charging system is an industrial air liquefaction plant in which electricity is used to drive a Claude cycle. The latter is a refrigeration-liquefaction process which combines compression of air followed by refrigeration and throttling. The latter step is such that due to Joule-Thompson effect temperature is further lowered, leading to the liquefaction of a fraction of the air flow rate previously compressed. Industrial air liquefaction plants are extensively used worldwide. Linde – one of the main commercial players in this sector – has designed and built more than 3000 air liquefaction units over the globe ("Linde - Air Separation Plants," 2020). Presently, such units are dedicated to production of industrial liquefied gas, such as nitrogen (ammonia production) or oxygen (primary steelmaking).

The second and third stages of LAES process are the storage and the discharge stages, respectively. Storage is performed by collecting the liquefied air in cryogenic tanks. These are commercially available in a range of sizes and used extensively in existing air liquefactions units and LNG terminal. During the discharge stage liquid air previously stored in the tanks is pumped at high pressure (in the range 50÷100 bar) before being evaporated using ambient heat or WH from a nearby source (e.g., industrial processes). The resulting stream of gaseous air then drives gas turbines to generate electricity.

LAES technology was first demonstrated in 2010, though at pilot scale of 350 kW/2.5 MWh. The pilot proved the feasibility of the process and the technology was further consolidated in 2018 with the operation of a 5 MW/15 MWh pre-commercial plant ("Highview Power," 2020). In late 2019 Highview Power has announced that it will build a first full-scale LAES system in the north of England. The system will have a capacity of 50 MW/250 MWh ("Highview Power - Cryobattery," 2020).

Horizon 2020
European Union Funding
for Research & Innovation

This project has received funding from
the European Union's Horizon 2020 research and innovation
programme under grant agreement No 847097

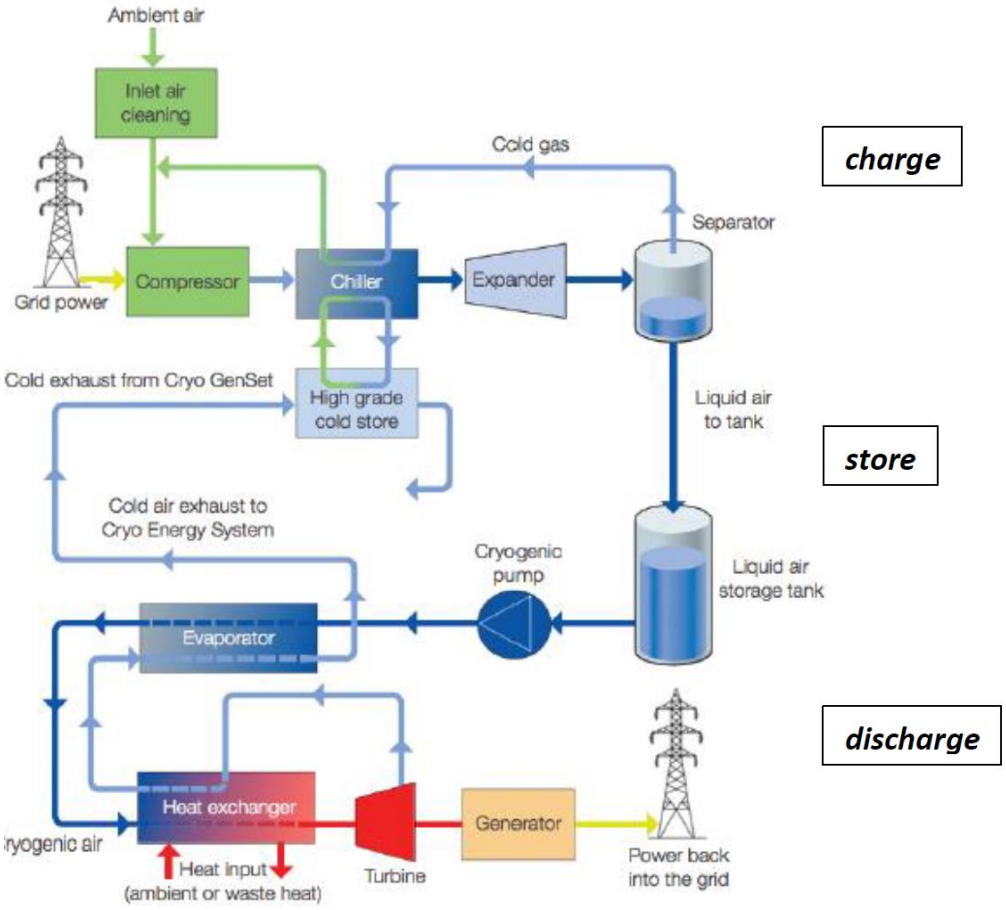

Figure 204: Schematic of a LAES system (Mark Akhurst et al., 2013).

Table 84 summarizes the typical range of performance parameters for LAES plants (X. Luo, Wang, Dooner, & Clarke, 2015) (Evans, Strezov, & Evans, 2012). Performance parameters are significantly enhanced through integration of WH/C from sources nearby the LAES plant. Potential heat sources include ICEs, power generation and industrial processes. The cryogenic temperatures of LAES are key, enabling exploitation of low-grade streams below 100°C. Roundtrip efficiency is expected to increase by 10 percentage points, every 50°C increase in the temperature of the external heat source (Yongliang Li, 2011). Waste cold at -160°C can be recovered from NG regasification terminals or at higher temperatures from industrial process. In all these cases, the absence of geographical constraints to LAES deployment is a decisive advantage for process co-location.

Table 84: Typical range of performance parameters for a liquid air energy storage plant (X. Luo et al., 2015)(Evans et al., 2012).

Parameter	Range	Notes
Storage capacity	1 MWh ÷ 1 GWh	/
Power delivered	1 MW ÷ 100 MW	GW range within reach
Power absorbed	100 kW ÷ 100 MW	Independent from power delivered; tailored to application
Energy/power ratio	1 h ÷ 8 h	Tailored to application
Roundtrip efficiency	45% ÷ 60%	Up to 70% with external WH integration
Energy density	130 MWh/L ÷ 220 MWh/L	1 OdM higher than CAES and 2 OdM higher than PHES
Response time	2 min ÷ 10 min	Size dependent; analogous to gas-fired power plant
Reheating T range	50°C ÷ 400°C	Depending on the number of compression stages

Horizon 2020
European Union Funding
for Research & Innovation

This project has received funding from
the European Union's Horizon 2020 research and innovation
programme under grant agreement No 847097

Cold recycle T range	-185°C ÷ -15°C	High-grade cold recycle is necessary
Lifetime	30 years ÷ 40 years	Well-proven components

5.8.1.2 LAES Applications – Integration with waste heat and waste cold processes

Integration with thermal plants

As previously mentioned, LAES can utilize external WH stream available during the discharge process. The WH stream is injected into the expanding air stream, which leads to an increase of the LAES power output and LAES round trip efficiency. Thus, LAES offers opportunities of heat-to-power for the valorisation of WH streams. It is however important to emphasize that the WH source should be sufficiently large to be injected into LAES. The latter is a MW-scale thermo-mechanical process, thus its integration with WH streams is not suitable for small scale WH sources.
The higher the grade of WH available, the more effective is the integration of WH streams with LAES. A WH stream at about 300°C is estimated to increase LAES round trip efficiency from 60% to 70% (Yongliang Li et al., 2014). Such feature makes LAES particularly suitable to recover WH from thermal plants co-located at the same LAES site. This is the case of open cycle gas turbine (OCGT) plant where the exhaust heat from the gas turbine can be injected into the LAES process. This has a double benefit; on one side LAES efficiency is increased but also the overall efficiency of the LAES plus OCGT site. Similar synergies can be explored also for other thermal plants such as combined cycles.

Integration with LNG terminals

During LAES charging process air is refrigerated and liquefied before it is stored in cryogenic tanks. Waste cold near LAES plant can be therefore harnessed to reduce the amount of cooling necessary for the air liquefaction process. Such recovery of waste cold reduces the amount of electricity spent to operate the LAES charge, effectively increasing the round trip efficiency of LAES while valorising waste cold. This type of LAES integration (Figure 205) is particularly attractive when vast amount of waste cold is available, such in the case of liquefied natural gas (LNG) facilities. In traditional LNG terminals regasification process converts LNG from about -160°C to ambient temperature. This is commonly done using sea water as hot source, causing the cold thermal energy of the LNG stream to be effectively dissipated into the sea water near the LNG terminal. Such cold thermal energy can be utilized to intercool compression and provide refrigeration to the charging process of LAES. If WH is also available at the LNG site, it can be also recovered as discussed in the previous section. Such integration of both waste cold and waste heat increases the (apparent) round trip efficiency of LAES up to 100%.

Horizon 2020
European Union Funding
for Research & Innovation

This project has received funding from
the European Union's Horizon 2020 research and innovation
programme under grant agreement No 847097

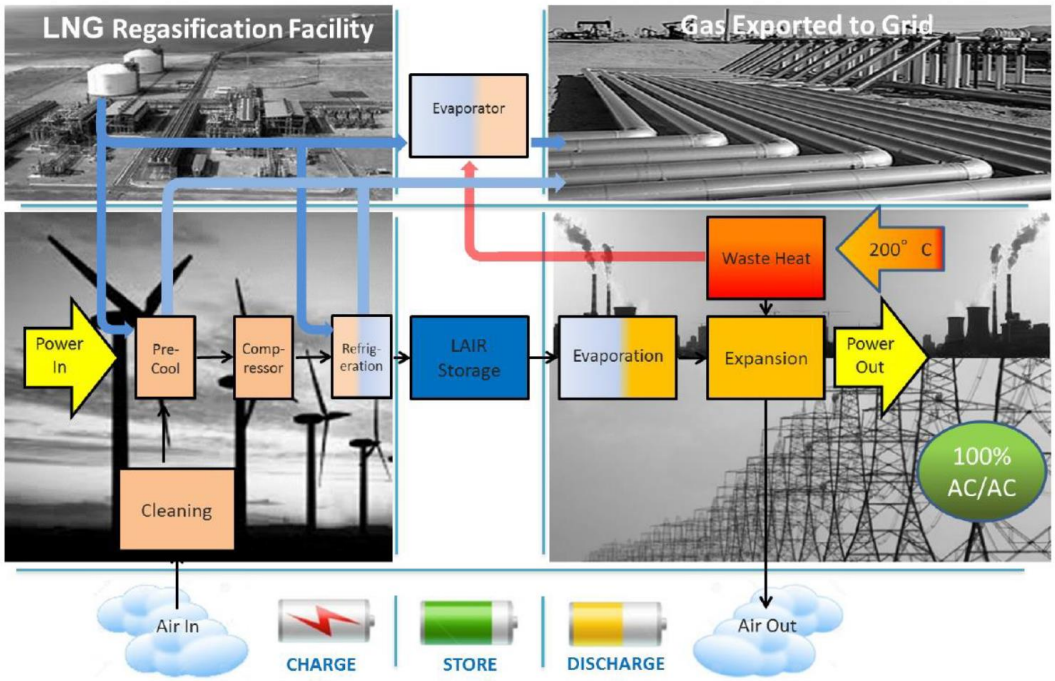

Figure 205: Integration of LAES with waste cold and waste heat source ("Highview Power," 2020).

5.8.2 Dearman engine (DEN)

5.8.2.1 Technological features and performance

Dearman engine (DEN) is a small-scale, zero-emission piston engine that uses liquid/gaseous nitrogen (or air) as working fluid (i.e. fuel). Ambient or low grade WH is used to vaporize liquid nitrogen (LN). The DEN is a near-to-market technology developed and distributed by Clean Cold Power UK Ltd. At the time this report is written Clean Cold Power UK Ltd is trialing DENs in collaboration with potential end users of the technology ("Dearman," 2020). Figure 206 shows a picture of a DEN.

Figure 207 presents the working principle of the DEN technology as well as its key parts (Mark Akhurst et al., 2013). Starting from the return stroke, a warm fluid is injected into the engine chamber filling the dead volume. At this stage LN is injected into the engine cylinder, mixing with the warm working fluid, thus exchanging heat by direct contact. The large temperature difference between the hot fluid and LN (about -190°C) causes the latter to instantaneously vaporizing, turning into gaseous Nitrogen (N_2). The liquid-to-gas volumetric expansion of nitrogen drives the engine piston down, producing motive power at the engine shaft. The expansion step takes place at near constant temperature due to the direct contact of the hot fluid and nitrogen, which allows to increase the overall efficiency of the cycle. Finally, at the bottom of the cycle mixture of hot fluid and gas exits the cylinder. The hot working fluid is recovered and used in the following cycle while the gas (N_2) is exhausted.

Horizon 2020
European Union Funding
for Research & Innovation

This project has received funding from
the European Union's Horizon 2020 research and innovation
programme under grant agreement No 847097

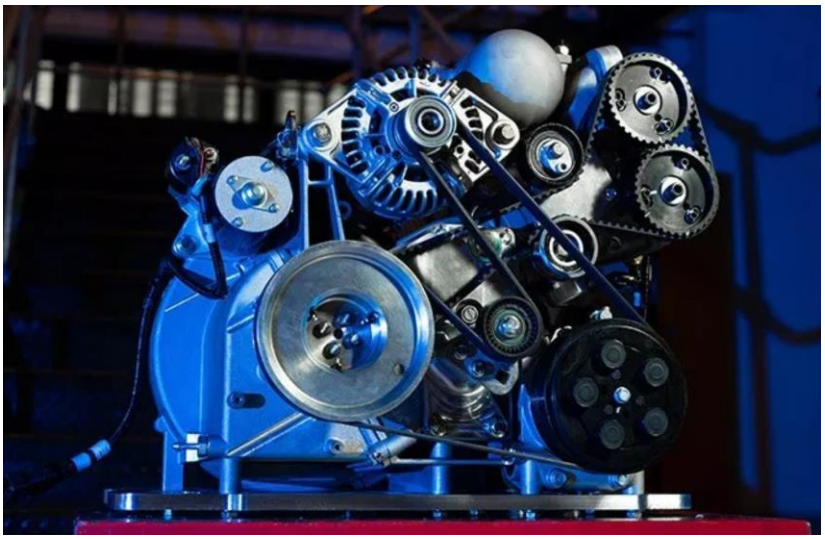

Figure 206: A Dearman engine manufactured by Clean Cold Power UK Ltd ("Dearman," 2020).

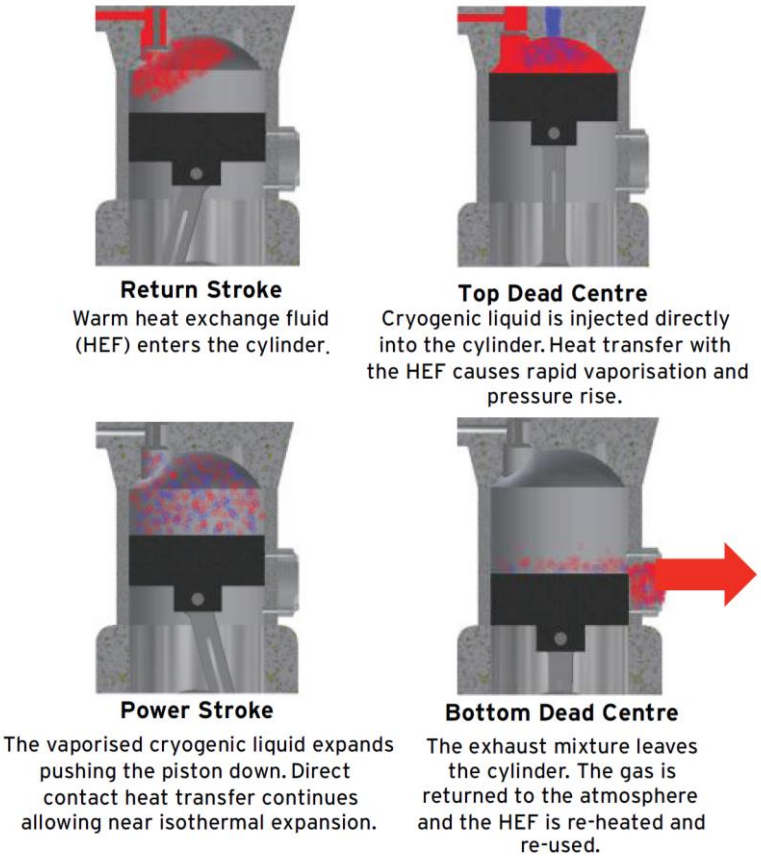

Figure 207: Working principle of the Dearman engine (Mark Akhurst et al., 2013).

The key novelty of the DEN consists of the direct heat exchange between the hot working fluid and the LN, directly in within the cylinder of the engine. This avoids to use external HEs, which leads to a more compact, economic and thermodynamically efficient system. Furthermore, direct heat transfer gives rise to a near-isothermal expansion, which produces a higher specific work output compared with traditional adiabatic expansion, as illustrated in Figure 208.

Horizon 2020
European Union Funding
for Research & Innovation

This project has received funding from
the European Union's Horizon 2020 research and innovation
programme under grant agreement No 847097

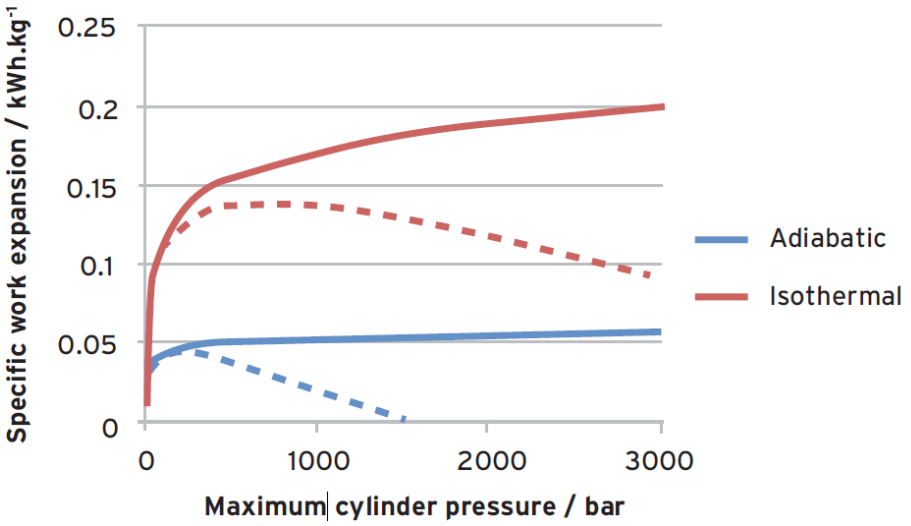

Figure 208: Specific work from the expansion of liquid nitrogen (Mark Akhurst et al., 2013).

5.8.2.2 DEN Applications – Stand-alone application and integration with waste heat sources

The energy density of LN (0.77 MJ/kg) is relatively low compared to fuels such as Diesel currently used in piston engines. This implies that the DEN technology finds applications primarily as an auxiliary engine, supporting a primary energy generator (Mark Akhurst et al., 2013). Such integration is particularly suitable when the primary generator produces waste heat and/or when there is a cooling demand at the location where the DEN is installed. The paragraphs below illustrate the main applications so far developed for DEN technology.

DEN 'heat hybrid' – waste heat recovery and cooling

Since DEN is driven by the vaporization of LN, its power output can be increased by the addition of WH from a nearby heat source. Since the temperature of LN at room pressure is -196°C, WH from low to high grade can be recovered by integration with a DEN unit. One of the applications developed by Clean Cold Power UK Ltd (developer and supplier of DEN technology) is the integration of DEN with conventional internal combustion engines (ICEs) (Centre for Low Carbon Futures and Liquid Air Energy Network, 2013). Figure 209 from one of the patents belonging to Clean Cold Power UK Ltd illustrates the DEN 'heat hybrid' concept. ICEs waste approximatively two thirds of the fuel primary energy in the form for low grade WH dissipated through the radiator (approximatively at about 100°C). In the DEH 'heat hybrid' application WH form the ICE is transferred from the ICE radiator to the hot heat transfer fluid employed in the DEN. The recovered WH is therefore converted into extra power available at the shaft of the DEN, effectively making the latter a heat-to-power recovery technology. The ICE-DEN hybrid has been initially conceived for use on heavy duty vehicles such as trucks, buses and lorries (Centre for Low Carbon Futures and Liquid Air Energy Network, 2013) as well as for stationary ICE (stationary generators). Finally, it is important to emphasize that since DEN uses LN as 'fuel', a supply of LN thus is necessary in both mobile and stationary applications. On-board LN tank is required for mobile applications while stationary applications can rely on local supply of LN.

Horizon 2020
European Union Funding
for Research & Innovation

This project has received funding from
the European Union's Horizon 2020 research and innovation
programme under grant agreement No 847097

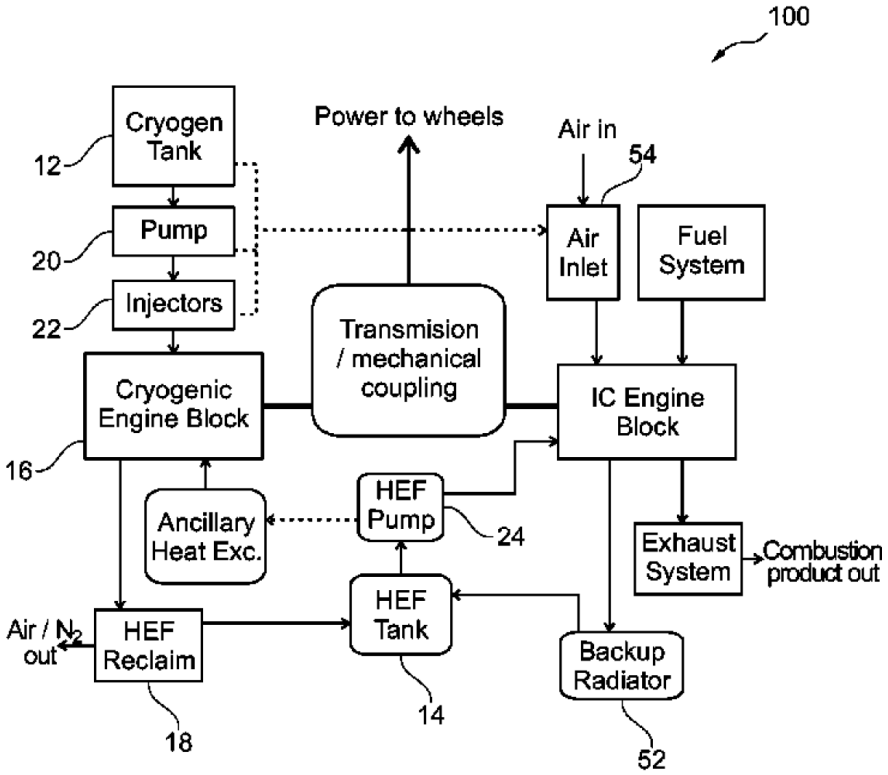

Figure 209: Integration of ICE with a Dearman engine; WH from the ICE is recovered and converted in power available at the shaft of the DEN (Cryogenic Engine Block in the figure) (Patent No. US 10260379 B2, 2019).

DEN as power and cooling unit

The DEN can also operate as combined cooling and power unit for transport refrigeration units (Centre for Low Carbon Futures and Liquid Air Energy Network, 2013) installed on trucks, lorries and shipping containers. Presently, the vast majority of transport refrigeration units are powered directly or indirectly through Diesel engines. This can be in the form of vapour compression cycle driven by the main Diesel engine of trucks/lorries/etc. or by a stand-alone refrigeration unit, which can account up to 20% of the fuel consumption of the truck/lorry/etc. (Centre for Low Carbon Futures and Liquid Air Energy Network, 2013). Figure 210 illustrates the concept for such application. LN is stored in an on-board cryogenic tank before it is pumped at about 40 bar prior to flowing and evaporated into the HE (evaporator). The evaporation of LN provides the cooling to the refrigerated container. Nitrogen, now in gaseous form, flows from the outlet of the HE to drive a DEN unit. The power output of the DEN can be then utilized to drive auxiliary components or the compressor of a conventional refrigeration cycle in order to provide further cooling effect. The DEN therefore displaces the consumption of Diesel fuel needed to operate the refrigeration system leading to reduction in CO_2, NO_x and particulate emissions.

Horizon 2020
European Union Funding
for Research & Innovation

This project has received funding from
the European Union's Horizon 2020 research and innovation
programme under grant agreement No 847097

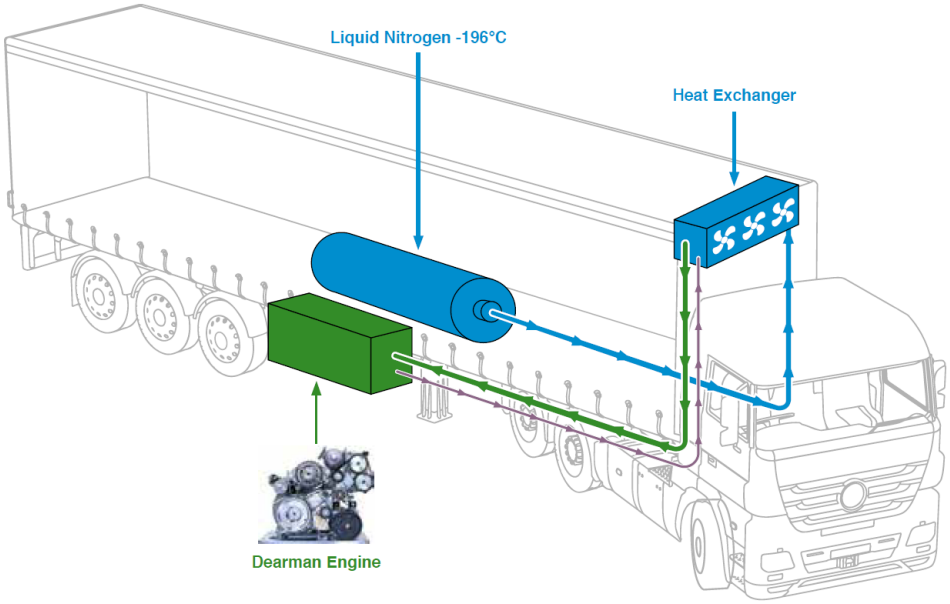

Figure 210: Dearman transport refrigeration system (Dearman, 2017).

5.8.3 Cost aspects

Costing of LAES is based on established technologies such as pumps, compressors, turbines and heat exchangers which are readily available in the supply chain for the required operating range (Morgan, Nelmes, Gibson, & Brett, 2015)(Georgiou, Shah, & Markides, 2018). Component investments typically scale with device size, according to a 0.6 exponent, allowing for economies of scale. Another advantage of LAES is that the size of charge, discharge and storage sections can be designed independently, which allows to tailor the plant to the specific application. Typical financial indicators for LAES are reported in Table 85. Projections assuming a 17.5% learning rate were used to characterize the price evolution with technology deployment, for a 10th-of-a-kind plant.

Table 85: Typical range of cost metrics for a liquid air energy storage plant.

Parameter	Range	
	1st-of-a-kind	10th-of-a-kind
CAPEX (per unit capacity)	250 ÷ 850 €/kWh	150 ÷ 450 €/kWh
CAPEX (per unit power)	1500 €/kW ÷ 2500 €/kW	800 ÷ 1300 €/kW
OPEX	1% ÷ 2% CAPEX per year	
Levelised cost of storage (LCOS)	36 ÷ 24 c€/kWh	27 ÷ 18 c€/kWh

Horizon 2020
European Union Funding
for Research & Innovation

This project has received funding from
the European Union's Horizon 2020 research and innovation
programme under grant agreement No 847097

5.9 Summary – Waste heat to power technologies

The systematic review highlighted that the existing waste heat to power (WHTP) technologies are a blend of well established (commercial) products with large adoption, commercial technologies with niche applications and near-to-market technologies. All of them share the same fundamental operating principle of converting heat into power (electricity), although different physical processes are exploited to do so depending on the technology considered. In the following the key findings for each WHTP technology are briefly summarized:

- Steam Rankine Cycle (SRC). Well proven large scale technology commonly used at scale in the power sector (thermal plant). It employs water-steam thermodynamic cycle to produce power through steam turbines. Only suitable for large scale, high grade WH sources (>400°C). Given its scale the technology usually requires significant investment and it is not typically suitable for retrofitting interventions.
- Organic Rankine Cycles (ORC) and low temperature Kalina Cycles (LT KCs). Low temperature power cycles that use organic fluids (ORC) and ammonia-water working fluids (KC). Suitable for conversion of WH typically at ~ 80÷250°C. These technologies have been fully demonstrated in industrial environment and a limited number of commercial suppliers currently exists, although adoption is still somehow limited. Given their low conversion efficiency ORC and low temperature KC are economically viable at medium scale (100 kW to a few MW). Small scale still remains economically prohibitive and research and development in this area is aimed at cost reduction.
- Supercritical CO_2 power cycles (sCO2) and high temperature Kalina Cycles (HT KCs). Due to the varying temperature in the heating process they allow an improved thermal match with the waste heat source compared to steam. However, the distillation/condensation subsystem in the KCs and the addition of more components and flow splits in the sCO2, which are required to enhance their performance make these systems quite complex with only a few full scale installations.
- Stirling Engine. Reciprocating, externally heated engine (no internal combustion); highly efficient although this is strongly related to the efficiency of one of the key subcomponent of the system (regenerator heat exchanger). The technology has been extensively trialed for high temperature solar thermal applications but a limited number of WH recovery applications currently exists, mostly around WHR from internal combustion engines. Commercial products are currently available from a limited number of suppliers.
- Thermo-electric generators (TEG) and thermo-photovoltaic generator (TPV). Technologies usually employed to convert medium to high-grade WH (200 to 1000°C) through Seebeck effect (TEG) or very high-grade WH (>1000°C) through photovoltaic cells (TPV). Both technologies are characterized by the absence of moving parts and have the advantage of modular design, enabling applications from few Watts up to hundreds of kW, although conversion efficiency is very low. Commercial TEG systems are currently available and have been employed in industrial applications (e.g., waste heat recovery from continuous casting, rotary kiln). On the other hand, a few prototypes of TPV have been developed and the technology remains at development stage.
- Liquid air energy storage (LAES) and Dearman Engine (DEN). Cryogenic energy technologies with potential of integration with WH sources. Both technologies employ cryogenic fluids with working temperature well below -100°C, which can be exploited as thermal sinks for low-grade WH. LAES is a large scale (>10 MW) storage process which can integrate WH from existing large scale industrial facilities or thermal plants in order to increase overall efficiency. Interestingly, LAES enables recovery of waste cold in particular from LNG terminal or gas stations. DEN is a small scale piston engine (~ 10 kW) which uses liquid nitrogen as working fluid. DEN can be

Horizon 2020
European Union Funding
for Research & Innovation

This project has received funding from
the European Union's Horizon 2020 research and innovation
programme under grant agreement No 847097

integrated with conventional internal combustion engines to recover WH from the latter and simultaneously produce power and cooling. The technology is mostly suitable for mobile applications (e.g., refrigerated trucks). Both LAES and DEN are currently near-to-market technologies with full commercial installations expected in the very short term.

Horizon 2020
European Union Funding
for Research & Innovation

This project has received funding from
the European Union's Horizon 2020 research and innovation
programme under grant agreement No 847097

6 Heat upgrade technologies

Three main technologies are covered in this Section: Vapour Compression Heat Pumps, Absorption Heat Pumps and Absorption Heat Transformers. The focus is on how low grade WH sources can improve the performance or drive these heat upgrade technologies that can provide useful heat not only for the residential/commercial sectors but also for the industrial sector.

6.1 Heat pumps (HPs)

A Heat Pump (HP) is an energy device whose primary aim is to upgrade heat from a heat source to a heat sink at higher temperature. This is done in general at the expense of consuming some extra high-quality energy, for example electricity. The working principle of HPs is therefore very similar and for various instances identical to refrigeration or air conditioning systems, with the crucial difference that the amount of upgraded heat is the desired effect in HP systems. HPs can collect heat from a variety of sources, such as air, water and ground to deliver heating for residential and commercial buildings ((Hussam Jouhara et al., 2018)(Deng, Wei, Liang, He, & Zhang, 2019a)). In the context of WH recovery, HPs are employed to valorise low-grade WH and upgrade it to higher temperatures, and thus making it more utilizable, for example as process heat.

Figure 211 illustrates the principle of HPs utilization for the purpose of WH recovery and valorisation. WH is the source from which the heat pump draws heat and the upgrade it making it valuable, i.e. increasing the temperature at which it is available. This is done, in the example presented in Figure 211, at the expense of electricity used to drive the compression process. Crucial parameters are the heat source temperature T_L (WH temperature in Figure 211) and the heat sink temperature T_H (usable heat temperature) across which the HP is capable to operate across. Such temperatures largely dictate the type of HP which can be utilized and the type of application. For this reason, various classes of HPs have been developed and commercialized. The following subsections present the HP classes most relevant for WHR applications.

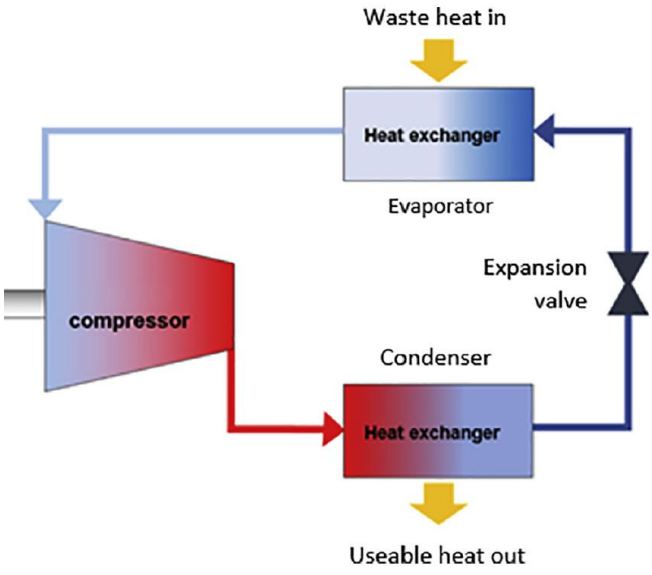

Figure 211: Heat pump utilization in the context of waste heat recovery (Hussam Jouhara et al., 2018).

Horizon 2020
European Union Funding
for Research & Innovation

This project has received funding from
the European Union's Horizon 2020 research and innovation
programme under grant agreement No 847097

6.1.1 Technological features and performance of vapour compression and absorption heat pumps

6.1.1.1 Vapour compression heat pumps (VCHPs)

1) Air source heat pumps

Air source heat pumps (ASHPs) employ the outdoor air as heat source, thus drawing heat from the environment. ASHPs are commercially available at scale and widely used worldwide across a variety of applications, predominantly for heating in buildings and for DHW. Table 86 reports typical applications for ASHPs. It can be observed that ASHPs can upgrade low-grade heat, around 20÷40°C. However, the temperature of heat source greatly impacts on ASHPs performance. It can be noted that the COP reported for ASHPs (see Table 86) may vary significantly, from about 1 to above 4, mostly due to the variation of the heat source, that is the variation of outdoor temperature. This makes ASHPs particularly sensitive to operating conditions and location of installation (e.g., cold or hot climates) (Q. Zhang, Zhang, Nie, & Li, 2017) (Yaning Zhang, Ma, Li, Fan, & Fu, 2017) (Xiao, He, et al., 2020). The availability of a low grade WH streams in place of ambient air could markedly improve the COP of the ASHP and it is of particular interest for this project. In particular, the WH generated in the data centres can be profitably used by AHSP providing space heating for adjacent buildings. In the feasibility study carried out by (Deymi-Dashtebayaz & Valipour-Namanlo, 2019) for a data centre in Mashhad (Iran) a COP of 5.1 was calculated when choosing R134a as WF and considering a temperature of 28°C of the cooling air leaving the data centre and entering the evaporator of the heat pump. The evaporation load was also useful to decrease the electricity consumption of the chiller that provides cooling air at 13°C for the data centre. In the application proposed by (Davies, Maidment, & Tozer, 2016b) the WH from data centres in the London area is upgraded by air source heat pumps and supplied to a DHN.

Table 86: Air source heat pumps (ASHPs): application, temperature of the heat source, temperature of the heat supplied, size and performance.

TRL	Heat source		Heat sink		Qheat (kW)	COP	Reference
	Application	Tin (°C)	Application	Tout (°C)			
N/A	Outdoor air	-10 ÷ 15	floor radiant heating, air convective heating and radiator heating	45	/	2.37 ÷ 4.62	(Q. Zhang et al., 2017)
4	Outdoor air	-20.9 ÷ -10.9	air convective heating	21.9 ÷ 27.3	≈2	1.04 ÷ 2.44	(Yaning Zhang et al., 2017)
4	Outdoor air	-20 ÷ 7	air convective heating and radiator heating	35 ÷ 48	≈2	1.67 ÷ 2.28	(Xiao, He, et al., 2020)
N/A	Outdoor air	2 ÷ 32	water heater	70 ÷ 80	≈10	2.07 ÷ 2.96	(Xiao, Chang, He, Zhao, & Shu, 2020)
N/A	Ambient air inside a room	25	water heater	65	14	3.5	(Nakayama, 2017)
9	Outdoor air	/	space heating and DHW	55	40	2.44[a]	(Popa, Ion, & Popa, 2016)
N/A	Outdoor air	16[a]	DHW	60	/	2.83[a] ÷ 3.02[a]	(X. Guo & Goumba, 2018)

Horizon 2020 European Union Funding for Research & Innovation
This project has received funding from the European Union's Horizon 2020 research and innovation programme under grant agreement No 847097

9	Ambient air in the hotel basement	/	domestic hot water (DHW)	55 ÷ 60	70	2.57[a]	(Liang et al., 2019)
9	Outdoor air	4.8[b]	space heating	/	/	2.58[b]	(Deng et al., 2019a)
N/A	Waste heat from data centre	28	space heating	/	58	4.4 ÷ 5.1	(Deymi-Dashtebayaz & Valipour-Namanlo, 2019)
N/A	Waste heat from data centre	35	District heating network	70	3500	4.1	(Davies et al., 2016b)

[a] average annual; [b] average of 11 different sites.

Figure 212: Photo of an ASHP for space and water heating installed in a school in Romania (Popa et al., 2016).

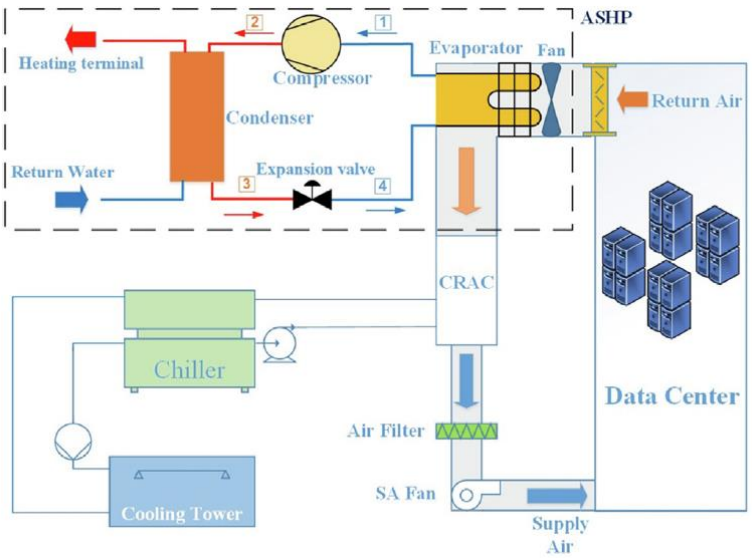

Figure 213: Coupling of an ASHP with the cooling system of a data centre (Deymi-Dashtebayaz & Valipour-Namanlo, 2019).

Horizon 2020
European Union Funding
for Research & Innovation

This project has received funding from
the European Union's Horizon 2020 research and innovation
programme under grant agreement No 847097

2) Water source heat pumps

Water source heat pumps (WSHPs) take advantage of heat sources in form of liquid, in most instances water, rather than outdoor air as in the case of ASHPs. The use of water-based sources has a dual benefit: the temperature of the source is relatively more stable (i.e., smaller fluctuations) and less affected by outdoor conditions (e.g., summer versus winter). Furthermore, yearly averaged temperature of water sources tend to be higher than those of air sources. As a result, WSHPs reach higher COPs than ASHPs, often exceeding value of 4÷5 (Deng et al., 2019a)(Pal, 2017). As a drawback, installation of WSHPs is somehow constrained as it clearly necessitates the presence of the water-based heat source.

Typical heat sources are aquifers and seawater for large scale centralized installation of WSHPs, such as in the case of integration with DHNs. As an example of application, three HPs with an overall capacity of 1.2 MW using aquifer water at 14°C below the Wandsworth Riverside Quarter in south-west London have been installed and designed to operate at COP of 4 (Foster, 2016). A system at Duindorp (The Hague, Netherlands) consisting of 2 HPs having each a capacity of 1.2 MW uses the heat of seawater at 3°C to supply heat at 11°C to a local low temperature network.

Of particular interest in the context of WHR and valorisation is the utilization of sewage or wastewater streams as heat sources for WSHPs. Sewage, wastewater and more generally low-temperature water streams are common carriers of low-grade WH from industrial processes, often difficult to be recovered since typically available in the range 10÷30°C (Foster, 2016)(Pal, 2017)(Popovac, Moretti, Lauermann, & Zottl, 2017)(Hu et al., 2017) (see also Table 87). In such a context, the utilization of WSHPs is therefore particularly valuable for the upgrading of WH carried by sewage and waste water. As an example, Figure 214 illustrates the integration of WSHPs for the upgrade of WH from wastewater from a chemical industrial process (Shijiazhuang, China). The heat was upgraded at about 45°C and then injected into a DHN. The HPs reached a COP of 6.95 and delivered about 1.7 MW of upgraded heat. In a similar manner, a large sewage source system composed by 5 HPs with an overall capacity of 84 MW_t was installed in Helsinki to preheat the DH return flow from 50°C to 62°C using sewage at 10°C and having a COP of 3.51 (Foster, 2016). Further relevant applications are reported in Table 87. It is worth to notice how WSHPs, in comparison with ASHPs, deliver better performance (COP) but are suitable for larger centralized installations, with size ranging from hundreds of kW to MW of thermal power.

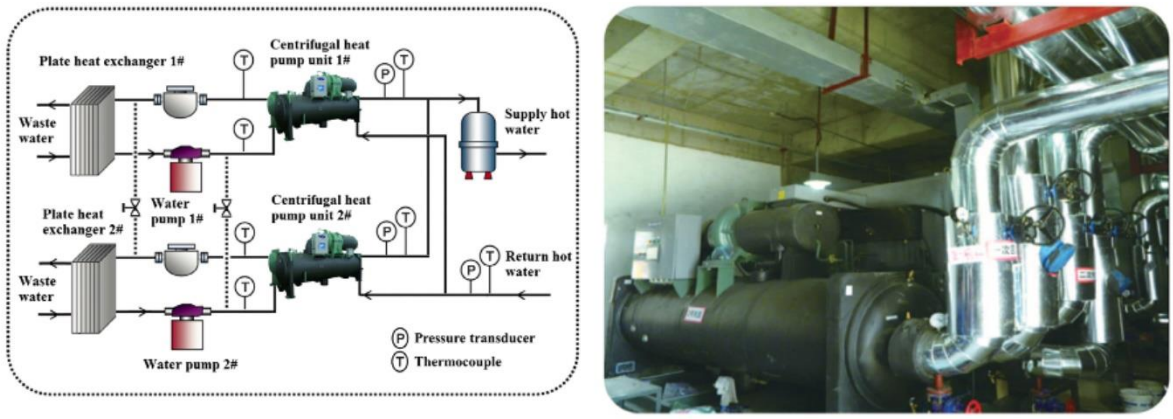

Figure 214: Integration of water source heat pumps for upgrade of WH from wastewater (Hu et al., 2017).

Horizon 2020
European Union Funding
for Research & Innovation

This project has received funding from
the European Union's Horizon 2020 research and innovation
programme under grant agreement No 847097

Table 87: Water source heat pumps (WSHPs): application, temperature of the heat source, temperature of the heat supplied, size and performance.

TRL	Heat source		Heat sink		Qheat (kW)	COP	Reference
	Application	Tin (°C)	Application	Tout (°C)			
9	Seawater and sewage	16.2[a]	space heating	/	/	4.64[a]	(Deng et al., 2019a)
9	Sewage	10	preheat the district return flow	62	16780	3.51	(Foster, 2016)
9	Aquifer	14	space heating	45	1200	4	(Foster, 2016)
9	Seawater	3	heat supply to a low temperature network	11	2400	11	(Foster, 2016)
9	Seawater	0.8	space heating	39.9	635	2.43	(H. Shu et al., 2015)
9	wastewater	12	space heating	32	3800	6.52[b]	(Pal, 2017)
9	wastewater	17.7	low temperature heating network	36.6	218	5.33[b]	(Popovac et al., 2017)
9	Industrial wastewater	23.7	floor radiation heating	45.1	1715	6.95	(Hu et al., 2017)
8	wastewater	30	district or industrial heating	60	9958	6.87	(Hu et al., 2019)
4	water	20	DHW	45 ÷ 65	≈ 5	3.72 ÷ 5.22	(Ju et al., 2018)
4	water	12	space heating	45 ÷ 55	3.3	3.13 ÷ 3.64	(Z. Sun et al., 2019)

[a] average of 5 different sites; [b] seasonal COP.

3) Ground source heat pumps

The ground and soil at shallow depths is another common heat source for HPs, in this instance called ground source heat pumps (GSHPs). A ground pipeline loop or vertical boreholes are used to extract heat from the ground, which is then upgraded though the operation of the HP. The main advantage is that the ground stays at relatively constant temperature during the year (Szulgowska-Zgrzywa & Fidorów-Kaprawy, 2017), which allows GSHPs to operate at a relatively constant COP throughout the year, with values of about 4 for shallow depths, with increasing values as deeper geothermal installations are considered. Overall, the vast majority of GSHPs applications is for space heating, either at individual building or at community level (for example coupled with district heating).

Application of GSHPs for WH recovery and valorisation is more challenging than for WSHPs due to the impossibility to use the WH stream directly as a heat source for the GSHP, since the heat exchange elements are buried into the ground. Therefore, valorisation of WH with GSHPs may be considered only at system level and indirectly. For example, the WH of the flue gases from a boiler or the exhaust gases from a thermal engine could be recovered to increase the ground temperature and, ultimately, the COP of a GSHP. The working principle is basically the same as that of coupling a solar seasonal storage system with GSHP aimed at preventing the decrease of the soil temperature and the deterioration of the heating performance (Liu, Zhu, & Zhao, 2016). However, in these novel systems the solar heat is replaced by the WH and the purpose is to obtain a significant temperature increase of the ground at shallow depths and, in turn, a significant increase of the COP. In this way, the COP of a shallow depth GSHP could approach that of a medium depth GSHP (see Table 88). In the system analysed in (Babak Dehghan, Wang, Motta, & Karimi, 2019), the WH of the flue gases leaving the

Horizon 2020 European Union Funding for Research & Innovation
This project has received funding from the European Union's Horizon 2020 research and innovation programme under grant agreement No 847097

boiler of a small biomass combustion plant is first stored into the ground and then upgraded through a GSHP system during the cold season. Water heated by the flue gases is pumped into the ground through 50 m depth U-tube ground HEs at a constant temperature of 60°C for three months continuously. By pumping hot water into the ground, heat was transferred by conduction from the borehole wall into the ground and the temperature of the ground around the HEs increased from the original value of 18°C. After completing the storage process, the stored heat was extracted from the ground and upgraded by a GSHP system. Figure 215 shows the temperature of the ground between two adjacent boreholes located at a distance of 6 m. A similar system was investigated in (Dehghan B., 2017) using the WH from the exhausts of a micro gas turbine (Figure 216). The WH was stored in ground through spiral ground HEs during warm climate and then recovered in cold climate using a GSHP system for supplying heating demands of the buildings. Another possibility for valorisation of WH is represented by the operation of reversible GSHPs. In this instance, WH when available and but utilized is stored in the ground through the operation of the GSHPs, to be then retrieved at a later time when needed in the premises of the GSHP installation. Table 88 shows the main features and performance of GSHPs.

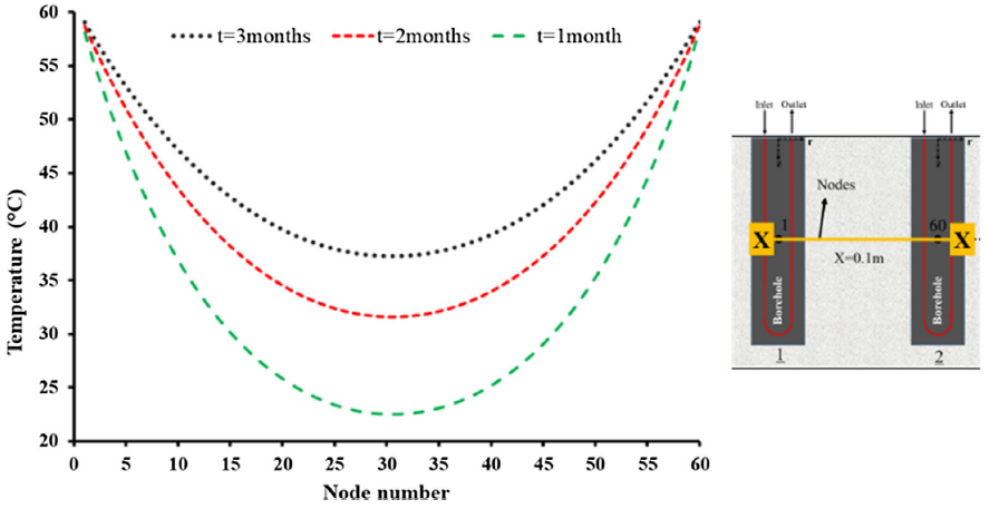

Figure 215: Variation of the ground temperature between two adjacent ground heat exchangers at the end of the first, second and third month of water injection at 60°C (Babak Dehghan et al., 2019).

Horizon 2020
European Union Funding
for Research & Innovation

This project has received funding from
the European Union's Horizon 2020 research and innovation
programme under grant agreement No 847097

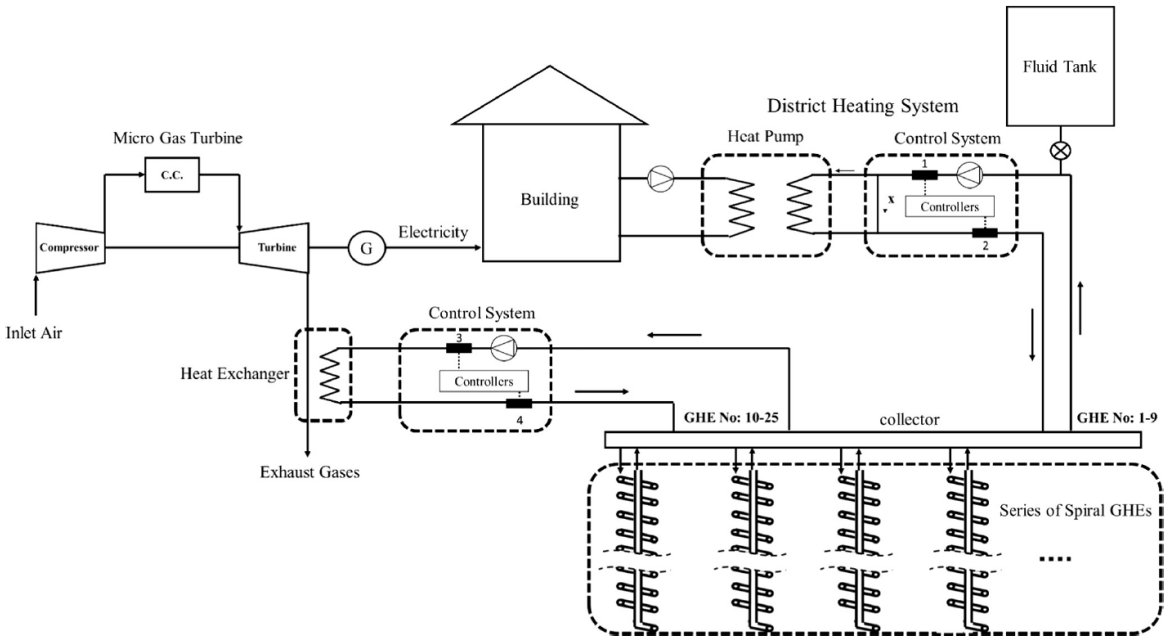

Figure 216: GSHP coupled with a WHR system that increases the temperature of the ground and the COP of the HP.

Table 88: Ground source heat pumps (GSHPs): application, temperature of the heat source, temperature of the heat supplied, size and performance.

TRL	Heat source		Heat sink		Qheat (kW)	COP	Reference
	Application	Tin (°C)	Application	Tout (°C)			
9	shallow depth	10.6[a]	space heating	/	/	3.72[a]	(Deng et al., 2019a)
9	shallow depth	6 ÷ 10	space heating and hot water	55	40	3.2	(Foster, 2016)
9	shallow depth	10.8 ÷ 11.7	floor space heating	40	≈17	3.53[b] ÷ 4.34[b]	(Szulgowska-Zgrzywa & Fidorów-Kaprawy, 2017)
9	shallow depth	/	space heating and hot water	/	/	3.24[b] ÷ 5[b]	(X. Liu, Malhotra, & Im, 2017)
7	low depth (300÷380 m)	12	floor heating	28	/	9.7	(Gasser et al., 2017)
9	medium depth (>2 km)	24.8[c]	space heating	/	/	5.15[c]	(Deng et al., 2019a)
9	medium depth (2÷3 km)	20 ÷ 34.7	space heating	39.2 ÷ 41.8	1040 ÷ 5680	4.35 ÷ 5.7	(Deng, Wei, Liang, He, & Zhang, 2019b)

[a] average of 8 installation sites; [b] seasonal COP; [c] average of 4 installation sites.

4) High temperature and very high temperature heat pumps

As illustrated in the previous Sections air, water and ground source heat pumps utilize heat sources up to ~35°C and upgrade heat to maximum temperature around 70÷80°C. Consequently, they are mostly used for valorisation of low grade WH, or in the context of space and water heating. This makes ASHPs, WSHPs and GSHPs unsuitable for upgrade and valorisation of WH to temperatures above 80°C, which are commonly required in industrial sectors such as Pulp & Paper, Food & Beverages, and Textile (Arpagaus, Bless, Uhlmann, Schiffmann, & Bertsch, 2018). In such contexts, high temperature heat pumps (HTHPs) and very high temperature heat pumps (VHTHPs) are of particular interest for

Horizon 2020
European Union Funding
for Research & Innovation

This project has received funding from
the European Union's Horizon 2020 research and innovation
programme under grant agreement No 847097

industrial applications and upgrade of WH from industrial processes. According to the classification originally proposed by (Peureux, Sicard, & Bobelin, 2014)(IEA Task 35, 2014) (see Figure 217) HTHPs commonly refers to HPs capable to reach a maximum temperature of ~100°C, while VHTHPs push the operational envelop up to ~160°C.

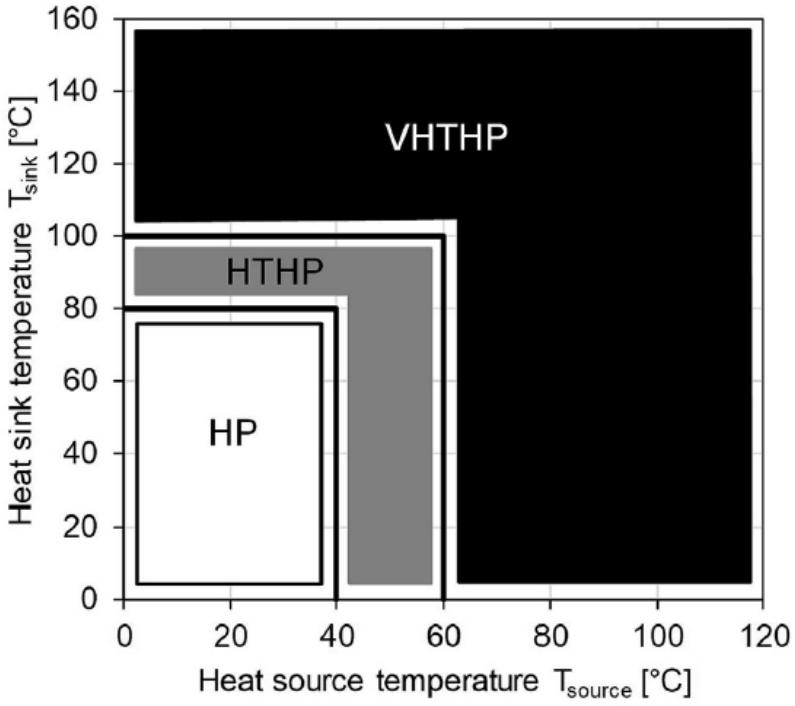

Figure 217: Development of temperature levels for compression heat pumps. HP: conventional heat pump; HTHP: high temperature heat pump; VHTHP: very high temperature heat pump (IEA Task 35, 2014)*(Arpagaus et al., 2018).*

Common HTHP configurations are single stage cycles and cascade cycles (two-stages), as illustrated in Figure 218 (Arpagaus et al., 2018). Such cycles are operated with refrigerant fluids, mostly hydrofluorocarbons (R134a, R245fa, etc.) or ammonia. Cascade cycles allows to employ separate loops with different WFs, which increases the temperature lift and thus allows to upgrade WH available at temperature below 70°C.

Horizon 2020
European Union Funding
for Research & Innovation

This project has received funding from
the European Union's Horizon 2020 research and innovation
programme under grant agreement No 847097

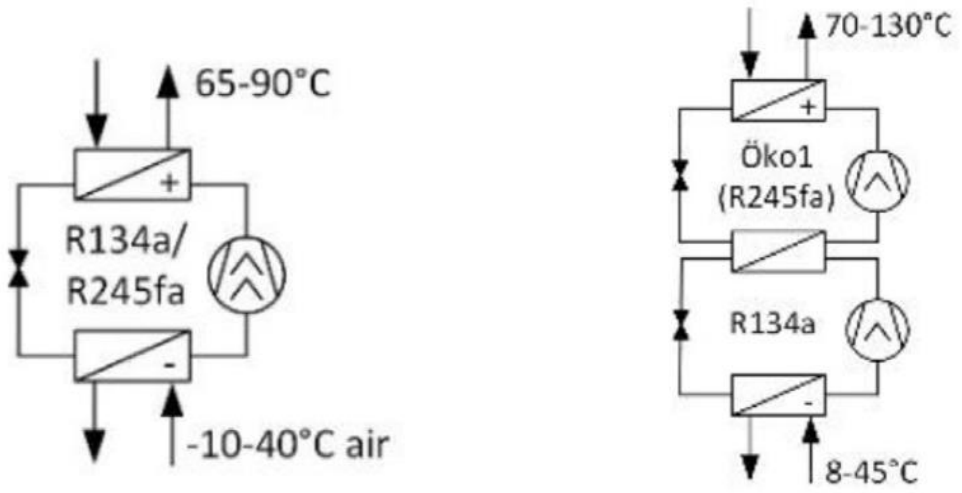

a) *b)*

Figure 218: HTHP cycle configurations: a) single stage cycle; b) double stage cycle (Arpagaus et al., 2018).

From technological stand point HTHPs are an established technology (often using common WFs such as R134a (Assaf, Zoughaib, Sapora, Peureux, & Clodic, 2010)) and with an established supply chain. Thirteen manufacturers and more than twenty HPs able to upgrade heat to at least 90°C have been identified in (Arpagaus et al., 2018). Manufacturers include Vicking Heating Engines AS, Hybrid Energy AS and Ochsner Energie Technik GmbH, with products ranging from 20 kW to >1 MW in heating capacity (i.e., amount of WH upgraded). Figure 219 summarizes the commercially available HTHPs and rank them by maximum temperature at which heat is delivered. Table 89 summarizes typical applications of HTHPs for valorization of industrial WH.

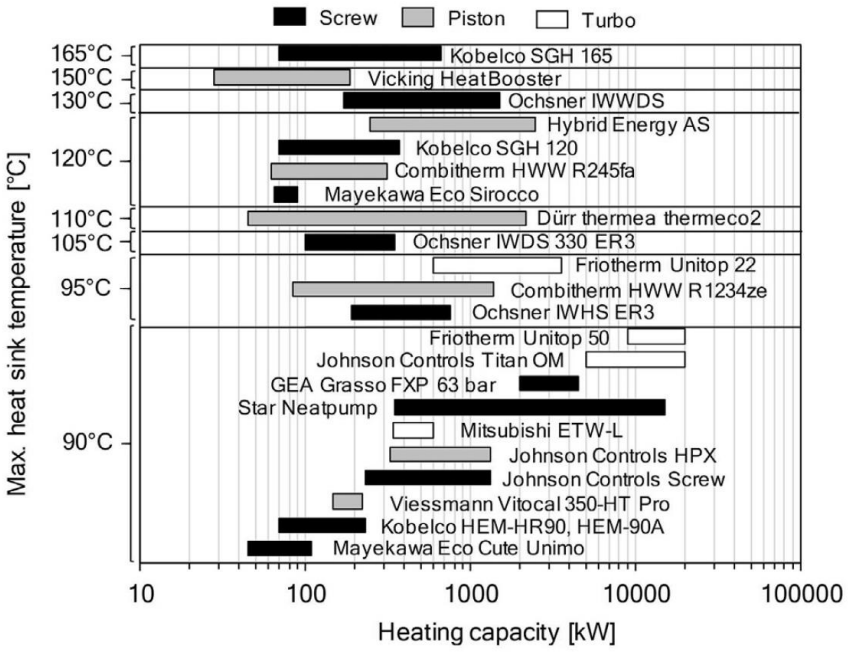

Figure 219: Industrial HTHP commercially available (Arpagaus et al., 2018).

Horizon 2020
European Union Funding
for Research & Innovation

This project has received funding from
the European Union's Horizon 2020 research and innovation
programme under grant agreement No 847097

Table 89: High temperature heat pumps (HTHPs): application, temperature of the heat source, temperature of the heat supplied, size and performance.

TRL	Heat source		Heat sink		Qheat (kW)	COP	Reference
	Application	Tin (°C)	Application	Tout (°C)			
9	Ambient air inside a room	≈25[a]	keep warm the dairy products	85	≈14	2.73[a]	(Nakayama, 2017)
9	WH from a data centre	35	supply of DH	80	3600	3.7	(Porkka, 2017)
9	WH of the exhaust air	20	fish feeding pellets drying	70÷80	1500	3.7	(Porkka, 2017)
6	WH streams in food industries	30 ÷ 50	hot process water for pasteurization, mashing in food industry	75	500	3 ÷ 4.5	(Assaf et al., 2010)
4	WH from industrial processes and geothermal DH systems	≈45	food drying, chemical distillation, ceramics production	≈75	≈ 4	2.89 ÷ 3.54	(S. Zhang, Wang, & Guo, 2010)
4	Outdoor air	7 ÷ 25	hot water supply	80	≈ 4	3.3 ÷ 4	(Watanabe, 2017)
9	WH from bio-refinery	70	preheat feedwater	90	2000	6.1	("Hybrid Energy (HTHP in Borregaard, Norway)," 2019)
9	WH from solar facility	35	district heating	100	1300	4.3	("Hybrid Energy (HTHP in Løgumkloster, Denmark)," 2019)

[a] annual average.

VHTHPs for heat upgrade above 120°C currently remain subject of R&D projects and only a handful of commercially viable products are available. Several R&D project have been conducted recently in Europe (DryFiciency ("H2020 DryFiciency," 2019); PACO ("EDF ANR Project PACO," 2019); HeatUp ("Sintef HeatUP," 2019); (Mateu-Royo, Navarro-Esbrí, Mota-Babiloni, Molés, & Amat-Albuixech, 2019)), in China ((Xiaoqiong Li et al., 2019)(X. Wu, Xing, He, Wang, & Chen, 2016)(Yan Zhang et al., 2017)(Xuelian Ma et al., 2018)) and Korea ((Kang, Na, Yoo, Lee, & Kim, 2019)), with a focus on the development of advanced layouts (Arpagaus et al., 2018), new working fluids (Yan Zhang et al., 2017)(Xiaoqiong Li et al., 2019) and adequate compressors (Chamoun, Rulliere, Haberschill, & Peureux, 2014)(O. Bamigbetan, Eikevik, Nekså, Bantle, & Schlemminger, 2019). Presently, literature reports the highest temperatures of heat upgrade in the range of 160÷180°C. The maximum temperature of 168°C was reached by a VHTHP prototype using a novel mixture (BY6) in the upper cycle (Xiaoqiong Li et al., 2019) in place of R245fa. Similarly, a prototype developed by a Norwegian company (Tveit, 2017) that uses a reverse Stirling cycle achieve a temperature of 183°C. Table 90 reports further prototypes and pilot installations of VHTHPs for industrial WH valorisation.

Table 90: Very high temperature heat pumps (VHTHPs): application, temperature of the heat source, temperature of the heat supplied, size and performance.

TRL	Heat source		Heat sink		Qheat (kW)	COP	Reference
	Application	Tin (°C)	Application	Tout (°C)			
5	paper drying, distillation	≈90	replace burning fossil fuel	≈ 119	≈ 300	4.7 ÷ 5.1	(Chamoun et al., 2014)

Horizon 2020 European Union Funding for Research & Innovation

This project has received funding from the European Union's Horizon 2020 research and innovation programme under grant agreement No 847097

5	pulp and paper and food industries	≈60	pulp and paper and food industries	≈ 95	≈ 100 ÷ 200	4.48	(Bobelin, Bourig, & Peureux, 2012)
4	milk production plant	30 ÷ 60	pressurized hot water production	115	20	2.1 ÷ 3.1	(O. Bamigbetan et al., 2019)
N/A	WH from industrial processes	70 ÷ 75	drying, pasteurization, distillation, sterilization	115 ÷ 125	20	2.0 ÷ 3.4	(Opeyemi Bamigbetan, Eikevik, Nekså, Bantle, & Schlemminger, 2018)
4	WH	70	steam generation	115 ÷ 125	12	2.95 ÷ 3.6	(Kang et al., 2019)
4	WH	55	reboiler for refining and chemical industry, steel rolling mill, pulp, paper, and food industries	100 ÷ 168.4	≈ 20	2.35 ÷ 3.17	(Xiaoqiong Li et al., 2019)
4	WH dyeing industry	74	production of hot water for the dyeing process	97.3	108	4.2	(X. Wu et al., 2016)
4	ICE jacket cooling water	60 ÷ 80	steam or pressurized water useful for the industrial processes	90 ÷ 140	≈ 15	2.23 ÷ 3.41	(Mateu-Royo et al., 2019)
4	distillation, rubber production	70 ÷ 80	distillation, rubber production	110 ÷ 130	≈ 18	2.54 ÷ 3.09	(Yan Zhang et al., 2017)
N/A	industrial WH	≈60	production of steam	≈ 125	≈ 75	2.56 ÷ 3.62	(Mikielewicz & Wajs, 2019)
4	petroleum refining industry	50	petroleum refining industry	101 ÷ 141	≈ 17	1.73 ÷ 2.97	(Xuelian Ma et al., 2018)
4	WH	≈81	production of pressurized water for industry	114	10	5.18	(Huang, Liang, & Zhuang, 2017)
7	WH from the paper production process	60	production of low pressure steam for the process	111 ÷ 138	160	1.9 ÷ 3.6	(Wemmers, Haasteren, Kremers, & Kamp, 2017)
7	heat from DHN	85	production of low/medium pressure steam for a dairy plant	183	450	2.1	(Tveit, 2017)
N/A	geothermal water	≈65	steam generation	≈120	/	3.22 ÷ 3.79	(Lu, Gong, Yao, Luo, & Ma, 2019)

Horizon 2020
European Union Funding
for Research & Innovation

This project has received funding from
the European Union's Horizon 2020 research and innovation
programme under grant agreement No 847097

6.1.1.2 Absorption heat pumps (AHPs)

Absorption heat pumps (AHPs) are a class of HPs that are thermally driven. The compression stage, present in vapour compression HPs, is replaced by the Generator/Absorber components in which the working fluid, i.e. a sorption solution is concentrated/diluted. A single effect configuration of AHP is shown in Figure 220. The key components are the generator (G), the evaporator (E), the condenser (C) and the absorber (A). Unlike the previous WHR systems, two heat sources at different temperatures are needed to operate continuously the AHP. A high temperature source drives the generation, while a low temperature heat source is absorbed at the evaporator. The net useful result of the AHP is a heat output at an intermediate temperature, which is delivered at the condenser and absorber. The high-grade driving heat source typically at temperatures in the range 80÷150°C is supplied to the generator, whereas the low-grade heat source supplied to the evaporator is close to ambient temperature. The high grade heat source can be industrial WH, heat supplied by a DHN, renewable energy (solar, geothermal, biomass) (W. Wu, Wang, Shi, & Li, 2014a).

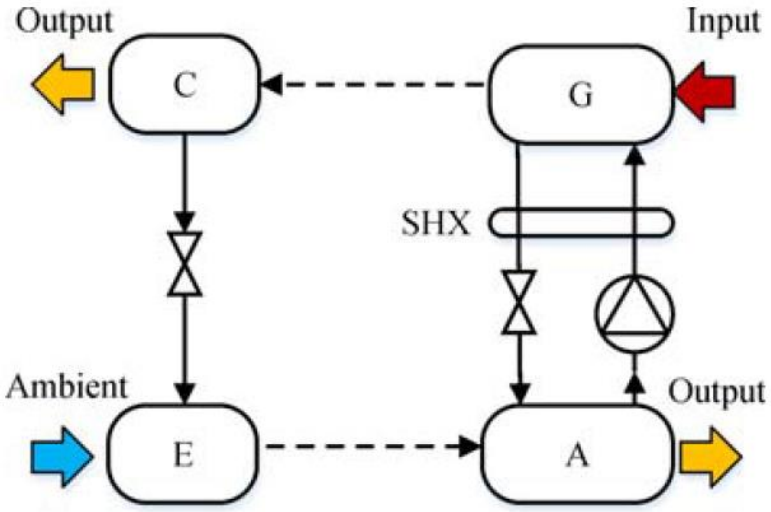

Figure 220: Single stage absorption heat pump (Z. Xu & Wang, 2017).

The working fluids commonly used in AHPs are solutions of H_2O/LiBr or NH_3/H_2O. In the generator the solution is heated, generating a high temperature high-pressure vapour refrigerant (H_2O in the H_2O/LiBr system, or NH_3 in the NH_3/H_2O system). This enters the condenser releasing the condensation heat to the heat user. The condensed liquid then flows through an expansion valve from the high to the low pressure side of the system and enters the evaporator where it absorbs low-temperature heat. Finally, the low pressure vapour refrigerant flows to the absorber where it mixes with the dilute solution and is absorbed by the solution in an exothermic process. The heat of absorption is released to the heat user as well.

Single stage AHPs typically achieve a *thermal* Coefficient-of-Performance (COP_t) in the range 1.5÷1.8 with generation, condensation and absorption temperatures attesting around 130°C, 70°C, 70°C, and 30-50°C (S. Jeong, Kang, & Karng, 1998)(Keil, Plura, Radspieler, & Schweigler, 2008). Although COPs of AHPs appear significant lower than those of VCHPs, it is important to remember that AHPs are thermally driven systems. This means that COP_t quantifies the ratio between the useful heat released in the condenser and absorber divided by the heat supplied to the generator driving the AHP.

Alongside single stage AHPs a few other cycle configurations have been developed in order to improve the performance of single stage AHPs. Table 91 summarizes the most common AHP cycle

Horizon 2020
European Union Funding
for Research & Innovation

This project has received funding from
the European Union's Horizon 2020 research and innovation
programme under grant agreement No 847097

configurations. Multiple stages configurations employ multiple Generators and Condensers to split generation and condensation across different pressure levels. This has the benefit to allow reintegration of heat (form high to low pressure) internally to the cycle, leading to higher COPs. Alternatively, two-stage layouts can be also optimized to maximize the temperature at which the heat output is delivered (double lift cycle). Other configurations include GAX Generation-absorption heat pump (suitable with ammonia and no risk of crystallization) and open cycle configurations.

Table 91: Summary of cycle configurations for absorption heat pumps (Z. Xu & Wang, 2017).

Configuration	Features	COP
Single effect	Basic cycle, widely used	1.5 ÷ 1.8
Double effect	High COP, research	2.14 ÷ 2.2
Double lift	Large temperature lift, research	1.34
GAX	High COP, feasible with ammonia-water	1.6 ÷ 2.2
Open cycle	Simple system, work with moist gas	1.55 ÷ 1.97

Table 92 summarizes the main applications of AHPs for upgrade and valorisation of WH. Capacity of AHP ranges from tens of kW to MW scale; for example, Figure 221 shows one of the largest AHP installation using six steam-driven LiBr-water AHPs, each one with a rated heating capacity of 48.5 MW. In such installation heat extracted from steam turbine of a nearby power plant is used as heat source for AHPs. Cooling water from the condenser of the power plant is used as the low-temperature heat source for the AHPs. This installation shows one of the key benefits of AHPs; AHPs are thermally driven systems, thus they allow integration of multiple heat sources at different temperatures, creating synergies between individual sub-processes, enabling better matching of different WH sources and sinks. Another example of such synergies can be appreciated for the installation developed in Munich (Germany). In this instance, the low-grade heat (<45°C) dissipated by a seasonal water solar storage is upgraded by an AHP to 55°C and supplied to the local DHN (Keil et al., 2008). Nevertheless, in absence of an industrial low-grade heat source, AHPs can operate by using air, soil, surface water (W. Wu, Ran, Shi, Wang, & Li, 2016)(Mirl, Schmid, Bierling, & Spindler, 2020)(Xianting Li, Wu, Zhang, Shi, & Wang, 2012), which therefore closely resemble the operation of conventional air-source or water source heat pumps.

Table 92: Thermally driven AHPs: temperature of the low grade and driving heat sources, temperature of the heat supplied and performance.

TRL	Low grade heat source		Driving heat source		Heat sink		Qheat (kW)	COP_t	Reference
	Application	Tin (°C)	Application	Tin (°C)	Application	Tout (°C)			
9	heat from steam condensation	35	steam extraction from the turbine	126 (2.5 bar)	district heating	80	63570	1.77	(Z. Y. Xu, Mao, Liu, & Wang, 2018)
9	residual heat in a solar hot water seasonal TES	10 ÷ 45	hot water from the DHN	90 ÷ 120	local heating network	55	/	1.7	(Keil et al., 2008)

Horizon 2020
European Union Funding
for Research & Innovation

This project has received funding from
the European Union's Horizon 2020 research and innovation
programme under grant agreement No 847097

6	industrial wastewater	51.4	hot water from the DHN	86.3	space heating	55	1000	1.88	(J. Sun, Ge, & Fu, 2017)
4	water heated by the residual heat in the boiler flue gases	30	hot water produced by the boiler	95.8	hot water supplied to the natural gas boiler	57.5	66	1.4	(Qu, Abdelaziz, & Yin, 2014)
N/A	wastewater in a chemical plant	38	steam	130	heat demands in the chemical plant	60	5000	1.70	(S. Jeong et al., 1998)
N/A	wastewater	25 ÷ 40	steam	145 ÷ 167	/	63 ÷ 72	≈1200	1.67 ÷ 1.73	(Jian, Lin, & Shigang, 2010)

Figure 221: Large scale (290 MW_t) steam driven AHP for district heating in Lanzhou (China) (Z. Y. Xu et al., 2018).

6.1.2 Cost aspects

The investment costs of VCHPs are widely available, also from previous EU projects. Thus, this Section focuses on the cost of AHPs. The investment cost of the large scale AHP project in Lanzhou, China (Figure 221) amounts to ≈130 million yuan. By considering the number of AHP units (6) and the heating capacity of each unit, a specific investment cost of 43.5 €/kW_t is obtained for very large (tens MWs) heat driven customized AHP units. The costs provided in other studies describing medium scale (from hundreds kW to 1 MW) thermally driven AHPs are cost estimates based on the heat load in the evaporator. For instance a cost of 600 yuan per kW_t of evaporation is assumed by (J. Sun et al., 2017), which results in a specific investment cost of 35.8 €/kWt when referred to the heating capacity. A baseline specific cost of 1500 yuan per kWt of heating capacity is considered in the detailed techno-economic analysis by (W. Wu, Wang, Shi, & Li, 2014b) with a possible range between 1000÷3000 yuan per kWt. For residential/small commercial units and in the US context, the unit cost of the AHPs was estimated as $400/kW (Qu et al., 2014) starting from the market price of absorption chillers. Finally,

Horizon 2020
European Union Funding
for Research & Innovation

This project has received funding from
the European Union's Horizon 2020 research and innovation
programme under grant agreement No 847097

the unit price of residential gas driven AHPs units is 83 €/kW_t (Robur, 2019). In summary, from the cost data summarized in Table 93, it appears that the unit cost of customized AHPs stabilizes after a 1 MW capacity and that thermally driven units are more expensive than gas fired units.

Table 93: Specific investment cost of thermally driven and gas driven AHPs.

TRL	Type	Cost (€)	Heating capacity (kW_t)	Specific investment cost (€/kW_t)	Reference
9	large heat driven	2762500	63570	43.5	(Z. Y. Xu et al., 2018)
6		35700	997	35.8	(J. Sun et al., 2017)
N/A	medium heat driven	/	≈ 300÷400	190	(W. Wu et al., 2014b)
4	small heat driven	/	66	350	(Qu et al., 2014)
9	small gas driven	1498	18	83	(Robur, 2019)

Horizon 2020
European Union Funding
for Research & Innovation

This project has received funding from
the European Union's Horizon 2020 research and innovation
programme under grant agreement No 847097

6.2 Absorption heat transformers (AHTs)

6.2.1 Technological features and performance

Figure 222 presents the working principle of absorption heat transformers (AHT). An AHT uses WH at low/medium temperature typically in the range 60÷95°C and transforms it into two separate thermal energy streams: high temperature heat and low temperature heat. Thus, AHTs valorise WH by upgrading part of it to higher temperature, hence making it more utilizable, but also producing a secondary low temperature thermal energy stream which might be used for cooling purposes. Up to 50% of the WH can be upgraded (Yin, Shi, Zhu, & Han, 2000)(Indus3Es H2020, 2019) through AHTs at the expenses of minimal electricity consumption.

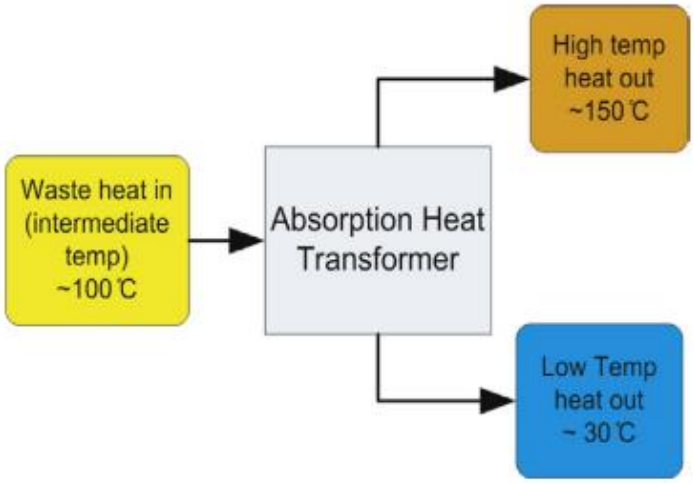

Figure 222: Input and output streams of an AHT (Donnellan, Cronin, & Byrne, 2015).

The simplest implementation of AHT is a single stage heat transformer (SSHT) (Donnellan et al., 2015)(Rivera, Best, Cardoso, & Romero, 2015); the layout and key components of a SSHT are presented in Figure 223. A WH source is used to supply heat to the Generator, in which sorbate (more volatile component) is separated from the absorbent. A typical pair utilized in AHTs is LiBr-H_2O solution (Parham, Khamooshi, Tematio, Yari, & Atikol, 2014). The sorbate is then condensed, releasing the corresponding latent heat producing a cooling effect (i.e., low temperature heat source). The sorbate (liquid at the outlet of the condenser) is evaporated (evaporator) and directed to the Absorber where it recombines with the liquid absorbent. The recombination process is exothermic, releasing the heat of absorption. This provides higher-grade heat at the Absorber. A temperature lift in the range of 30÷60°C is typically achieved (Parham et al., 2014). The cycle is closed by the diluted absorbent flowing back to the Generator. Overall, it is worthy to notice that a SSHT is in its essence an absorption heat pump operated in reverse (Srikhirin, Aphornratana, & Chungpaibulpatana, 2000).

Horizon 2020
European Union Funding
for Research & Innovation

This project has received funding from
the European Union's Horizon 2020 research and innovation
programme under grant agreement No 847097

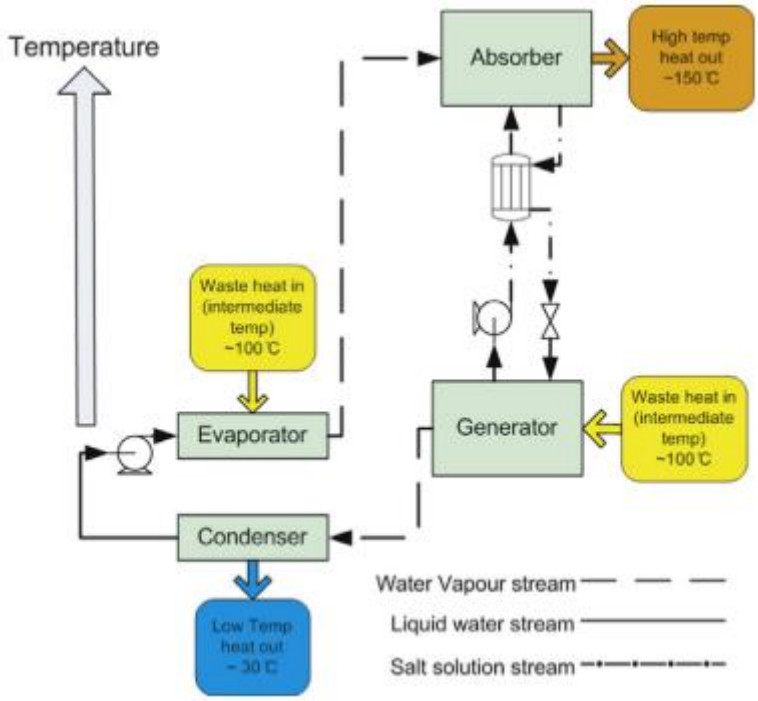

Figure 223: Layout of a single stage AHT (Donnellan et al., 2015).

SSHT provides WH upgrade typically in the range of 30÷60°C. In order to attain higher temperature lifts more complex AHT architectures have been also developed (Rivera, Huicochea, Romero, & Lozano, 2018)(Hanzhi Wang, Li, Bu, & Wang, 2017)(Hanzhi Wang, Li, Bu, & Wang, 2016). Table 94 summarizes the main AHTs layouts and it provides a high-level cross comparison with the SSHT architecture. Working fluids selections also vary. Table 95 reports the WFs more commonly considered in AHTs. Due to similar working principles, the working fluids for AHTs closely resemble those employed in AHPs, with lithium bromide – water pair (LiBr-H_2O) being the most commonly adopted.

Table 94: Summary of absorption heat transformer architectures.

Absorption heat transformer architecture	Features	Typical temperature lift [°C]	COP
Single stage AHT	/	30÷50	0.40÷0.50
Double stage AHT	Absorber coupled to the evaporator (internal heat recovery); use of two Absorbers, one acting as intermediate Evaporator	80÷90	0.25÷0.30
Double absorption heat transformer (DHAT)	Similar to double stage, but shared generator and condensers	50÷70	0.25 ÷ 0.32
Triple stage AHT	Two absorbers/condensers at different temperature	125	0.20

Horizon 2020
European Union Funding
for Research & Innovation

This project has received funding from
the European Union's Horizon 2020 research and innovation
programme under grant agreement No 847097

Table 95: Summary of working fluids for absorption heat transformers.

Working fluid	Reference
lithium bromide – water (LiBr-H_2O)	(S. J. Hong et al., 2018)(Xuehu Ma et al., 2003)(Fujii, Kawamura, Sakano, Uchida, & Nishiguchi, 2008)(Parham et al., 2014)
sodium hydroxide – water (NaOH-H_2O)	(Scott, Jernqvist, & Aly, 1999)(Abrahamsson, Gidner, & Jernqvist, 1995)
calcium chloride – water ($CaCl_2$-H_2O)	(Barragán, Arellano, Heard, Best, & Holland, 1997)
water - ammonia (H_2O-NH_3)	(Garone, Toppi, Guerra, & Motta, 2017)(Best, Eisa, & Holland, 1987)(S. Yang, Qian, Wang, & Yang, 2017)
Refrigerants (tri-fluoroethanol)	(Z. Zhao, Zhang, & Ma, 2005)(Ayou et al., 2014)
LiBr – ethylene glycol – water mixture	(Ibarra-Bahena et al., 2015)(Ibarra-Bahena, Dehesa-Carrasco, Montiel-González, Romero, & Venegas-Reyes, 2017)(Rivera, 2000)

6.2.2 Example of applications and technology maturity

AHT technology has been demonstrated and fully integrated with the industrial process in a small number of cases (Xuehu Ma et al., 2003)(Fujii et al., 2008)(IEA Task 35, 2014). In such instances, AHT has been reported to achieve PBT of ~2 ÷ 5 years and deliver significant energy savings, although economic viability of AHT still need to be fully documented and it is case dependent (Donnellan et al., 2015). Commercial uptake has therefore been lagging and it appears that no commercial products are currently available on the market. Furthermore, it has been reported that AHT are still not utilized in industry because "they are till an unknown entity" (Donnellan et al., 2015). Furthermore, AHT systems currently manifest a mixture of advantages and disadvantages which might increase the uncertainty around their adoption. Advantages/disadvantages are summarized in Table 96. Identified working fluids are difficult to handle due to corrosiveness and potential toxicity. Size of component might be large with in part unproven costs. On the other side, AHTs are usually robust (low maintenance) and are thermally driven system, with minimal electrical input.

Table 96: Main pros and cons of Absorption Heat Transformers.

Benefits	Disadvantages
Up to 50% of waste heat upgrade	Hazardous working fluids
Thermally driven system	Bulky equipment
Low maintenance	Demonstrated at scale only in few cases

Table 97 summarizes the main operating and performance parameters of the most relevant real scale AHT plants (TRL=9) and AHT experimental projects (TRL=4÷6) using the single stage AHT layout. Most of the full scale installations were developed in the eighties/nineties (Figure 224 and Figure 225). A more recent installation in an hydraulic machinery factory in Japan is reported in (Fujii et al., 2008). At lab scale/ small pilot scale (1÷20 kW) AHT has been recently investigated experimentally to a good extent. Among the advanced pilot, the one developed within the project Indus3Es (Indus3Es H2020, 2019) appears particularly relevant and promising. The system is illustrated in Figure 226 and it consists of a single effect AHT with a capacity of 200 kW_t and a nominal temperature lift of 40°C. A PBT target of 2÷4 years is expected for future commercialization.

Horizon 2020
European Union Funding
for Research & Innovation

This project has received funding from
the European Union's Horizon 2020 research and innovation
programme under grant agreement No 847097

Table 97: Single stage AHTs: applications, temperatures and performance.

TRL	Driving heat source		Heat sink		Qheat (kW)	COP_t	Reference
	Application	Tin (°C)	Application	Tout (°C)			
9	WH in a synthetic rubber plant	98	production of hot water	110	2350	0.47	(Xuehu Ma et al., 2003)
9	cooling water from a gas engine	90	low pressure (3 bar) steam generation for heating, cleaning, drying	137	150	0.484	(Fujii et al., 2008)
9	saturated steam at 1 bar ethylene amine plant	100	production of low pressure steam (4.6 bar)	145	6700	0.490	(IEA Task 35, 2014)
9	cooling water of the furnaces of the hot rolling strip mill	90	production of low pressure steam (2.7 bar)	130	4100	0.456	(IEA Task 35, 2014)
9	dryer vapour	90	production of low pressure steam for a food dryer	145	2150	0.483	(Mostofizadeh & Kulick, 1998)
9	vapour in a pulp and paper mill	100	production of low pressure steam	123	100	0.45	(Abrahamsson et al., 1995)
6	implementation in an oil refinery	95	production of useful for the oil refinery	135	200	0.45	(Indus3Es H2020, 2019)
4	WH from industry	85 ÷ 95	industry	115÷ 140	≈20	0.42 ÷ 0.47	(Cudok, Ciganda, Kononenko, & Drescher, 2017)
4	WH from industry	60÷64	district heating networks	73÷88	≈3	0.400 ÷ 0.475	(Garone et al., 2017)
4	WH	92÷93	direct steam generation at 2÷2.5 bar	114 ÷ 124	≈20	0.20 ÷ 0.38	(F. Liu, Sui, Liu, & Jin, 2017)
4	WH from industrial sectors and RES (geothermal, solar)	60 ÷ 80	heat-driven thermal distillation	<100	≈ 5	0.30 ÷ 0.38	(Sekar & Saravanan, 2011)
4	WH from industrial processes	95	heating of thermal oil	110 ÷ 140	≈ 5	0.27 ÷ 0.43	(Merkel, Bücherl, Zimmermann, Wagner, & Schaber, 2018)
4	WH	≈ 90	water purification	≈100 ÷ 105	≈ 1	0.26 ÷ 0.35	(Ibarra-Bahena et al., 2015)

Horizon 2020
European Union Funding
for Research & Innovation

This project has received funding from
the European Union's Horizon 2020 research and innovation
programme under grant agreement No 847097

Figure 224: Single stage 5 MW AHT installed in a synthetic rubber plant (Xuehu Ma et al., 2003).

Figure 225: Heat transformer installed in the nineties in the Netherlands to upgrade the WH released in a hot rolling strip mill (IEA Task 35, 2014).

Horizon 2020
European Union Funding
for Research & Innovation

This project has received funding from
the European Union's Horizon 2020 research and innovation
programme under grant agreement No 847097

Figure 226: Picture of the 200 kW AHT developed within the EU project Indus3ES (Indus3Es H2020, 2019).

When the industrial process requires temperature higher than 140°C or when the temperature lift is higher than 50°C more advanced layouts are required, like the double stage (or lift) AHT or the double AHT (Table 98). The feasibility of the double lift system was demonstrated at lab and pilot scale (Figure 227) showing the feasibility of steam generation at 8÷10 bar at COP ≈ 0.30 (Lubis, Giannetti, Yamaguchi, Saito, & Inoue, 2017)(Saito et al., 2015)(Moriwaki, Takigiri, Yamaguchi, & Saito, 2017). The double AHT was experimentally investigated in (Rivera et al., 2018) and it combines a rather simple layout with a high temperature lift. The integration of a double lift system in a pulp and industry plant was theoretically investigated by (Costa, Bakhtiari, Schuster, & Paris, 2009). For generation of process heat at temperatures >200°C a triple stage layout was investigated in (Donnellan, Cronin, Acevedo, & Byrne, 2014) for upgrade of waste streams in an oil refinery.

Table 98: Advanced AHTs architectures: applications, temperatures and performance.

TRL	Layout	Driving heat source		Heat sink		Qheat (kW)	COP_t	Reference
		Application	Tin (°C)	Application	Tout (°C)			
6	Double lift	waste heat	88	generation of process steam at 8 bar	180	200	0.278	(Saito et al., 2015)
4			80 ÷ 90		170 ÷ 172	14	0.237 ÷ 0.320	(Lubis et al., 2017)
4			88	steam at 10 bar	180	14	0.30 ÷ 0.33	(Moriwaki et al., 2017)
4	Double AHT	waste heat	70 ÷ 80	industry	90 ÷ 118	<1	0.12 ÷ 0.37	(Rivera et al., 2018)
N/A	Double lift	waste contaminated steam in the Kraft pulping process	96	generation of steam at 4 bar	144	10000	0.35	(Costa et al., 2009)
N/A	Triple stage	small oil refinery	120 ÷ 179	heating of a thermal oil loop	210	4500	0.21	(Donnellan et al., 2014)

Horizon 2020
European Union Funding
for Research & Innovation

This project has received funding from
the European Union's Horizon 2020 research and innovation
programme under grant agreement No 847097

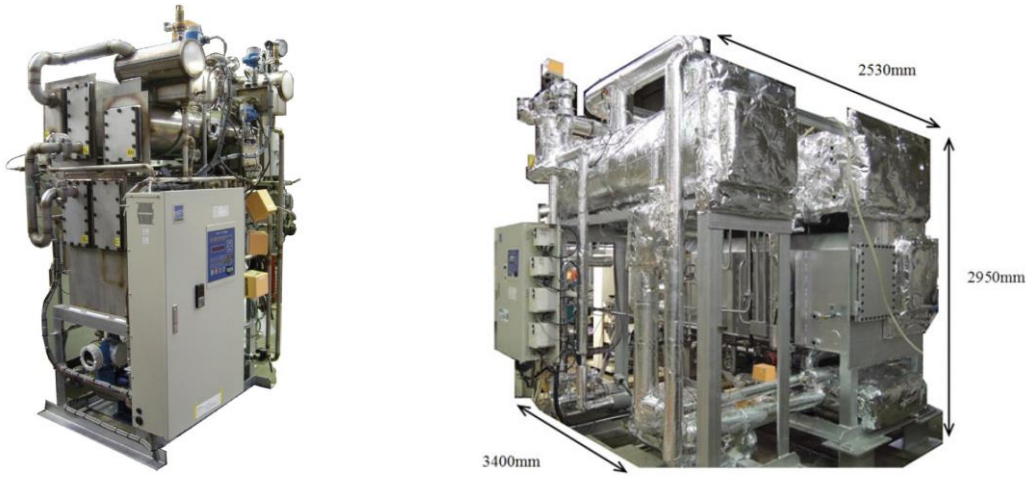

a) *b)*

Figure 227: Double lift AHT capable of generating steam at 8 bar from WH at 80÷90°C: a) experimental prototype (14 kW) and b) practical scale prototype (Lubis et al., 2017)(Saito et al., 2015).

6.2.3 Cost aspects

Table 99 shows the specific investment costs of AHTs reported in the literature. The specific investment cost of single stage AHTs varies in the range 190÷500 €/kW. Higher values are reported for double lift and triple stage systems due to the higher number of plant components. The use of NaOH/H_2O as working pair appears a more convenient option compared to LiBr/H_2O due to the lower corrosivity.

Table 99: Specific investment costs of AHTs having different layouts and operating with different working pairs.

Layout	Working pairs	Heating capacity (kW)	Specific investment cost (€/kW)	Reference
Single stage	LiBr/H_2O	3700	274	(K. Zhang et al., 2014)
Single stage	LiBr/H_2O	4100	498	(IEA Task 35, 2014)
Single stage	NaOH/ H_2O	42200	190	(Scott et al., 1999)
Single stage	LiBr/H_2O	42200	307	(Scott et al., 1999)(Berghmans, 1990)
Single stage	LiBr/H_2O	2350	331	(Xuehu Ma et al., 2003)
Single stage	NaOH/ H_2O	100	365	(Abrahamsson et al., 1995)
Single stage	LiBr/H_2O	200	/	(Indus3Es H2020, 2019)
Modified single stage	LiBr/H_2O	2150	400	(Mostofizadeh & Kulick, 1998)
Cascade	NH_3/H_2O (low T stage) LiBr/H_2O (high T stage)	2700	157[a] 302[b]	(S. Yang et al., 2017)
Double lift	LiBr/H_2O	≈ 10000	670	(Costa et al., 2009)
Triple stage	LiBr/H_2O	4500	1178[a] 4667[b]	(Donnellan et al., 2014)

[a] equipment purchase cost; [b] total installed cost.

Horizon 2020 European Union Funding for Research & Innovation

This project has received funding from the European Union's Horizon 2020 research and innovation programme under grant agreement No 847097

6.3 Summary – heat upgrade technologies

The systematic review identified that this technological class is dominated by two specific technologies: Heat pumps (HPs) and Absorption heat transformers (AHTs). For the vast majority HPs are fully commercially available with a large number of suppliers. Commercial HPs are mostly electrically driven systems (vapor compression HPs) for low temperature applications (upgrade to < 100°C). Such technology is particularly attractive as it enables coupling of heat and electrical systems, opening possibilities of business cases for WHR which go beyond the simple reutilization of WH. Of particular relevance for industrial WHR are the high temperature HPs where a limited number of commercial products exists for upgrade up to about 120÷130°C, while current development efforts are aimed at increasing the upgrade temperature above 140°C.

Absorption heat transformers are a near-to-market technology. Bespoken application of AHTs have been fully demonstrated at MW scale in industrial environment although full commercialization has not followed the demonstration stage, likely for a combination of lack of awareness of this technology by industrial stakeholders and of specialized knowledge needed to design, install and operate the AHT. The technology has the benefit of being purely thermally driven (electricity consumption usually negligible) and to also produce cooling as a by product of WH upgrade. As a drawback, thermal COP is usually limited (<0.5). Current effort is directed at developing "plug-and-play" AHT and abating costs.

Technology	Benefits	Drawbacks
	Heat upgrade technologies	
Heat pumps	Fully developed technology for low temperature vapor compression cycles (air, water) and domestic application; highly efficient. Enables alternative business cases through heat-electricity coupling. High temperature heat pumps (~80÷130°C) particularly attractive for industrial applications. Absorption heat pumps attractive for purely thermal driven installations	Performance might deteriorate with variation of WH source temperature; very high temperature heat pumps (> 140°C) still under development.
Absorption heat transformers	Technology demonstrated at MW scale in large industries but limited number of installations; operate as an inverse absorption heat pump to simultaneously produce high grade heat (~150°C) and low grade heat (~ 30°C) from a mid-temperature WH source (~60°÷90°C)	Limited awareness of this technology among industrial stakeholders; relatively low coefficient of performance; current development efforts directed at providing "plug-and-play" transformers and at reducing costs

Horizon 2020
European Union Funding
for Research & Innovation

This project has received funding from
the European Union's Horizon 2020 research and innovation
programme under grant agreement No 847097

7 Conclusions

Five different classes of WH/C recovery technologies have thoroughly been reviewed in this document. The selected classes encompass passive technologies as well as active technologies. Furthermore, beside established and commercial technologies also near-to-market ones have been identified and reviewed to capture current trends in technological development which could lead to new commercial technologies in the short term. The main findings and trends emerged for each technology are summarized in the Table below. The findings and the data collected for each technology within this report will feed directly into the SO-WHAT technology database that will be integrated in the final version of the SO-WHAT tool. Specifically, the finding presented in this report allows to:

i. assess technology readiness level of each technology, and thus differentiate the database into fully commercial technologies and those (near-to-market) that might reach market in the short term, hence enabling alternative routes for WH/C recovery;
ii. quantify typical operating conditions, nominal size and performance indicators of each technology, and thus allow to pre-select the most technically adequate technology for a given WH source temperature and size;
iii. identify the economic parameters for each technology considered necessary for the assessment of WH recovery business case.

The findings gathered in this report also support and can be utilized in the next steps of the SO-WHAT tool development and beyond. In particular, the document reports systematically an extensive collection of applications and integration cases for each one of the WHR technology considered. Such findings therefore inform the development of WH/C recovery scenarios and the development of accurate business models. Furthermore, the report gives a comprehensive cross-comparison of the WH/C recovery technologies, therefore helping in increasing the awareness among relevant stakeholders about the current technological state-of-the-art, as well as of existing WH/C recovery solutions that might be replicated.

Technology	Benefits	Disadvantages
Heat to heat technologies		
District heating heat exchangers	Well proven technology based on conventional heat exchangers; used on a wide scale and fully commercially available.	District heating infrastructure needs to be in place and it needs to reach waste heat sources
Condensation heat recovery	Direct and direct condensing economizers are available commercially; well proven.	Stream of condensed liquid need to be handled adequately and disposed if necessary
Economizers	Well proven technology based on conventional gas-liquid heat exchangers	Use limited to pre-heat boilers feed water; possible large foot print due to heat transfer limitations
Waste heat boilers	Well proven technology with fully developed supply chain	Technological option only feasible when there is a demand of steam to be met
Recuperators and Regenerators	Medium to high temperature heat exchangers to recover WH from flue gases; proven technology with several designs available	Possible issues with high operating temperatures and fouling. Moving parts for certain type of designs

Horizon 2020
European Union Funding
for Research & Innovation

This project has received funding from
the European Union's Horizon 2020 research and innovation
programme under grant agreement No 847097

Heat pipe heat exchangers	Near to market technology, about 300 full scale installations. Higher recovery capacity compared with traditional heat exchangers	Limited number of supplies; specialized knowledge needed for design and installation
Thermal energy storage technologies		
Sensible thermal storage	Well proven technology; Used at scale for T < 100°C (water tanks) and T ~ 300 – 500°C (molten salt tanks). Near to market solid media systems (rocks, concrete)	Possible low energy storage density and self-discharge (heat losses)
Latent thermal storage	Higher energy storage density, wide range of storage temperature, cold thermal storage; it can provide energy flexibility opportunities (e.g. peak/off peak)	Storage materials (PCMs) commercially available mostly in the range -20 – 120°C; Require specialists for fully engineered system; higher costs that sensible storage.
Thermochemical storage	Highest energy storage density; no thermal losses; possibility of long duration storage of heat; suitable and demonstrated for mobile applications	Currently at pilot scale, limited number of suppliers. Possible high system complexity. Development and demonstration needed to abate costs and establish long term performance
Heat to cold technologies		
Absorption chillers	Thermal driven refrigeration systems; proven within trigeneration systems	Multi-component, multiphase working fluid; cold sink necessary; COP might be limited
Heat to power technologies		
Steam Rankine cycles	Well proven technology and used at scale commonly in power station	Necessitate high-grade (>400°C) and large source of WH (~ MW); Water based cycle.
Organic Rankine cycles	Proven technology for power output in the range (~ 100 kW – a few MW). Can convert WH typically at ~80-250°C	Economically prohibitive at small scale (kW); utilizes organic fluids with potential environmental hazards) (e.g. R series); low conversion efficiency
Kalina cycles	Can convert low grade WH (<100°C); improved efficiency compared with ORCs; use ammonia-water working fluid. Improved thermal efficiency compared to the SRC for medium/high temperature WH	Proprietary technology; requires specialists to develop bespoken solution
Supercritical CO_2 cycles	Compactness and wide temperature range (200÷650°C)	Complex architectures required for WHR
Thermoelectric and thermophotovoltaic generators	TEG: technology demonstrated for industrial WH recovery up to ~ 100 kW; does not require a specific grade of WH, as long as a temperature difference is ensured; modular design and no moving parts TPV: enables direct conversion of radiant energy from thermal sources	TEG: very low efficiency and reliance on rare materials; typically used in high end specialized applications where cost is not the primary criterium TPV: few prototypes developed; technology still under R&D investigation; very low efficiency.
Stirling Engines	Reciprocating, externally heated engine – no internal combustion; highly efficient	Limited applications for waste heat recovery; an efficient

Horizon 2020 European Union Funding for Research & Innovation

This project has received funding from the European Union's Horizon 2020 research and innovation programme under grant agreement No 847097

		regenerator is the key component of the system
Liquid Air Energy Storage	Near to market energy storage technology that uses cryogenic fluids; offer possibility for recovery of very low grade waste heat; possibility for waste cold recovery	Only suitable for large scale applications; e.g. integration with large industrial processes and with energy storage needs.
Dearman engine	Near to market engine driven by liquid nitrogen; it offer possibility for recovery of waste heat particularly in transport application	Technology developed primarily to complement refrigeration systems on truck, lorries, containers
Heat upgrade technologies		
Heat pumps	Fully developed technology for low temperature vapor compression cycles (air, water) and domestic application; highly efficient. Enables alternative business cases through heat-electricity coupling. High temperature heat pumps (~70-130°C) particularly attractive for industrial applications. Absorption heat pumps attractive for purely thermal driven installations	Performance might deteriorate with variation of WH source temperature; very high temperature heat pumps (> 140°C) still under development.
Absorption heat transformers	Technology demonstrated at MW scale but in large scale industries but limited number of installations; operate as an inverse absorption heat pump to simultaneously produce high grade heat (~150°C) and low grade heat (~ 30°C) from a mid-temperature WH source (~60°-90°C)	Limited awareness of this technology among industrial stakeholders; relatively low coefficient of performance; current development efforts directed at providing "plug-and-play" transformers and at reducing costs

Horizon 2020
European Union Funding
for Research & Innovation

This project has received funding from
the European Union's Horizon 2020 research and innovation
programme under grant agreement No 847097

References

Aalborg Portland's supply of surplus heat from production in the form of district heating. (2020). Retrieved February 13, 2020, from http://climateyourbusiness.eu/project/aalborg-portland/

ABB. (2012). *The pulp mill that became a major energy supplier*.

Abhat, A. (1983). Low temperature latent heat thermal energy storage: Heat storage materials. *Solar Energy*. https://doi.org/10.1016/0038-092X(83)90186-X

Abrahamsson, K., Gidner, A., & Jernqvist, Å. (1995). Design and experimental performance evaluation of an absorption heat transformer with self-circulation. *Heat Recovery Systems and CHP*, *15*(3), 257–272. https://doi.org/10.1016/0890-4332(95)90010-1

AC Boilers. (2019). Retrieved from https://www.acboilers.com/en/products/heat-recovery-steam-generators/

ACT - Advanced Cooling Technologies. (2020). https://doi.org/https://www.1-act.com/innovations/heat-pipes/

AEInnova. (2019). AEInnova. Retrieved from https://aeinnova.com/

Ahmed, N., Elfeky, K. E., Lu, L., & Wang, Q. W. (2019). Thermal and economic evaluation of thermocline combined sensible-latent heat thermal energy storage system for medium temperature applications. *Energy Conversion and Management*. https://doi.org/10.1016/j.enconman.2019.03.040

Ahn, Y., Bae, S. J., Kim, M., Cho, S. K., Baik, S., Lee, J. I., & Cha, J. E. (2015). Review of supercritical CO_2 power cycle technology and current status of research and development. *Nuclear Engineering and Technology*, *47*(6), 647–661. https://doi.org/10.1016/j.net.2015.06.009

Alfa Laval - Plate and Shell HXs. (2020). Retrieved February 13, 2020, from https://www.alfalaval.com/products/heat-transfer/plate-heat-exchangers/Welded-plate-and-shell-heat-exchangers/

Alfa Laval - Spiral heat exchangers. (2020). Retrieved February 13, 2020, from https://www.alfalaval.co.uk/products/heat-transfer/plate-heat-exchangers/welded-spiral-heat-exchangers/

Alfa Laval - Waste heat recovery. (2020). Retrieved January 30, 2020, from https://www.alfalaval.co.uk/industries/marine-and-transportation/marine/waste-heat-recovery/

Alovisio, A., Chacartegui, R., Ortiz, C., Valverde, J. M., & Verda, V. (2017). Optimizing the CSP-Calcium Looping integration for Thermochemical Energy Storage. *Energy Conversion and Management*. https://doi.org/10.1016/j.enconman.2016.12.093

Altamirano, A., Pierrès, N. Le, & Stutz, B. (2019). Review of small-capacity single-stage continuous absorption systems operating on binary working fluids for cooling: Theoretical, experimental and commercial cycles. *International Journal of Refrigeration*. https://doi.org/10.1016/j.ijrefrig.2019.06.033

Altieri R., Campana F., V. R. (2014). *Waste Heat Valorisation for More Sustainable Energy Intensive IndustrieS*.

Alva, G., Lin, Y., & Fang, G. (2018). An overview of thermal energy storage systems. *Energy*. https://doi.org/10.1016/j.energy.2017.12.037

Amiri Rad, E., & Mohammadi, S. (2018). Energetic and exergetic optimized Rankine cycle for waste heat recovery in a cement factory. *Applied Thermal Engineering*, *132*, 410–422. https://doi.org/10.1016/j.applthermaleng.2017.12.076

Aneke, M., Agnew, B., Underwood, C., Wu, H., & Masheiti, S. (2012). Power generation from waste heat in a food processing application. *Applied Thermal Engineering*. https://doi.org/10.1016/j.applthermaleng.2011.12.023

Angerer, M., Becker, M., Härzschel, S., Kröper, K., Gleis, S., Vandersickel, A., & Spliethoff, H. (2018). Design of

Horizon 2020 European Union Funding for Research & Innovation

This project has received funding from the European Union's Horizon 2020 research and innovation programme under grant agreement No 847097

a MW-scale thermo-chemical energy storage reactor. *Energy Reports*. https://doi.org/10.1016/j.egyr.2018.07.005

Angerer, M., Djukow, M., Riedl, K., Gleis, S., & Spliethoff, H. (2018). Simulation of Cogeneration-Combined Cycle Plant Flexibilization by Thermochemical Energy Storage. *Journal of Energy Resources Technology*, *140*(2), 020909. https://doi.org/10.1115/1.4038666

Araiz, M., Casi, Á., Catalán, L., Martínez, Á., & Astrain, D. (2020). Prospects of waste-heat recovery from a real industry using thermoelectric generators: Economic and power output analysis. *Energy Conversion and Management*. https://doi.org/10.1016/j.enconman.2019.112376

Arpagaus, C., Bless, F., Uhlmann, M., Schiffmann, J., & Bertsch, S. S. (2018). High temperature heat pumps: Market overview, state of the art, research status, refrigerants, and application potentials. *Energy*. https://doi.org/10.1016/j.energy.2018.03.166

Ashouri, M., Khoshkar Vandani, A. M., Mehrpooya, M., Ahmadi, M. H., & Abdollahpour, A. (2015). Techno-economic assessment of a Kalina cycle driven by a parabolic Trough solar collector. *Energy Conversion and Management*, *105*, 1328–1339. https://doi.org/10.1016/j.enconman.2015.09.015

Assaf, K., Zoughaib, A., Sapora, E., Peureux, J.-L., & Clodic, D. (2010). Experimental simulation of a heat recovery heat pump system in food industries. *International Refrigeration and Air Conditioning Conference*, (June 2015), 1–7.

Ayala Delgado, R. (1992). *An experimental study of heat driven absorption cooling systems*.

Ayou, D. S., Currás, M. R., Salavera, D., García, J., Bruno, J. C., & Coronas, A. (2014). Performance analysis of absorption heat transformer cycles using ionic liquids based on imidazolium cation as absorbents with 2,2,2-trifluoroethanol as refrigerant. *Energy Conversion and Management*. https://doi.org/10.1016/j.enconman.2014.04.077

Babaelahi, M., Mofidipour, E., & Rafat, E. (2019). Design, dynamic analysis and control-based exergetic optimization for solar-driven Kalina power plant. *Energy*, *187*. https://doi.org/10.1016/j.energy.2019.115977

Babak Dehghan, B., Wang, L., Motta, M., & Karimi, N. (2019). Modelling of Waste Heat Recovery of a Biomass Combustion Plant through Ground Source Heat Pumps- Development of an Efficient Numerical Framework. *Applied Thermal Engineering*. https://doi.org/10.1016/j.applthermaleng.2019.114625

Bamigbetan, O., Eikevik, T. M., Nekså, P., Bantle, M., & Schlemminger, C. (2019). The development of a hydrocarbon high temperature heat pump for waste heat recovery. *Energy*. https://doi.org/10.1016/j.energy.2019.02.159

Bamigbetan, Opeyemi, Eikevik, T. M., Nekså, P., Bantle, M., & Schlemminger, C. (2018). Theoretical analysis of suitable fluids for high temperature heat pumps up to 125 °C heat delivery. *International Journal of Refrigeration*. https://doi.org/10.1016/j.ijrefrig.2018.05.017

Bao, J., & Zhao, L. (2013). A review of working fluid and expander selections for organic Rankine cycle. *Renewable and Sustainable Energy Reviews*. https://doi.org/10.1016/j.rser.2013.03.040

Barragán, R. M., Arellano, V. M., Heard, C. L., Best, R., & Holland, F. A. (1997). Experimental performance of the system water/magnesium chloride in a heat transformer. *International Journal of Energy Research*, *21*(2), 139–151. https://doi.org/10.1002/(SICI)1099-114X(199702)21:2<139::AID-ER226>3.0.CO;2-1

Bass, J. C., Elsner, N. B., & Leavitt, F. A. (1995). *Performance of the 1 kW thermoelectric generator for diesel engines*. 295–298. https://doi.org/10.1063/1.46818

Bauer, T., Forbes, I., & Pearsall, N. (2004). The potential of thermophotovoltaic heat recovery for the UK industry. *International Journal of Ambient Energy*, *25*(1), 19–25. https://doi.org/10.1080/01430750.2004.9674933

Horizon 2020
European Union Funding
for Research & Innovation

This project has received funding from
the European Union's Horizon 2020 research and innovation
programme under grant agreement No 847097

Bauer, T., Forbes, I., Penlington, R., & Pearsall, N. (2003). *The Potential of Thermophotovoltaic Heat Recovery for the Glass Industry*.

Bause, T., Campana, F., Filippini, L., Foresti, A., Monti, N., & Pelz, T. (2015). Cogeneration with ORC at Elbe-Stahlwerke Feralpi EAF shop. *Iron and Steel Technology*, *12*(5), 290–299.

Bayon, A., Bader, R., Jafarian, M., Fedunik-Hofman, L., Sun, Y., Hinkley, J., … Lipiński, W. (2018). Techno-economic assessment of solid–gas thermochemical energy storage systems for solar thermal power applications. *Energy*. https://doi.org/10.1016/j.energy.2017.11.084

Bayón, R., Rojas, E., Valenzuela, L., Zarza, E., & León, J. (2010). Analysis of the experimental behaviour of a 100 kWth latent heat storage system for direct steam generation in solar thermal power plants. *Applied Thermal Engineering*. https://doi.org/10.1016/j.applthermaleng.2010.07.011

BCS, I. (2008). *Waste Heat Recovery: Technology and Opportunities in U.S. Industry*.

Beausoleil-Morrison, I., Kemery, B., Wills, A. D., & Meister, C. (2019). Design and simulated performance of a solar-thermal system employing seasonal storage for providing the majority of space heating and domestic hot water heating needs to a single-family house in a cold climate. *Solar Energy*. https://doi.org/10.1016/j.solener.2019.08.034

Bellan, S., Alam, T. E., González-Aguilar, J., Romero, M., Rahman, M. M., Goswami, D. Y., & Stefanakos, E. K. (2015). Numerical and experimental studies on heat transfer characteristics of thermal energy storage system packed with molten salt PCM capsules. *Applied Thermal Engineering*. https://doi.org/10.1016/j.applthermaleng.2015.07.056

Bellos, E., Tzivanidis, C., Pavlovic, S., & Stefanovic, V. (2017). Thermodynamic investigation of LiCl-H2O working pair in a double effect absorption chiller driven by parabolic trough collectors. *Thermal Science and Engineering Progress*. https://doi.org/10.1016/j.tsep.2017.06.005

Berghmans, J. (1990). *High temperature industrial heat pumps -Final report prepared for the IEA Advanced Heat Pumps Annex IX*.

Bert, J., Chrenko, D., Sophy, T., Le Moyne, L., & Sirot, F. (2014). Simulation, experimental validation and kinematic optimization of a Stirling engine using air and helium. *Energy*. https://doi.org/10.1016/j.energy.2014.10.061

Best, R., Eisa, M. A. R., & Holland, F. A. (1987). Thermodynamic design data for absorption heat transformers-III. Operating on ammonia-water. *Heat Recovery Systems and CHP*. https://doi.org/10.1016/0890-4332(87)90139-6

Bianchi, G., & Tassou, S. A. (2019). sCO2 applications for high grade heat to power conversion. *ETN October Workshop 2019*.

Bianchi, Giuseppe, Kennedy, S., Zaher, O., Tassou, S. A., Miller, J., & Jouhara, H. (2018). Numerical modeling of a two-phase twin-screw expander for Trilateral Flash Cycle applications. *International Journal of Refrigeration*. https://doi.org/10.1016/j.ijrefrig.2018.02.001

Bianchi, M., Branchini, L., De Pascale, A., Melino, F., Peretto, A., Archetti, D., … Rossetti, N. (2019). Feasibility of ORC application in natural gas compressor stations. *Energy*. https://doi.org/10.1016/j.energy.2019.01.127

Bianchi, M., & De Pascale, A. (2011). Bottoming cycles for electric energy generation: Parametric investigation of available and innovative solutions for the exploitation of low and medium temperature heat sources. *Applied Energy*. https://doi.org/10.1016/j.apenergy.2010.11.013

Blanco-Rodríguez, P., Rodríguez-Aseguinolaza, J., Gil, A., Risueño, E., D'Aguanno, B., Loroño, I., & Martín, L. (2015). Experiments on a Lab Scale TES Unit using Eutectic Metal Alloy as PCM. *Energy Procedia*. https://doi.org/10.1016/j.egypro.2015.03.087

Horizon 2020
European Union Funding
for Research & Innovation

This project has received funding from
the European Union's Horizon 2020 research and innovation
programme under grant agreement No 847097

Blanco-Rodríguez, P., Rodríguez-Aseguinolaza, J., Risueño, E., & Tello, M. (2014). Thermophysical characterization of Mg-51%Zn eutectic metal alloy: A phase change material for thermal energy storage in direct steam generation applications. *Energy*. https://doi.org/10.1016/j.energy.2014.05.058

Bobelin, D., Bourig, A., & Peureux, J. (2012). Experimental results of a newly developed very high temperature industrial heat pump (140°C) equipped with scroll compressors and working with a new blend refrigerant. *International Refrigeration and Air Conditioning Conference*, *2012*, 1–10.

Bode, C., Friedrichs, J., Somdalen, R., Köhler, J., Büchter, K.-D., Falter, C., … Kožulovic, D. (2017). Potential of Future Thermoelectric Energy Recuperation for Aviation. *Journal of Engineering for Gas Turbines and Power*, *139*(10). https://doi.org/10.1115/1.4036527

Bogdanović, B., Ritter, A., Spliethoff, B., & Straßburger, K. (1995a). A process steam generator based on the high temperature magnesium hydride/magnesium heat storage system. *International Journal of Hydrogen Energy*, *20*(10), 811–822. https://doi.org/10.1016/0360-3199(95)00012-3

Bogdanović, B., Ritter, A., Spliethoff, B., & Straßburger, K. (1995b). A process steam generator based on the high temperature magnesium hydride/magnesium heat storage system. *International Journal of Hydrogen Energy*. https://doi.org/10.1016/0360-3199(95)00012-3

Böhm, H., & Lindorfer, J. (2019). Techno-economic assessment of seasonal heat storage in district heating with thermochemical materials. *Energy*. https://doi.org/10.1016/j.energy.2019.04.177

Bombarda, P., Invernizzi, C. M., & Pietra, C. (2010). Heat recovery from Diesel engines: A thermodynamic comparison between Kalina and ORC cycles. *Applied Thermal Engineering*, *30*(2–3), 212–219. https://doi.org/10.1016/j.applthermaleng.2009.08.006

Bosch Thermotechnology. (2019). Retrieved January 30, 2020, from https://www.bosch-thermotechnology.com/global/media/country-pool/commercial_industrial_media/service/catalogue/en/br_steamboilers_en.pdf

Bott, C., Dressel, I., & Bayer, P. (2019). State-of-technology review of water-based closed seasonal thermal energy storage systems. *Renewable and Sustainable Energy Reviews*. https://doi.org/10.1016/j.rser.2019.06.048

Boudéhenn, F., Bonnot, S., Demasles, H., Lefrançois, F., Perier-Muzet, M., & Triché, D. (2016). Development and Performances Overview of Ammonia-water Absorption Chillers with Cooling Capacities from 5 to 100 kW. *Energy Procedia*. https://doi.org/10.1016/j.egypro.2016.06.234

BOYD corporation - Heat Pipe Technology. (2020). Retrieved January 31, 2020, from https://www.boydcorp.com/thermal-management/heat-pipe-technology.html

Braimakis, K., & Karellas, S. (2018). Exergetic optimization of double stage Organic Rankine Cycle (ORC). *Energy*, *149*, 296–313. https://doi.org/10.1016/j.energy.2018.02.044

Branchini, L., De Pascale, A., & Peretto, A. (2013). Systematic comparison of ORC configurations by means of comprehensive performance indexes. *Applied Thermal Engineering*. https://doi.org/10.1016/j.applthermaleng.2013.07.039

Brough, D., & Jouhara, H. (2020). The aluminium industry: A review on state-of-the-art technologies, environmental impacts and possibilities for waste heat recovery. *International Journal of Thermofluids*, *1–2*. https://doi.org/10.1016/j.ijft.2019.100007

Brough, D., Mezquita, A., Ferrer, S., Segarra, C., Chauhan, A., Almahmoud, S., … Jouhara, H. (2020). An experimental study and computational validation of waste heat recovery from a lab scale ceramic kiln using a vertical multi-pass heat pipe heat exchanger. *Energy*, *208*. https://doi.org/10.1016/j.energy.2020.118325

Brun, K., Friedman, P., & Dennis, R. (2017). Fundamentals and Applications of Supercritical Carbon Dioxide (SCO2) Based Power Cycles. In *Fundamentals and Applications of Supercritical Carbon Dioxide (SCO2)*

Horizon 2020 European Union Funding for Research & Innovation

This project has received funding from the European Union's Horizon 2020 research and innovation programme under grant agreement No 847097

Based Power Cycles.

Butcher, T. A., Hammonds, J. S., Horne, E., Kamath, B., Carpenter, J., & Woods, D. R. (2011). Heat transfer and thermophotovoltaic power generation in oil-fired heating systems. *Applied Energy*. https://doi.org/10.1016/j.apenergy.2010.10.033

Byworth - Waste heat boilers. (2020). Retrieved January 30, 2020, from https://byworth.co.uk/industrial-boilers-by-type/industrial-heat-recovery-waste-heat-boilers/

Campos Rodríguez, C. E., Escobar Palacio, J. C., Venturini, O. J., Silva Lora, E. E., Cobas, V. M., Marques Dos Santos, D., … Gialluca, V. (2013). Exergetic and economic comparison of ORC and Kalina cycle for low temperature enhanced geothermal system in Brazil. *Applied Thermal Engineering*. https://doi.org/10.1016/j.applthermaleng.2012.11.012

Cannon Boiler Works. (2020). Retrieved February 6, 2020, from http://cannonboilerworks.com/boiler-economizers/heavy-duty-boiler-economizers/

Cannon Bono Energia. (2019). Retrieved from https://www.cannonbonoenergia.com/case-history/

Carbon Trust. (2019). *How to implement industrial heat recovery equipment*. Retrieved from https://www.carbontrust.com/media/147123/j7958_ctl037_industrial_heat_recovery_equipment_aw.pdf

Carlson, F., Davidson, J. H., Tran, N., & Stein, A. (2019). Model of the impact of use of thermal energy storage on operation of a nuclear power plant Rankine cycle. *Energy Conversion and Management*. https://doi.org/10.1016/j.enconman.2018.11.058

Cartif. (2020). Retrieved February 11, 2020, from https://www.cartif.com/en/

Casci, C., Angelino, G., Ferrari, P., Gaia, M., Giglioli, G., & Macchi, E. (1981). Heat recovery in a ceramic kiln with an organic rankine cycle engine. *Journal of Heat Recovery Systems*. https://doi.org/10.1016/0198-7593(81)90027-8

Centre for Low Carbon Futures and Liquid Air Energy Network. (2013). *Liquid Air Technologies – a guide to the potential*. Retrieved from http://www.lowcarbonfutures.org/sites/default/files/potential-guide.pdf

Cervantes, M., Sauceda, D., Velázquez, N., Lara, F., & Pando, G. (2016). Efecto De La Temperatura De Generacion En Un Ciclo De Absorcion Avanzado Branched-Gax. *Revista Mexicana de Ingeniería Química*, *15*.

Chahartaghi, M., Golmohammadi, H., & Shojaei, A. F. (2019). Performance analysis and optimization of new double effect lithium bromide–water absorption chiller with series and parallel flows. *International Journal of Refrigeration*. https://doi.org/10.1016/j.ijrefrig.2018.08.011

Chamoun, M., Rulliere, R., Haberschill, P., & Peureux, J. L. (2014). Experimental and numerical investigations of a new high temperature heat pump for industrial heat recovery using water as refrigerant. *International Journal of Refrigeration*. https://doi.org/10.1016/j.ijrefrig.2014.04.019

Chan, C. W., Ling-Chin, J., & Roskilly, A. P. (2013). A review of chemical heat pumps, thermodynamic cycles and thermal energy storage technologies for low grade heat utilisation. *Applied Thermal Engineering*. https://doi.org/10.1016/j.applthermaleng.2012.06.041

Chaudhry, H. N., Hughes, B. R., & Ghani, S. A. (2012). A review of heat pipe systems for heat recovery and renewable energy applications. *Renewable and Sustainable Energy Reviews*, *16*(4), 2249–2259. https://doi.org/10.1016/j.rser.2012.01.038

Che, D., Liu, Y., & Gao, C. (2004). Evaluation of retrofitting a conventional natural gas fired boiler into a condensing boiler. *Energy Conversion and Management*. https://doi.org/10.1016/j.enconman.2004.01.004

Chen, Q., Finney, K., Li, H., Zhang, X., Zhou, J., Sharifi, V., & Swithenbank, J. (2012). Condensing boiler applications in the process industry. *Applied Energy*. https://doi.org/10.1016/j.apenergy.2010.11.020

Horizon 2020
European Union Funding
for Research & Innovation

This project has received funding from
the European Union's Horizon 2020 research and innovation
programme under grant agreement No 847097

Chen, X., Zhang, Z., Qi, C., Ling, X., & Peng, H. (2018). State of the art on the high-temperature thermochemical energy storage systems. *Energy Conversion and Management*. https://doi.org/10.1016/j.enconman.2018.10.011

Cheng, C. H., Yang, H. S., & Keong, L. (2013). Theoretical and experimental study of a 300-W beta-type Stirling engine. *Energy*. https://doi.org/10.1016/j.energy.2013.06.060

Chew, J. M., Reddy, C. C. S., & Rangaiah, G. P. (2014). Improving energy efficiency of dividing-wall columns using heat pumps, Organic Rankine Cycle and Kalina Cycle. *Chemical Engineering and Processing: Process Intensification*, *76*, 45–59. https://doi.org/10.1016/j.cep.2013.11.011

Chuang Wu, Xiao-jiang Yan, Shun-sen Wang, Kun-lun Bai, Juan Di, Shang-fang Cheng, & Jun Li. (2016). System optimisation and performance analysis of CO2 transcritical power cycle for waste heat recovery. *Energy*, *100*, 391–400.

Chucherd, P., & Kittisupakorn, P. (2017). Devise of an exhaust gas heat exchanger for a thermal oil heater in a palm oil refinery plant. *AIP Conference Proceedings*, *1879*. https://doi.org/10.1063/1.5000462

Climator. (2019). Retrieved from https://www.climator.com/en/pcm-climsel/product-data-sheets

Cochran UK. (2019). Retrieved from https://cochran.co.uk/products/heat-recovery-boilers.aspx

Colella, F., Sciacovelli, A., & Verda, V. (2012). Numerical analysis of a medium scale latent energy storage unit for district heating systems. *Energy*. https://doi.org/10.1016/j.energy.2012.03.043

Colonna, P., Casati, E., Trapp, C., Mathijssen, T., Larjola, J., Turunen-Saaresti, T., & Uusitalo, A. (2015). Organic Rankine Cycle Power Systems: From the Concept to Current Technology, Applications, and an Outlook to the Future. *Journal of Engineering for Gas Turbines and Power*, *137*(10). https://doi.org/10.1115/1.4029884

Comtes FP7. (2016). Retrieved from GA ID: 295568 website: http://comtes-storage.eu/comtes-project/

Copper Alliance - Aurubis. (2020). Retrieved February 12, 2020, from https://copperalliance.eu/coppers-role-transition-low-carbon-economy/

Corgnale, C., Hardy, B., Motyka, T., Zidan, R., Teprovich, J., & Peters, B. (2014). Screening analysis of metal hydride based thermal energy storage systems for concentrating solar power plants. *Renewable and Sustainable Energy Reviews*. https://doi.org/10.1016/j.rser.2014.07.049

Costa, A., Bakhtiari, B., Schuster, S., & Paris, J. (2009). Integration of absorption heat pumps in a Kraft pulp process for enhanced energy efficiency. *Energy*. https://doi.org/10.1016/j.energy.2008.07.019

Coutts, T. J. (1999). Review of progress in thermophotovoltaic generation of electricity. *Renewable & Sustainable Energy Reviews*. https://doi.org/10.1016/S1364-0321(98)00021-5

Crane, D., Lagrandeur, J., Jovovic, V., Ranalli, M., Adldinger, M., Poliquin, E., … Maranville, C. (2013). TEG on-vehicle performance and model validation and what it means for further teg development. *Journal of Electronic Materials*, *42*(7), 1582–1591. https://doi.org/10.1007/s11664-012-2327-8

Crane, D. T., Koripella, C. R., & Jovovic, V. (2012). Validating steady-state and transient modeling tools for high-power-density thermoelectric generators. *Journal of Electronic Materials*, *41*(6), 1524–1534. https://doi.org/10.1007/s11664-012-1955-3

CREATE H2020. (2020). Retrieved from GA ID: 721065 website: http://www.createproject.eu/

Crespo, A., Barreneche, C., Ibarra, M., & Platzer, W. (2019). Latent thermal energy storage for solar process heat applications at medium-high temperatures – A review. *Solar Energy*. https://doi.org/10.1016/j.solener.2018.06.101

Cristopia. (2019). Retrieved from https://www.ciat.uk.com/product/cristopia-energy-storage/

Cudok, F., Ciganda, J. L. C., Kononenko, N., & Drescher, E. (2017). Experimental results of an absorption heat

Horizon 2020 European Union Funding for Research & Innovation

This project has received funding from the European Union's Horizon 2020 research and innovation programme under grant agreement No 847097

transformer. *12th IEA Heat Pump Conference*, 1–12.

Cunningham, P., & Chambers, H. (2002). Waste heat/cogen opportunities in the cement industry. *Cogeneration and Competitive Power Journal*, *17*(3), 31–51. https://doi.org/10.1092/BJMW-P3Q1-GHRF-YAB3

Dadollahi, M., & Mehrpooya, M. (2017). Modeling and investigation of high temperature phase change materials (PCM) in different storage tank configurations. *Journal of Cleaner Production*. https://doi.org/10.1016/j.jclepro.2017.05.171

Dahash, A., Ochs, F., Janetti, M. B., & Streicher, W. (2019). Advances in seasonal thermal energy storage for solar district heating applications: A critical review on large-scale hot-water tank and pit thermal energy storage systems. *Applied Energy*. https://doi.org/10.1016/j.apenergy.2019.01.189

Dal Magro, F., Savino, S., Meneghetti, A., & Nardin, G. (2017). Coupling waste heat extraction by phase change materials with superheated steam generation in the steel industry. *Energy*. https://doi.org/10.1016/j.energy.2017.04.051

Daneshvar, H., Prinja, R., & Kherani, N. P. (2015). Thermophotovoltaics: Fundamentals, challenges and prospects. *Applied Energy*. https://doi.org/10.1016/j.apenergy.2015.08.064

Danieli, P., Rech, S., & Lazzaretto, A. (2019). Supercritical CO2 and air Brayton-Joule versus ORC systems for heat recovery from glass furnaces: Performance and economic evaluation. *Energy*, *168*, 295–309. https://doi.org/10.1016/j.energy.2018.11.089

Danstoker - Waste heat recovery boilers (WHRB). (2019). Retrieved January 30, 2020, from http://danstoker.com/product-search/waste-heat-recovery-boilers-whrb/

Davies, G. F., Maidment, G. G., & Tozer, R. M. (2016a). Using data centres for combined heating and cooling: An investigation for London. *Applied Thermal Engineering*. https://doi.org/10.1016/j.applthermaleng.2015.09.111

Davies, G. F., Maidment, G. G., & Tozer, R. M. (2016b). Using data centres for combined heating and cooling: An investigation for London. *Applied Thermal Engineering*, *94*, 296–304. https://doi.org/10.1016/j.applthermaleng.2015.09.111

Dawo, F., Wieland, C., & Spliethoff, H. (2019). Kalina power plant part load modeling: Comparison of different approaches to model part load behavior and validation on real operating data. *Energy*, *174*, 625–637. https://doi.org/10.1016/j.energy.2019.02.173

De Jong, A. J., Van Vliet, L., Hoegaerts, C., Roelands, M., & Cuypers, R. (2016). Thermochemical Heat Storage - From Reaction Storage Density to System Storage Density. *Energy Procedia*. https://doi.org/10.1016/j.egypro.2016.06.187

Dearman. (2017). *Dearman - A Technical Introduction*.

Dearman. (2020). Retrieved February 11, 2020, from https://dearman.co.uk/

Dearman, P., Dearman, M., Old, D., Clarke, H., & Zhao, D. (2019). *Patent No. US 10260379 B2*.

Dehghan B., B. (2017). Performance assessment of ground source heat pump system integrated with micro gas turbine: Waste heat recovery. *Energy Conversion and Management*, *152*, 328–341. https://doi.org/10.1016/j.enconman.2017.09.058

Delpech, B., Axcell, B., & Jouhara, H. (2019). Experimental investigation of a radiative heat pipe for waste heat recovery in a ceramics kiln. *Energy*, *170*, 636–651. https://doi.org/10.1016/j.energy.2018.12.133

Delpech, B., Milani, M., Montorsi, L., Boscardin, D., Chauhan, A., Almahmoud, S., … Jouhara, H. (2018). Energy efficiency enhancement and waste heat recovery in industrial processes by means of the heat pipe technology: Case of the ceramic industry. *Energy*, *158*, 656–665. https://doi.org/10.1016/j.energy.2018.06.041

Horizon 2020
European Union Funding
for Research & Innovation

This project has received funding from
the European Union's Horizon 2020 research and innovation
programme under grant agreement No 847097

Delta Energy & Environment Ltd. (2016). *Evidence Gathering: Thermal Energy Storage (TES) Technologies*.

Deng, J., Wei, Q., Liang, M., He, S., & Zhang, H. (2019a). Does heat pumps perform energy efficiently as we expected: Field tests and evaluations on various kinds of heat pump systems for space heating. *Energy and Buildings*. https://doi.org/10.1016/j.enbuild.2018.10.014

Deng, J., Wei, Q., Liang, M., He, S., & Zhang, H. (2019b). Field test on energy performance of medium-depth geothermal heat pump systems (MD-GHPs). *Energy and Buildings*. https://doi.org/10.1016/j.enbuild.2018.12.006

Der Minassians, A., & Sanders, S. R. (2011). Stirling engines for distributed low-cost solar-thermal-electric power generation. *Journal of Solar Energy Engineering, Transactions of the ASME*, *133*(1). https://doi.org/10.1115/1.4003144

Deymi-Dashtebayaz, M., & Valipour-Namanlo, S. (2019). Thermoeconomic and environmental feasibility of waste heat recovery of a data center using air source heat pump. *Journal of Cleaner Production*. https://doi.org/10.1016/j.jclepro.2019.02.061

Dimplex. (2019). Retrieved from https://www.dimplex.co.uk/storage-heaters

Ding, J., Wang, Y., Gu, R., Wang, W., & Lu, J. (2019). Thermochemical storage performance of methane reforming with carbon dioxide using high temperature slag. *Applied Energy*. https://doi.org/10.1016/j.apenergy.2019.05.064

Dinker, A., Agarwal, M., & Agarwal, G. D. (2017). Heat storage materials, geometry and applications: A review. *Journal of the Energy Institute*. https://doi.org/10.1016/j.joei.2015.10.002

DiPippo, R. (2004). Second Law assessment of binary plants generating power from low-temperature geothermal fluids. *Geothermics*. https://doi.org/10.1016/j.geothermics.2003.10.003

DOE. (2011). *Thermochemical heat storage for concentrated solar power - thermochemical system reactor design for thermal energy storage*.

Dolz, V., Novella, R., García, A., & Sánchez, J. (2012). HD Diesel engine equipped with a bottoming Rankine cycle as a waste heat recovery system. Part 1: Study and analysis of the waste heat energy. *Applied Thermal Engineering*. https://doi.org/10.1016/j.applthermaleng.2011.10.025

Donnellan, P., Cronin, K., Acevedo, Y., & Byrne, E. (2014). Economic evaluation of an industrial high temperature lift heat transformer. *Energy*. https://doi.org/10.1016/j.energy.2014.06.059

Donnellan, P., Cronin, K., & Byrne, E. (2015). Recycling waste heat energy using vapour absorption heat transformers: A review. *Renewable and Sustainable Energy Reviews*. https://doi.org/10.1016/j.rser.2014.11.002

Doty, S., & Turner, W. C. (2013). *Energy Management Handbook*.

Drescher, U., & Brüggemann, D. (2007). Fluid selection for the Organic Rankine Cycle (ORC) in biomass power and heat plants. *Applied Thermal Engineering*. https://doi.org/10.1016/j.applthermaleng.2006.04.024

Dresser-Rand & Supercritical CO2. (2016). *SCO2 Symposium 2016 (San Antonio, Texas)*.

Durisch, W. (2003). *Small self-powered grid-connected thermophotovoltaic prototype system*.

E-Hub FP7. (2013). Retrieved from GA ID: 260165 website: https://www.e-hub.org/

Ease, & EERA. (2017). *European Energy Storage Technology Development*.

Echogen Power Systems. (2020). Retrieved February 17, 2020, from https://www.echogen.com/

Eco-Tech Ceram. (2019). Retrieved from https://www.ecotechceram.com/

Econotherm. (2020). Retrieved January 31, 2020, from https://www.econotherm.eu/

Horizon 2020
European Union Funding
for Research & Innovation

This project has received funding from
the European Union's Horizon 2020 research and innovation
programme under grant agreement No 847097

EDF ANR Project PACO. (2019). Retrieved from https://www.edf.fr/en/the-edf-group/world-s-largest-power-company/activities/research-and-development/flagship-projects/a-very-high-temperature-water-cooled-industrial-heat-pump

EERA TES Technologies. (2018). Retrieved from https://eera-es.eu/wp-content/uploads/2018/08/JPES-SP3-Technology-Factsheets-Brochure.pdf

Egilegor, B., Jouhara, H., Zuazua, J., Al-Mansour, F., Plesnik, K., Montorsi, L., & Manzini, L. (2019). ETEKINA: Analysis of the potential for waste heat recovery in three sectors: Aluminium low pressure die casting, steel sector and ceramic tiles manufacturing sector. *International Journal of Thermofluids*. https://doi.org/10.1016/j.ijft.2019.100002

EnergyNest. (2019). Retrieved from https://energy-nest.com/

Engin, T., & Ari, V. (2005). Energy auditing and recovery for dry type cement rotary kiln systems - A case study. *Energy Conversion and Management*. https://doi.org/10.1016/j.enconman.2004.04.007

EPRI. (2002). *Stirling Engine Assessment*.

EPRI. (2010). *Waste Heat Recovery in Industrial Facilities - Opportunities for Combined Heat and Power and Industrial Heat Pumps*.

Esaki, T., Yasuda, M., & Kobayashi, N. (2017). Experimental evaluation of the heat output/input and coefficient of performance characteristics of a chemical heat pump in the heat upgrading cycle of CaCl2 hydration. *Energy Conversion and Management*. https://doi.org/10.1016/j.enconman.2017.08.013

ETEKINA H2020. (2020). Retrieved from https://www.etekina.eu/

Evans, A., Strezov, V., & Evans, T. J. (2012). Assessment of utility energy storage options for increased renewable energy penetration. *Renewable and Sustainable Energy Reviews*. https://doi.org/10.1016/j.rser.2012.03.048

Farid, M. M., Khudhair, A. M., Razack, S. A. K., & Al-Hallaj, S. (2004). A review on phase change energy storage: Materials and applications. *Energy Conversion and Management*. https://doi.org/10.1016/j.enconman.2003.09.015

Feng, L., Lin, D., Lin, F., & Xiling, Z. (2019). Application of absorption heat pump and direct-contact total heat exchanger to advanced-recovery flue-gas waste heat for gas boiler. *Science and Technology for the Built Environment*, *25*(2), 149–155. https://doi.org/10.1080/23744731.2018.1506676

Feng, Y., Hung, T. C., Greg, K., Zhang, Y., Li, B., & Yang, J. (2015). Thermoeconomic comparison between pure and mixture working fluids of organic Rankine cycles (ORCs) for low temperature waste heat recovery. *Energy Conversion and Management*. https://doi.org/10.1016/j.enconman.2015.09.042

Fergani, Z., Touil, D., & Morosuk, T. (2016). Multi-criteria exergy based optimization of an Organic Rankine Cycle for waste heat recovery in the cement industry. *Energy Conversion and Management*. https://doi.org/10.1016/j.enconman.2015.12.083

Fernández, R., Ortiz, C., Chacartegui, R., Valverde, J. M., & Becerra, J. A. (2019). Dispatchability of solar photovoltaics from thermochemical energy storage. *Energy Conversion and Management*. https://doi.org/10.1016/j.enconman.2019.03.074

Ferrari, C., Melino, F., Pinelli, M., & Spina, P. R. (2014). Thermophotovoltaic energy conversion: Analytical aspects, prototypes and experiences. *Applied Energy*. https://doi.org/10.1016/j.apenergy.2013.08.064

Fiaschi, D., Manfrida, G., Russo, L., & Talluri, L. (2017). Improvement of waste heat recuperation on an industrial textile dryer: Redesign of heat exchangers network and components. *Energy Conversion and Management*. https://doi.org/10.1016/j.enconman.2017.05.053

Fleer, M., Lorentsen, O. A., Harvey, W., Palsson, H., & Saevarsdottir, G. (2010). Heat recovery from the exhaust gas of aluminum reduction cells.

Horizon 2020
European Union Funding
for Research & Innovation

This project has received funding from
the European Union's Horizon 2020 research and innovation
programme under grant agreement No 847097

Fleischanderl, A., Steinparzer, T., & Trunner, P. (2017). Waste heat recovery for EAF - Innovative concepts and industrial implementation. *AISTech - Iron and Steel Technology Conference Proceedings*, *1*, 103–112.

Florides, G. A., Tassou, S. A., Kalogirou, S. A., & Wrobel, L. C. (2002). Review of solar and low energy cooling technologies for buildings. *Renewable and Sustainable Energy Reviews*. https://doi.org/10.1016/S1364-0321(02)00016-3

Fopah Lele, A., Kuznik, F., Opel, O., & Ruck, W. K. L. (2015). Performance analysis of a thermochemical based heat storage as an addition to cogeneration systems. *Energy Conversion and Management*. https://doi.org/10.1016/j.enconman.2015.10.068

Foster, S. (2016). *Heat Pumps in District Heating - Case Studies*.

FP7 PITAGORAS. (2017). Retrieved from GA ID: 314596 website: https://pitagoraspro ject.eu/

Fraas, L. M., Avery, J. E., & Huang, H. X. (2003). Thermophotovoltaic furnace-generator for the home using low bandgap GaSb cells. *Semiconductor Science and Technology*, *18*(5). https://doi.org/10.1088/0268-1242/18/5/316

Fraas, Lewis M. (2014). Economic potential for thermophotovoltaic electric power generation in the steel industry. *2014 IEEE 40th Photovoltaic Specialist Conference, PVSC 2014*, 766–770. https://doi.org/10.1109/PVSC.2014.6925031

Frauscher thermal motors. (2019). Retrieved from https://www.frauscher-motors.com/

Frederiksen, S., & Werner, S. (2013). *District heating and cooling*. Lund Studentlitteratur.

Frobenius, F., Gaiser, G., Rusche, U., & Weller, B. (2016). Thermoelectric Generators for the Integration into Automotive Exhaust Systems for Passenger Cars and Commercial Vehicles. *Journal of Electronic Materials*, *45*(3), 1433–1440. https://doi.org/10.1007/s11664-015-4059-z

Fujii, T., Kawamura, H., Sakano, Y., Uchida, S., & Nishiguchi, A. (2008). A single-effect absorption heat transformer for waste heat recovery in industrial use. *International IEA Heat Pump Conference, 2008, Zürich, Switzerland*, (May), 20–22.

Ganapathy, V. (2014). Steam generators and waste heat boilers: For process and plant engineers. In *Steam Generators and Waste Heat Boilers: For Process and Plant Engineers*. https://doi.org/10.1201/b17519

Ganesh, H. S., Ezekoye, O. A., Edgar, T. F., & Baldea, M. (2019). Heat integration and operational optimization of an austenitization furnace using concentric-tube radiant recuperators. *AIChE Journal*, *65*(7). https://doi.org/10.1002/aic.16414

Garimella, S., Keinath, C. M., Delahanty, J. C., Hoysall, D. C., Staedter, M. A., Goyal, A., & Garrabrant, M. A. (2016). Development and demonstration of a compact ammonia-water absorption heat pump prototype with microscale features for space-conditioning applications. *Applied Thermal Engineering*, *102*, 557–564. https://doi.org/10.1016/j.applthermaleng.2016.03.169

Garimella, S., Ponkala, M. J., Goyal, A., & Staedter, M. A. (2019). Waste-heat driven ammonia-water absorption chiller for severe ambient operation. *Applied Thermal Engineering*. https://doi.org/10.1016/j.applthermaleng.2019.03.098

Garone, S., Toppi, T., Guerra, M., & Motta, M. (2017). A water-ammonia heat transformer to upgrade low-temperature waste heat. *Applied Thermal Engineering*. https://doi.org/10.1016/j.applthermaleng.2017.08.082

Gas Technology Institute. (2013). *Energy and water recovery with transport membrane condenser*.

Gasser, L., Flück, S., Kleingries, M., Meier, C., Bätschmann, M., & Wellig, B. (2017). High efficiency heat pumps for low temperature lift applications. *12th IEA Heat Pump Conference*, 11.

GE Power - Heat recovery steam generators. (2020). Retrieved January 31, 2020, from

Horizon 2020 European Union Funding for Research & Innovation

This project has received funding from the European Union's Horizon 2020 research and innovation programme under grant agreement No 847097

https://www.ge.com/power/gas/hrsg

Georgiou, S., Shah, N., & Markides, C. N. (2018). A thermo-economic analysis and comparison of pumped-thermal and liquid-air electricity storage systems. *Applied Energy*, *226*, 1119–1133. https://doi.org/10.1016/j.apenergy.2018.04.128

Gesmex. (2020). Retrieved February 13, 2020, from http://www.gesmex.com/index.php/en/products/xps-plate-and-shell-en

Ghalandari, V., Majd, M. M., & Golestanian, A. (2019). Energy audit for pyro-processing unit of a new generation cement plant and feasibility study for recovering waste heat: A case study. *Energy*. https://doi.org/10.1016/j.energy.2019.02.102

Ghosh, S., Margatan, K., Ahn, C. H., & Bahk, J. H. (2018). Radiant heat recovery by thermoelectric generators: A theoretical case-study on hot steel casting. *Energy Conversion and Management*. https://doi.org/10.1016/j.enconman.2018.08.106

Gil, A., Medrano, M., Martorell, I., Lázaro, A., Dolado, P., Zalba, B., & Cabeza, L. F. (2010). State of the art on high temperature thermal energy storage for power generation. Part 1-Concepts, materials and modellization. *Renewable and Sustainable Energy Reviews*. https://doi.org/10.1016/j.rser.2009.07.035

Global Geothermal. (2019). *Kalina Cycle - Enhanced Energy Efficiency Solutions Iron & Steel Industry*.

Global Geothermal - Advanced Waste Heat Engineering. (2019). Global Geothermal - Advanced Waste Heat Engineering. Retrieved from http://www.globalgeothermal.com/Applications.aspx

Gómez-Aláez, S. L., Brizzi, V., Alfani, D., Silva, P., Giostri, A., & Astolfi, M. (2017). Off-design study of a waste heat recovery ORC module in gas pipelines recompression station. *Energy Procedia*. https://doi.org/10.1016/j.egypro.2017.09.205

Gorog, J. P. (2007). *Improved materials and operation of recuperators for aluminum melting furnaces*.

Goyal, A., Staedter, M. A., Hoysall, D. C., Ponkala, M. J., & Garimella, S. (2017). Experimental evaluation of a small-capacity, waste-heat driven ammonia-water absorption chiller. *International Journal of Refrigeration*, *79*, 89–100. https://doi.org/10.1016/j.ijrefrig.2017.04.006

Green`s Power Economisers. (2019). Retrieved February 6, 2019, from https://greenspower.co.uk/economisers-flue-gas-coolers/

Groth, T., Marinitsch, G., & Newman, S. (2012). Applications of a Stirling engine based wood chip fired trigeneration system in UK supermarkets. *20th European Biomass Conference & Exhibition*.

Guo, C., & Zhang, W. (2008). Numerical simulation and parametric study on new type of high temperature latent heat thermal energy storage system. *Energy Conversion and Management*. https://doi.org/10.1016/j.enconman.2007.10.025

Guo, S., Liu, Q., Zhao, J., Jin, G., Wu, W., Yan, J., … Jin, H. (2018). Mobilized thermal energy storage: Materials, containers and economic evaluation. *Energy Conversion and Management*. https://doi.org/10.1016/j.enconman.2018.09.070

Guo, S., Zhao, J., Wang, W., Yan, J., Jin, G., & Wang, X. (2017). Techno-economic assessment of mobilized thermal energy storage for distributed users: A case study in China. *Applied Energy*. https://doi.org/10.1016/j.apenergy.2016.08.137

Guo, X., & Goumba, A. P. (2018). Air source heat pump for domestic hot water supply: Performance comparison between individual and building scale installations. *Energy*. https://doi.org/10.1016/j.energy.2018.09.065

Güven, M., Bedir, H., & Anlaş, G. (2019). Optimization and application of Stirling engine for waste heat recovery from a heavy-duty truck engine. *Energy Conversion and Management*. https://doi.org/10.1016/j.enconman.2018.10.096

Horizon 2020
European Union Funding
for Research & Innovation

This project has received funding from
the European Union's Horizon 2020 research and innovation
programme under grant agreement No 847097

H2020 DryFiciency. (2019). Retrieved from http://dry-f.eu/

Haraldsson, L. B. (2019). *Viability of a district heating system in Fjarðabyggð using waste heat from Alcoa Fjarðaál*. Reykjavík University.

Hauer, A. (1997). *Thermal energy storage with zeolite for heating and cooling applications*.

Hauer, A. (2002). *Thermal energy storage with zeolite for heating and cooling applications*.

Hauer, A., Gschwander, S., Kato, Y., Martin, V., Schossig, P., & Setterwall, F. (2010). *Transportation of energy by utilization of thermal energy storage technology*.

He, C., Liu, C., Gao, H., Xie, H., Li, Y., Wu, S., & Xu, J. (2012). The optimal evaporation temperature and working fluids for subcritical organic Rankine cycle. *Energy*. https://doi.org/10.1016/j.energy.2011.12.022

He, Q., & Zhang, W. (2001). A study on latent heat storange exchangers with the high-temperature phase-change material. *International Journal of Energy Research*, *25*(4), 331–341. https://doi.org/10.1002/er.683

HEAT-R. (2019). HEAT-R. Retrieved from https://cordis.europa.eu/project/id/697982

Heat is Power Association. (2019). Retrieved from http://www.heatispower.org/about/

HEATRECAR FP7. (2013). HEATRECAR FP7. Retrieved from https://cordis.europa.eu/project/id/218541/reporting

Held, T. J. (2014). Initial test results of a megawatt-class supercritical co2 heat engine. *The 4th International Symposium - Supercritical CO2 Power Cycles*.

Held, T. J. (2015). Supercritical CO2 cycles for gas turbine combined cycle power plants. *Power Gen International*.

Held, T. J., Vermeersch, M. L., Xie, T., & Miller, J. D. (2011). *Patent No. WO 2011/119650 A2*.

Held, T., Zdankiewicz, E., Kacludis, A., & Persichilli, M. (2012). Supercritical CO2 Power Cycle Developments and Commercialization: Why SCO2 Can Displace Steam. *Supercritical CO2 Power Cycle Symposium*. Retrieved from http://www.sco2powercyclesymposium.org/resource_center/system_concepts/supercritical-co2-power-cycle-developments-and-commercialization-why-sco2-can-displace-steam

Herold, K. E., Radermacher, R., & Klein, S. A. (2016). Absorption Chillers and Heat Pumps. In *Absorption Chillers and Heat Pumps*. https://doi.org/10.1201/b19625

Hesselgreaves, J. E., Law, R., & Reay, D. A. (2017). *COMPACT HEAT EXCHANGERS Selection, Design and Operation* (Butterworth-Heinemann, Ed.).

Hi-Z Technology. (2019). Hi-Z Technology. Retrieved from https://hi-z.com/

Highview Power. (2020). Retrieved February 11, 2020, from https://www.highviewpower.com/

Highview Power - Cryobattery. (2020). Retrieved February 11, 2020, from https://www.theengineer.co.uk/highview-power-energy-storage/

Hong, H., Gao, J., Qu, W., Sun, J., Kang, Q., & Li, Q. (2017). Thermodynamic analyses of the solar-driven Kalina cycle having a variable concentration ratio. *Applied Thermal Engineering*, *126*, 997–1005. https://doi.org/10.1016/j.applthermaleng.2017.07.160

Hong, S. J., Lee, C. H., Kim, S. M., Kim, I. G., Kwon, O. K., & Park, C. W. (2018). Analysis of single stage steam generating absorption heat transformer. *Applied Thermal Engineering*. https://doi.org/10.1016/j.applthermaleng.2018.08.104

Horne, W. E. (2003). *500 Watt Diesel Fueled TPV Portable Power Supply*. 91–100. https://doi.org/10.1063/1.1539367

Hoshi, A., Mills, D. R., Bittar, A., & Saitoh, T. S. (2005). Screening of high melting point phase change materials

Horizon 2020
European Union Funding
for Research & Innovation

This project has received funding from
the European Union's Horizon 2020 research and innovation
programme under grant agreement No 847097

(PCM) in solar thermal concentrating technology based on CLFR. *Solar Energy*. https://doi.org/10.1016/j.solener.2004.04.023

Hu, B., Liu, H., Wang, R. Z., Li, H., Zhang, Z., & Wang, S. (2017). A high-efficient centrifugal heat pump with industrial waste heat recovery for district heating. *Applied Thermal Engineering*. https://doi.org/10.1016/j.applthermaleng.2017.07.030

Hu, B., Xu, S., Wang, R. Z., Liu, H., Han, L., Zhang, Z., & Li, H. (2019). Investigation on advanced heat pump systems with improved energy efficiency. *Energy Conversion and Management*. https://doi.org/10.1016/j.enconman.2019.04.031

Hua, J., Chen, Y., Wang, Y., & Roskilly, A. P. (2014). Thermodynamic analysis of ammonia-water power/chilling cogeneration cycle with low-grade waste heat. *Applied Thermal Engineering*. https://doi.org/10.1016/j.applthermaleng.2013.12.043

Hua, J., Chen, Y., Wu, J., Zhi, Z., & Dong, C. (2015). Waste heat supply-side power regulation with variable concentration for turbine in Kalina cycle. *Applied Thermal Engineering*. https://doi.org/10.1016/j.applthermaleng.2015.08.048

Huang, M., Liang, X., & Zhuang, R. (2017). Experimental Investigate on the Performance of High Temperature Heat Pump Using Scroll Compressor. *12th IEA Heat Pump Conference 2017, Rotterdam*, 1–8.

Hui, L., Edem, N. K., Nolwenn, L. P., & Luo, L. (2011). Evaluation of a seasonal storage system of solar energy for house heating using different absorption couples. *Energy Conversion and Management*. https://doi.org/10.1016/j.enconman.2010.12.049

Hybrid Energy (HTHP in Borregaard, Norway). (2019). Retrieved from https://www.hybridenergy.no/referenceplants/borregaard-norway/

Hybrid Energy (HTHP in Løgumkloster, Denmark). (2019). Retrieved from https://www.hybridenergy.no/referenceplants/logumkloster-denmark/

I-Therm H2020. (2019). Retrieved from http://www.itherm-project.eu/public/

Ibarra-Bahena, J., Dehesa-Carrasco, U., Montiel-González, M., Romero, R. J., & Venegas-Reyes, E. (2017). Feasibility analysis of a hot water solar system coupled to an absorption heat transformer. *Applied Thermal Engineering*. https://doi.org/10.1016/j.applthermaleng.2016.05.140

Ibarra-Bahena, J., Romero, R. J., Cerezo, J., Valdez-Morales, C. V., Galindo-Luna, Y. R., & Velazquez-Avelar, L. (2015). Experimental assessment of an absorption heat transformer prototype at different temperature levels into generator and into evaporator operating with water/Carrol mixture. *Experimental Thermal and Fluid Science*. https://doi.org/10.1016/j.expthermflusci.2014.09.013

ICF International. (2019). Retrieved from https://www.icf.com/

IEA-ECES. (2018). Applications of Thermal Energy Storage in the Energy Transition - Benchmarks and Developments. In *Public Report of IEA ECES Annex 30*.

IEA Task 32. (2007). *Laboratory Prototypes of Thermo-Chemical and Sorption Storage Units*.

IEA Task 35. (2014). *Application of Industrial Heat Pumps*.

Incropera, F. P., Prescott, P. J., & Voelkel, D. D. (1985). Hybrid systems for furnace waste heat recovery: I. Use of a radiation recuperator with a Rankine cycle. *Journal of Heat Recovery Systems*. https://doi.org/10.1016/0198-7593(85)90006-2

Indus3Es H2020. (2019). Indus3Es H2020. Retrieved from http://www.indus3es.eu/

INTEGRAL H2020. (2019). INTEGRAL H2020. Retrieved from http://www.integral-h2020.eu/

Ionkin, I. L., Roslyakov, P. V., & Luning, B. (2018). Application of Condensing Heat Utilizers at Heat-Power

Horizon 2020
European Union Funding
for Research & Innovation

This project has received funding from
the European Union's Horizon 2020 research and innovation
programme under grant agreement No 847097

Engineering Objects (Review). *Thermal Engineering*, *65*(10), 677–690. https://doi.org/10.1134/S0040601518100038

IRENA. (2013). *Thermal Energy Storage Technology Brief*.

ISSHIKI, S., SATO, H., KONNO, S., SHIRAISHI, H., ISSHIKI, N., FUJII, I., & MIZUI, H. (2008). The Experimental Study of Atmospheric Stirling Engines Using Pin-Fin Arrays' Heat Exchangers. *Journal of Power and Energy Systems*, *2*(5), 1198–1208. https://doi.org/10.1299/jpes.2.1198

Jakob, U., Spiegel, K., Pink, W., Manager, G., & Gmbh, P. (2008). Development and experimental investigation of a novel 10 kW ammonia/water absorption chiller - Chillii PSC - for air-conditioning and refrigeration systems. *International IEA Heat Pump Conference Volume 9*, 1–8. Retrieved from http://www.solarnext.eu/pdf/ger/publications_presentations/jakob/HPC2008_s5_p32.pdf

Jeffrey Snyder, G. J. (2006). Thermoelectric Power Generation: Efficiency and Compatibility. In *Thermoelectrics handbook - macro to nano*. Boca Raton, FL.

Jeong, K., Kessen, M. J., Bilirgen, H., & Levy, E. K. (2010). Analytical modeling of water condensation in condensing heat exchanger. *International Journal of Heat and Mass Transfer*. https://doi.org/10.1016/j.ijheatmasstransfer.2010.02.004

Jeong, S., Kang, B. H., & Karng, S. W. (1998). Dynamic simulation of an absorption heat pump for recovering low grade waste heat. *Applied Thermal Engineering*. https://doi.org/10.1016/s1359-4311(97)00040-9

jhc specialized solutions. (2019). Retrieved January 31, 2020, from https://www.jhcss.com.au/products-1/thermal-management/heat-pipes-heat-exchangers

Ji, C., Qin, Z., Dubey, S., Choo, F. H., & Duan, F. (2017). Three-dimensional transient numerical study on latent heat thermal storage for waste heat recovery from a low temperature gas flow. *Applied Energy*. https://doi.org/10.1016/j.apenergy.2017.07.101

Jian, S., Lin, F., & Shigang, Z. (2010). Performance calculation of single effect absorption heat pump using LiBr + $LiNO_3$ + H_2O as working fluid. *Applied Thermal Engineering*. https://doi.org/10.1016/j.applthermaleng.2010.07.018

Jiang, L., Wang, L., Wang, R., Zhu, F., Lu, Y., & Roskilly, A. P. (2017). Experimental investigation on an innovative resorption system for energy storage and upgrade. *Energy Conversion and Management*. https://doi.org/10.1016/j.enconman.2017.02.014

Jiménez-García, J. C., & Rivera, W. (2018). Parametric analysis on the performance of an experimental ammonia/lithium nitrate absorption cooling system. *International Journal of Energy Research*, *42*(14), 4402–4416. https://doi.org/10.1002/er.4185

Johansson, M. T., & Söderström, M. (2011). Options for the Swedish steel industry - Energy efficiency measures and fuel conversion. *Energy*. https://doi.org/10.1016/j.energy.2010.10.053

Jouhara, H., Chauhan, A., Nannou, T., Almahmoud, S., Delpech, B., & Wrobel, L. C. (2017). Heat pipe based systems - Advances and applications. *Energy*, *128*, 729–754. https://doi.org/10.1016/j.energy.2017.04.028

Jouhara, Hussam. (2016). Heat pipe heat exchangers for industrial heat recovery. *PowerPoint Presentation "Heat Pipe Based Systems for Waste Heat Recovery and Renewable Energy."* London: Brunel University.

Jouhara, Hussam, Almahmoud, S., Chauhan, A., Delpech, B., Bianchi, G., Tassou, S. A., … Arribas, J. J. (2017). Experimental and theoretical investigation of a flat heat pipe heat exchanger for waste heat recovery in the steel industry. *Energy*, *141*, 1928–1939. https://doi.org/10.1016/j.energy.2017.10.142

Jouhara, Hussam, Bertrand, D., Axcell, B., Montorsi, L., Venturelli, M., Almahmoud, S., … Chauhan, A. (2021). Investigation on a full-scale Heat Pipe Heat Exchanger in the ceramics industry for waste heat recovery. *Energy*, 120037. https://doi.org/10.1016/j.energy.2021.120037

Jouhara, Hussam, Khordehgah, N., Almahmoud, S., Delpech, B., Chauhan, A., & Tassou, S. A. (2018). Waste

Horizon 2020 European Union Funding for Research & Innovation

This project has received funding from the European Union's Horizon 2020 research and innovation programme under grant agreement No 847097

heat recovery technologies and applications. *Thermal Science and Engineering Progress*, *6*, 268–289. https://doi.org/10.1016/j.tsep.2018.04.017

Ju, F., Fan, X., Chen, Y., Wang, T., Tang, X., Kuang, A., & Ma, S. (2018). Experimental investigation on a heat pump water heater using R744/R290 mixture for domestic hot water. *International Journal of Thermal Sciences*. https://doi.org/10.1016/j.ijthermalsci.2018.05.043

Jung, H. C., Krumdieck, S., & Vranjes, T. (2014). Feasibility assessment of refinery waste heat-to-power conversion using an organic Rankine cycle. *Energy Conversion and Management*. https://doi.org/10.1016/j.enconman.2013.09.057

Júnior, E. P. B., Arrieta, M. D. P., Arrieta, F. R. P., & Silva, C. H. F. (2019). Assessment of a Kalina cycle for waste heat recovery in the cement industry. *Applied Thermal Engineering*. https://doi.org/10.1016/j.applthermaleng.2018.10.088

JX Crystals. (2019). JX Crystals. Retrieved from https://jxcrystals.com/wp/

Kacludis, A., Lyons, S., Nadav, D., & Zdankiewicz, E. (2012). Waste Heat to Power (WH2P) Applications Using a Supercritical CO 2 -Based Power Cycle. *Power-Gen International*, *2*(December), 1–10.

Kaibe, H., Makino, K., Kajihara, T., Fujimoto, S., & Hachiuma, H. (2012). Thermoelectric generating system attached to a carburizing furnace at Komatsu Ltd., Awazu Plant. *AIP Conference Proceedings*, *1449*, 524–527. https://doi.org/10.1063/1.4731609

Kaibe, Hiromasa, Kajihara, T., & Fujimoto, S. (2011). Recovery of Plant Waste Heat by a Thermoelectric Generating System. *Komatsu Technical Report*, *57*(164), 26–30. Retrieved from http://dcnwis78.komatsu.co.jp/CompanyInfo/profile/report/pdf/164-E-05.pdf

Kakac, S., Liu, H., & Pramuanjaroenkij, A. (2012). *HEAT EXCHANGERS - Selection, Rating, and Thermal Design* (CRC Press, Ed.).

Kalfrisa - Convective recuperators. (2020). Retrieved February 7, 2020, from http://kalfrisa.es/convective_recuperators.aspx

Kalfrisa - Radiation recuperators. (2020). Retrieved February 7, 2020, from http://kalfrisa.es/radiationrecuperators.aspx

Kalina, A. I. (1984). Combined-Cycle System With Novel Bottoming Cycle. *Journal of Engineering for Gas Turbines and Power*.

Kalina, A. I., & Leibowitz, H. M. (1988). The design of a 3MW kalina cycle experimental plant. *Proceedings of the ASME Turbo Expo*, *3*. https://doi.org/10.1115/88-GT-140

Kalina, A. I., Leibowitz, H. M., Markus, D. W., & Pelletier, R. I. (1991). Further technical aspects and economics of a utility-size Kalina bottoming cycle. *Proceedings of the ASME Turbo Expo*, *4*. https://doi.org/10.1115/91-gt-365

Kalina, A., Kaiina, M., Dickson, J., & Moore, S. (2014). Evaluation and comparisons of currently available binary cycle geothermal power systems. *Transactions - Geothermal Resources Council*, *38*, 777–788.

Kalina Power. (2019). Retrieved from http://www.kalinapower.com/technology/

Kang, D. H., Na, S. I., Yoo, J. W., Lee, J. H., & Kim, M. S. (2019). Experimental study on the performance of a steam generation heat pump with the internal heat exchanging effect. *International Journal of Refrigeration*. https://doi.org/10.1016/j.ijrefrig.2019.09.003

Karabulut, H., Yücesu, H. S., Çinar, C., & Aksoy, F. (2009). An experimental study on the development of a β-type Stirling engine for low and moderate temperature heat sources. *Applied Energy*. https://doi.org/10.1016/j.apenergy.2008.04.003

Karamarković, V., Marašević, M., Karamarković, R., & Karamarković, M. (2013). Recuperator for waste heat

Horizon 2020 European Union Funding for Research & Innovation

This project has received funding from the European Union's Horizon 2020 research and innovation programme under grant agreement No 847097

recovery from rotary kilns. *Applied Thermal Engineering*. https://doi.org/10.1016/j.applthermaleng.2013.02.027

Karellas, S., Leontaritis, A. D., Panousis, G., Bellos, E., & Kakaras, E. (2013). Energetic and exergetic analysis of waste heat recovery systems in the cement industry. *Energy*. https://doi.org/10.1016/j.energy.2013.03.097

Kaşka, Ö. (2014). Energy and exergy analysis of an organic Rankine for power generation from waste heat recovery in steel industry. *Energy Conversion and Management*, *77*, 108–117. https://doi.org/10.1016/j.enconman.2013.09.026

Kehlhofer, R., Hannemann, F., Stirnimann, F., & Rukes, B. (2009). *Combined-Cycle Gas Steam Turbine Power Plants*.

Keil, C., Plura, S., Radspieler, M., & Schweigler, C. (2008). Application of customized absorption heat pumps for utilization of low-grade heat sources. *Applied Thermal Engineering*. https://doi.org/10.1016/j.applthermaleng.2008.04.012

Kelvion - Coils. (2020). Retrieved February 13, 2020, from https://www.kelvion.com/products/product/coils/

Kenisarin, M. M. (2010). High-temperature phase change materials for thermal energy storage. *Renewable and Sustainable Energy Reviews*. https://doi.org/10.1016/j.rser.2009.11.011

Khatita, M. A., Ahmed, T. S., Ashour, F. H., & Ismail, I. M. (2014). Power generation using waste heat recovery by organic Rankine cycle in oil and gas sector in Egypt: A case study. *Energy*. https://doi.org/10.1016/j.energy.2013.11.011

Kilinc¸, E., Kaya, D., Kilic¸, F. Ç., Eyidoğan, M., Özkaymak, M., Taylan, O., & Pedrycz, W. (2014). An energy efficiency analysis of an industrial reheating furnace and an implementation of efficiency enhancements methods. *Energy Exploration and Exploitation*, *32*(6), 989–1003. https://doi.org/10.1260/0144-5987.32.6.989

Kimzey, G. (2012). Development of a Brayton Bottoming Cycle using Supercritical Carbon Dioxide as the Working Fluid. In *EPRI Report*.

Kishita, Y., Ohishi, Y., Uwasu, M., Kuroda, M., Takeda, H., & Hara, K. (2016). Evaluating the life cycle CO_2 emissions and costs of thermoelectric generators for passenger automobiles: A scenario analysis. *Journal of Cleaner Production*. https://doi.org/10.1016/j.jclepro.2016.02.121

Kizilkan, O. (2020). Performance assessment of steam Rankine cycle and sCO_2 Brayton cycle for waste heat recovery in a cement plant: A comparative study for supercritical fluids. *International Journal of Energy Research*. https://doi.org/10.1002/er.5138

Koehler, J., Tegethoff, W. J., Westphalen, D., & Sonnekalb, M. (1997). Absorption refrigeration system for mobile applications utilizing exhaust gases. *International Communications in Heat and Mass Transfer*, *32*(5), 333–340.

Köfinger, M., Schmidt, R. R., Basciotti, D., Terreros, O., Baldvinsson, I., Mayrhofer, J., … Pauli, H. (2018). Simulation based evaluation of large scale waste heat utilization in urban district heating networks: Optimized integration and operation of a seasonal storage. *Energy*. https://doi.org/10.1016/j.energy.2018.06.192

Konovšek, D., Fuzir, M., Slatinek, M., Šepul, T., Plesnik, K., & Lečnik, S. (2017). Process of optimization of district heat production by utilizing waste energy from metallurgical processes. *AIP Conference Proceedings*, *1866*. https://doi.org/10.1063/1.4994527

Konwar, D., & Gogoi, T. K. (2018). Performance of double effect H_2O–LiCl absorption refrigeration systems and comparison with H_2O–LiBr systems, Part 1: Energy analysis. *Thermal Science and Engineering Progress*. https://doi.org/10.1016/j.tsep.2018.08.008

Konwar, D., Gogoi, T. K., & Das, A. J. (2019). Multi-objective optimization of double effect series and parallel

Horizon 2020 European Union Funding for Research & Innovation

This project has received funding from the European Union's Horizon 2020 research and innovation programme under grant agreement No 847097

flow water–lithium chloride and water–lithium bromide absorption refrigeration systems. *Energy Conversion and Management*. https://doi.org/10.1016/j.enconman.2018.10.029

Kotzé, J. P., Von Backström, T. W., & Erens, P. J. (2013). High temperature thermal energy storage utilizing metallic phase change materials and metallic heat transfer fluids. *Journal of Solar Energy Engineering, Transactions of the ASME*, *135*(3). https://doi.org/10.1115/1.4023485

Krese, G., Koželj, R., Butala, V., & Stritih, U. (2018). Thermochemical seasonal solar energy storage for heating and cooling of buildings. *Energy and Buildings*. https://doi.org/10.1016/j.enbuild.2017.12.057

Krönauer, A., Lävemann, E., Brückner, S., & Hauer, A. (2015). Mobile sorption heat storage in industrial waste heat recovery. *Energy Procedia*. https://doi.org/10.1016/j.egypro.2015.07.688

Kühn, A. (2013). *THERMALLY DRIVEN HEAT PUMPS FOR HEATING AND COOLING*.

Kühn, A., Meyer, T., & Ziegler, F. (2008). OPERATIONAL RESULTS OF A 10 kW ABSORPTION CHILLER IN HEAT PUMP MODE. *Proceedings of the Ninth International IEA Heat Pump Conference*, (May), 20–22.

Kühn, A., Petersen, S., Ziegler, F., Kohlenbach, P., Harm, M., & Schweigler, C. (2005). OPERATIONAL RESULTS OF A 10 kW ABSORPTION CHILLER FOR LOW-GRADE DRIVING HEAT. *International Sorption Heat Pump Conference*, *ISHPC-051-*.

Kuroki, T., Kabeya, K., Makino, K., Kajihara, T., Kaibe, H., Hachiuma, H., … Fujibayashi, A. (2014). Thermoelectric generation using waste heat in steel works. *Journal of Electronic Materials*, *43*(6), 2405–2410. https://doi.org/10.1007/s11664-014-3094-5

Kuroki, T., Murai, R., Makino, K., Nagano, K., Kajihara, T., Kaibe, H., … Matsuno, H. (2015). Research and Development for Thermoelectric Generation Technology Using Waste Heat from Steelmaking Process. *Journal of Electronic Materials*, *44*(6), 2151–2156. https://doi.org/10.1007/s11664-015-3722-8

Laing, D., Bauer, T., Breidenbach, N., Hachmann, B., & Johnson, M. (2013). Development of high temperature phase-change-material storages. *Applied Energy*. https://doi.org/10.1016/j.apenergy.2012.11.063

Lance, B. W., & Carlson, M. D. (2018). Microchannel heat exchanger flow validation study. *Proceedings of the ASME Turbo Expo*, *9*. https://doi.org/10.1115/GT2018-77197

Landelle, A., Tauveron, N., Haberschill, P., Revellin, R., & Colasson, S. (2017). Organic Rankine cycle design and performance comparison based on experimental database. *Applied Energy*, *204*, 1172–1187. https://doi.org/10.1016/j.apenergy.2017.04.012

Larjola, J. (1995). Electricity from industrial waste heat using high-speed organic Rankine cycle (ORC). *International Journal of Production Economics*. https://doi.org/10.1016/0925-5273(94)00098-0

Le Lostec, B., Galanis, N., & Millette, J. (2012). Experimental study of an ammonia-water absorption chiller. *International Journal of Refrigeration*. https://doi.org/10.1016/j.ijrefrig.2012.05.012

Lecompte, S., Huisseune, H., Van Den Broek, M., Vanslambrouck, B., & De Paepe, M. (2015). Review of organic Rankine cycle (ORC) architectures for waste heat recovery. *Renewable and Sustainable Energy Reviews*. https://doi.org/10.1016/j.rser.2015.03.089

Lee, Y. R., Liu, L. W., Chang, Y. Y., & Hsieh, J. C. (2017). Development and application of a 200 kW ORC generator system for energy recovery in chemical processes. *Energy Procedia*, *129*, 519–526. https://doi.org/10.1016/j.egypro.2017.09.176

Lefebvre, D., & Tezel, F. H. (2017). A review of energy storage technologies with a focus on adsorption thermal energy storage processes for heating applications. *Renewable and Sustainable Energy Reviews*. https://doi.org/10.1016/j.rser.2016.08.019

Legmann, H. (2002). Recovery of industrial heat in the cement industry by means of the ORC process. *IEEE Cement Industry Technical Conference (Paper)*, 29–35. https://doi.org/10.1109/CITCON.2002.1006482

Horizon 2020
European Union Funding
for Research & Innovation

This project has received funding from
the European Union's Horizon 2020 research and innovation
programme under grant agreement No 847097

Lehar, M. A., & Michelassi, V. (2013). *System and method for recovery of waste heat from dual heat sources*. Retrieved from http://www.google.com/patents/US20130247570

Leibowitz, H. M., & Micak, H. A. (1999). Design of a 2 MW Kalina cycle binary module for installation in Husavik, Iceland. *Transactions - Geothermal Resources Council*, *23*, 75–80.

Lemmens, S. (2016). Cost engineering techniques & their applicability for cost estimation of organic rankine cycle systems. *Energies*, *9*(7). https://doi.org/10.3390/en9070485

Lewis, W. E., & Ralph, M. (2002). A DOE-Funded Design Study for Pioneer Baseload Application of an Advanced Geothermal Binary Cycle at a Utility Plant in Western Utah. *Transactions - Geothermal Resources Council*, 695–699.

Li, C., Li, Q., & Ding, Y. (2019a). Carbonate salt based composite phase change materials for medium and high temperature thermal energy storage: From component to device level performance through modelling. *Renewable Energy*. https://doi.org/10.1016/j.renene.2019.03.005

Li, C., Li, Q., & Ding, Y. (2019b). Investigation on the thermal performance of a high temperature packed bed thermal energy storage system containing carbonate salt based composite phase change materials. *Applied Energy*. https://doi.org/10.1016/j.apenergy.2019.04.031

Li, G. (2016). Sensible heat thermal storage energy and exergy performance evaluations. *Renewable and Sustainable Energy Reviews*. https://doi.org/10.1016/j.rser.2015.09.006

Li, G., Hwang, Y., Radermacher, R., & Chun, H. H. (2013). Review of cold storage materials for subzero applications. *Energy*. https://doi.org/10.1016/j.energy.2012.12.002

Li, S., & Dai, Y. (2014). Thermo-economic comparison of Kalina and CO2 transcritical power cycle for low temperature geothermal sources in China. *Applied Thermal Engineering*. https://doi.org/10.1016/j.applthermaleng.2014.04.067

Li, S. F., Liu, Z. hua, & Wang, X. J. (2019). A comprehensive review on positive cold energy storage technologies and applications in air conditioning with phase change materials. *Applied Energy*. https://doi.org/10.1016/j.apenergy.2019.113667

Li, T., Tang, D., Li, Z., Du, J., Zhou, T., & Jia, Y. (2012). Development and test of a Stirling engine driven by waste gases for the micro-CHP system. *Applied Thermal Engineering*. https://doi.org/10.1016/j.applthermaleng.2011.09.020

Li, T. X., Xu, J. X., Wu, D. L., He, F., & Wang, R. Z. (2019). High energy-density and power-density thermal storage prototype with hydrated salt for hot water and space heating. *Applied Energy*. https://doi.org/10.1016/j.apenergy.2019.04.114

Li, Xianting, Wu, W., Zhang, X., Shi, W., & Wang, B. (2012). Energy saving potential of low temperature hot water system based on air source absorption heat pump. *Applied Thermal Engineering*. https://doi.org/10.1016/j.applthermaleng.2011.12.045

Li, Xiaoqiong, Zhang, Y., Ma, X., Deng, N., Jin, Z., Yu, X., & Li, W. (2019). Performance analysis of high-temperature water source cascade heat pump using BY3B/BY6 as refrigerants. *Applied Thermal Engineering*. https://doi.org/10.1016/j.applthermaleng.2019.113895

Li, Yemao, Xia, J., Fang, H., Su, Y., & Jiang, Y. (2016). Case study on industrial surplus heat of steel plants for district heating in Northern China. *Energy*. https://doi.org/10.1016/j.energy.2016.02.105

Li, Yongliang. (2011). Cryogen Based Energy Storage : Process Modelling and Optimisation. *PhD Thesis. University of Leeds*, (September).

Li, Yongliang, Cao, H., Wang, S., Jin, Y., Li, D., Wang, X., & Ding, Y. (2014). Load shifting of nuclear power plants using cryogenic energy storage technology. *Applied Energy*. https://doi.org/10.1016/j.apenergy.2013.08.077

Horizon 2020
European Union Funding
for Research & Innovation

This project has received funding from
the European Union's Horizon 2020 research and innovation
programme under grant agreement No 847097

Liang, X.-Y., Cheng, J.-H., He, Y.-J., Wang, L., Li, H., Shao, L.-L., & Zhang, C.-L. (2019). Study on annual energy performance of transcritical CO2 heat pump water heating systems in Shanghai. *International Journal of Refrigeration*. https://doi.org/10.1016/j.ijrefrig.2019.07.016

Liao, T., Cai, L., Zhao, Y., & Chen, J. (2016). Efficiently exploiting the waste heat in solid oxide fuel cell by means of thermophotovoltaic cell. *Journal of Power Sources*. https://doi.org/10.1016/j.jpowsour.2015.12.080

Libby, C. (2010). *Solar Thermocline Storage Systems: Preliminary Design Study*. https://doi.org/Report no. 1019581, EPRI, California

Lin, Y., Alva, G., & Fang, G. (2018). Review on thermal performances and applications of thermal energy storage systems with inorganic phase change materials. *Energy*. https://doi.org/10.1016/j.energy.2018.09.128

Lin, Y. P., Wang, W. H., Pan, S. Y., Ho, C. C., Hou, C. J., & Chiang, P. C. (2016). Environmental impacts and benefits of organic Rankine cycle power generation technology and wood pellet fuel exemplified by electric arc furnace steel industry. *Applied Energy*. https://doi.org/10.1016/j.apenergy.2016.08.183

Linde - Air Separation Plants. (2020). Retrieved February 11, 2020, from https://www.linde-engineering.com/en/process-plants/air-separation-plants/index.html?gclid=EAIaIQobChMI-479g5O45wIVibbtCh1fRw4sEAAYASAAEgI90PD_BwE

Linnemann, M., Priebe, K. P., Heim, A., Wolff, C., & Vrabec, J. (2020). Experimental investigation of a cascaded organic Rankine cycle plant for the utilization of waste heat at high and low temperature levels. *Energy Conversion and Management*. https://doi.org/10.1016/j.enconman.2019.112381

Liu, F., Sui, J., Liu, H., & Jin, H. (2017). Experimental studies on a direct-steam-generation absorption heat transformer built with vertical falling-film heat exchangers. *Experimental Thermal and Fluid Science*. https://doi.org/10.1016/j.expthermflusci.2016.11.033

Liu, M., Steven Tay, N. H., Bell, S., Belusko, M., Jacob, R., Will, G., … Bruno, F. (2016). Review on concentrating solar power plants and new developments in high temperature thermal energy storage technologies. *Renewable and Sustainable Energy Reviews*. https://doi.org/10.1016/j.rser.2015.09.026

Liu, X., Deng, Y. D., Li, Z., & Su, C. Q. (2015). Performance analysis of a waste heat recovery thermoelectric generation system for automotive application. *Energy Conversion and Management*. https://doi.org/10.1016/j.enconman.2014.11.015

Liu, X., Malhotra, M., & Im, P. (2017). *Performance Analysis of Ground Source Heat Pump Demonstration Projects in the United States*. Retrieved from http://hpc2017.org/wp-content/uploads/2017/05/P.2.7.16-Performance-Analysis-of-Ground-Source-Heat-Pump-Demonstration-Projects-in-the-United-States.pdf

Liu, Z., Xie, N., & Yang, S. (2020). Thermodynamic and parametric analysis of a coupled LiBr/H2O absorption chiller/Kalina cycle for cascade utilization of low-grade waste heat. *Energy Conversion and Management*. https://doi.org/10.1016/j.enconman.2019.112370

Lizana, J., Friedrich, D., Renaldi, R., & Chacartegui, R. (2018). Energy flexible building through smart demand-side management and latent heat storage. *Applied Energy*. https://doi.org/10.1016/j.apenergy.2018.08.065

Llamas, S. U., Herrera, J. V., Cuevas, R., Gómez, V. H., García-Valladares, O., Cerezo, J., & Best, R. (2007). Development of a small capacity ammonia-lithium nitrate absorption refrigeration system. *2nd International Conference Solar Air-Conditioning*, 470–475.

Louvet, Y., Fischer, S., Furbo, S., Giovannetti, F., Helbig, S., Köhl, M., … Vajen, K. (2019). Economic comparison of reference solar thermal systems for households in five European countries. *Solar Energy*. https://doi.org/10.1016/j.solener.2019.09.019

Lu, Z., Gong, Y., Yao, Y., Luo, C., & Ma, W. (2019). Development of a high temperature heat pump system for steam generation using medium-low temperature geothermal water. *Energy Procedia*. https://doi.org/10.1016/j.egypro.2019.01.513

Horizon 2020
European Union Funding
for Research & Innovation

This project has received funding from
the European Union's Horizon 2020 research and innovation
programme under grant agreement No 847097

Lubis, A., Giannetti, N., Yamaguchi, S., Saito, K., & Inoue, N. (2017). Experimental performance of a double-lift absorption heat transformer for manufacturing-process steam generation. *Energy Conversion and Management*. https://doi.org/10.1016/j.enconman.2017.05.074

Lumenion. (2019). Retrieved from https://lumenion.com/?lang=en

Luo, Q., Li, P., Cai, L., Zhou, P., Tang, D., Zhai, P., & Zhang, Q. (2015). A Thermoelectric Waste-Heat-Recovery System for Portland Cement Rotary Kilns. *Journal of Electronic Materials*, *44*(6), 1750–1762. https://doi.org/10.1007/s11664-014-3543-1

Luo, X., Wang, J., Dooner, M., & Clarke, J. (2015). Overview of current development in electrical energy storage technologies and the application potential in power system operation. *Applied Energy*. https://doi.org/10.1016/j.apenergy.2014.09.081

Ma, F., & Zhang, P. (2017). Investigation on the performance of a high-temperature packed bed latent heat thermal energy storage system using Al-Si alloy. *Energy Conversion and Management*. https://doi.org/10.1016/j.enconman.2017.08.040

Ma, Xuehu, Chen, J., Li, S., Sha, Q., Liang, A., Li, W., … Feng, Z. (2003). Application of absorption heat transformer to recover waste heat from a synthetic rubber plant. *Applied Thermal Engineering*. https://doi.org/10.1016/S1359-4311(03)00011-5

Ma, Xuelian, Zhang, Y., Fang, L., Yu, X., Li, X., Sheng, Y., & Zhang, Y. (2018). Performance analysis of a cascade high temperature heat pump using R245fa and BY-3 as working fluid. *Applied Thermal Engineering*. https://doi.org/10.1016/j.applthermaleng.2018.05.052

Ma, Zhao, Yang, W. W., Yuan, F., Jin, B., & He, Y. L. (2017). Investigation on the thermal performance of a high-temperature latent heat storage system. *Applied Thermal Engineering*. https://doi.org/10.1016/j.applthermaleng.2017.04.085

Ma, Zheshu, Yang, D., & Guo, Q. (2012). Conceptual design and performance analysis of an exhaust gas waste heat recovery system for a 10000TEU container ship. *Polish Maritime Research*, *19*(2), 31–38. https://doi.org/10.2478/v10012-012-0012-8

Ma, Zhiwei, Bao, H., & Roskilly, A. P. (2019). Seasonal solar thermal energy storage using thermochemical sorption in domestic dwellings in the UK. *Energy*. https://doi.org/10.1016/j.energy.2018.10.066

Madlool, N. A., Saidur, R., & Rahim, N. A. (2012). Investigation of Waste Heat Recovery in Cement Industry: A Case Study. *International Journal of Engineering and Technology*, *4*(5), 665–667. https://doi.org/10.7763/ijet.2012.v4.457

MAGENTA H2020. (2019). MAGENTA H2020. Retrieved from https://www.magenta-h2020.eu/

MAN Diesel & Turbo. (2014). *Thermo Efficiency System for Reduction of Fuel Consumption and CO2 Emission*.

Manente, G., & Lazzaretto, A. (2014). Innovative biomass to power conversion systems based on cascaded supercritical CO2 Brayton cycles. *Biomass and Bioenergy*, *69*, 155–168. https://doi.org/10.1016/j.biombioe.2014.07.016

Manente, G., Lazzaretto, A., & Bonamico, E. (2017). Design guidelines for the choice between single and dual pressure layouts in organic Rankine cycle (ORC) systems. *Energy*, *123*. https://doi.org/10.1016/j.energy.2017.01.151

Manente, G., Lazzaretto, A., Tavian, A., Molinari, I., Bronzini, F., & Ferraresi, F. (2018). The district heating system of the municipality of ferrara: Reduction of pumping energy consumption. *ECOS 2018 - Proceedings of the 31st International Conference on Efficiency, Cost, Optimization, Simulation and Environmental Impact of Energy Systems*.

Manente, Giovanni, & Costa, M. (2020). On the conceptual design of novel supercritical CO2 power cycles for waste heat recovery. *Energies*, *13*(2). https://doi.org/10.3390/en13020370

Horizon 2020
European Union Funding
for Research & Innovation

This project has received funding from
the European Union's Horizon 2020 research and innovation
programme under grant agreement No 847097

Manente, Giovanni, & Fortuna, F. M. (2019). Supercritical CO2 power cycles for waste heat recovery: A systematic comparison between traditional and novel layouts with dual expansion. *Energy Conversion and Management*, *197*, 111777. https://doi.org/10.1016/j.enconman.2019.111777

Manente, Giovanni, Lazzaretto, A., Molinari, I., & Bronzini, F. (2019). Optimization of the hydraulic performance and integration of a heat storage in the geothermal and waste-to-energy district heating system of Ferrara. *Journal of Cleaner Production*. https://doi.org/10.1016/j.jclepro.2019.05.146

Manickam, K., Mistry, P., Walker, G., Grant, D., Buckley, C. E., Humphries, T. D., … Felderhoff, M. (2019). Future perspectives of thermal energy storage with metal hydrides. *International Journal of Hydrogen Energy*. https://doi.org/10.1016/j.ijhydene.2018.12.011

Marchionni, M., Saravi, S. S., Bianchi, G., & Tassou, S. A. (2019). Modelling and performance analysis of a supercritical CO2 system for high temperature industrial heat to power conversion at off-design conditions. *3rd European SCO2 Conference*. Retrieved from https://duepublico2.uni-due.de/receive/duepublico_mods_00048908

Marchionni, Matteo, Bianchi, G., & Tassou, S. A. (2018). Techno-economic assessment of Joule-Brayton cycle architectures for heat to power conversion from high-grade heat sources using CO2 in the supercritical state. *Energy*. https://doi.org/10.1016/j.energy.2018.02.005

Marguerite, C., Andresen, G. B., & Dahl, M. (2018). Multi-criteria analysis of storages integration and operation solutions into the district heating network of Aarhus – A simulation case study. *Energy*. https://doi.org/10.1016/j.energy.2018.06.013

Marini, D., Buswell, R. A., & Hopfe, C. J. (2019). Sizing domestic air-source heat pump systems with thermal storage under varying electrical load shifting strategies. *Applied Energy*. https://doi.org/10.1016/j.apenergy.2019.113811

Marinitsch, G., Bovin, J., Gørtz, T., Mygind, K., & Carlsen, H. (2011). CO2 neutral, low emission small scale biomass CHP plants based on updraft gasification and stirling engines – Technology development. *19th European Biomass Conference & Exhibition*, 981–990.

Marinova, M., Beaudry, C., Taoussi, A., Trépanier, M., & Paris, J. (2008). Economic Assessment of Rural District Heating by Bio-Steam Supplied by a Paper Mill in Canada. *Bulletin of Science, Technology & Society*, *28*(2), 159–173. https://doi.org/10.1177/0270467607313953

Mark Akhurst, Andy Atkins, Ian Arbon, & michael Ayres et al. (2013). *Liquid Air in the energy and transport systems - Opportunities for industry and innovation in the UK Full Report*. Retrieved from www.liquidair.org.uk

Marlow Industries. (2019). Marlow Industries. Retrieved from https://www.marlow.com/products/power-generators

Marston, C. H. (1989). Parametric analysis of the Kalina cycle. *Proceedings of the ASME Turbo Expo*, *4*. https://doi.org/10.1115/89GT-218

Martić, I. I., Budimir, S. J., Mitrović, N. R., Maslarević, A. M., & Marković, M. D. (2016). Application and design of an economizer for waste heat recoveryin a co-generation plant. *Thermal Science*, *20*(4), 1355–1362. https://doi.org/10.2298/TSCI141113211M

Mateu-Royo, C., Navarro-Esbrí, J., Mota-Babiloni, A., Molés, F., & Amat-Albuixech, M. (2019). Experimental exergy and energy analysis of a novel high-temperature heat pump with scroll compressor for waste heat recovery. *Applied Energy*. https://doi.org/10.1016/j.apenergy.2019.113504

Matjanov, E. (2020). Gas turbine efficiency enhancement using absorption chiller. Case study for Tashkent CHP. *Energy*. https://doi.org/10.1016/j.energy.2019.116625

Matsuda, K. (2013). Low Heat Power Generation System. *Chemical Engineering Transactions*.

Horizon 2020
European Union Funding
for Research & Innovation

This project has received funding from
the European Union's Horizon 2020 research and innovation
programme under grant agreement No 847097

Matsuda, Kazuo. (2014). Low heat power generation system. *Applied Thermal Engineering*. https://doi.org/10.1016/j.applthermaleng.2014.03.037

McCaffrey, R. (2018). DG Khan Khairpur: The 'self-sufficient' cement plant. *Global Cement Magazine*.

Meda, L., Romzek, M., Zhang, Y., & Cleary, M. (2016). Development of a 1kW Exhaust Waste Heat Thermoelectric Generator. *SAE International Journal of Commercial Vehicles*, *9*(1), 21–30. https://doi.org/10.4271/2016-01-1273

Melissa Poerner, P. E., Musgrove, G., & Beck, G. (2016). Liquid co2 formation, impact, and mitigation at the inlet to a supercritical CO2 compressor. *Proceedings of the ASME Turbo Expo*, *9*. https://doi.org/10.1115/GT2016-56513

MERITS FP7. (2015). Retrieved from GA ID: 295983 website: https://www.merits.eu/project

Merkel, N., Bücherl, M., Zimmermann, M., Wagner, V., & Schaber, K. (2018). Operation of an absorption heat transformer using water/ionic liquid as working fluid. *Applied Thermal Engineering*. https://doi.org/10.1016/j.applthermaleng.2017.11.147

Merlin, K., Soto, J., Delaunay, D., & Traonvouez, L. (2016). Industrial waste heat recovery using an enhanced conductivity latent heat thermal energy storage. *Applied Energy*, *183*, 491–503. https://doi.org/10.1016/J.APENERGY.2016.09.007

Michel, B., Neveu, P., & Mazet, N. (2014). Comparison of closed and open thermochemical processes, for long-term thermal energy storage applications. *Energy*. https://doi.org/10.1016/j.energy.2014.05.097

Microgen Engine Corporation. (2019). Retrieved from https://www.microgen-engine.com/

Mikielewicz, D., & Wajs, J. (2019). Performance of the very high-temperature heat pump with low GWP working fluids. *Energy*. https://doi.org/10.1016/j.energy.2019.05.203

Miol, D., De Miol, M., Bianchi, G., Henry, G., Holaind, N., & Tassou Arthur Leroux, S. A. (2018). *Design of a single-shaft compressor, generator, turbine for small-scale supercritical CO2 systems for waste heat to power conversion applications DESIGN OF A SINGLE-SHAFT COMPRESSOR, GENERATOR, TURBINE FOR SMALL-SCALE SUPERCRITICAL Co2 SYSTEMS FOR WASTE H*. https://doi.org/10.17185/duepublico/46086

Mirl, N., Schmid, F., Bierling, B., & Spindler, K. (2020). Design and analysis of an ammonia-water absorption heat pump. *Applied Thermal Engineering*. https://doi.org/10.1016/j.applthermaleng.2019.114531

Miró, L., Gasia, J., & Cabeza, L. F. (2016). Thermal energy storage (TES) for industrial waste heat (IWH) recovery: A review. *Applied Energy*. https://doi.org/10.1016/j.apenergy.2016.06.147

Mirolli, M. D. (2005). The Kalina cycle for cement kiln waste heat recovery power plants. *2005 IEEE Cement Industry Technical Conference Record*, *2005*, 330–336. https://doi.org/10.1109/CITCON.2005.1516374

Mirolli, M. D. (2007). Ammonia-water based thermal conversion technology: Applications in waste heat recovery for the cement industry. *2007 IEEE Cement Industry Technical Conference Record*, 234–241. https://doi.org/10.1109/CITCON.2007.359001

Mirolli, M., & Gibbons, T. B. (2012). Kalina Cycle Power Systems in Waste Heat Recovery. *Conference and Exhibition on Waste Heat Recovery for the Cement and Allied Industries*.

Mitsubishi Heavy Industries - waste heat recovery systems. (2020). Retrieved from https://www.mhi-mme.com/products/boilerturbine/whrs.html

Mlcak, H., Mirolli, M., Hjartarson, H., Húsavíkur, O., & Ralph, M. (2002). Notes from the North: A Report on the Debut Year of the 2 MW Kalina Cycle® Geothermal Power Plant in Húsavík, Iceland. *Transactions - Geothermal Resources Council*, 715–718.

Modi, A., Andreasen, J. G., Kærn, M. R., & Haglind, F. (2015). Part-load performance of a high temperature Kalina cycle. *Energy Conversion and Management*, *105*, 453–461.

Horizon 2020
European Union Funding
for Research & Innovation

This project has received funding from
the European Union's Horizon 2020 research and innovation
programme under grant agreement No 847097

https://doi.org/10.1016/j.enconman.2015.08.006

Modi, A., Knudsen, T., Haglind, F., & Clausen, L. R. (2014). Feasibility of using ammonia-water mixture in high temperature concentrated solar power plants with direct vapour generation. *Energy Procedia*. https://doi.org/10.1016/j.egypro.2014.10.192

Mohagheghi, M., & Kapat, J. (2013). Thermodynamic Optimization of Recuperated S-Co2 Brayton Cycles for Waste Heat Recovery Applications. *The 4th International Symposium - Supercritical CO2 Power Cycles*, *53*(9), 1689–1699. https://doi.org/10.1017/CBO9781107415324.004

Mohammadkhani, F., Yari, M., & Ranjbar, F. (2019). A zero-dimensional model for simulation of a Diesel engine and exergoeconomic analysis of waste heat recovery from its exhaust and coolant employing a high-temperature Kalina cycle. *Energy Conversion and Management*, *198*. https://doi.org/10.1016/j.enconman.2019.111782

Moreira, L. F., & Arrieta, F. R. P. (2019). Thermal and economic assessment of organic Rankine cycles for waste heat recovery in cement plants. *Renewable and Sustainable Energy Reviews*. https://doi.org/10.1016/j.rser.2019.109315

Morgan, R., Nelmes, S., Gibson, E., & Brett, G. (2015). An analysis of a large-scale liquid air energy storage system. *Proceedings of Institution of Civil Engineers: Energy*, *168*(2), 135–144. https://doi.org/10.1680/ener.14.00038

Moriwaki, R., Takigiri, M., Yamaguchi, S., & Saito, K. (2017). Performance Evaluation of Double-Lift Absorption Heat Transformer for Generation of Steam at 180 ° C. *12th IEA Heat Pump Conference*, 1–10.

Mostofizadeh, C., & Kulick, C. (1998). Use of a new type of heat transformer in process industry. *Applied Thermal Engineering*. https://doi.org/10.1016/s1359-4311(97)00115-4

Musgrove, G. O., Le Pierres, R., & Nash, J. (2014). Heat Exchangers for Supercritical CO2 Power Cycle Applications. *The 4th International Symposium for Supercritical CO2 Power Cycles*.

Nag, P. K., & Gupta, A. V. S. S. K. S. (1998). Exergy analysis of the kalina cycle. *Applied Thermal Engineering*, *18*(6), 427–439. https://doi.org/10.1016/S1359-4311(97)00047-1

Nakayama, Y. (2017). *Field test study on the performance of air source heat pump installed at various industrial processes in Japan*.

Narayanan, S., Kim, H., Umans, A., Yang, S., Li, X., Schiffres, S. N., … Hidrovo, C. H. (2017). A thermophysical battery for storage-based climate control. *Applied Energy*. https://doi.org/10.1016/j.apenergy.2016.12.003

Narayanan, S., Li, X., Yang, S., Kim, H., Umans, A., McKay, I. S., & Wang, E. N. (2015). Thermal battery for portable climate control. *Applied Energy*. https://doi.org/10.1016/j.apenergy.2015.03.101

Nardin, G., Meneghetti, A., Dal Magro, F., & Benedetti, N. (2014). PCM-based energy recovery from electric arc furnaces. *Applied Energy*. https://doi.org/10.1016/j.apenergy.2014.07.052

Navarro-Esbrí, J., Peris, B., Collado, R., & Molés, F. (2013). Micro-generation and micro combined heat and power generation using "free" low temperature heat sources through organic rankine cycles. *Renewable Energy and Power Quality Journal*, *1*(11), 624–629. https://doi.org/10.24084/repqj11.390

Niamsuwan, S., Kittisupakorn, P., & Mujtaba, I. M. (2013). A newly designed economizer to improve waste heat recovery: A case study in a pasteurized milk plant. *Applied Thermal Engineering*. https://doi.org/10.1016/j.applthermaleng.2013.06.056

Nicholson, R. (1983). Recuperative and regenerative techniques at high temperature. *Journal of Heat Recovery Systems*, *3*(5), 385–404. https://doi.org/10.1016/0198-7593(83)90053-X

Nilsson, E., & Rohdin, P. (2019). Performance evaluation of an industrial borehole thermal energy storage (BTES) project – Experiences from the first seven years of operation. *Renewable Energy*. https://doi.org/10.1016/j.renene.2019.05.020

Horizon 2020
European Union Funding
for Research & Innovation

This project has received funding from
the European Union's Horizon 2020 research and innovation
programme under grant agreement No 847097

Nomura, T., Okinaka, N., & Akiyama, T. (2010). Waste heat transportation system, using phase change material (PCM) from steelworks to chemical plant. *Resources, Conservation and Recycling*. https://doi.org/10.1016/j.resconrec.2010.02.007

Nord, L., & Bolland, O. (2012). Steam bottoming cycles offshore - Challenges and possibilities. *Journal of Power Technologies*, *92*(3), 201--207. Retrieved from http://papers.itc.pw.edu.pl/index.php/JPT/article/view/346

Nord, L. O., & Montañés, R. M. (2018). Compact steam bottoming cycles: Model validation with plant data and evaluation of control strategies for fast load changes. *Applied Thermal Engineering*. https://doi.org/10.1016/j.applthermaleng.2018.07.012

Oak Ridge National Laboratory. (2015). *Waste Heat to Power Market Assessment*.

Obernberger, I. (2010). Trends and opportunities of micro-CHP technologies based on biomass combustion. *18th European Biomass Conference. Lyon 2010*, 1–9. Retrieved from http://bioenergy2020.eu/files/publications/pdf/Obernberger-2010-Lyon-Micro-CHP.pdf

Oberweis, S., & Al-Shemmeri, T. (2012). Performance Evaluation of a Lithium-Chloride Absorption Refrigeration and an Assessment of Its Suitability for Biomass Waste Heat. *Applied Sciences*, *2*(4), 709–725. https://doi.org/10.3390/app2040709

Odenthal, C., Klasing, F., & Bauer, T. (2017). Demonstrating Cost Effective Thermal Energy Storage in Molten Salts: DLR's TESIS Test Facility. *Energy Procedia*, *135*, 14–22. https://doi.org/10.1016/j.egypro.2017.09.483

Ogriseck, S. (2009). Integration of Kalina cycle in a combined heat and power plant, a case study. *Applied Thermal Engineering*. https://doi.org/10.1016/j.applthermaleng.2009.02.006

OkoFEN. (2019). Retrieved from http://www.okofen-e.com/en/pellet_boiler/

Orcan Energy AG. (2020). Retrieved February 27, 2020, from https://www.orcan-energy.com/en/applications-marine.html

Ortiz, C., Valverde, J. M., Chacartegui, R., Perez-Maqueda, L. A., & Giménez, P. (2019). The Calcium-Looping ($CaCO_3/CaO$) process for thermochemical energy storage in Concentrating Solar Power plants. *Renewable and Sustainable Energy Reviews*. https://doi.org/10.1016/j.rser.2019.109252

Pal, K. (2017). Efficient solution for large heat pumps: wastewater heat recovery. *12th IEA Heat Pump Conference 2017*, 1–11. Retrieved from http://hpc2017.org/wp-content/uploads/2017/05/P.3.7.1-Efficient-Solution-For-Large-Heat-Pumps-Wastewater-Heat-Recovery.pdf

Pan, C., Vermaak, N., Romero, C., Neti, S., Hoenig, S., Chen, C. H., & Bonner, R. (2018). Cost estimation and sensitivity analysis of a latent thermal energy storage system for supplementary cooling of air cooled condensers. *Applied Energy*. https://doi.org/10.1016/j.apenergy.2018.04.080

Pan, Z. H., & Zhao, C. Y. (2017). Gas–solid thermochemical heat storage reactors for high-temperature applications. *Energy*. https://doi.org/10.1016/j.energy.2017.04.102

Pantaleo, A. M., Fordham, J., Oyewunmi, O. A., De Palma, P., & Markides, C. N. (2018). Integrating cogeneration and intermittent waste-heat recovery in food processing: Microturbines vs. ORC systems in the coffee roasting industry. *Applied Energy*. https://doi.org/10.1016/j.apenergy.2018.04.097

Pardo, P., Deydier, A., Anxionnaz-Minvielle, Z., Rougé, S., Cabassud, M., & Cognet, P. (2014). A review on high temperature thermochemical heat energy storage. *Renewable and Sustainable Energy Reviews*. https://doi.org/10.1016/j.rser.2013.12.014

Parham, K., Khamooshi, M., Tematio, D. B. K., Yari, M., & Atikol, U. (2014). Absorption heat transformers - A comprehensive review. *Renewable and Sustainable Energy Reviews*. https://doi.org/10.1016/j.rser.2014.03.036

PCM Products Ltd. (2019). Retrieved from http://www.pcmproducts.net/

Horizon 2020 European Union Funding for Research & Innovation

This project has received funding from the European Union's Horizon 2020 research and innovation programme under grant agreement No 847097

Pellegrino, J. L. (2002). *Energy and Environmental Profile of the U.S. Glass Industry*.

Pereira da Cunha, J., & Eames, P. (2016). Thermal energy storage for low and medium temperature applications using phase change materials - A review. *Applied Energy*. https://doi.org/10.1016/j.apenergy.2016.05.097

Peris, B., Navarro-Esbrí, J., Molés, F., & Mota-Babiloni, A. (2015). Experimental study of an ORC (organic Rankine cycle) for low grade waste heat recovery in a ceramic industry. *Energy*. https://doi.org/10.1016/j.energy.2015.03.065

Persichilli, M., Held, T., Hostler, S., & Zdankiewicz, E. (2011). Transforming Waste Heat to Power through Development of a CO2 - Based Power Cycle. *16th International Symposium, Compressor Users-Manufacturers*, 8–10.

Peureux, J.-L., Sicard, F., & Bobelin, D. (2014). French industrial heat pump developments applied to heat recovery. *11th IEA Heat Pump Conference, May 12, 2014, Montréal, Canada*.

Phase energy Ltd. (2019). Retrieved from http://phase-energy.com/

Pilodia, N. K., Wanve, S., Maheshwari, A., & Kumar, M. (2018). Kalina Cycle (waste heat recovery applications) – A Review. *International Journal of Advanced in Management, Technology and Engineering Sciences*, *8*(Iii), 1369–1376.

Pineda, D. D. (2017). *Thermoelectric Energy Conversion Basic Concepts and Device Applications*.

PLUSS. (2019). Retrieved from https://www.pluss.co.in/product-range-PCM.php

Popa, V., Ion, I., & Popa, C. L. (2016). Thermo-Economic Analysis of an Air-to-Water Heat Pump. *Energy Procedia*, *85*, 408–415. https://doi.org/10.1016/j.egypro.2015.12.221

Popovac, M., Moretti, I., Lauermann, M., & Zottl, A. (2017). *Monitoring and optimization of an existing heat pump system using waste water as the heat source*. 1–8.

Porkka, A. (2017). *Practical experience of feasibility in some real industrial waste heat recycling utilizing heat pumps*.

Qiu, G. (2012). Selection of working fluids for micro-CHP systems with ORC. *Renewable Energy*. https://doi.org/10.1016/j.renene.2012.06.006

Qiu, K., & Hayden, A. C. S. (2012). Development of a novel cascading TPV and TE power generation system. *Applied Energy*. https://doi.org/10.1016/j.apenergy.2011.09.041

Qnergy. (2019). Retrieved from https://www.qnergy.com/

Qu, M., Abdelaziz, O., & Yin, H. (2014). New configurations of a heat recovery absorption heat pump integrated with a natural gas boiler for boiler efficiency improvement. *Energy Conversion and Management*. https://doi.org/10.1016/j.enconman.2014.06.083

Quoilin, S., Broek, M. Van Den, Declaye, S., Dewallef, P., & Lemort, V. (2013). Techno-economic survey of organic rankine cycle (ORC) systems. *Renewable and Sustainable Energy Reviews*. https://doi.org/10.1016/j.rser.2013.01.028

Rahbar, K., Mahmoud, S., Al-Dadah, R. K., Moazami, N., & Mirhadizadeh, S. A. (2017). Review of organic Rankine cycle for small-scale applications. *Energy Conversion and Management*. https://doi.org/10.1016/j.enconman.2016.12.023

Rakib, M. I., Saidur, R., Mohamad, E. N., & Afifi, A. M. (2017). Waste-heat utilization – The sustainable technologies to minimize energy consumption in Bangladesh textile sector. *Journal of Cleaner Production*, *142*, 1867–1876. https://doi.org/10.1016/j.jclepro.2016.11.098

Ramirez, M., Epelde, M., De Arteche, M. G., Panizza, A., Hammerschmid, A., Baresi, M., & Monti, N. (2017). Performance evaluation of an ORC unit integrated to a waste heat recovery system in a steel mill. *Energy*

Horizon 2020
European Union Funding
for Research & Innovation

This project has received funding from
the European Union's Horizon 2020 research and innovation
programme under grant agreement No 847097

Procedia. https://doi.org/10.1016/j.egypro.2017.09.183

Ravindra, N. M. (2019). *Thermoelectrics - Fundamentals, Materials Selection, Properties, and Performance*.

Rayaprolu, K. (2009). Boilers for Power and Process. In *Boilers for Power and Process*. https://doi.org/10.1201/ebk1420075366

Rea, J. E., Oshman, C. J., Olsen, M. L., Hardin, C. L., Glatzmaier, G. C., Siegel, N. P., … Toberer, E. S. (2018). Performance modeling and techno-economic analysis of a modular concentrated solar power tower with latent heat storage. *Applied Energy*. https://doi.org/10.1016/j.apenergy.2018.02.067

Rea, J. E., Oshman, C. J., Singh, A., Alleman, J., Parilla, P. A., Hardin, C. L., … Toberer, E. S. (2018). Experimental demonstration of a dispatchable latent heat storage system with aluminum-silicon as a phase change material. *Applied Energy*. https://doi.org/10.1016/j.apenergy.2018.09.017

Reay, D. A. (1981). A review of gas-gas heat recovery systems. *Journal of Heat Recovery Systems*, *1*(1), 3–41. https://doi.org/10.1016/0198-7593(81)90003-5

Recurrent Engineering LLC. (2013). *THE KALINA CYCLE - A Major Breakthrough in Efficient Heat to Power Generation*.

Reddy, K. S., Mudgal, V., & Mallick, T. K. (2018). Review of latent heat thermal energy storage for improved material stability and effective load management. *Journal of Energy Storage*. https://doi.org/10.1016/j.est.2017.11.005

Reinalter, W., Ulmer, S., Heller, P., Rauch, T., Gineste, J. M., Fernere, A., & Nepveu, F. (2008). Detailed performance analysis of a 10kW dish/stirling system. *Journal of Solar Energy Engineering, Transactions of the ASME*, *130*(1), 0110131–0110136. https://doi.org/10.1115/1.2807191

Reis, M. M. L., & Gallo, W. L. R. (2018). Study of waste heat recovery potential and optimization of the power production by an organic Rankine cycle in an FPSO unit. *Energy Conversion and Management*. https://doi.org/10.1016/j.enconman.2017.12.015

Ren, L., & Wang, H. (2019). Parametric optimization and thermodynamic performance comparison of organic trans-critical cycle, steam flash cycle, and steam dual-pressure cycle for waste heat recovery. *Energies*, *12*(24). https://doi.org/10.3390/en12244623

Reslag H2020. (2019). Retrieved from http://www.reslag.eu/

RESTRUCTURE FP7. (2016). Retrieved from https://cordis.europa.eu/project/rcn/100980/factsheet/en

RETD, I. E. A. T. C. P. (2017). *Fostering renewable energy integration in the industry (RE-INDUSTRY)*.

Riahi, S., Jovet, Y., Saman, W. Y., Belusko, M., & Bruno, F. (2019). Sensible and latent heat energy storage systems for concentrated solar power plants, exergy efficiency comparison. *Solar Energy*. https://doi.org/10.1016/j.solener.2018.12.072

Risseh, A. E., Nee, H.-P., Erlandsson, O., Brinkfeldt, K., Contet, A., Frobenius lng, F., … Dellrud, J. (2017). Design of a Thermoelectric Generator for Waste Heat Recovery Application on a Drivable Heavy Duty Vehicle. *SAE International Journal of Commercial Vehicles*, *10*(1), 26–44. https://doi.org/10.4271/2017-01-9178

Rivera, W. (2000). Experimental evaluation of a single-stage heat transformer used to increase solar pond's temperature. *Solar Energy*. https://doi.org/10.1016/s0038-092x(00)00107-9

Rivera, W., Best, R., Cardoso, M. J., & Romero, R. J. (2015). A review of absorption heat transformers. *Applied Thermal Engineering*. https://doi.org/10.1016/j.applthermaleng.2015.08.021

Rivera, W., Huicochea, A., Romero, R. J., & Lozano, A. (2018). Experimental assessment of double-absorption heat transformer operating with H2O/LiBr. *Applied Thermal Engineering*. https://doi.org/10.1016/j.applthermaleng.2017.12.117

Horizon 2020
European Union Funding
for Research & Innovation

This project has received funding from
the European Union's Horizon 2020 research and innovation
programme under grant agreement No 847097

Robur. (2019). Robur. Retrieved from https://www.robur.com/heat_pumps

Rogdakis, E. D., Antonakos, G. D., & Koronaki, I. P. (2012). Thermodynamic analysis and experimental investigation of a Solo V161 Stirling cogeneration unit. *Energy*. https://doi.org/10.1016/j.energy.2012.03.012

Rowe, T. M. (2006). *Thermoelectrics Handbook - macro to nano*.

Rubitherm. (2019). Retrieved from https://www.rubitherm.eu/en/index.php/productcategory/organische-pcm-rt

Saghafifar, M., Omar, A., Mohammadi, K., Alashkar, A., & Gadalla, M. (2019). A review of unconventional bottoming cycles for waste heat recovery: Part I – Analysis, design, and optimization. *Energy Conversion and Management*. https://doi.org/10.1016/j.enconman.2018.10.047

Saito, K., Inoue, N., Nakagawa, Y., Fukusumi, Y., Yamada, H., & Irie, T. (2015). Experimental and numerical performance evaluation of double-lift absorption heat transformer. *Science and Technology for the Built Environment*, *21*(3), 312–322. https://doi.org/10.1080/23744731.2014.998937

SaltX. (2019). Retrieved from http://saltxtechnology.com/

Sanaye, S., Khakpaay, N., Chitsaz, A., Hassan Yahyanejad, M., & Zolfaghari, M. (2020). A comprehensive approach for designing, modeling and optimizing of waste heat recovery cycle and power generation system in a cement plant: A thermo-economic and environmental assessment. *Energy Conversion and Management*. https://doi.org/10.1016/j.enconman.2019.112353

Sartor, K., & Dewallef, P. (2018). Integration of heat storage system into district heating networks fed by a biomass CHP plant. *Journal of Energy Storage*. https://doi.org/10.1016/j.est.2017.12.010

Sathish, S., Kumar, P., Nagarathinam, L., Swami, L., Namburi, A. N., Bandarupalli, V. S., & Gopi, P. C. (2019). *Brayton Cycle Supercritical CO2 Power Block for Industrial Waste Heat Recovery*. https://doi.org/10.1115/gtindia2019-2347

Scapino, L., Zondag, H. A., Van Bael, J., Diriken, J., & Rindt, C. C. M. (2017). Sorption heat storage for long-term low-temperature applications: A review on the advancements at material and prototype scale. *Applied Energy*. https://doi.org/10.1016/j.apenergy.2016.12.148

Schaube, F., Wörner, A., & Tamme, R. (2011). High temperature thermochemical heat storage for concentrated solar power using gas-solid reactions. *Journal of Solar Energy Engineering, Transactions of the ASME*, *133*(3). https://doi.org/10.1115/1.4004245

Schneider, T., Müller, D., & Karl, J. (2018). Biomass conversion with a fluidized bed-fired stirling engine in a micro-scale chp plant. *European Biomass Conference and Exhibition Proceedings*, *2018*(26thEUBCE), 630–634.

sCO2-HeRo H2020. (2018). Retrieved from GA ID: 662116 website: https://cordis.europa.eu/project/id/662116

sCO2flex H2020. (2019). Retrieved from https://www.sco2-flex.eu/

SCORES - D 2.3 Market analysis on hybrid storage components. (2019).

SCORES H2020. (2020). Retrieved from GA ID: 766464 website: http://www.scores-project.eu/

SCORES PROJECT - "Self Consumption Of Renewable Energy by hybrid Storage systems." (2019). *Winter 2019 European Energy Innovation*.

Scott, M., Jernqvist, Å., & Aly, G. (1999). Experimental and theoretical study of an open multi-compartment absorption heat transformer for different steam temperatures. Part III: Application to process industry. *Applied Thermal Engineering*. https://doi.org/10.1016/S1359-4311(98)00061-1

Seitz, M., Johnson, M., & Hübner, S. (2017). Economic impact of latent heat thermal energy storage systems

Horizon 2020
European Union Funding
for Research & Innovation

This project has received funding from
the European Union's Horizon 2020 research and innovation
programme under grant agreement No 847097

within direct steam generating solar thermal power plants with parabolic troughs. *Energy Conversion and Management*. https://doi.org/10.1016/j.enconman.2017.03.084

Sekar, S., & Saravanan, R. (2011). Experimental studies on absorption heat transformer coupled distillation system. *Desalination*. https://doi.org/10.1016/j.desal.2011.01.064

Sharma, H., Kumar, A., Varun, & Khurana, S. (2014). A review of metallic radiation recuperators for thermal exhaust heat recovery. *Journal of Mechanical Science and Technology*, *28*(3), 1099–1111. https://doi.org/10.1007/s12206-013-1186-4

Sharma, R. K., Ganesan, P., Tyagi, V. V., Metselaar, H. S. C., & Sandaran, S. C. (2015). Developments in organic solid-liquid phase change materials and their applications in thermal energy storage. *Energy Conversion and Management*. https://doi.org/10.1016/j.enconman.2015.01.084

Shen, Z. G., Tian, L. L., & Liu, X. (2019). Automotive exhaust thermoelectric generators: Current status, challenges and future prospects. *Energy Conversion and Management*. https://doi.org/10.1016/j.enconman.2019.05.087

Shiue, A., Hu, S. C., & Chiang, K. H. (2018). Effect of operating variables on performance of an absorption chiller driven by heat from municipal solid waste incineration. *Sustainable Energy Technologies and Assessments*. https://doi.org/10.1016/j.seta.2018.04.008

Shoaei, E. (2016). Performance assessment of thermophotovoltaic application in steel industry. *Solar Energy Materials and Solar Cells*. https://doi.org/10.1016/j.solmat.2016.05.012

Shu, G., Wang, X., & Tian, H. (2016). Theoretical analysis and comparison of rankine cycle and different organic rankine cycles as waste heat recovery system for a large gaseous fuel internal combustion engine. *Applied Thermal Engineering*. https://doi.org/10.1016/j.applthermaleng.2016.07.070

Shu, H., Duanmu, L., Shi, J., Jia, X., Ren, Z., & Yu, H. (2015). Field measurement and energy efficiency enhancement potential of a seawater source heat pump district heating system. *Energy and Buildings*. https://doi.org/10.1016/j.enbuild.2015.07.069

Siemens - Heat Recovery Steam Generators. (2020). Retrieved January 31, 2020, from https://assets.new.siemens.com/siemens/assets/api/uuid:de018f2c6d8afb5eb38368c053103c2cf4d30c18/version:1530610338/hrsg-interactive-pdf-v40.pdf

Sintef HeatUP. (2019). Retrieved from https://www.sintef.no/projectweb/heatup/

Skagestad, B., & Mildenstein, P. i. (2002). *District Heating and Cooling Connection Handbook*. Retrieved from http://dedc.dk/sites/default/files/programme_of_research_development_and_demonstration_on_district_heating_and_cooling.pdf

Smallbone, A., Jülch, V., Wardle, R., & Roskilly, A. P. (2017). Levelised Cost of Storage for Pumped Heat Energy Storage in comparison with other energy storage technologies. *Energy Conversion and Management*. https://doi.org/10.1016/j.enconman.2017.09.047

Smartrec H2020. (2019).

SOCRATCES H2020. (2020). Retrieved from GA ID: 727348 website: https://socratces.eu/

Soffiato, M., Frangopoulos, C. A., Manente, G., & Lazzaretto, A. (2014). Design and performance evaluation of an organic rankine cycle system exploiting the low grade waste heat of the main engines in a LNG carrier. *Proceedings of the 27th International Conference on Efficiency, Cost, Optimization, Simulation and Environmental Impact of Energy Systems, ECOS 2014*.

Soffiato, M., Frangopoulos, C. A., Manente, G., Rech, S., & Lazzaretto, A. (2015). Design optimization of ORC systems for waste heat recovery on board a LNG carrier. *Energy Conversion and Management*, *92*, 523–534. https://doi.org/10.1016/j.enconman.2014.12.085

Söğüt, Z., Oktay, Z., & Karakoç, H. (2010). Mathematical modeling of heat recovery from a rotary kiln. *Applied*

Horizon 2020
European Union Funding
for Research & Innovation

This project has received funding from
the European Union's Horizon 2020 research and innovation
programme under grant agreement No 847097

Thermal Engineering, *30*(8–9), 817–825. https://doi.org/10.1016/j.applthermaleng.2009.12.009

Sondex - Plate and shell HX. (2020). Retrieved February 13, 2020, from https://www.danfoss.com/en-gb/products/heat-exchangers/dhs/welded-heat-exchangers/sondex-plate-and-shell-heat-exchangers-sps/#tab-overview

Sondex - Plate heat exchanger. (2020). Retrieved February 13, 2020, from https://www.danfoss.com/en-gb/products/heat-exchangers/dhs/gasketed-heat-exchangers/traditional-plate-heat-exchangers/#tab-overview

Song, J., Li, Y., Gu, C. wei, & Zhang, L. (2014). Thermodynamic analysis and performance optimization of an ORC (Organic Rankine Cycle) system for multi-strand waste heat sources in petroleum refining industry. *Energy*. https://doi.org/10.1016/j.energy.2014.05.014

Song, Y., Zhang, N., Jing, Y., Cao, X., Yuan, Y., & Haghighat, F. (2019). Experimental and numerical investigation on dodecane/expanded graphite shape-stabilized phase change material for cold energy storage. *Energy*. https://doi.org/10.1016/j.energy.2019.116175

Song, Z., Chen, J., & Yang, L. (2015). Heat transfer enhancement in tubular heater of Stirling engine for waste heat recovery from flue gas using steel wool. *Applied Thermal Engineering*. https://doi.org/10.1016/j.applthermaleng.2015.05.028

Spirax Sarco. (2020). Retrieved January 31, 2020, from https://www.spiraxsarco.com/global/en-GB

Spoelstra, S., Haije, W. G., & Dijkstra, J. W. (2002). Techno-economic feasibility of high-temperature high-lift chemical heat pumps for upgrading industrial waste heat. *Applied Thermal Engineering*. https://doi.org/10.1016/S1359-4311(02)00077-7

Srikhirin, P., Aphornratana, S., & Chungpaibulpatana, S. (2000). A review of absorption refrigeration technologies. *Renewable and Sustainable Energy Reviews*. https://doi.org/10.1016/S1364-0321(01)00003-X

Sripakagorn, A., & Srikam, C. (2011). Design and performance of a moderate temperature difference Stirling engine. *Renewable Energy*. https://doi.org/10.1016/j.renene.2010.12.010

Staedter, M. A., & Garimella, S. (2018). Development of a micro-scale heat exchanger based, residential capacity ammonia–water absorption chiller. *International Journal of Refrigeration*, *89*, 93–103. https://doi.org/10.1016/j.ijrefrig.2018.02.016

Steinmann, W.-D., Laing, D., & Tamme, R. (2010). Latent heat storage systems for solar thermal power plants and process heat applications. *Journal of Solar Energy Engineering, Transactions of the ASME*, *132*(2), 0210031–0210035. https://doi.org/10.1115/1.4001405

Steinmann, W. D., Bauer, D., Jockenhöfer, H., & Johnson, M. (2019). Pumped thermal energy storage (PTES) as smart sector-coupling technology for heat and electricity. *Energy*. https://doi.org/10.1016/j.energy.2019.06.058

Stobart, R. K., & Yang, Z. (2018). The Development of Skutterudite-Based Thermoelectric Generators for Vehicles. *SAE Technical Papers*, *2018-April*. https://doi.org/10.4271/2018-01-0788

Storch, G., & Hauer, A. (2006). Cost-effectiveness of a heat energy distribution system based on mobile storage units: two case studies. *Proceedings of the ECOSTOCK Conference*, 1–8.

Strasser, M. N., & Selvam, R. P. (2014). A cost and performance comparison of packed bed and structured thermocline thermal energy storage systems. *Solar Energy*. https://doi.org/10.1016/j.solener.2014.07.023

Sun, F., Li, J., Fu, L., Li, Y., Wang, R., & Zhang, S. (2020). New configurations of district heating and cooling system based on absorption and compression chillers driven by waste heat of flue gas from coke ovens. *Energy*. https://doi.org/10.1016/j.energy.2019.116707

Sun, J., Ge, Z., & Fu, L. (2017). Investigation on LiBr-H2O double evaporation-absorption heat pump (DEAHP)

Horizon 2020
European Union Funding
for Research & Innovation

This project has received funding from
the European Union's Horizon 2020 research and innovation
programme under grant agreement No 847097

for heat recovery under lower driving sources. *Applied Thermal Engineering*. https://doi.org/10.1016/j.applthermaleng.2017.07.061

Sun, Z., Cui, Q., Wang, Q., Ning, J., Guo, J., Dai, B., … Xu, Y. (2019). Experimental study on CO2/R32 blends in a water-to-water heat pump system. *Applied Thermal Engineering*. https://doi.org/10.1016/j.applthermaleng.2019.114303

Sung, T., Yun, E., Kim, H. D., Yoon, S. Y., Choi, B. S., Kim, K., … Kim, K. C. (2016). Performance characteristics of a 200-kW organic Rankine cycle system in a steel processing plant. *Applied Energy*. https://doi.org/10.1016/j.apenergy.2016.09.018

Swedish Stirling AB. (2019). Retrieved from https://swedishstirling.com/en/

Szulgowska-Zgrzywa, M., & Fidorów-Kaprawy, N. (2017). Performance analysis of a brine-to-water heat pump and of its boreholes' temperature change during three years of operation. *Applied Thermal Engineering*. https://doi.org/10.1016/j.applthermaleng.2017.07.129

Szybist, J., Davis, S., Thomas, J., & Kaul, B. C. (2018). Performance of a Half-Heusler Thermoelectric Generator for Automotive Application. *SAE Technical Papers*, *2018-April*. https://doi.org/10.4271/2018-01-0054

Tartière, T., & Astolfi, M. (2017). A World Overview of the Organic Rankine Cycle Market. *Energy Procedia*. https://doi.org/10.1016/j.egypro.2017.09.159

TASIO H2020. (2019). Retrieved from GA ID: 637189 website: https://cordis.europa.eu/project/id/637189

Tauveron, N., Colasson, S., & Gruss, J. (2015). Conversion of waste heat to electricity: cartography of possible cycles due to hot source characteristics. *Proceedings of ECOS 2015 - The 28th International Conference on Efficiency, Cost, Optimization, Simulation and Environmental Impact of Energy Systems*, 1–13.

Tchanche, B. F., Lambrinos, G., Frangoudakis, A., & Papadakis, G. (2011). Low-grade heat conversion into power using organic Rankine cycles - A review of various applications. *Renewable and Sustainable Energy Reviews*. https://doi.org/10.1016/j.rser.2011.07.024

Teap. (2019). Retrieved from https://www.teappcm.com/products.htm

TECTEG. (2019). TECTEG. Retrieved from https://tecteg.com/

TEGMART. (2019). TEGMART. Retrieved from https://www.tegmart.com/

The Insight Partners. (2019). Waste Heat Boiler Market to 2027. Retrieved from https://www.theinsightpartners.com/reports/waste-heat-boiler-market

Thermax - Waste heat recovery boilers. (2019). Retrieved January 30, 2020, from https://www.thermaxglobal.com/process-heating-solutions-industrial-heaters-manufacturers/waste-heat-recovery-boiler/

ThermTech. (2020). Retrieved February 6, 2020, from http://thermtech.co.uk/category/case-studies/

Thomson, A., & Claudio, G. (2019). The Technical and Economic Feasibility of Utilising Phase Change Materials for Thermal Storage in District Heating Networks. *Energy Procedia*. https://doi.org/10.1016/j.egypro.2018.12.042

Thulukkanam, K. (2013). Heat Exchanger Design Handbook. In *Heat Exchanger Design Handbook*. https://doi.org/10.1201/b14877

Toffolo, A., Lazzaretto, A., Manente, G., & Paci, M. (2014). A multi-criteria approach for the optimal selection of working fluid and design parameters in Organic Rankine Cycle systems. *Applied Energy*, *121*, 219–232. https://doi.org/10.1016/j.apenergy.2014.01.089

Trojanowski, R., Butcher, T., Worek, M., & Wei, G. (2016). Polymer heat exchanger design for condensing boiler applications. *Applied Thermal Engineering*. https://doi.org/10.1016/j.applthermaleng.2016.03.004

Horizon 2020
European Union Funding
for Research & Innovation

This project has received funding from
the European Union's Horizon 2020 research and innovation
programme under grant agreement No 847097

Turboden. (2019). Retrieved from https://www.turboden.com/case-histories

Tveit, T.-M. (2017). Application of an industrial heat pump for steam generation using district heating as heat source. *12th IEA Heat Pump Conference, Rotterdam, The Netherlands*, 1–9.

U.S. Department of Energy. (2007). *Considerations When Selecting a Condensing Economizer*.

U.S. Department of Energy. (2017a). *Absorption Chillers for CHP Systems*.

U.S. Department of Energy. (2017b). *Microturbines*.

U.S. Department of Energy. (2020). STEP project. Retrieved February 21, 2020, from https://www.gti.energy/step-demo/step-demo-project/

U.S. Environmental Protection Agency. (2012). *Waste heat to power systems*.

Unterhaching. (2019). Retrieved from http://www.thinkgeoenergy.com/tender-sale-of-up-to-3-4-mwe-kalina-geothermal-power-plant-technology-of-unterhaching/

Utlu, Z. (2019). Thermophotovoltaic applications in waste heat recovery systems: example of GaSb cell. *International Journal of Low-Carbon Technologies*, *00*, 1–10.

Utlu, Z., Paralı, U., & Gültekin, Ç. (2018). Applicability of Thermophotovoltaic Technologies in the Iron and Steel Sectors. *Energy Technology*, *6*(6), 1039–1051. https://doi.org/10.1002/ente.201700607

Vahterus. (2020). Retrieved February 13, 2020, from https://vahterus.com/products

Van Essen, V. M., Zondag, H. A., Cot Gores, J., Bleijendaal, L. P. J., Bakker, M., Schuitema, R., … Rindt, C. C. M. (2009). Characterization of $MgSO_4$ hydrate for thermochemical seasonal heat storage. *Journal of Solar Energy Engineering, Transactions of the ASME*, *131*(4), 0410141–0410147. https://doi.org/10.1115/1.4000275

Varga, Z., & Csaba, T. (2018). Techno-economic evaluation of waste heat recovery by organic Rankine cycle using pure light hydrocarbons and their mixtures as working fluid in a crude oil refinery. *Energy Conversion and Management*. https://doi.org/10.1016/j.enconman.2018.08.031

Ventas, R., Lecuona, A., Vereda, C., & Rodriguez-Hidalgo, M. C. (2017). Performance analysis of an absorption double-effect cycle for power and cold generation using ammonia/lithium nitrate. *Applied Thermal Engineering*. https://doi.org/10.1016/j.applthermaleng.2016.12.102

Ventas, R., Lecuona, A., Zacarías, A., & Venegas, M. (2010). Ammonia-lithium nitrate absorption chiller with an integrated low-pressure compression booster cycle for low driving temperatures. *Applied Thermal Engineering*. https://doi.org/10.1016/j.applthermaleng.2010.02.022

Viessmann Vitomax 200-RS - waste heat boiler for generating steam. (2020). Retrieved January 30, 2020, from https://www.viessmann.ae/en/industry/waste-heat-boilers/steam-generation/vitomax-200rs.html

Vigants, E., Prodanuks, T., Vigants, G., Veidenbergs, I., & Blumberga, D. (2017). Modelling of Technological Solutions to 4th Generation DH Systems. In *Environmental and Climate Technologies*. https://doi.org/10.1515/rtuect-2017-0007

Vigants, G., Galindoms, G., Veidenbergs, I., Vigants, E., & Blumberga, D. (2015). Efficiency Diagram for District Heating System with Gas Condensing Unit. *Energy Procedia*. https://doi.org/10.1016/j.egypro.2015.06.017

Villar, A., Parrondo, J., & Arribas, J. J. (2014). District heating from industrial surplus heat in Avilés (Spain). *Environmental Progress and Sustainable Energy*, *33*(4), 1380–1388. https://doi.org/10.1002/ep.11883

Vnukov, A. K., & Rozanova, F. A. (2013). The improvement of the effectiveness of using natural gas in hot-water boilers by means of condensing economizers. *Thermal Engineering (English Translation of Teploenergetika)*, *60*(7), 499–505. https://doi.org/10.1134/S0040601513070136

Volpi, G., Penati, M., & Silva, G. (2005). Heat Recovery Steam Generators for large combined cycle plants (250

Horizon 2020
European Union Funding
for Research & Innovation

This project has received funding from
the European Union's Horizon 2020 research and innovation
programme under grant agreement No 847097

MWe GT output): experiences with different design options and promising improvements by once-through technology development. *Power Gen Europe 2005, Milan, 28-30 June 2005*, (June), 1–16.

Wabtec corporation - Radiation recuperators. (2020). Retrieved February 7, 2020, from https://www.wabtec.com/products/7689/radiation-recuperators

Wahlroos, M., Pärssinen, M., Manner, J., & Syri, S. (2017). Utilizing data center waste heat in district heating – Impacts on energy efficiency and prospects for low-temperature district heating networks. *Energy*, *140*, 1228–1238. https://doi.org/10.1016/j.energy.2017.08.078

Walmsley, T. G., Atkins, M. J., Walmsley, M. R. W., Philipp, M., & Peesel, R.-H. (2018). Process and utility systems integration and optimisation for ultra-low energy milk powder production. *Energy*, *146*, 67–81. https://doi.org/10.1016/j.energy.2017.04.142

Walnum, H. T., Nekså, P., Nord, L. O., & Andresen, T. (2013). Modelling and simulation of CO2 (carbon dioxide) bottoming cycles for offshore oil and gas installations at design and off-design conditions. *Energy*, *59*, 513–520. https://doi.org/10.1016/j.energy.2013.06.071

Walsh, C., & Thornley, P. (2012). The environmental impact and economic feasibility of introducing an organic Rankine cycle to recover low grade heat during the production of metallurgical coke. *Journal of Cleaner Production*. https://doi.org/10.1016/j.jclepro.2011.12.024

Wang, C., He, B., Sun, S., Wu, Y., Yan, N., Yan, L., & Pei, X. (2012). Application of a low pressure economizer for waste heat recovery from the exhaust flue gas in a 600 MW power plant. *Energy*, *48*(1), 196–202. https://doi.org/10.1016/j.energy.2012.01.045

Wang, C., He, B., Yan, L., Pei, X., & Chen, S. (2014). Thermodynamic analysis of a low-pressure economizer based waste heat recovery system for a coal-fired power plant. *Energy*, *65*, 80–90. https://doi.org/10.1016/j.energy.2013.11.084

Wang, D., Bao, A., Kunc, W., & Liss, W. (2012). Coal power plant flue gas waste heat and water recovery. *Applied Energy*. https://doi.org/10.1016/j.apenergy.2011.10.003

Wang, E., & Yu, Z. (2016). A numerical analysis of a composition-adjustable Kalina cycle power plant for power generation from low-temperature geothermal sources. *Applied Energy*, *180*, 834–848. https://doi.org/10.1016/j.apenergy.2016.08.032

Wang, Hanzhi, Li, H., Bu, X., & Wang, L. (2016). Optimum performance of a double absorption heat transformer. *Energy Conversion and Management*. https://doi.org/10.1016/j.enconman.2016.05.095

Wang, Hanzhi, Li, H., Bu, X., & Wang, L. (2017). Effects of the generator and evaporator temperature differences on a double absorption heat transformer—Different control strategies on utilizing heat sources. *Energy Conversion and Management*. https://doi.org/10.1016/j.enconman.2017.01.076

Wang, Huarong, Xu, J., Yang, X., Miao, Z., & Yu, C. (2015). Organic Rankine cycle saves energy and reduces gas emissions for cement production. *Energy*. https://doi.org/10.1016/j.energy.2015.03.112

Wang, Jiangfeng, Dai, Y., & Gao, L. (2009). Exergy analyses and parametric optimizations for different cogeneration power plants in cement industry. *Applied Energy*. https://doi.org/10.1016/j.apenergy.2008.09.001

Wang, Jiangfeng, Yan, Z., Zhou, E., & Dai, Y. (2013). Parametric analysis and optimization of a Kalina cycle driven by solar energy. *Applied Thermal Engineering*. https://doi.org/10.1016/j.applthermaleng.2012.09.002

Wang, Jianxiang, Ye, H., Wu, X., Wang, H., & Xu, X. (2013). Experimental investigation and feasibility analysis of a thermophotovoltaic cogeneration system in high-temperature production processes. *Frontiers in Energy*, *7*(2), 146–154. https://doi.org/10.1007/s11708-013-0253-y

Wang, S. sen, Wu, C., & Li, J. (2018). Exergoeconomic analysis and optimization of single-pressure single-stage

Horizon 2020
European Union Funding
for Research & Innovation

This project has received funding from
the European Union's Horizon 2020 research and innovation
programme under grant agreement No 847097

and multi-stage CO2 transcritical power cycles for engine waste heat recovery: A comparative study. *Energy*, *142*, 559–577. https://doi.org/10.1016/j.energy.2017.10.055

Wang, W. (2010). *Mobilized thermal energy storage for heat recovery for distributed heating*.

Wang, W., Guo, S., Li, H., Yan, J., Zhao, J., Li, X., & Ding, J. (2014). Experimental study on the direct/indirect contact energy storage container in mobilized thermal energy system (M-TES). *Applied Energy*. https://doi.org/10.1016/j.apenergy.2013.12.058

Wang, W., Hu, Y., Yan, J., Nyström, J., & Dahlquist, E. (2010). Combined heat and power plant integrated with mobilized thermal energy storage (M-TES) system. *Frontiers of Energy and Power Engineering in China*, *4*(4), 469–474. https://doi.org/10.1007/s11708-010-0123-9

Wang, X., Liu, J., Zhang, Y., Di, H., & Jiang, Y. (2006). Experimental research on a kind of novel high temperature phase change storage heater. *Energy Conversion and Management*. https://doi.org/10.1016/j.enconman.2005.12.004

Wang, Y., Yu, K., & Ling, X. (2019). Experimental and modeling study on thermal performance of hydrated salt latent heat thermal energy storage system. *Energy Conversion and Management*. https://doi.org/10.1016/j.enconman.2019.111796

Warren, I. (1982). Ljungstrom heat exchangers for waste heat recovery. *Journal of Heat Recovery Systems*. https://doi.org/10.1016/0198-7593(82)90019-4

Wasabi Energy Limited. (2010). *Commissioning of world's first solar thermal Kalina Cycle power plant, during Expo 2010 in Shanghai, China*.

Watanabe, c. (2017). *Theoretical and Experimental Study on High-Temperature Heat Pumps Using a Low GWP Refrigerant*.

Wei, G., Wang, G., Xu, C., Ju, X., Xing, L., Du, X., & Yang, Y. (2018). Selection principles and thermophysical properties of high temperature phase change materials for thermal energy storage: A review. *Renewable and Sustainable Energy Reviews*. https://doi.org/10.1016/j.rser.2017.05.271

Wemmers, A. K., Haasteren, A. W. M. B., Kremers, P., & Kamp, P. an der. (2017). Test results R600 pilot heat pump. *12th IEA Heat Pump Conference*, 1–9. Retrieved from http://hpc2017.org/wp-content/uploads/2017/05/O.3.5.3-Test-results-R600-pilot-heat-pump.pdf

Werner, A., Klemencic, G., Flegkas, S., Haider, M., & Helmut Leibinger. (2016). Comparison of conventional and CO2 power generation cycles for waste heat recovery. *The 5th International Symposium - Supercritical CO2 Power Cycles*, 1–15.

Werner, S. (2017a). District heating and cooling in Sweden. *Energy*, *126*, 419–429. https://doi.org/10.1016/j.energy.2017.03.052

Werner, S. (2017b). International review of district heating and cooling. *Energy*, *137*, 617–631. https://doi.org/10.1016/j.energy.2017.04.045

Wilkes, J. C. (2018). *Tutorial: Fundamentals of Supercritical CO2* (Southwest Research Institute, Ed.).

William B. Stine and Richard B. Diver. (1994). *A Compendium of Solar Dish/Stirling Technology*.

Wright, S.A., Davidson, C. L., & Scammel, W. . (2016). Thermo Economic Analysis of Four sCO2 Waste Heat Recovery Power Systems. *Supercritical CO2 Power Cycle Symposium*.

Wright, Steven A, Davidson, C. S., & Husa, C. (2018). Off-design performance modeling results for a supercritical CO 2 waste heat recovery power system. *The 6th International Supercritical CO2 Power Cycles Symposium*, 1–10.

Wu, M., Xu, C., & He, Y. L. (2014). Dynamic thermal performance analysis of a molten-salt packed-bed thermal energy storage system using PCM capsules. *Applied Energy*.

Horizon 2020
European Union Funding
for Research & Innovation

This project has received funding from
the European Union's Horizon 2020 research and innovation
programme under grant agreement No 847097

https://doi.org/10.1016/j.apenergy.2014.01.085

Wu, S., Zhou, C., Doroodchi, E., Nellore, R., & Moghtaderi, B. (2018). A review on high-temperature thermochemical energy storage based on metal oxides redox cycle. *Energy Conversion and Management*. https://doi.org/10.1016/j.enconman.2018.05.017

Wu, W., Ran, S., Shi, W., Wang, B., & Li, X. (2016). NH3-H2O water source absorption heat pump (WSAHP) for low temperature heating: Experimental investigation on the off-design performance. *Energy*. https://doi.org/10.1016/j.energy.2016.09.058

Wu, W., Wang, B., Shi, W., & Li, X. (2014a). Absorption heating technologies: A review and perspective. *Applied Energy*. https://doi.org/10.1016/j.apenergy.2014.05.027

Wu, W., Wang, B., Shi, W., & Li, X. (2014b). Techno-economic analysis of air source absorption heat pump: Improving economy from a design perspective. *Energy and Buildings*. https://doi.org/10.1016/j.enbuild.2014.06.018

Wu, X., Xing, Z., He, Z., Wang, X., & Chen, W. (2016). Performance evaluation of a capacity-regulated high temperature heat pump for waste heat recovery in dyeing industry. *Applied Thermal Engineering*. https://doi.org/10.1016/j.applthermaleng.2015.10.075

Wuerth, M., Becker, M., Ostermeier, P., Gleis, S., & Spliethoff, H. (2019). Development of a continuous fluidized bed reactor for thermochemical energy storage application. *Journal of Energy Resources Technology, Transactions of the ASME*, *141*(7). https://doi.org/10.1115/1.4043629

Xia, J., Zhu, K., & Jiang, Y. (2016). Method for integrating low-grade industrial waste heat into district heating network. *Building Simulation*, *9*(2), 153–163. https://doi.org/10.1007/s12273-015-0262-3

Xiao, B., Chang, H., He, L., Zhao, S., & Shu, S. (2020). Annual performance analysis of an air source heat pump water heater using a new eco-friendly refrigerant mixture as an alternative to R134a. *Renewable Energy*. https://doi.org/10.1016/j.renene.2019.09.143

Xiao, B., He, L., Zhang, S., Kong, T., Hu, B., & Wang, R. Z. (2020). Comparison and analysis on air-to-air and air-to-water heat pump heating systems. *Renewable Energy*. https://doi.org/10.1016/j.renene.2019.08.033

Xu, B., Li, P., & Chan, C. (2015). Application of phase change materials for thermal energy storage in concentrated solar thermal power plants: A review to recent developments. *Applied Energy*. https://doi.org/10.1016/j.apenergy.2015.09.016

Xu, L., Torrens, J. I., Guo, F., Yang, X., & Hensen, J. L. M. (2018). Application of large underground seasonal thermal energy storage in district heating system: A model-based energy performance assessment of a pilot system in Chifeng, China. *Applied Thermal Engineering*, *137*, 319–328. https://doi.org/10.1016/j.applthermaleng.2018.03.047

Xu, Z., & Wang, R. (2017). Absorption heat pump for waste heat reuse: current states and future development. *Frontiers in Energy*, *11*(4), 414–436. https://doi.org/10.1007/s11708-017-0507-1

Xu, Z. Y., Mao, H. C., Liu, D. S., & Wang, R. Z. (2018). Waste heat recovery of power plant with large scale serial absorption heat pumps. *Energy*. https://doi.org/10.1016/j.energy.2018.10.052

Yağli, H., Koç, Y., Koç, A., Görgülü, A., & Tandiroğlu, A. (2016). Parametric optimization and exergetic analysis comparison of subcritical and supercritical organic Rankine cycle (ORC) for biogas fuelled combined heat and power (CHP) engine exhaust gas waste heat. *Energy*. https://doi.org/10.1016/j.energy.2016.05.119

Yan, T., Wang, R. Z., Li, T. X., Wang, L. W., & Fred, I. T. (2015). A review of promising candidate reactions for chemical heat storage. *Renewable and Sustainable Energy Reviews*. https://doi.org/10.1016/j.rser.2014.11.015

Yang, H., Xu, C., Yang, B., Yu, X., Zhang, Y., & Mu, Y. (2020). Performance analysis of an Organic Rankine Cycle system using evaporative condenser for sewage heat recovery in the petrochemical industry. *Energy*

Horizon 2020
European Union Funding
for Research & Innovation

This project has received funding from
the European Union's Horizon 2020 research and innovation
programme under grant agreement No 847097

Conversion and Management. https://doi.org/10.1016/j.enconman.2019.112402

Yang, S., Qian, Y., Wang, Y., & Yang, S. (2017). A novel cascade absorption heat transformer process using low grade waste heat and its application to coal to synthetic natural gas. *Applied Energy*. https://doi.org/10.1016/j.apenergy.2017.04.028

Yang, Z., Zhang, Y., Dong, Q., Lin, J., Lin, G., & Chen, J. (2018). Maximum power output and parametric choice criteria of a thermophotovoltaic cell driven by automobile exhaust. *Renewable Energy*. https://doi.org/10.1016/j.renene.2018.01.009

Yin, J., Shi, L., Zhu, M. S., & Han, L. Z. (2000). Performance analysis of an absorption heat transformer with different working fluid combinations. *Applied Energy*. https://doi.org/10.1016/S0306-2619(00)00024-6

Yu, C., & Chau, K. T. (2009). Thermoelectric automotive waste heat energy recovery using maximum power point tracking. *Energy Conversion and Management*. https://doi.org/10.1016/j.enconman.2009.02.015

Yu, M. (2018). *Waste Heat Recovery from Aluminium Production*. Reykjavík University.

Yu, N., Wang, R. Z., & Wang, L. W. (2013). Sorption thermal storage for solar energy. *Progress in Energy and Combustion Science*. https://doi.org/10.1016/j.pecs.2013.05.004 Review

Yue, C., Han, D., Pu, W., & He, W. (2015). Comparative analysis of a bottoming transcritical ORC and a Kalina cycle for engine exhaust heat recovery. *Energy Conversion and Management*, *89*, 764–774. https://doi.org/10.1016/j.enconman.2014.10.029

Zalba, B., Marín, J. M., Cabeza, L. F., & Mehling, H. (2003). Review on thermal energy storage with phase change: Materials, heat transfer analysis and applications. *Applied Thermal Engineering*. https://doi.org/10.1016/S1359-4311(02)00192-8

Zamora, M., Bourouis, M., Coronas, A., & Vallès, M. (2014). Pre-industrial development and experimental characterization of new air-cooled and water-cooled ammonia/lithium nitrate absorption chillers. *International Journal of Refrigeration*, *45*, 189–197. https://doi.org/10.1016/j.ijrefrig.2014.06.005

Zamora, M., Bourouis, M., Coronas, A., & Vallès, M. (2015). Part-load characteristics of a new ammonia/lithium nitrate absorption chiller. *International Journal of Refrigeration*. https://doi.org/10.1016/j.ijrefrig.2014.11.005

Zebik, A., Baliko, S., & Mont, J. (1997). Heat recovery from industry. *Energy Engineering: Journal of the Association of Energy Engineering*, *94*(5), 61–72. https://doi.org/10.1080/01998595.1997.10530389

Zeinelabdein, R., Omer, S., & Gan, G. (2018). Critical review of latent heat storage systems for free cooling in buildings. *Renewable and Sustainable Energy Reviews*. https://doi.org/10.1016/j.rser.2017.10.046

Zhang, H., Baeyens, J., Cáceres, G., Degrève, J., & Lv, Y. (2016). Thermal energy storage: Recent developments and practical aspects. *Progress in Energy and Combustion Science*. https://doi.org/10.1016/j.pecs.2015.10.003

Zhang, K., Liu, Z., Li, Y., Li, Q., Zhang, J., & Liu, H. (2014). The improved CO2 capture system with heat recovery based on absorption heat transformer and flash evaporator. *Applied Thermal Engineering*, *62*(2), 500–506. https://doi.org/10.1016/j.applthermaleng.2013.10.007

Zhang, P., Ma, F., & Xiao, X. (2016). Thermal energy storage and retrieval characteristics of a molten-salt latent heat thermal energy storage system. *Applied Energy*. https://doi.org/10.1016/j.apenergy.2016.04.012

Zhang, Q., Zhang, L., Nie, J., & Li, Y. (2017). Techno-economic analysis of air source heat pump applied for space heating in northern China. *Applied Energy*. https://doi.org/10.1016/j.apenergy.2017.06.083

Zhang, S., Wang, H., & Guo, T. (2010). Experimental investigation of moderately high temperature water source heat pump with non-azeotropic refrigerant mixtures. *Applied Energy*. https://doi.org/10.1016/j.apenergy.2009.11.001

Horizon 2020
European Union Funding
for Research & Innovation

This project has received funding from
the European Union's Horizon 2020 research and innovation
programme under grant agreement No 847097

Zhang, Yan, Zhang, Y., Yu, X., Guo, J., Deng, N., Dong, S., … Ma, X. (2017). Analysis of a high temperature heat pump using BY-5 as refrigerant. *Applied Thermal Engineering*. https://doi.org/10.1016/j.applthermaleng.2017.08.072

Zhang, Yaning, Ma, Q., Li, B., Fan, X., & Fu, Z. (2017). Application of an air source heat pump (ASHP) for heating in Harbin, the coldest provincial capital of China. *Energy and Buildings*. https://doi.org/10.1016/j.enbuild.2016.12.044

Zhang, Yanliang, Cleary, M., Wang, X., Kempf, N., Schoensee, L., Yang, J., … Meda, L. (2015). High-temperature and high-power-density nanostructured thermoelectric generator for automotive waste heat recovery. *Energy Conversion and Management*. https://doi.org/10.1016/j.enconman.2015.08.051

Zhao, X., Fu, L., Sun, T., Wang, J. Y., & Wang, X. Y. (2017). The recovery of waste heat of flue gas from gas boilers. *Science and Technology for the Built Environment*, *23*(3), 490–499. https://doi.org/10.1080/23744731.2016.1223976

Zhao, Z., Zhang, X., & Ma, X. (2005). Thermodynamic performance of a double-effect absorption heat-transformer using TFE/E181 as the working fluid. *Applied Energy*. https://doi.org/10.1016/j.apenergy.2004.10.012

Zheng, X. F., Liu, C. X., Yan, Y. Y., & Wang, Q. (2014). A review of thermoelectrics research - Recent developments and potentials for sustainable and renewable energy applications. *Renewable and Sustainable Energy Reviews*. https://doi.org/10.1016/j.rser.2013.12.053

Zhi, L. H., Hu, P., Chen, L. X., & Zhao, G. (2019). Parametric analysis and optimization of transcritical-subcritical dual-loop organic Rankine cycle using zeotropic mixtures for engine waste heat recovery. *Energy Conversion and Management*. https://doi.org/10.1016/j.enconman.2019.05.062

Zhu, K., Xia, J., Xie, X., & Jiang, Y. (2014). Total heat recovery of gas boiler by absorption heat pump and direct-contact heat exchanger. *Applied Thermal Engineering*, *71*(1), 213–218. https://doi.org/10.1016/j.applthermaleng.2014.06.047

Zhu, S., Zhang, K., & Deng, K. (2019). A review of waste heat recovery from the marine engine with highly efficient bottoming power cycles. *Renewable and Sustainable Energy Reviews*. https://doi.org/10.1016/j.rser.2019.109611

Ziemele, J., Blumberga, D., Talcis, N., & Laicane, I. (2012). Industrial research of condensing unit for natural gas boiler house. *Environmental and Climate Technologies*, *10*(1), 34–38. https://doi.org/10.2478/v10145-012-0023-9

Zondag, H., Kikkert, B., Smeding, S., Boer, R. de, & Bakker, M. (2013). Prototype thermochemical heat storage with open reactor system. *Applied Energy*. https://doi.org/10.1016/j.apenergy.2013.01.082

Horizon 2020
European Union Funding
for Research & Innovation

This project has received funding from
the European Union's Horizon 2020 research and innovation
programme under grant agreement No 847097